ELLIPSOMETRY OF ANODIC FILM GROWTH

Craig Gordon Smith
(Ph. D. thesis)

August 1978

Prepared for the U. S. Department of Energy
under Contract W-7405-ENG-48

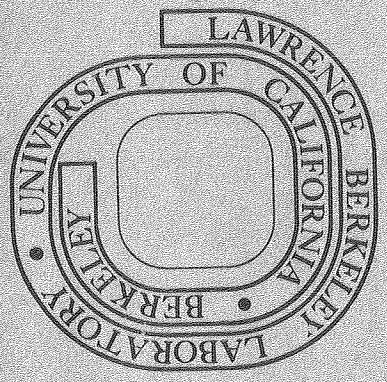

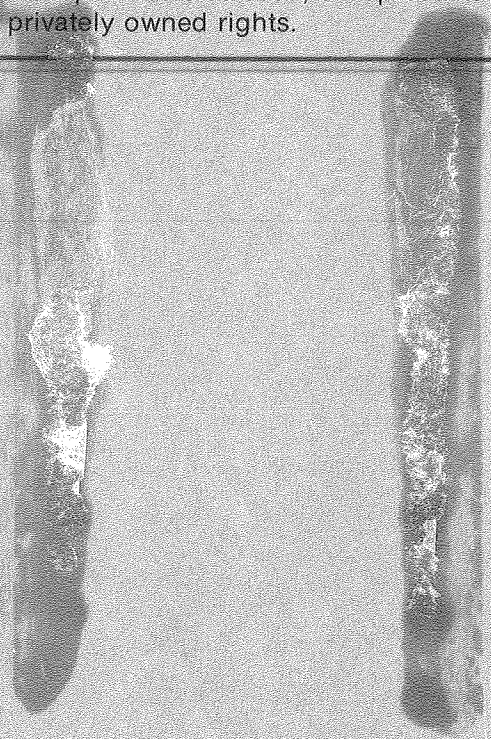

ELLIPSOMETRY OF ANODIC FILM GROWTH

Craig Gordon Smith

Lawrence Berkeley Laboratory
University of California
Berkeley, California

ELLIPSOMETRY OF ANODIC FILM GROWTH

TABLE OF CONTENTS

Ellipsometry of Anodic Film Growth

Craig Gordon Smith

Materials and Molecular Research Division, Lawrence Berkeley Laboratory
and Department of Chemical Engineering, University of California,
Berkeley, California 94720

ABSTRACT

An automated computer interpretation of ellipsometer measurements of anodic film growth has been developed. Continuous mass and charge balances are used to utilize more fully the time-dependence of the ellipsometer data and the current and potential measurements. A multiple-film model is used to characterize the growth of films which proceeds via a dissolution-precipitation mechanism; the model also applies to film growth by adsorption and nucleation mechanisms. Characteristic parameters describing the film growth are evaluated by a fitting routine in a multidimensional space, and error limits for the values are assigned. The characteristic parameters describe homogeneous and heterogeneous crystallization rates, film porosities and degree of hydration, and the supersaturation of ionic species in the electrolyte. Additional descriptions which may be chosen are patchwise film formation, non-stoichiometry of the anodic film, and statistical variations in the size and orientation of secondary crystals. Theories were developed to describe the optical effects of these processes.

An automatic, self-compensating ellipsometer has been used to study the growth in alkaline solution of anodic films on silver, cadmium, and zinc. Mass-transport conditions included stagnant electrolyte and forced convection in a flow channel. Single crystal and polycrystalline

electrodes were used. Multiple films are needed to characterize the optical properties of these films. Anodic films grow from an electrolyte supersaturated in the solution-phase dissolution product. The degree of supersaturation of the solution-phase species depends on transport conditions and has a major effect on the structure of the film. Anodic reaction rates are limited by the transport of charge carriers through a primary surface layer. Film porosities derived from ellipsometer measurements agree with film conductivity inferred from electrode potential measurements. The primary layers on silver, zinc, and cadmium all appear to be non-stoichiometric, containing excess metal. Diffusion coefficients, transference numbers, and the free energy of adsorption of zinc oxide have been derived from ellipsometer measurements.

John Newman

II. Introduction

Ellipsometry is a surface-sensitive technique which allows *in situ* observations to be conducted during electrode reactions. While this technique has been known since the turn of the century, the fact that the use of manual ellipsometers required about 5 minutes to make a measurement restricted the applications of this technique to observations of static or slowly-changing surfaces. Automatic ellipsometers, which have recently been developed, have measurement periods on the order of one millisecond, and are now able to provide accurate information about the optical properties of rapidly growing anodic films.

A systematic investigation of the effects on anodic film formation of mass-transport conditions, alkaline concentration, electrode current density, and the crystallographic orientation of the metal substrate has been undertaken. Film formation on silver, zinc, and cadmium has been studied. These metals have practical applications towards battery technology, and conventional electrical measurements have not provided sufficient information about the reaction mechanisms involved, or about the effects surface layers have on the electrode process.

III. Literature Review

A. Silver Oxide Literature Review

Extensive investigations have been performed on the $Ag/Ag_2O/AgO$ system in alkaline solutions (A1-A3). Nevertheless, the reaction mechanism still remains uncertain. In situ measurements have been restricted to classical electrochemical techniques (current, potential, and impedence measurements). Characterizations have also been performed by X-ray, electron, and neutron diffraction, and scanning electron microscopy, all of which require transfer of the sample into vacuum.

Kinetics

Potential measurements in the galvanostatic mode yield three distinct plateaus (A4). X-ray and electron diffraction studies (A5-A9) indicate the products of the first two plateaus are Ag_2O and AgO. Neutron-diffraction (A10) indicates AgO is actually composed of the monovalent and trivalent silver; the divalent state is not present as indicated by the diamagnetic properties of silver. At the third plateau, oxygen is the primary product (A4), with possible simultaneous Ag_2O_3 formation. The potential during Ag_2O formation for a smooth, uncycled sheet is higher than on a cycled sheet, and a maximum or overshoot prior to the first plateau is observed (A4, A11).

Current measurements during potential sweeps yield additional information. A peak prior to Ag_2O formation has been suggested as being due to the formation of $AgOH$ (A12, A13). When no AgO is present, only Ag_2O and Ag_2O_3 peaks were observed (A14). The trivalent

product Ag_2O_3 has been isolated from acid solution (A15), but not from alkaline solution. On the cathodic sweep, AgO is formed from Ag_2O_3 (A14). In general, the potential peaks and the magnitude of the current density depend upon sweep rates, temperature, and alkaline concentration (A12, A14-A17).

Overpotential measurements indicate two distinct behaviors during the Ag_2O plateau. In 1 M KOH and at low current densities, Tafel behavior is observed with a slope of 20 to 30 mV/decade and an exchange current density of 10^{-8} to 10^{-6} A/cm^2 (A11). At high current densities and larger alkaline concentration the potential-current relationship is linear. The limiting thickness of the Ag_2O film at which the transition to AgO formation occurs shows corresponding behaviors: for i less than 0.25 mA/cm^2 the limiting thickness varies linearly with current densities, while for larger current densities, the limiting thickness varies linearly with the logarithm of the current density (A11). Open circuit potential decays ($i = 0.4$ mA/cm^2) indicate that of 30 to 40 mV total overpotential, the first 10 to 15 mV had Tafel slopes of 12 to 23 mV/decade, with the lowest slope occurring at the middle of the Ag_2O plateau. The remaining overpotential decayed very slowly and had slopes of 30 to 9 mV/decade (A11). A subsequent investigation indicated the initial fast decay was followed by <u>two</u> slower decays (A18).

<u>Physical Characteristics</u>

The total charge passed during the galvanostatic formation of Ag_2O is usually less than for the subsequent formation of AgO . On

the first cycle, the Ag_2O plateau is always shorter than for subsequent cycles (A19-A21). The capacity of the electrode (charge passed before initiation of O_2 evolution) increases over the first 25 cycles (A22, A23). The onset of oxygen evolution is determined by the thickness of the Ag_2O film, which in turn depends upon the amount of Ag_2O present and the conditions underwhich it has been formed, the current density, alkaline concentration, and the history of the electrode. The thickness of the Ag_2O layer increases as the current density decreases (A24, A25). Maximum oxides are formed in 30 to 35% KOH solutions (A26, A5). Thickness of the layers ranges up to 3 μm (A4, A11). In concentrated alkaline, the films are porous, very rough, and slightly amorphous. At 0.7 M NaOH , low current densities, and with stirring, glassy films up to 7000 Å thick were reported (A11). The thickness of the layers increase with cycling, with initial conditions of the electrode playing an important role (A11). Ag_2O forms as distinct crystals, whose size decreases with increasing current density (0.1 to 10 μm), (A8, A9). At low current densities, the growth of Ag_2O is not uniform, but forms in patches (A4, A5).

An excellent scanning electron micrograph study (A3, A27) indicated that a primary layer of distinct crystals forms prior to the growth of a secondary layer. Electron diffraction patterns of the primary layer consist of rings of uniform intensity. The thickness of this layer was 50-100 Å, based on coulometric estimates. The variation of size of the crystals composing the secondary layer were greatest on the (100) and polycrystal silver electrodes, with the least variation on

the (111) face. The (111) faces of the oxides tended to be parallel to the (100) faces of the metal. The number density of crystals increases with current density. X-ray diffraction indicated a faint $d = 3.35$ Å line at glancing incidence, which was suggested as being due to the 110 face of the oxide.

The increase in potential to the AgO plateau is due to transport through the primary layer (A3). This is evident by an incomplete surface coverage of the secondary layer at the transition. This is in agreement with A-C impedence measurements (A28) which indicate that dissolution is limited by diffusion of Ag^+ through the primary layer. Scanning electron microscopy is unable to give information on the growth of the primary layer after secondary crystal growth has begun.

The surface layer is oxygen rich (A29,A9). The existence of an oxide intermediate between Ag_2O and the monoclinic AgO has been reported. This oxide has a NaCl type lattice (A30).

Reaction Mechanisms

The overall reaction for Ag_2O formation is (A31,A12,A32,A7)

$$2Ag + 2OH^- = Ag_2O + H_2O + 2e^-$$

and for AgO formation is

$$Ag_2O + 2OH = 2AgO + H_2O + 2e^- .$$

The standard potentials (vs H_2) for these reactions are 0.342 V for Ag/Ag_2O and 0.604 V for Ag_2O/AgO (A33,A34). The Pourbaix diagram is given in Ref. (A35).

Solid-State Mechanism

In this postulated mechanism, hydroxyl groups react at the electrode surface with surface ions (A12,A32). The film thickens by O_2^- diffusing into the bulk. Modifications are that Ag^+ or both Ag^+ and O_2^- are the charge carrier. (A21,A36).

Pore-Filling Mechanism

This mechanism regards O_2^- as the moving species, but allows for a porous film. The increase in the resistence of the film is due to the filling of the pores (A37).

Dissolution-Precipitation Mechanism

In this mechanism, dissolution of ionic silver is the initiating step. Ag_2O formation occurs by precipitation of dissolved material from the supersaturated electrolyte. A dependence of the reaction rate on negatively charged ions in solution has been observed (A38,A24). Possible intermediate for the reaction are AgOH (A12) and $Ag(OH)_2^-$ (A12,A24,A39,A13,A40). In a recent investigation in which transport conditions were controlled using a flow cell and rotating disc electrodes, the electrical measurements were fit using this model (A41). The consideration of distinct nucleation sites is central to various modifications (A42,A41).

It has been suggested that two mechanisms are involved (A2), the dissolution-precipitation mechanism for large current densities, and the solid-state mechanism for current densities less than 0.25 mA/cm^2. This logic cites duplex film models for the silver system (A43) and the cadmium system (A44) as support.

Passivation

It is being recognized that surface layers are probably responsible for passivation of the electrode. Chemisorbed O_2 (A43) and OH^- (A45) have been suggested.

Soluble Species

Maximums in the solubility dependencies of Ag_2O with alkaline concentration have been reported (A33,A23): values of 4.8×10^{-4} M in 6 M KOH (A33) and 3.3×10^{-4} in 4.12 (A23). Rotating disc studies during reduction of AgO in 1 M KOH indicate a value of 8.7×10^{-4} M (A46) for the solubility of AgO . The diffusion coefficient for the soluble species associated with Ag_2O formation decreases with alkaline concentration from a value of 8.7×10^{-6} cm^2/s (1 M KOH), (A23).

A1. P. Ruetschi, Zinc-Silver Oxide Batteries, A. Fleicher and J. Lander, ed (John Wiley & Sons, New York, 1971) pp. 117-130.

A2. G. D. Nagy and E. J. Casey, ibid., pp. 133-151.

A3. H. R. Thirsk and D. Lax, ibid., pp. 153-179.

A4. B. D. Cahan, J. Ockerman, R. F. Amlie, and P. Ruetschi, J. Electrochem. Soc. 107, 725 (1960).

A5. J. Burbank and C. P. Wales, J. Electrochem. Soc. 112, 13 (1965).

A6. P. Jones, H. R. Thirsk, W. F. K. Wynne-Jones, Trans. Faraday Soc. 52, 1003 (1956).

A7. C. P. Wales and J. Burbank, J. Electrochem. Soc. 106, 885 (1959).

A8. C. P. Wales and J. Burbank, ibid., 111, 131 (1964).

A9. S. Yoshizawa and Z. Takehara, J. Electrochem. Soc. Japan 31 (3), 91 (1963).

A10. J. A. McMillan, J. Inorg. Nucl. Chem. 13, 28-31 (1960).

A11. M. J. Dignam, H. M. Barrett, G. D. Nagy, Can. J. Chem., 47 4253 (1969).

A12. T. P. Dirkse and D. B. DeVries, J. Phys. Chem. 63, 107 (1959).

A13. J. Ambrose and R. G. Barradas, Electrochim. Acta 19, 781 (1974).

A14. R. H. McClelland and M. Shaw, Extended Abstracts, Electrochem. Soc., Inc., Battery Division 10, 32 (1965).

A15. T. Palagyi and I. Naray-Szabo, Acta. Chim. Acad. Sci. Hung. 30, 1 (1962).

A16. H. Sasaki and S. Toshima, Electrochim. Acta 20, 201 (1975).

A17. P. Stonehart and F. P. Portante, Electrochim. Acta 13, 1805 (1968).

A18. A. A. Yakovleva, T. K. Borisova, and V. I. Veselovskii, Zh. Fiz. Khim 36, 1426 (1962).

A19. I. A. Denison, Trans. Electrochem. Soc. 90, 387 (1946).

A20. A. Hickley and S. Hill, Discussions Far. Soc. 1, 236 (1946).

A21. C. P. Wales, J. Electrochem. Soc. 108, 395 (1961).

A22. T. P. Hoar and C. K. Dyer, Electrochim. Acta 17, 1563 (1972).

A23. B. Miller, J. Electrochem. Soc. 117, 491 (1970).

A24. T. P. Dirkse, D. DeWitt, and R. Shoemaker, J. Electrochem. Soc. 115, 442 (1968); 114, 1196.

A25. C. P. Wales and J. Burbank, J. Electrochem. Soc. 111, 1002 (1964).

A26. C. P. Wales and J. Burbank, ibid., 109, 1119 (1962).

A27. G. W. Briggs, M. Fleischamnn, D. J. Lax, and H. R. Thirsk, Trans. Faraday Soc. 64, 3120 (1968).

A28. B. N. Kabanov and D. I. Leikis, Z. Electrochim. 62, 660 (1958).

A29. G. M. Arcand, N67-25332 (1967).

A30. K. Gossner and H. Polle, Z. Phys. Chem 54, 93 (1967).

A31. G. T. Croft, J. Electrochemical Soc. 106, 278 (1959).

A32. T. P. Dirkse, J. Electrochem. Soc. 106, 453 (1959); 106, 920 (1959).

A33. R. F. Amlie and P. Ruetschi, J. Electrochemical Soc. 108, 813 (1961).

A34. J. F. Bonk and A. B. Garrett, J. Electrochem. Soc. 106, 612 (1959).

A35. P. Delahay, M. Pourbaix, and P. Van Rysselberghe, J. Electrochem. Soc. 98, 65 (1951).

A36. V. I. Veselovskii, T. K. Borisova, A. A. Jakoleva, S. O. Izidinov, Electrochim. Acta 10, 325 (1965).

A37. T. P. Dirkse and G. J. Werkema, J. Electrochem. Soc. 106, 88 (1959).

A38. T. P. Dirkse and J. B. DeRoos, Z. Phys. Chem. 41, 1 (1964).

A39. R. D. Giles, J. A. Harrison, and H. R. Thirsk, J. Electroanalytic Chem. 22, 375 (1969).

A40. N. A. Hampson, K. I. MacDonald, J. B. Lee, J. Electroanalytic Chem. 45, 149 (1973).

A41. D. B. Gibbs, B. Rao, R. A. Griffin, and M. J. Dignam, J. Electrochem. Soc. 122, 1167 (1975).

A42. B. V. Tilek, R. S. Perkins, H. A. Kozlowska, and B. E. Conway, Electrochim. Acta 17, 1447 (1972).

A43. G. L. Vidovich, D. I. Leikis, and D. N. Kabanov, Dokl. Akad. Nauk, SSSR, 142, 109 (1962).

A44. P. E. Lake and E. J. Casey, J. Electrochem Soc. 106, 913 (1959).

A45. T. P. Dirkse, J. Electrochem. Tech. 5, 18 (1967).

A46. E. F. Zavgorodnyaya, T. Yu Inyutim, and Yu. M. Povarov, Soviet Elect. 13, 332 (1977).

B. Zinc Oxide Literature Review

Kinetics

Studies of the effect of the concentration of the electroactive species on the exchange current density i_o, indicate a two-step dissolution reaction (Z1, Z2)

$$Zn + 2\,OH^- \rightarrow Zn(OH)_2 + 2e$$

$$Zn(OH)_2 + 2OH^- = Zn(OH)_4^{=} \quad .$$

The equilibrium constant for the formation of zincate from the hydroxide has a value β given by (Z3)

$$\beta = \frac{[Zn(OH)_4^{=}]}{[OH^-]^2\,[Zn(OH)_2]} = 10^{15.38}$$

At low overpotentials, impedence measurements indicate the rate of ion exchange at the surface is controlled by the flux of adsorbed zinc surface atoms (Z4, Z5, Z6) and depends upon characteristics of the metal. The exchange current density for the (0001) face is about 1/3 the value for polycrystal electrodes. The exchange current is independent of the soluble zinc concentration (Z7) [$i_o(Zn^{++}=0.016M) = 0.238$; $i_o(Zn^{++}=0.64M) = 0.224$], but depends on the hydroxyl concentration as given by

$$\frac{\partial\, \ell n\, i_o}{\partial\, \ell n\, (OH^-)} = 0.2$$

At high overpotentials, Tafel behavior is observed (Z5, Z8, Z9). The slope of 42 to 49 mV/decade is too high for the overpotential to be pure charge-transfer (30 mV/decade for the 2 electron step). The rest potential has been correlated with the zincate activity and has the form (Z9)

$$E^{o} = 0.441 - 0.1182\ pH + 0.0295 \log \alpha_{Zn(OH)_4^{=}}$$

Soluble Species

The solubility of ZnO in KOH increases with the alkaline concentration (Z10), but does not depend on temperature. The temperature independence suggests zinc is in a colloid form, although the optical clarity of the electrolyte contradicts this. NMR and light scattering were used (Z11), and the authors claim that no colloids or solids exist. Both $Zn(OH)_3^-$ and $Zn(OH)_4^{=}$ appear to be present in strong alkaline electrolytes (Z12, Z13). At larger KOH concentrations, the predominant form is $Zn(OH)_4^{=}$ (Z14). The phase diagram is presented in Ref. (Z15). The thermodynamic solubility, based on the γ-hydroxide intermediate, has the form (Z16)

$$\log\ Zn(OH)_4^{=} = -29.78 + 2pH \quad .$$

Solutions supersaturated in the zinc species are easily formed electrochemically. A white precipitate occurs in battery electrolytes during discharge (Z17, Z18). Concentrations corresponding to twice

the equilibrium value of ZnO are common. On standing, ZnO is eventually formed as the hydroxides [six forms exist (Z19)] are unstable with respect to the oxide (Z20, Z21). The decay of the hydroxides to the oxide is reduced by lithium and silicate ions (Z22). Over a very limited range of silicate concentrations, homogeneous nucleation is strongly promoted (Z23, Z24). The α-hydroxide has been found on the surface of anodes (Z25).

Supersaturation has been studied by Raman spectroscopy (Z26). The zincate species has tetrahedral symmetry (Z27). Polarization modes indicate the bands are depolarized. Only one major form, $Zn(OH)_4^{=}$, is present. For a 70% increase in dissolved zinc species, only a 12% increase in $Zn(OH)_4^{=}$ was observed, or only 1/6 of the dissolved zinc was converted to the zincate.

Passivation

At large current densities, dissolution becomes limited by mass-transport (Z28,Z29). Passivated electrodes become blocked for zinc dissolution by a passive film (Z30 - Z43). Three mechanisms have been suggested for the formation of the passivating film: 1] An absorption model (Z41, Z44); 2] Nucleation and two-dimensional growth of crystals (Z8); and 3] The dissolution-precipitation mechanism. Breiter and Powers (Z45, Z46) have shown that the anodic film is composed of two layers. Type I is a loose, flocculent precipitated film. Below this is a Type II film, which is dark and perhaps only 1 monolayer thick.

Some authors consider the films to be orthorhombic forms of

$Zn(OH)_2$ (Z38). Electron diffraction indicates ZnO is present with grain sizes of between 1 - 3 μm (Z36). The overall stoichiometry is rarely ZnO. Dark, zinc-rich films have been observed at low current densities (Z38, Z39). X-ray transmission and electron diffraction indicate γ-$Zn(OH)_2$ is present. ZnO_2 has been postulated, but not isolated (Z38, Z43). Excess oxygen in the film occurs at high current densities (Z43). It has been postulated that the blackening of the film (excess zinc) is due to the deposition of finely divided zinc by the disproportionation of $Zn(OH)_2^-$ to Zn and $Zn(OH)_4^=$ (Z50).

Passivation times have been correlated by use of the following equation (Z33, Z34, Z41, Z42, Z43, Z47, Z48).

$$(i - i_\ell)\ t_p^{1/2} = k$$

This applies at constant current. i_ℓ is the current density below which no passivation occurs. The constant $t_p^{1/2}$ can be justified by considering the Sand equation for diffusion (Z5). The data are not very reproducible at long times (Z34), but are better at short times ($t < 30s$), (Z42). This equation applies for both natural convection (Z38, Z42) and for pure diffusion (Z37). For natural convection, k and i_ℓ have maximums at about 9 M KOH. A theoretical derivation of the equation has been presented (Z49). Rotating disc studies (Z43) indicate that at passivation, the zincate concentration is about 0.16 times the hydroxyl concentration. The value of t_p is affected little by saturating the electrolyte, implying large supersaturations occur, or that the saturating species is not the passivating species.

Z1. T. P. Dirkse, Zinc-Silver Oxide Batteries (John Wiley & Sons, NY [1969]) A. Fleischer and J. L. Lander, ed., pp. 19-28.

Z2. H. Gerischer, Z. Physik. Chem. 202, 302 (1953).

Z3. T. Sekine, Acta Chem. Scand. 19, 1526 (1965).

Z4. J. P. G. Farr and N. A. Hampson, Trans. Farraday Soc. 62, 3493 (1966).

Z5. N. A. Hampson, Reference 1, pp 37-62.

Z6. R. D. Armstrong and M. F. Bell, J. Electroanal. Chem. 55, 201 (1974).

Z7. J. P. G. Farr and N. A. Hampson, ibid, 13, 443 (1967).

Z8. R. D. Armstrong and G. M. Bulman, ibid, 25, 121 (1970).

Z9. J. O'M. Bockris, Z. Nagy, and A. Damjanovic, J. Electrochem. Soc. 119, 285 (1972).

Z10. T. P. Dirkse, A D - 820273.

Z11. W. Van Doorne and T. P. Dirkse, J. Electrochem. Soc. 122, 1 (1975).

Z12. T. P. Dirkse, ibid, 102, 497 (1955).

Z13. F. Kunschert, Z. Anorg. Chem. 41, 337 (1904).

Z14. T. P. Dirkse, C. Postmus Jr., and R. Vandenbosch, J. Am. Chem. Soc. 76, 6022 (1954).

Z15. T. P. Dirkse, J. Electrochem. Soc. 106, 154 (1959).

Z16. M. Pourbaix, Atlas of Electrochemical Equilibria (Pergamon Press, NY 1966), p. 408.

Z17. T. P. Dirkse, J. Electrochem. Soc. 102, 497 (1955).

Z18. V. N. Flerov, Zh. Fiz. Khim. 31, 49 (1957).

Z19. W. Fleitknecht, Helv. Chim. Acta 13, 314 (1930).

Z20. G. F. Huettig and H. Moeldner, Z. Anorg. Allgem. Chem. 211, 368 (1933).

Z21. R. Fricke and B. Wallhorst, ibid, 205, 127 (1932).

Z22. A. Fischbach and A. L. Almerini, U. S. Pat. 2,811,572 (Oct. 29, 1957).

Z23. A. Marshall, N. A. Hampson, J. Electroanal. Chem. 59, 19 (1975).

Z24. A. Marshall, N. A. Hampson and M. P. Saunders, ibid, 78, 307 (1977).

Z25. T. Inoue, M. Sato, and F. Ishii, J. Electrochem. Soc. Japan, 22, 679 (1954).

Z26. J. F. Jackovitz and A. Langer, Reference 1, pp. 29-36.

Z27. J. S. Fordyce and R. L. Baum, J. Chem. Phys. 43, 843 (1965).

Z28. R. Landsberg, L. Mueller, Wiss. Z. Tech. Hochsch. Chem. Leuna-Merseburg 2, 103 (1959).

Z29. E. D. Farmer and A. H. Webb, J. Appl. Electrochem. 2, 123 (1972).

Z30. F. Jolas, Electrochim. Acta 13, 2207 (1968).

Z31. T. P. Dirkse, J. Electrochem. Soc. 328 (1954).

Z32. T. P. Dirkse, ibid, 102, 497 (1955).

Z33. S. Dmitriev, Ref. Zh. Khim, 9, Pt. 1 (1966).

Z34. M. Eisenberg, H. F. Baumann, and D. M. Brettner, J. Electrochem. Soc. 108, 909 (1961).

Z35. H. Fischer and N. Budiloff, Z. Mettalik 32, 100 (1940).

Z36. H. Fry and M. Whitaker, J. Electrochem. Soc. 106, 606 (1959).

Z37. H. A. Hampson and M. J. Tarbox, ibid, 110, 95 (1962).

Z38. H. A. Hampson, M. J. Tarbox, J. T. Lilley, and J. P. G. Farr, Electrochem. Tech. 2, 309 (1964).

Z39. K. Huber, J. Electrochem. Soc., 100, 376 (1953).

Z40. Z. A. Iofa, S. Ya Mirlina, and N. B. Moiseeva, Zh Prikl Khim 35, 1571 (1961).

Z41. B. N. Kabanov, Electrochim. Acta 6, 253 (1962).

Z42. R. Landsberg and H. Barlett, Z. Electrochem. 61, 1162 (1957).

Z43. T. I. Popeva, V. S. Bagotskii, and B. N. Kabanov, Zh. Fiz. Khim. 36, 766 (1962).

Z44. M. N. Hull, J. E. Ellison, and J. E. Toni, J. Electrochem. Soc. 117, 192 (1970).

Z45. R. W. Powers and M. W. Breiter, ibid, 116, 719 (1969).

Z46. M. W. Breiter, Electrochim. Acta 16, 1169 (1971).

Z47. T. P. Dirkse and N. A. Hampson, ibid, 16, 2049 (1971).

Z48. J. P. Elder, J. Electrochem. Soc. 116, 757 (1969).

Z49. N. A. Hampson, P. C. Jones, and R. F. Phillips, Can. J. Chem 45, 2039 (1967).

Z50. G. S. Vozdvizhenskii and E. D. Kochman, Zh. Fiz. Chem. 39 (3), 657 (1965).

C. Cadmium Hydroxide Literature Review

Cadmium hydroxide is the major product formed by anodizing cadmium in alkaline solutions. Two major uncertainties regarding the electrode process remain, although many investigations have been conducted: 1.] The mechanism by which electrode passivation occurs, and 2.] The possible formation of CdO.

Soluble Species

Cadmium has a small solubility in concentrated bases (C1-C4). The predominant form of the soluble species is $Cd(OH)_4^{=}$ (C4). At very low alkaline concentrations (10^{-2}M), a minimum in the solubility curve occurs. This is possible evidence that at very low KOH concentrations, $Cd(OH)^{+}$ may be formed (C3, C6).

Solid Phase Products

The major product formed is β - $Cd(OH)_2$ (C7-C9). The basal plane tends to orient parallel to the surface, depending on the overpotential (C10-C12). Values of the lattice parameters are not reproducible, and this variation has been attributed to the inclusion of water in the lattice (C13). The monoclinic γ-$Cd(OH)_2$ has also been observed (C14,C15).

The presence of CdO has been debated, but no conclusive evidence exists (C11). The only evidence for the oxide is that the anodic films are dark or yellowish, in contrast to the white hydroxides (C12, C16). Several authors, therefore, suggest that the hydroxide layer is formed through a primary oxide layer. Thermodynamic arguments indicate that CdO should not exist at the hydroxide potentials (C17, C2).

Active Dissolution

A rotating ring-disc study (C18) indicates that the electrolyte has a 10-fold supersaturation prior to film formation. After the formation of a surface layer, dissolution rates are greatly decreased. A tafel slope of 20 mV/decade has been measured (C17) compared with the expected 30 mV slope for a $2e^-$ reaction. Impedence measurements give a solubility of 5.3×10^{-6} in 1 M NaOH (C19) and values of 3.23×10^{-4} (C19) and 2.5×10^{-4} (C20) in 10 M NaOH. A diffusion coefficient of 5.32×10^{-7} cm^2/s has been similarly determined (C20).

Passivating Film Formation

Except at short times, the parabolic law describes the growth of the solid phase products (C21). The growth mechanism has been suggested as being the solid-state mechanism (C22) and the dissolution-precipitation mechanism (C23) in which cadmium oxide is first formed. The time to reach passivation depends strongly upon temperature and electrode current density (C24). Experiments conducted at constant potential suggest the film grows by the successive deposition of monolayers (C8).

The results of ring-disc experiments were consistent with the dissolution-precipitation mechanism (C18). Potential sweeps on ring-discs (C17) indicated that the current-potential curves did not vary within the 30% experimental error with rotation rate. The authors cite this as proof that the solid-state mechanism applies. However, due to the small dissolution current, this conclusion should not be highly regarded. A combined solid-state/dissolution-precipitation mechanism has recently been discussed (C25), in which a thin underlayer

is covered by the γ and β hydroxides. The underlayer is non-stoichiometric, as shown by studies conducted using Auger spectroscopy (C26).

C1. P. E. Lake and J. M. Goodings, Canad. J. Chem. 36, 1089 (1958).

C2. P. C. Milner and U. B. Thomas, Advances in Electrochemistry and Electrochemical Engineering (Interscience, NY, 1967), C. W. Tobias, Ed., Vol. 5, pp. 58-69.

C3. D. E. Ryan, J. R. Dean, and R. M. Cassiday, Canad. J. Chem. 43, 999 (1965).

C4. D. Dryssen and P. Lumme, Acta Chem. Scand. 16, 1785 (1962).

C6. K. H. Gayer and L. Wootner, J. Phys. Chem. 61, 364 (1957).

C7. K. Haber, Z. Electrochem. 62, 675 (1958).

C8. M. Fleischmann, K. S. Rajagopalan, and H. R. Thirsk, Trans. Faraday Soc. 59, 741 (1963).

C9. R. D. Armstrong, E. H. Boult, D. F. Porter, and H. R. Thirsk, Electrochim. Acta 12, 1245 (1967).

C10. S. U. Falk, J. Electrochem. Soc. 107, 661 (1960).

C11. K. Huber, Helv. Chim. Acta 51, 1343 (1968).

C12. P. E. Lake and E. J. Casey, J. Electrochem. Soc. 106, 913 (1959), 105, 52 (1958).

C13. M. Fleischmann and H. R. Thirsk, ibid, 110, 688 (1963).

C14. P. M. deWolff, Acta Cryst. 21, 432 (1966).

C15. P. M. deWolff, ibid, 22, 441 (1967).

C16. M. W. Breiter and J. L. Weininger, J. Electrochem. Soc. 113, 651 (1966).

C17. R. D. Armstrong and G. D. West, J. Electroanal. Chem. 30, 385 (1971).

C18. Y. Okinawa, J. Electrochem. Soc. 117, 289 (1970).

C19. R. D. Armstrong, J. D. Milewski, W. P. Race, and H. R. Thirsk, J. Electroanal. Chem. 21, 517 (1969).

C20. R. D. Armstrong and K. Edmondson, ibid, 53, 371 (1974).

C21. G. T. Croft, J. Electrochem. Soc. 106, 278 (1959).

C22. G. T. Croft and D. Toumi, ibid, 108, 915 (1961).

C23. M. A. Devanathan and S. Lahshmanan, Electrochim. Acta 13, 667 (1968).

C24. H. Y. Kang, J. Electrochem. Soc. 118, 462 (1971).

C25. E. J. Casey and C. L. Gardner, ibid, 122, 851 (1975).

C26. T. P. Hoar, M. Talerman, and E. Trad, Nature 244, 41 (1973).

IV. Representation of the Electrode Processes

A. Introduction

The anodic processes at the electrode in general consist of a series of partial reactions. The reactions include at least one electrochemical reaction in which charge is transferred, and possibly chemical reactions and phase changes following or preceding the charge transfer step. The slowest reaction step limits the rate of the overall electrode process. Conventional electrode kinetics can be used to model possible reactions and to attempt to predict or at least reproduce experimental current-potential relationships. This approach is not unambiguous, as indicated by the uncertainties cited in the literature.

The kinetic electrode overpotential is related to the driving forces which cause the reactions to occur at finite rates and will be dominated by the rate limiting step. As given in Vetter (G1), the total overpotential may be divided into charge transfer, diffusion, reaction, and crystallization overpotentials. The definition used for overpotential is the difference between the active potential when current is flowing and the equilibrium potential established at open circuit. This assumes equilibrium conditions are reached at open circuit. Charge transfer overpotential has been associated with the work required to transport charge across the electrical double layer at the electrode-electrolyte interface. At high anodic potentials, the Tafel equation relates this overpotential to the electrode current density. A reaction overpotential is associated with reactions whose rates depend only on concentrations and is independent of the potential. Either homogeneous or heterogeneous reactions may give

polarization effects; heterogeneous reactions generally exhibit poor reproducibility. The Nernst equation relates changes in activities to the overpotential. At high anodic potentials, the current potential relationship has the form of a Tafel equation. Diffusion overpotentials are associated with processes in which depletion or accumulation of reactants or products occurs in the electrolyte due to slow mass-transport processes. The concentration difference between the bulk electrolyte and the interface is related through the Nernst equation to the overpotential. Crystallization overpotentials are associated with the incorporation of adatoms into a crystal lattice, and surface concentrations are relative to the overpotential. Both diffusion and crystallization reactions exhibit Tafel behavior as well.

Resistance polarization is defined separately because of the lack of a reference equilibrium state. This polarization is due to ohmic drops within the electrolyte and possible surface layers. Electron and/or ion conductivity must be considered. Within surface layers, high electric field strengths may occur, and Ohm's law may not apply. Instead the current will vary with the logarithm of the potential drop across the film (G2-G5).

Because all of the overpotentials considered (charge transfer, diffusion, reaction, and crystallization) have the forms at high anodic potentials of Tafel expressions, experimental potential measurements have been used in this work mainly to distinguish between possible reaction products. The above review was presented to accommodate discussion of the structural characteristics of the following model.

Preliminary Computations

The model discussed in the remainder of this section was developed through a sequence of preliminary interpretations. Figure 1a shows eight models which were considered. Model 1 represents the anodic film as a single homogeneous film of constant optical properties. Models 2, 3, and 4 add the mass-transport boundary layer, a second homogeneous film, and roughness of the metal substrate. Model 5, which is discussed in more detail in Appendix C , interprets the top film as a polymer layer and uses mass and charge balances to relate the anodic film formation products to the electrode current density. Models 6 and 7 add roughness to the metal substrate and a second dual solid film. Model 8, which is discussed in detail, adds secondary crystals and the hydrate layer. Models 5 through 8 use an automated computer interpretation to evaluate characteristic parameters. Only Model 8 (Fig. 1b) was found to be able to reproduce the experimental data over large ranges of film thicknesses using optical constants consistent with the anodic film formation products assigned to the electrode potentials measured experimentally. A discussion of the models is given in Section V.

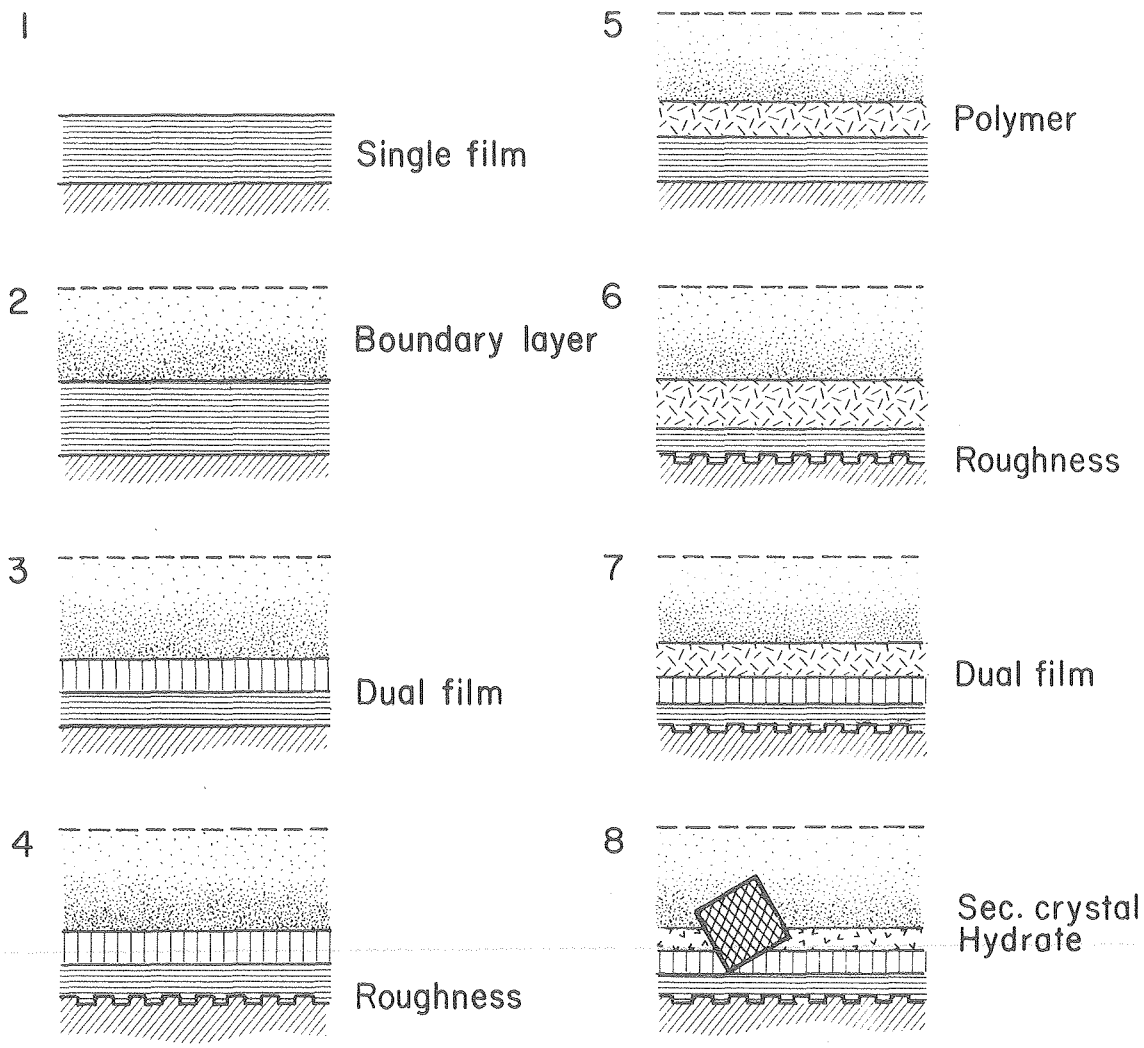

Figure 1a. Models of anodic films investigated for the interpretation of ellipsometer measurements.

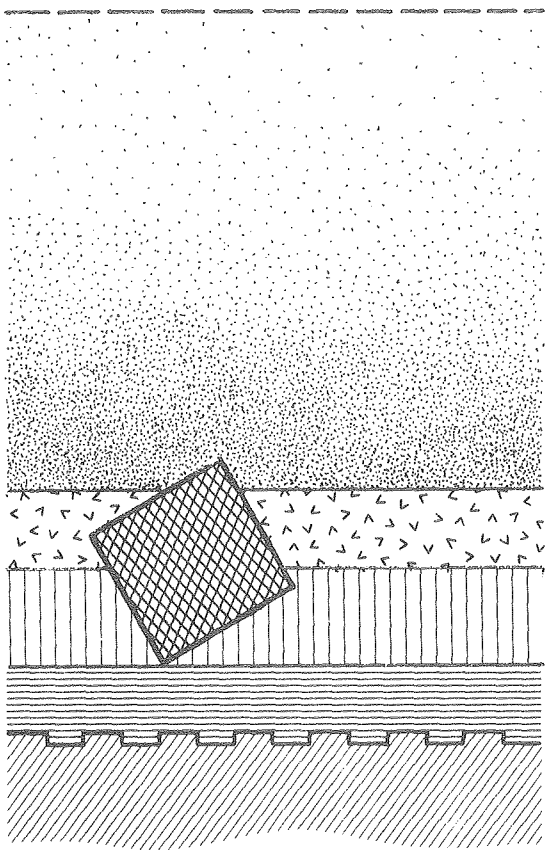

Figure 1b. Anodic film model (Number 8) used in the interpretation of film growth.

B. Generalized Structure of the Anodic Film Formation Products: Six Layers

Mass-Transport Boundary Layer

Previous work (G6, G7) has shown that the concentration profile across the mass-transport boundary layer (MTBL) can have significant effects on the ellipsometer measurements. The MTBL describes the flux by convective diffusion of ionic species away from the electrode surface. Both the rate expression for the flux density and the optical treatment of the refractive index (concentration) profile have been established (Appendix D). The major uncertainty involved is the degree of supersaturation of ionic species at the electrode surface.

The Hydrate Layer

This layer allows for the accumulation of products in the electrolyte adjacent to the electrode which is not accounted for by the MTBL. If the electrode process occurs by the dissolution-precipitation mechanism, the electrolyte will have a degree of supersaturation, and it is possible that a colloidal suspension forms by homogeneous nucleation (G8, G9). A previous model (Appendix C) indicated that a layer with optical properties consistent with a colloidal layer greatly improved the reproduction of experimental observations on silver. The formation of anion complexes such as $Ag(OH)_2^-$, $Cd(OH)_4^=$, and $Zn(OH)_4^=$ (Ref. A13, C4, Z12) would enhance the accumulation at the positive electrode.

Type II Primary Layer

This nomenclature was chosen to conform with work done by Breiter and Powers (Z46) on the dissolution of zinc in alkaline solution. This is the lowermost layer of reaction products, immediately above the metal substrate. The Type II layer is conceived as forming by crystallization onto heterogeneous nucleation sites. Fleischmann and Thirsk (A27) indicate that this layer forms before the secondary crystals (see below) and used electron diffraction to gain evidence that this layer consists of crystals of about 50 to 100 Å diameter. The use of scanning electron microscopy cannot provide quantitative information on the thickness of this film, but ion-etching offers the possibility for such a confirmation.

Secondary Crystals

These crystals are also formed by crystallization onto heterogeneous nucleation sites. Figure 2 shows scanning electron micrographs of crystals formed on silver, cadmium, and zinc. As cited in the literature, the number density and size of these crystals depend strongly on the anodic current density and the electrolyte composition.

Type I Primary Layer

This is the primary layer which grows after the onset of secondary crystal growth. It is conceived that this film is formed by homogeneous nucleation and subsequent precipitation, but the model is flexible enough to allow for the continued growth of the Type II film. Scanning electron micrographs indicate that the electrode can passivate before the secondary crystals completely cover the surface. This

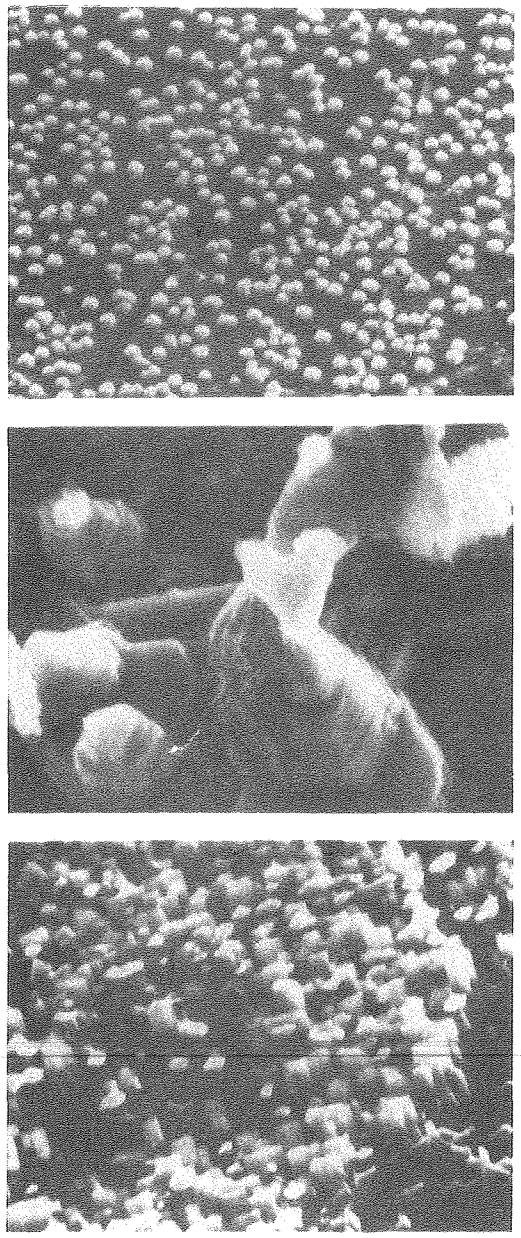

Figure 2. Secondary crystals formed on silver, zinc, and cadmium single crystal electrodes during anodic oxidation in 6 M KOH.

implies that the anodic process eventually becomes limited, via resistance polarization, by the transport of the charge carriers across the primary films (Type I and Type II).

Roughness of the Metal Substrate

This layer describes the optical effect of surface roughness. The roughening rate will vary strongly with the grain size and the number density of lattice imperfections in the substrate. Single crystal electrodes of close-packed orientation were used to minimize this roughness. Section F discusses the optical treatment of this layer.

Sequential Formation of the Structural Layers

Figure 3 indicates the sequences of formation of the six layers. Starting with an initially film-free surface, the electrode first dissolves by the formation of cations, with simultaneous roughening of the metal substrate. For sufficiently large current densities, the electrolyte becomes supersaturated and nucleation of Type II film begins. After growth of the Type II film to a limiting thickness, the secondary crystals begin forming. After an induction period during which the hydrated species accumulated, precipitation of the Type I film begins. Both the secondary crystals and the Type I film continue to grow.

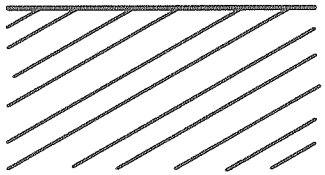

1. Bare Metal

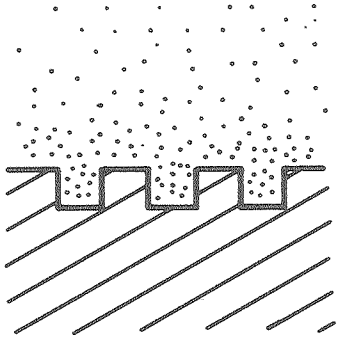

2. Rough Metal, Mass Transport Boundary Layer

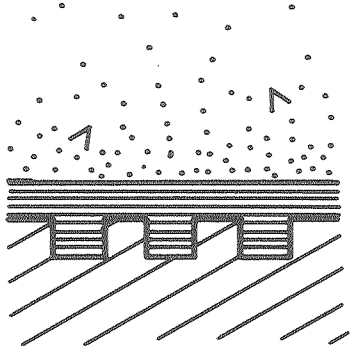

3. Growth of Type II Film

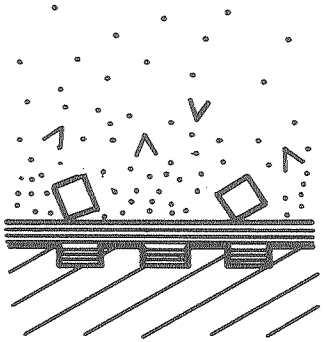

4. Nucleation of Secondary Crystals

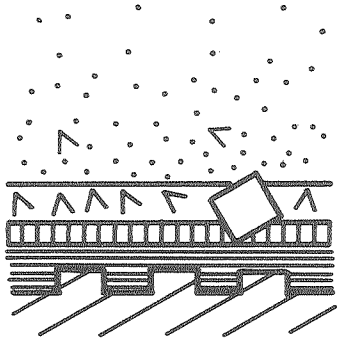

5. Type I Hydrate and Film Begin

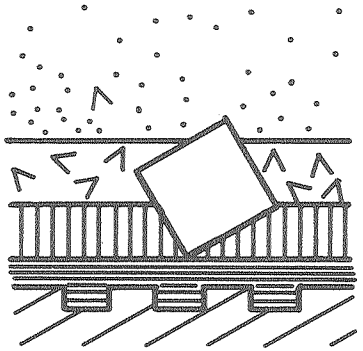

6. Growth of Secondary Crystals, Type I Film

Figure 3. Time sequence of events in anodic film formation (Model 8).

XBL 787-9519

C. Flux Densities Between Layers

Simplified equations have been used for the flux densities between layers because insufficient detail is known about the electrode kinetics. The major assumption made in the following expressions is that the concentrations of the reactants and products reach a constant, steady state value after transient increases in the concentration. The flux densities are defined as current densities entering each layer.

Layer	Flux Density	
Type II Film	$i_{IIF} = C_{IIF}$	(1)
Secondary Crystals	$i_{sc} = C_{sc}(A_c/A_b)$	(2a)
or	$i_{sc} = C'_{sc}$	(2b)
Type I film	$i_{IF} = f_R i_{IH}$	(3)
Boundary Layer	$i_D = \frac{zFD(C_{ss}-C)}{(1-t_+)\delta(t)}$	(4)
Type I Hydrate	$i_{IH} = i-i_D-i_{sc}$ (or i_{IIF})	(5)

For the type II Film, i_{IIF} has assumed a constant interfacial concentration and the neglect of changes in surface area. The flux density for the secondary crystals has two limiting expressions: In the first case, the flux density to the secondary crystals is proportional to the surface area of the crystals A_c relative to the superficial electrode area A_b. This flux corresponds to rate control by crystallization from a constant concentration of surface adatoms.

The second expression Eq. (2b) would correspond to crystal growth limited by transport of reactants to the crystal surface. The flux density for the Type I Film Eq. (3) assumes zero order kinetics for the dehydration of the Type I hydrate and would also be valid for constant concentration of the hydrate. In the flux density for the boundary layer Eq. (4), transient effects are modelled by the time dependence of the boundary layer thickness $\delta(t)$ (see below). The flux density into the hydrate layer is found by a linear combination of the total electrode current density and the five previously defined flux densities. This prevents overspecification of the system. Formalization of the hydrate layer flux density would require describing the kinetics for the formation of polymers and anions and the corresponding unsteady-state mass-transport within an electric field.

The flux densities have units of mA/cm^2. Areas have been normalized to a radius of influence of the secondary crystals defined by

$$R_i = \frac{10^8 \text{ Å}}{2\sqrt{N_o}} \tag{6}$$

where N_o is the number of crystals per sq. cm. The radius R_i is the half distance between adjacent crystal centers.

D. Unsteady State Effects

Mass-Transport Boundary Layer

For constant-current experiments, the boundary layer thickness initially increases with time. Approximate solutions of the convective diffusion equation, which assume constant transport properties, have been used. For stagnant electrolytes, the Sand equation gives (G10)

$$\delta = 1.129 \sqrt{Dt} \tag{7}$$

For forced convection in a flow cell, a series solution by Rosebrugh and Miller (G11) for a finite boundary layer was used. A characteristic time constant α is defined as

$$\alpha = \frac{\pi D}{4\delta_{bl}^2} \tag{8}$$

where δ_{bl} is the limiting, steady state boundary layer thickness given by Sherwood number correlations,

$$\delta_{bl} = d_h/Sh \tag{9}$$

where d_h is the hydraulic diameter. For $\alpha < 0.5$, the series solution is approximated by the Sand equation, and the growth of the boundary layer is described by Eq. (7).

It is assumed that the electrolyte must be supersaturated before film formation begins. The time to reach an ionic supersaturation C_{ss} is t_{ss}.

For $0 < t < t_{ss}$ the increase in interfacial ion concentration for stagnant electrolyte is given by (G10),

$$C_i = C_b + \frac{1.129\ \sqrt{Dt}}{zFD}\ (1-t_+)i \tag{10}$$

and for forced convection (G11) by

$$C_i = C_b + i\ \frac{\delta_{bl}}{zFD}\left[1 - \frac{8}{\Pi^2}\ e^{-\alpha t}\right] . \tag{11}$$

The time t_{ss} to reach the steady-state interfacial ion concentration C_{ss} is given by (stagnant electrolyte),

$$t_{ss} = \left[\frac{zFD(C_{ss}-C_b)}{1.129\ i(1-t_+)D^{1/2}}\right]^2 \tag{12}$$

and for forced convection by

$$t_{ss} = \frac{-1}{\alpha}\ \ell n\left[\frac{\Pi^2}{8}\ \ 1 - (C_{ss}-C_b)\ \frac{zFD}{i(1-t_+)\delta_{bl}}\right] . \tag{13}$$

Before t_{ss} no film is formed, and after t_{ss}, the interfacial ion concentration is assumed constant.

The Sherwood Number correlations used for the limiting forced convection boundary layer thicknesses are (G7):

$$Sh = 1.40\,(ReSc\,d_h/X)^{1/3} \qquad Re < 3000 \qquad (14)$$

$$1.40\,(3000Scd_h/X)^{1/3} \qquad 3000 \leq Re < 5000 \qquad (15)$$

$$0.042Re^{0.743}Sc^{1/3} \qquad 5000 \leq Re \qquad (16)$$

For the constant potential experiments, the time dependence of the boundary layer thickness was approximated by the Cottrell-Stefan solution to the diffusion equation (G13)

$$\delta = \sqrt{\pi Dt} \qquad (17)$$

This was used for both stagnant and forced convection transport conditions. For forced convection, the limiting thickness given by Eqs (14-16) is used for large times. The interfacial ion concentration C_i as a function of time is computed from the concentration overpotential η_c:

$$\eta_c = \frac{0.0257}{z} \ln \frac{C_i}{C_s} \qquad (18)$$

To obtain η_c, the experimental value of the total overpotential η is corrected for surface overpotential (charge transfer, reaction, crystallization) and resistance polarization. The surface overpotential is computed from a Tafel equation

$$i = i_o \exp\left(\alpha z \eta_s / kT\right) \qquad (19)$$

with the exchange current density i_o evaluated by the computational procedure. The resistance polarization for surface films is computed

assuming Ohm's law applies. For both the Type I and Type II films, effective conductivities are calculated by assuming parallel resistances to transfer through pores and through the solid film. The total resistance is a series resistance across the Type II and Type I layers:

$$\eta_r = i\left[\sigma_{IIe}T_{FII} + \sigma_{Ie}T_{FI}\ (1 - f_{sc})^{-1}\right] \qquad (20)$$

Blockage effects due to secondary crystal growth are included in the fractional surface coverage f_{sc}. Using experimental values of the electrode current density in Eq. (20), use of Eqs. (21), (20), and (19) gives

$$\eta_c = \eta - \eta_s - \eta_r \ . \qquad (21)$$

Type II Film

The Type II film is assumed to be the only surface layer forming during the time period $t_{ss} < t < t_{NUC}$. The time to reach supersaturation t_{ss} is calculated as outlined above from the steady state degree of supersaturation of the ionic species D_{ss}, for the experimental transport conditions. The time at which secondary crystal growth begins, t_{NUC} and D_{ss}, are determined by the interpretation procedure.

Type I Film

Growth of the Type I film begins at t_{NUC}. The growth rate is characterized by dehydration of the Type I hydrate. As the flux density into the hydrate layer [Eq. (3)] depends on the flux density

into the secondary crystals, the growth rate of the Type I film is therefore inversely proportional to the growth rate of the secondary crystals. The Type I film can reach a limiting thickness for $i_{sc} = i$.

Type I Hydrate

Although the hydrate layer accounts for the homogeneous formation of polymers and anions, the growth rate of this layer is determined by the residual charge remaining after ionic transport and heterogeneous nucleation and crystallization have been accounted for. For the optical treatment of this layer, a characteristic time T_{diff} is evaluated by the computational procedure. T_{diff} is the time to reach the minimum porosity of the hydrate layer.

Secondary Crystals

Nucleation of the secondary crystals begins at time t_{NUC}. Three kinetic treatments of the crystal growth may be chosen for the computational procedure: [1] growth rate increases with surface area (crystallization control), [2] growth rate constant (transport control), [3] mixed kinetics where initially crystallization control applies until a characteristic time T_{KIN} (evaluated by the computation procedure) after which transport control applies.

Surface Roughness

Measurements of film-free surfaces can be interpreted by use of independently determined optical constants and the effect of a finite surface roughness. A square-ridge model has been used for roughness of the metal substrate. Three empirical parameters are required to des-

cribe the growth of the layer representing the roughness: [1] the initial peak to peak roughness, [2] an initial porosity or area fraction of the "valleys", and [3] the fraction of the current density which creates void volume (product of area fraction of valleys and peak to peak roughness) during the dissolution process. Two treatments of the growth process may be chosen for the computational procedure; the thickness of the layer remains constant and the increase in voids results in an increase in porosity, or the porosity of the layer remains constant and the increase in void and volume is used to compute an increase in the thickness of the layer. The computer program (Appendix G) allows changes in this layer to stop at the onset of secondary crystal growth t_{NUC} or the layer may continue to grow indefinitely.

E. Mass and Charge Balances

The flux densities defined above describe the current densities into each type of layer. Changes in volumes for the layers are computed by the use of Faraday's law, bulk densities, molecular weights, valence, and the number density of secondary crystals. The general proportionality factor P_i is

$$P_i = \frac{M_i \times 10^8}{z\rho(0.965)N_o} . \qquad (22)$$

This factor gives volume changes in cubic angstroms per radius of influence of secondary crystal for current densities in mA cm^{-2}, density ρ in g cm^{-3}, and number density N_o in crystals μm^{-2}. The incremental changes in volumes are then:

Layer	dV_i ($Å^3$ per secondary crystal site)	
Type II Film	$dV_{IIF} = P_{IIF}\, i_{IIF}\, dt$, $t \leq t_{nuc}$	(23)
	$= 0$, $t > t_{nuc}$	
Type I Film	$dV_{IF} = 0$, $t \leq t_{nuc}$	(24)
	$= P_{IF} f_R (i - i_d - i_{sc})dt$, $t > t_{nuc}$	
Type I Hydrate	$dV_{IH} = P_{IH}(i - i_d - i_{IIF})dt$, $t \leq t_{nuc}$	(25)
	$= (1-f_R)P_{IH}(i - i_d - i_{sc})dt$, $t > t_{nuc}$	
Secondary Crystals	$dV_{sc} = 0$, $t \leq t_{nuc}$	(26)
	$dV_{sc} = P_{sc} i_{sc} dt$, $t > t_{nuc}$	

Dimensions of the Layers

The thicknesses of the Type II Film, Type I Film and Hydrate, and the size of the secondary crystals are computed from the volumes of the solids as defined above and the volume fractions of solution (porosities or hydration degree). For the Type I Film and Hydrate, a correction is included for inhomogeneous effects by assuming the porosity $\in$ increases parabolically in the direction normal to the surface from $\in_i$ at the bottom to $\in_b$ at the top.

$$\in - \in_i = (\in_b - \in_i)(1 - y/T)^2 \tag{27}$$

The time increments used to compute V_i are taken from the experimental

values input to the program.

Layer	Thickness	
Type II Film	$T_{IIF} = V_{IIF}(1-\varepsilon_{IIF})^{-1}A_B^{-1}$	(28)
Type I Film	$T_{IF} = V_{IF}[1-(2/3\varepsilon_{IF}+1/3\varepsilon_{IH})]^{-1}A_{BC}^{-1}$	(29)
Type I Hydrate	$T_{IH} = 1.5V_{IH}(1-\varepsilon_{IH})^{-1}(A_{BC}+A_C)^{-1}$	(30)
Secondary Crystals	$T_{sc} = \left[V_{sc}P^{-2}(1-\varepsilon_{sc})^{-1}\right]^{1/3}$	(31)

The areas involved are:

$$A_B = 10^8/N_o \quad (32)$$

$$A_{BC} = (1-f_{sc})A_B \quad (33)$$

$$A_C = (4P+2P^2)T_{sc} \quad (34)$$

For N_o in secondary crystals cm^{-2}, A_B is in square angstroms. A_{BC} is the surface area not covered by the secondary crystals, and A_C is the surface area of crystals having height T_{sc} and width $P\ T_{sc}$. For $P = 1$, the crystals are cubes.

F. Optical Treatment of the Layers

Principles of Ellipsometry

Changes in the state of polarization caused by reflection are expressed by the ratio ρ of the reflection coefficients r_p and r_s for the electric field components parallel and normal to the plane of

incidence. The plane of incidence is defined by the incident and specularly reflected beams. The complex quantity ρ is conveniently described by a relative amplitude change $\tan \psi$ and a relative phase change Δ (Eq. 35); Δ and ψ are experimentally measured.

$$\rho = \frac{r_p}{r_s} = \tan \psi \, e^{i\Delta} \tag{35}$$

For ideal (planar, smooth, isotropic) bare surfaces, the reflection coefficients are given by the Fresnel equations [Eq. (36), (37)] which involve the angle of incidence ϕ (angle between incident light beam and surface normal) and the angle of refraction ϕ' (angle between transmitted beam and surface normal).

$$r_p = \frac{\tan (\phi - \phi')}{\tan (\phi + \phi')} \tag{36}$$

$$r_s = -\frac{\sin (\phi - \phi')}{\sin (\phi + \phi')} \tag{37}$$

The angle of refraction ϕ' can be obtained from the angle of incidence ϕ and the refractive indices of incident medium n_o and reflecting medium n_s by the use of Snell's law of refraction:

$$\sin \phi' = \frac{n_o}{n_s} \sin \phi' \tag{38}$$

For a light absorbing surface such as a metal, the refractive index n_s and the angle of refraction ϕ' are complex quantities (G14). The sign convention followed in this work is such that the imaginary part

of the complex refractive index is negative,

$$n_s \equiv n - i\,k \tag{39}$$

For a surface covered by a homogeneous and isotropic film (G15), r_p and r_s can be determined by use of the Drude equations:

$$r_\nu = \frac{r_{1\nu} + r_{2\nu}\, e^{-i\tau}}{1 + r_{1\nu} r_{2\nu} e^{-i\tau}} \quad , \tag{40}$$

where ν is either s or p. As shown in Figure 4, $r_{1\nu}$ is the reflection coefficient [Eq. (36), (37)] for the top surface of the film and $r_{2\nu}$ is the reflection coefficient at the base of the film. The phase τ has the form (Eq. 41)

$$\tau = \frac{4\Pi}{\lambda}\, T_f\, n_{cf} \cos \phi_{cf} \quad . \tag{41}$$

T_f is the film thickness, n_{cf} the complex film refractive index, and $\cos \phi_{cf}$ the cosine of the complex angle of transmission through the film (relative to the surface normal).

Mass Transport Boundary Layer

The optical effect of a mass-transport boundary layer on light reflected from an underlying substrate is illustrated in Fig. 5. Computationally the continuously varying concentration in the

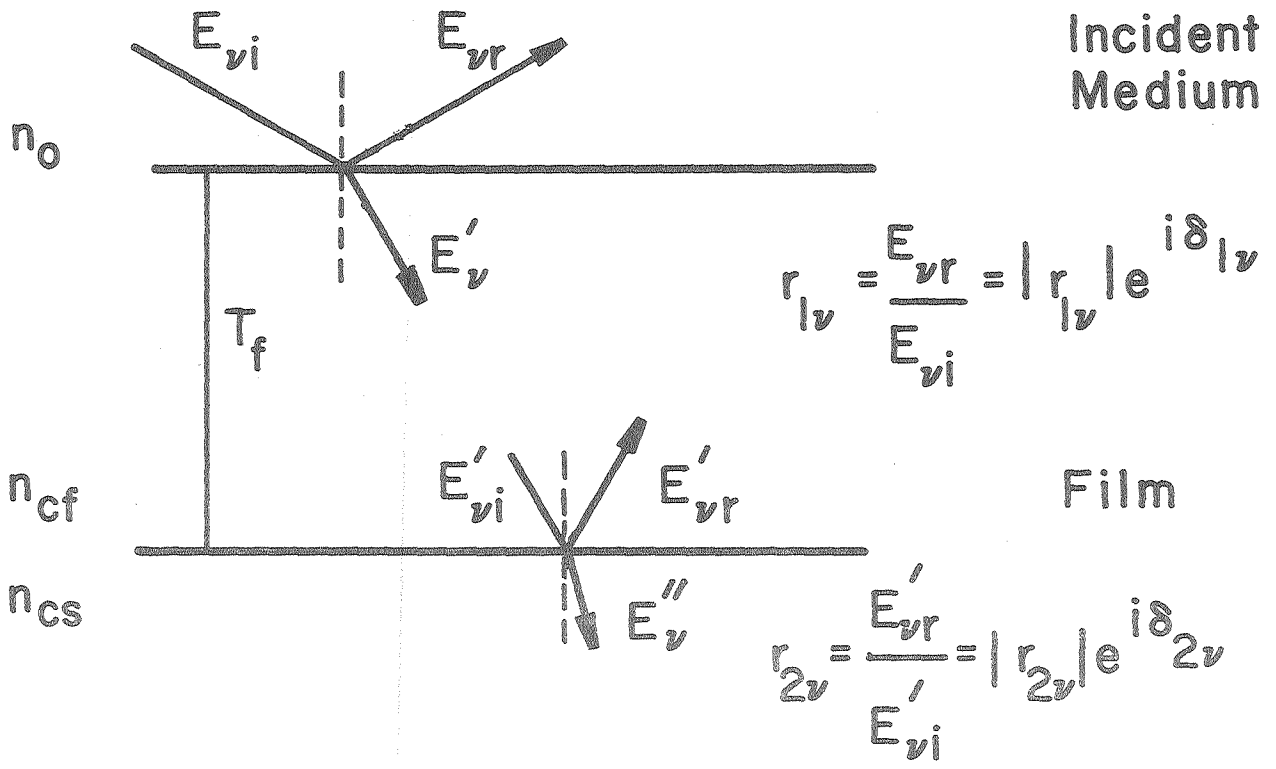

Figure 4. Definition of the reflection coefficients used in the Drude equations. Reflection of light at the top film boundary is described by $r_{1\nu}$, while reflection of light at the bottom film boundary is described by $r_{2\nu}$, where ν refers to s or p component.

XBL 787-9523

optically inhomogeneous) boundary layer can be represented by a series of (optically homogeneous) layers of uniform refractive index, with refraction and reflection of the light beam taking place at each interface between layers. Three approximations for the MTBL were considered:

[1] The refractive index in the boundary layer decreases parabolically from the surface to the bulk electrolyte as given by Eq. (42).

$$n = (n_i - n_b)\ (1 - y/\delta)^2 + n_b \qquad (42)$$

[2] The refractive index decreases linearly as given by Eq. (43).

$$n = (n_i - n_b)\ (1 - y/\delta) + n_b \qquad (43)$$

The Nernst boundary layer thickness was used for the linear profile, $\delta_N = 1/2\delta$, which gives the same interfacial concentration gradient as does the parabolic profile when used in the Sherwood number correlations (Eqs. 14-16).

[3] A homogeneous film approximation was used with the same interfactial refractive index n_i and the Nernst boundary layer thickness. The multiple-film method (G7, G16) was used to treat the inhomogeneity described by Eqs. (42) and (43).

Figure 6 shows results of the computations for the three approximate representations of the MTBL. A constant interfacial refractive index n_i was maintained as the boundary layer thickness was increased. For thick boundary layers, the values of Δ and ψ converge to a limit-

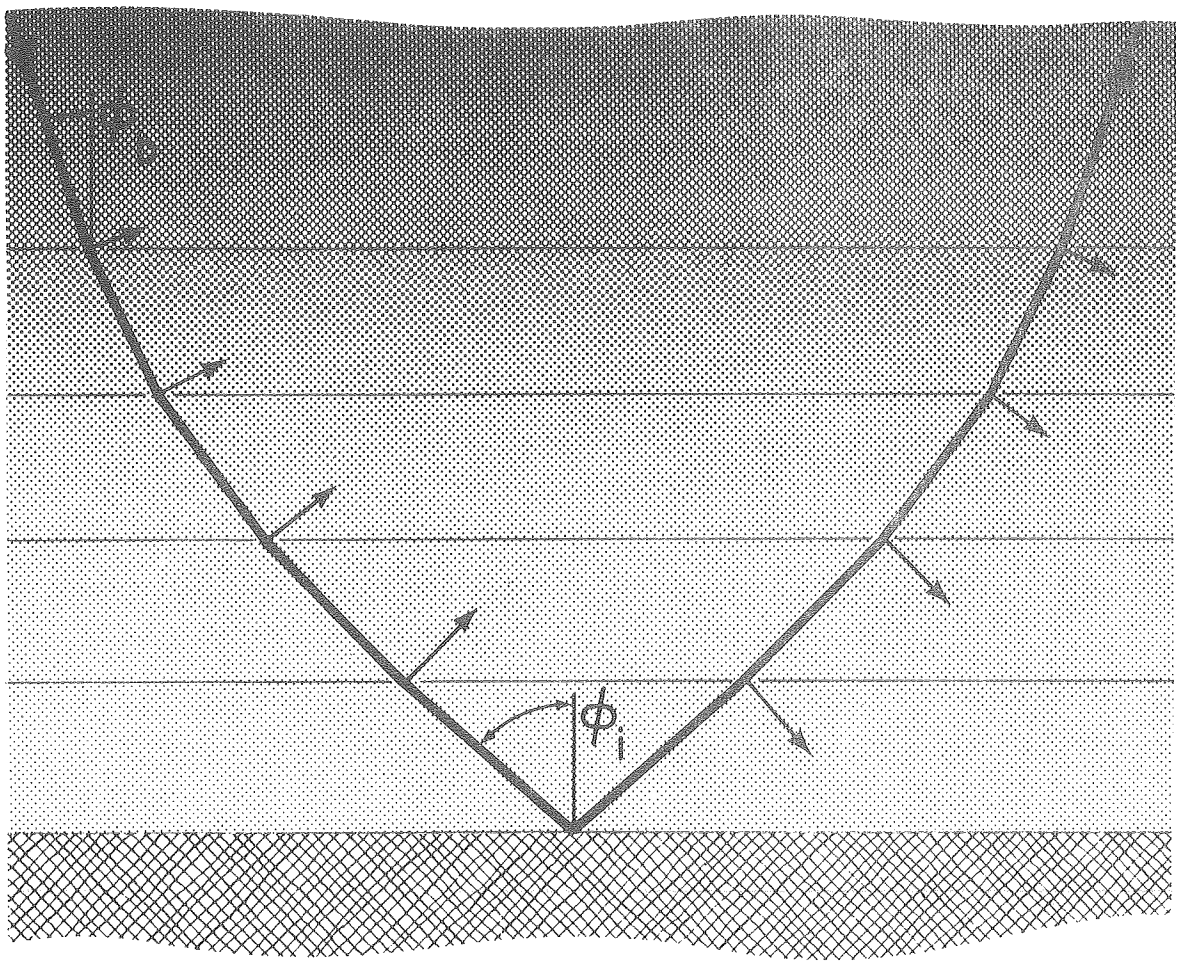

XBL7611-4369

Figure 5. Representation of the optically inhomogeneous boundary layer by multiple homogeneous films with light reflection and refraction taking place at the interface between layers. ϕ_b is the angle of incidence upon the boundary layer, ϕ_i the angle of incidence upon the substrate (solid phase).

ing value for the inhomogeneous film representations. Reflection within the MTBL becomes negligible (G6, G7) and the principal optical effect is a change in the angle of incidence ϕ_i on the substrate. This effect depends on the refractive indices in the bulk fluid n_b and at the interface n_i, and can be determined from the angle of incidence outside the boundary layer ϕ_o by use of Snell's law.

$$\sin \phi_i = \frac{n_b}{n_i} \sin \phi_o \tag{44}$$

For very thin boundary layers, the homogeneous film does approximate the inhomogeneities described by Eqs. (42) and (43). The homogeneous film approximates the linear profile for about 1/4 of a cycle of oscillation. The boundary layer thickness at this point is given by Eq. (45) (G7).

$$\delta = \frac{\lambda_o}{2(n_i^2 - n_b^2 \sin^2 \phi_o)^{1/2}} \tag{45}$$

The optical effect of the MTBL was determined by using the two limiting approximations indicated above. For boundary layers thinner than the thickness given by Eq. (45), the MTBL was treated as a homogeneous film having the refractive index n_i. Thicker boundary layers were treated by modifying the angle of incidence according to Eq. (44). For short times, prior to the formation of the hydrate layer, the refractive index n_i corresponds to the concentration of ionic species at the interface. When the hydrate layer is present, n_i depends on the

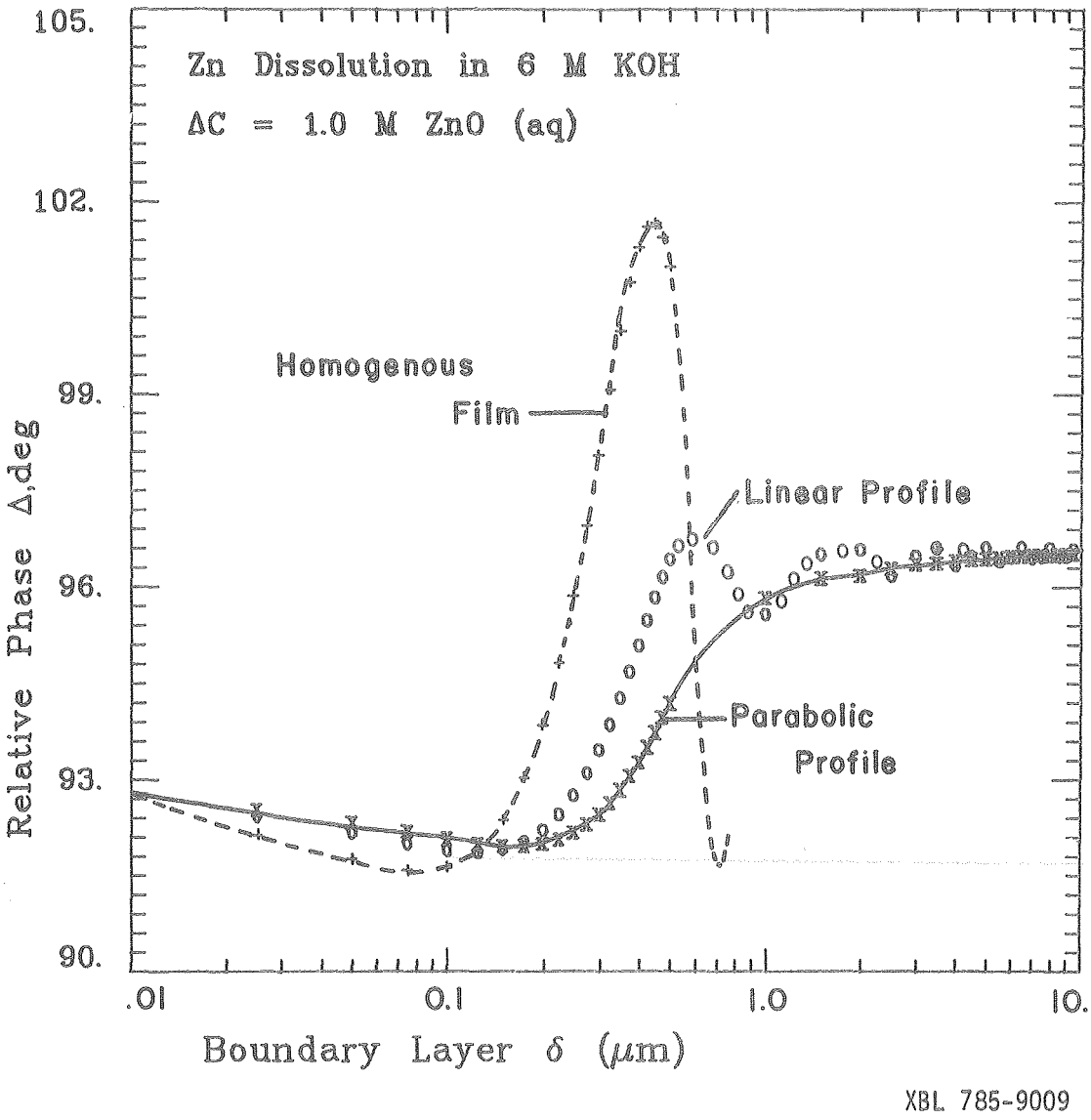

Figure 6a. Effect of mass-transport boundary layer of thickness δ, on ellipsometer parameter Δ. Zinc dissolution in KOH, Δc the concentration difference between interface and bulk. Computations for parabolic and linear refractive index profiles and the homogeneous film approximation.

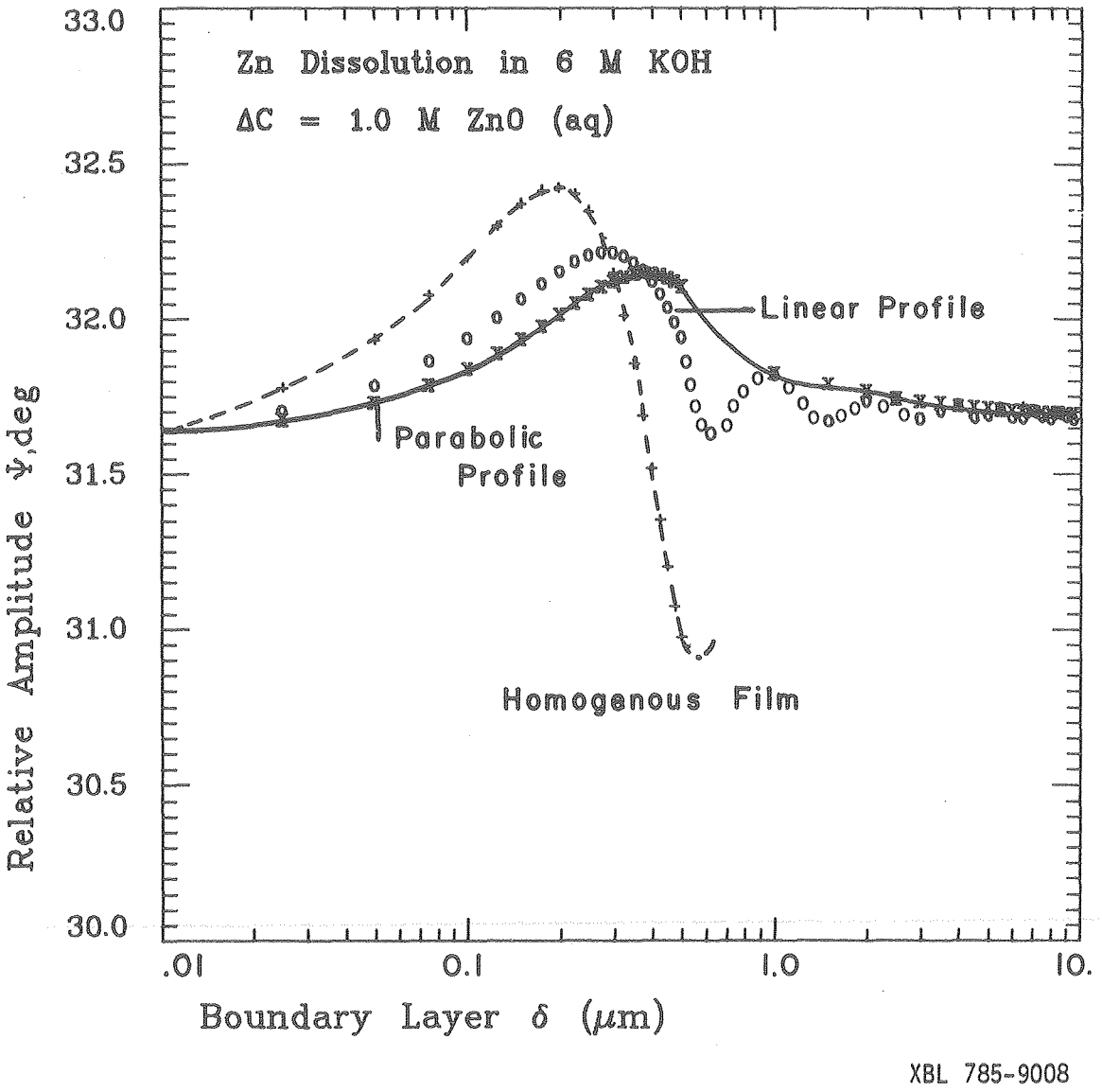

Figure 6b. Effect of mass-transport boundary layer of thickness δ, on ellipsometer parameter ψ. Zinc dissolution in KOH, Δc the concentration difference between interface and bulk. Computations for parabolic and linear refractive index profiles and the homogeneous film approximation.

treatment of the hydrate layer (see below).

Hydrate Layer

Either of three descriptions of the optical effect of the hydrate layer may be chosen for the computational procedure;

[1] The hydrate layer is a homogeneous film with refractive index n_H and the thickness given by Eq. (30). The refractive index is a linear average of the solid refractive index of the hydrated species n_{ppt} (specified as input to the computer program) and the refractive index of the electrolyte n_{soln}, as given by Eq. (46).

$$n_H = (1 - \epsilon_H)\, n_{ppt} + \epsilon_H\, n_{soln} \qquad (46)$$

For this treatment, the refractive index n_i of the MTBL is given by the concentration of ionic species at the MTBL-Hydrate layer interface.

[2] The hydrate layer is viewed as an extension of the MTBL. The reflection at the MTBL-Hydrate interface is neglected to represent a gradual change in refractive index between the two layers. The refractive index n_H (calculated as specified above) becomes n_i for the MTBL.

[3] The hydrate layer is an inhomogeneous film with a parabolic distribution of porosity [Eq. (27)]. The multiple-film method is used (G7, G16) with five equivalent homogeneous films. The refractive index of each homogeneous film is determined by the use of Eqs. (27) and (46). The refractive index n_i of the MTBL is the same as described in case [1].

Type I Film and Type II Film

The type I film is treated as a homogeneous film of thickness T_{IF} as given by Eq. (29). The refractive index of the film is computed by a linear average [Eq. (46)] of the solid film refractive index n_{IFS} and the electrolyte refractive index n_{soln}. The constant porosity of the film $\in_{IF}$ used in the linear average is determined by the computations.

The type II film is also treated as a homogeneous film. The thickness T_{IIF} is given by Eq. (28) and the refractive index again is the linear average of the solid film refractive index n_{IIFS} and the electrolyte refractive index n_{soln}. For the computational procedure, the porosity of this layer can be set to the constant value of 0.21 (corresponding to close-packed spheres), or allowed to decrease to 0.21 linearly with time until the value t_{nuc}. The decrease with time is an approximate treatment of patchwise film formation on the scale of the coherent length ℓ_c of the light beam (see below).

Secondary Crystals

The optical treatment of the secondary crystals is determined by the number density of crystals, or equivalently, by the size of the crystals. Three general regimes of crystal sizes T_{sc} are distinguished (G17):

$$T_{sc} << \lambda_i = \frac{\lambda}{n_i} = O(100\text{Å}) \tag{47}$$

$$T_{sc} = O(\lambda_i) \tag{48}$$

$$T_{sc} \gg \lambda_i = O(\ell_c) \tag{49}$$

Where λ_i is the wavelength of light in the material i, λ the wavelength in vacuum, and ℓ_c the lateral coherence of light. For very small crystals or large number densities [$N_o = O(10^{10} cm^{-2})$], the crystals are not individually distinguishable. Crystals on the order of the wavelength of light (λ = 546.1 nm) must be treated by the coherent superposition of light reflected from distinct crystals. Crystals having sizes larger than the lateral coherence of light must be treated by the incoherent superposition of reflection from two regions. Unfortunately, no adequate theory for the optical effect of crystals in the latter two regions is available in the literature, but theories have been developed for this dissertation.

Small crystals

In this regime of the secondary crystal sizes, homogeneous films are used to represent the optical effect of the layer of crystals. The thickness of the layer T_{sc} is given by Eq. (31). As the surface between the crystals is covered by the Type I film and the hydrate layer, the layer of secondary crystals is divided into two sublayers having thicknesses T_{IF} (Eq. 29), and $T_{sc}-T_{IF}$. The refractive indices of the films are linear functions of the optical surface coverage of the crystals as given by Eq. (50).

$$n_{sce} = C_c n_c + (1 - C_c) n_{uc} \tag{50}$$

For the bottom layer n_{uc} is the Type I film, while

for the top sublayer, n_{uc} is the hydrate material. (If $T_{IH} < T_{sc} - T_{IF}$ a third sublayer is included).

Two methods were used to compute the optical surface coverage of the crystals. The first method uses the projection onto the surface when viewed along the surface normal. The second method uses the projection along the propagation vector of the light and includes the angle of incidence ϕ_o. Two angles specify the orientation of the cubes (Fig. 7). The angle between the surface and the side of the crystal is α, and the smallest angle from the s-plane to a crystal face is β. The use of two angles assumes a line of contact between the surface and the crystals. The coverage projected along the surface normal is:

$$C_c = \left(\frac{T_{sc} \, (P \cos \alpha + \sin \alpha)}{2 \, R_i} \right)^2 \tag{51}$$

The coverage projected along the propagation direction is:

$$C_c = \frac{P \, T_{sc}^{\,2} \tan \phi_o \, (1 + P^2)^{1/2} \sin(\alpha+45) [\cos\beta + \cos(90-\beta)]}{2 \, R_i^{\,2}} \tag{52}$$

To calculate the optical effect of the complete structure given in Figure 1, the multiple-film method was used for the 5 (or 4, depending on the treatment of the hydrate layer) homogeneous layers of the roughness, type II film, type I film, secondary crystals and hydrate layer covered by the MTBL.

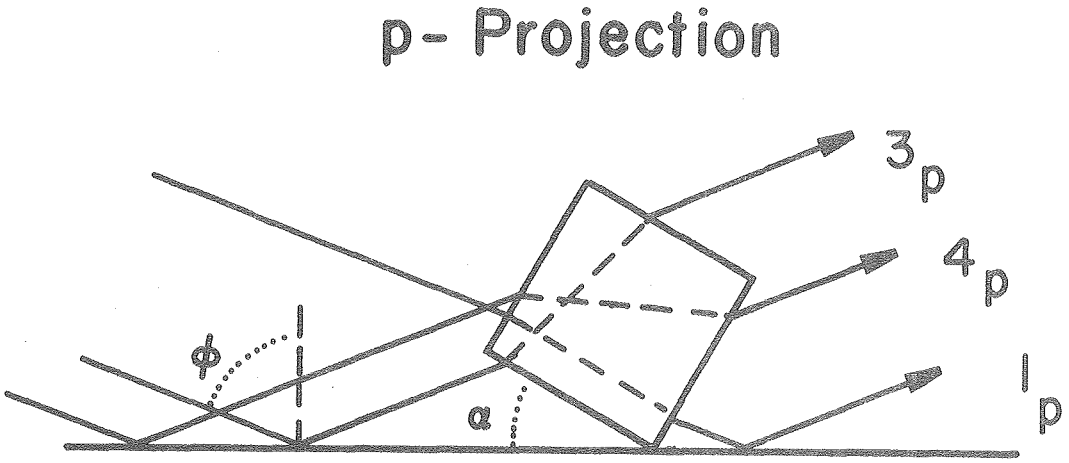

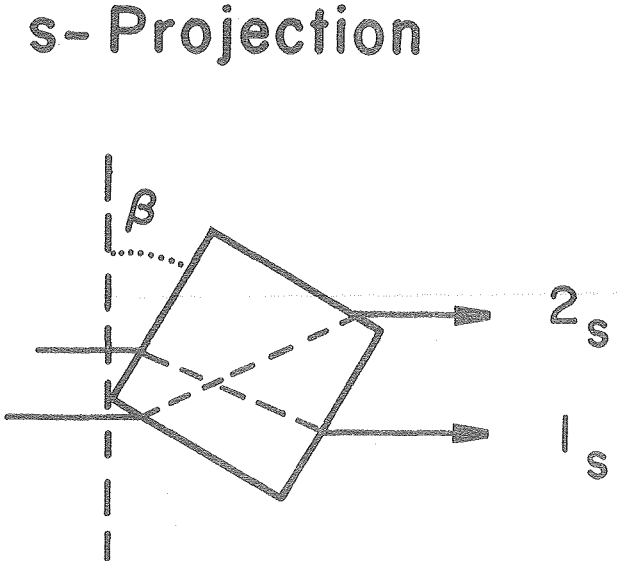

XBL 786-9164

Figure 7. Projected angles in the p and s planes specifying the orientation of secondary crystals on the electrode surface. The observer is looking across the electrode surface for the p-projection, and straight down at the surface for the s-projection.

Coherent Superposition from Distinct Crystals

Crystal sizes in this regime are treated by computing the reflection coefficients r_p and r_s from an area average of the reflection coefficients for the surface covered by the secondary crystals and the uncovered surface, as given by Eq. (53) where ν is either s or p .

$$r_\nu = C_c r_{\nu c} + (1-C_c) r_{\nu b} \quad . \tag{53}$$

The coverage projected along the propagation direction [Eq. (52)] was used. Two models were used to represent the crystal-covered surface.

The first model treats the cubes as a homogeneous film having thickness T_{sc} . The multiple-film method is used separately for the covered and uncovered surfaces, and $r_{\nu c}$ and $r_{\nu b}$ are combined by use of Eq. (53).

The second model uses a ray method to describe light transmission through the cubes (Appendix B).

Incoherent Superposition from Distinct Crystals

This regime applies when the crystal sizes are larger than the lateral coherence of the light beam. The lateral coherence can be estimated by Eq. (54)(G18)

$$\sigma_c = \frac{0.16\ S\lambda}{D_d} \quad . \tag{54}$$

For source dimension D_d resulting from the pinhole diameter following the light source of 1 mm and a distance S (focal length of collimator) of

fifteen cm(λ = 546.1 nm), a lateral coherence of 13 μm is determined for the ellipsometer (see Equipment section).

Incoherent superposition is treated as an intensity average of the reflectance ratios ρ_i [Eq. (35)] for the covered and uncovered portions of the surface, as given by Eq. (55).

$$\rho = \frac{C_c I_c \rho_c + (1 - C_c) I_b \rho_b}{C_c I_c + (1 - C_c) I_b} \tag{55}$$

The two methods described in the coherent superposition section were used to treat the optical effects of the cubes. The intensities I_d are given by Eq. (56).

$$I_d = (r_{sd} r_{sd}^* + r_{pd} r_{pd}^*) \tag{56}$$

Statistical Variations in the Secondary Crystal Size

The effect of random variations in the number density (size) and orientation (α and β) of the secondary crystals may be investigated for assumed distribution functions. Three points in the Gaussian distribution space were used, $X = \mu$ and $X - \mu = \pm \sigma$, where the probability of X (number density, α, or β) is given by

$$f(x, \mu, \sigma) = \frac{1}{\sqrt{2\Pi}} \exp\left(-1/2 \left(\frac{x-\mu}{\sigma}\right)^2\right) \tag{57}$$

For random variations in the intermediate range of crystal sizes, Eq. (53) is used to determine r_s and r_p for each value of the statistical quantity, and a weighted average is computed using Eqs. (57)

and (58).

$$r_\nu = \sum_{i=1}^{3} f(X_i)\, r_\nu\,(X_i) \qquad (58)$$

For random variations in the incoherent superposition regime, Eq. (55) is used to determine ρ for each value of the statistical quantity, and a weighted average is computed using Eqs. (56), (57), and (59).

$$\rho = \frac{1}{\sum_{i=1}^{3} f(X_i) I(X_i)} \sum_{i=1}^{3} f(X_i) I(X_i) \rho(X_i) \qquad (59)$$

Statistical Variations in the Nucleation of Secondary Crystals

The use of a uniform distribution on the surface in the number density of secondary crystals as outlined above results in a uniform thickness for the Type II film. An alternate approach allows for variations in the Type II film thickness at different points on the electrode surface: The time of the onset of crystal growth t_{NUC} is allowed to be a statistical quantity having three values, the mean value μ and $\mu \pm \sigma$. At each experimental value of time, the three computed curves resulting from the three values of t_{NUC} are incoherently superimposed using Eqs. (56), (57), and (59).

Depletion of the Hydrate Layer

The formation of secondary crystals will tend to deplete the dissolved material which accumulates in the hydrate layer prior to the nucleation of the crystals. To account for the optical effect of the depletion of the hydrate layer, the porosity of the hydrate layer may be increased from the minimum value at T_{DIFF} until 0.999 at a characteristic time T_{PACK}. The increase is a linear function of time, and T_{PACK} is evaluated by the computational procedure.

Patchwise Film Formation

Under certain conditions, most notably low current densities (see the results for cadmium hydroxide formation), anodic film will form preferentially on localized regions of the electrode. To model this patchwise film formation, the electrode surface is divided into a fraction covered by secondary crystals and a fraction assumed free of secondary crystals. The fraction of coverage (of secondary crystals) increases from a value COVII at T_{NUC} parabolically with time until T_{DISS}, a characteristic time evaluated by the computational procedure.

As nucleation at preferred regions is probably due to variations of surface composition, the model allows for films to be present on the electrode surface before the current is initiated. For the computation procedure, the initial surface layer may cover only the fraction COVII or cover the total electrode surface. The thickness of the initial layer, T_{FICCO} is evaluated by the computational procedure. This initial layer is the first phase of the Type II film.

During anodic film formation, the volume of material forming secondary crystals (eq. 2, 22, 26) is divided by the fractional coverage before the crystal sizes are computed by use of eq. 31. The hydrate layer is assumed to cover the total electrode surface.

For the computation procedure, the Type I film may either cover the total electrode surface or only the fraction covered by secondary crystals.

Variations in Surface Composition

To account for changes of the primary layer composition (Type II and Type I Films), two different refractive indices may be used for the portions of the surface covered and not covered by the secondary crystals. The refractive index describing non-stoichiometry may be determined in either of two ways: 1) Both the real and imaginary parts are evaluated by the computational procedure. 2) Excess metal is considered to be the cause of the non-stoichiometry,and the refractive index is computed using the Lorenz-Lorenz equation (eq. (60)), (Appendix C) to average the metal optical constants with the input oxide optical constants

$$\frac{n_e^2 - 1}{n_e^2 + 2} = \rho_e \left[\frac{f_1}{\rho_1} \frac{n_1^2 - 1}{n_1^2 - 2} + \frac{(1-f_1)}{\rho_2} \frac{n_2^2 - 1}{n_2^2 + 2} \right]. \qquad (60)$$

Bulk densities ρ_i are used, and f_1 is the volume fraction of component 1 calculated from the mole fraction of component 1 (evaluated by the computational procedure) by assuming additivity of molar volumes.

The regions having different primary layer compositions can be averaged either coherently (eq. (53) with C_c as the area fraction of the patches) or incoherently (eqs. (55), (56)).

Changes with time of the primary layer composition are modeled in two ways: (1) The fraction of the surface covered by the non-stoichiometric patches increases parabolically with time from the value COVII at TPACK to 0.999 at TDISS. (2) The mole fraction of excess metal in the films increases linearly with time from an initial value (determined by the computational procedure) from TPACK to unity at TDISS.

Adsorption of Dissolved Species

Film formation has been restricted to begin after the metal cation concentration exceeded the solubility limit of the metal in the electrolyte by a supersaturation required for nucleation or precipitation. Kinetics approximating an adsorption mechanism for film formation may be used for the computational procedure by the evaluation of the parameter VADS. This parameter, fulfilling the same role as C_{IIF} in eq. (1), describes the flux density entering the Type II film for the time interval $0 < t < t_{ss}$, where t_{ss} is the time to reach supersaturation of the metal cation (eq. (12), (13)).

Another consideration is the optical effect of adsorbed species on the electrode surface. Two approaches may be used for the computational procedure. The first approach forms a monolayer coverage of Type II film at a rate determined by VADS introduced above. The film is optically distinct from the mass-transport boundary layer, the refractive index of which is determined by the concentration of cations in the electrolyte at the surface.

The second optical treatment of adsorbed species assumes that there is no discontinuous change in refractive index between the boundary layer and the adsorbed sub-monolayer film. For this case, the interfacial refractive index of the mass-transport boundary layer is determined by the coverage of adsorbed species, using a linear average of the electrolyte and the adsorbed species refractive indices. The coverage of adsorbed species is calculated using an adsorption isotherm of the form of eq. (61)

$$\theta = f(a_1, e^{-\Delta G/RT}) \tag{61}$$

where a_i is the activity of the dissolved species in the electrolyte at the interface and ΔG is the free energy of adsorption. ΔG is evaluated by the computational procedure, and a_i requires use of an activity coefficient-concentration relationship.

G. Computation Procedure

Interpretation of the experimental data is accomplished by finding values of characteristic parameters in the model which will best reproduce the experimental values of Δ and ψ. The computer program (Appendix G) is a subroutine which calculates an error term (for fixed values of the characteristic parameters) defined as the average distance per point between experiment and theory, as given by Eq. (62)

$$\varepsilon_\ell = \frac{1}{(n-i)} \sqrt{\sum_{j=i}^{n} (\Delta_e - \Delta_t)_j^2 + (\psi_e - \psi_t)_j^2} \; . \tag{62}$$

The subroutine is designed to be used with a program which evaluates characteristic parameters by minimizing the error term.

The minimizing program used (MINUIT) was available as a library program (Library (Minuit73)) at the Lawrence Berkeley Laboratory. Simplex (G19) and Davidon variable matrix (G20) algorithms are used to evaluate all (or specifically chosen) parameters. Two versions are available, accommodating 15 and 55 variables. Parabolic error estimates are used to provide limits of uncertainty for the parameters. A parabola is fitted through the partial derivative of each parameter near the minimum. A measure of uncertainty is given by the change in parameter value necessary to change ε_ℓ (the distance between experimental and calculated points) by a specified value. In addition, a Monte Carlo routine (G21) may be used to search randomly the multidimensional space for multiple roots. In the routine, new initial values for the iteration process for the parameters being evaluated are chosen at random, and a new minimization is conducted.

The characteristic parameters in the model which may be evaluated by the computational procedure are given in Table IA. In practice, only a few of these parameters are simultaneously evaluated, with the remaining parameters becoming input variables.

Table IA. Parameters which may be Derived from Ellipsometer Measurements

Parameter	Description
VCRYS2	Crystallization Rate of the Type II Film
POREI	Porosity of the Type II Film
RATF	Dehydration Rate of Hydrate Layer
POREF2	Porosity of Hydrate Layer
POREFØ	Porosity of Type I Film (Initial)
CNØ	Number Density of Secondary Crystals
VCRYS	Crystallization Rate of Secondary Crystals
HYDR	Hydration of Secondary Crystals
FRUFF	Rate of Void Formation in Roughness Layer
POREØ	Porosity of Roughness Layer
TMØ	Initial Thickness of Roughness Layer
TF1CCØ	Initial Thickness of Type II Film
P	Width to Height Ratio of Secondary Crystals
DSSAT	Degree of Supersaturation of Metal Cations
AITAF	Charge-Transfer Exchange Current Density
ALPH, BETA	Orientation Angles for the Secondary Crystals
TNUC	Time, Onset of Secondary Crystal Growth
TDIFF	Time, Minimum Porosity of Hydrate Layer
FPACK	Final Porosity of Type I Film
TPACK	Time for Compaction of Type I Film
TDISS	Characteristic Time Describing Depletion of Hydrate Layer, Patchwise Film Formation, or Developing Non-Stoichiometry
TNFR, TNFI	Complex Refractive Index Describing Non-Stoichiometry
COVII	Initial Coverage for Patchwise Film Formation
SIGCN	Standard Deviation in CNØ
SIGTN	Standard Deviation in TNUC
SIGALF	Standard Deviation in ALPH
SIGBET	Standard Deviation in BETA
FARRAY	Limiting Coverage of Secondary Crystals
BADS	Free Energy of Adsorption
VADS	Rate of Adsorption of Type II Film
PADS	Adsorption Parameter for 2-Parameter Isotherms

V. Experimental Equipment and Procedures

A. Equipment

Automatic Self-Compensating Ellipsometer

The ellipsometer (G22) is a self-compensating instrument. The basic arrangement is illustrated in Fig. 8 . With the quarter wave compensator set at ± 45°, the polarizer azimuth is adjusted to give linearly polarized light after reflection from the sample. The analyzer azimuth is crossed at 90° to the reflected azimuth, giving a minimum intensity in the light transmitted to the photomultiplier. The experimental parameters, the relative amplitude tan ψ and the relative phase Δ, are computed from the polarizer and analyzer azimuths (G25). Figure 9 shows the arrangement of components for the automatic ellipsometer. Faraday cells, driven by 150 ampere bipolar programmable power supplies, rotate the planes of polarization to maintain the minimum in intensity. The instrument has a response time of 1 ms and a resolution of 0.001 deg. in azimuth. It has a slew rate of 1600 deg/sec, which corresponds to μm/sec film growth.

Electrochemical Current Supplies

Experiments were conducted at constant current and constant potential modes. For galvanostatic operation, a Fluke Model 382A regulated power supply was used. Six digits may be set over a 0-2A range. The compliance rating is 50 volts. Potentiostatic measurements were performed using a Magna Model 4700M potentiostat. This is a dual channel power supply with a 5A/20V range to control potential over a ± 3V range.

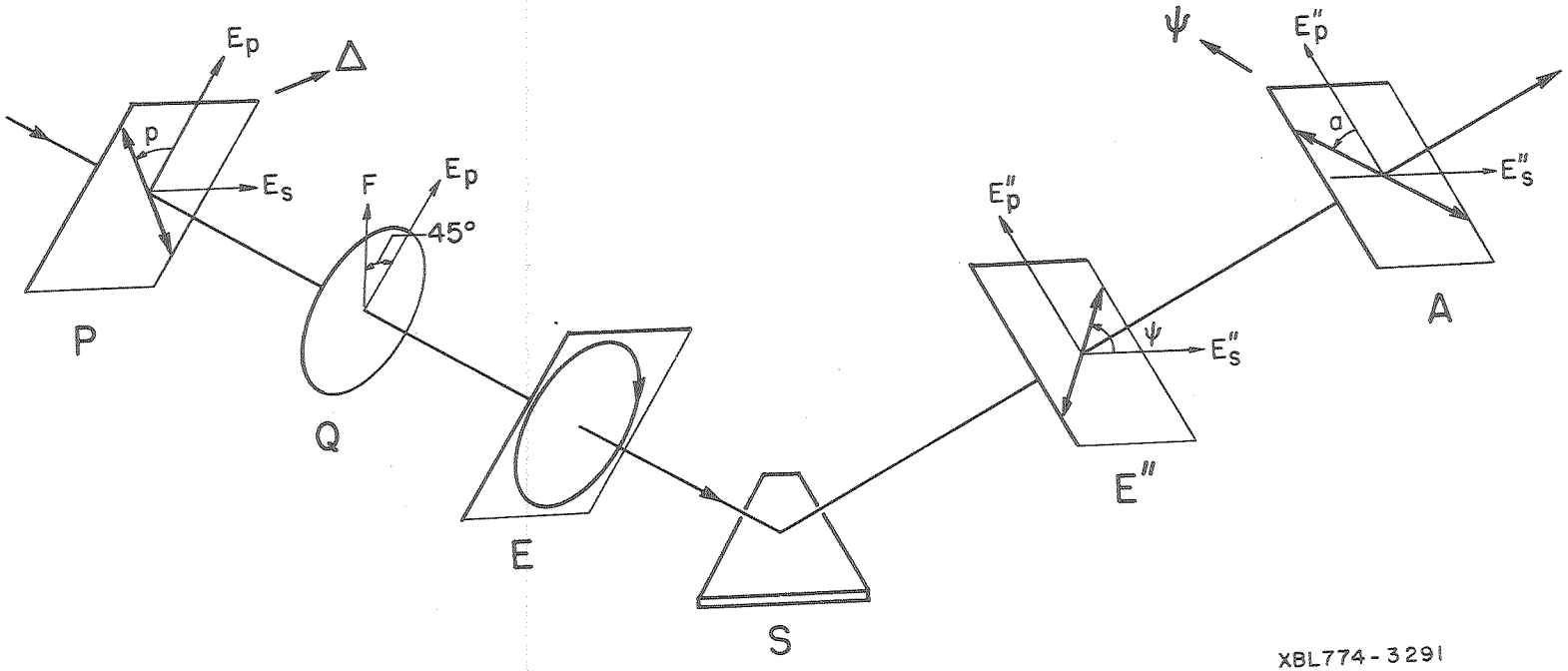

Figure 8. Azimuths of ellipsometer components at compensation. P, Q, S, A, refer to the polarizer, quarter-wave compensator, specimen, and analyzer. E represents elliptic polarization incident on the surface and E" represents linear polarization after reflection.

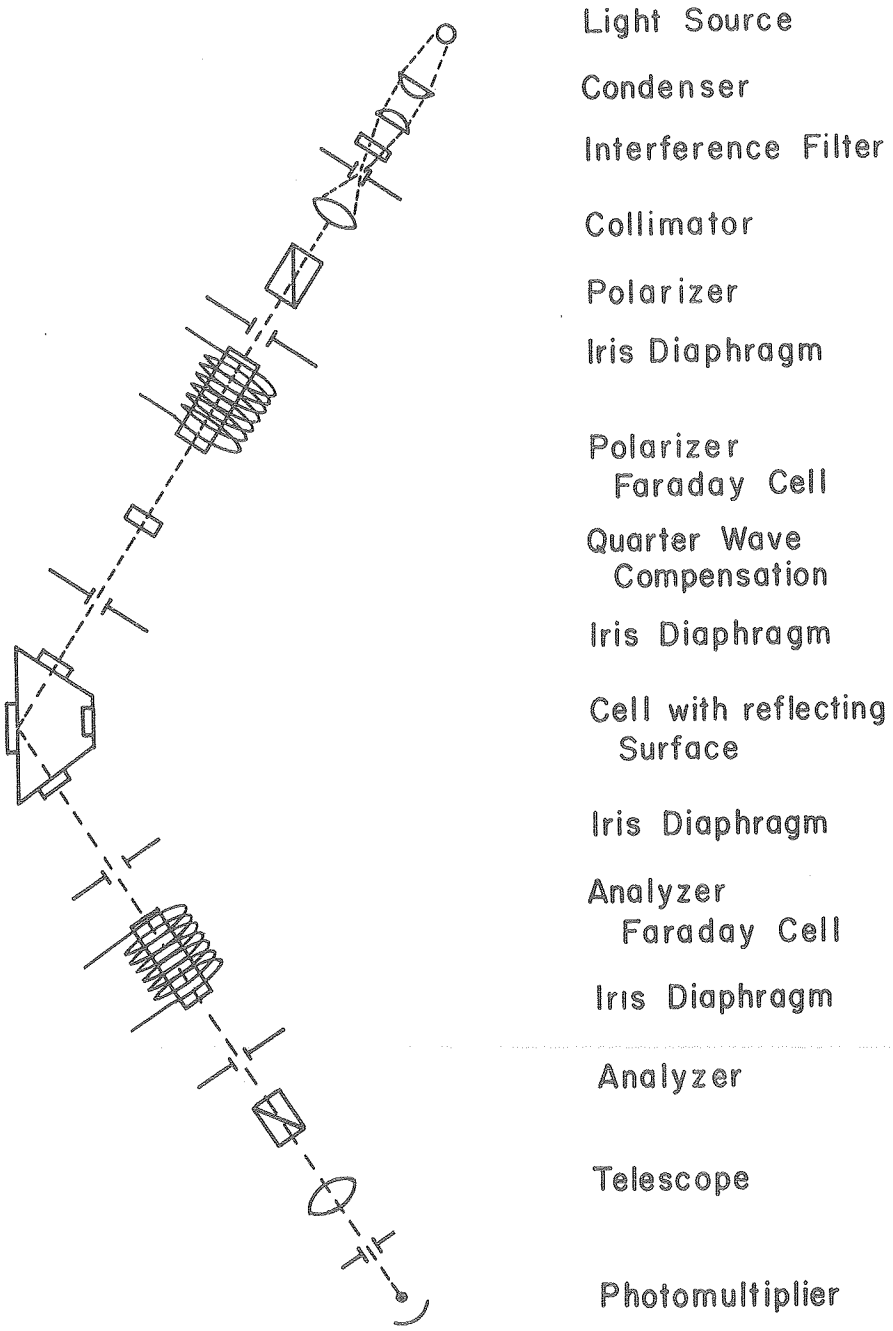

Figure 9. Arrangement of components for the automatic self-compensating ellipsometer.

Flowmeter and Flowsystem

An ultrasonic flowmeter (Series 240, Controlatron Corp.) was used to monitor fluid velocity during forced convection experiments. The flowmeter measures the Doppler shift in the ultrasonic beam travelling across the pipe. Readings are taken every 20 ms over a range of 0.01 to 333 gpm. A 0-10 V analog signal is used for recording. The flow system is illustrated in Fig. 10 . The holding tank and the 3/4 in.sch 80 pipe are made of polypropylene, while the flow cell and the degassing chamber are made of plexiglass. The magnetically-coupled pump (Gorman-Rupp, Model 14520) has a polypropylene drive assembly. 10 μm polypropylene elements are used in an in-line filter.

Recorder

Hard-copy outputs of the polarizer and analyzer azimuths, flow velocity, electrode potential, and cell current are obtained in analog form with a Honeywell (Model 1108) galvanometer recorder. The input voltages deflect mirrors in the galvanometers to direct light beams onto photo-sensitive paper. The pre-amplifier to the recorder has an input impedance of 20 KΩ. For potential measurements, a 10 MΩ pre-amplifier is used in series with the recorder. Signals for recording the polarizer and analyzer azimuths (current to the Faraday cells) and the cell current are generated by precision shunts. A 0-10 V output is generated by the flowmeter controller.

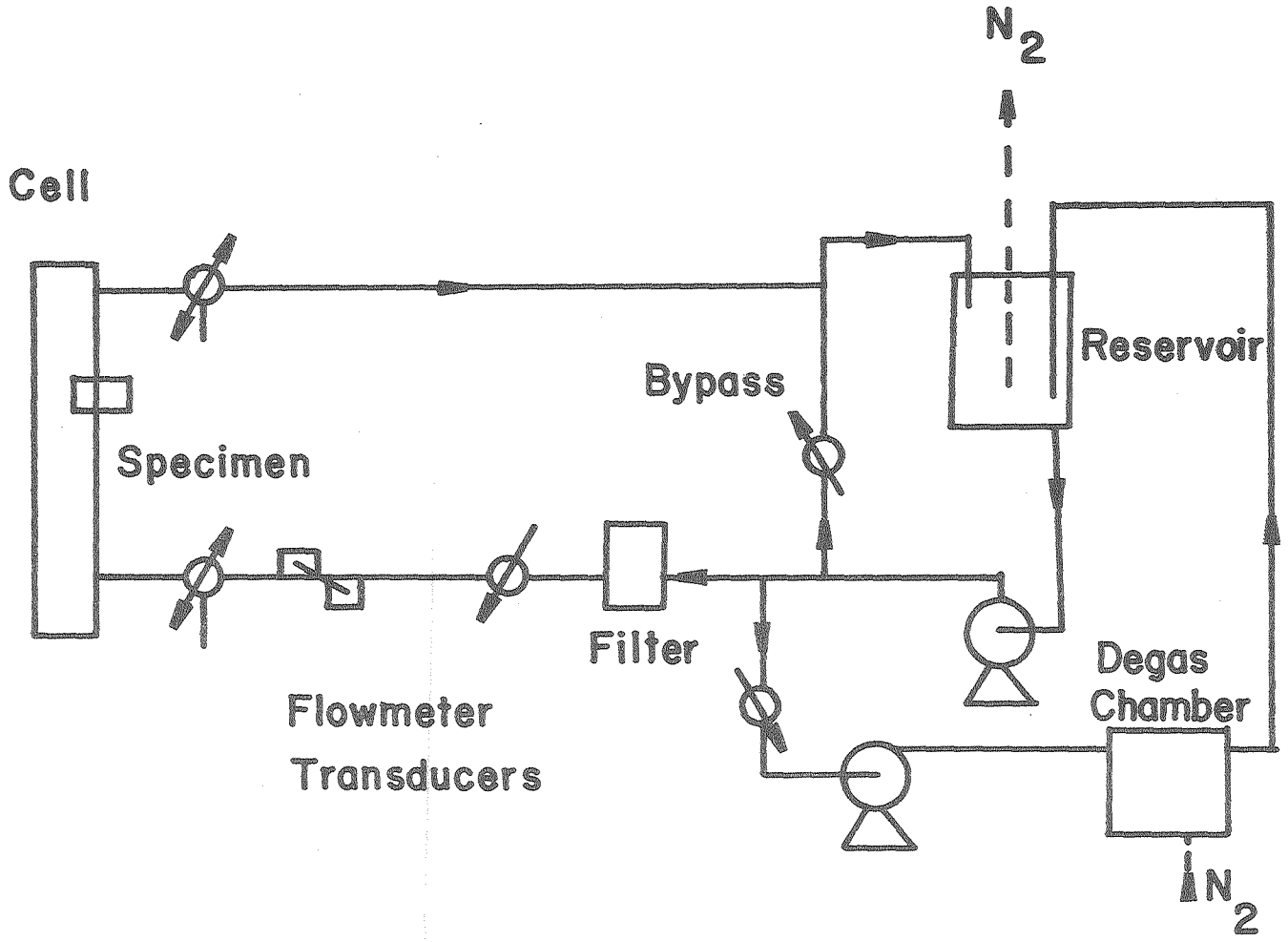

Figure 10. Flow system used for forced-convection experiments in flow channel.

XBL 787-9524

B. Electrode Preparation

Electrodes were formed from high-purity (99.999%) silver, zinc, and cadmium metals. Polycrystalline and single crystal electrodes were designed to be used in a single electrode holder which is used with both the stagnant and flow cell. Polycrystalline electrodes were milled to give 1.2 x 3 cm surface area. Silver, zinc, and cadmium single crystals (purchased from Orion Chemical Co.) were cut using electrical discharge (EDM, Model C1000, South Bend, Indiana). Laue x-ray diffraction was used to orient all crystals for cutting and mounting. Brass screws (1/4-20) were silver-soldered to the polycrystalline samples, and silver epoxied to the single crystal electrodes. They served to attach the electrodes to the holder and to make electrical contact. The electrodes were cast in epoxy mounts of 1.5 in. diameter.

The initial surface preparation for all electrodes was identical: rough polishing through a series of silicon carbide papers to the 0000 grit. A jig was used to keep the surface perpendicular to the cylinder axis. Anodic dissolution in aqueous 1M H_2SO_4 was used to remove 10 μm of damaged surface from the single crystals prior to the final polish with 1 μm diamond paste. Prior to placement in the cell, all electrodes were cleaned of organic materials left by the polishing sequence by evolving hydrogen at 100 mA/cm^2 in 1 M NaOH for three minutes in a beaker.

C. Electrolyte Preparation

Analytical-grade chemicals and glass-distilled, deionized water

were used to prepare the electrolytes used for the experiments. The molarity of the KOH solutions was determined by titration with a standard 1 M HCl solution. A degassing chamber (Fig. 11) was used to remove dissolved oxygen from the electrolyte by stripping with water-saturated nitrogen for 30 minutes. This procedure was used to decrease the oxygen content of the electrolyte by at least 3 orders of magnitude.

Design of the Degassing Chamber

The design was treated as a batchwise stripping of two liters of electrolyte by a stream of 1 mm diameter bubbles. The change in concentration of oxygen with time is

$$\frac{dC}{dt} = \frac{Ak_c C}{V_e} \tag{63}$$

where A is the surface area for transfer, V_e the volume of electrolyte (2 liters), and k_c the mass-transport coefficient. The transfer area A is given by the hold up volume of the gas stream V_g and the bubble diameter d_p,

$$A = 6V_g/d_p \ .$$

Substituting into eq. (63) gives

$$\frac{C}{C_o} = \exp\left(-\frac{6V_g}{V_l}\frac{k_c}{d_p}t\right) . \tag{64}$$

The mass transport coefficient is evaluated from (G23)

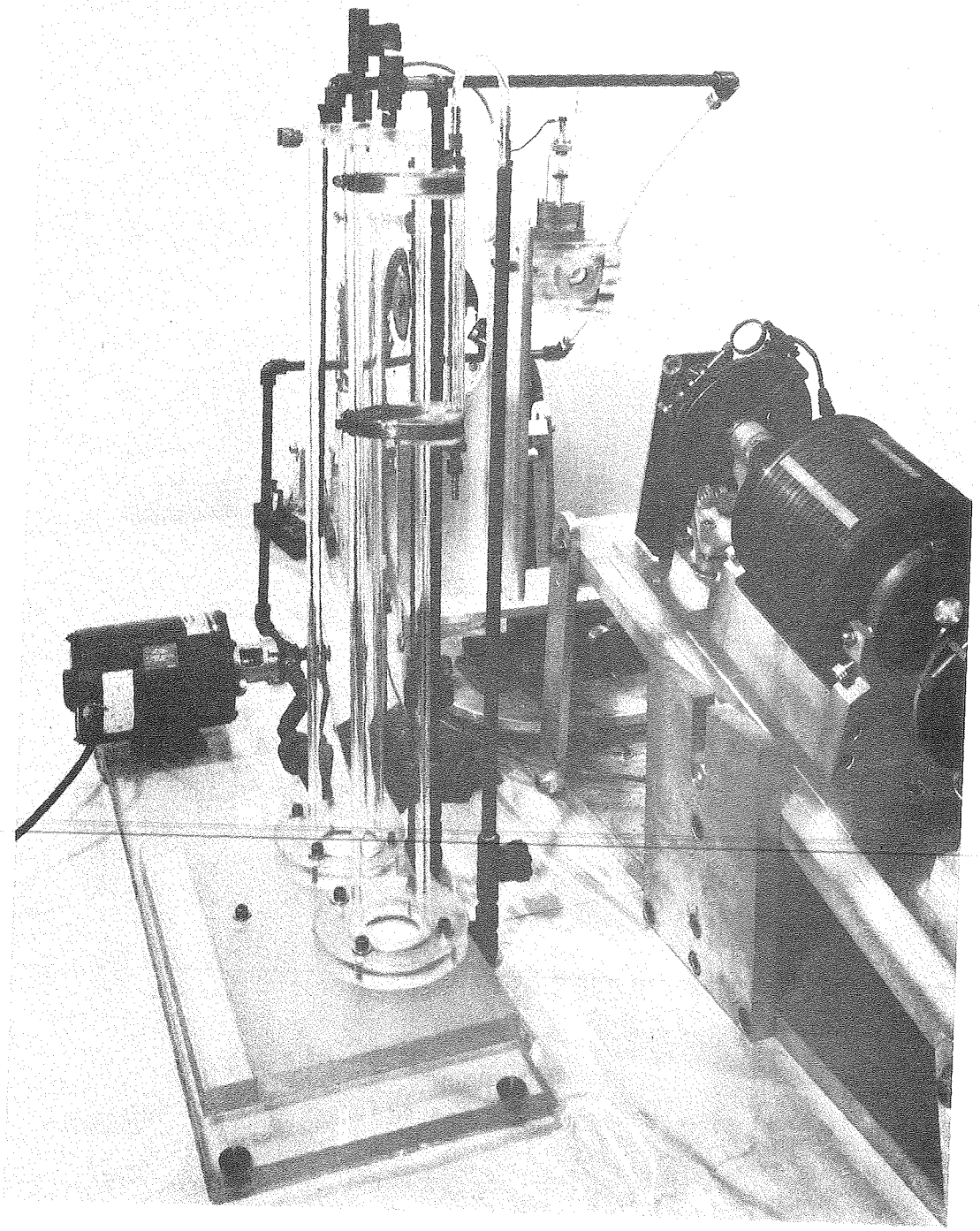

XBB 764-3743

Figure 11. Degassing chamber for removing dissolved oxygen from the electrolyte. Nitrogen is saturated with water in the nearest column, and then dispersed as bubbles into the electrolyte in the second column.

$$\frac{k_c d_p}{D} = 1.13\left(\frac{d_p \bar{u}}{D}\right)^{1/2}\left(\frac{d_p}{0.45 + 0.2\, d_p}\right). \qquad (65)$$

The rise velocity $\bar{u}$ for 1 mm bubbles (Fig. 6.14) (G23) is 15 cm/s. For a diffusivity of 2×10^{-5} cm^2/s, k_c = 0.0138 cm/s .

Equation (65) indicates for a gas holdup volume of 0.252 ℓ, 1.4 min is required to reduce the oxygen content by a factor of 1000. 5 mm diameter bubbles require 3.2 min at a hold up of 0.58 ℓ. Thirty minutes was used in practice for an average bubble diameter of 3 mm and a gas holdup of 0.4 ℓ.

D. Electrochemical Cells

Two cells were used to provide defined mass-transport conditions, a stagnant cell and a flow cell. The cell windows are oriented at right angles to the path of the incident and reflected light beam to prevent polarization changes which would affect the ellipsometer measurements. The cells were constructed for observations at 75 deg. angle of incidence.

The stagnant cell is shown in Fig. 12. The counterelectrode is a 2×2 cm platinum sheet located 8 cm from the working electrode. Inlet and outlet ports connect the cell to the degassing column, in which a centrifugal pump (Flotec Model R2P11104V) is used to transfer the electrolyte to and from the degassing chamber, which serves as a reservoir. A capillary is used for the reference electrode connection (Hg/HgO for KOH electrolyte). The cell is mounted with the working electrode directed face-up (pure diffusion) or face-down (natural

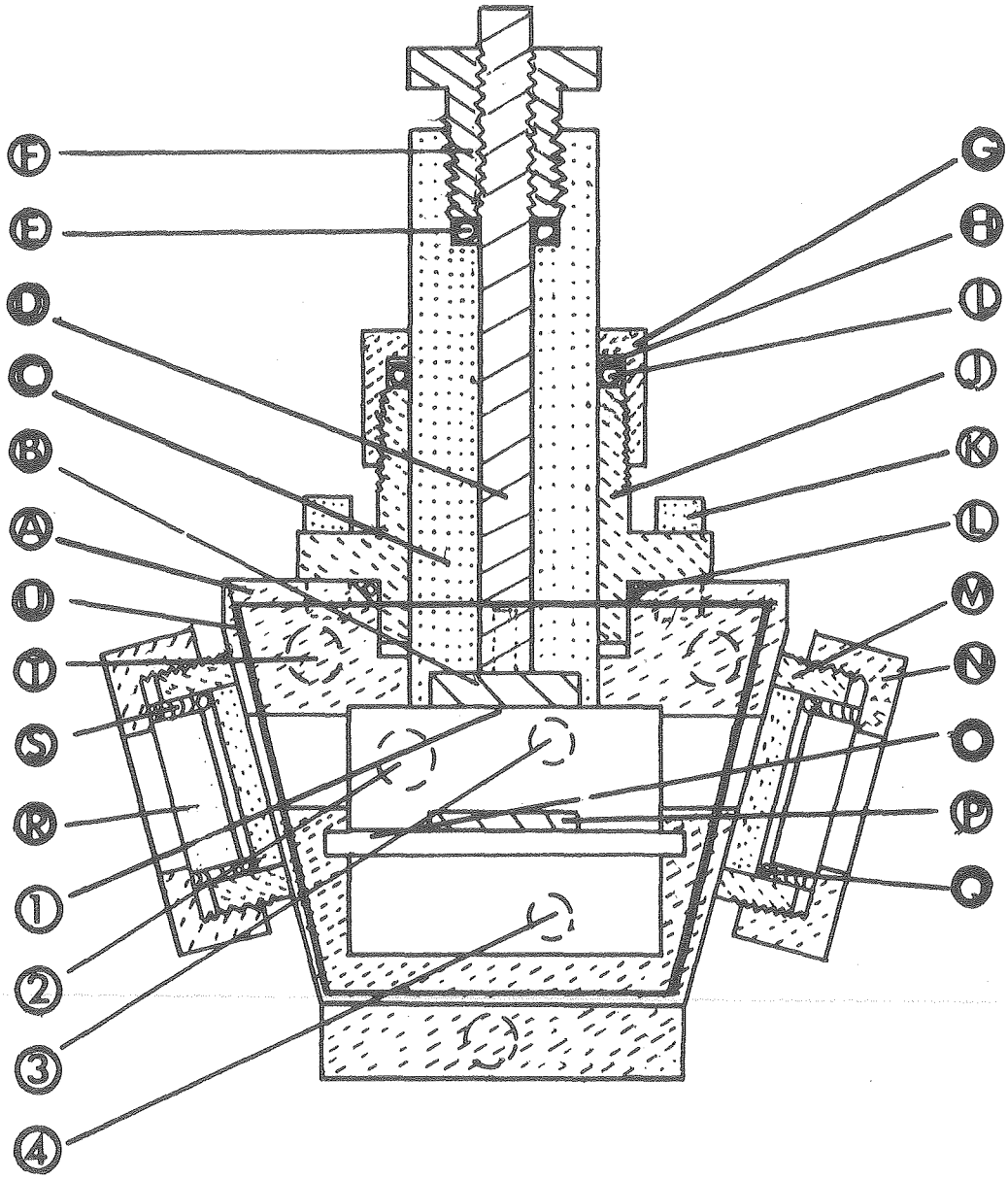

Figure 12. See caption on page 75

Figure 12. Cross-section of stagnant solution cell.

A cell body
B observed electrode approximately 1×3 cm^2 area
C body for electrode (acrylic, exchangeable)
D electrical connection to electrode (chrome-plated brass)
E O-ring seal
F adjustable body for controlling electrode depth (chrome-plated brass)
G sealing nut for electrode body (aluminum)
H washer (Teflon)
I O-ring for electrode body (silicone rubber)
J holder for electrode body (polypropylene)
K screws for attaching holder to cell body
L O-ring seal for holder
M frame for window (acrylic, glued to cell body)
N sealing nut for window (acrylic)
O support for counter electrode (acrylic); also position for diaphram
P counter electrode, copper
Q O-ring for cell window
R cell window
S pressure sleeve for cell window
T screws for attaching fourth side
U O-ring seal for fourth side
1 capillary for reference electrode
2-4 inlet and outlet for electrolyte and nitrogen

convection) on a coordinate table giving x-y translations. The coordinate table is mounted on an adjustable tripod base giving three-dimensional rotations.

The flow cell is shown in Fig. 13 . The trapezoidal cross-section of hydraulic diameter 1.21 cm include a 75 cm entrance length to establish fully-developed flow. The working electrode and stainless steel counterelectrode are vertical. A 0.030 in. capillary located downstream from the electrode is used for potential measurements. The cell mounts on an aluminum plate which uses three push-pull screw arrangements for alignment with respect to the ellipsometer.

E. Experimental Procedures

The ellipsometer components are first aligned for observations under the appropriate transport conditions. Auto-collimation is done using a precision trapezoidal prism (accurate to 16 sec. of 75 degrees) with reflection coated end pieces located at the specimen position. A light beam is directed along the optical axis by use of a special eyepiece which introduces the beam from the side by reflection from a partially-transmitting mirror. With the prism stationary, each sub-assembly of components is adjusted separately until the light reflecting from the prism returns along the optical axis (G24).

The electrodes were then introduced into the cells and polarized 10 mV negative to the bare metal potential (with electrolyte) to remove air-formed oxides and prevent corrosion processes. The cell is then aligned with respect to the ellipsometer by centering the light

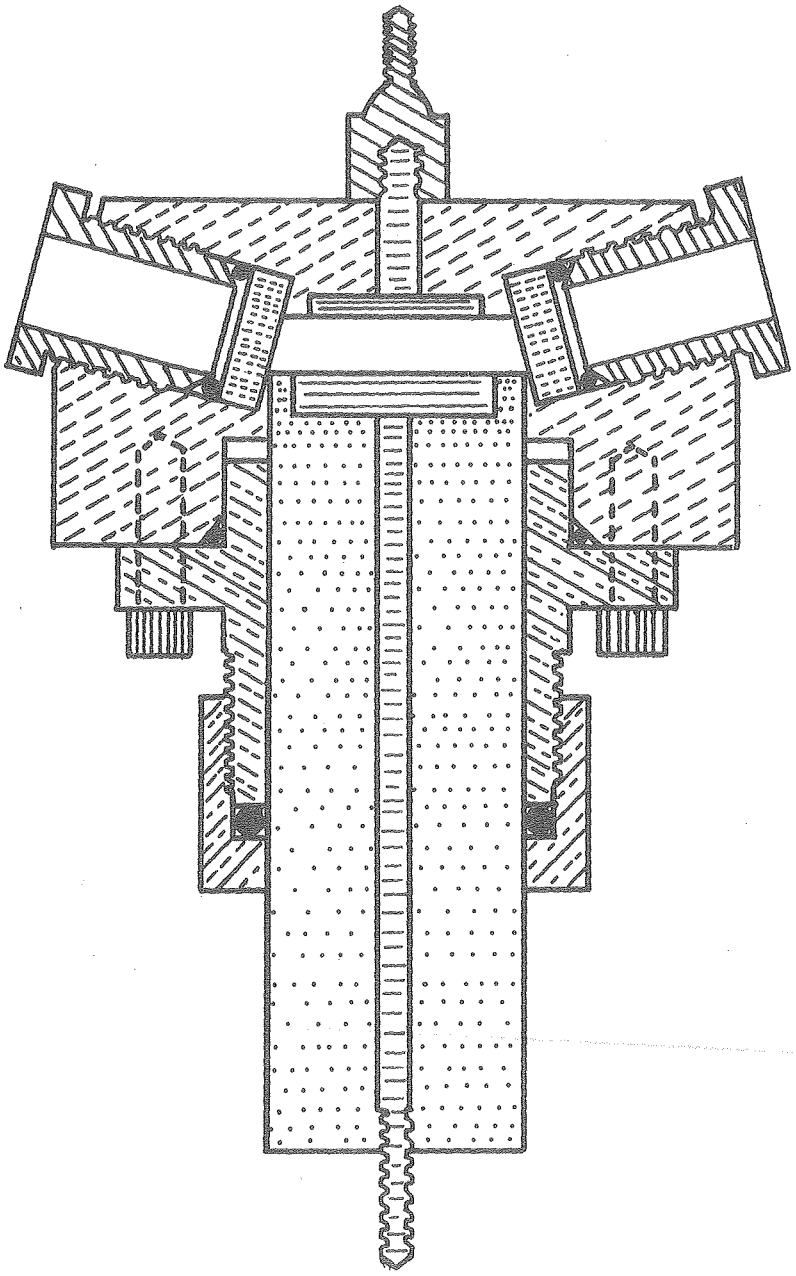

XBL 741-34A

Figure 13. Cross-section of flow cell. Materials of construction and seals are similar to those in the stagnant cell, Figure 12. The same electrode bodies can be used in both.

beam on the electrode and positioning the reflected beam through the optical axis of the second sub-assembly of ellipsometer components.

The chosen transport conditions are obtained. For forced-convection experiments, the volumetric flow rate associated with the chosen Reynolds number is set by adjusting the valves in the flow system. For convection-free experiments, the pump circulating electrolyte from the degassing chamber is stopped.

A four-zone measurement is taken to allow determination of specimen misalignment errors (G25). The recorder is turned on and the electrical current initiated to perform the experiment. For conditions in which relatively slow changes in the optical properties of the electrode surface occur (low current densities) and result in slow changes in the polarizer and analyzer Faraday cell compensation, the azimuths of the Glan-Thompson prisms in the fixed polarizer and analyzer may be stepped manually to follow changes greater than the present ± 22 degree electrical compensation of the ellipsometer.

The values of the analyzer and polarizer, current, electrode potential, and volumetric flow rates as functions of time are read from the recorder. The relative amplitude parameter tan Ψ and the relative phase Δ were calculated from the polarizer, analyzer, and quarter wave plate azimuths by use of a linearized theory accounting for optical imperfections in the ellipsometer (G25).

VI. Results of Experimental Observations

A. Induction Periods at Low Current Densities

During constant current experiments in stagnant electrolyte, detailed structure in the $\Delta - \psi$ curve becomes apparent at low current densities. Figure 14 shows changes in the slope of the experimental curve ($0.05\ mA/cm^2$) occurring at times designated as θ_1 and θ_2. Prior to time θ_1, changes in Δ may be explained by roughening of the silver surface. During this time, the electrode potential is increasing and reaches the value of 0.22 V (0.244 is the Ag/Ag_2O plateau) at θ_1. The curve between θ_1 and θ_2 may be explained in terms of increasing surface coverage of an adsorbed layer of either Ag_2O or AgOH. Film growth begins at θ_2, with the $\Delta - \psi$ curve agreeing exactly with the slope calculated using compact Ag_2O optical constants.

Due to the low solubility of silver oxide, an increase in the concentration of silver ions during this time period cannot be detected because the change in refractive index at the interface would be too small to observe. However, the times θ_1 and θ_2 can be correlated by use of the Sand equation (eq. 12) which applies for these experimental conditions. By assuming the solubility limit of Ag_2O is reached at θ_1, a diffusion coefficient for the ionic species of $1.14\times10^{-5} cm^2/s$ is calculated. Using this value of the diffusion coefficient, an interfacial concentration of 2.30 times $C_s (= 1.5\times10^{-4} M)$ is calculated from θ_2. This indicates a minimum degree of supersaturation of 2.3 is required for the heterogeneous crystallization of silver oxide.

This correlation applies for other metals as indicated in Figure 15. Diffusion coefficients were determined from the first slope change in

the $\Delta - \psi$ curve at low current densities (appropriate to the solubility of the ionic species) for Zn, Ag, Cd, Pb, and Cu . A value of $C^*(\equiv C/C_s)$ was then determined from the second slope change. The solubilities and diffusion coefficients corresponding to Figure 15 are given in Table I.

At larger current densities, this structure becomes less distinct, as shown by the 0.1 mA/cm^2 curve in Figure 14. The values of θ_2 indicate that supersaturations larger than 10 occur at higher current densities.

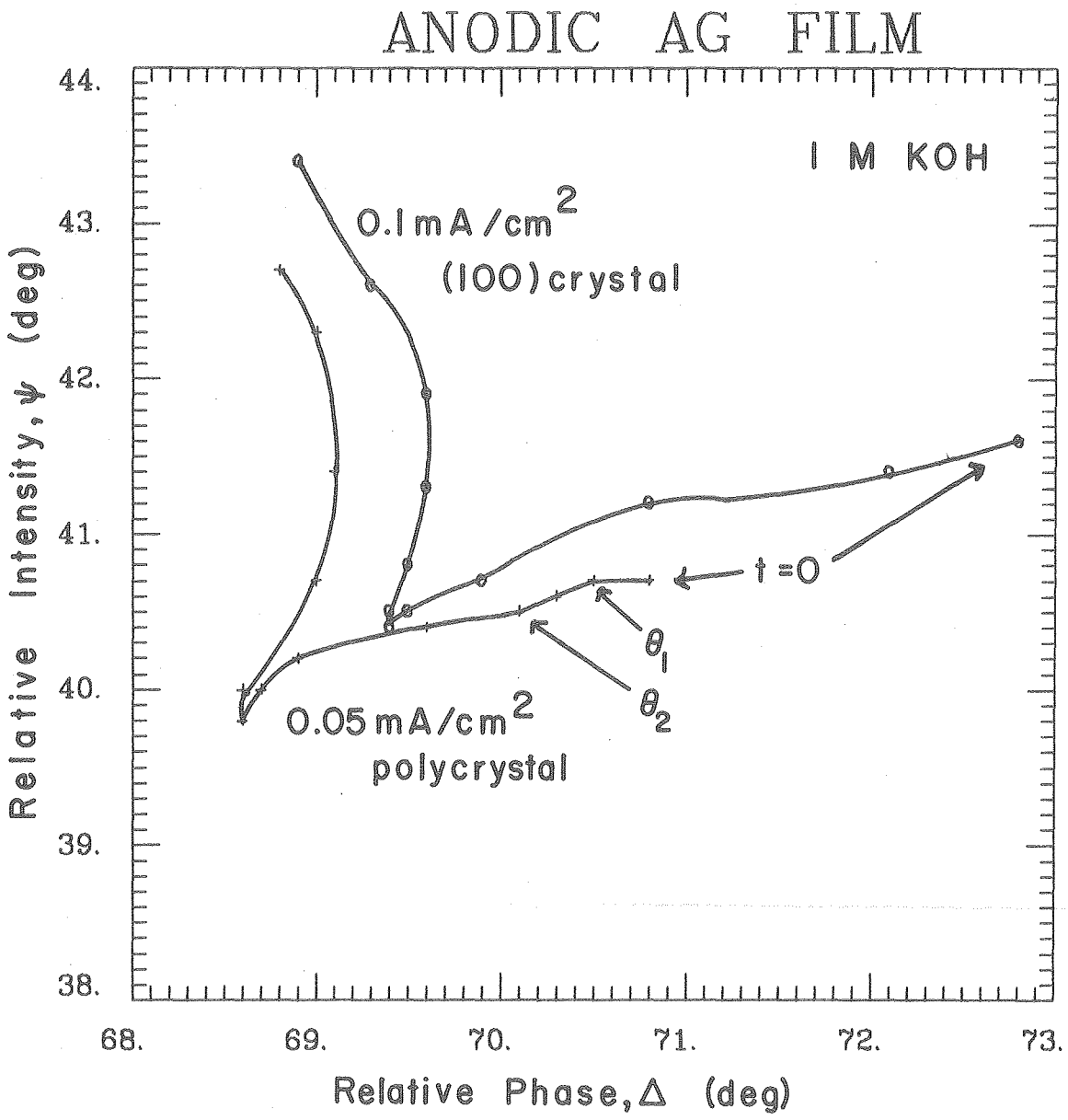

XBL 774-8331

Figure 14. Induction periods for correlating interfacial concentrations. At time θ_1, the solubility limit of the ionic species in the electrolyte is reached. Heterogeneous crystallization begins at θ_2.

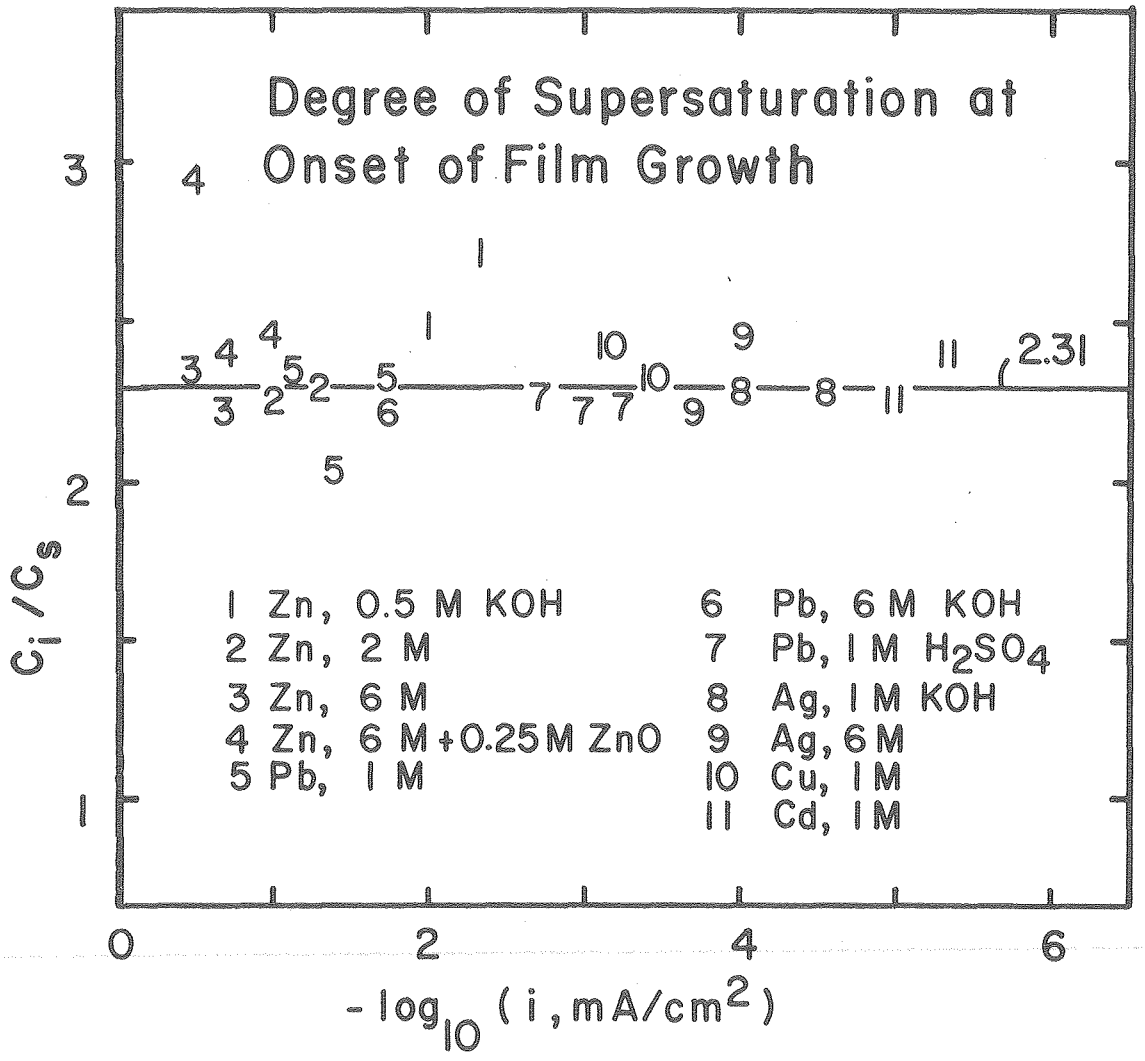

XBL 786-9226

Figure 15. Supersaturation of electrolyte at onset of anodic film growth. Concentrations determined from θ_2 values in Figure 14. (Abscissa should read amps cm^{-2}.)

Table I. Diffusion Coefficients Indicated by Ellipsometer Transients (Solubilities obtained from the literature (Appendix F))

Metal	Electrolyte	Solubility (moles/liter)	D (cm^2/s)
Ag	1 M KOH	1.5×10^{-4}	11.4×10^{-6}
	6 M KOH	4.7×10^{-4}	
Zn	0.5 M KOH	4.1×10^{-3}	9.7×10^{-6}
	2 M KOH	6.6×10^{-2}	
	6 M KOH	0.6	
Cd	1 M KOH	5×10^{-6}	8.6×10^{-6}
Pb	1 M KOH	1.6×10^{-2}	11.3×10^{-6}
	1 M H_2SO_4	4.3×10^{-3}†	
Cu	1 M KOH	1.9×10^{-3}	7.8×10^{-6}

†Calculated using diffusion coefficient obtained from 1M KOH experiment.

B. Computations for Developmental Models

To illustrate the relative merits of the models presented in Figure 1a, the average deviation between experimental and computed values of the relative amplitude parameter ψ and the relative phase Δ was computed for the anodic oxidation of silver in 6M KOH at 1 mA/cm^2 (stagnant electrolyte). These results are presented in Table II. Computations were omitted for Model 5, which is discussed in Appendix C.

Table II. Deviation between Experiment and Theory for Models of Anodic Film Formation (Exp. Ag 80-30).

Model No. (Fig. 1a)	Ave. Deviation (deg)
1	56.23
2	56.22
3	62.02
4	9.06
6	6.03
7	7.75
8	4.90

Model 1 uses a single homogeneous film having a refractive index corresponding to porous silver oxide. The addition of the mass-transport boundary layer in Model 2 does not improve the deviation between experiment and theory, as the solubility of silver is too low to give a concentration of ions having a significant optical effect. The use of two homogeneous films (Model 3) representing films of different

porosity also gives very poor agreement with experimental observations.

Model 4 includes a roughness layer and two porous oxide layers. The top oxide refractive index of 1.42 - 0.02 i is similar to the colloidal layer described in Appendix C. Model 6 uses a non-absorbing top layer, of refractive index 1.41, an intermediate oxide layer, the porosity of which decreases with time from 0.85 to 0, and a roughness layer with refractive index 1.22 - 0.60 i. The use of an additional porous oxide in Model 7 does not give an improvement over Model 6. For the computations in Model 8, the roughness layer was neglected and a constant porosity was used for the Type I film. A detailed discussion of Model 8 is given below.

Models 6 and 8 give the smallest deviations between experiment and theory. The optical effect of the growing secondary crystals in Model 8 is similar to the decreasing porosity of the oxide layer in Model 6. The porous Type II film in Model 8 and the roughness layer in Model 6 also appear to have similar optical effects.

C. Silver Oxide (Ag_2O) Formation

Qualitative Aspects

The effects of electrode current density, alkaline concentration, electrolyte flow velocity, and the crystallographic orientation of the silver substrate on the optical properties of the anodic film are shown qualitatively in Figures 16, 17, 18, and 19. Scanning electron micrographs of the electrode surfaces are shown for comparison in Figures 20, 21 and 22. The 1.0 mA/cm^2 curve of Figure 16 is characteristic of the electrode surface being covered with large number densities

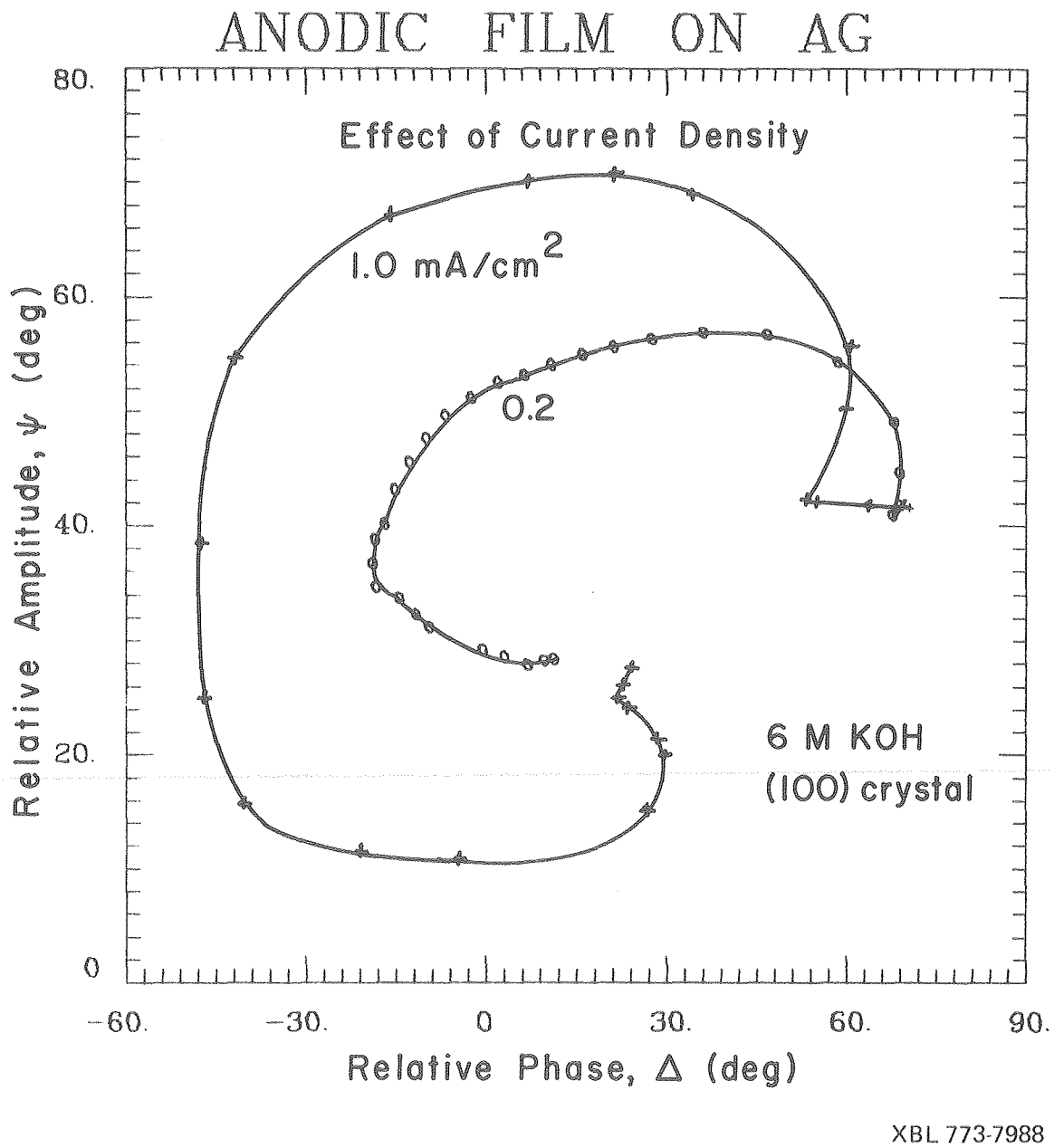

Figure 16. Differences in the optical properties of anodic films formed at different current densities as indicated by the ellipsometer measurements Δ and ψ. Times at endpoints (lower left) 1.0 A/cm^2 - 109 s, 0.2 mA/cm^2 - 680 s.

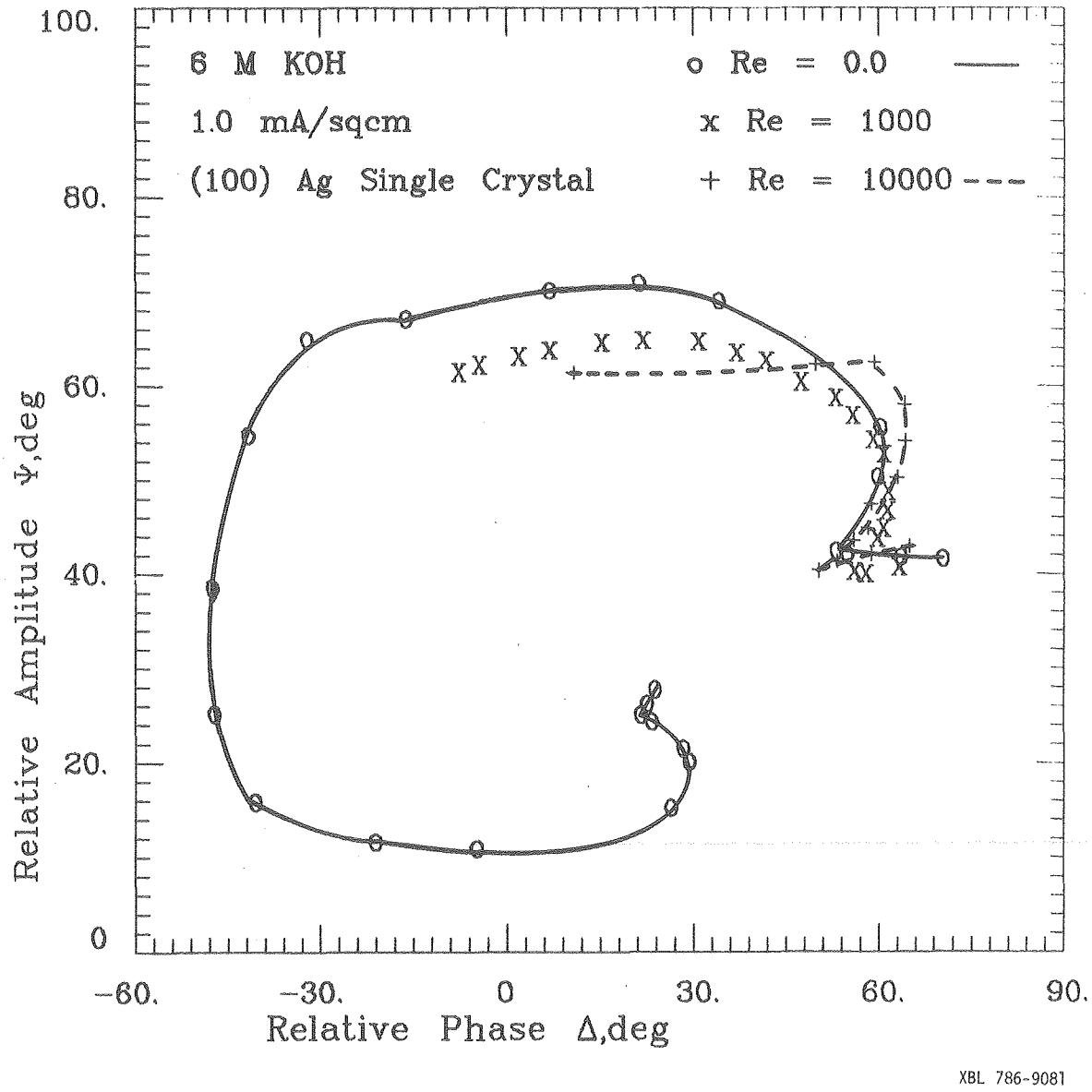

Figure 18. Differences in the optical properties of anodic films formed at different electrolyte flow rates, as indicated by the ellipsometer parameters Δ and ψ. Times at endpoints (left) 0 Re - 109 s , 1000 Re - 33 s , 10000 Re - 30 s .

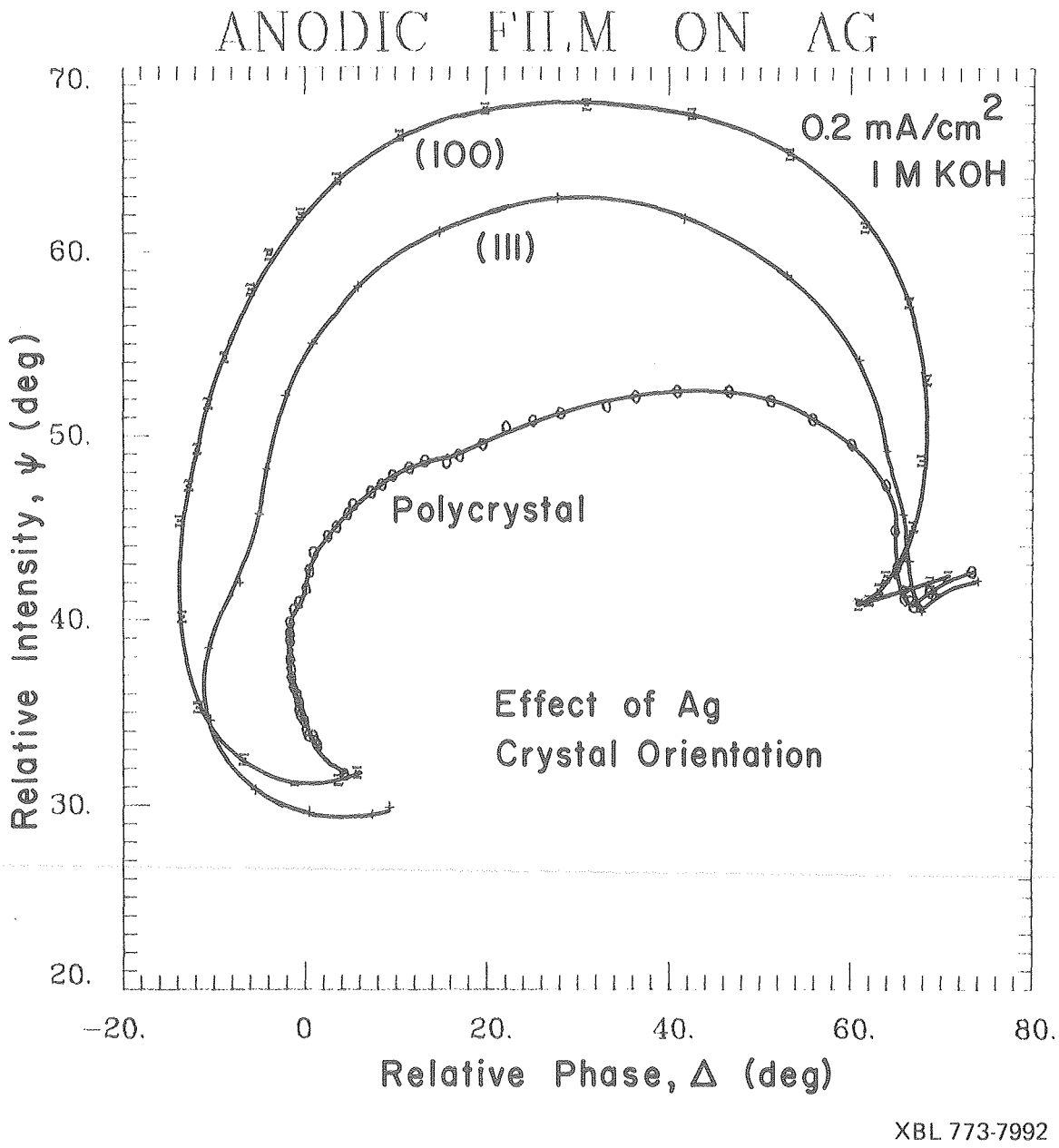

Figure 19. Differences in the optical properties of anodic films formed on different metal substrates, as indicated by the ellipsometer parameters Δ and ψ. Times at end-points (lower left) (100) - 660 s, (111) - 660 s, polycrystal - 670 s.

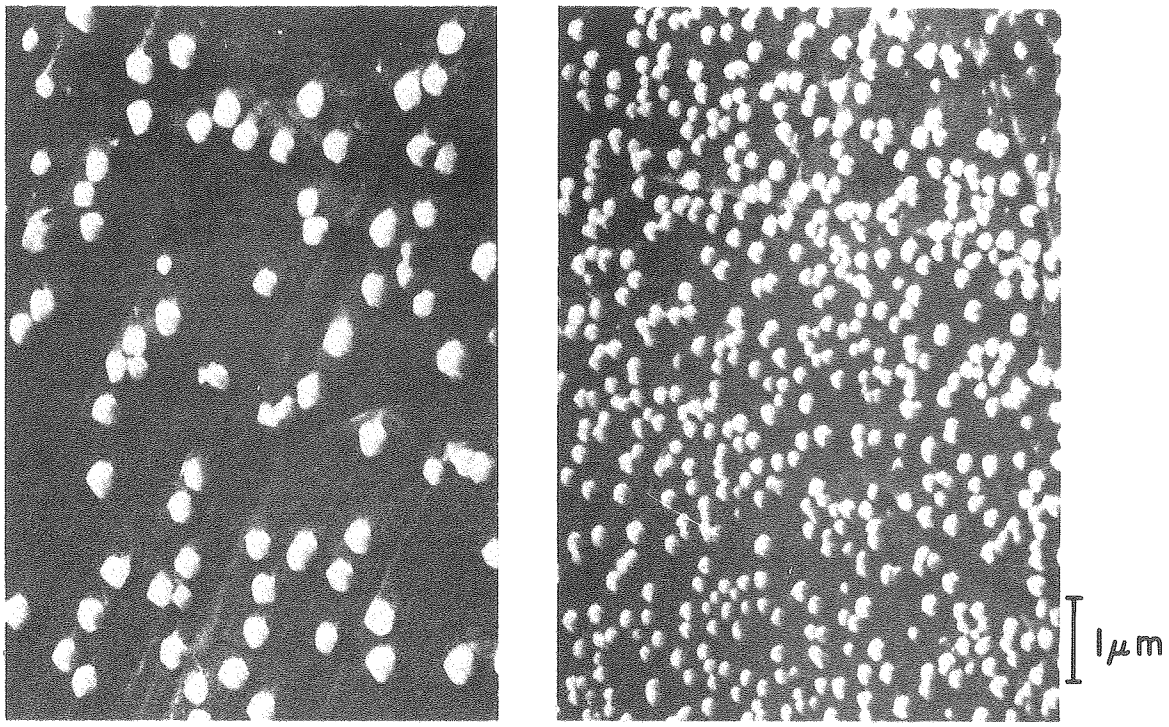

Figure 20. Higher number density of secondary crystals with higher current density.

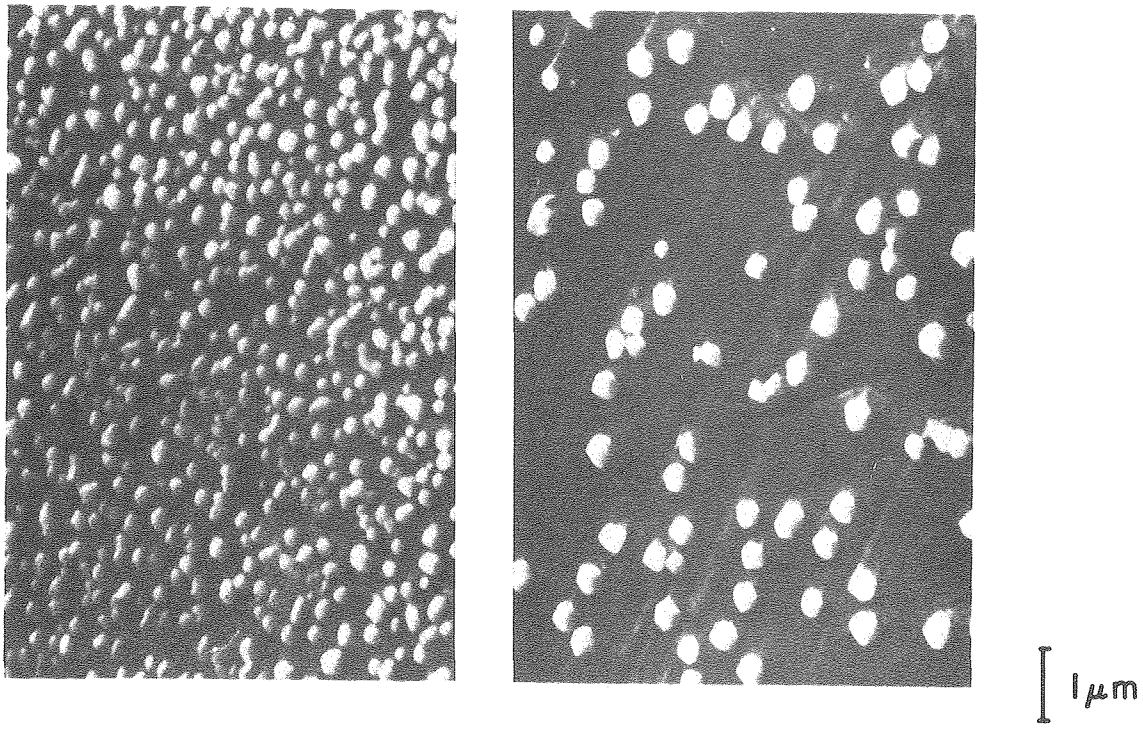

XBB 786-6979

Figure 21. Higher number density of secondary crystals with lower solubility.

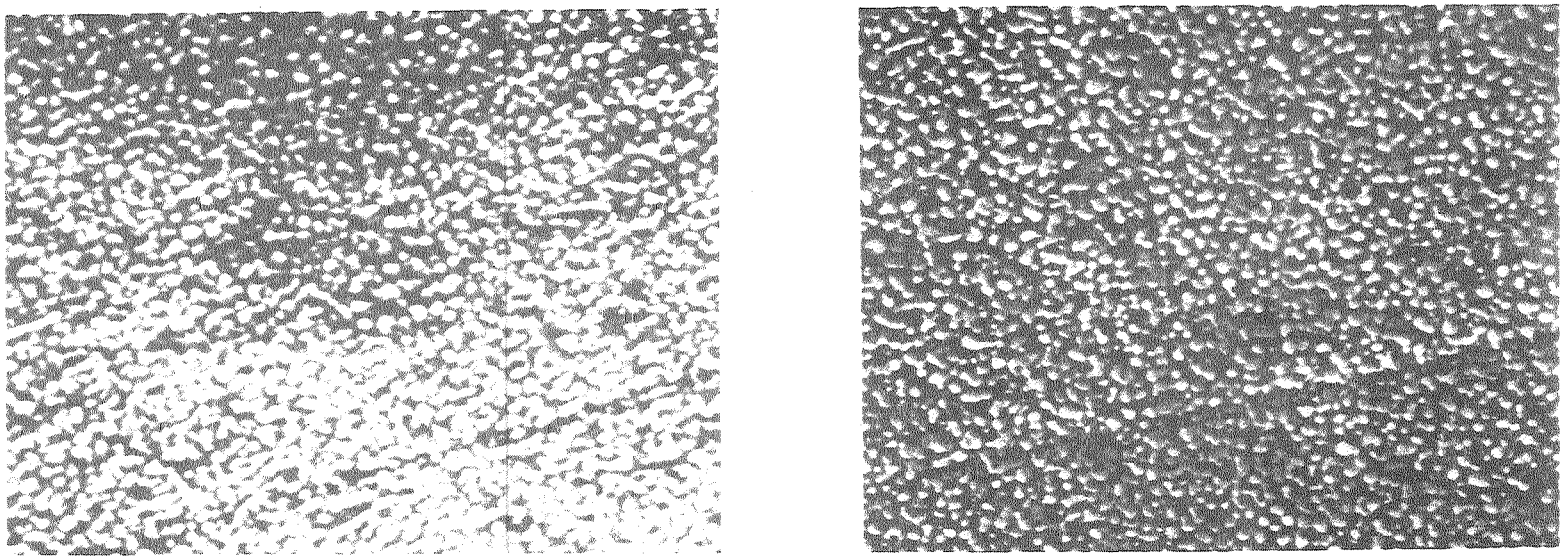

Figure 22. Higher number density of secondary crystals with lower flow rate.

of secondary crystals. Large changes in ψ and Δ result from the growth of the anodic film. The 0.2 mA/cm^2 curve (Fig. 16) is characteristic of small number densities of secondary crystals being present on the electrode surface. The ranges of Δ and ψ are much smaller.

The increase in the number density of secondary crystals with increasing electrode current density, decreasing alkaline concentration, and decreasing flow velocity is readily explained by large number densities being associated with large degrees of supersaturation of the solution-phase silver species. The effect of crystallographic orientation is less obvious, but still consistent. SEM observations indicate larger number densities of secondary crystals on the (100) electrode than on the (111) electrode. However, a large distribution in crystal sizes is also observed on the (100) and polycrystalline electrodes.

The trends illustrated by Figs. 16-22 are very reproducible for the experimental procedures given in Sec. V. This reproducibility is a further indication that solution-side processes are dominant, as the electrode surface is less easily controlled than is the electrolyte.

Quantitative Interpretations

For the interpretations presented below, the optical model shown in Fig. 1b was used. Unless stated otherwise, the following assumptions were made for the representation of the electrode process (Section IV): 1) The porosity of the Type I film was constant with time. The porosity of the hydrate layer decreased until time TDIFF, afterwhich it remained constant. 2) The growth rate of the secondary crystals was proportional to their surface area (eq. 2a). 3) Type I film formation and the optical effect of the hydrate layer began at the same time (t_{NUC}) that secondary crystal growth began. 4) The optical effect of the secondary crystals was calculated using coherent superposition from distinct crystals (eq. 53) with the cubes being represented as homogeneous films. The surface coverage was determined from eq. 52, which uses the projection along the propagation direction. 5) The hydrate layer was treated as an asymptotically thick MTBL.

The number density of secondary crystals was determined from SEM photographs. The value used for the refractive index of bulk argentous oxide, 2.18 - 0.28 i, was determined from ellipsometer measurements on compressed analytical grade powder. The hydrate layer was assumed to be porous silver hydroxide; the bulk refractive index of 1.87 was calculated from the oxide using molar refractivities (Appendix F). Appendix G contains the computer output describing the interpretations.

Film Growth in 6M KOH Electrolyte

Stagnant Electrolyte, 1 mA/cm^2 (Exp. Ag 80-30)

Figures 23 and 24 show the interpretation of ellipsometer measurements of an anodic film containing a large number density ($4.7\times10^8/cm^2$) of secondary crystals. The average deviation between experimental and theoretical $\Delta - \psi$ points was 4.90 deg. Figure 24 presents the values of the parameters evaluated by the computational procedure. The measure of uncertainty corresponds to changes in parameter values which shift the average deviation 0.5 deg away from the minimum value of 4.90 deg; the experimental error as determined by the error analysis for the ellipsometer is 0.5 deg. The crystallization rate of the secondary crystals can be determined to within about 12%. The porosity of the Type I film and the hydration of the secondary crystals have experimental uncertainties of about ±0.05 volume fraction electrolyte. The time for the onset of secondary crystal growth has large uncertainty limits. Two factors contribute to this large uncertainty: 1) The crystals have to reach a finite size before they have an optical effect. a) The assumption that Type I film formation begins at the same moment as secondary crystal growth appears to be invalid, as will be discussed later.

The porosity of the hydrate layer of 0.999 is a consequence of the assumption that the hydrate layer reaches and maintains a minimum porosity; the hydrate layer appears to be depleted by later stages of film growth.

The left-hand portion of the curve in Figure 23, where the theoretical points lie to the left of the experimental points, is the region of major discrepancy. It is likely that this discrepancy is caused by non-stoichiometry of the Type I film, which begins precipitating at the point where the experimental and theoretical curves diverge. At this point, the electrode potential decreases from 0.38 to 0.33 volts. This non-stoichiometry is discussed further for the 0.2 mA/cm^2 experimental results presented below.

At the end of the curve of Figure 23 ((Δ,ψ) coordinates $(26°,15°)$) the thickness of the Type I film was 1400 Å and the size of the secondary crystals was 1200 Å. The calculated crystal sizes are generally smaller than the crystal dimensions measured from SEM photographs. The disagreement between secondary crystal sizes can be a result of the statistical variation in the size found on the (100) electrode. As the crystals are light absorbing, the larger crystals are opaque and give no contribution to the light intensity reaching the photodetector. Computations using statistical variations in the secondary crystal sizes did not reduce the average deviation between experiment and theory. This again is an indication that the deviation between experiment and theory results from properties of the primary layer not accounted for by the present analysis.

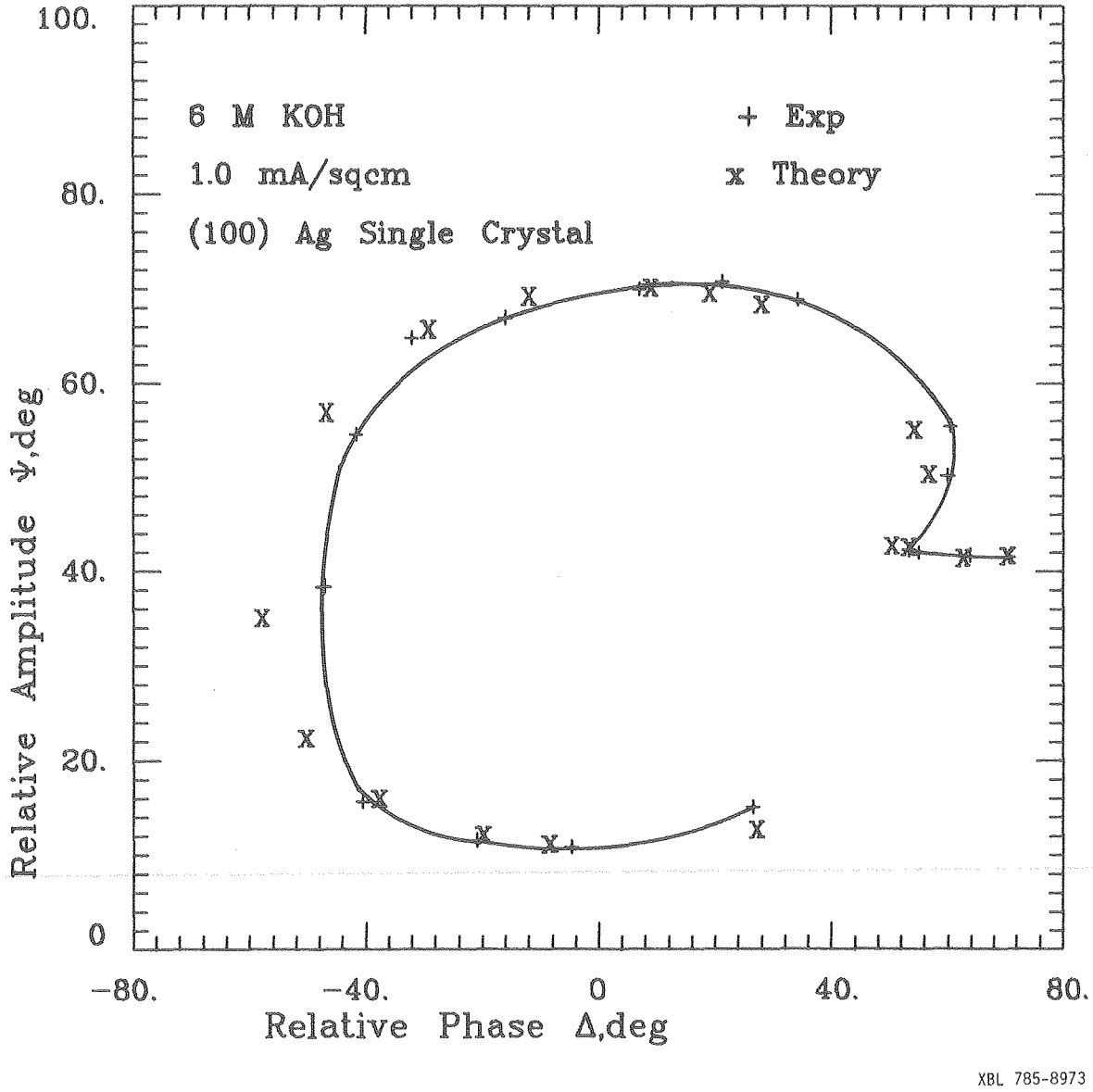

Figure 23. Interpretation of ellipsometer measurements (Exp. Ag 80-30).

Anodic Oxidation of Silver
Parameters Derived from Ellipsometer Interpretation
6 M KOH stagnant, 1 mA/cm^2, Ag(100)

Parameter	Value	Measure of Uncertainty†	
		Positive	Negative
Crystallization Rate of Type II Film	0.012 mA/cm^2	0.013	0.003
Crystallization Rate of Secondary Crystals	0.158 mA/cm^2	0.008	0.019
Porosity of Type I Film	0.260	0.046	0.073
Porosity of Hydrate Layer	0.999	>0.001	0.013
Dehydration of Hydrate Layer	1.00 mA/cm^2	>0.001	0.043
Onset of Secondary Crystal Growth	6.13 s	4.23	3.25
Hydration of Secondary Crystals	0.40	0.053	0.012
Time to reach steady state hydrate concentration	13.05 s	—	—

† Change in Parameter Value resulting in 0.5 deg. deviation.

Figure 24. Film parameters and their measure of uncertainty for the interpretation shown in Fig. 23 (Exp. Ag 80-30).

XBL 787-9522

Stagnant Electrolyte, 0.2 mA/cm^2 (Exp. Ag 80-32)

Figures 25, 26, and 27 show interpretations of an anodic film containing a small number density of secondary crystals.

For Figs. 25 and 26 a constant porosity was used for the Type I film. The secondary crystals were treated as homogeneous films in Figure 25 and the ray model (Appendix B) was used for the computations presented in Figure 26. Very poor agreement with experiment is obtained in both situations.

For the computations presented in Figure 27, the optical effect of the secondary crystals was neglected. The experimental data were interpreted in two stages, curves $\overline{AB}$ and curves $\overline{BC}$. Along curve $\overline{AB}$, the electrode potential is increasing to the value 0.29 V at point B. Beginning at point B(t = 100s), the electrode potential drops 40 mV over a 140s time interval.

The primary layer growing along curve $\overline{AB}$ was treated as an inhomogeneous film with the solid volume fraction decreasing parabolically from 0.874 (evaluated by the computational procedure) at the metal surface to 0.013, the solid fraction in the hydrate layer. Five films were used to describe the inhomogeneity. This optical treatment is consistent with a primary layer consisting of optically indistinct crystals. The thickness of this layer at point B is 30 Å.

The theoretical curve $\overline{BC}$ was obtained from the patchwise growth of a non-stoichiometric Type I film. The initial fraction of the surface covered by the patches was 0.36, and the time at which the surface coverage was complete, TDISS = 321s, corresponds very closely

to the experimental time of 300s at which the electrode potential reached a stable plateau of 0.26 V. The porosity of this film decreased from 0.73 to 0.60, and the refractive index of the hydrate layer decreased from 1.420 to 1.386 (the refractive index of the electrolyte) during the same compaction period. The refractive index of the solid non-stoichiometric film material determined by the computational procedure was 2.19-1.04 i; the refractive index of the final porous Type I film was 1.71-0.42 i.

Measures of uncertainty were not computed for the parameters evaluated by the computational procedure in order to keep the interpretation qualitative until verification of the non-stoichiometry by Auger spectroscopy (Appendix A) can be sought.

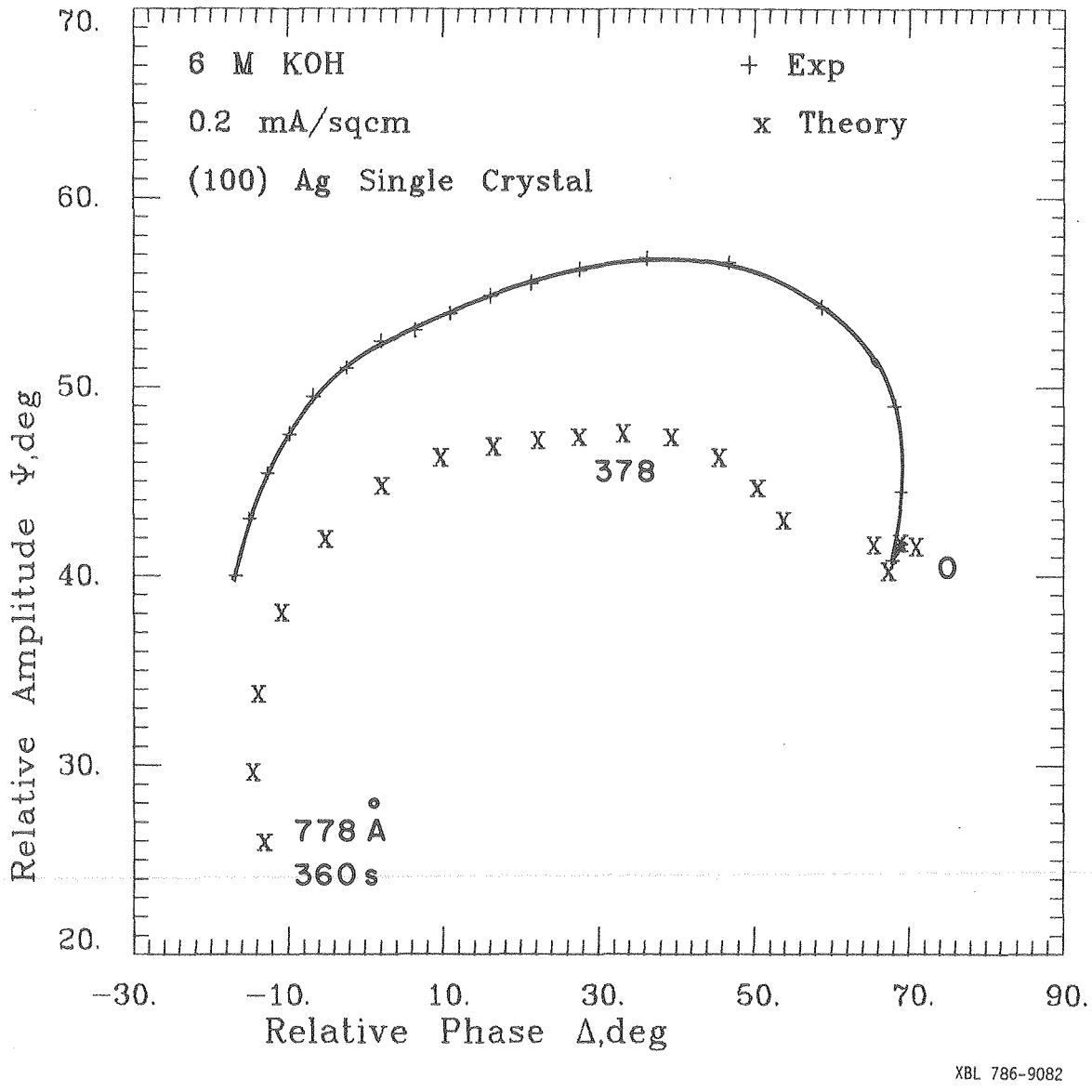

Figure 25. Interpretation of ellipsometer observations (Exp. Ag 80-32). Secondary crystals treated as homogeneous films.

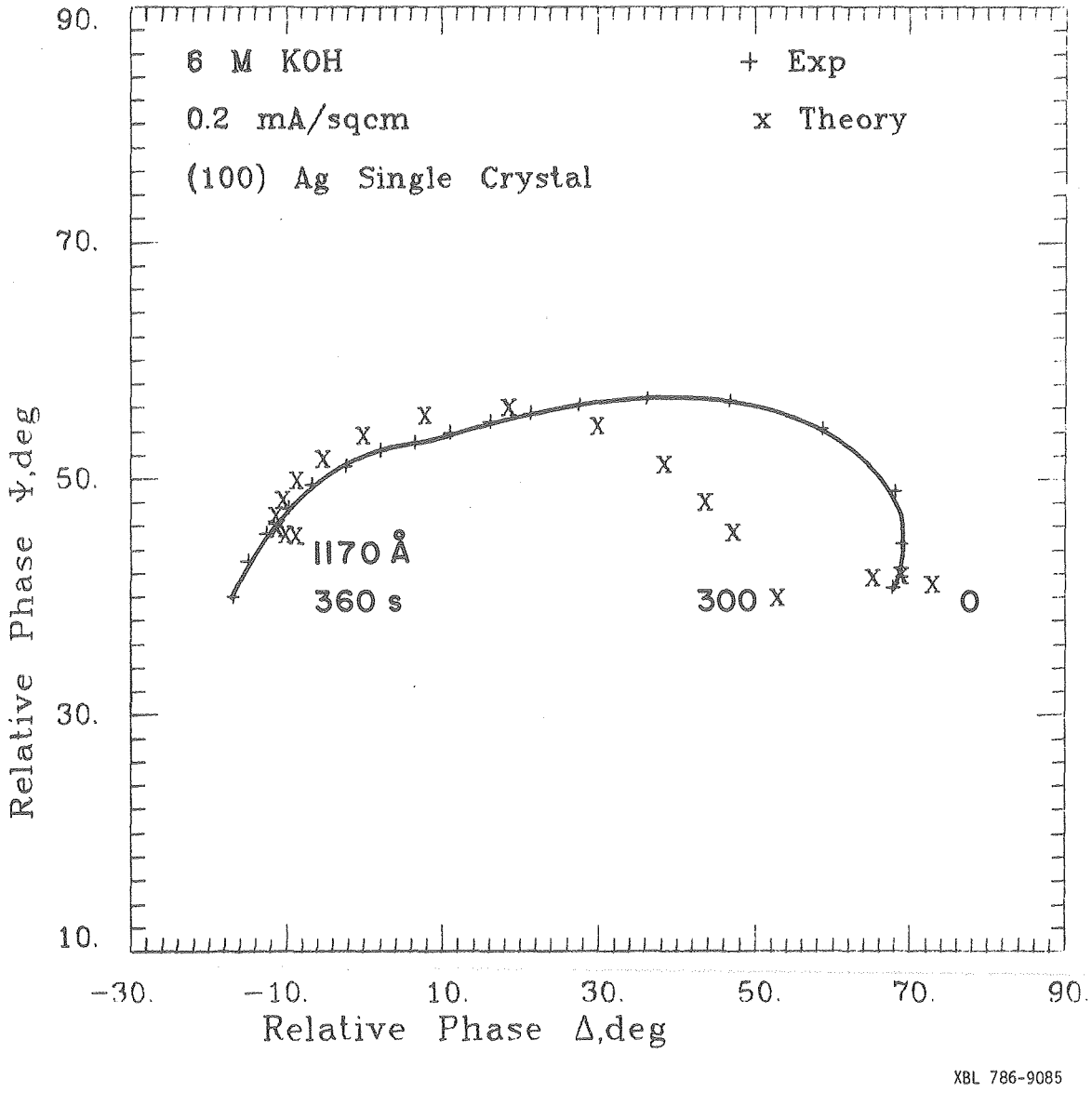

Figure 26. Interpretation of ellipsometer observations (Exp. Ag 80-32). Optical effect of secondary crystals computed using the ray model described in Appendix B.

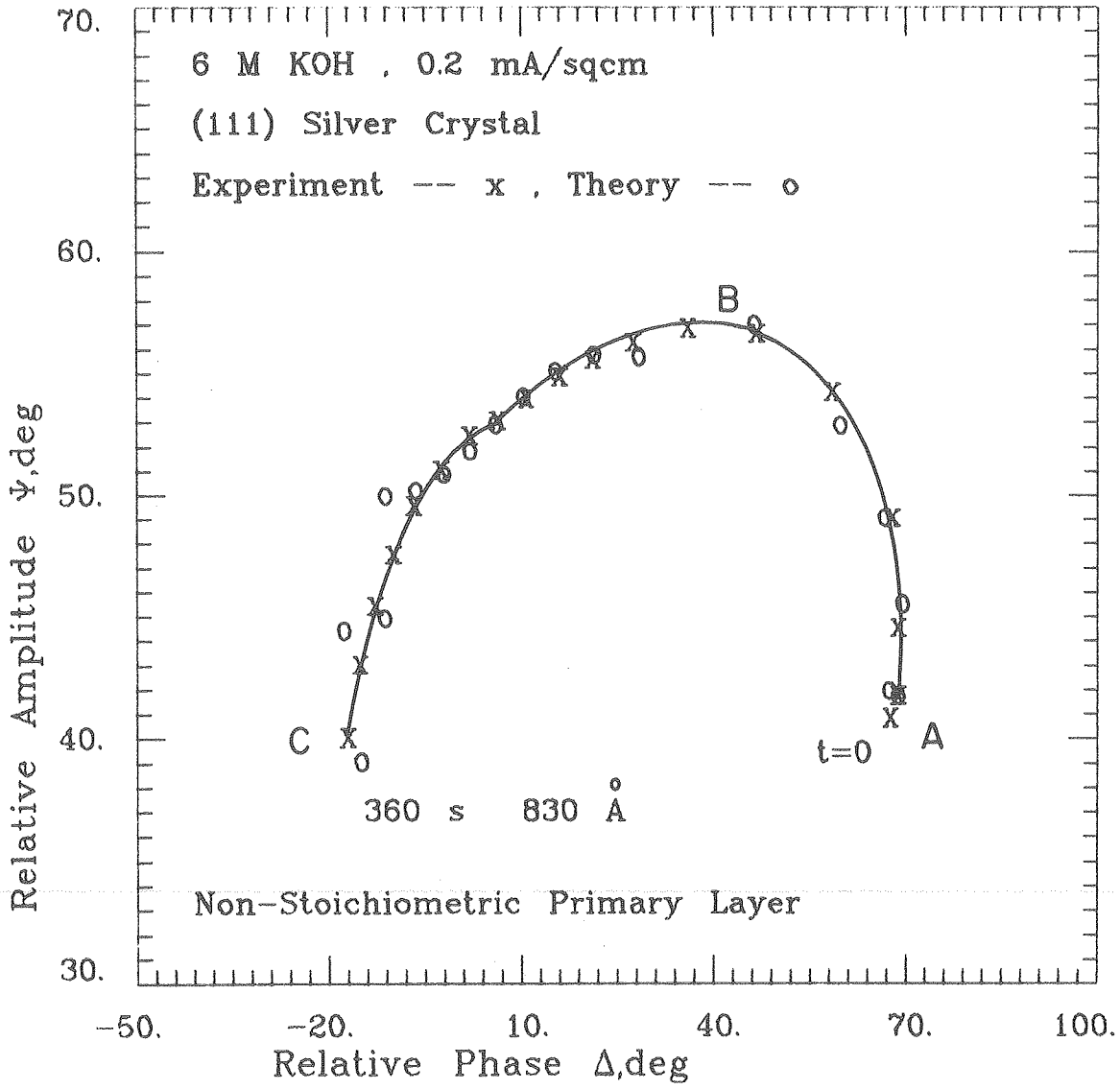

Figure 27. Interpretation of ellipsometer observations (Exp. Ag 80-32). The optical effect of secondary crystals has been neglected. At 360s, the primary layer is 830 Å thick. Micrograph of large secondary crystals shown in Fig. 20. Patchwise film formation.

1000 Re, 1.0 mA/cm^2 (Exp. Ag 300-16)

The interpretation of ellipsometer observations of the growth of an anodic film with flowing electrolyte is given in Figure 28 and Table III. The major change in the growth characteristics of the film is that a steady state condition is reached and the film stops growing for a significant period of time. This steady state condition was reached at 32 sec. for the experiment presented in Fig. 28. At this point the primary layer was 700 Å thick, and no indication of non-stoichiometry was observed. Under laminar flow, film growth at a much reduced rate will usually begin after as long as a 30 second arrest, while under turbulent flow the steady state condition may continue indefinitely.

The average deviation between experimental and theoretical points was 1.25 deg. The parameter values determined from the computational procedure and their measures of uncertainty are presented in Table III. The porosity of the primary layer and the hydration of the secondary crystals agree very well with the values computed for the stagnant electrolyte experiment (Ag 80-30). The porosity of the hydrate layer is significantly smaller for the forced convection experiment, and the crystallization rate of the secondary crystals is correspondingly higher.

The nomenclature for the primary layers should perhaps be modified at this point. The primary layer showing no signs of non-stoichiometry, which continues to grow after the onset of secondary crystals, will still be called a Type II film, while the non-stoichiometric primary layer which beings growing when the electrode potential drops will be called

a Type I film. The primary layer computed for Fig. 28 is stoichiometric, and the electrode potential has reached a stable plateau (at 0.29 V) with no subsequent decrease in potential. It is possible, however that the large number density of secondary crystals is concealing the non-stoichiometry of the primary layer.

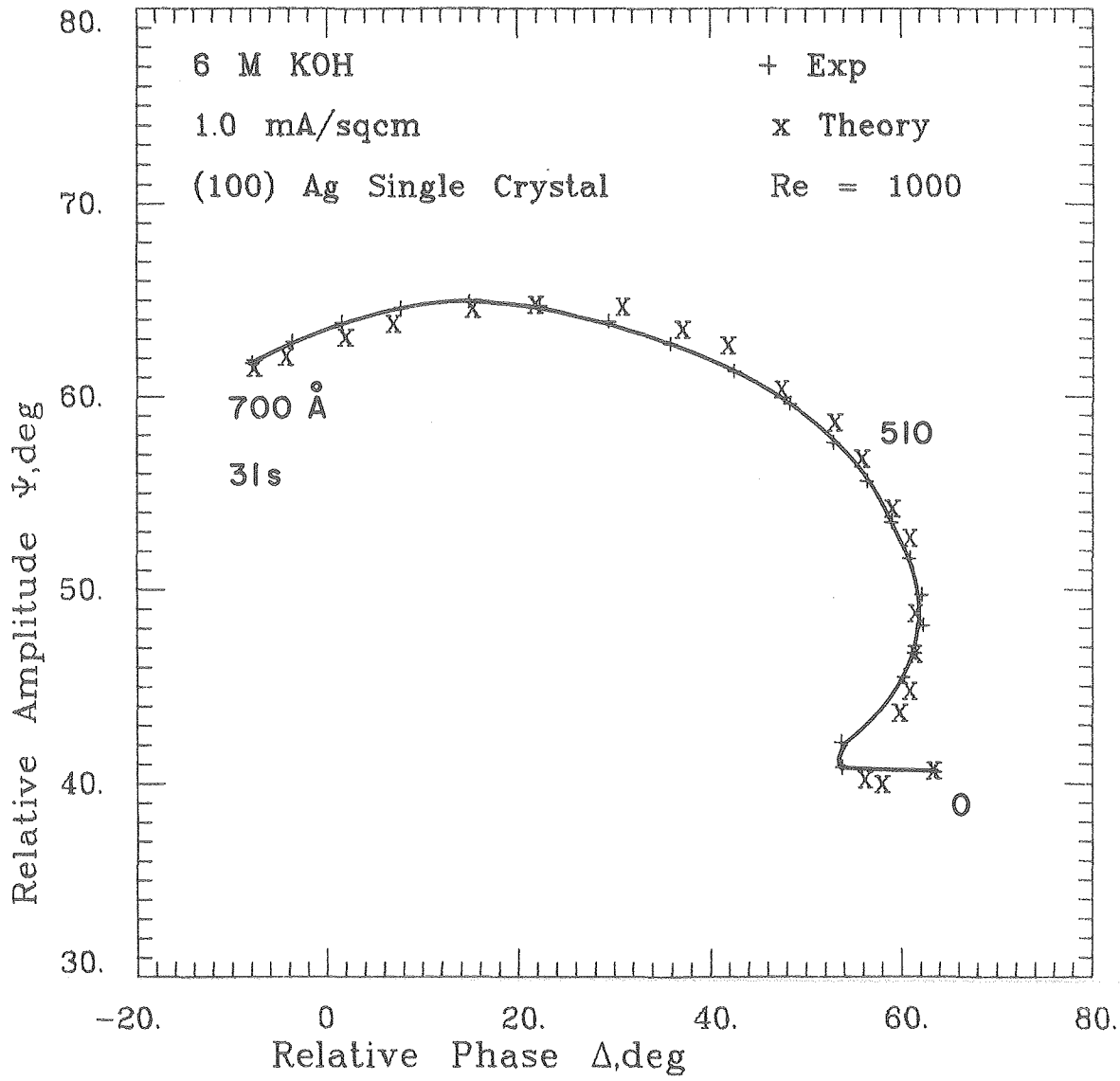

Figure 28. Interpretation of ellipsometer observations (Exp. Ag 300-16). Primary layer thickness indicated along the curve, forced convection.

Table III. Anodic Oxidation of Silver Parameters Derived from Ellipsometer Interpretation 6M KOH, Re = 1000, 1 mA/cm^2, Ag(100).

Parameter	Value	Measure of Uncertainty†	
		Positive	Negative
Crystallization Rate of Type II Film	0.056 mA/cm^2	0.015	0.012
Crystallization Rate of Secondary Crystals	0.328 mA/cm^2	0.011	0.047
Porosity of Type II Film	0.247	0.034	0.069
Porosity of Hydrate Layer	0.913	0.015	0.022
Dehydration of Hydrate Layer	0.933 mA/cm^2	>0.012	0.067
Onset of Secondary Crystal Growth	5.63s	2.87	3.10
Hydration of Secondary Crystals	0.41	0.021	0.052
Time to reach steady state hydrate concentration	18.53s	4.48	8.43

†Change in parameter value resulting in 0.5 deg deviation.

10500 Re, 1.0 mA/cm^2 (Exp. Ag 300-2)

The transport of solution-phase species downstream by flowing electrolyte leads to variations in film properties along the flow direction. The theoretical curve in Figure 29 only qualitatively reproduces the experimental values of Δ and ψ. Figure 30 illustrates that the thickness of the primary layer and the number density of secondary crystals both increase in the downstream direction.

Of the non-uniformities in secondary crystal growth described in Section IV, only the statistical variation in the time of the onset of secondary crystals improves the agreement between experiment and theory for forced convection experiments. This formalism does allow for variations in the thickness of the primary layer, which has been assumed to begin growth simultaneously with the crystals.

Removal of this last assumption should lead to a more accurate interpretation of Exp. Ag 300-2 (Fig. 29). Table IV shows the rather modest improvements resulting from the use of statistical variations in TNUC.

Table IV. Statistical Variation in the Onset of Secondary Crystals Growth.

Experiment	Re	i(mA/cm^2)	Ag	Ave. Deviation between Experiment and Theory	
				Statistics	No Statistics
Ag 300-3	10500	0.6	(100)	2.88 deg	4.47 deg
Ag 300-6	4600	0.6	(111)	7.54	8.18
Ag 300-7	4600	0.6	(100)	4.12	5.86

The remaining discrepancies between experiment and theory could result from non-stoichiometry of the primary layer and different times for the onset of secondary crystal and Type I primary layer growth. It is instructive that the use of statistical variations in t_{NUC} does not lead to improved interpretations for stagnant electrolyte experiments.

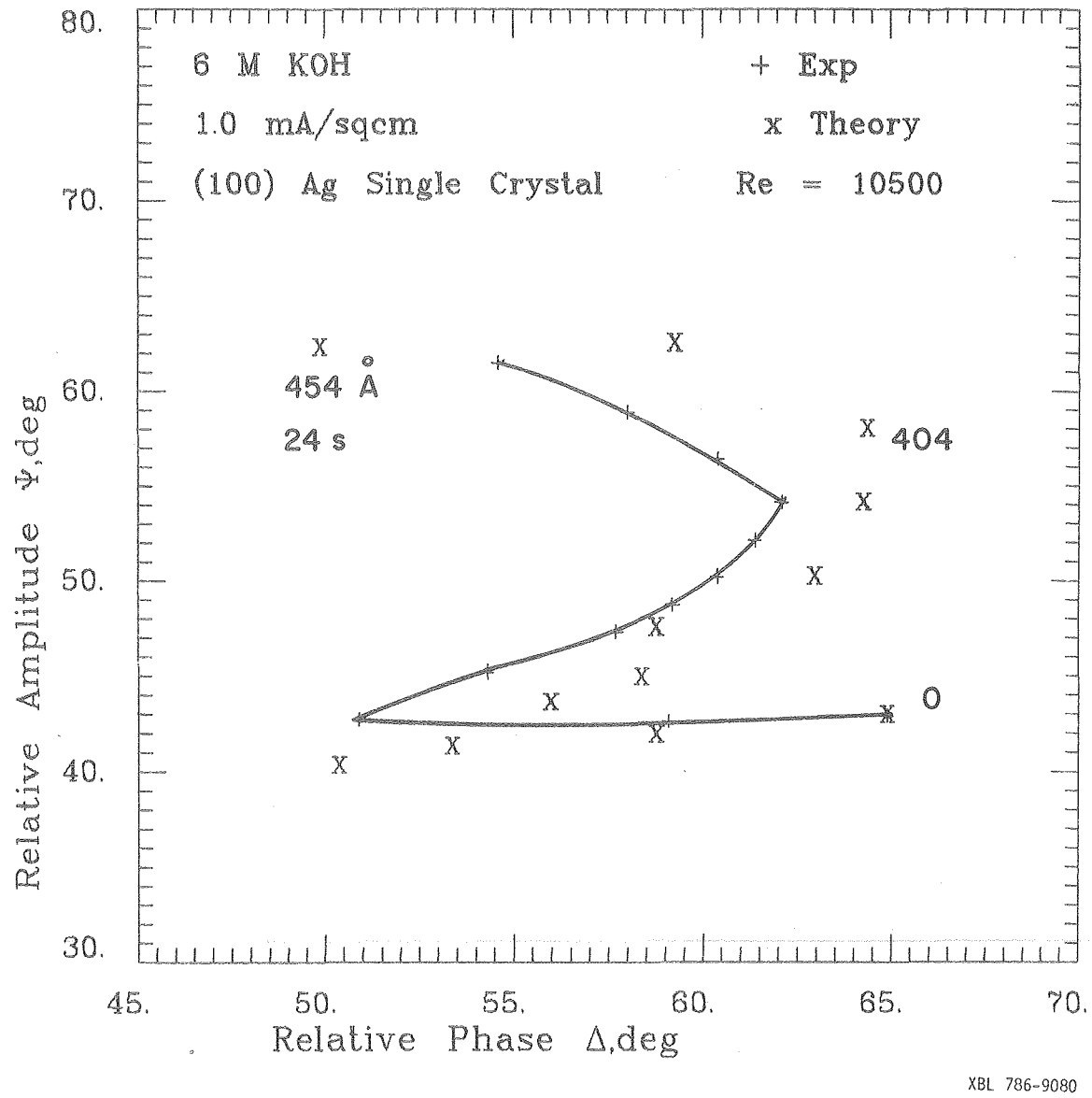

Figure 29. Interpretation of ellipsometer observations (Exp. Ag 300-2). Primary layer thickness indicated along the computed points. Variation with distance from leading edge of film properties not considered.

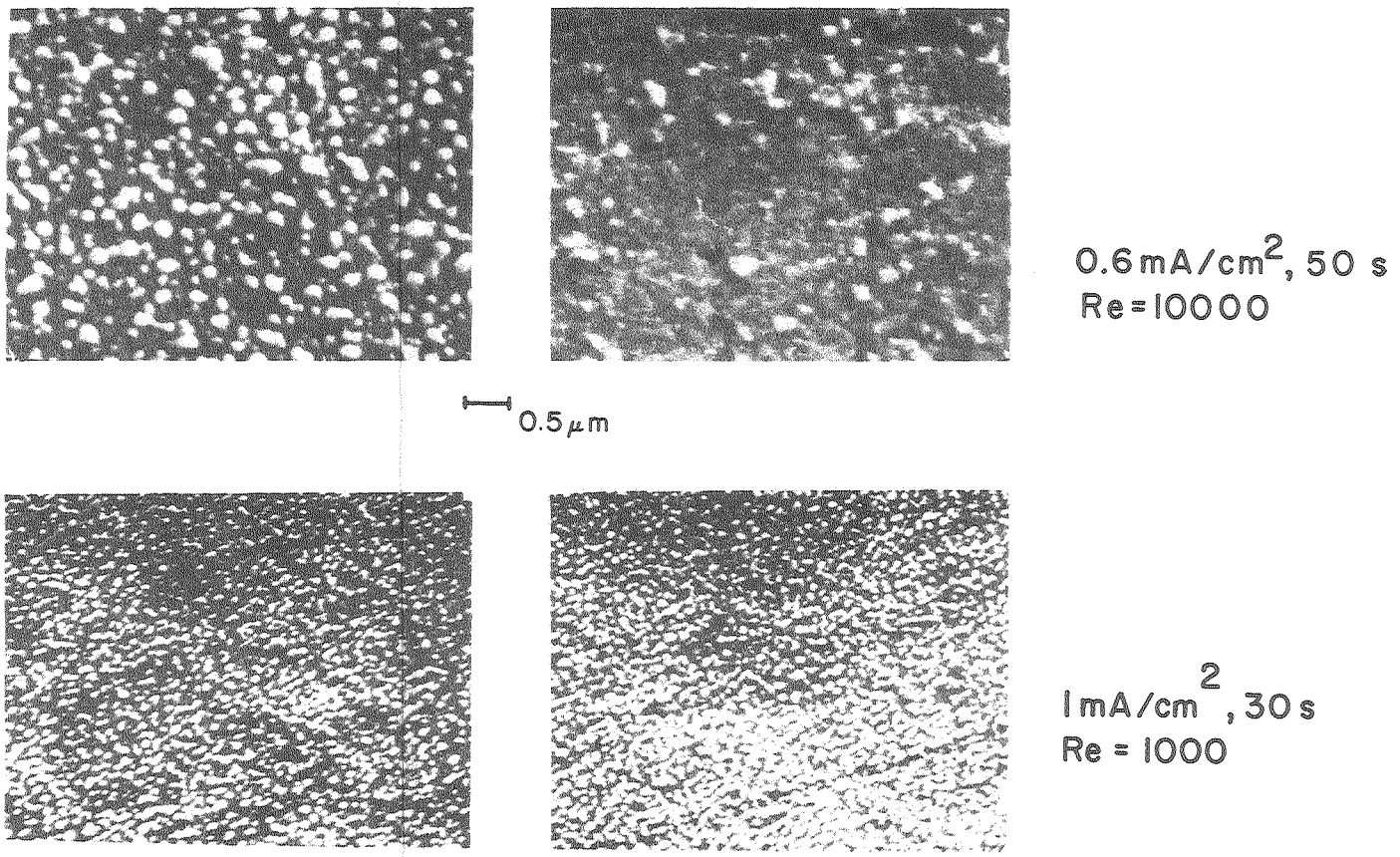

Figure 30. Scanning electron micrographs of argentous oxide, effect of distance from leading edge.

Film Growth in 0.1 M KOH Electrolyte

Stagnant Electrolyte, 0.2 mA/cm^2 (Exp. Ag 80-18)

The current densities at which the electrode passivates in 0.1 M KOH are approximately 10 times smaller than the current densities in 6 M KOH. This is a consequence of the decreased solubility of the silver ion in 0.1 M KOH. Figure 31 shows the experimental curve characteristic of large number densities of secondary crystals (Fig. 21). The major disagreement between experiment and theory is in the initial portion of the curve, where the experimental points are to the right of the theoretical points. The use of a porosity of the hydrate layer which increases with time, which describes depletion of the layer, would decrease the disagreement. The 1400 Å thick primary layer was taken to be stoichiometric.

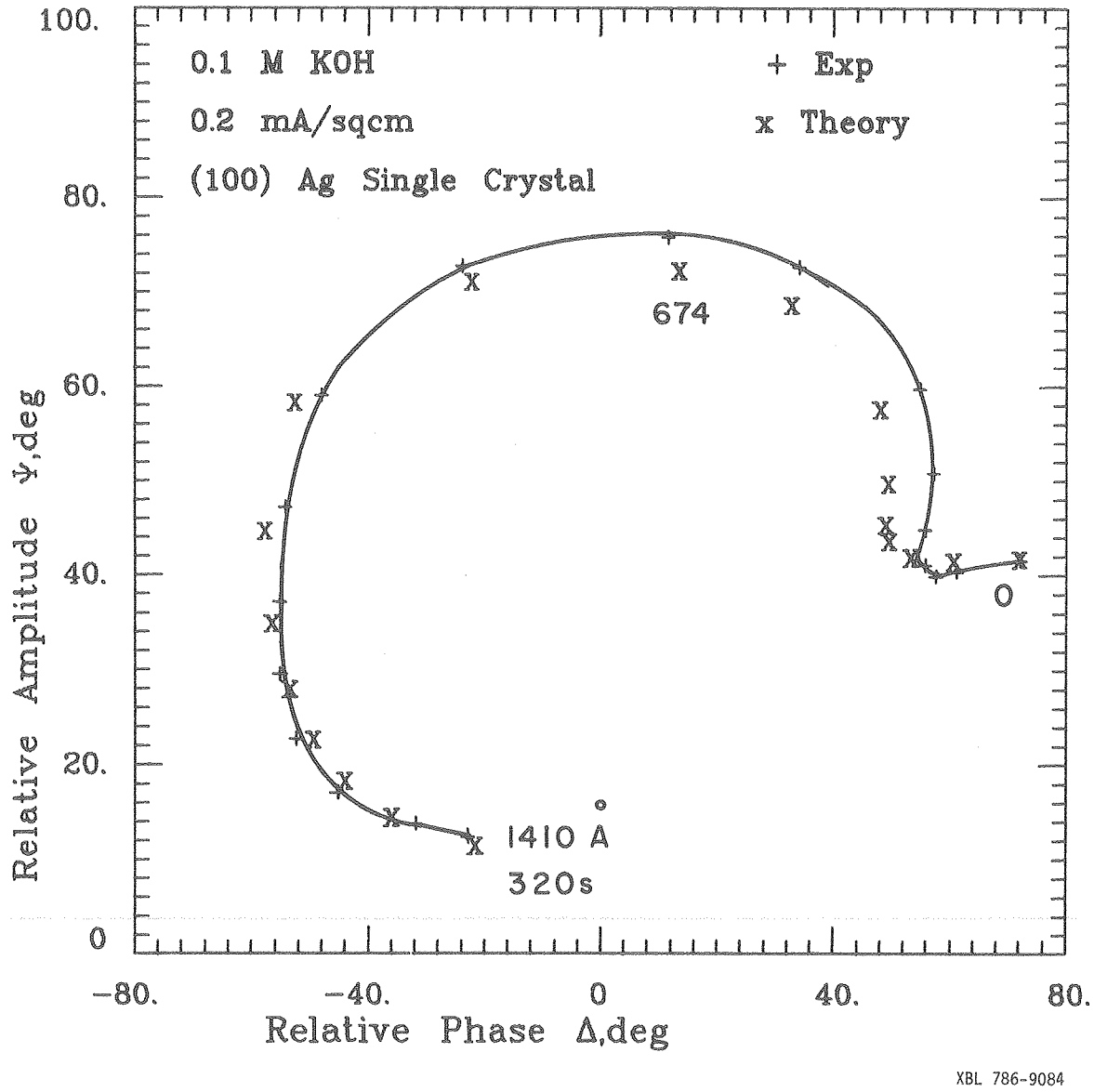

Figure 31. Interpretation of ellipsometer measurements (Exp. Ag 80-18). Primary layer thickness indicated along the curve, small secondary crystals (Fig. 21).

Film Growth in 1 M KOH Electrolyte

The solubility of silver ion in 1 M KOH is intermediate to the solubilities in 0.1 M and 6 M KOH. The optical properties of the anodic films again show a very strong dependence on the degree of supersaturation of the solution-phase species: larger current densities yield a larger number density of secondary crystals. There does appear to be a decrease in the degree of the non-stoichiometry of the primary layer which indicates a dependence on the hydroxyl ion concentration. The electrode potential also does not pass through a maximum, which correlated well with the presence of the non-stoichiometric film in 6 M KOH.

Stagnant Electrolyte, 0.4 mA/cm^2 (Exp. Ag 80-4)

Figure 32 shows the comparison between experimental and calculated points. The primary layer (Type I Film) was compact, and reached a thickness of 580 Å after 70s. Experimental curves for comparable number densities of secondary crystals in 6 M KOH were diverging more towards the right at the last point of Figure 32.

Stagnant Electrolyte, 0.2 mA/cm^2 (Exp. Ag 80-3)

For the results presented in Figure 33, the major deviation between experiment and theory is along the right-hand portion of the curve. An increasing porosity with time of the hydrate layer would decrease this disagreement.

Stagnant Electrolyte, 0.34 volts vs Hg/HgO (Exp. Ag 80-12)

The constant potential experiment shown in Figure 34 certainly indicates that the properties of the primary layer change with time. For the interpretation, a time-invariant porosity of 0.25 as evaluated by the computational procedure gives very poor agreement along the left-hand portion of the curve. The deviation of the theoretical curves is analogous to the effects produced by non-stoichiometry in the 6 M KOH electrolyte. As the potential of 0.34 volts will result in very large supersaturations of the silver ion (assuming charge-transfer overpotential is negligible), this is evidence that the production of the non-stoichiometric film is proportional to the silver ion concentration.

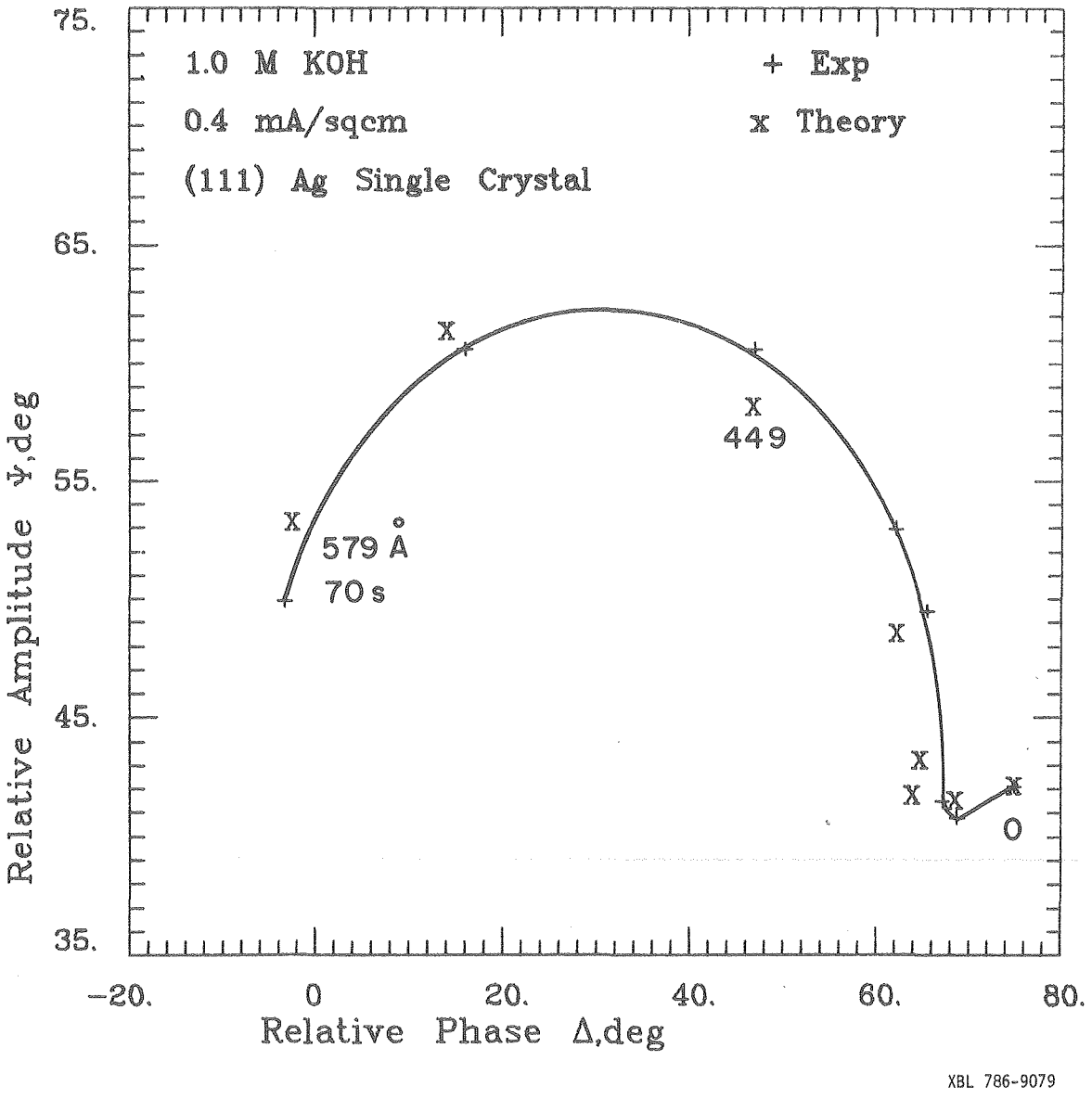

Figure 32. Interpretation of ellipsometer measurements (Exp. Ag 80-4). Primary layer thickness indicated along the curve.

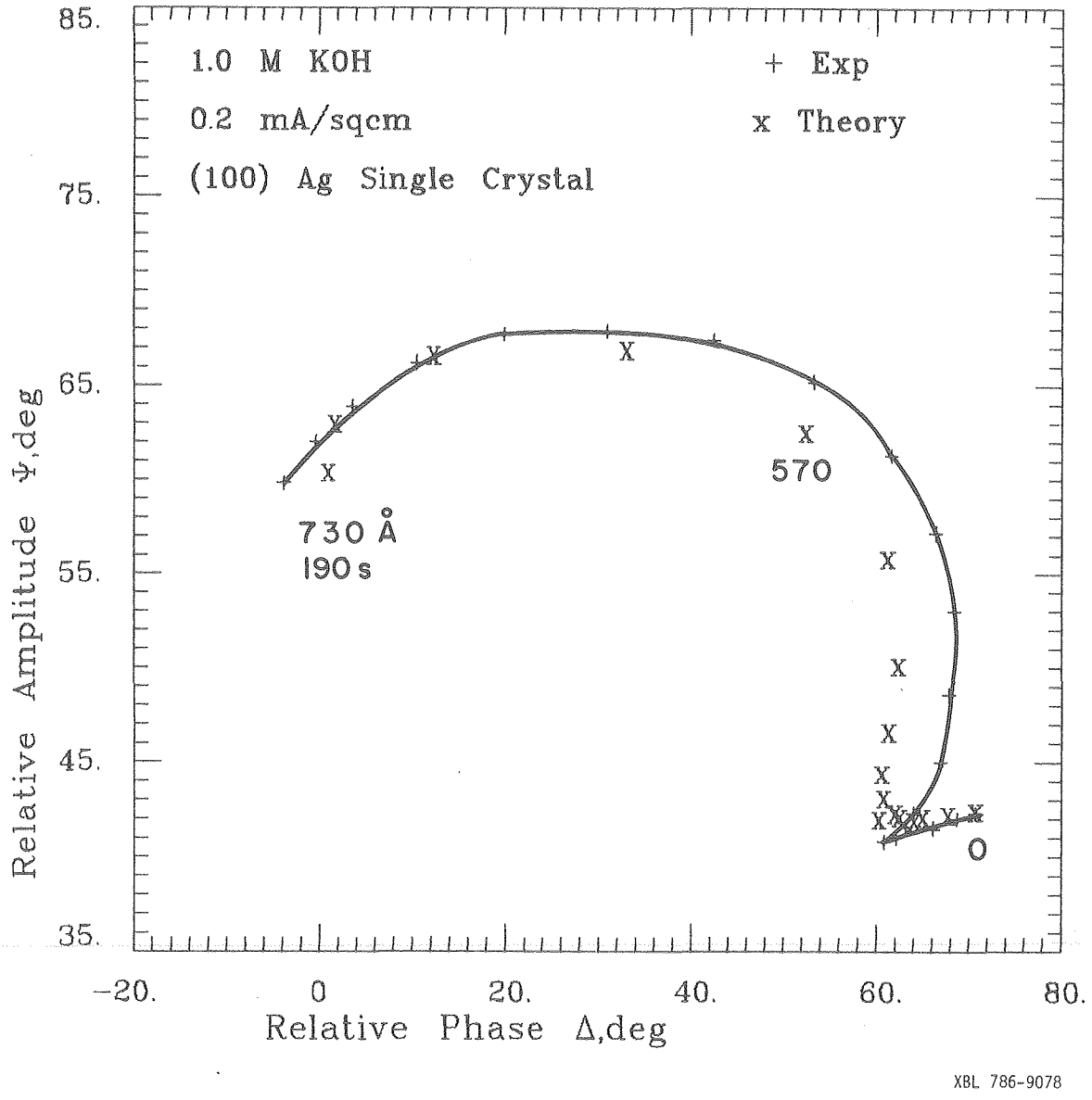

Figure 33. Interpretation of ellipsometer measurements (Exp. Ag 80-3). Primary layer thickness indicated along the curve.

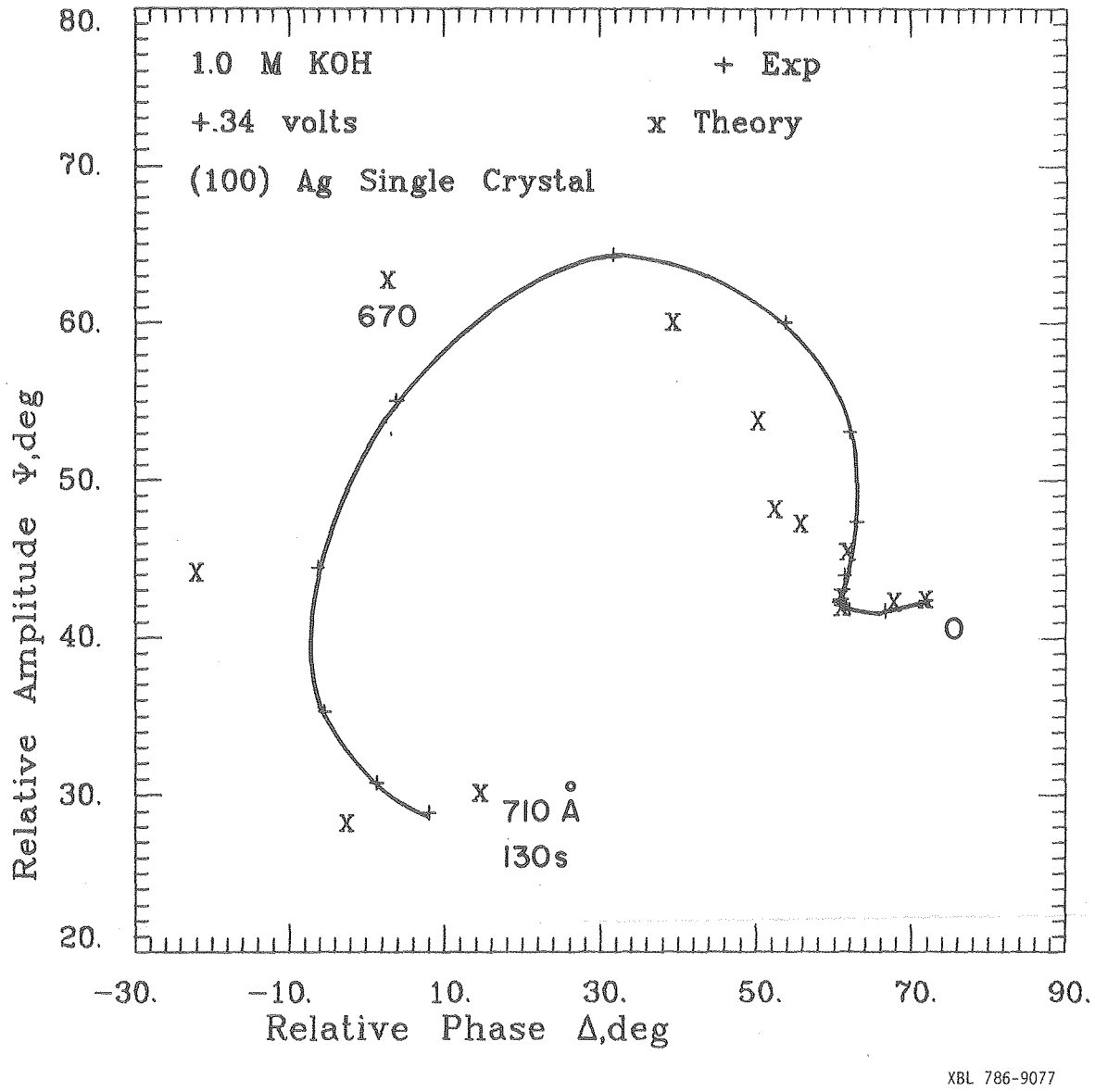

Figure 34. Interpretation of ellipsometer measurements (Exp. Ag 80-12). Primary layer thickness indicated along the curve, constant potential.

Stagnant Electrolyte, 0.55 volts vs Hg/HgO (Exp. Ag 80-13)

The potential of 0.55 volts lies above the plateau assigned to AgO formation (0.49 volts). However, the interpretation presented in Fig. 35 modeled the film growth as the formation of argentous oxide. The current density decreases along the horizontal portion of the curve from 20 to 10 mA/cm^2 and then increases to 15 mA/cm^2 at 21.5s.

The currents to the Faraday cells of the automatic ellipsometer were at maximums at the last point of Figure 35. New power supplies are under construction which will extend the range of the instrument and allow ellipsometer observations over a longer experimental period.

Comparison of Primary Layer Porosity and Conductivity

It was noted above that under forced convection, a steady state situation is reached in which anodic film formation stops. At steady state, the degree of supersaturation of ionic species can be calculated from the electrode current density and the mass-transfer rate corresponding to the transport conditions. Assuming that charge transfer overpotential is negligible, the steady-state electrode potential will be composed of concentration polarization and resistence polarization. Use of the degree of supersaturation of ionic species allows computation of the resistence polarization, from which conductivities of the primary layer can be obtained.

Table V presents a comparison of the primary layer porosities determined from ellipsometer measurements and film conductivities computed at the steady state, no film growth conditions. The surface

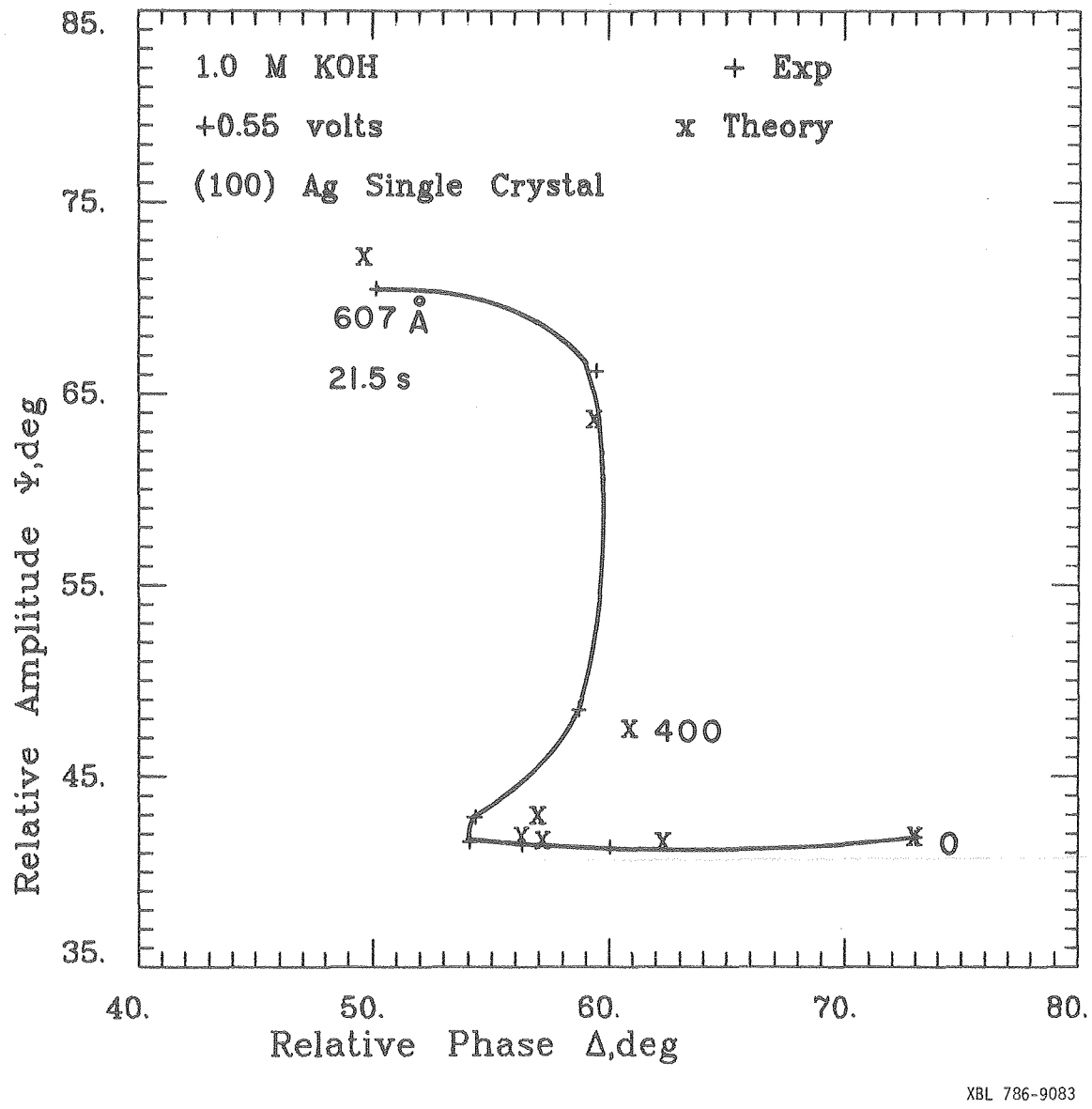

Figure 35. Interpretation of ellipsometer measurements (Exp. Ag 80-13). Primary layer thickness indicated along the curve. Constant potential, high initial current density.

Table V. Comparison of Primary Layer Porosity and Conductivity.

	Ag 300-16	Ag 300-13	Ag 300-7	Ag 300-6	Ag 300-5	Ag 300-3	Ag 300-2
i, mA/cm^2	1.0	1.0	0.6	0.6	0.6	0.6	1.0
Re	1000	1000	4600	4600	4600	10000	10000
Ag	(100)	(100)	(111)	(100)	(111)	(100)	(100)
Surface Area Correction	1.41	1.16	1.98	2.18	1.49	1.49	1.06
Ionic Supersaturation	13.5	16.5	2.75	2.51	3.66	2.17	5.10
Concentration Overpotential (mV)	67	72	26	24	33	20	42
Resistence Polarization (mV)	3	8	54	56	57	60	78
Primary Layer Thickness (Å)	700	616	680	484	622	605	454
Porosity of Primary Layer	0.24	0.20	0.02	0.01	0.02	0.02	0.02
Conductivity $\Omega^{-1}cm^{-1}\times10^7$	250	81	13.4	11.0	8.4	7.9	6.0

area correction in the fourth row is the ratio of the secondary crystals and primary layer surface areas to the superficial electrode area. The concentration overpotential has been computed using the Nernst equation (eq. 18) and the degree of supersaturation of monovalent argentous ions. The resistence polarization is the difference between the experimental electrode overpotential (a rest potential of 0.22 vs Hg/HgO volts was used) and the concentration overpotential. The film conductivities were calculated using the ellipsometrically determined film thicknesses and by assuming the transport of charge occurs only across the portion of the electrode surface not covered by the secondary crystals.

The first column of Table V supports the assumption that charge-transfer overpotential is negligible, as the concentration overpotential is within the 10 mV experimental error of the total electrode overpotential. The seventh and ninth rows indicate that ellipsometer measurements show compact primary layers only when significant resistence polarizations are observed. As the porosity of the primary layer has been determined to within only approximately 0.05 volume fraction electrolyte, it is not possible to differentiate quantitatively between solid state and solution phase charge transport mechanisms for the compact primary layers. However, it is apparent that when porous primary layers are present, the transport mechanism is the solution-phase diffusion of argentous ions. For the computation of the concentration overpotential in Table V, the following values were used: $D = 1.14\times10^{-5}$ cm^2/s, $\nu = 0.015$ cm^2/s , and the solubility of argentous ion, $C_s = 4.7\times10^{-4}$ M .

D. Cadmium Hydroxide Formation

Qualitative Aspects

The physical and optical properties of anodic cadmium hydroxide films are strongly affected by the initial state of the electrode surface. The base metal cadmium corrodes in alkaline solution, as significant changes in Δ and ψ occur when no current is being passed. The corrosion rate is greatly enhanced by the presence of dissolved oxygen. The degassing chamber was designed to treat the 2 liters of electrolyte used with the stagnant cell and seemed inadequate to treat the 20 liters of electrolyte used in the flow system. As a result, increasing the flow rate of the electrolyte, which would increase the transport rate of dissolved oxygen to the electrode surface, increases the corrosion rate. The growth rate of anodic films also varies significantly for different electrodes of the same crystallographic orientation. An air-formed oxide is possibly responsible for these latter variations in anodic film growth characteristics.

The most striking feature of scanning electron micrographs of anodic films formed on cadmium is the non-uniformity of the film. This patchwise film formation is illustrated in Figures 36, 37 and 38. A competition between nucleation and crystallization occurs on a local level, leading to islands with large number densities of secondary crystals. The patchwise film formation is probably a consequence of the initial state of the electrode surface generated by corrosion processes.

The growth characteristics of the cadmium hydroxide secondary crystals are similar to these of silver oxide. Increasing the

supersaturation of the solution-phase dissolution product increases the number density of secondary crystals. Larger number densities are associated with larger current densities (Fig. 39), less concentrated alkaline solutions (comparison of Figs. 36 and 37), and lower flow rates (Fig. 40). Experiments were performed only on (0001) single crystal electrodes.

The properties of the anodic films vary significantly along the flow direction for forced convection experiments, as shown in Figure 41. Transport of material downstream leads to larger number densities of secondary crystals and a thicker film away from the leading edge of the electrode. The film downstream is also darker, both to the eye and to the SEM.

Quantitative Interpretations

For the following interpretations of ellipsometer measurements made during the growth of anodic cadmium hydroxide films, the patchwise film formation described in Sec. IV (p. 59) was used. The electrode surface at the moment at which the anodic current was initiated was covered by patches of cadmium hydroxide. The refractive index of cadmium hydroxide used for the computational procedure, 2.13, was computed from the refractive index of cadmium oxide. The cadmium oxide refractive index, 2.51, was determined from ellipsometer measurements on compressed powders (Appendix F).

Figure 42 shows the changes in the ellipsometer parameters Δ and ψ resulting from the anodic film growth of cadmium hydroxide.

The computed curve for the compact hydroxide is shown for comparison. The latter part of the curve shows a periodic behavior (with respect to film thickness) in Δ and ψ. In this region, the secondary crystals appear to be optically dominant. The interpretations presented below exclude this region of the curve in order to emphasize primary layer film growth characteristics.

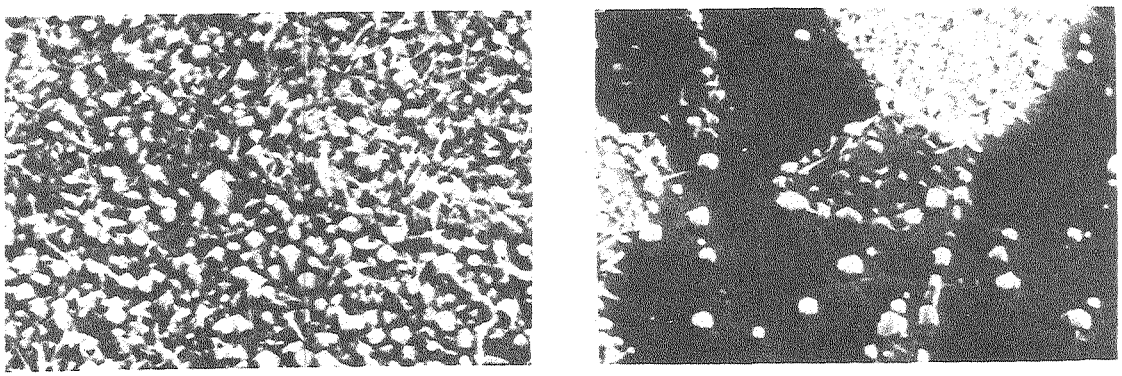

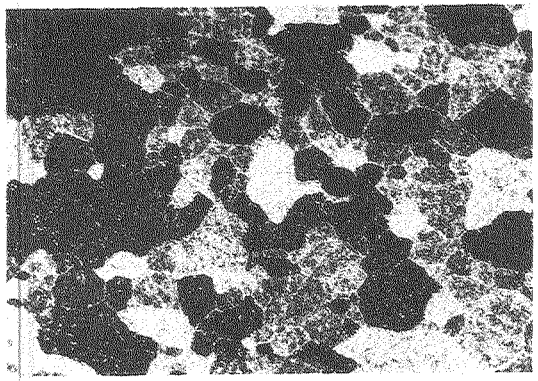

ANODIC CADMIUM HYDROXIDE

1 M KOH, stagnant, (0001) Cd
0.1 mA/cm^2, 150 s

XBB 786-7633

Figure 36. Scanning electron micrographs of anodic cadmium hydroxide. Magnification of bottom picture is 10 times smaller than the magnification of the top pictures, for which the scale applies.

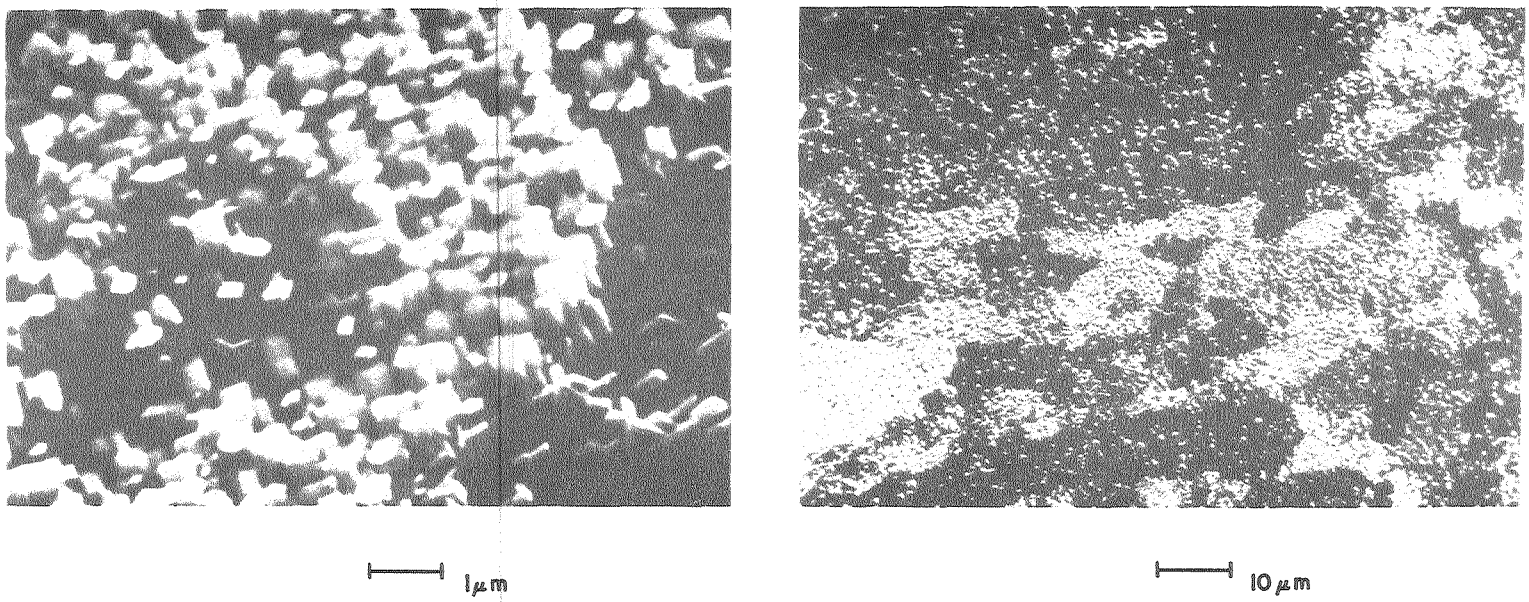

XBB 786-7627

Figure 37. Scanning electron micrographs of anodic cadmium hydroxide.

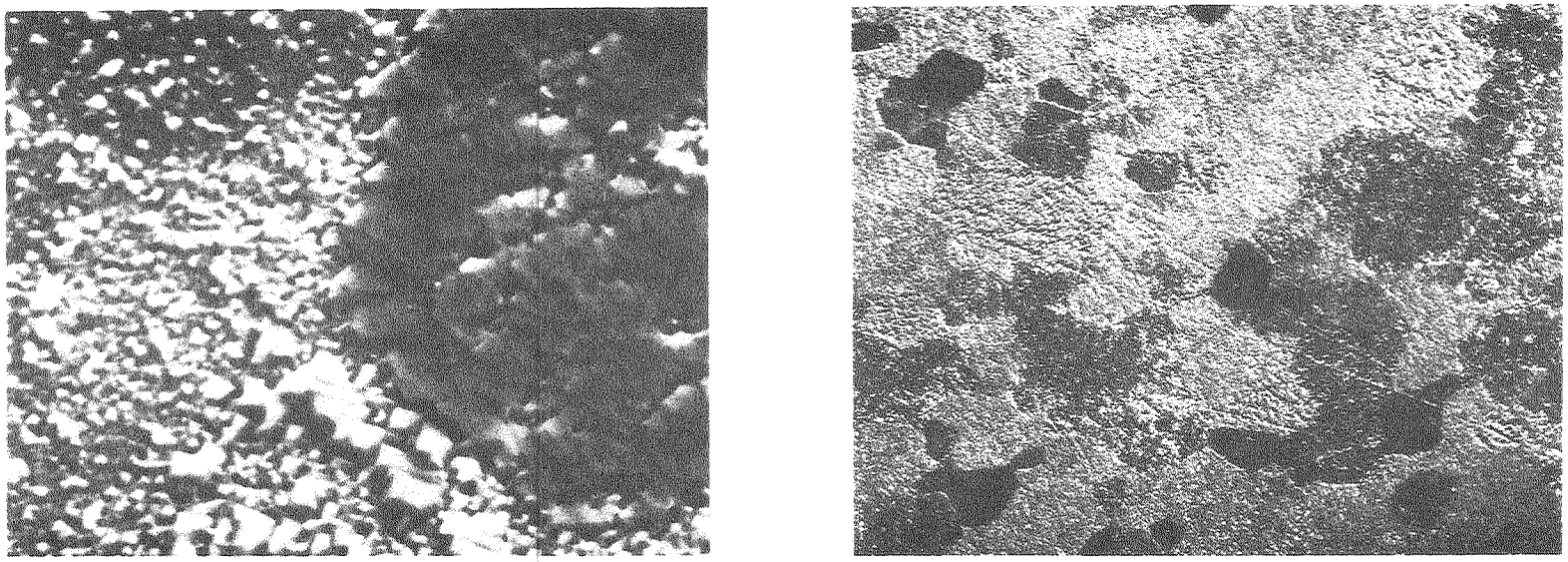

Figure 38. Scanning electron micrographs of anodic cadmium hydroxide.

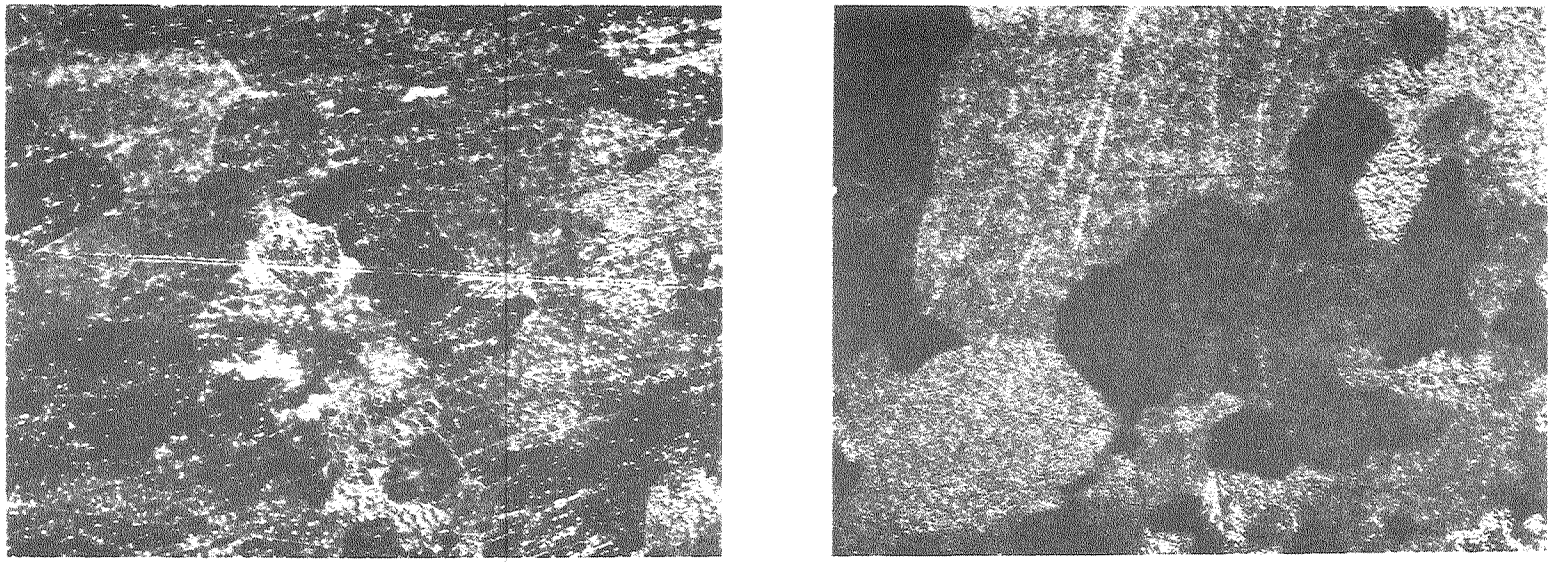

XBB 786-7620

Figure 39. Scanning electron micrographs of anodic cadmium hydroxide.

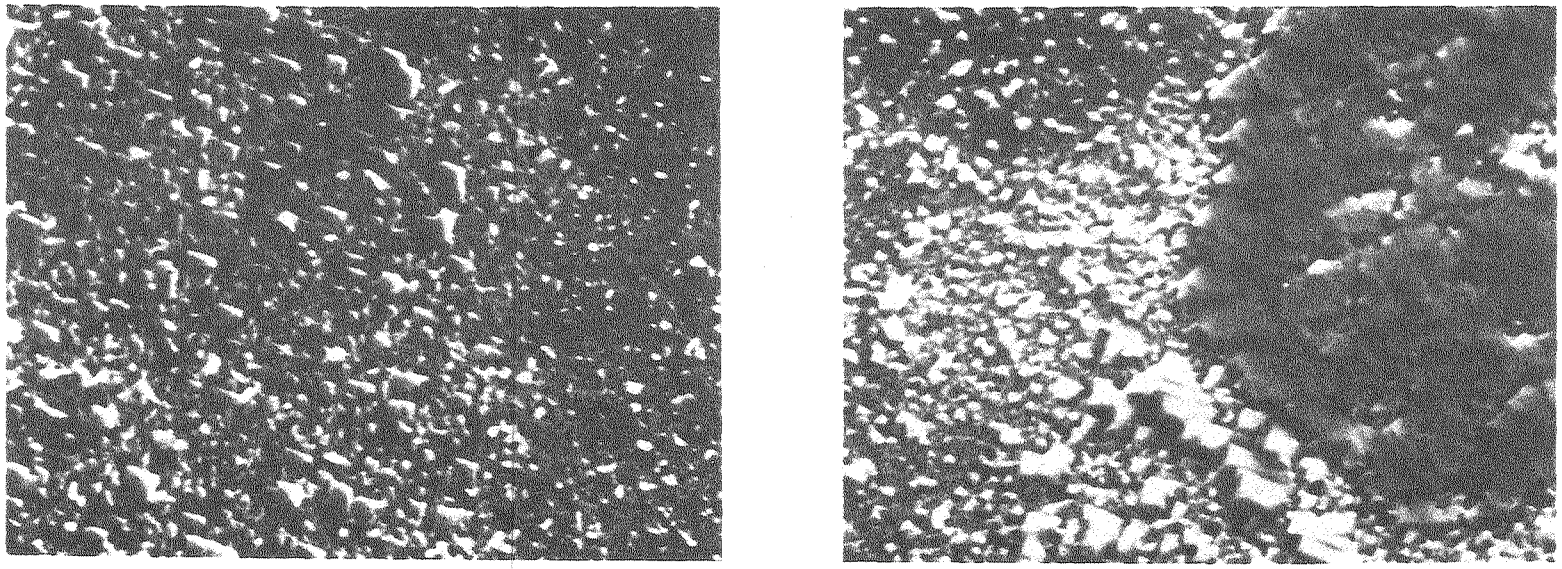

XBB 786-7621

Figure 40. Scanning electron micrographs of anodic cadmium hydroxide.

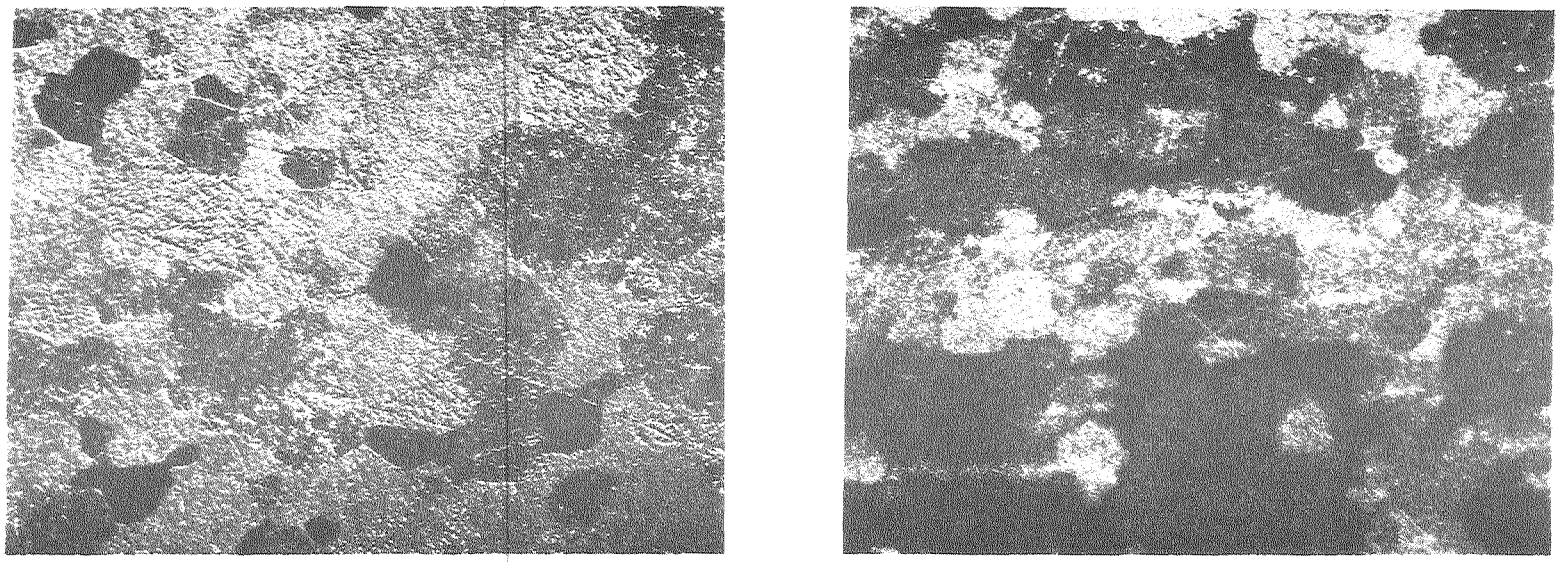

XBB 786-7623

Figure 41. Scanning electron micrographs of anodic cadmium hydroxide.

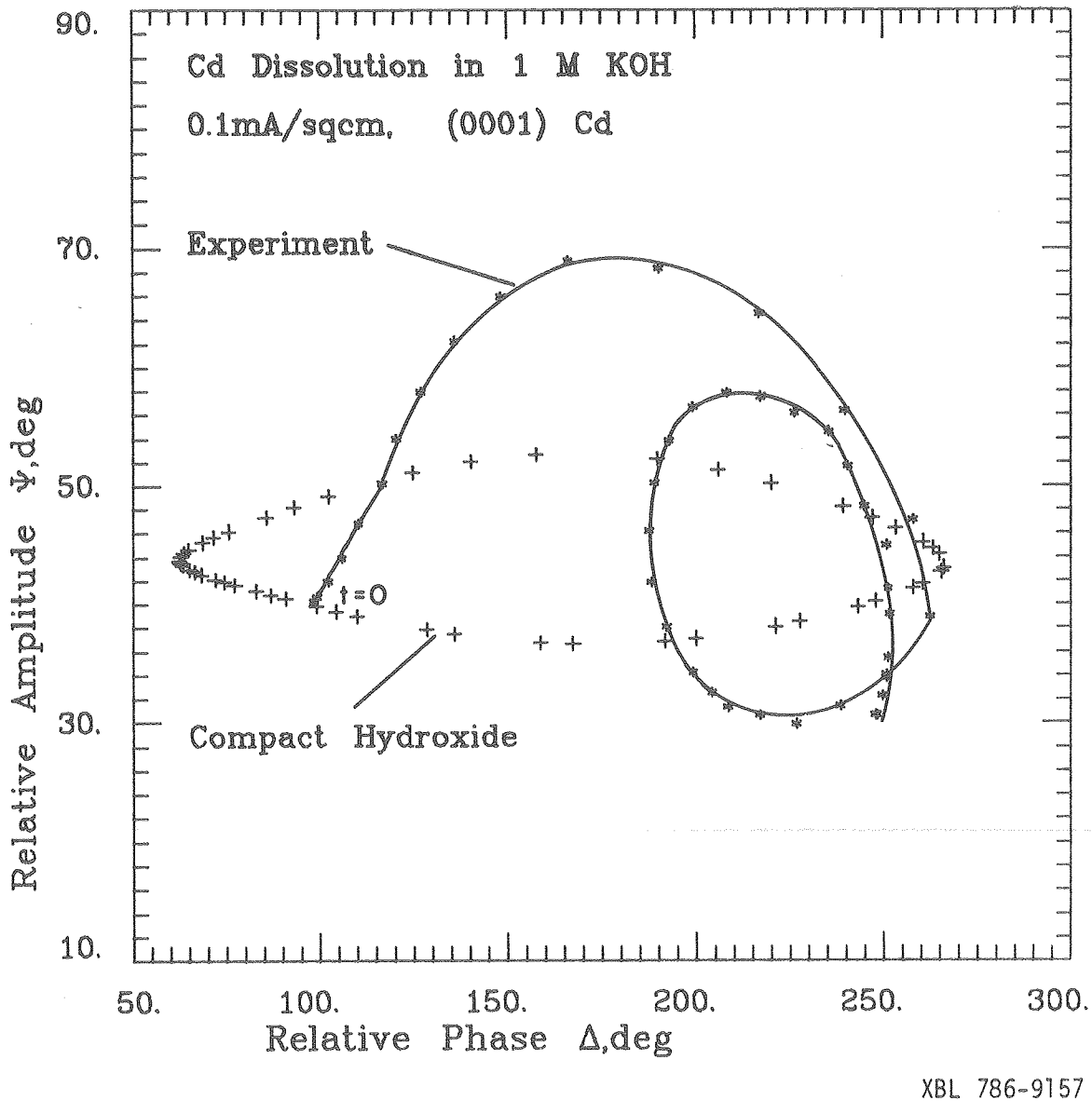

Figure 42. Ellipsometer observations of anodic cadmium hydroxide growth. Computation for a compact, isotropic film.

Film Growth in 1 M KOH

Stagnant Electrolyte, 0.1 mA/cm^2 (Exp. Cd 100-26)

Figure 43 shows the interpretation of ellipsometer observations. At t = 0 , 37% of the electrode surface was covered by patches of a porous (0.20 volume fraction electrolyte) Type II film 150 Å thick. After 120s, all of the electrode surface was covered by a 400 Å thick film. This period of time covers the linear portion of the curve in Figure 43. During this same interval, the porosity of the hydrate layer increased from 0.70 to 0.99. This increasing hydrate layer porosity probably represents a compaction of the primary layer, from an initial inhomogeneous state to a final more homogeneous state. Another indication of the primary layer becoming more dense with time is that the Type I film, which begins forming after 60s, has a porosity of only 0.01.

The computer output for this experiment (Appendix G) gives a surface coverage of secondary crystals (coverage projected along surface normal) of only 3.5% after 420s. This is perhaps an artifact of the optical treatment of the secondary crystals, as Fig. 36 indicates that in regions of the electrode surface, the coverage of the secondary crystals is much larger.

The latter part of the curve is qualitatively reproduced by the theoretical growth of a compact Type I film which reaches a thickness of 950 Å after 420s. Further work is necessary in order to resolve whether the discrepancy between experiment and theory is due to variations in the optical properties across the electrode surface, such as

light scattering from secondary crystals, or whether the discrepancy is due to variations in the chemical composition of the film in the direction normal to the surface.

Effective substrate refractive indices are determined by using the bare substrate reflection coefficients (Eqs. 35-38) to compute the refractive index which gives the initial value of Δ and ψ. The use of effective substrate refractive indices for cadmium metal gives very poor results, as indicated in Figure 44. It is impossible to reach the large experimental values of ψ (68 deg is the maximum in Figures 44 and 43) by using effective substrate optical constants.

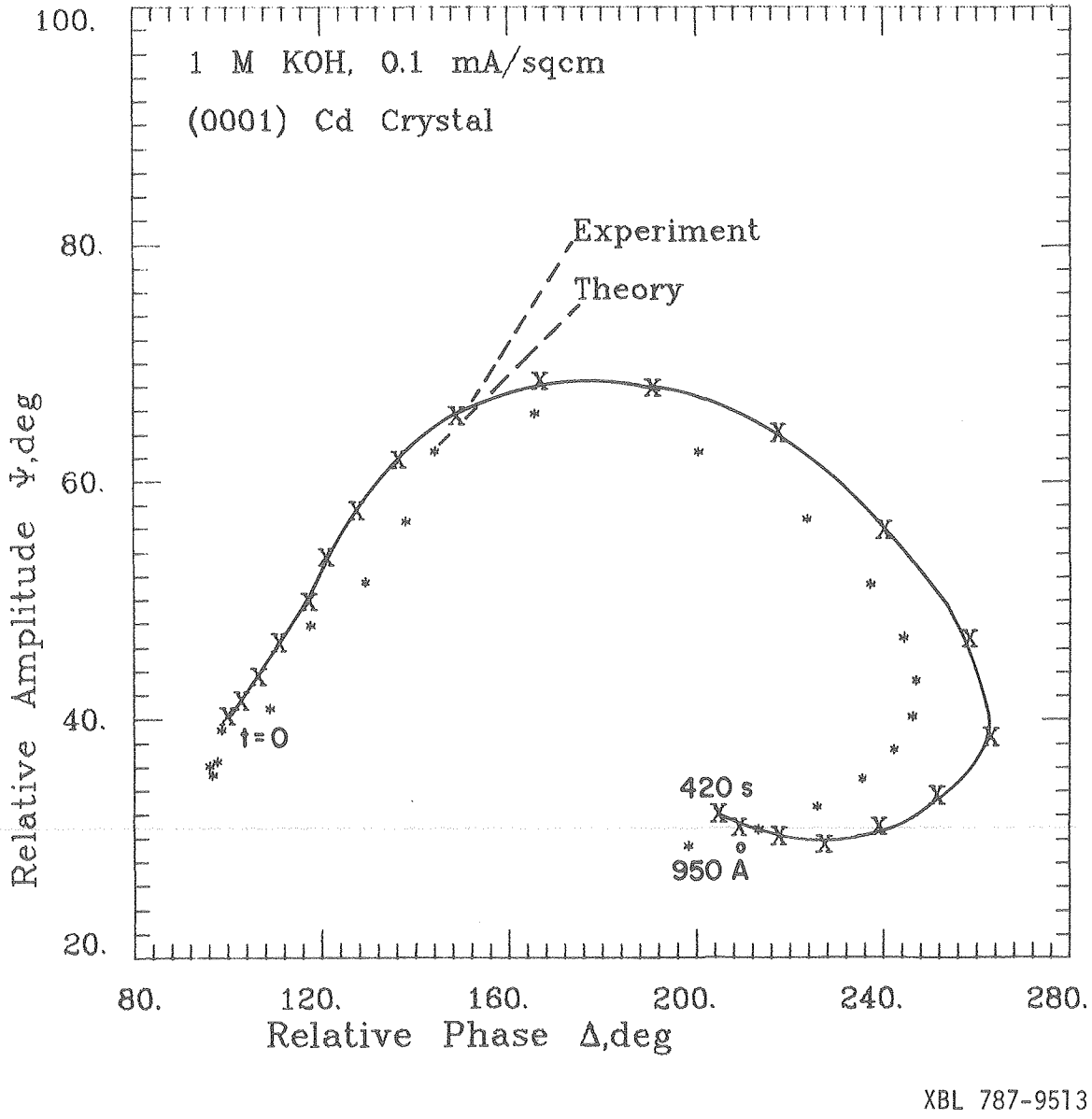

Figure 43. Interpretation of ellipsometer measurements (Exp. Cd 100-26). Primary layer thickness indicated along the curve. Patchwise film formation.

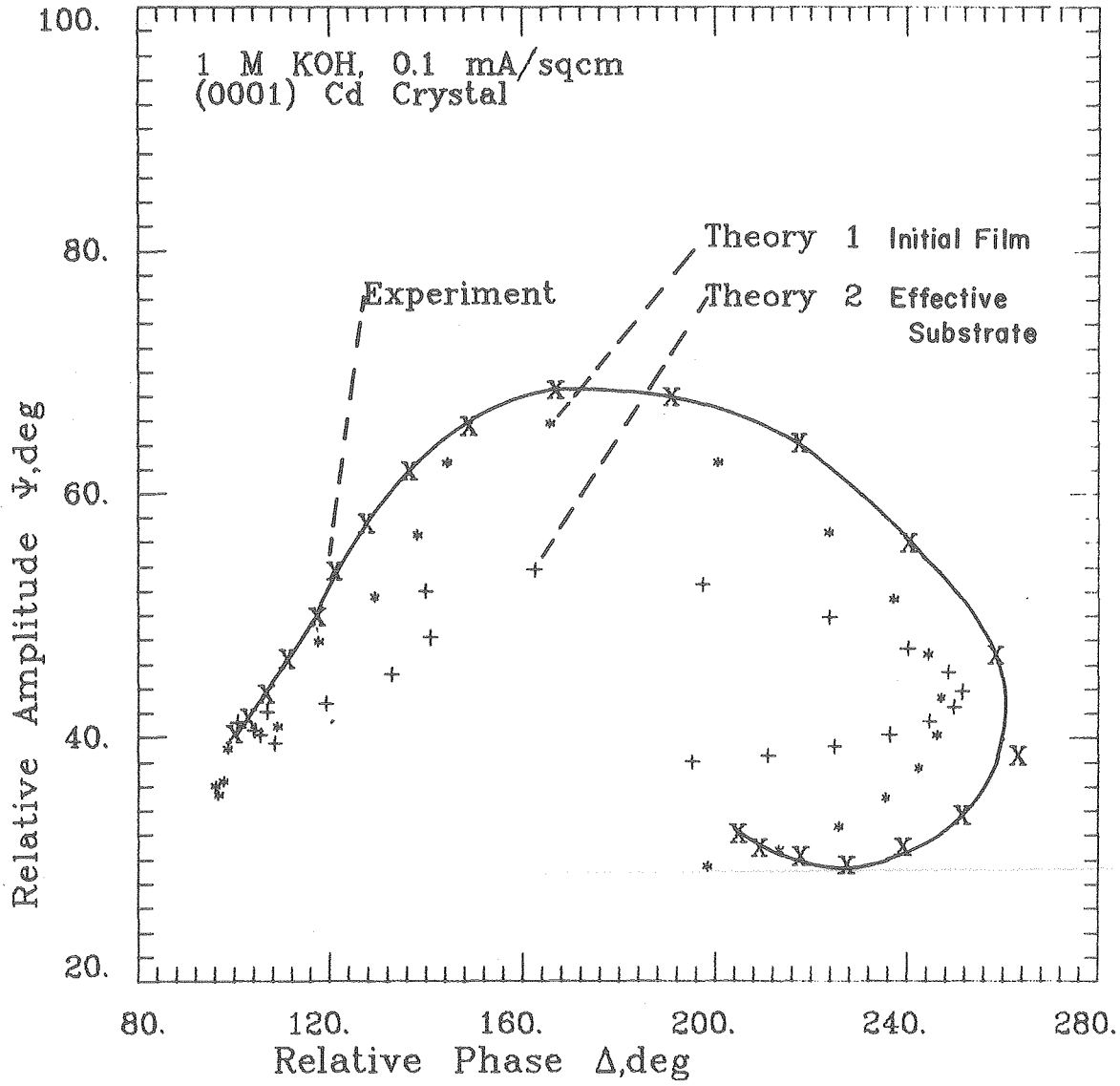

Figure 44. The use of effective substrate optical constants gives poor agreement with theory, in comparison to the use of an initial film (Fig. 43), covering 37% of the surface and 150 Å thick.

Stagnant Electrolyte, 0.2 mA/cm^2 (Exp. Cd 100-25)

For the interpretation presented in Figure 45 and Table VI, 62% of the electrode surface was initially covered by a 320 Å thick, 20% porous cadmium hydroxide film. After 60 seconds, when the electrode passivated, the assumed linear increase with time of the surface coverage leads to a 87% coverage of the primary layer. During this interval of time, the thickness of the primary layer increased by only 9 Å .

The small values for the crystallization rate of the secondary crystals and the dehydration rate of the hydrate layer (Table VI) would seem to indicate only a very small fraction of the current results in film formation. However, it is possible that the secondary crystals act as light scatterers or occupy too small a portion of the electrode surface to have any significant optical effect. The 500 Å dimensions for the secondary crystals given in the computer output are by no means representative of the 1 μm crystal sizes shown in scanning electron micrographs.

Stagnant Electrolyte, 0.4 mA/cm^2 (Exp. Cd 100-15)

For the interpretation presented in Figure 46, 38% of the electrode surface was initially covered by a 300 Å thick hydroxide layer. The secondary crystals have a very small optical effect, as their final surface coverage is only 4%. The time at which the surface coverage of the compact primary layer becomes complete, TDISS = 90.8s, agrees exactly with the experimental time at which the electrode passivates.

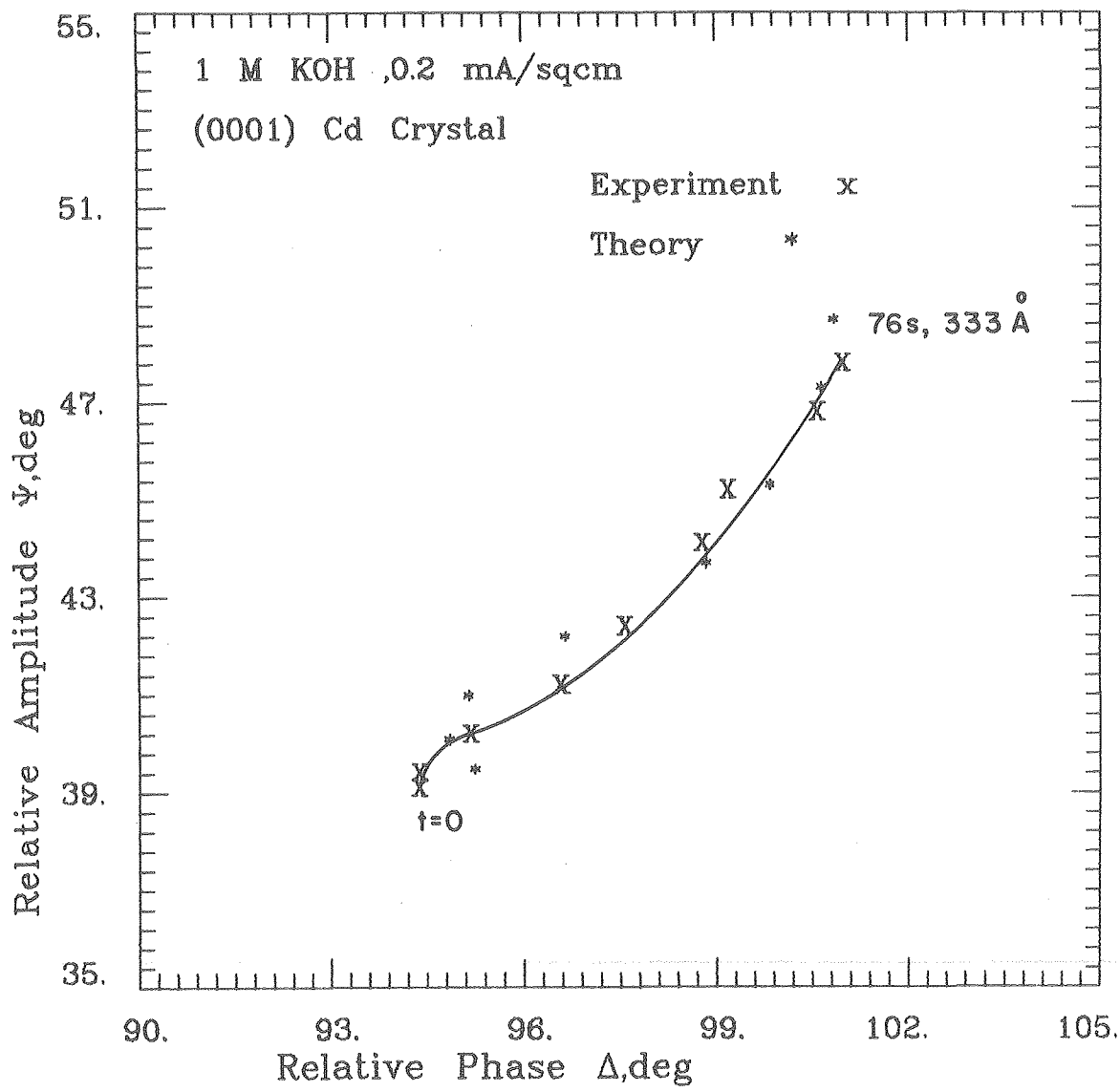

XBL 787-9531

Figure 45. Interpretation of ellipsometer measurements (Exp. Cd 100-25). Primary layer thickness indicated along the curve. Spreading of initial layer.

Table VI. Anodic Cadmium Hydroxide Parameters Derived from Ellipsometer Measurements. 1 M KOH stagnant, 0.2 mA/cm^2, Cd (0001)

Initial Film Thickness	318 ± 61 Å†
Initial Film Coverage	0.62 ± 0.11
Initial Porosity of Hydrate Layer	0.83 ± 0.02
Time to Complete Film Coverage	92 ± 12s
Time to Dissipate Hydrate Layer	99 ± 15s
Number Density of Secondary Crystals	2.11×10^9 ± 0.26 crystals/cm^2
Crystallization Rate of Secondary Crystals	0.0042 ± 0.006 mA/cm^2
Dehydration Rate of Hydrate Layer	0.0010 ± 0.0014 mA/cm^2

†Uncertainty gives 0.5 deg change in the average deviation.

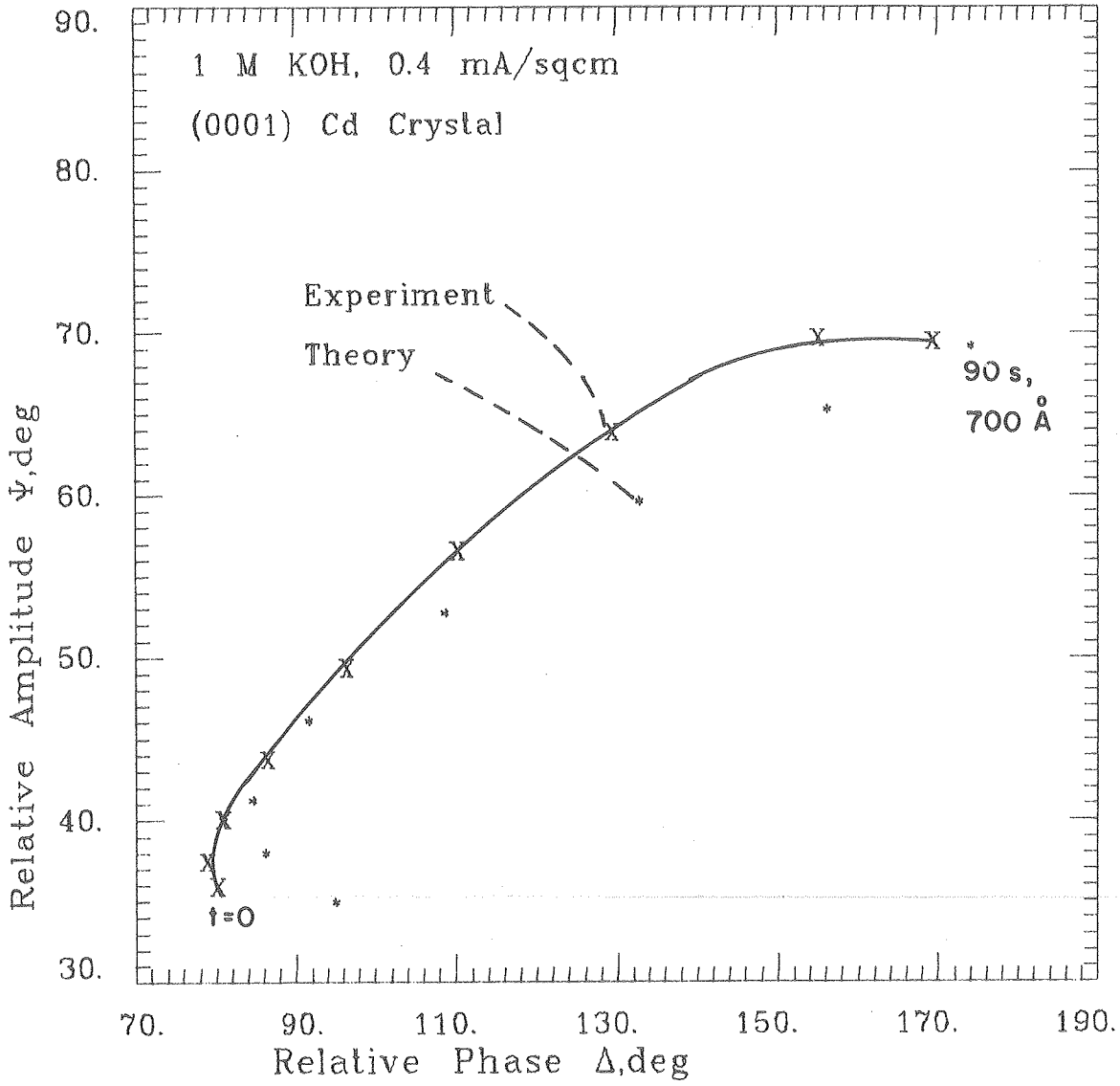

XBL 787-9533

Figure 46. Interpretation of Ellipsometer measurements (Exp. Cd 100-15). Primary layer thickness indicated along the curve. Passivation associated with complete coverage by primary layer. Spreading and growth of primary layer.

Stagnant Electrolyte, 0.6 mA/cm^2 (Exp. Cd 100-24)

Figure 47 illustrates the dependence of the film growth characteristics on the history of the electrode surface. For Cycle 1, the experimental curve initially shows the patchwise film formation trend, and then the relative phase Δ decreases rapidly as the electrode passivates. The decrease in Δ corresponds to the growth of about a 20 Å thick compact hydroxide layer which completely covers the electrode surface. After the current was stopped, the ellipsometer parameters Δ and ψ drifted to the values corresponding to $t = 0$ for the second cycle.

For the second cycle, 90% of the surface was initially covered by a 390 Å thick film. After 50s, the primary layer completely covers the surface and is 550 Å thick. Once again, the time at which complete coverage is reached agrees exactly with the time at which the electrode passivates, as indicated by potential measurements.

Stagnant Electrolyte, 1 mA/cm^2 (Exp. Cd 100-22)

For Figure 48, 63% of the electrode surface was initially covered with a 450 Å thick film. The time to reach complete patch coverage, TDISS = 9.1s, agrees exactly with the experimental time for the passivation of the electrode surface. The electrode potential rises 1.3 volts between 9 and 12s, and during this period the primary layer thickness increased by 6 Å.

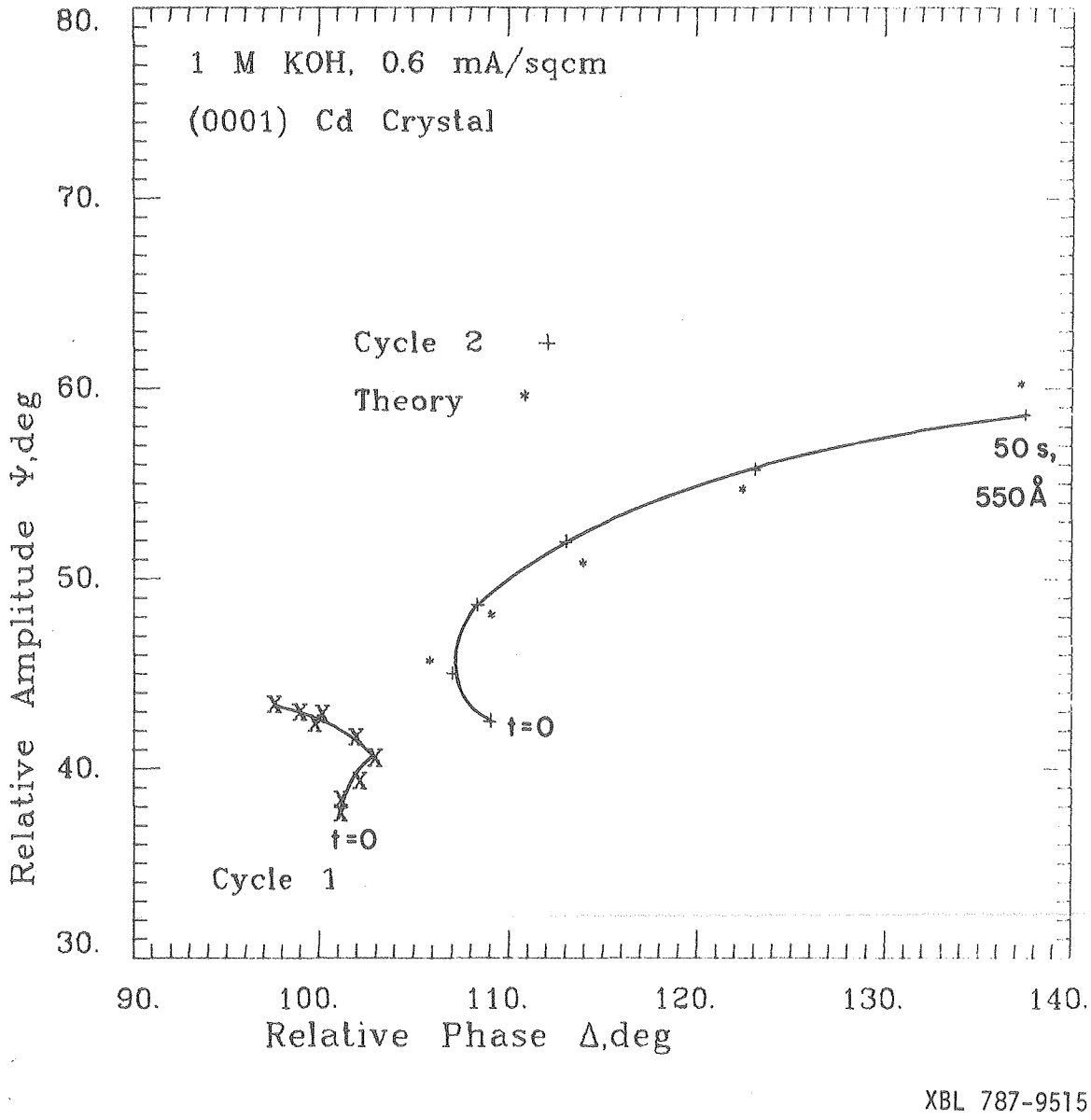

Figure 47. Interpretation of ellipsometer measurements (Exp. Cd 100-24). Primary layer thickness indicated along the curve. Film formation on previously passivated cadmium.

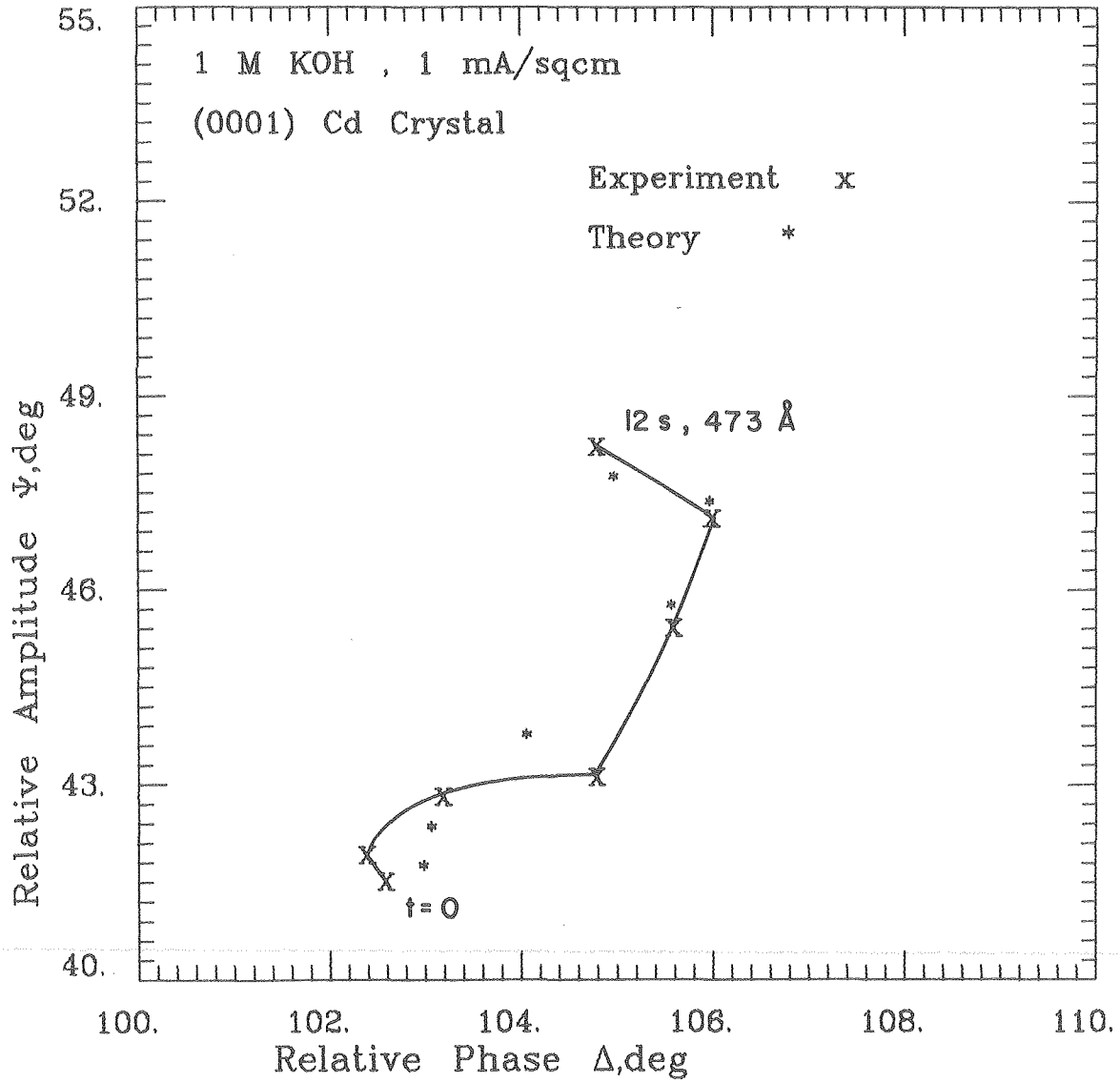

XBL 787-9532

Figure 48. Interpretation of ellipsometer measurements (Exp. Cd 100-22). Primary layer thickness indicated along the curve. Passivation upon merging of patches.

Film Formation in 6 M KOH Electrolyte

Stagnant Electrolyte, 0.6 mA/cm^2 (Exp. Cd 100-33)

The experimental observations presented in Figure 49 were interpreted in two sections. The first five theoretical points were computed using patchwise film formation. The surface coverage increased from 77% initially to complete coverage 54 seconds after the current was turned on. The primary layer thickness increased from the initial value of 460 Å to the value 700 Å after 50s. The initial porosity of the primary layer was 0.15, and the porosity of the Type I film decreased from 0.134 to 0.100 volume fraction electrolyte. The secondary crystals had a negligible optical effect.

After about 50s, the optical properties of the anodic film change. The continued growth of the porous hydroxide film would lead to increasing values of Δ with only a minor decrease in the relative amplitude parameter ψ. The experimental curve instead shows a large decrease in ψ with a small increase in Δ. Although it may be possible that this change in the optical properties of the anodic film is the result of secondary crystal growth, none of the optical treatments of the secondary crystals outlined in Section IV was able to reproduce this change.

The latter part of the experimental curve in Figure 49 was reproduced using non-stoichiometry. The primary layer was slightly absorbing, with a refractive index of 1.86 - 0.001 i. However, beneath the primary layer a very strongly light absorbing film (n = 1.48 - 1.41 i) grew to a thickness of 400 Å at 110 seconds. This bottom layer was modeled

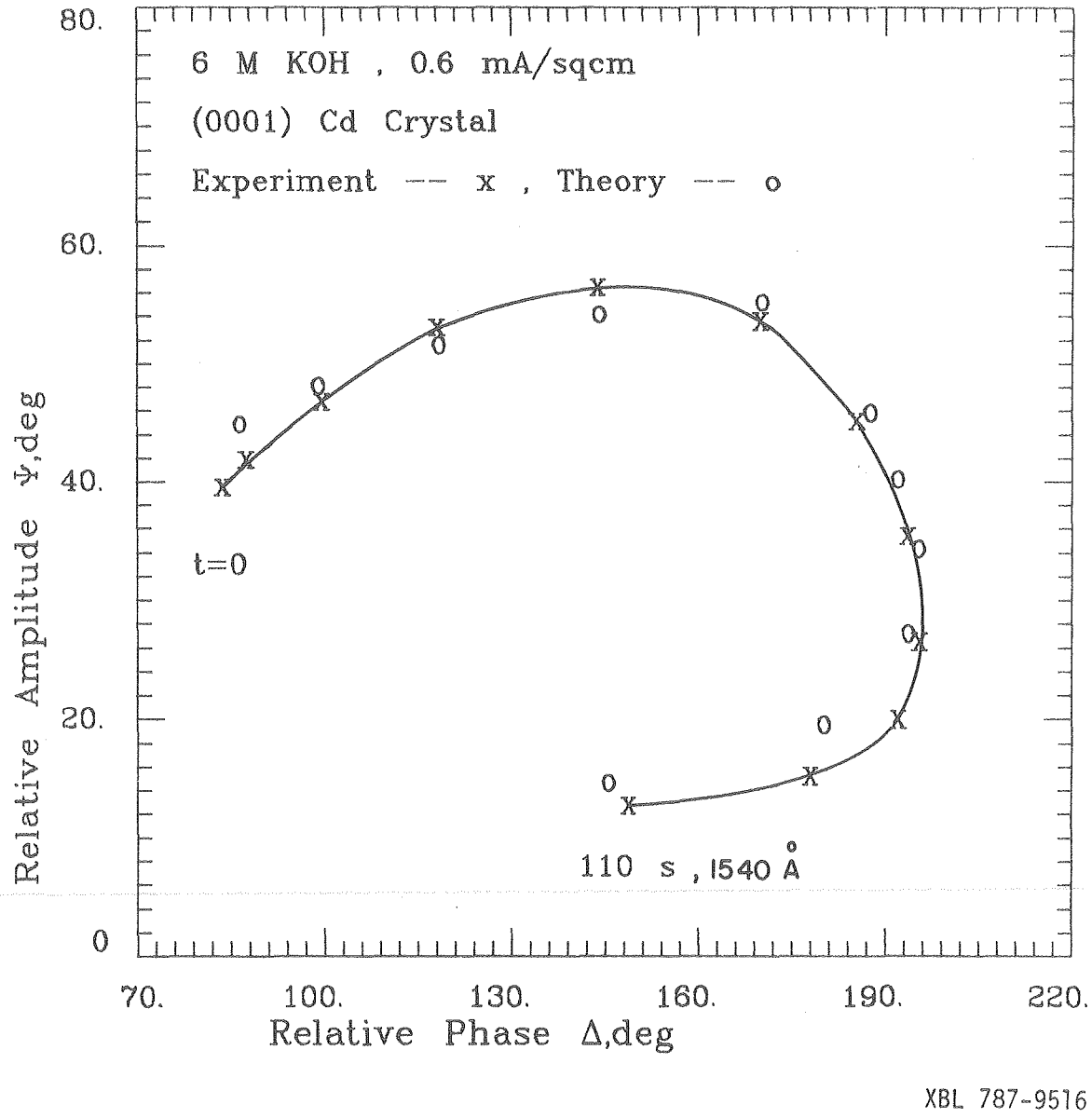

Figure 49. Interpretation of ellipsometer measurements (Exp. Cd 100-33). Primary layer thickness indicated along the curve. Interpretation in 2 segments.

as the growth of a porous, rough layer. This optical behavior is very typical of stagnant, 6 M KOH experiments.

Stagnant Electrolyte, 1 mA/cm^2 (Exp. Cd 100-30)

The two-part reproduction of experimental observations described above (Exp. CD 100-33) was used for the interpretation presented in Figure 50. The initial stoichiometric hydroxide layer was compact, in comparison to the porous (10%) layer formed at 0.6 mA/cm^2.

The degree of non-stoichiometry of the primary layer formed at latter stages was much larger than the film formed at 0.6 mA/cm^2. The refractive index of 2.65 - 0.28 i corresponds to a metal mole fraction of 0.59. A patchwise development of non-stoichiometry was used, in which the fraction of the surface covered by the absorbing film increased from 0.91 at 67s to 1.0 at 138 seconds.

Stagnant Electrolyte, 2 mA/cm^2 (Exp. Cd 100-32)

The interpretation presented in Figure 51 can be viewed as the growth of an inhomogeneous film with variations in both porosity and chemical composition in the direction normal to the surface. The porosities (constant with time) of the hydrate layer, Type I film, and Type II film were 0.86, 0.47, and 0.15. The refractive indices of the three films and the rough layer were 1.489, 1.81 - 0.005 i, 2.17 - 0.01 i, and 1.45 - 1.09 i. Light absorption in the film was modelled by patches of film occupying 5% of the surface and containing 5 mole percent metal. After 70s, the Type I film was 1300 Å thick, the Type II film was 390 Å thick, and the rough layer was 950 Å thick

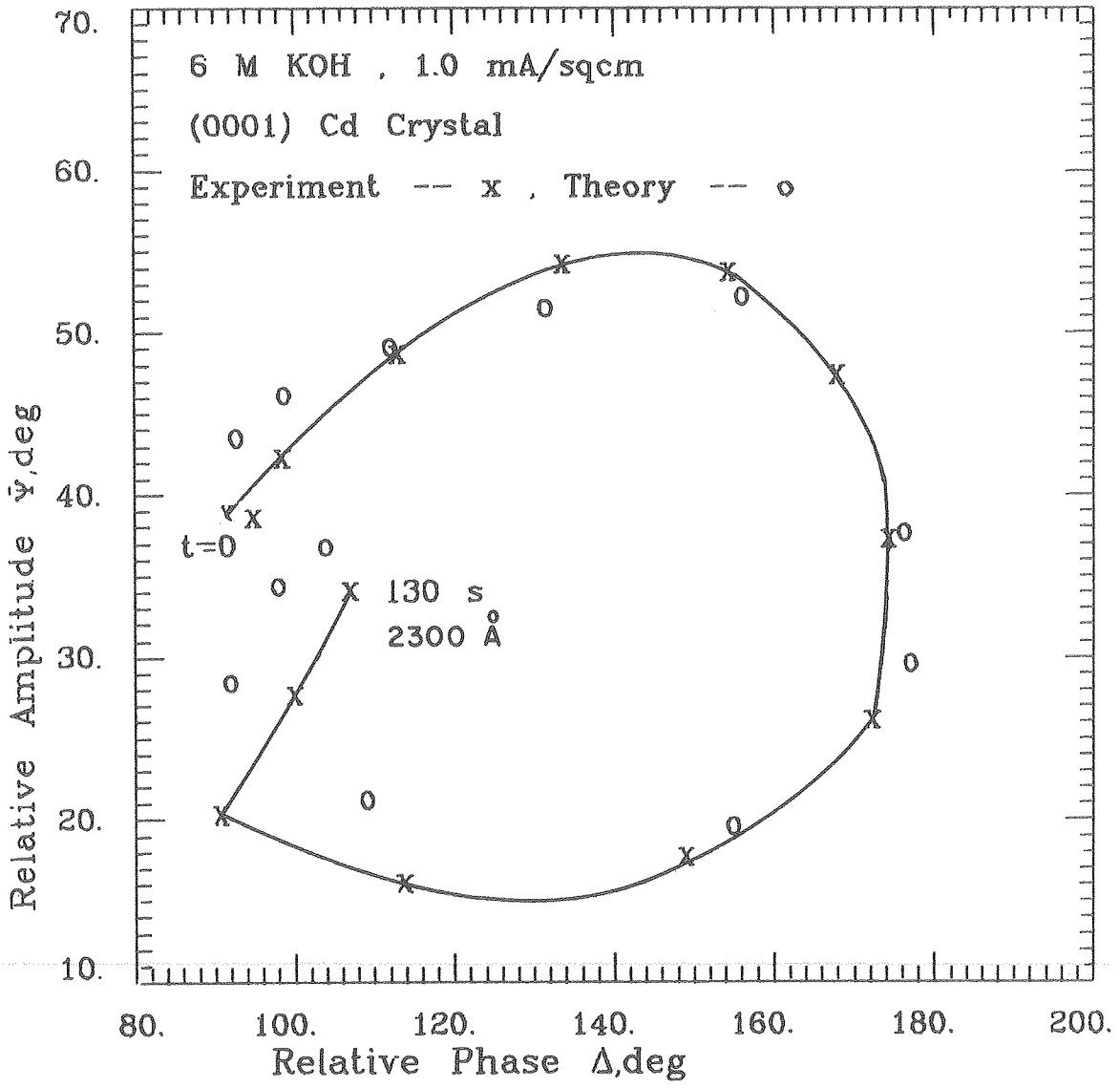

XBL 787-9537

Figure 50. Interpretation of ellipsometer measurements (Exp. Cd 100-30). Primary layer thickness along curve. Interpretation in 2 segments.

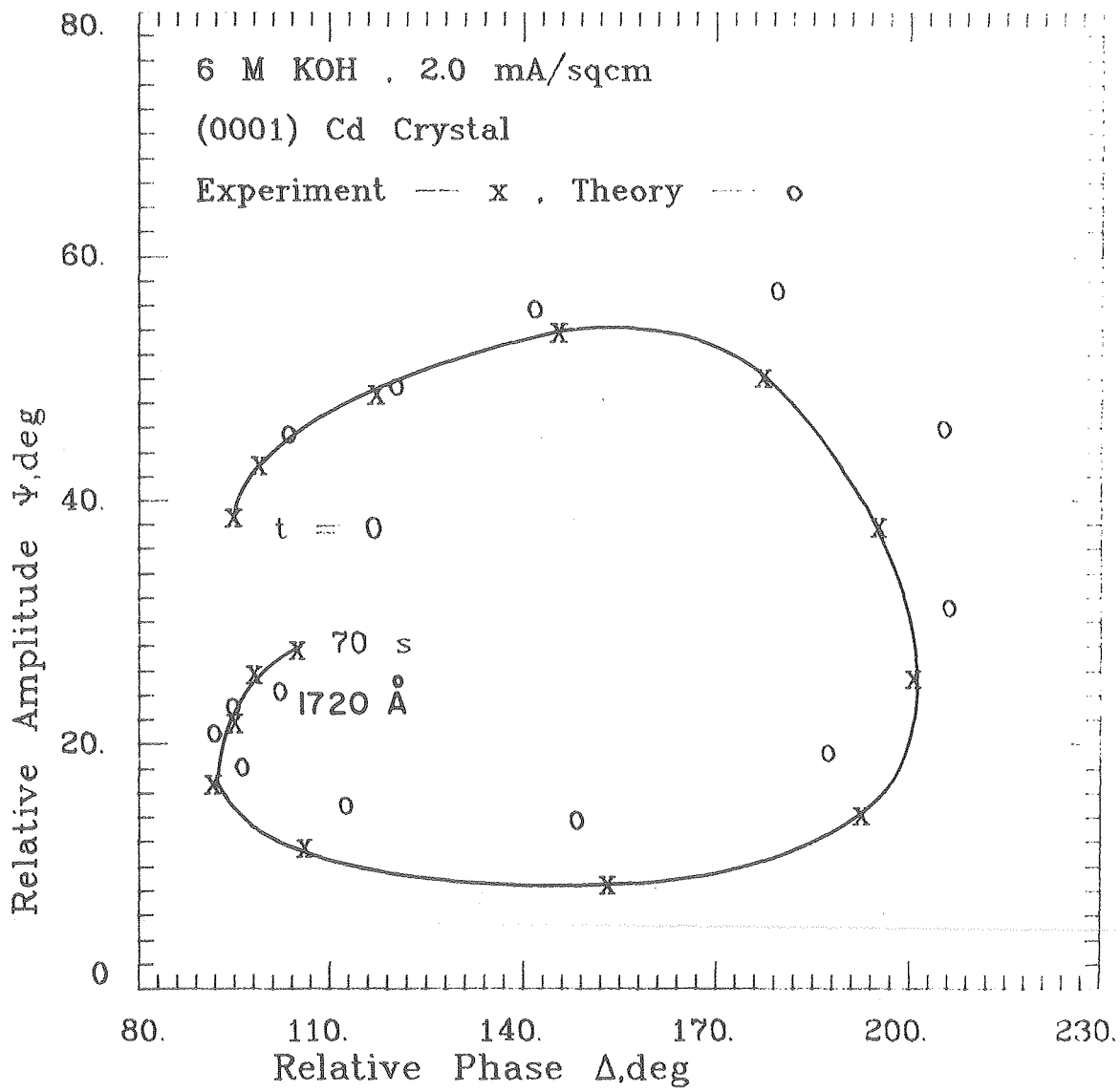

XBL 787-9538

Figure 51. Interpretation of ellipsometer measurements (Exp. Cd 100-32). Primary layer thickness along curve. Interpretation in one part.

1140 Re, 0.2 mA/cm^2 (Exp. Cd 400-15)

For the initial portion of the experimental curve presented in Figure 52, the theoretical values of Δ and ψ were computed using patchwise film formation with roughening of the substrate. A compact 180 Å thick hydroxide film initially covered 43% of the electrode surface. The porosity of the Type I film decreased from an initial value of 0.79 to 0.02 after 107 seconds. The refractive index of the roughness layer was 1.70 - 1.59 i.

In order to interpret the latter part of the experimental curve, non-stoichiometric patches containing excess metal and a thinner and less porous roughness layer were used. Patches containing 82 mole percent metal initially occupy 2% of the electrode surface, and the surface coverage of the patches was 77% after 250s. Dark regions are observed on scanning electron micrographs. The refractive index of the roughness layer was 1.60 - 3.37 i.

1140 Re, 1 mA/cm^2 (Exp. Cd 400-16)

Figure 53 shows deviations between experiment and theory similar to those indicated in Figure 52, which are an indication of developing non-stoichiometry in the anodic film. The rapid rise in ψ at the point at which the divergence begins is probably the result of excess metal in the primary layer (Figs. 39 and 40).

7000 Re, 0.4 mA/cm^2 (Exp. Cd 400-11)

For the interpretation presented in Figure 54, 27% of the electrode surface was initially covered by a compact, 490 Å thick hydroxide film.

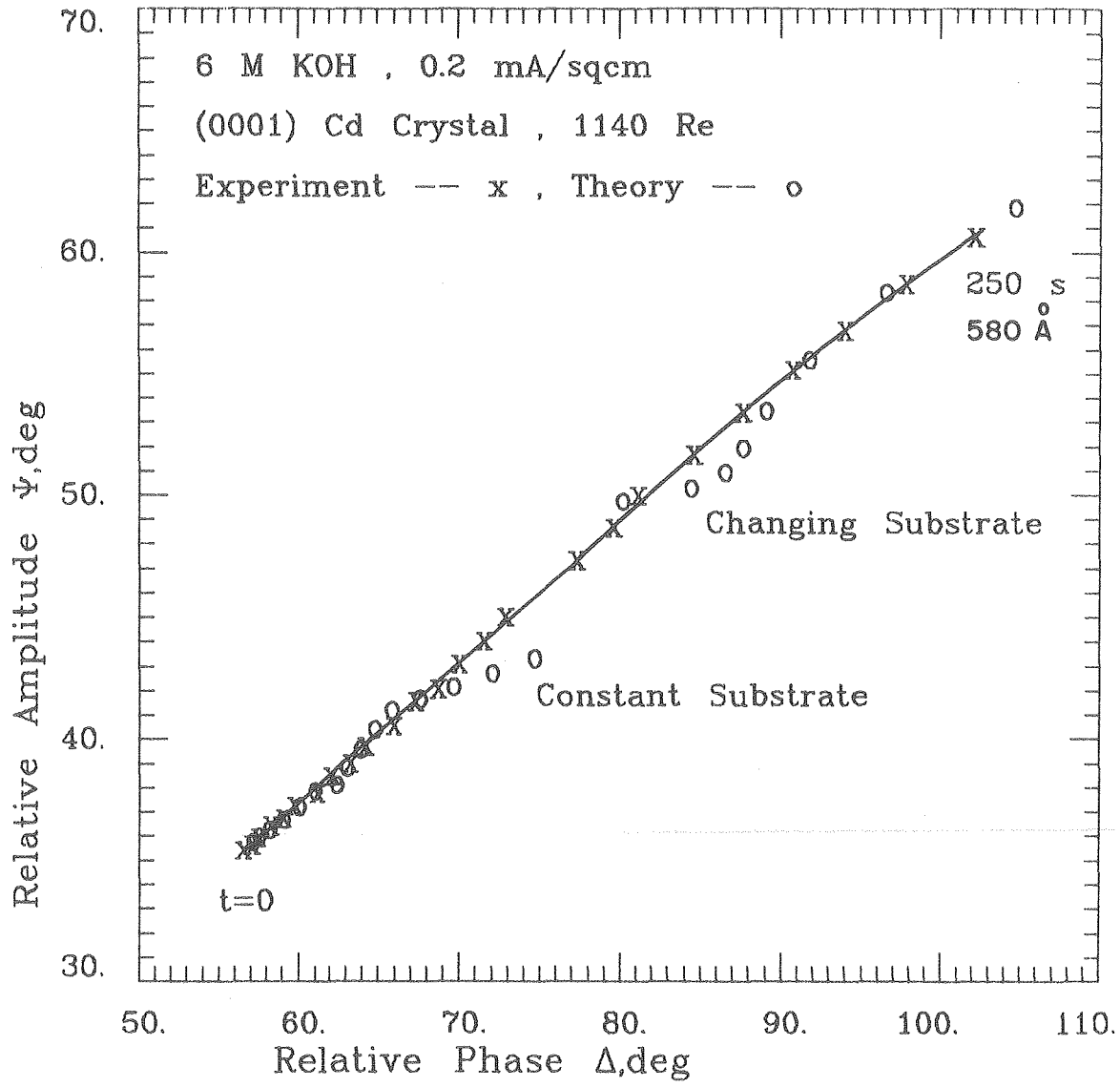

XBL 787-9517

Figure 52. Interpretation of ellipsometer measurements (Exp. Cd 400-15). Primary layer thickness along curve. Non-stoichiometry in film and changing substrate optical constants.

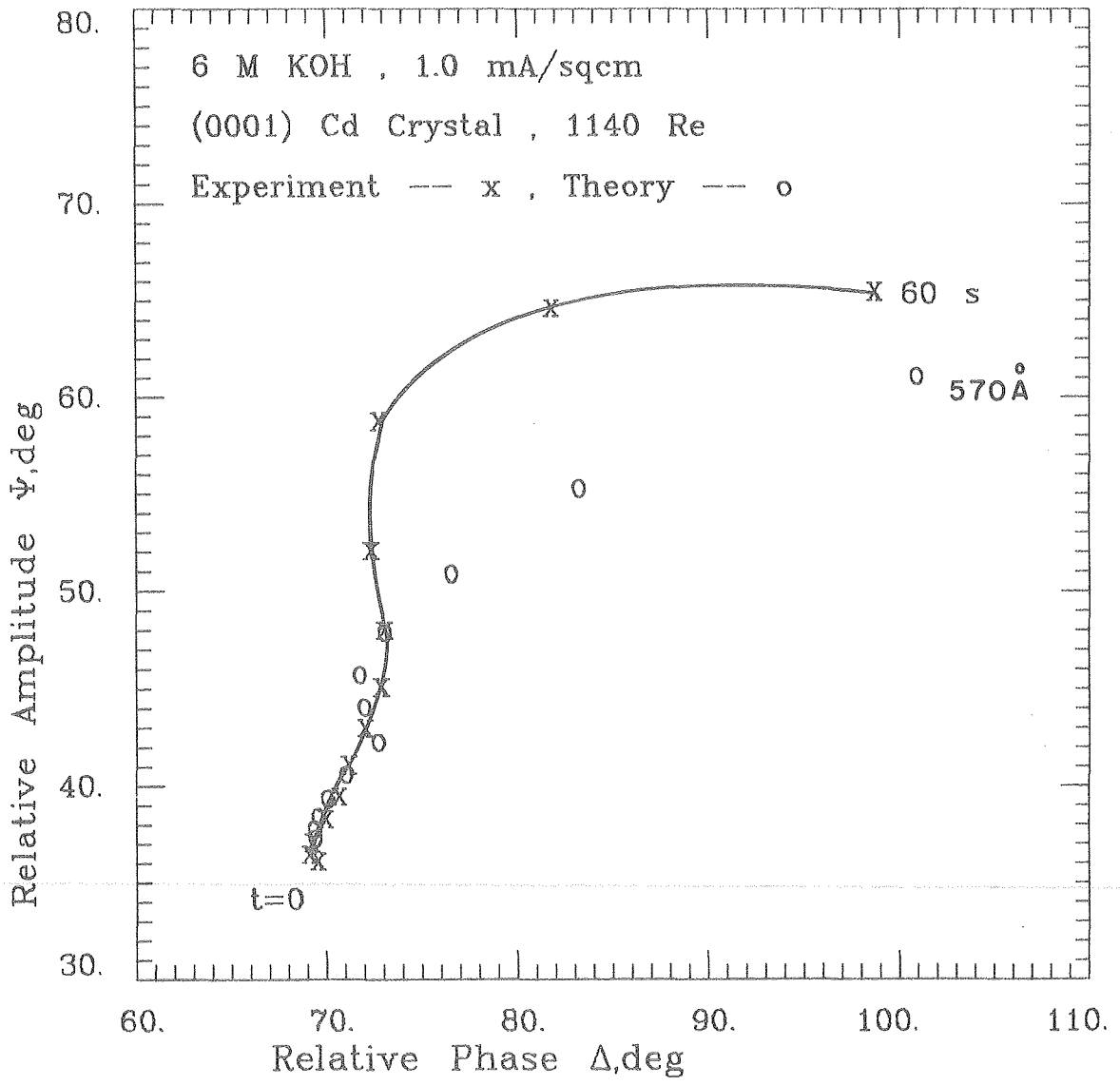

XBL 787-9535

Figure 53. Interpretation of ellipsometer measurements (Exp. Cd 400-16). Primary layer thickness along computed points. Developing non-stoichiometry.

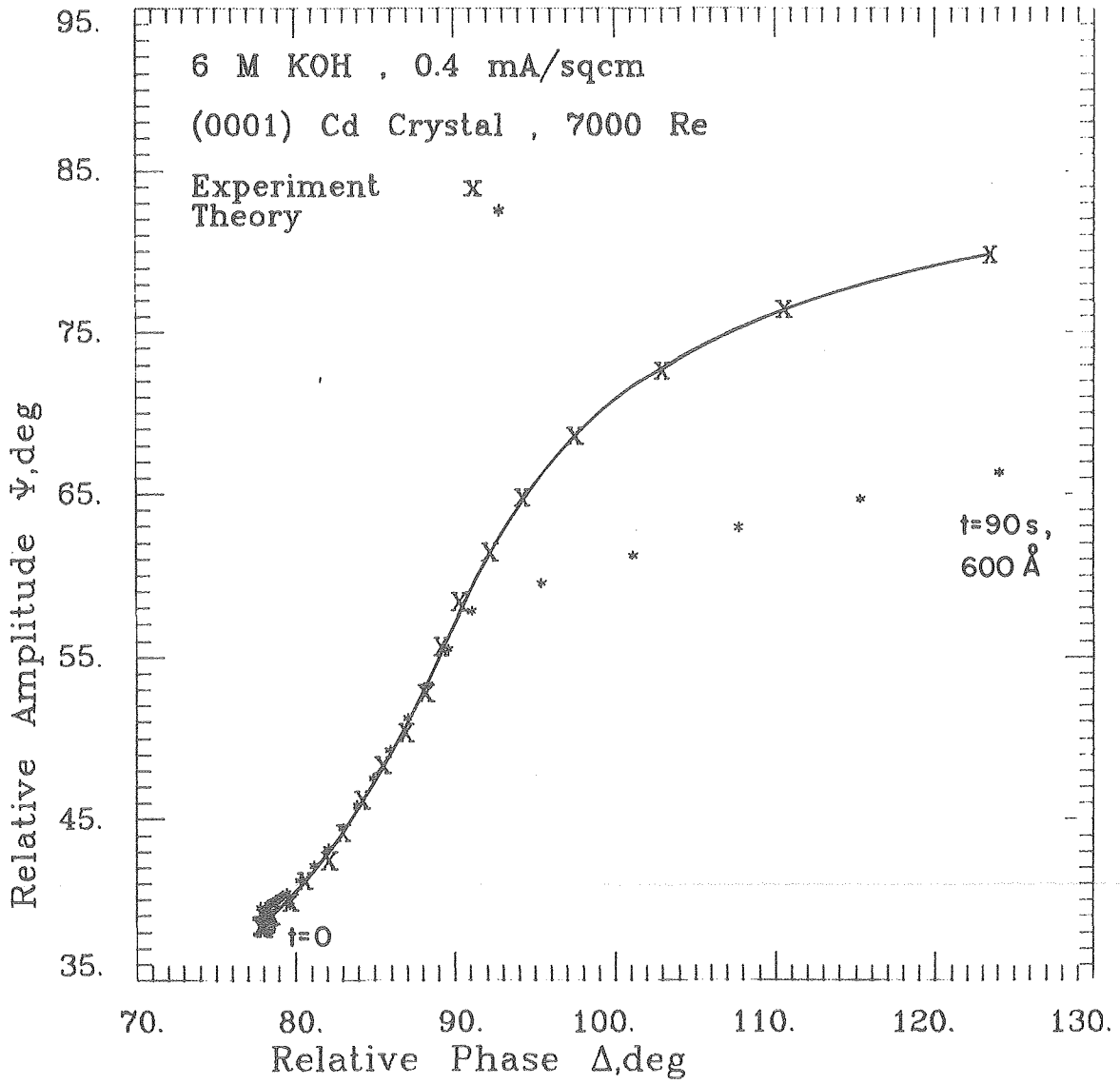

XBL 787-9528

Figure 54. Interpretation of ellipsometer measurements (Exp. Cd 400-11). Primary layer thickness along computed points. Deviation after merging of patches.

The point at which the experimental and theoretical curves diverge corresponds to the time at which the primary layer completely covers the electrode surface, 66 seconds. At this point the compact primary layer is 550 Å thick.

7000 Re,1 mA/cm^2 (Exp. Cd 400-10)

The experimental curve in Figure 55 has a discontinuity at the Δ, ψ coordinates (87.2°, 50.5°). At this point, the potential rises abruptly as the electrode passivates. The rapid rise in ψ occurring simultaneously with passivation is an indication that excess cadmium metal allows the film to become an electron conductor.

7000 Re, 4 mA/cm^2 (Exp. Cd 400-9)

For the interpretation presented in Figure 56, the initial 122 Å thick hydroxide layer which occupied 76% of the electrode surface completely covered the surface after 6.6 seconds. At this value of time, the electrode potential jumped from -0.50 volts to +0.86 volts. A change in the slope of the experimental $\Delta - \psi$ curve occurs at the third data point. At this moment, the electrode potential shifts from -0.90 to -0.75 volts.

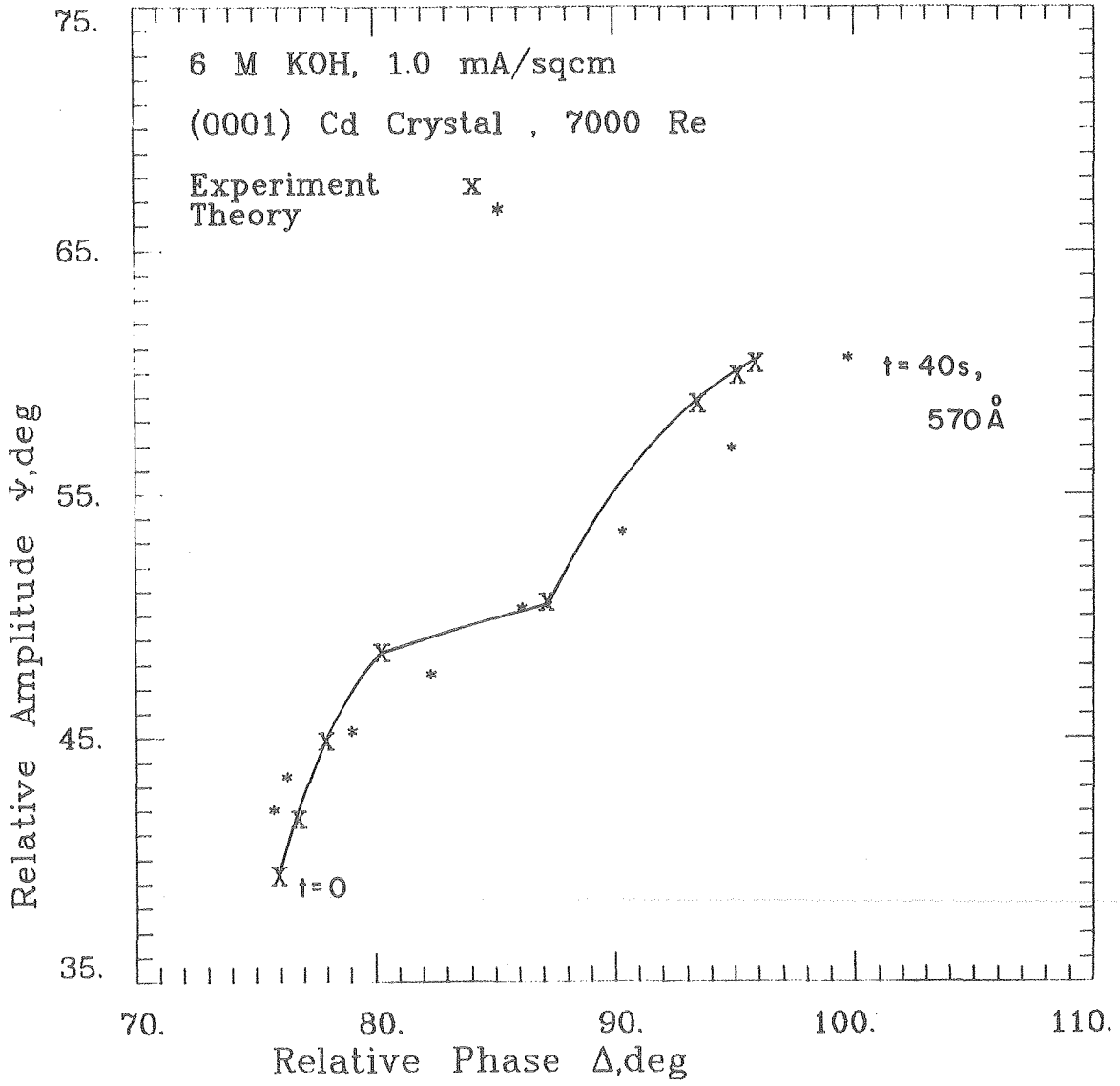

XBL 787-9529

Figure 55. Interpretation of ellipsometer measurements (Exp. Cd 400-10). Passivation at kink in experimental curve.

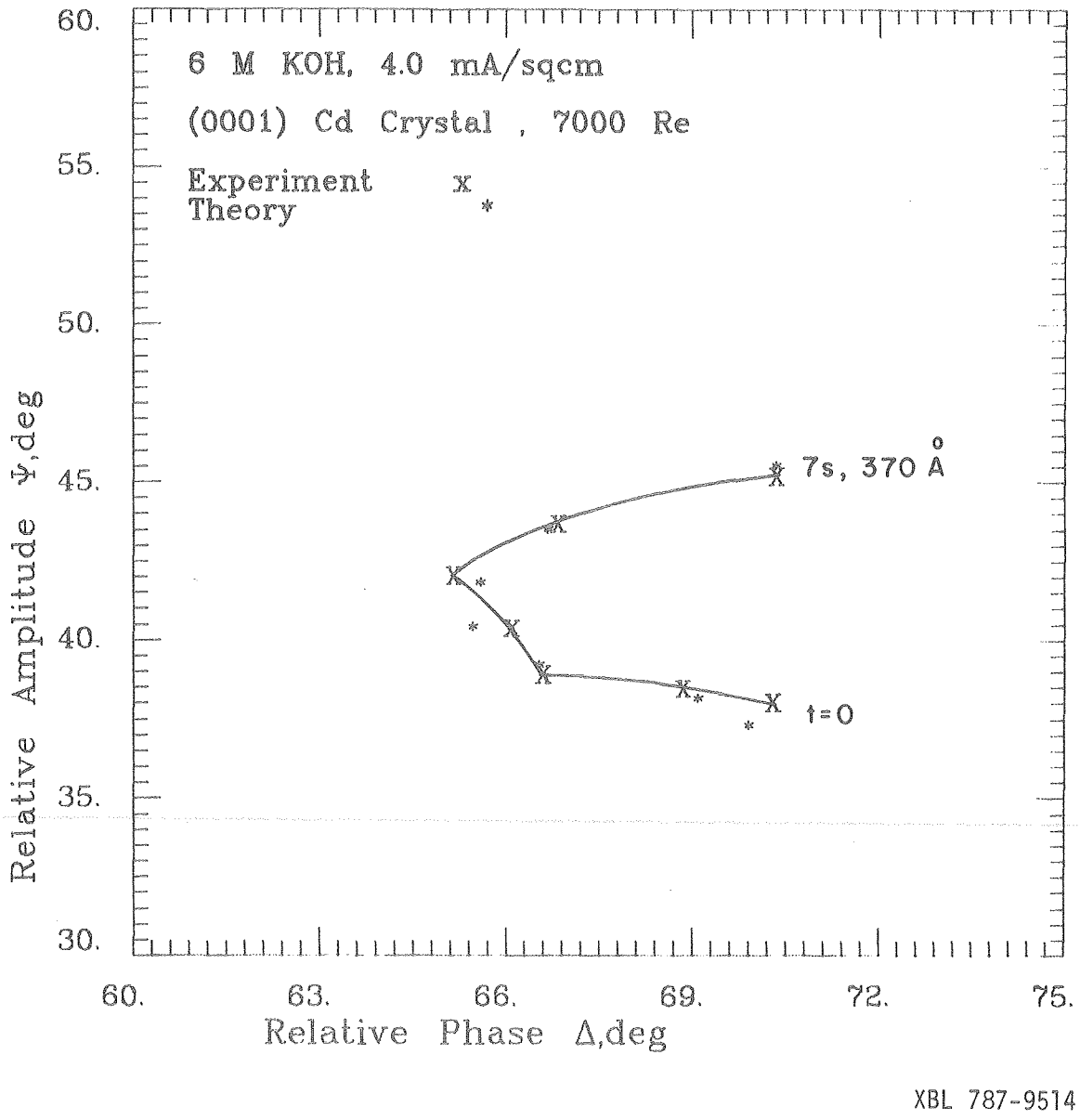

Figure 56. Interpretation of ellipsometer measurements (Exp. Cd 400-9). Changes in potential at changes in slope of $\Delta - \psi$ curve,

E. Zinc Oxide Formation

Qualitative Aspects

Due to the formation of zincate, $Zn(OH)_4^{=}$, the solubility of zinc in alkaline solution is a strong function of the alkaline concentration. In 6M KOH, the solubility of zinc is three orders of magnitude greater than the solubilities of silver and cadmium, and as a result, the anodic electrode current densities used to study film formation were as large as 750 mA/cm^2.

Zinc corrodes in alkaline solution. The following observations in 6M KOH indicate that a surface phase is formed on the electrode surface as a result of the corrosion processes. When the zinc electrode is cathodically protected at -1.7 Volts (approximately 1 mA/cm^2 current density) with electrolyte flowing at 1.7 cm/s linear velocity, oscillations in the ellipsometer parameters occur. The magnitude of the oscillations for both Δ and ψ are 2 degrees, with a frequency of approximately 2 seconds. When the cathodic protection is removed, the potential shifts to -1.35 V, the relative amplitude parameter ψ increases by about 5 degrees, and Δ remains constant. If anodic current is immediately passed, ψ decreases by the same 5 degrees and the initial electrode behavior is that of a growing mass-transport boundary layer with negligible roughening of the metal substrate. When the cathodic protection is maintained at -1.37 V, no oscillations in Δ and ψ occur, and no shift in ψ is observed when the cathodic protection is removed. When anodic current is passed, major roughening of the metal substrate occurs, which is greatly accentuated by portions of the electrode surface being passivated by a surface layer.

The primary layer formed on zinc in 0.5 M KOH has a glassy appearance in scanning electron micrographs. Major voids are apparent, possibly caused by secondary crystals which detached from the surface during the period when the electrode was being removed from the cell. Localized dark regions are observed by SEM. The dark regions are more pronounced at high current densities.

In 6M KOH, the anodic film is localized rather than uniformly covering the total electrode surface. Scanning electron microscopy cannot provide quantitative information about the primary layer formed over the regions of the electrode surface not covered by the secondary crystal growth.

Quantitative Interpretation

Film Formation in 0.5 M KOH (Stagnant)

-1.2 V vs Hg/HgO (Exp. Zn 70-25)

The ellipsometer observations presented in Figure 57 were interpreted in four sections in order to describe changes with time in the optical properties of the anodic film. For comparison, the general features of an anodic film formed by approximately reproducing the current vs. time behavior is shown in Figure 58.

The theoretical values of Δ and ψ for the initial portion of the curve (points A in Fig. 57) were computed using patchwise film formation with roughening of the metal substrate. Compact zinc oxide began forming on 52% of the electrode surface, and after 65 seconds covered 94% of the surface. The thickness of the primary layer at this time was 325 Å. During this same time interval the porosity of

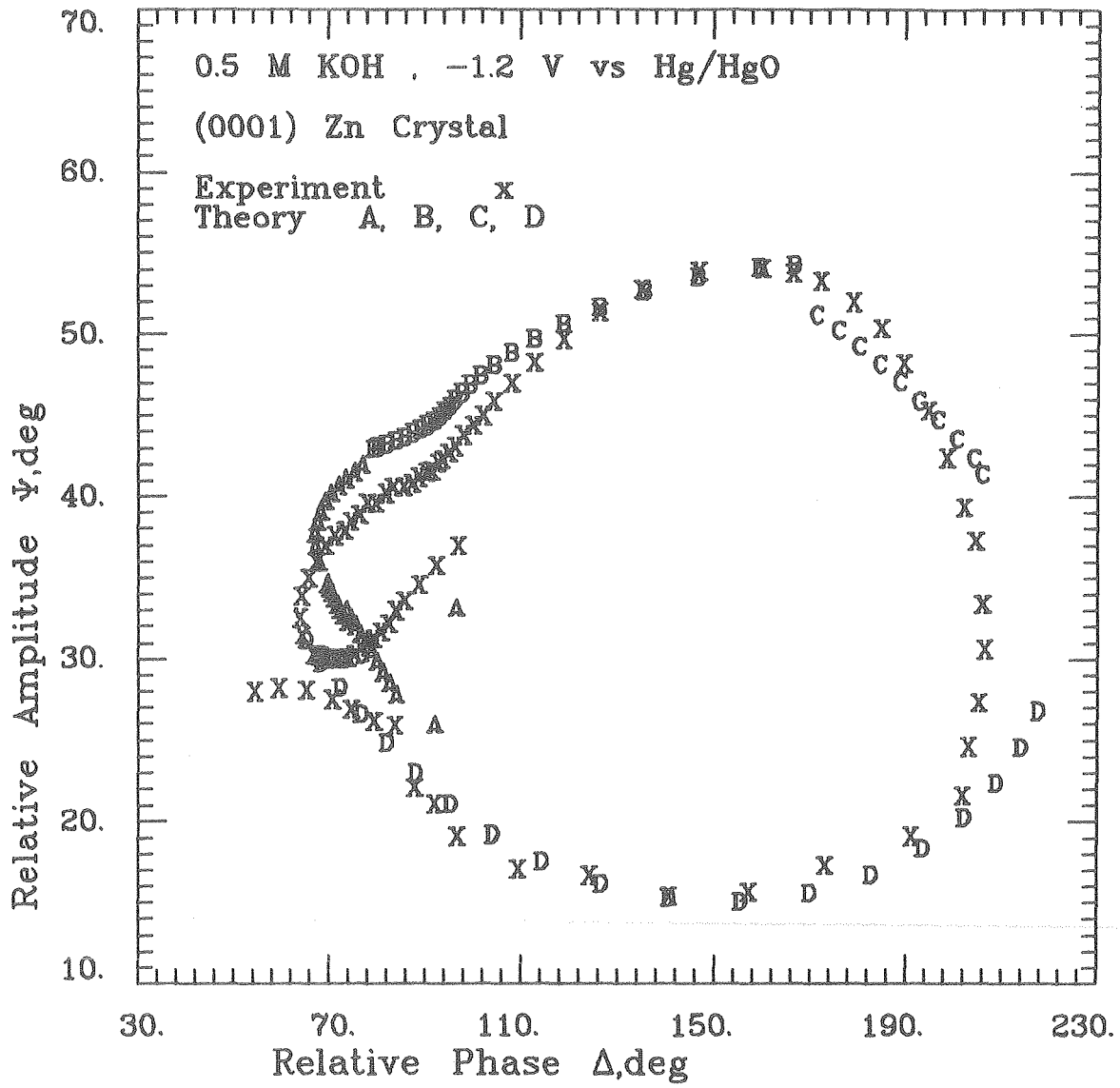

Figure 57. Interpretation of ellipsometer measurements (Exp. Zn 70-25).

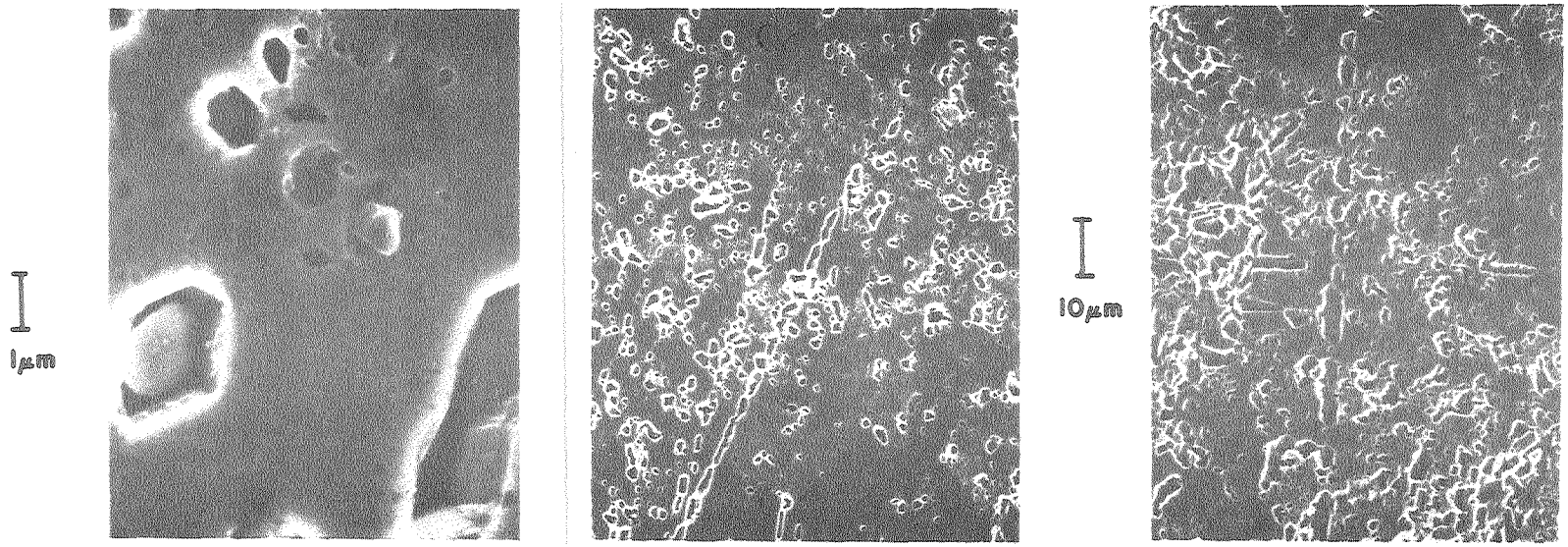

Figure 58. Scanning electron micrographs of porous zinc oxide.

the hydrate layer increased from 0.88 to 0.99 volume fraction electrolyte. Roughening of the substrate was modeled as the growth of a layer of a constant porosity of 16 volume percent metal. As indicated in Fig. 57, the initial slope of the computed curve is too steep; a larger volume fraction of metal would give better agreement with the initial slope of the experimental curve. The small value of the metal volume fraction possibly indicates that undercutting of the oxide layer occurs, resulting in a metal fraction which decreases with time.

The second portion of the theoretical curve (points B) was computed using the growth of compact zinc oxide. Secondary crystals occupied only 7.5% of the electrode surface and had a minor optical effect. The thickness of the primary layer after 305 seconds was 780 Å. The constant metal volume fraction in the roughness layer was 0.38. At the end of this portion of the curve, the theoretical points computed as outlined diverge from the experimental curve, with the computed values of ψ being too large.

The third portion of the theoretical curve (points C), which at best only qualitatively reproduces the experimental curve, was computed using a dual film structure for the zinc oxide. A Type II film 220 Å thick completely covered the surface. A compact Type I film 700 Å thick expanded across the surface. The metal volume fraction was unity for the roughness layer (no roughness).

The last part of the theoretical curve (points D) was computed using a non-stoichiometric primary layer. The mole fraction metal in the film was 0.087, giving a refractive index of 2.10 - 0.061 i.

Secondary crystals of hydration 0.63 volume fraction water occupied about 40% of the electrode surface. After 450 seconds, the primary layer was 3000 Å thick and the height of the secondary crystals was 2800 Å. The final thickness of the roughness layer was 330 Å and the layer contained 94 volume fraction metal. The localized black regions in Fig. 58 are probably the source of the non-stoichiometry indicated by the computations.

-1.0 V vs Hg/HgO (Exp. Zn 70-23)

The experimental curve in Figure 59 shows three distinct regions. Roughening of the metal substrate during the time interval $0 < t < 1.5$ s leads to the decreasing values of ψ. At 1.5 s, the discontinuity in the experimental curve indicates a sudden onset of film formation.

The second portion of the experimental curve covers the time interval $1.5 \text{ s} < t < 50 \text{ s}$. The theoretical values of Δ and ψ computed using a primary layer which completely covers the electrode does not reproduce the rise in ψ values observed experimentally. The use of patchwise film formation would probably improve the agreement with experiment. Beginning at $t = 3.5$ s ((Δ,ψ) coordinate (94.3,33.9)) the relative phase Δ decreases simultaneously with a decrease in electrode current density from 3.3 to 0.11 mA/cm^2. The behavior of the ellipsometer parameters is consistent with either the compaction of an approximately 70 Å thick primary layer or the formation of an approximately 5 Å thick primary layer.

Beginning at $t = 50$ s, the electrode current density doubles to 0.2 mA/cm^2 and Δ and ψ both begin to decrease. The theoretical

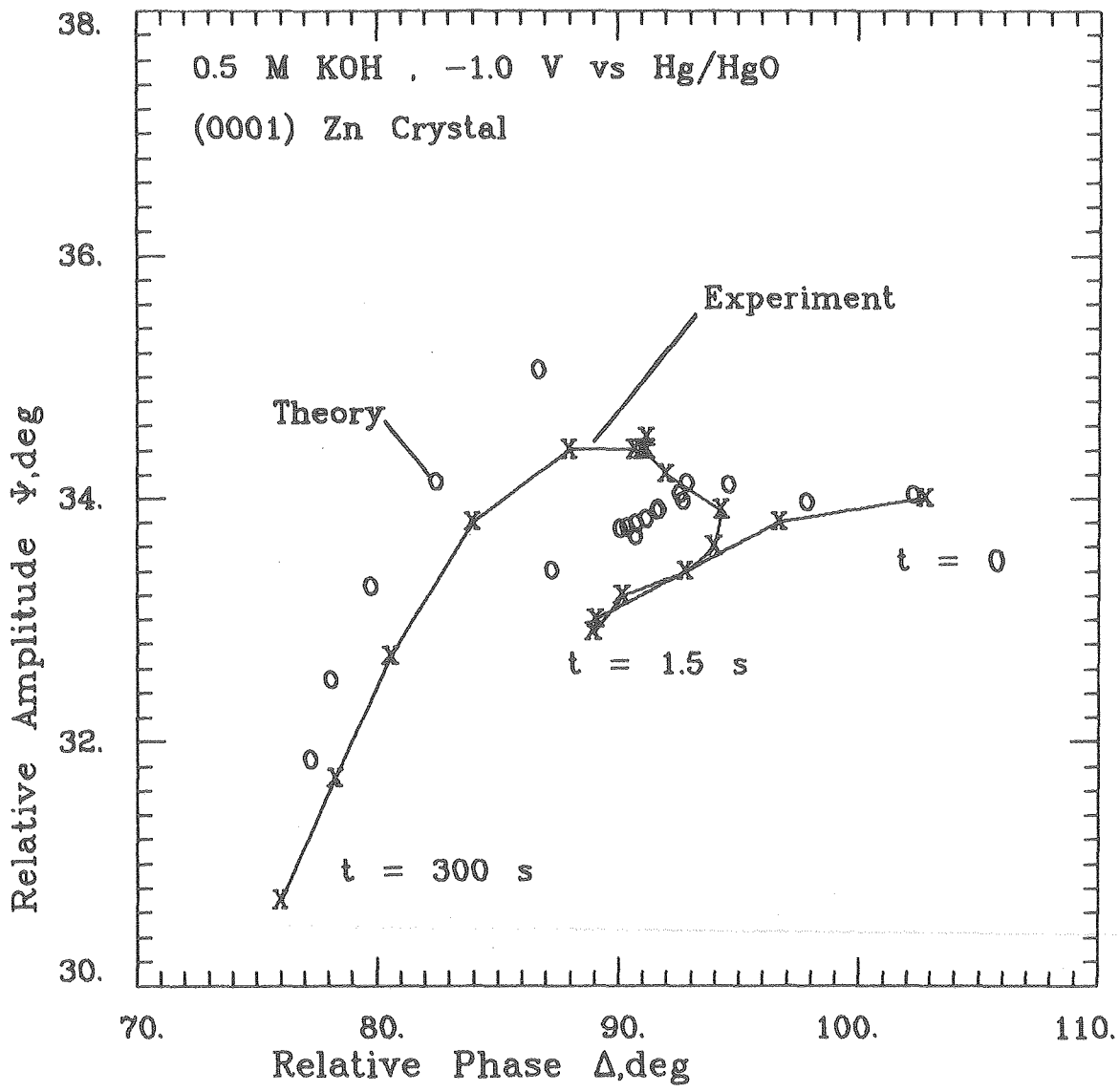

XBL 787-9511

Figure 59. Interpretation of ellipsometer measurements (Exp. Zn 70-23). Segment t = 0 to 1.5 s due to substrate roughening.

values of Δ and ψ presented in Figure 59 were computed using the growth of a roughness layer covered by a 109 Å, 19% porous primary layer. The volume fraction of metal in the roughness layer was 0.51. The roughness layer could describe developing non-stoichiometry in the interior of the film.

10 mA/cm^2 (Exp. 70-10)

The interpretation presented in Figure 60 used patchwise film formation to compute the theoretical values of Δ and ψ. Film formation began on 20% of the electrode surface and after 15 seconds, the 440 Å thick primary layer covered 70% of the surface. During this interval, the porosity of the primary layer decreased from 14.3% (volume) electrolyte to 5.6%. The roughness layer containing 48% (volume) metal was 100 Å thick at the end of this period.

Figure 60 indicates that the theoretical curve is shifted to the left of the experimental curve. The hydrate layer contained 98% electrolyte. The use of an initially concentrated hydrate layer which is depleted with time would eliminate much of the deviation between experiment and theory.

The optical effect cannot be due to zinc cations, as the initial concentration necessary to shift Δ by 10 deg is about 2.5 M (Fig. 6a), while the solubility of zinc is only 10^{-3} M.

Film Formation in 6 M KOH Electrolyte

Stagnant Electrolyte, 100 mA/cm^2 (Exp. Zn 70-61)

The topography of the anodic film formed at 100 mA/cm^2 is shown in Figures 61 and 62. The secondary crystals have a pyramidal shape

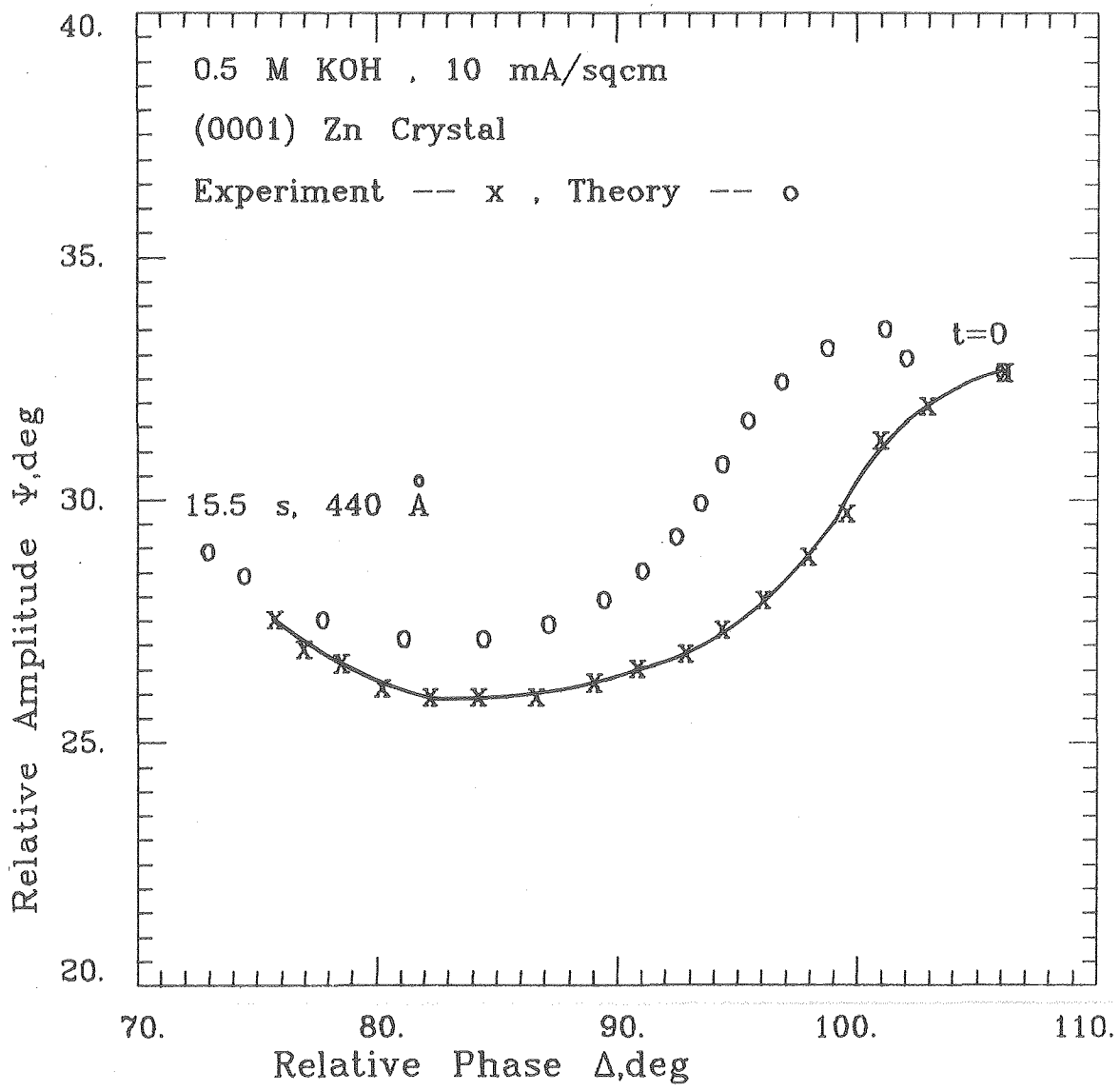

XBL 787-9536

Figure 60. Interpretation of ellipsometer measurements (Exp. Zn 70-10), without consideration of hydrate layer. Primary layer thickness along the curve.

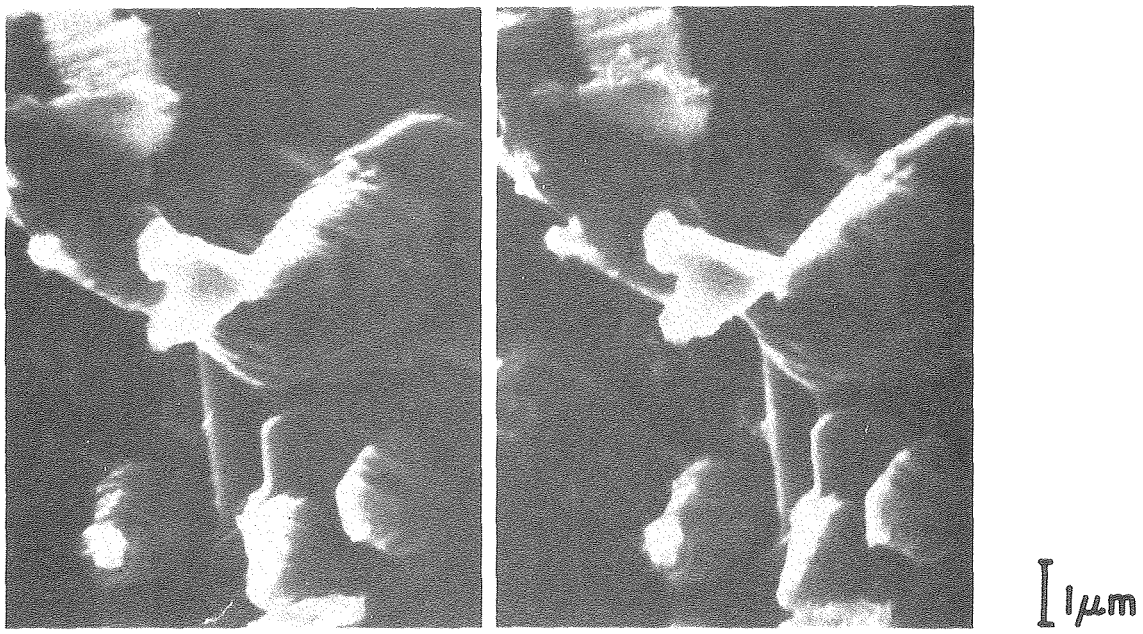

ANODIC ZINC OXIDE

Stagnant 6 M KOH, 100 mA/cm^2, 120 s, (0001) Zn

XBB 786-6978

Figure 61. Scanning electron micrographs of zinc oxide. Stereo pair. Pyramidal shape of secondary oxide crystals.

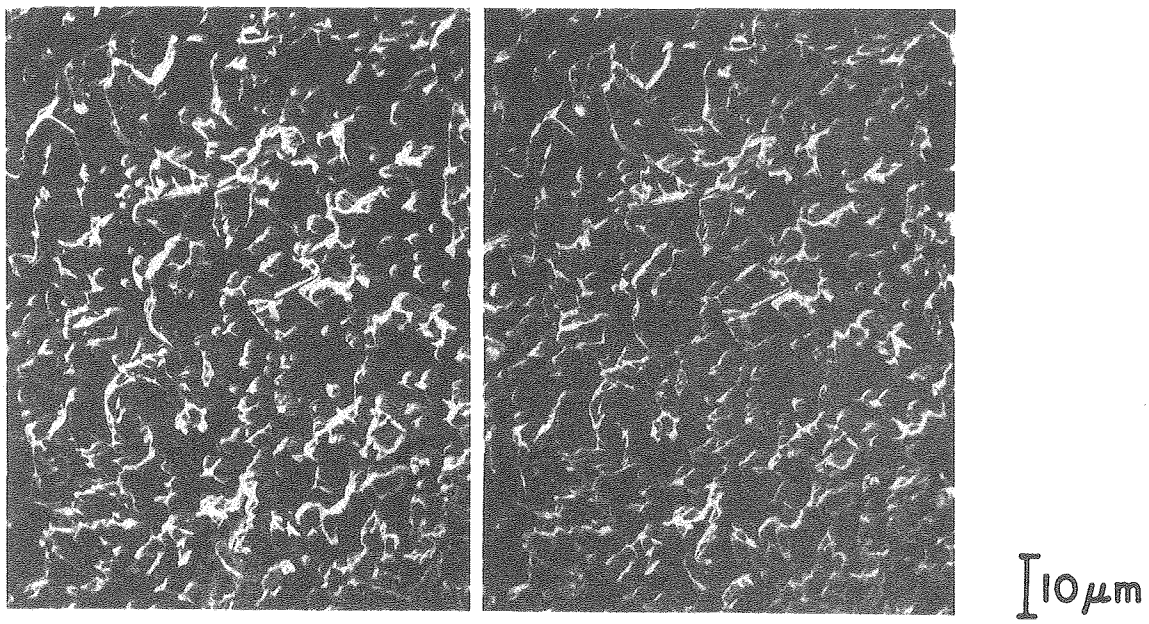

XBB 786-6977

Figure 62 Scanning electron micrographs of zinc oxide. Stero pair, uniformity of secondary crystal distribution.

and do not completely cover the electrode surface. Ellipsometer observations are presented in Figure 63. Three portions of the experimental curve are distinguishable.

The initial portion of the experimental curve was interpreted using roughening of the metal substrate and the growth of a MTBL with the interfacial refractive index determined by the surface coverage of adsorbed zinc oxide. The large initial decrease in ψ between the first and second experimental points was not satisfactorily reproduced by the square-ridge roughness model (Section IV). The observations cited in the qualitative zinc oxide results (p. 155) indicate it is possible that the initial decrease in ψ is due to the removal of a surface phase produced by corrosion which fractionally covers the electrode surface.

The surface coverage of adsorbed species θ was computed using a Langmuir isotherm ((G 26), Section IV, p.)

$$\frac{\theta}{1 - \theta} = a_i e^{-\Delta G/RT} . \qquad (66)$$

The activity of the zinc species in the electrolyte having the interfacial concentration determined from the Sand equation was computed using eq. (67)

$$a = 0.735 + 6.13\ C . \qquad (67)$$

Equation 67 is a least-squares fit of experimental data found in the literature (G27).

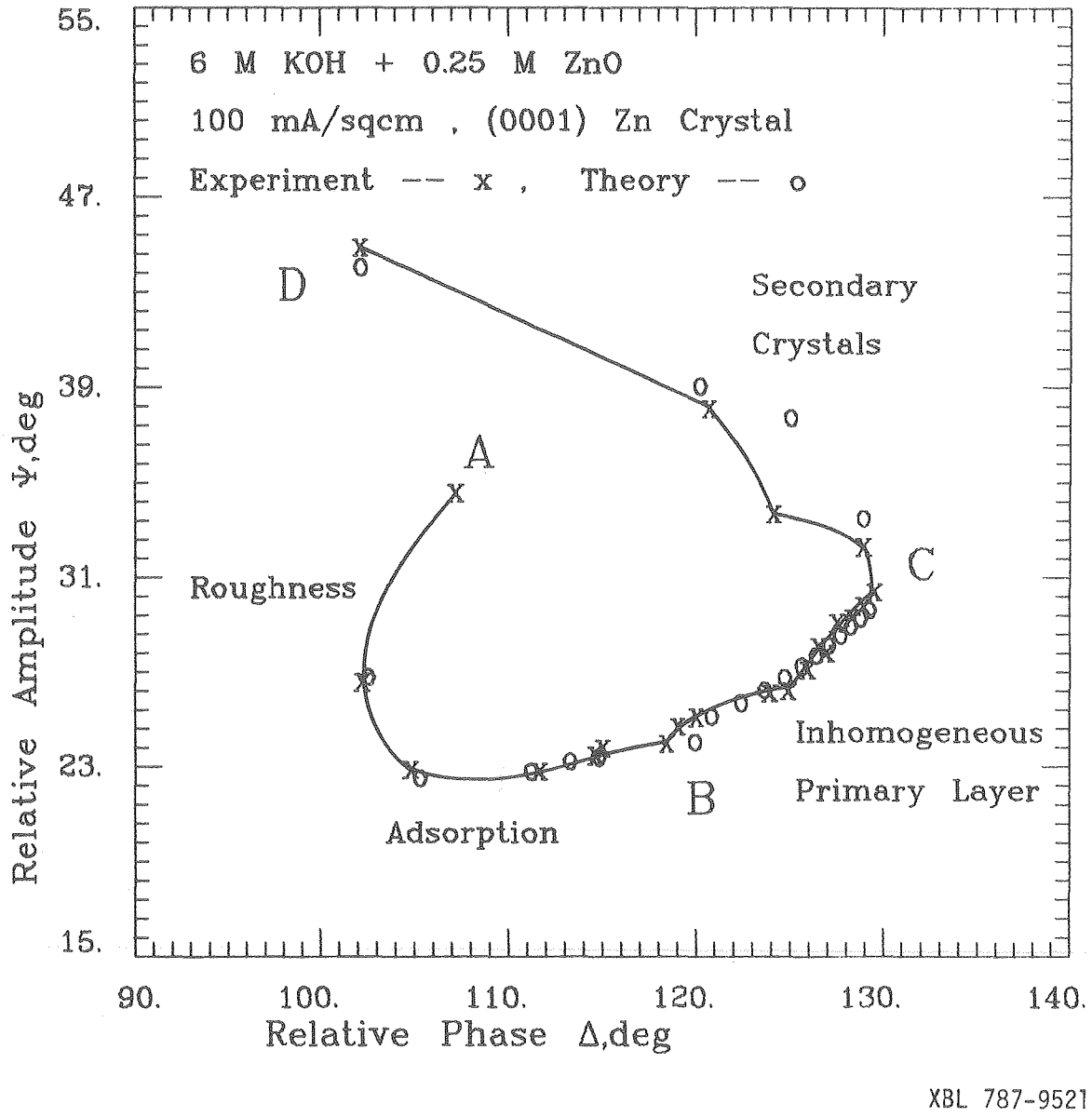

Figure 63. Interpretation of ellipsometer measurements (Exp. Zn 70-61). Optically dominant processes indicated along the curve.

The parameters evaluated by the computational procedure are given in Table VII.

Table VII. Adsorption of Zinc Oxide Parameters Derived from Ellipsometer Measurements. 6 M KOH (stagant), 100 mA/cm^2, (0001) Zn.

Free Energy of Adsorption	1.47 ± 0.24 kcal/mole
Volume Fraction Metal in Roughness Layer	0.39 ± 0.07
Current Fraction Forming Roughness	0.14 ± 0.02

At point B in Figure 63 (t = 30 s), an inhomogeneous Type I film begins forming. The porosity of the film was assumed to increase parabolically with film thickness, and the film was divided into five sublayers to describe the inhomogeneity. The porosity at the bottom of the film was 0.30% (volume) electrolyte, and the porosity at the top of the film was 85%. At point C, (130 s) the primary layer was 57 Å thick. Secondary crystals were growing during this period, but their optical effect was negligible.

The optical effect of the secondary crystals becomes important at point C. For the theoretical values of Δ and ψ along segment $\overline{CD}$, the crystallization rate of the secondary crystals was 93 mA/cm^2, the width to height ratio of the crystals was 0.13, and the crystals were strongly hydrated, containing 75% (volume) water. The crystals were treated optically as homogeneous films, and coherent superposition was used to average the reflection coefficients for the covered and

uncovered portions of the surface. The surface coverages were computed using the projection along the light propagation vector.

Stagnant Electrolyte, 200 mA/cm^2 (Exp. Zn 70-62)

For the first 5 experimental points in Figure 64, the electrode potential was constant at -0.93 volts. The free energy of adsorption determined by the interpretation was 1.76 ± 0.28 kcal/mole. This value agrees exactly with the free energy computed for another 200 mA/cm^2 experiment, 70-58. After 10 seconds, the potential begins increasing in correspondence to a change in slope of the $\Delta - \psi$ curve. An abrupt decrease in Δ occurs at time $t = 30$ s , and at this moment the potential jumps from -0.72 v to + 1.00 volts. The thickness of the compact primary layer at passivation was computed as 206 Å.

The anodic current was turned off immediately upon passivation. Figure 64 shows major changes in the ellipsometer parameters occurring after the current interruption. This portion of the experimental curve is uniquely characteristic of the growth of a compact primary layer which completely covers the electrode surface.

Stagnant Electrolyte, 500 mA/cm^2 (Exp. Zn 70-63 B)

The theoretical values of Δ and ψ in Figure 65 only qualitatively reproduce the experimental values. The downward trend in ψ is an indication that roughening of the electrode is significant. Film growth certainly continued after the current was interrupted upon passivation. The free energy of adsorption determined from the measurements was 6.3 ± 3.3 kcal/mole.

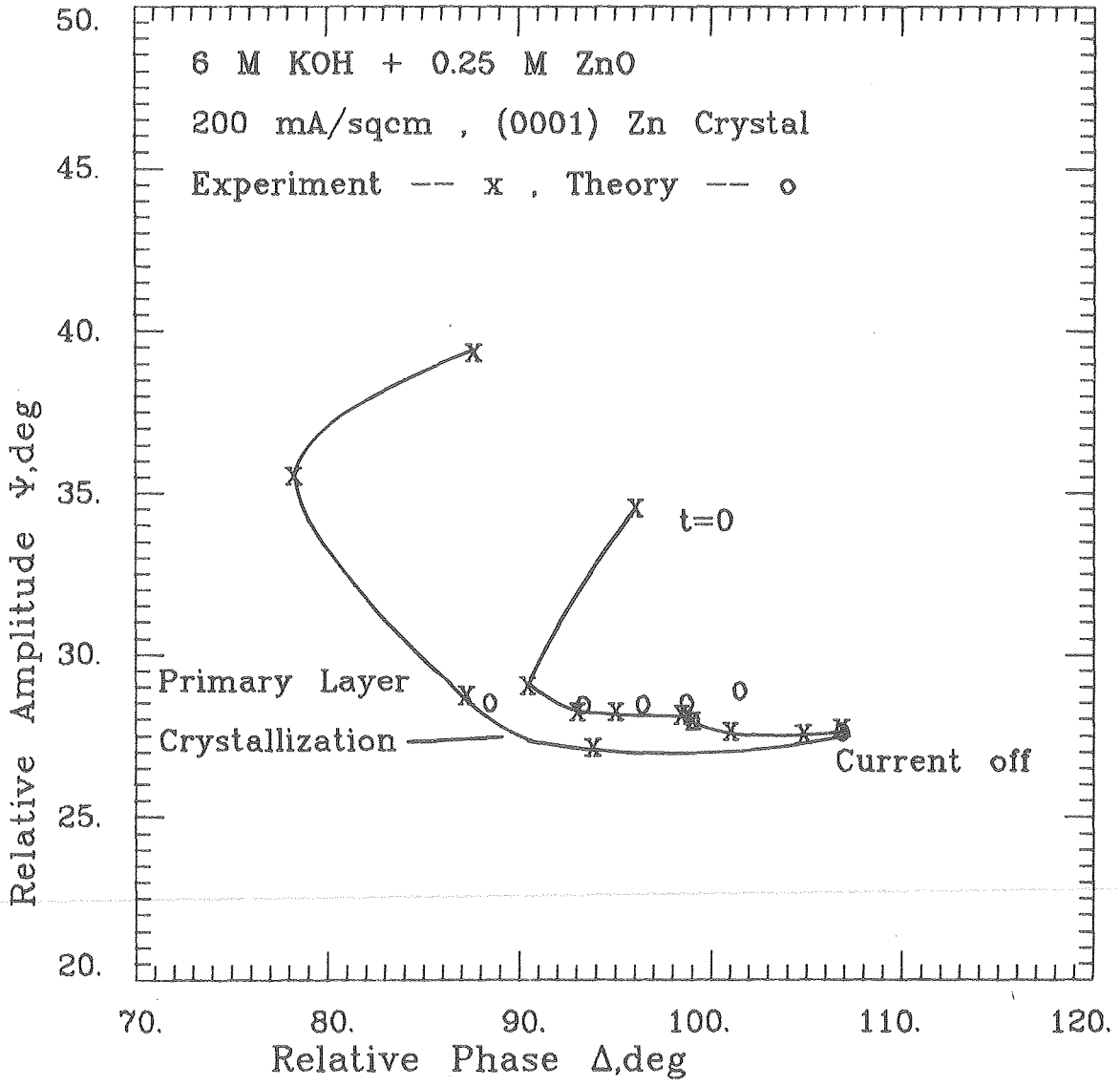

Figure 64. Interpretation of ellipsometer measurements (Exp. Zn 70-62). Growth of compact film after current is turned off.

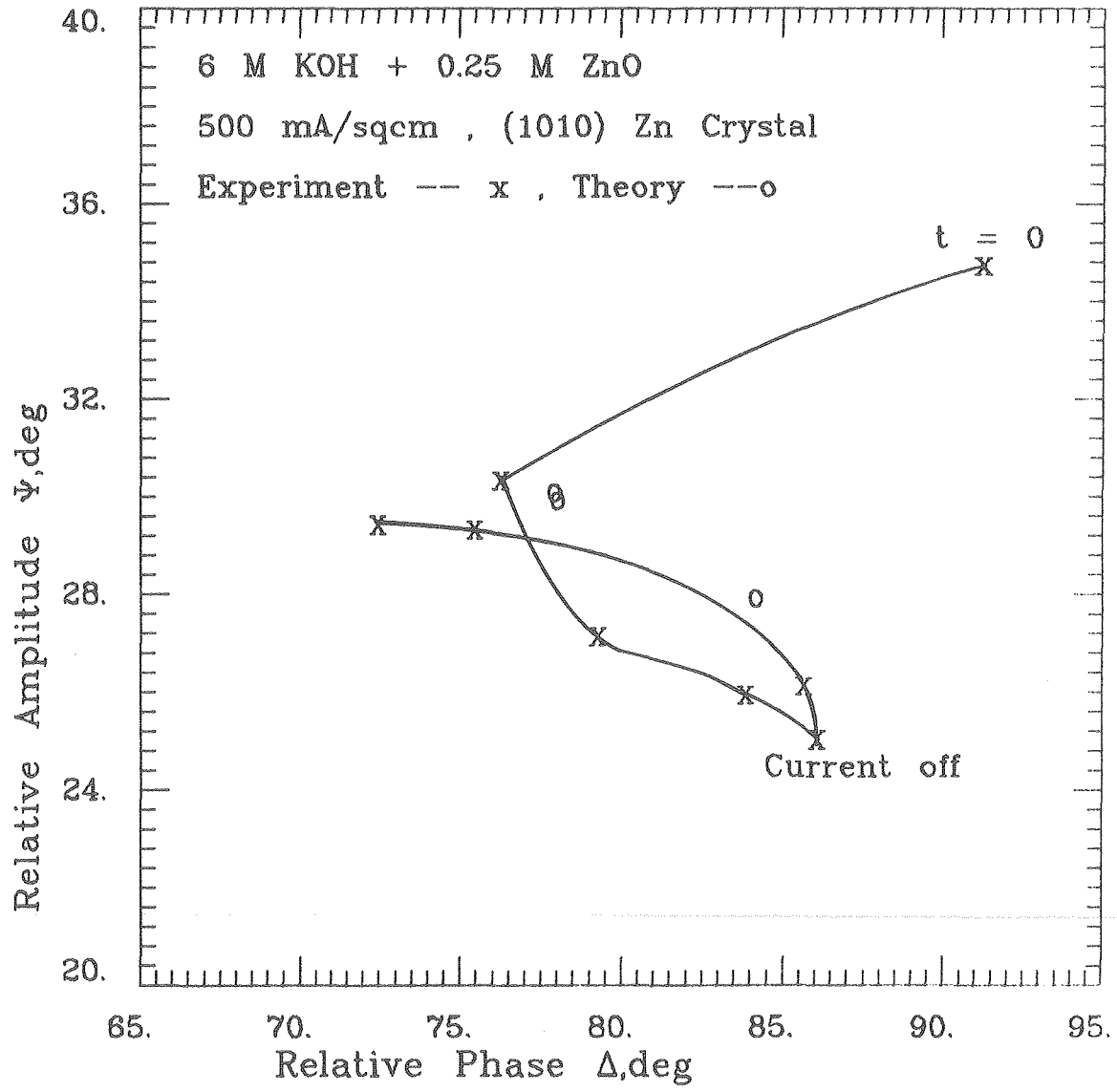

XBL 787-9534

Figure 65. Interpretation of ellipsometer measurements (Exp. Zn 70-63B). Continued film growth after current interruption.

Forced Convection Experiments (6 M KOH)

Figures 66-70 show scanning electron micrographs of anodic films formed under forced convection mass transport conditions. Lateral growth is favored over the pyramidal growth observed in stagnant electrolyte. The films are thicker and more compact downstream, indicating that dissolved species are being transported. The films are more compact at high current densities and low Reynolds numbers. The film morphology is greatly affected by the crystallographic orientation of the zinc substrate. Film formation is absent at high Reynolds numbers (Fig. 70) unless the current density is large enough to provide the degree of supersaturation necessary for film formation.

900 Re, 400 mA/cm^2 (Exp. Zn 200-21)

The general features of the experimental $\Delta - \psi$ curve shown in Figure 71 are similar to the curves for stagnant electrolyte, with the exceptions that the inhomogeneous Type I film and the initial decrease in ψ are absent. For the time interval $0 < t < 6.3$ s, the theoretical values of Δ and ψ were computed using adsorption of zinc oxide. The only parameter determined by the computational procedure, the free energy of adsorption, had the value 3.25 ± 0.43 kcal/mole. The average deviation between experiment and theory was 0.97 deg.

Beginning at time $t = 6.3$ seconds, the rapid formation of a porous (0.36 volume % electrolyte) primary layer leads to the passivation of the electrode. The thickness of this layer reaches 2500 Å after 2 seconds.

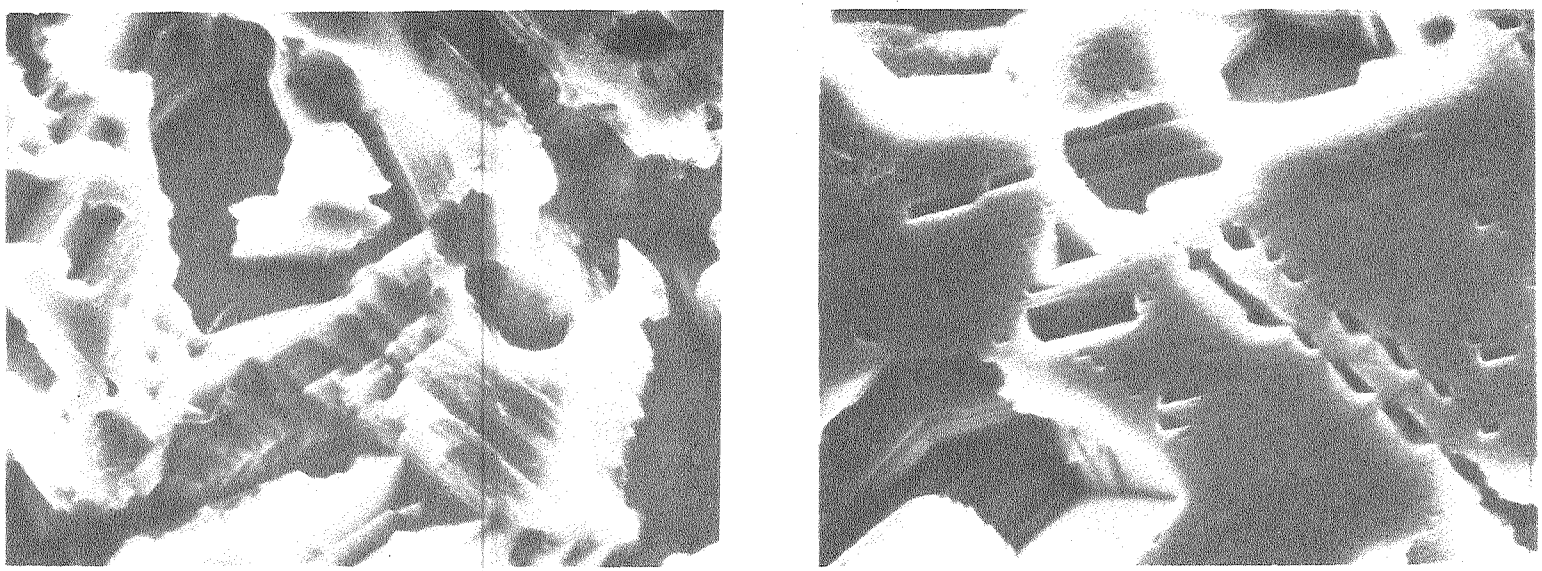

Figure 66. Scanning electron micrographs of zinc oxide. Effect of distance from the leading edge.

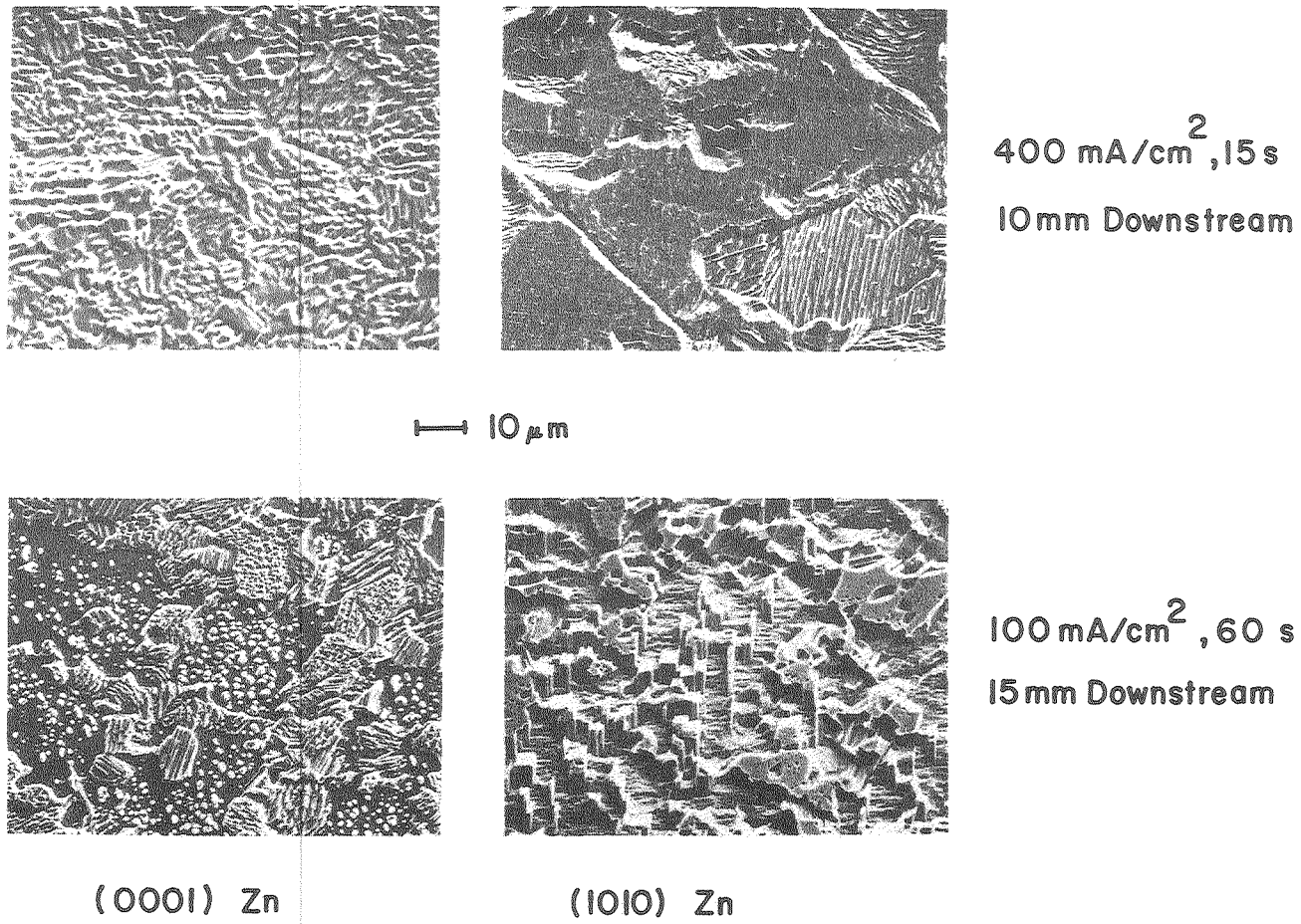

Figure 67. Scanning electron micrographs of zinc oxide. Effect of distance from the leading edge.

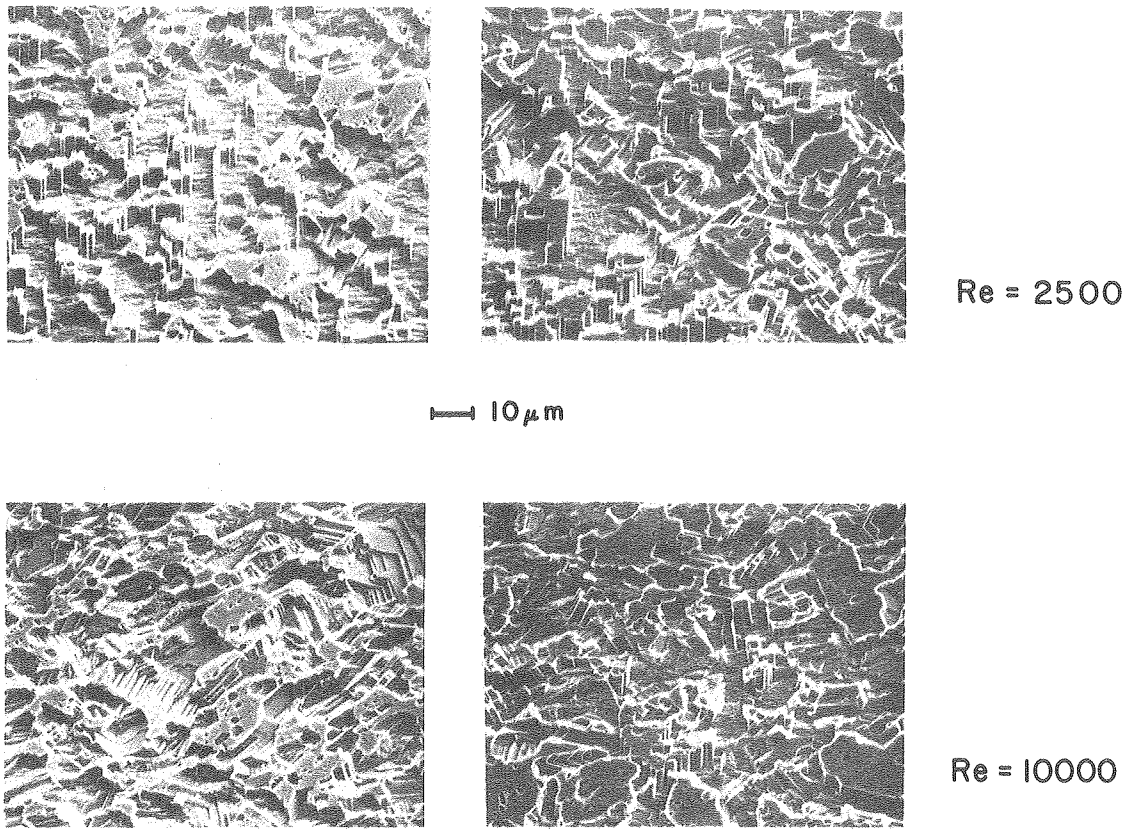

XBB 786-7629

Figure 68. Scanning electron micrographs of zinc oxide. Effect of distance from the leading edge.

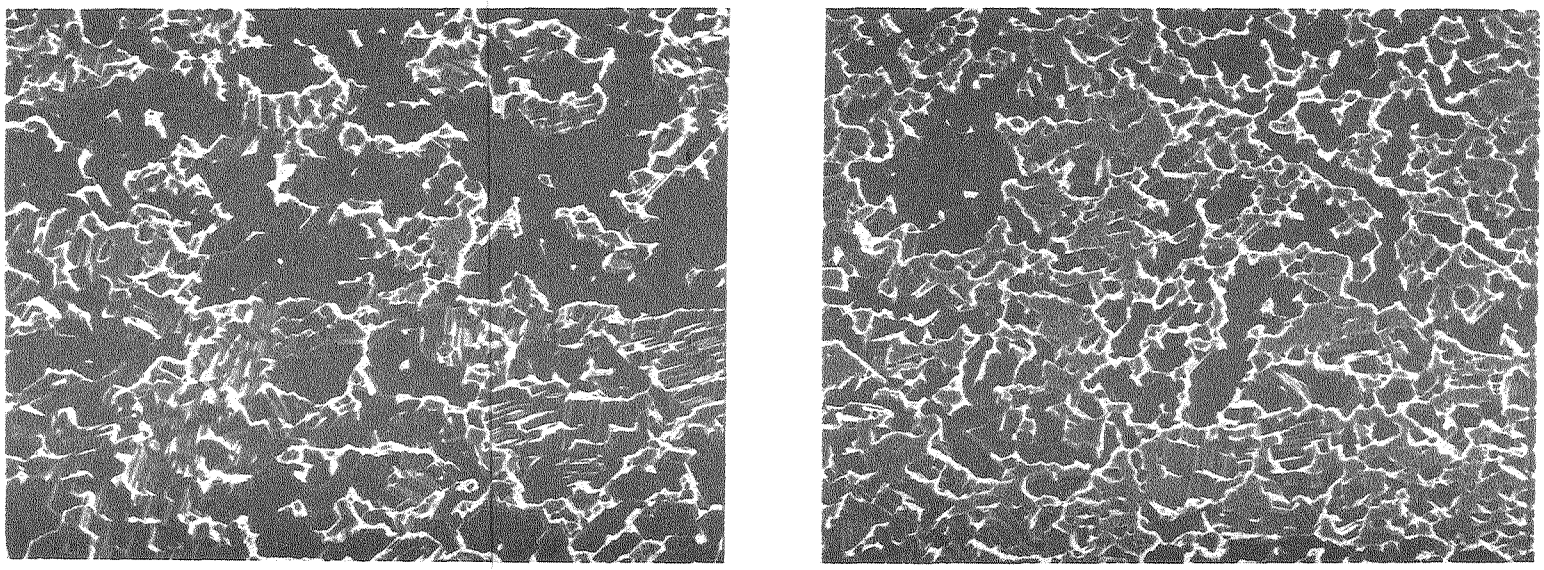

Figure 69. Scanning electron micrographs of zinc oxide. Effect of distance from the leading edge.

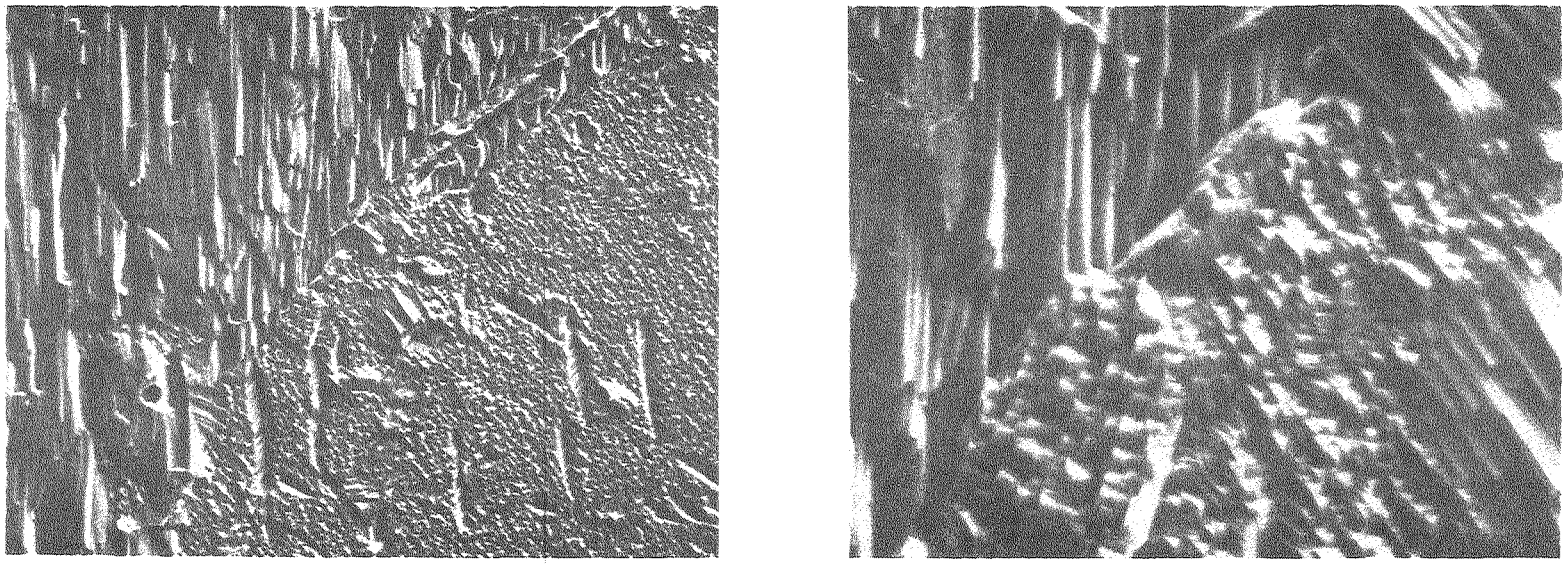

XBB 786-7625

Figure 70. Topography of polycrystalline zinc substrate near a grain boundary.

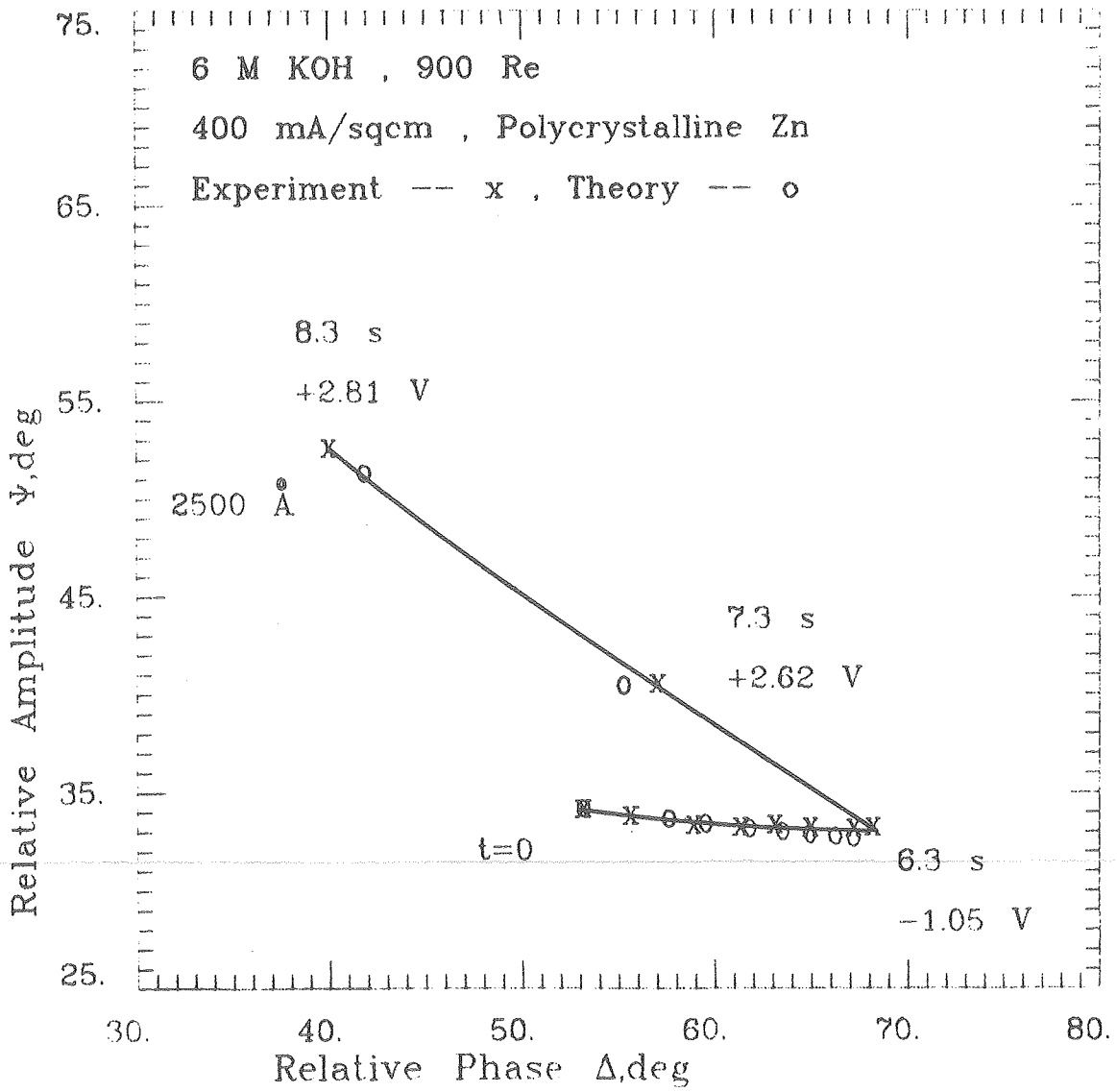

Figure 71. Interpretation of ellipsometer measurements (Exp. Zn 200-21). Primary layer thickness indicated along the curve. Absence of Type I film under flow conditions.

3000 Re, 200 mA/cm^2 (Exp. Zn 200-18)

The free energy of adsorption determined by the interpretation of the curve $\overline{AB}$ in Figure 72 had the value 2.72 ± 0.05 kcal/mole . The average deviation between experiment and theory was 1.5 deg. The curve $\overline{BC}$ was interpreted using the growth of secondary crystals containing 67% (volume) water. The thickness of the layer after 55 seconds was 1 μm.

4500 Re, 458 mA/cm^2 (Exp. Zn 200-22)

The free energy of adsorption for the initial portion of the experimental curve presented in Figure 73 was 3.11 ± 0.37 kcal/mole . The electrode passivates after 4 seconds, and the thickness of a 24% porous primary layer was 2100 Å at $t = 5.7$ s.

9000 Re, 500 mA/cm^2 (Exp. Zn 200-39)

For the interpretation of the experiment presented in Figure 74, the free energy of adsorption was 3.74 ± 0.43 kcal/mole . The electrode does not passivate, which illustrates the role of mass-transport in the anodic processes. After 15 seconds the thickness of a 15% porous primary layer was 2600 Å, and the secondary crystal layer was 16 μm thick.

11000 Re, 472 mA/cm^2 (Exp. Zn 200-34)

For the interpretation of the initial increase in Δ observed experimentally (Figure 75), adsorption was negligible. The increase in Δ is due to ionic zinc, as indicated in Figure 76. The concentration

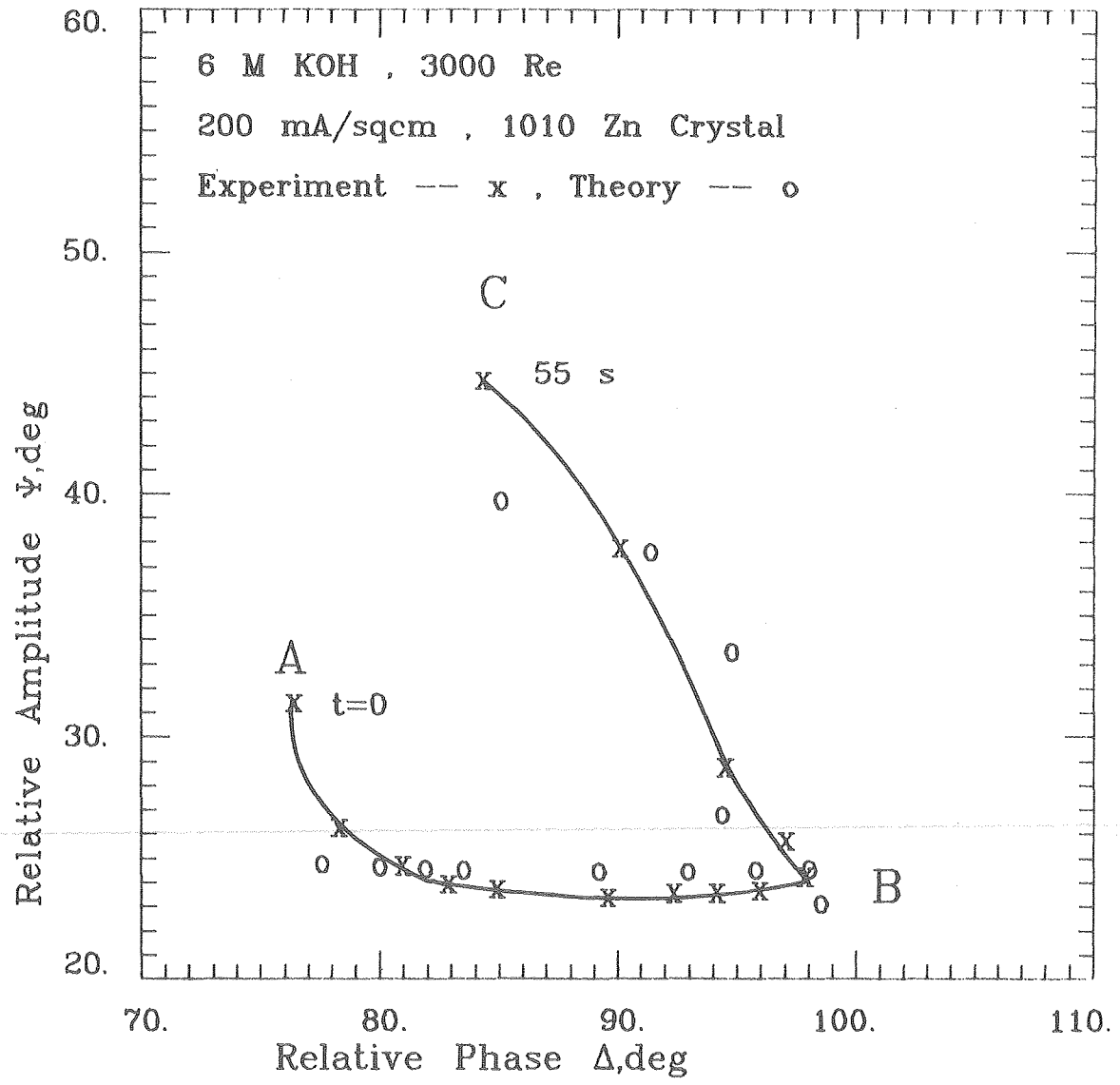

XBL 787-9664

Figure 72. Interpretation of ellipsometer measurements (Exp. Zn 200-18). Accumulation of dissolved species followed by film formation.

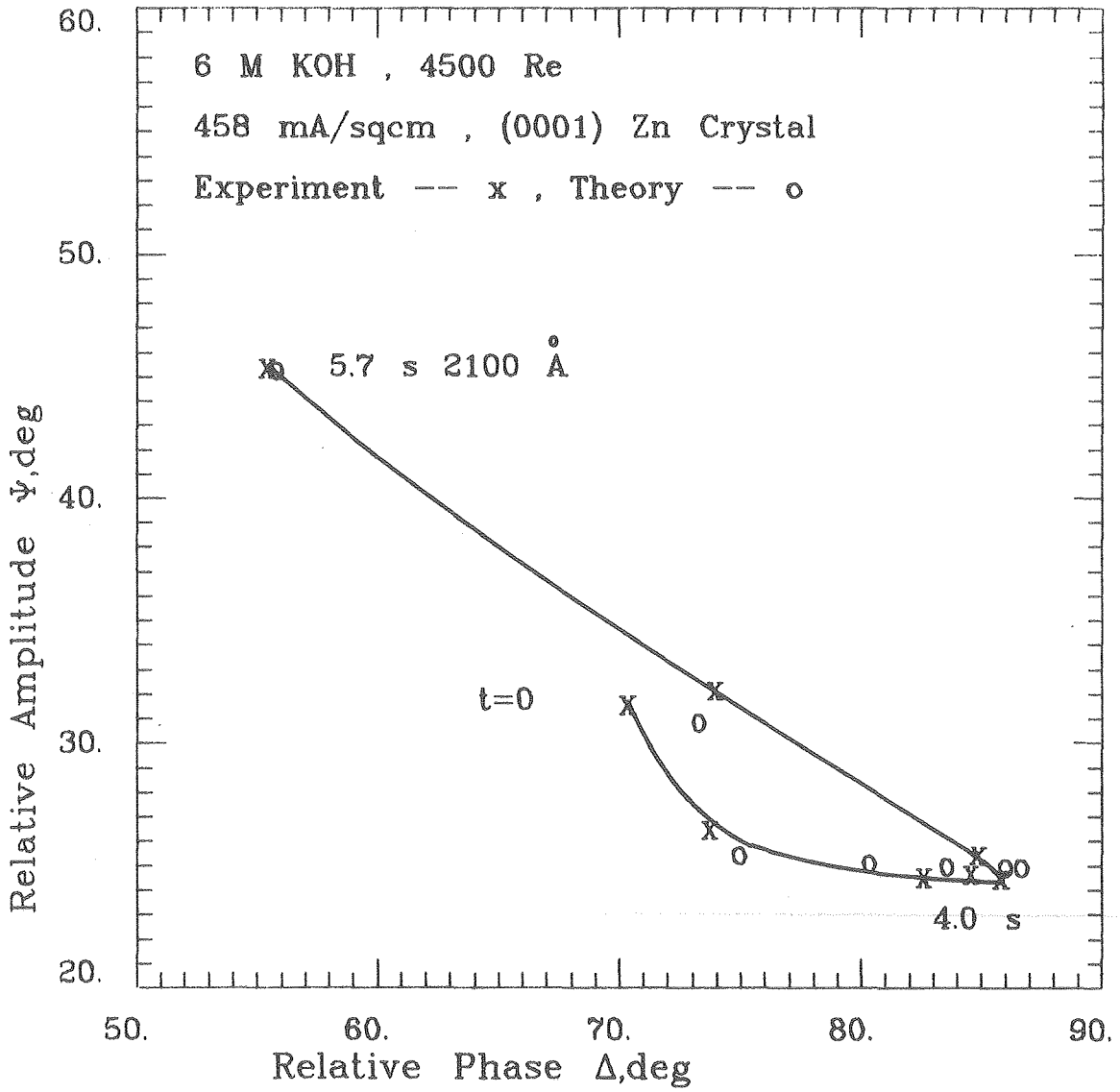

Figure 73. Interpretation of ellipsometer measurements (Exp. Zn 200-22). Primary layer thickness indicated along the curve.

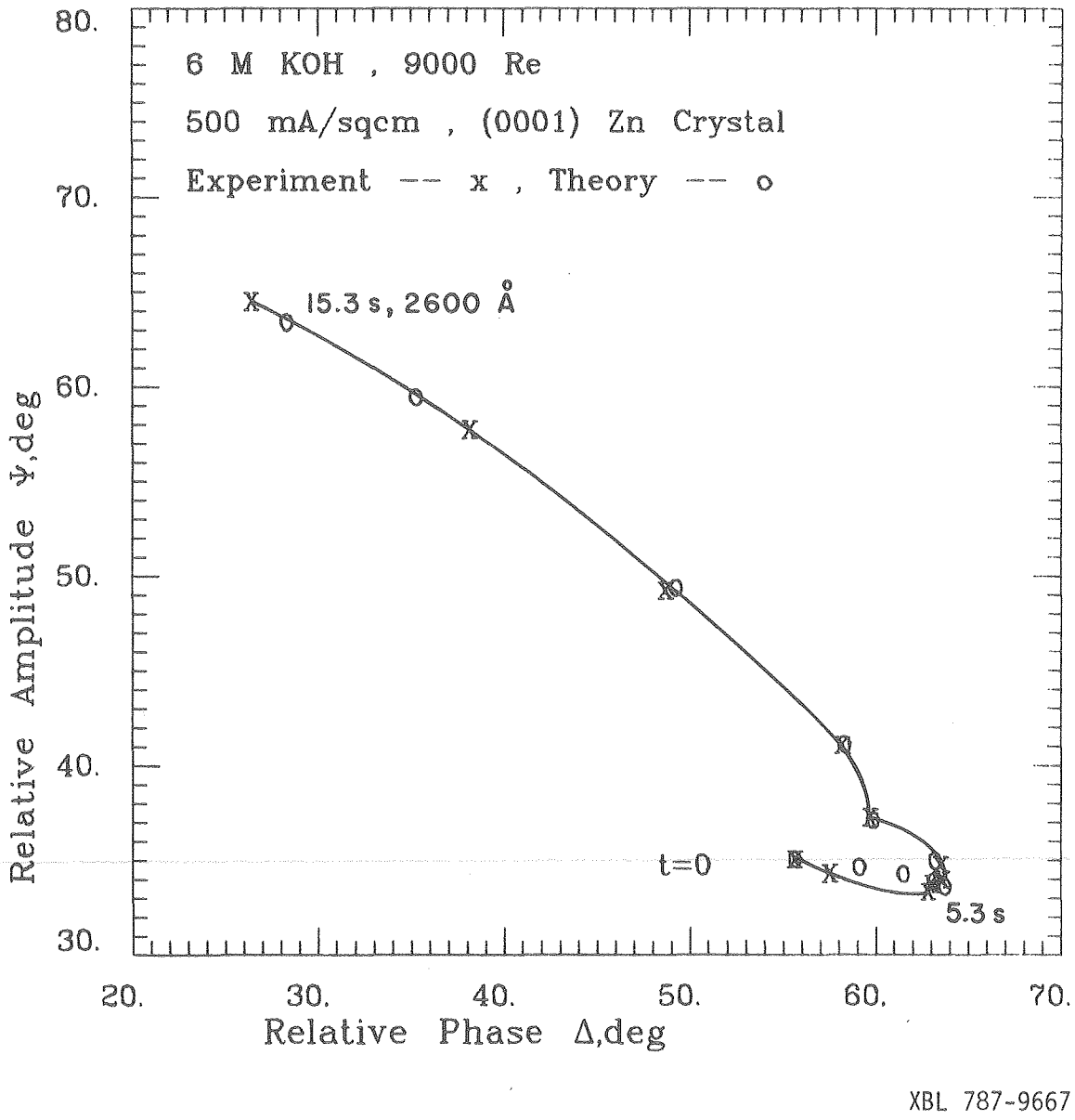

Figure 74. Interpretation of ellipsometer measurements (Exp. Zn 200-39). Primary layer thickness indicated along the curve.

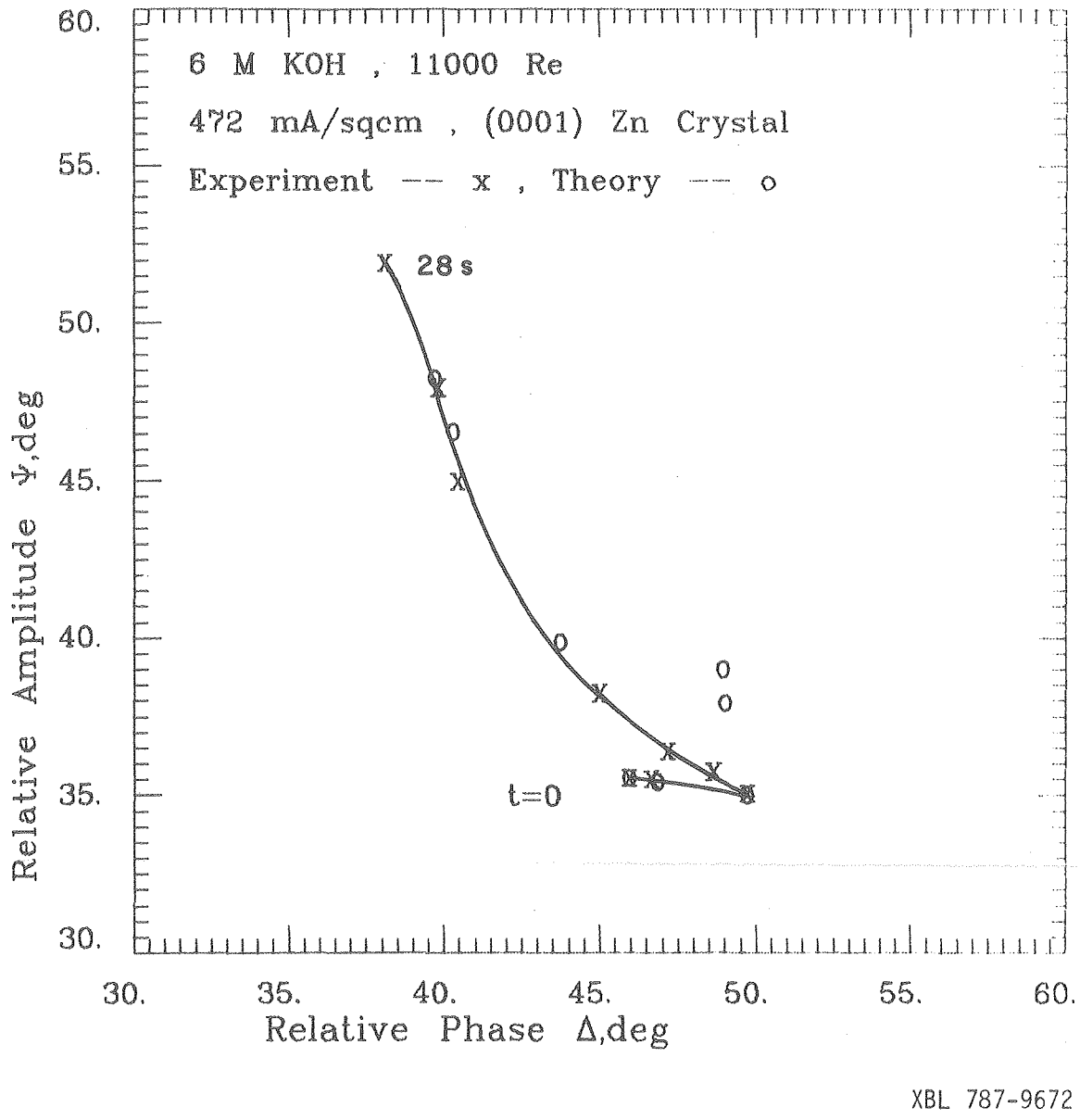

Figure 75. Interpretation of ellipsometer measurements (Exp. Zn 200-34).

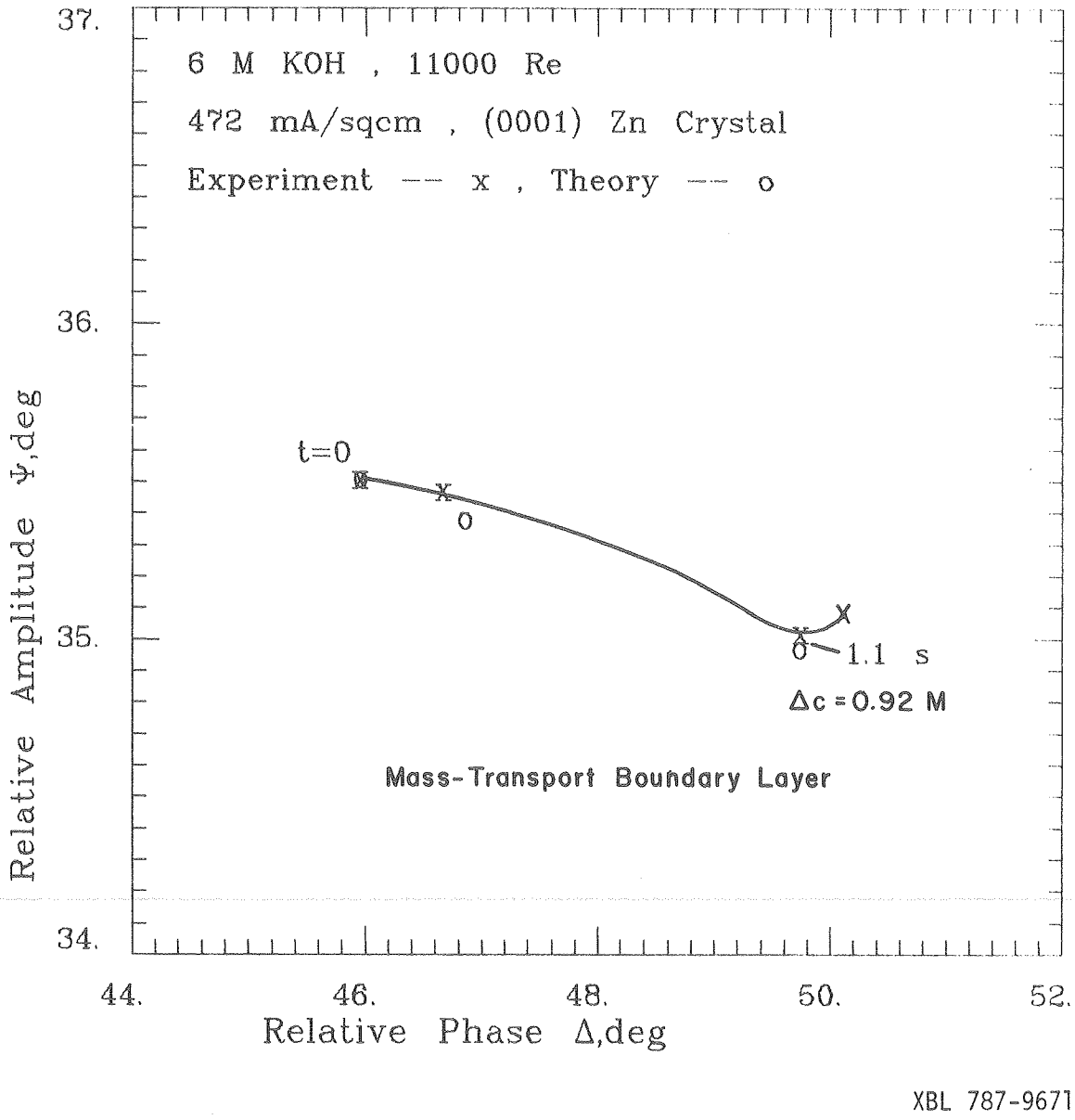

Figure 76. Optical effect of the mass-transport boundary layer formed during zinc dissolution.

of zinc at the interface reached 0.92 M after 1.1 seconds. The use of the Sand equation (eq. 12) to describe the change with time of the interfacial concentration resulted in an average deviation between experiment and theory of 0.13 deg.

The growth of the anodic film (Fig. 75) was only qualitatively reproduced by theoretical computations. After 28 seconds, a compact primary layer 540 Å thick completely covered the surface, and a 21 μm thick layer of secondary crystals (75 volume percent water) fractionally covered the surface.

Qualitative Comparisons

Figures 77-80 indicate the effects of electrode current density, electrolyte flow velocity, and substrate crystallographic orientation on ellipsometer observations. In Figure 77, the 200 mA/cm^2 curve rises more sharply than the 400 mA/cm^2 curve in the region where zinc oxide formation is dominant. This is characteristic of a more patchy or porous film forming at lower current densities. As the current density is increased, the rates of film formation become so fast that further increases produce only minor differences in the film characteristics, as indicated in Figure 78.

As increased electrolyte flow rates increase the mass-transport rate of the solution-phase zinc species, the supersaturation of zincate is lower at higher flow rates. Figure 79 illustrates that a very compact primary layer passivates the electrode at the lower Reynolds number, while at the high Reynolds number, a more porous film grows on the active electrode.

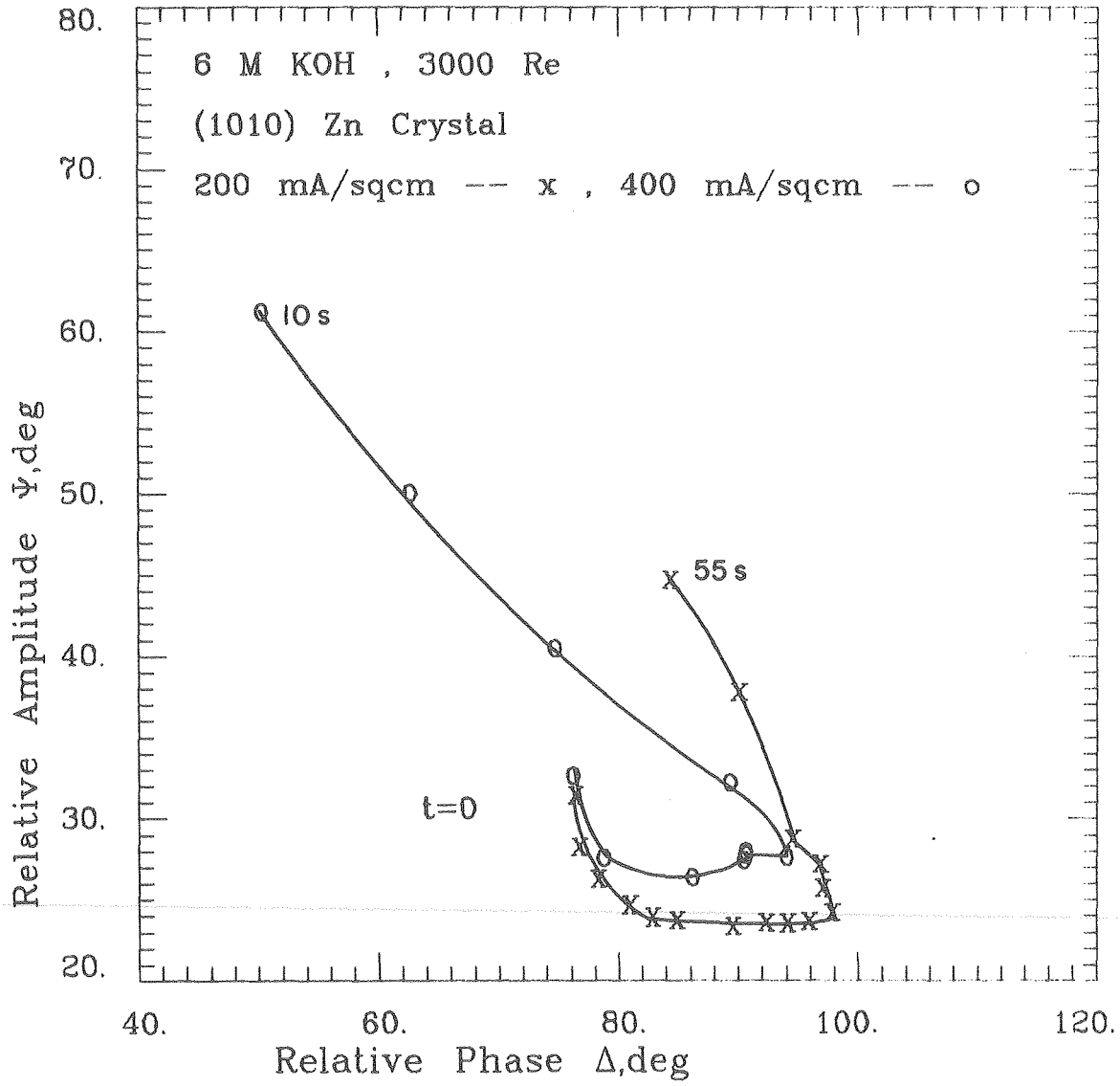

Figure 77. Variations in the optical properties of anodic zinc oxide films formed at different current densities experiments.

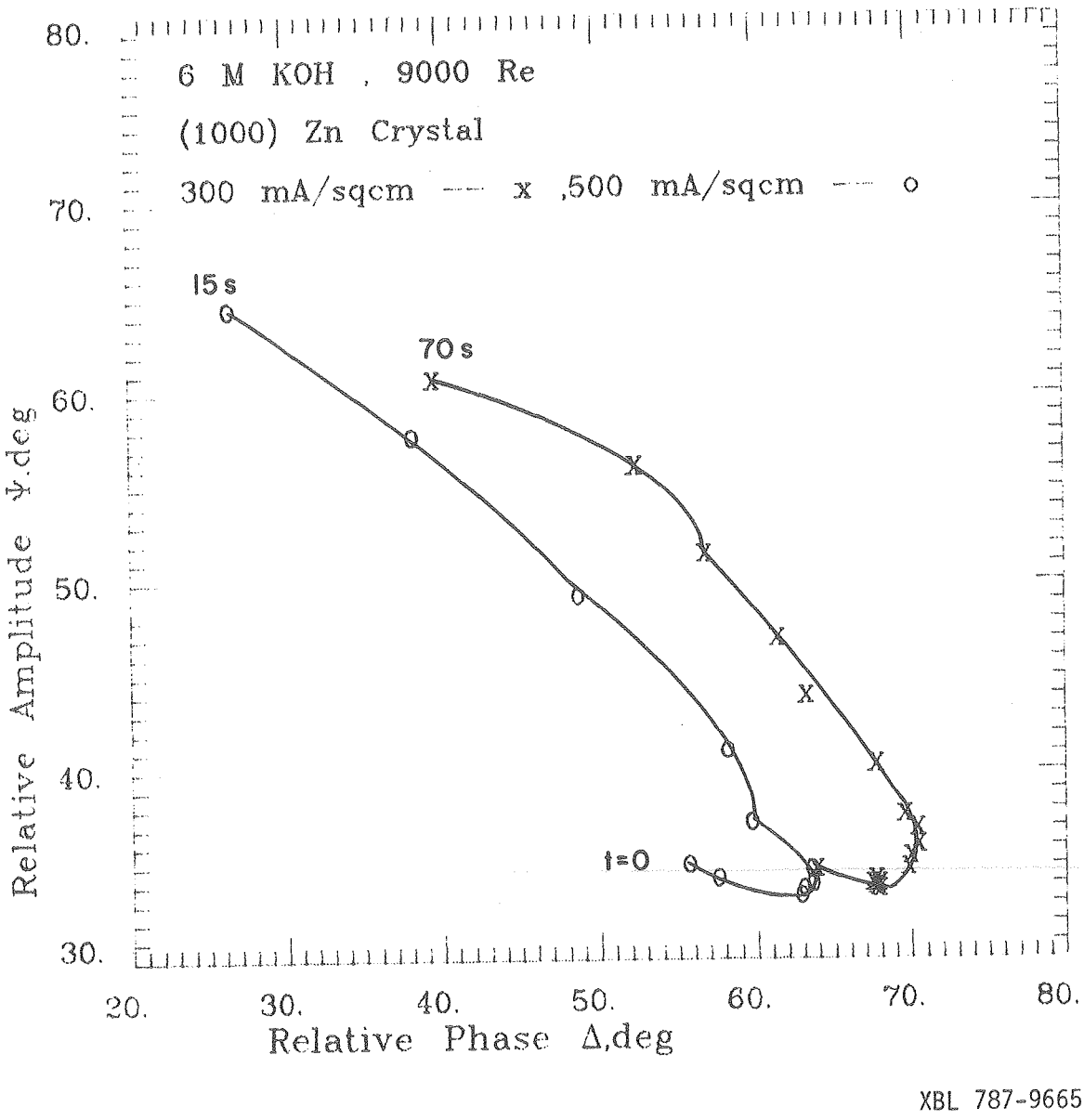

Figure 78. Variations in the optical properties of anodic zinc oxide films formed at different current densities experiments.

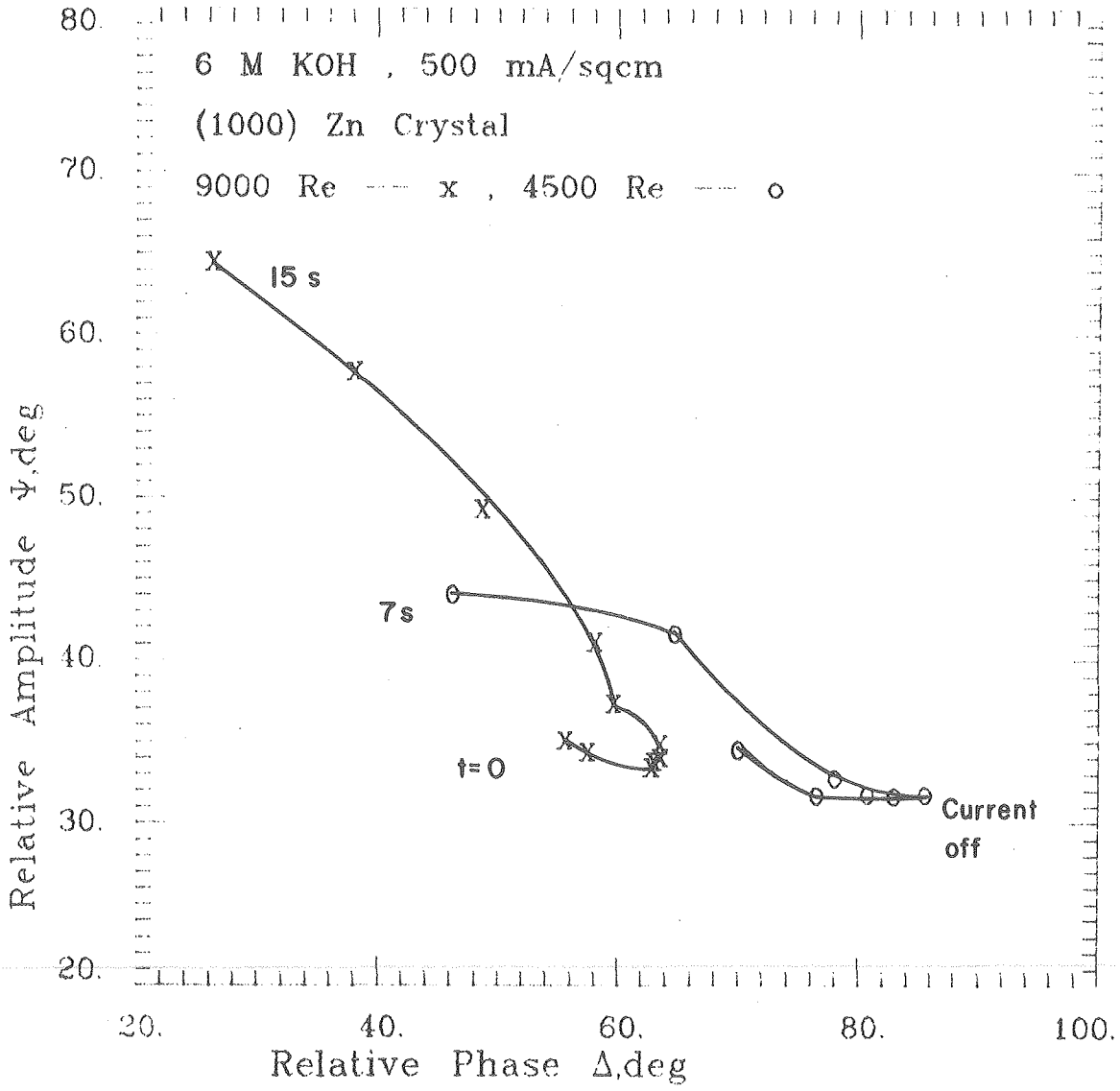

XBL 787-9668

Figure 79. Variations in the optical properties of anodic zinc oxide films formed under different mass-transport conditions. Passivation at lower flow rate indicated by current off.

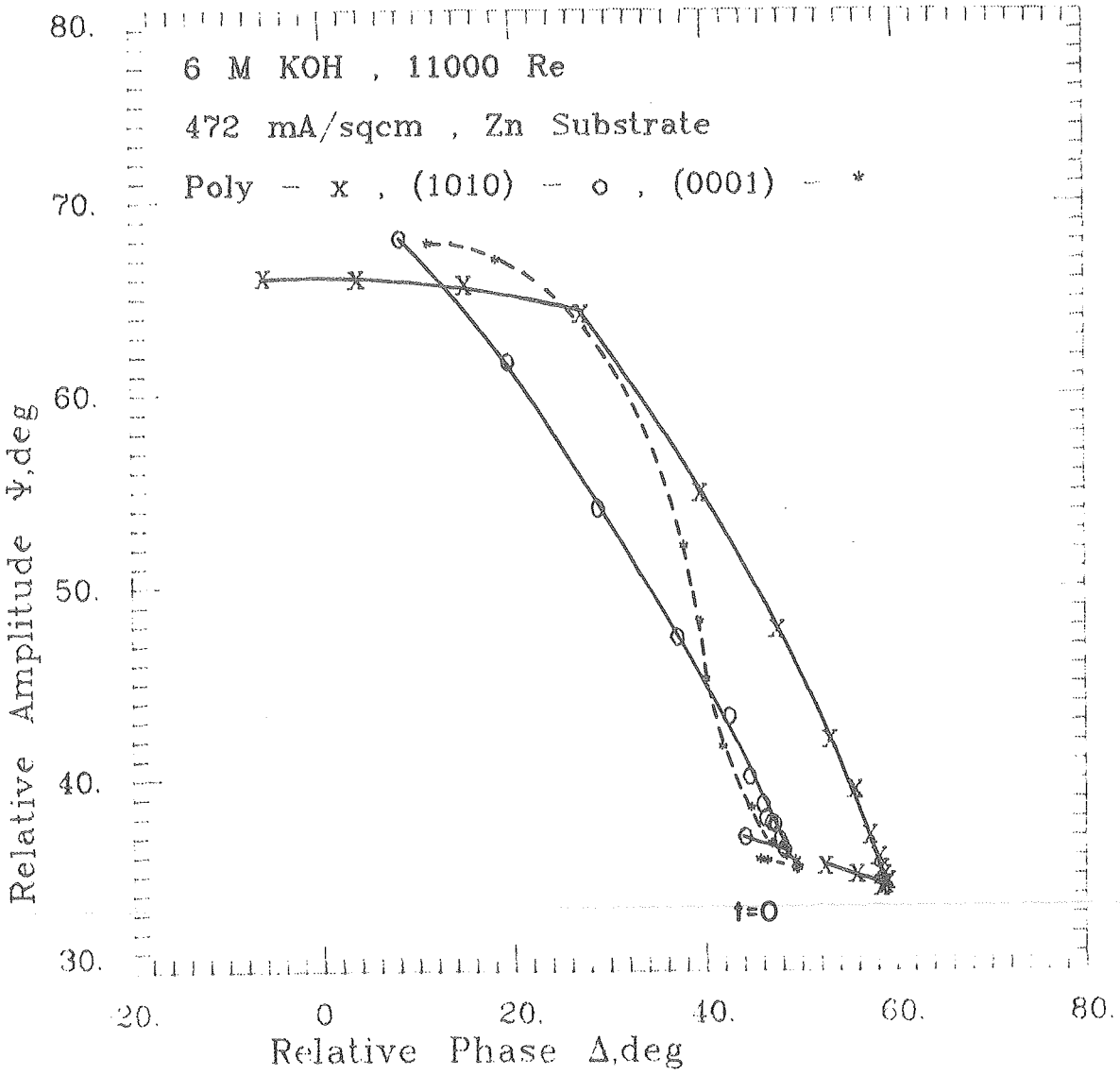

Figure 80. Variations with substrate orientation of the optical properties of anodic zinc oxide films.

for number sequence only

Only minor differences in the ellipsometer curves for different electrode orientations are observed, as shown in Figure 80. Macroscopic differences are apparent in scanning electron micrographs (Fig. 67). The large degree of disorder on a lateral scale larger than the wavelength of light is probably scattering much of the light beam. The anodic film shown in Figure 81 is not typical, but would scatter much less light. This film was observed on the downstream corner of an electrode. Immediately upstream, the electrode surface was not covered by an anodic film.

Interfacial Concentrations During Zinc Dissolution

The current interruption technique outlined in Appendix D was used to measure the interfacial concentrations of zinc during anodic dissolution in the flow cell. The results are given in Table VIII. Interfacial concentrations were computed for comparison using equations 14-16. Migration effects were neglected.

The interfacial concentrations measured in 1M KOH were consistently lower than the theoretical values, with the average deviation being about 20%. If depletion of the hydroxyl ion by complexing with zinc is negligible, the measurements indicate that the transference number ranges from 0.19 to 0.23. The solubility of zinc in 1 M KOH is about 10^{-2} M (Z16), and yet interfacial concentrations of 0.6 M were observed.

The interfacial concentrations measured in 6 M KOH agreed very well with theoretical values, especially at large flow rates (Re = 11400). In certain instances, notably the results obtained at a Reynolds number of 2700, adsorption of zinc appears to be present, as the measured

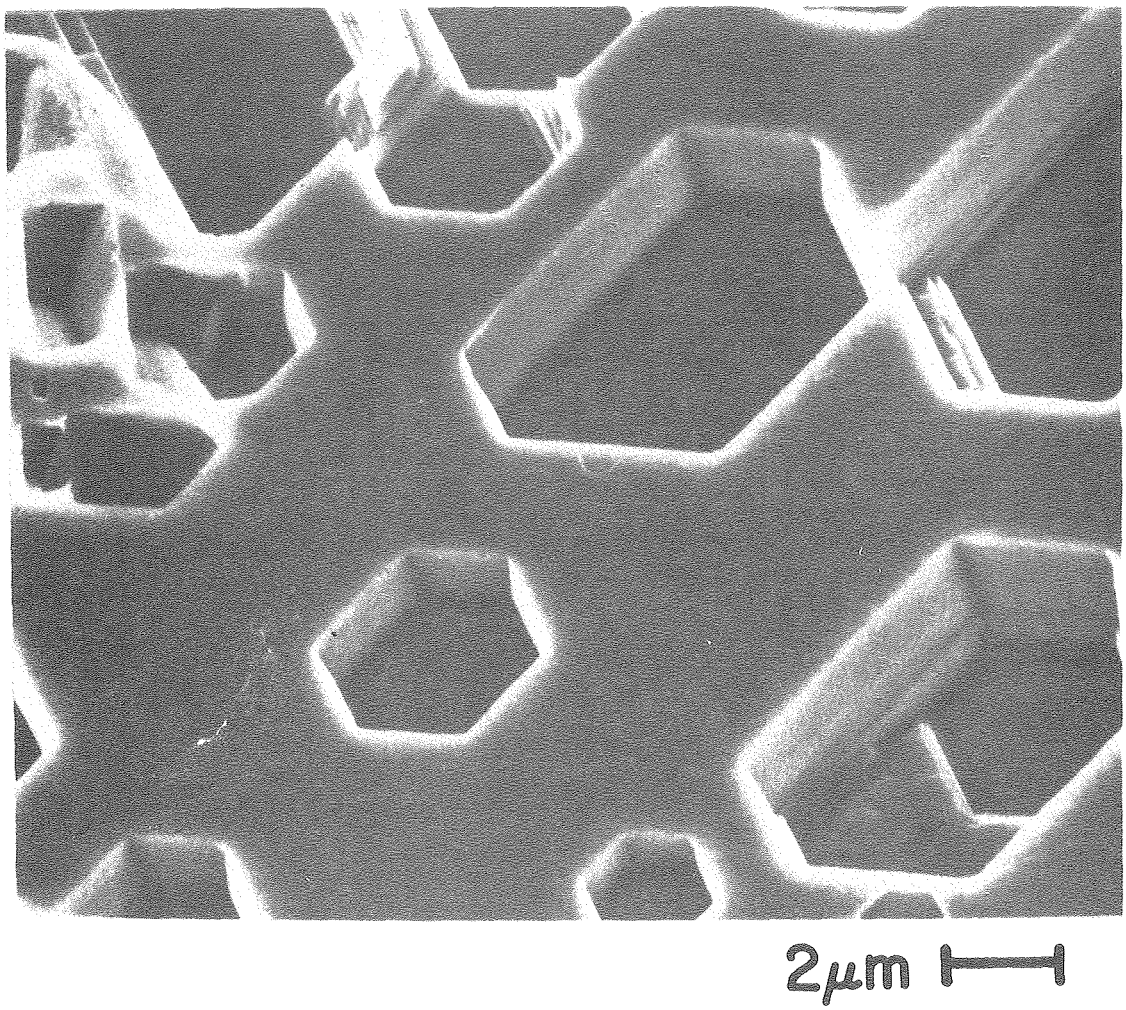

XBB 787-8247

Figure 81. Scanning electron micrograph of anodic zinc oxide.

interfacial refractive index would correspond to 2.75 M while the theoretical value is 1.47 M, and the solubility is 0.66 M.

For the computations, a diffusion coefficient of 9.7×10^{-6} cm^2/s was used. The refractive index of zincate solutions, as measured by a refractometer (G28) is a linear function of concentration,

$$n = n_{ref} + 0.00575\ C \tag{68}$$

where n_{ref} is the refractive index of the KOH solution in the temperature range $20° < T < 30°C$ and the wavelength of light range $435.8 < \lambda < 589.2$ nm . The refractive index-concentration relationship was measured for zincate concentrations up to 0.6 M. The linear relationship was extrapolated into the concentration ranges covered in Table VIII (Appendix F).

Table VIII. Interfacial Concentrations of Zinc Derived from Ellipsometer Measurements

Electrolyte	Re	i (mA/cm^2)	c_i(theory)	c_i(experiment)
1.025 M KOH	900	170	0.73 M	0.67
	2800	180	0.52	0.39
		250	0.72	0.60
	3000	241	0.69	0.62
	8000	180	0.31	0.25
		232	0.40	0.31
6.01 M KOH	1640	500	1.74	1.66
		750	2.61	3.00
	2700	400	1.18	1.41
		500	1.47	2.75
	3200	400	1.11	1.68
	3400	500	1.36	1.42
	11400	500	0.66	0.66
		750	0.99	0.99

VII. Discussion

Induction Periods at Low Current Densities

The major assumption which was used to correlate the induction periods with interfacial concentrations and diffusion coefficients is that film formation begins when the solubility limit of the cation is reached. If small but finite degrees of supersaturation are present, the interfacial concentrations are underestimated in eq. (10), and the diffusion coefficients in Table I are larger than the true values.

Silver Oxide Formation

The deviations between experiment and theory for all of the interpretations are larger than the experimental error in the values of Δ and ψ of about 0.5 deg. This indicates the evaluation of six or seven parameters by the computational procedure does not overspecify the system of equations in the representation of the electrode process. At least 40 experimental quantities(values of time, current density, Δ and ψ for 10 points) were used for each interpretation.

When large number densities of secondary crystals were present on the electrode surface, the computed degree of hydration of the crystals was consistently between 0.37 and 0.43 volume fraction water. Assuming the additivity of molar volumes, the volume fraction of water in $Ag_2O \cdot H_2O$ is 0.34. This is strong evidence that the secondary crystals are formed by the crystallization of the hydroxide, which gives this degree of hydration. The rate expression for the growth of the secondary crystals which applied for all interpretations was eq. (2a), in which the rate is proportional to the surface area of the crystals.

The use of the constant rate (eq. (2b)) generally led to deviations between experiment and theory of 20 deg. when the use of eq. (2a) gave deviations of 5 deg. The average deviation was also very sensitive to the initial size of the crystals. The computations used the thickness of the Type II film for the initial secondary crystal dimension.

When small number densities of secondary crystals are present, ellipsometry is sensitive to the optical properties of the primary layer. The primary layer appears to be non-stoichiometric, as indicated in the discussion for experiment Ag 80-32. The refractive index of the solid, non-porous material evaluated by the interpretation was 2.19-1.04 i. The large imaginary part could indicate silver is present in a powder form, possibly resulting from a disproportionation reaction. One possible reaction mechanism is given in eqs. 69 and 70.

$$Ag^{+} + Ag(OH)_2^{-} \quad Ag_2(OH)_2 \tag{69}$$

$$Ag_2(OH)_2 \rightarrow Ag + AgO \cdot H_2O \ . \tag{70}$$

As neutron diffraction studies have indicated that AgO is actually composed of the monovalent and trivalent silver, the divalent state indicated above could be unstable. While AgO formation has been assigned to the 0.49 V peak, potential sweep measurements (A14) have shown that if no AgO is initially present, only peaks associated with the monovalent and trivalent states are observed. The reactions given in eqs. (69) and (70) are consistent with observations that the

non-stoichiometry is more prevalent in more alkaline electrolytes (6 M vs. 1 M), at larger Ag^+ concentrations (Exp. Ag 80-12), and occurs when a decrease in electrode potential (removal of concentration overpotential) is observed.

An interpretation which is alternative to the development of non-stoichiometry is that precipitation of the hydroxide occurs under the three conditions stated in the previous sentence. The theoretical $\Delta - \psi$ curves lie to the left of the experimental curves, and would be shifted to the right by the hydrate layer. Removal of the assumption that the hydrate layer and Type I film begin forming at the same time as secondary crystal growth begins would probably allow the computational procedure to reproduce the experimental observations.

The two non-idealities in the primary layer characteristics, non-stoichiometry vs. a precipitated hydroxide layer, probably cannot unambiguously be distinguished by the use of ellipsometry alone. If the samples can be transfered into vacuum without major changes occuring in the characteristics of the film, film profile studies (Appendix A) may be able to provide distinguishing information.

Properties of anodic films formed under forced convection vary along the direction of flow. Due to the transport of solution-phase silver downstream, the primary layer is thicker and the number density of secondary crystals is greater away from the leading edge of the electrode (Figure 30). The use of statistical variations in the time of the onset of secondary crystal growth, which also allows for variations in primary layer thickness, does reduce the deviation between

experiment and theory resulting from the use of a uniform film thickness and number density. This variation in properties is not actually random, and an alternate formalism is probably warranted.

The initial stages of film formation at +0.55 volts (Exp. Ag 80-13) was interpreted using the optical constants of the monovalent oxide, and very satisfactory agreement with experimental observations was obtained. The monovalent oxide should form if most of the overpotential is initially concentration overpotential. This indirectly implies that resistance polarization resulting from surface layers restricting ionic transport leads to the higher valence state formation at 0.49 volts.

The fact that steady state conditions are reached in forced convection experiments has allowed the computation of the crystalization overpotentials in Table V. By assuming that charge transfer overpotential is negligible, primary layer film conductivities were calculated which qualitatively agree with film porosities derived from ellipsometer measurements. Under forced convection, the film porosity increases with current density. An explanation for this behavior is that the large supersaturations of the solution-phase silver species at large current densities promote nucleation of particles, while at lower current densities, crystallization of material onto existing sites leads to a more dense phase.

The hydrate layer discussed in Sec. IV appears to have a minor optical effect. This conclusion is valid unless the effect interpreted as non-stoichiometry in the discussion of experiment Ag 80-32 is instead due to the precipitation of the hydroxide.

The size of the secondary crystals derived from ellipsometer measurements are generally smaller than the dimensions measured by scanning electron microscopy. Unless the crystals continue to grow after the current is interrupted, the theoretical descriptions of the optical effect of the crystals (Sec. IV) are therefore only qualitatively correct. It is in fact possible that ellipsometry is not sensitive to crystals larger than about 1000 Å because of light attenuation by absorption or because of light scattering effects. Ellipsometry measures the relative change in amplitude between the s and p components, and not absolute changes in amplitude. Reflectance measurements, in which the change in the intensity of the individual s or p component is monitored, are probably necessary for the quantitative description of secondary crystal growth. While the thickness and the optical properties of the primary layer are of present interest, a sensitivity to secondary crystal growth is required in order to use mass balances (Sec. IV) to derive kinetic parameters and to relate the thickness of the primary layer to the electrode current density.

Cadmium Hydroxide Formation

The results for the anodic formation of cadmium hydroxide films are more qualitative than the results for silver oxide formation. The interpretations of ellipsometer observations indicate that the electrode surface initially is covered by patches of film formed by a corrosion process. The initial film thickness is about 300 Å. A more

detailed study of the corrosion of cadmium is warranted, especially as the characteristics of anodic film formation depend strongly on the initial state of the surface. An initial film allows crystallization to occur and prevents the formation of the more compact, passivating layer resulting from the larger supersaturation of ionic species required for nucleation. The use of scanning wavelength or spectroscopic ellipsometer should allow the thickness and coverage of the initial film to be determined with greater accuracy and certainty.

Non-stoichiometry appears to be present in the lower most layer. The degree of non-stoichiometry increases as the primary layer thickness increases. The refractive index for the non-stoichiometric film indicates that the film is light absorbing, and possibly due to excess metal. Other investigators have suggested that the darkness of these films is due to cadmium oxide being present. However, as the oxide optical constants (Appendix F) do not provide the necessary degree of light absorption, and as no evidence for the oxide has ever been obtained, it is very probable that no oxide is being formed. Film profile studies (Appendix A) will be necessary to obtain more quantitative information.

Zinc Oxide Formation

The corrosion of zinc in alkaline electrolyte leads to roughening of the metal substrate and possibly to the formation of a patchy hydroxide or oxide layer. The initial values of Δ and ψ do not provide enough information to uniquely characterize the fractional coverage, thickness, and refractive index of an initial surface layer. The use of spectroscopic ellipsometry would provide additional information.

The ultrahigh vacuum system (Appendix A) would allow the determination of the refractive indices as a function of wavelength of zinc and zinc oxide compressed powder (Appendix F).

In 0.5 M KOH, the degree of non-stoichiometry of the anodic film increases as the film thickness increases. The blackening of the film has been postulated (Z50) as resulting from the deposition of finely divided zinc by the disproportionation of $Zn(OH)_2^-$ to Zn and $Zn(OH)_4^=$. In order to obtain quantitative information about the developing non-stoichiometry, film profile studies will be necessary, in conjunction with the use of scanning electron microscopy, as the film composition appears to vary across the electrode surface as well as in the direction normal to the surface.

The information obtained about the physical properties of the anodic films formed in 6 M KOH should be regarded as being qualitative. The structures assumed for the secondary crystals in Sec. IV are not strictly applicable to the pyramidal shapes observed by SEM (Fig. 61) for the films formed in stagnant electrolyte. In forced convection experiments, the metal substrate dissolves non-uniformly due to localized blockage of the surface by patches of the anodic film, leading to both roughening of the substrate and a highly disordered film (Fig. 66). The degree to which the water content of the film can be differentiated from void space is uncertain. Reflectance measurements would provide additional information. Experimental procedures could also be developed which would minimize the disorder in the film (Fig. 81). Saturating the electrolyte by electrochemically dissolving zinc would result in film formation at lower current densities.

Additional verification of the adsorption of zinc oxide, which was used to interpret the initial large increase in Δ for experiments conducted in 6 M KOH, should be sought. Scanning wavelength ellipsometry or simultaneous electrode impedence measurements would provide additional information.

VIII. Conclusions

The structures of anodic films formed on silver, cadmium, and zinc in alkaline solutions are quite complex. The films are not isotropic and homogeneous, as indicated in Figure 2, and any realistic model describing the optical properties of these films must reflect this structural detail. The multi-dimensional interpretation of ellipsometer measurements developed in this dissertation has three major assets: 1) The inclusion in the analysis of mass transport in the electrolyte, and electrical charge passed as a function of time, experimental information which has previously been disregarded by investigators, provides necessary constraints on the thickness of the anodic film. 2) The automated interpretation procedure, in which characteristic parameters (having physical meaning) are evaluated by minimizing the deviation between experiment and theory, provides a means to investigate and compare the effects of alternate assumptions made for the representation of the electrode process. 3) Measures of uncertainty determined by the computational procedure indicate the sensitivity of ellipsometry towards various physical processes.

Ellipsometry is sensitive to the optical properties of the primary layers covering the silver, zinc, and cadmium electrodes. The anodic reaction rates are limited by the transport of the charge carriers through the primary layer (see Table V, p.120, and the discussions for experiments Cd 100-15, p.136, and Zn 200-21, p.172). The primary layers on all three metals appear to contain excess metal, and film profiling studies combining ellipsometry, Auger spectroscopy, ion-etching, and scanning electron microscopy are warranted.

Quantitative information regarding the structure and composition of large (appoximately 1 μm dimension) secondary crystals probably cannot be obtained from ellipsometer measurements alone. Light scattering and absorption reduce the optical effect of these crystals relative to the primary layer. As knowledge of the secondary crystal sizes is required in order to use mass balances to relate the primary layer thickness to the electrode current density, future studies should combine reflectance measurements with ellipsometer and SEM observations.

The concentration of the solution-phase species at the electrode surface has a major effect on the structure of the anodic film. Large degrees of supersaturation promote nucleation and increase crystallization rates. Maximum electrode current densities can probably be maintained when the interfacial concentration is large enough to allow a disordered film structure resulting from continued nucleation (Table V).

Ellipsometry is sensitive towards the presence of solution-phase species. An accumulation of species at the electrode surface, in concentrations much larger than can result from the diffusion of positive species, appears to be present during the anodic dissolution of silver, zinc, and cadmium. For zinc, this accumulation was interpreted as resulting from zinc oxide adsorbing on the surface with a free energy of adsorption which increases from 1.5 to 6 kcal/mole as the current density increases from 100 to 500 mA/cm^2. At large electrolyte flow rates, the optical effect corresponds exactly to the interfacial concentration predicted by mass transport theory.

References

G1. K. J. Vetter, Electrochemical Kinetics, (Academic Press, NY, 1967), pp. 104-392.

G2. D. A. Vermilyea, J. Electrochem. Soc., 102, 655 (1955).

G3. E. J. W. Verwey, Physica, 2, 1059 (1935).

G4. N. F. Mott, Trans. Faraday Soc., 43, 429 (1947).

G5. N. Cabreva, J. Chim. Phys., 44, 172 (1947).

G6. R. H. Muller and C. G. Smith, Surf. Sci., 56, 440 (1976).

G7. C. G. Smith, LBL-3903 (M.S. Thesis, UCB) 1975.

G8. D. A. Vermilyea, "Anodic Films," in Advances in Electrochemistry and Electrochemical Engineering, Vol. III, P. Delahay, Ed., (Interscience Publishers, NY, 1963), p. 227.

G9. C. Wagner, J. Electrochem. Soc., 101, 60 (1954).

G10. H. J. S. Sand, Phil. Mag., 1 (6), 45 (1901).

G11. T. R. Rosebrugh and W. L. Miller, J. Phys. Chem., 14, 816 (1910).

G12. J. Newman, Electrochemical Systems, (Prentice-Hall, Inc., Englewood Cliffs, N.J., 1973), pp. 305-318.

G13. F. G. Cottrell, Z. Physikal. Chem., 42, 385 (1903).

G14. R. H. Muller, "Principles of Ellipsometry," in Advances in Electrochemistry and Electrochemical Engineering, Vol. IX, P. Delahay and C. W. Tobias, eds., (John Wiley & Sons, NY, 1973), pp. 167-226.

G15. P. Drude, Weber Oberflachenschickten, Ann. der Physik und Chemis, 36, 531-561, 865-897 (1889).

G16. O. S. Heavens, Optical Properties of Thin Solid Films, (Dover, NY, 1956), p. 63.

G17. O. Hunderi, J. De. Physique, Colleque, C5, 38, C5-89 (1977).

G18. M. Born and E. Wolf, Principles of Optics, (Macmillan, NY, 1964), p. 551.

G19. J. S. Nelder and R. A. Mead, Computer J., 7, 308 (1967).

G20. W. C. Davidon, Computer J., 10, 406 (1968).

G21. F. James, "Monte Carlo for Particle Physicists" (Sec. 6.1) in Methods in Subnuclear Physics, Vol. IV, Part 3, M. Nikolic, ed., (Gordon and Breach, London, 1970).

G22. H. J. Mathieu, D. E. McClure, and R. H. Muller, Rev. Sci. Instrum., 45, 798 (1974).

G23. T. K. Sherwood, R. Pigford, and C. Wilke, Mass Transfer, (McGraw-Hill, NY, 1975), p. 233.

G24. H. Gu, "Ellipsometry of Surface Layers," LBL-165 (M.S. Thesis, UCB), 1971, p. 133.

G25. C. G. Smith, J. S. Remer, and R. H. Muller, "Corrections for Component Imperfections and Azimuth Errors in an Automatic Self-Compensating Ellipsometer," LBL-7303, in preparation.

G26. P. Delahay, Double Layer and Electrode Kinetics, (Interscience, NY, 1965), p. 82.

G27. D. P. Boden, R. Wylie, and V. J. Spera, J. Electrochem. Soc., 118, 1298 (1971).

G28. Bausch and Lomb Precision Refractometer, Catalogue Number 33-45-03.

G29. C. G. Smith and R. H. Muller, "Interpretation of Ellipsometer Observations of Anodic Films," in Optical Polarimetry, Instrumentation, and Applications, Soc. Photo.-Opt. Instr. Engrs., Bellingham, Wash., Proc. Vol. 112 (1977); LBL-6640 (1977).

G30. W. N. Hansen, "Internal Reflection Spectroscopy in Electrochemistry," in Advances in Electrochemistry and Electrochemical Engineering, Vol. IX, P. Delahay and C. W. Tobias, eds. (Interscience Publishers, NY, 1973), p. 4.

Appendix A. Construction of an Ultrahigh Vacuum System for Film Profile Studies

The chemical composition of surface layers can usually not be determined unambiguously from ellipsometer measurements when the structural variations discussed in section IV are also present. In order to augment ellipsometer data, an ultraigh vacuum system has been built in which surface layers can gradually be thinned by ion etching, while being observed by ellipsometry. Elemental composition at various stages of thinning can be determined by Auger spectroscopy without realignment of the specimen. With this equipment, it will be possible to determine composition and porosity profiles of surface layers which can be transferred without alteration into a vacuum environment.

The whole vacuum system can readily be removed from and reconnected to the ellipsometer (Figure A1). The optical windows of the chamber are mounted on bellows to allow alignment normal to the beam. The three probes (light, electron, and ion beams) intersect at the focal point (radius of curvature) of the three-grid LEED optics, which serves as detector for the Auger signal. The beams are incident onto the sample at an angle of incidence of 75 degrees from the surface normal.

Vacuum System

Two sorption pumps[1] are used for rough pumping from atmospheric pressures to approximately 10^{-4} mm Hg . The pressure is monitored in this range by a thermocouple gauge.[2] A diode Vac-Ion pump[3] is used to obtain ultrahigh vacuum pressures of up to 10^{-11} mm Hg . The pressure

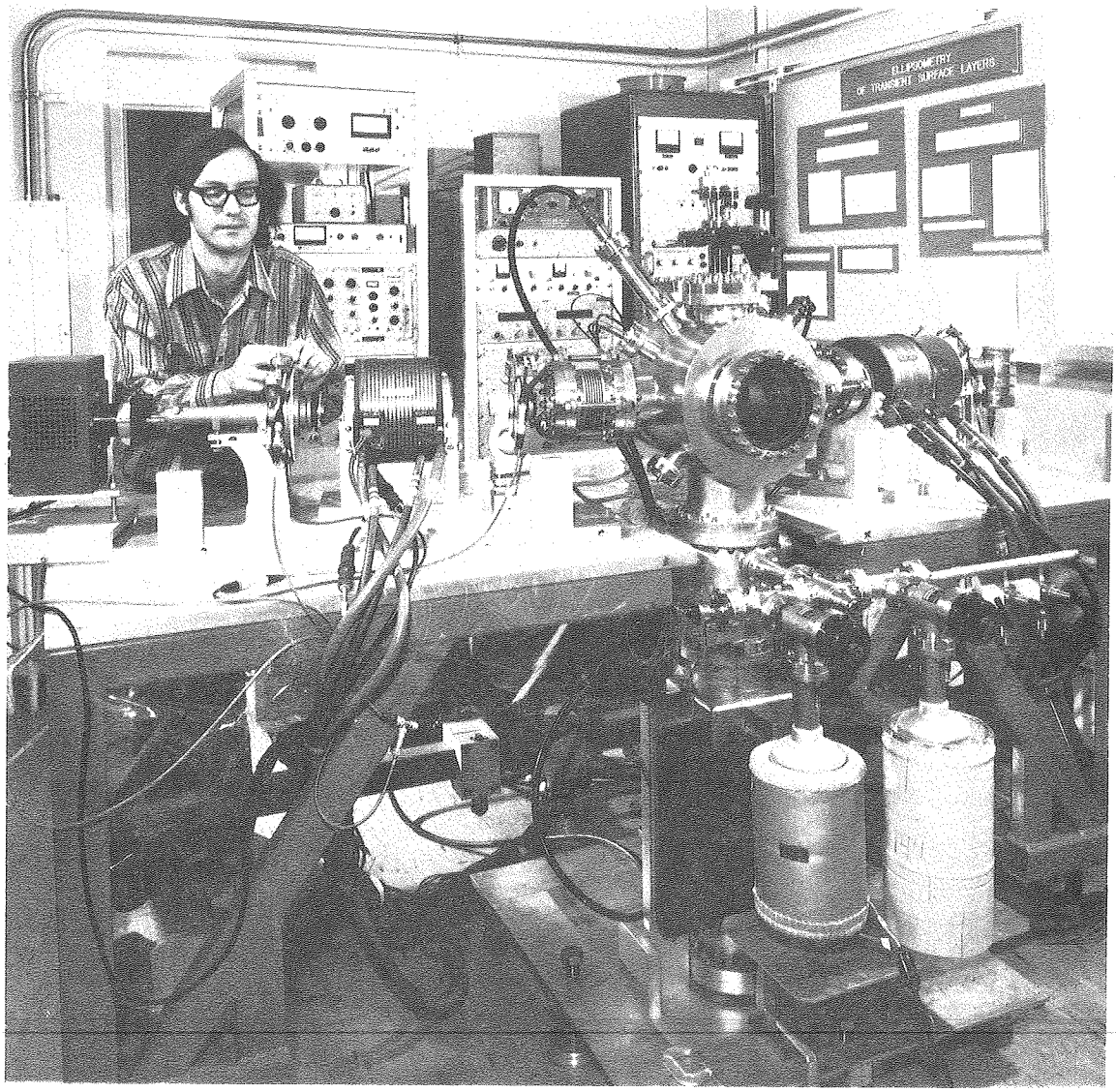

CBB 760-11054

Figure A1. Ultrahigh vacuum system for simultaneous use of ellipsometry, Auger spectroscopy, and ion-etching.

is monitored in this range by a vac-ion gauge.[4]

Electron Detection System

A schematic of the Auger electron detection system is shown in Figure A2. The retarding voltage (0 to 3 KV) to the second grid of the LEED optics[5] is modulated at a selected frequency and amplitude by the oscillator. A ramp generator is used to sweep the DC retarding voltage at rates from 1 to 500 volts/min. The current collected by the phosphor screen of the LEED optics is amplified and sent to a lock-in amplifier,[6] which is tuned to the first harmonic of the modulation frequency to measure the derivative of the Auger electron intensity with respect to the electron energy.[7] The oscilloscope[8] following the lock-in amplifier provides additional amplification of the signal prior to recording. The first and third grids are grounded.

Ion Etching

A leak valve[9] is used to introduce gases into the bell jar at controlled flow rates. The energy of the argon ion beam generated by the ion-bombardment gun[10] may be varied from 0 to 3 kV. The ion beam may be scanned over the sample by rastering to achieve uniform sputtering rates over an approximately 1 cm^2 area.

Sample Holder

The crystal manipulator[11] provides separate X-Y-Z translations plus rotation of the sample about an axis parallel to the ellipsometric p-plane. Power feedthroughs on the crystal manipulator may be used for resistive heating of the sample and thermocouple feedthroughs may be used to monitor the temperature of the sample.

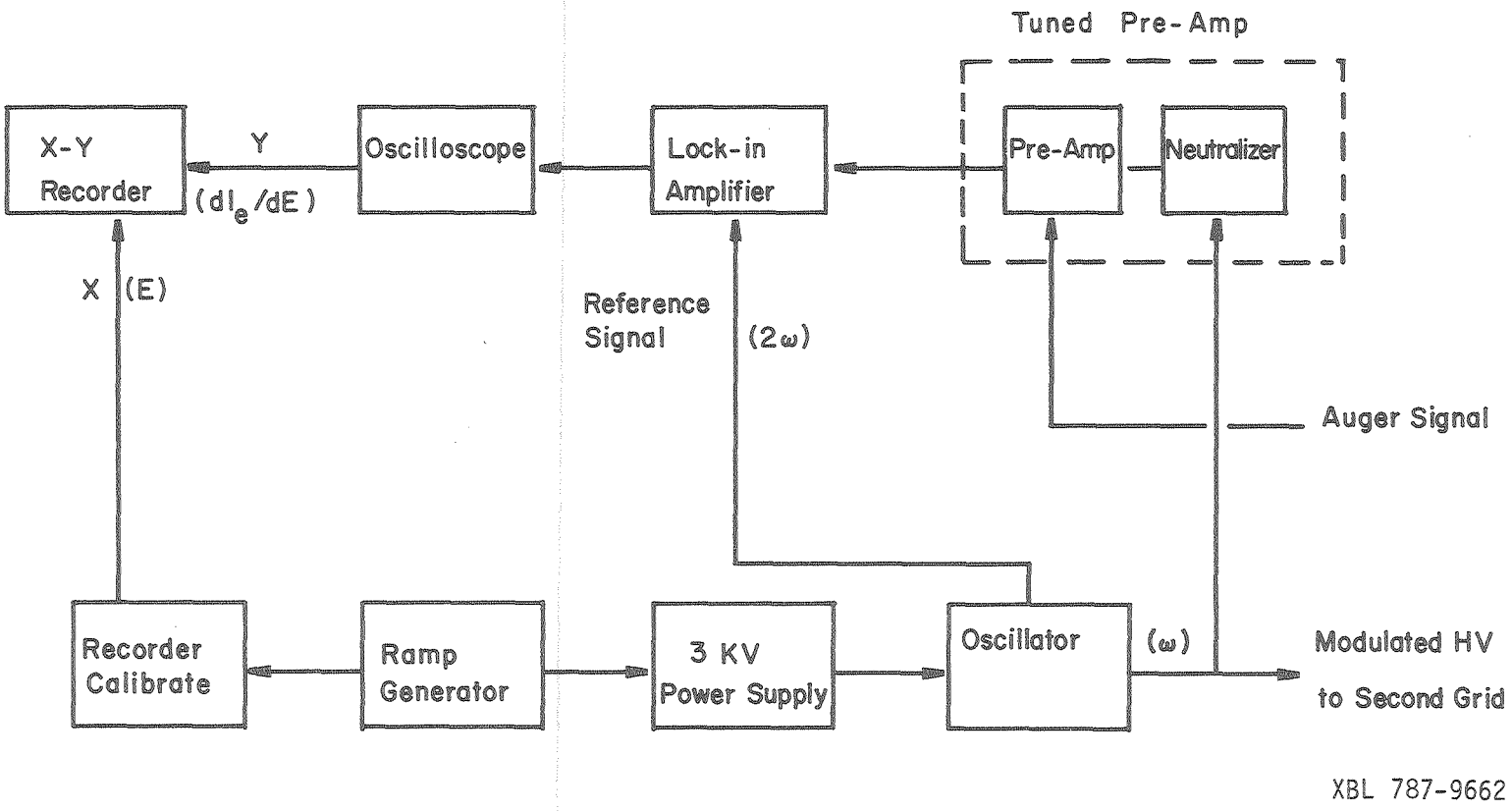

Figure A2. Schematic of the Auger electron detection system.

References

1. Varian Vac Sorb Pump, Model No. 941-6001.

2. Varian Thermocouple Guage, Model No. 0801-F2739-301.

3. Varian 280 l/s Diode Vac Ion Pump, Control Unit No. 921-0034.

4. Varian UHV-24 Nude Guage, Model No. 971-5008, Perkin-Elmer Ultek Digital Guage Control, Model No. 605-0002.

5. Varian LEED Optics, Model No. 981-0024.

6. PAR Lock-in Amplifier, Model No. 5101.

7. T. A. Carlson, Photoelectron and Auger Spectroscopy (Plenium Press, N.Y., 1975) pp. 45-48.

8. Tecktronix T922R Oscilloscope.

9. Varian Variable Leak Valve, Model No. 951-5106.

10. Varian 3 keV Ion Bombardment Gun and Beam Probe, Model No. 981-2043, Control Unit Model No. 981-2046.

11. Varian High Precision Sample Manipulator, Model No. 981-2536/7/8.

Appendix B. A Ray Model for Describing the Optical Effect of Brick-Shaped Crystals on Ellipsometer Measurements

This model attempts to describe changes in the state of polarization of a light beam specularly reflected from a surface covered by brick-shaped crystals. Only light rays whose propogation direction is not changed by transmission through the crystals are considered; scattered light, which does not reach the photodetector, is neglected. This constraint requires that a ray must enter and leave the crystals through coplanar faces. The light may reflect from the surface beneath the crystals either before or after transmission through the crystals.

Superposition of Six Rays

The crystals are assumed to contact the surface at a crystal edge. This leaves two angles necessary to specify the average orientation of a crystal. Figure 7 defines the angles α and β in terms of projections normal to the p plane and the surface. Six rays need to be considered (Fig. 7), 3 "p-rays" × 2 "s-rays". For $\alpha \leq 45$, two rays reflect from the surface before entering the crystal faces oriented at either β or $90-\beta$ degrees from the s-plane. A third ray transmits through the crystals before reflecting from the surface. For $\alpha \geq 45°$, two rays pass through the crystals before reflection and one ray reflects before transmission. The angle of the light ray relative to the surface normal is used to describe the effects of reflection and transmission on the state of polarization of light. Each of the six rays have different angles of incidence on the crystal faces. These may be determined using the cosine law (eq. B1) for the

angles normal to the surface in the p-projection (ϕ_α) and the s-projection (ϕ_β) .

$$\cos \phi_e = \cos \phi_\alpha \cos \phi_\beta \ . \tag{B1}$$

Figure B1 shows the three incident angles in the p-projection and Figure B2 shows the two incident angles in the s-projection. These angles are

$$\phi_{\alpha 1} = |\alpha + \phi - 90| \tag{B2}$$

$$\phi_{\alpha 2} = 90 - \phi_{\alpha 1} \tag{B3}$$

$$\phi_{\alpha 3} = |\phi - \alpha| \tag{B4}$$

$$\phi_{\alpha 4} = 90 - \phi_{\alpha 3} \tag{B5}$$

$$\phi_{\beta 1} = \beta \tag{B6}$$

$$\phi_{\beta 2} = 90 - \beta \tag{B7}$$

where ϕ is the angle of incidence on the surface beneath the crystals. $\phi_{\alpha 3}$ is used for $\alpha \leq 45°$ and $\phi_{\alpha 4}$ is used for $\alpha > 45°$. The six angles of incidence given by eq. (B1) are then

$$\phi_1 = \cos^{-1}[\cos |\alpha + \phi - 90| \cos \beta] \tag{B8}$$

$$\phi_2 = \cos^{-1}[\cos |\alpha + \phi - 90| \cos (90 - \beta)] \tag{B9}$$

$$\phi_3 = \cos^{-1}[\cos |\phi - \alpha| \cos \beta] \tag{B10}$$

$$\phi_4 = \cos^{-1}[\cos |\phi - \alpha| \cos (90 - \beta)] \tag{B11}$$

for $\alpha \geq 45$,

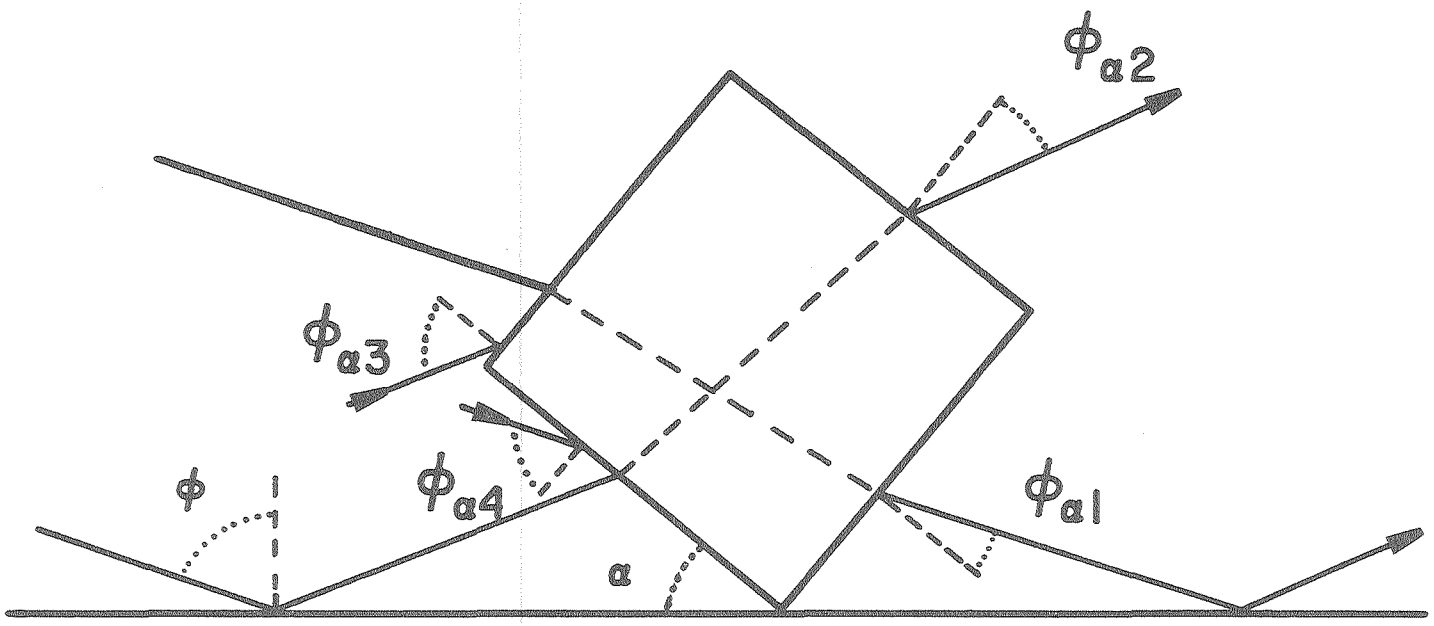

Figure B1. Angles of incidence on different faces of secondary crystals, p-projection. XBL 786-9163

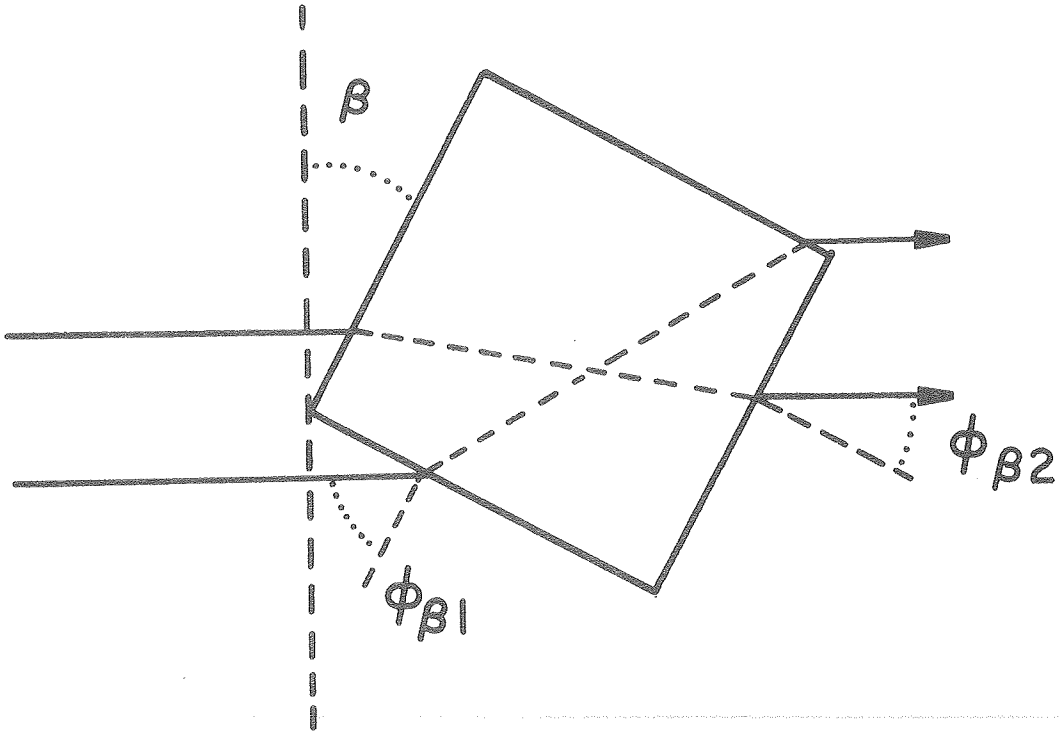

Figure B2. Angles of incidence on the different crystal faces of secondary crystal faces of secondary crystals, normal projection onto the electrode surface.

$$\phi_5 = \cos^{-1}[\cos(\alpha+\phi)\cos\beta], \text{ or } \cos^{-1}[\cos(180-\alpha-\phi)\cos\beta] \quad \text{(B12)}$$

$$\phi_6 = \cos^{-1}[\cos(\alpha+\phi)\cos(90-\beta)], \text{ or } \cos^{-1}[\cos(180-\alpha-\phi)\cos(90-\beta)] \quad \text{(B13)}$$

for $\alpha < 45°$,

$$\phi_5 = \cos^{-1}[\cos|\phi - \alpha|\cos\beta] \quad \text{(B14)}$$

$$\phi_6 = \cos^{-1}[\cos|\phi - \alpha|\cos(90 - \beta)] \quad \text{(B15)}$$

Transmission Coefficients

The transmission coefficients T_ν (ν is either s or p) for light passing through the crystals are the ratios of the complex electric field leaving the cube relative to the incident electric field. These coefficients describe amplitude changes and phase shifts resulting from entering, passing through, and leaving the crystals. Figure B3 shows that the exiting electric field may be viewed as a series of beams resulting from multiple reflections and transmissions. The first order beam N_1 will give a transmission coefficient of

$$t_\nu^1 = t_{1\nu}t_{2\nu}e^{-i\delta_1}$$
$$= (1 - r_{1\nu})(1 - r_{2\nu})e^{-i\delta_1} \quad \text{(B16)}$$

where $r_{1\nu}$ and $r_{2\nu}$ are the reflection coefficients at the first and second crystal faces (eqs. (36), (37)) and δ_1 is the phase shift given by

$$\delta_1 = \frac{2\pi}{\lambda} n_c \cos \phi_c L \ . \tag{B17}$$

The second reflection coefficient $r_{2\nu}$ has the opposite sign of $r_{1\nu}(r_{2\nu} = -r_{1\nu})$, and eq. (B16) becomes

$$t_\nu = \left(1 - r_{1\nu}^2\right) e^{-\delta_1} \ . \tag{B18}$$

For a large number of beams, the multiple beam series converges to the Drude equations (eq. (40)). The transmission coefficient for a film covered surface is (G 30),

$$t_\nu^\infty = \frac{t_{1\nu} t_{2\nu} e^{-i\delta_1}}{1 + r_{1\nu} r_{2\nu} e^{-2i\delta_1}}$$

$$= \frac{\left(1 - r_{1\nu}^2 e^{-i\delta_1}\right)}{1 - r_{1\nu}^2 e^{-2i\delta_1}} \ . \tag{B19}$$

The number of beams leaving the crystal can be shown to be given by eq. (B20) for $i = 1$ to 6.

$$N_i = 1/2 \left[\frac{1}{P \tan \phi_i} + 1\right] \tag{B20}$$

P is the ratio of the width to the height of the crystals, $P = h/w$. For $N_i \leq 1$, eq. (B16) is used for the transmission coefficient, while for $N_i \geq 3$, eq. (B19) is used. For $1 < N_i < 3$, the transmission coefficient is a weighted average of t_ν^1 and t_ν^∞ as given by eq. (B21)

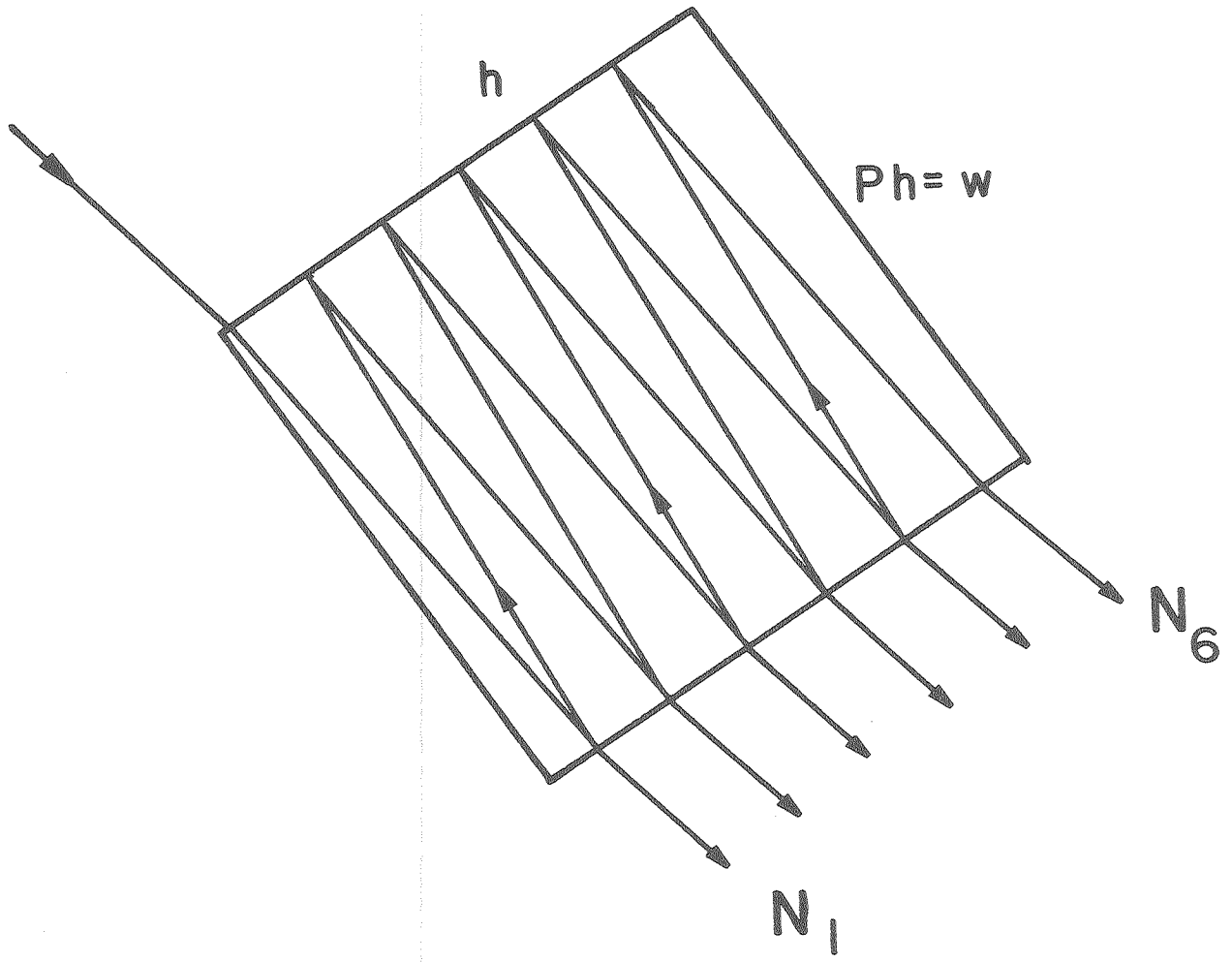

Figure B3. Multiple-beam representation of the electric field leaving secondary crystals. XBL 786-9161

$$2t_{\nu e} = (N_i-1)t_\nu^1 + (3-N_i)t_\nu^\infty \quad . \tag{B21}$$

Reflection and Transmission

The changes in amplitude and phase for a light beam passing through the crystals and reflecting from the surface are given by equation (B22)

$$R_i = \frac{\vec{E}_{refl.}}{\vec{E}_{inc.}} = t_{\nu i} R_b \quad . \tag{B22}$$

R_b is the reflection coefficient for the surface beneath the crystals (eq. (40)). If the crystals are covered by a film, $r_{1\nu}$ in eqs. (B16) and (B19) is computed using the Drude equations.

Area Fractions for the Six Rays

To superimpose the six rays, an effective reflection coefficient is formed from the coefficients for each ray by summing with respect to the active area fraction of the crystal surface. The active fraction is that portion of the area which allows the ray to exit from a crystal face parallel to the entrance face. The area fraction is composed of three factors, the area fractions in the p- and s-projections and the fraction of the exit face coplanar with the entrance face in the projection along the light beam. Figures B4 and B5 give the fractions for the s- and p-projections, Figure B6 the active area fraction f_a. The area fractions for the six rays are given in eqs. (B23) - (B32).

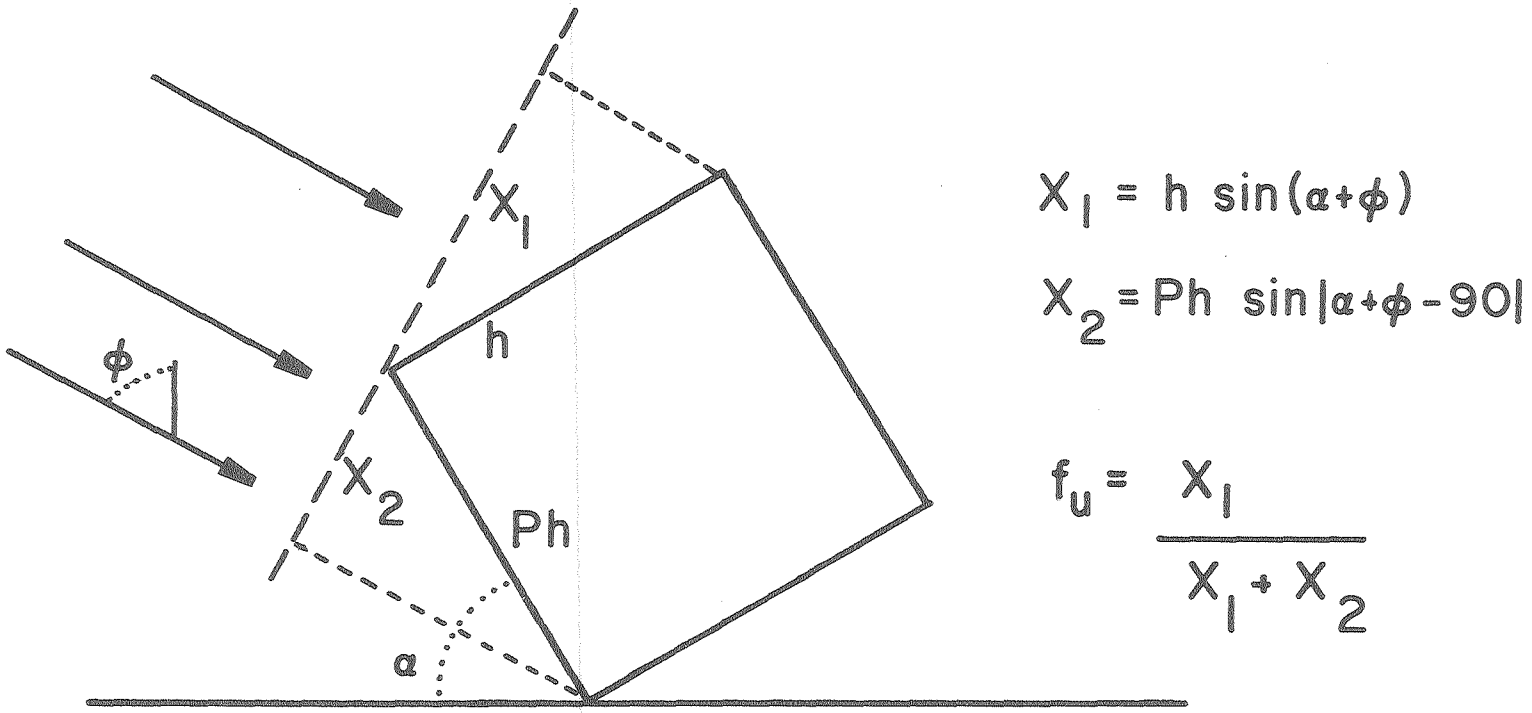

XBL 786-9159

Figure B4. Fraction of light f_u incident upon the upper crystal face of a secondary crystal, projection onto p-plane.

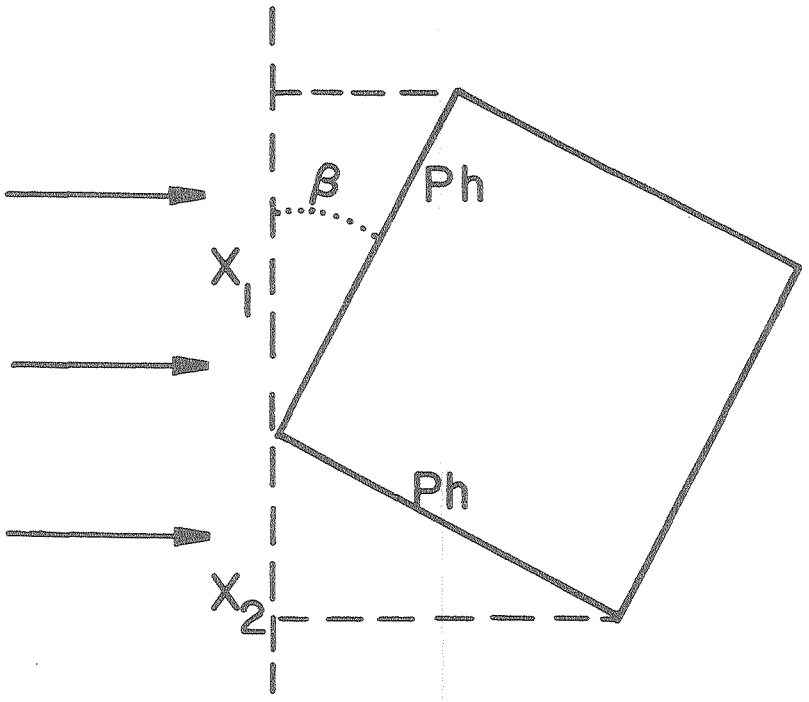

$$X_1 = Ph \cos\beta$$

$$X_2 = Ph \sin\beta$$

$$f_r = \frac{X_1}{X_1 + X_2}$$

XBL 786-9160

Figure B5. Fraction of light f_r incident upon the right crystal face of a secondary crystal, normal projection onto electrode surface.

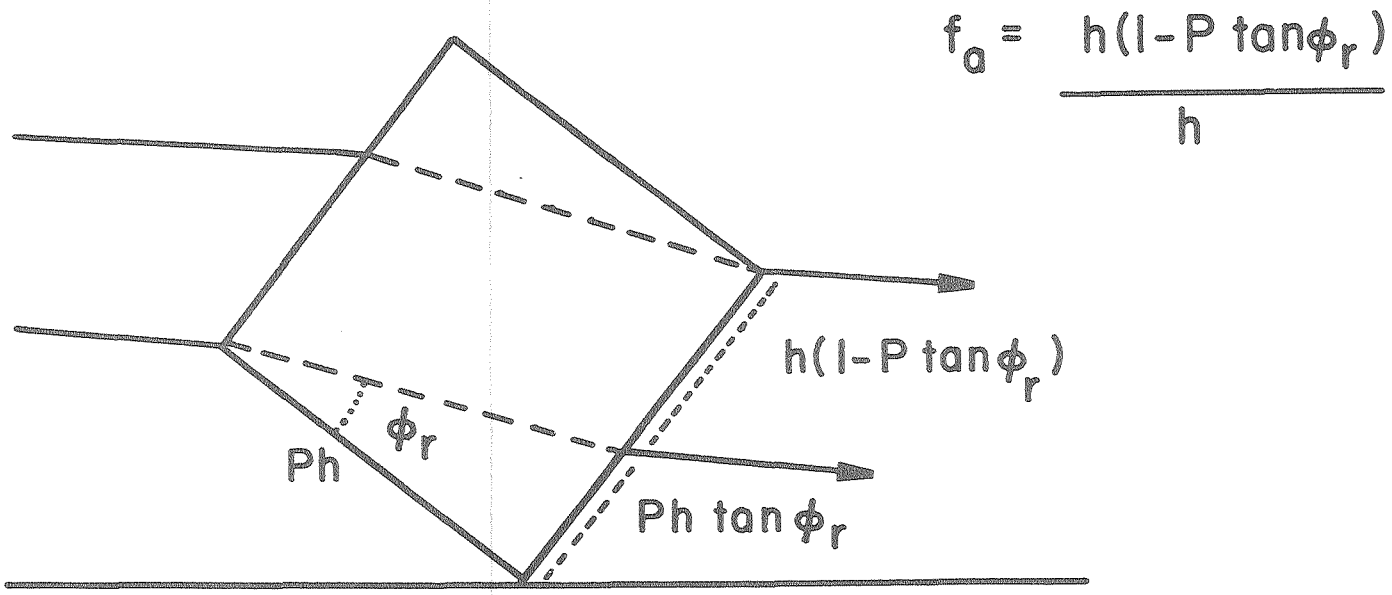

XBL 786-9158

Figure B6. Active area fraction f_a of a crystal face for which light enters and leaves the crystal through parallel faces.

$$A_1 = f_u f_r \qquad (1 - P \tan \phi_{1r}) \tag{B23}$$

$$A_2 = f_u(1-f_r) \qquad (1 - P \tan \phi_{2r}) \tag{B24}$$

$$A_3 = (1-f_u) f_r \qquad (1 - \tan \phi_{3r}/P) \tag{B25}$$

$$A_4 = (1-f_u)(1-f_r) \quad (1 - \tan \phi_{4r}/P) \tag{B26}$$

for $\alpha \geq 45°$,

$$A_5 = f_u f_r \qquad (1 - P \tan \phi_{5r}) \tag{B27}$$

$$A_6 = f_u(1-f_r) \qquad (1 - P \tan \phi_{6r}) \tag{B28}$$

for $\alpha < 45°$,

$$A_5 = (1-f_u) fr \qquad (1 - \tan \phi_{5r}/P) \tag{B29}$$

$$A_6 = (1-f_u)(1-f_r) \quad (1 - \tan \phi_{6r}/P) \tag{B30}$$

where

$$f_u = \frac{\sin (\alpha+\phi)}{P \sin |\alpha + \phi - 90| + \sin (\alpha+\phi)} \tag{B31}$$

$$f_r = \frac{\cos \beta}{\cos \beta + \sin \beta} \, . \tag{B32}$$

It should be noted that the angles ϕ_{ir} in the active area factors are the angles of refraction at the crystal faces, which must be computed from the complex angle of refraction ϕ_{icr} used in the reflection coefficients for absorbing crystals. The real angles are computed using equation (B33)

$$\phi_{ir} = \sin^{-1} \left(1 - A^2/B^2\right)^{1/2} \tag{B33}$$

where $$A = \text{Real } (n_c \cos \phi_{icr}) ,$$

$$B = (C - D + CD/A^2)^{1/2} ,$$

with

$$C = [\text{Real } (n_c)]^2$$

and

$$D = [\text{Imag } (n_c)]^2 .$$

The complex cosine $\cos \phi_{icr}$ is found using the complex form of Snells law and the trigonometric identity $\cos \phi = (1 - \sin^2\phi)^{1/2}$,

$$\cos \phi_{icr} = \text{CSQRT} \left(1 - n_o^2 \sin^2 \phi_i / n_c^2\right)$$

with n_o the (real) incident medium and ϕ_i as given by eqs. (B8) - (B15).

The effective reflection coefficient for an isolated crystal which has no interactions with other crystals is given by eq. (B34)

$$R_{\nu e} = (1 - q) R_{\nu b} + q \sum_{i=1}^{6} A_i t_{\nu i} R_{\nu b}$$

$$= R_{\nu b} \left[(1 - q) + q \sum_{i=1}^{6} A_i t_{\nu i} \right] . \tag{B34}$$

The fraction of the surface covered by the crystals q is given by eq. (52).

When the crystals are sufficiently close together, the light beam will have to pass through two crystals, before and after reflection. Squared terms should then be included in the summation, as indicated by (eq. B35)

$$R_{\nu e} = R_{\nu b}\left[1 - q + q\left[\sum_{i=1}^{6} A_i t_{\nu i} + F \sum_{i=1}^{2} A_i t_{\nu i} \sum_{j=3}^{6} A_j t_{\nu j}\right]\right] \quad \text{(B35a)}$$

for $\alpha < 45$, and for $\alpha \geq 45°$,

$$R_{\nu e} = R_{\nu b}\left[1 - q + q\left[\sum_{i=1}^{6} A_i t_{\nu i} + F \sum_{i=1,2,5,6} \sum A_i t_{\nu i} \sum_{j=3,4} A_j t_{\nu j}\right]\right] \quad \text{(B35b)}$$

The factor F may be included to describe the orderliness of the crystals. An ordered array will transmit more light than a disordered array.

Appendix C. A Preliminary Model for the Interpretation of Ellipsometer Observations of Anodic Films

This automated interpretation of ellipsometer observations (G 29) was developed to include mass-transport processes in the interpretation of ellipsometer measurements of anodic film formation and to more fully use electrochemical data collected simultaneously. The reaction rate at the electrode surface is derived from the current density, and the amount of reacted material accumulated at different distances from the substrate is obtained from a balance of mass fluxes. Electrode potential measurements are used to identify thermodynamically possible products and major changes in products with time.

Preliminary Interpretation

The potential usefulness of several simple optical models was initially evaluated by conventional computation. Figure C1 illustrates that homogeneous films with different complex refractive indices cannot account for the measurements. Assuming the existence of a colloidal suspension (see Hydrate Layer, section IV) near the solid film dramatically improves the agreement with observation, as shown in Figure C2 (the refractive index of this region is too high to be due to ionically dissolved silver, which has a solubility of only 4.7×10^{-4} M in this solution).

Calculations for uniaxial birefringence, with the optical axis normal to the surface (G29) do not fit the data. Calculations for biaxial anisotropy have not been conducted, but the deviations from isotropic single film behavior are much greater than birefringent effects presented by other investigators (G 29).

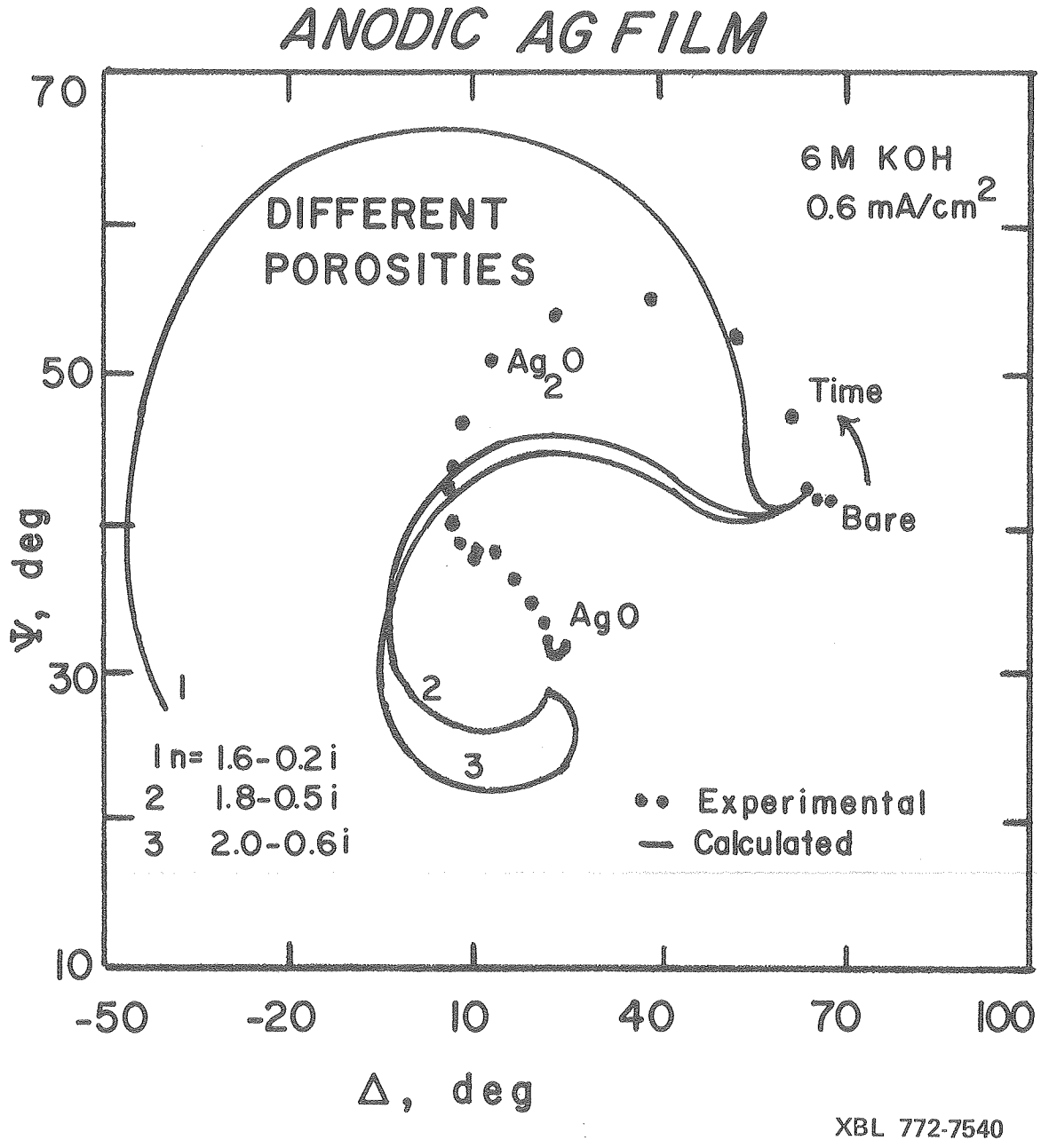

Figure C1. Anodic film formation on silver in alkaline solution. The calculated curves represent different film porosities. Monovalent and divant oxides are the products indicated by electrode potential measurements.

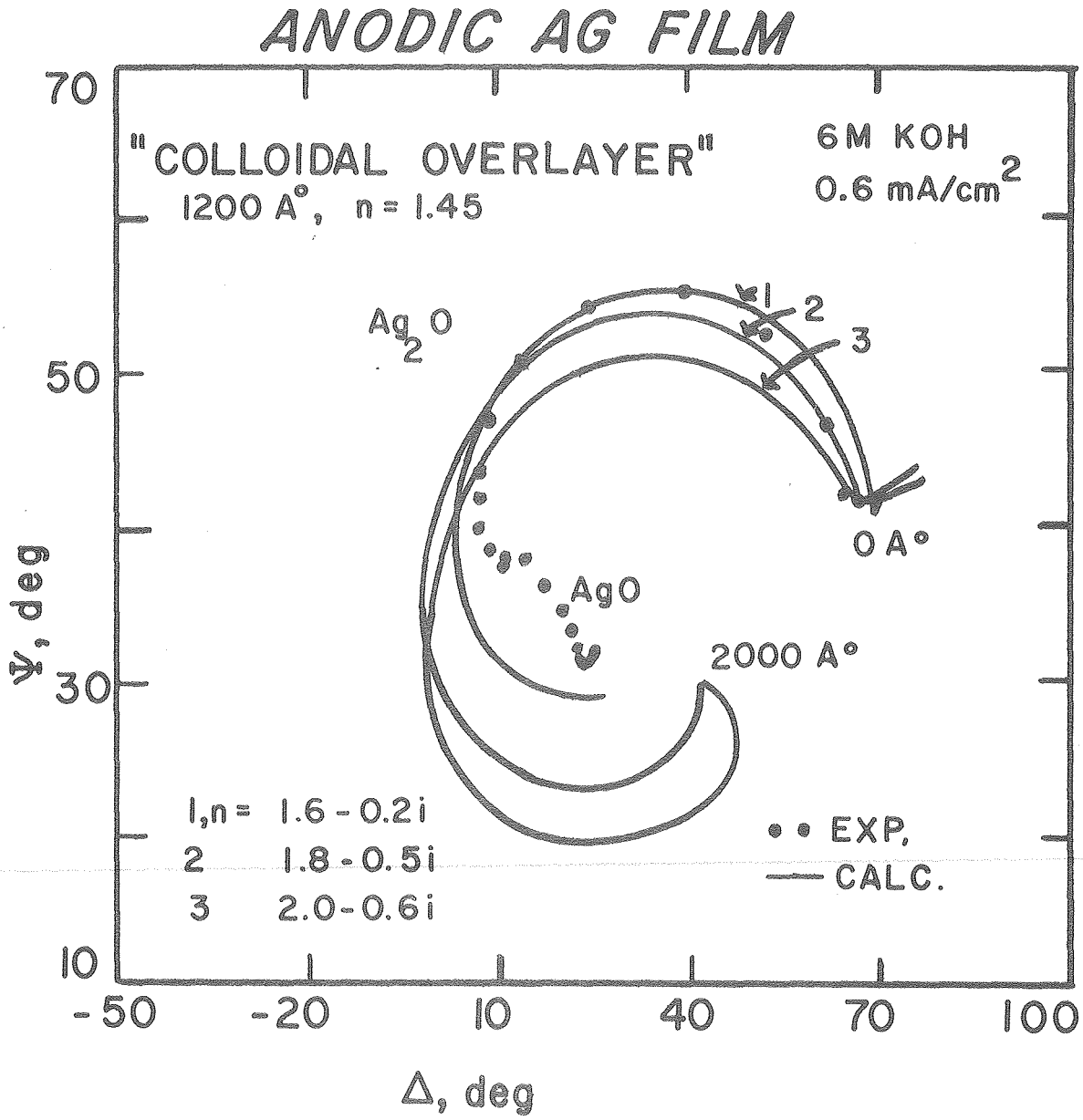

Figure C2. The use of a Colloidal Overlayer of constant refractive index n = 1.45 and constant thickness T_c = 1200 A° in a preliminary interpretation. Same film refractive indices as in Figure C1.

Optical Model

The optical film model used for the automated interpretation of ellipsometer measurements is illustrated in Fig. C3. It consists of a smooth substrate, a homogeneous solid film (which may be porous), a colloidal overlayer and a mass-transport boundary layer. A constant anodic current density i (based on macroscopic surface area) is passed across the electrolyte-metal interface and results in the production of an equivalent flux of dissolved primary reaction product. A fraction of this flux, corresponding to the current density i_c, enters the colloidal layer, the remainder is precipitated as solid film. Part of the dissolved material is precipitated in colloidal form, and the remainder (flux density j_D) enters the mass-transport boundary layer.

The Sand equation, valid for diffusion into a stagnant, semi-infinite medium, is used for determining the boundary layer thickness as a function of time:

$$\delta = 1.129 \sqrt{Dt} \ . \qquad \text{(C1)}$$

A uniform film porosity is modeled to decrease from an initial value of ε_o to zero at an adjustable film thickness of T_{fl}:

$$\varepsilon = \varepsilon_o (1 - T/T_{fl})^2 \ . \qquad \text{(C2)}$$

To account for a possible restriction in the removal of primary dissolution product by the growing film, the dissolution current i_c

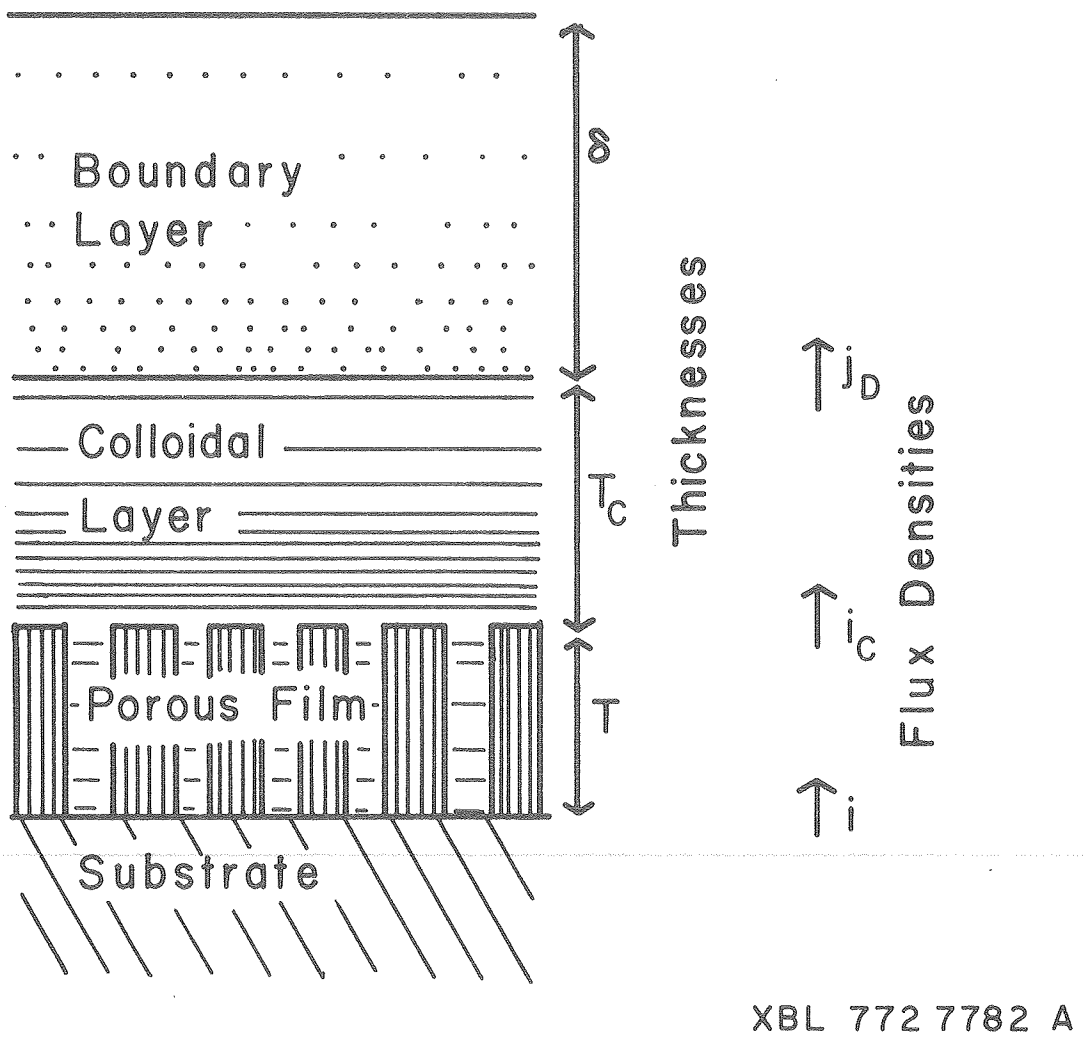

Figure C3. Preliminary optical model for automated interpretation of measurements with definitions of layer thicknesses and flux densities between layers. (Model 5, Figure 1a).

is modeled to decrease to zero at an adjustable thickness $T_{c\ell}$:

$$i_c = if(1 - T/T_{c\ell}) \quad . \tag{C3}$$

The refractive index n of the colloidal layer is assumed to remain constant, an approximation valid for a steady state process.

Neglecting ionic migration effects (valid due to the large excess of KOH), the diffusion flux across the boundary layer of dissolved reaction products is given by

$$j_D = - \frac{D\Delta C}{\delta} \tag{C4}$$

where ΔC is the concentration difference between the colloidal layer and the bulk solution. A value of 2.3 times the solubility of silver hydroxide has been used for the ionic concentration at the boundary between the colloidal layer and the bulk solution.

Table CI shows the parameters describing the film formation process which are evaluated by the computational procedure (see Section IV-G). From the values of $n_s - ik_f$, f, $T_{c\ell}$, n, ε_o, and T_{fl}, the time-dependent variables of j_D, i_c, ε, T_f, T_c, and $n_f - ik_f$ are determined. The porous film refractive index $n_f - ik_f$ is calculated using the Lorenz-Lorenz mixing rule (G29) to average $n_s - ik_s$ with the colloidal suspension in the pores (eq. C2). The film thickness T_f at each moment is determined by using the valence, molar volume, porosity, and charge consumed in film formation to calculate the volume per cm^2 of solid reaction products. The thickness of the colloidal

Table CI

Parameters of Anodic Film Formation Determined by the Automated Interpretation

Time-invariant parameters:

n_s-ik_s - Solid film refractive index.

f - Initial current fraction used for dissolution, eq. (3).

$T_{c\ell}$ - Film thickness for zero dissolution current, eq. (3).

n - Refractive index of colloidal overlayer.

ε_o - Initial film porosity, eq. (2).

T_{f1} - Film thickness for zero porosity, eq. (2).

Time-dependent variables (functions of the time-invariant parameters):

j_D - Ionic diffusion flux density, eq. (4).

i_c - Dissolution current density, eq. (3).

ε - Film porosity, eq. (2).

T_f - Thickness of porous film.

T_c - Thickness of colloidal overlayer.

n_f-ik_f - Refractive index of porous film.

overlayer of each moment is determined as follows:

The integrated difference between the dissolution current i_c and the diffusion flux j_D gives the charge used in colloid formation. Valence and molar volume then give the total volume of colloid particles formed. The volume fraction of colloid particles is calculated with the Lorenz-Lorenz mixing rule using the values of n (Table CI), the compact colloidal material refractive index $n_c (= 1.87)$, the bulk solution refractive index n_b, and the bulk densities of the electrolyte and the colloid material. The ratio of the volume per cm^2 and the volume fraction gives the thickness.

To reduce computation time, the optical effects of the inhomogeneous boundary and colloidal layers were represented by the two limiting models described in Section IV, p. 48.

Results

Shown in Figure C4 and Table CII are the results of an automated interpretation of ellipsometer observations of an experiment conducted on a (111) Ag substrate at $0.6\ mA/cm^2$ in stagnant 6 M KOH. A CDC 7600 computer required 5 seconds to evaluate all seven parameters. The accuracy of the fit (Fig. C4), an average distance of 0.5 deg between experimental and calculated points, agrees favorably with experimental uncertainties of ± 0.1 deg in Δ and ± 0.25 deg in ψ which were indicated by the error analysis for the automatic ellipsometer. However, the accuracy of the fit decreases if later portions of the curve are included.

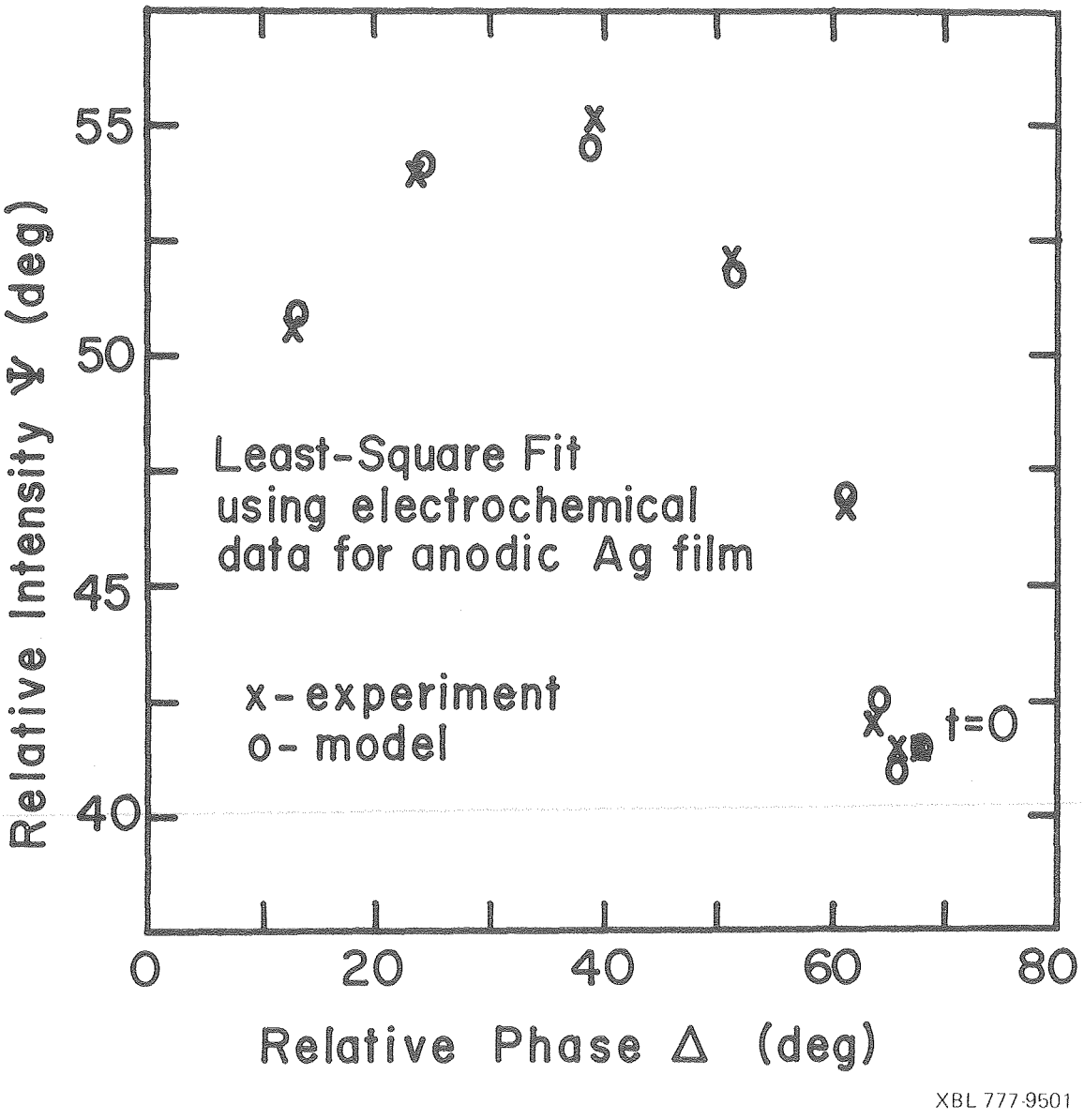

Figure C4. Least-squares fit of the initial portion of ellipsometer measurements of anodic film formation on silver.

Table CII

Least-Squares Fit of Anodic Film on Silver. Average distance between experimental and calculated points d: 0.50 deg.

Parameter			Value	Measure of Uncertainty† Positive	Negative
Solid Film Refractive Index	$n_s - ik_s$	n_s	1.474	+ 0.031	- 0.156
		k_s	0.306	+ 0.036	- 0.027
Initial Current Fraction Used for Dissolution		f	0.018	*	*
Film Thickness for Zero Dissolution Layer		$T_{c\ell}$	130 Å	*	*
Refractive Index of Colloidal Overlayer		n	1.448	+ 0.059	- 0.038
Initial Film Porosity		ε_o	0.272	+ 0.223	- 0.167
Film Thickness for Zero Porosity		T_{f1}	1,770 Å	4,250	*

†Change in parameter value resulting 0.83 deg change in d.
*Non parabolic behavior about the minimum, resulting in excessive number of iterations.

The minimum given by the parameters is the best obtained after numerous Monte Carlo searches (see Section IV, p. 63), supporting uniqueness of the solution. Although seven parameters are involved in fitting the $\Delta - \psi$ curve, various characteristics of the model provide additional constraints. Besides values of Δ and ψ, the shape of the curve and the charge passed as a function of time are 2 additional experimental quantities.

The value found for the refractive index of the compact film material, 1.47 - 0.31 i, is not the value for Ag_2O of 2.18 - 0.28 i determined independently from ellipsometer measurements. The large measures of uncertainty for f, $T_{c\ell}$ and T_{f1} as well as the non-parabolic behavior about the minimum for f and $T_{c\ell}$ are indications that the modeling of the colloid layer and the description of the compaction of the film (eq. (2)) are inadequate.

Appendix D. Interfacial Concentration Determined by Ellipsometry

Introduction

Ellipsometry is an optical technique in which monochromatic polarized light is reflected from a specimen surface. Changes in the state of polarization caused by the reflection are measured and interpreted in terms of physical properties of the reflecting surface [1]. The traditional use of ellipsometry has been restricted to the investigation of solid thin films and, until recently, was confined to slowly-changing phenomena due to the slow response (approx. 5 min.) of manually operated instruments.

The presence of mass-transfer boundary layers has been shown previously [2] to significantly affect the measurement of films and surfaces by ellipsometry. The recent development of automatic ellipsometers [3] has made it possible to use ellipsometry as a new technique for specifically observing mass-transport boundary layers on a local level. The technique samples an area of the interface which is determined by the intersection with the light beam (usually a few mm diameter) and doesn't interfere with transport processes. Since the measured parameters are sensitive to the refractive index of the liquid phase at the interface the technique is applicable to all transport processes which result in boundary layers of variable refractive index which includes heat transfer processes. An optically reflecting interface is necessary, preferably one which remains unaffected by the transport process, otherwise, interruption of the transport process can be used to establish changes in substrate optical properties.

The purpose of this paper is to demonstrate the validity of the technique by its application to electrolytic mass transport in the

deposition and dissolution of Cu from aqueous $CuSO_4$. Stagnant electrolyte and channel flow have been used.

Principles of Ellipsometry

Changes in the state of polarization caused by reflection are expressed by the ratio ρ of the reflection coefficients r_p and r_s for the electric field components parallel and normal to the plane of incidence. The complex quantity ρ is conveniently described by a relative amplitude change $\tan \psi$ and a relative phase change Δ (eq. 1); ψ and Δ are experimentally measured.

$$\rho = \frac{r_p}{r_s} = \tan \psi \, e^{i\Delta} \quad . \tag{1}$$

For ideal (planar, smooth, isotropic) bare surfaces, the reflection coefficients are given by the Fresnel equations (eqs. 2,3) which involve the angle of incidence ϕ (angle between incident or reflected light beam and surface normal) and the angle of refraction ϕ' (angle between transmitted beam and surface normal).

$$r_p = \frac{\tan (\phi - \phi')}{\tan (\phi + \phi')} \tag{2}$$

$$r_s = \frac{\sin (\phi - \phi')}{\sin (\phi + \phi')} \quad . \tag{3}$$

The angle of refraction ϕ' can be obtained from the angle of incidence ϕ and the refractive indices of incident medium n_o and reflecting medium n_s by use of Snell's law of refraction (eq. 4)

$$\sin \phi' = \frac{n_o}{n_s} \sin \phi' \quad . \tag{4}$$

For a light-absorbing substrate, such as a metal, the refractive index n_s and the angle of refraction ϕ' are complex quantities [1]. For a film-covered surface, r_p and r_s can be determined by use of the Drude equations [4] in place of the Fresnel equations.

Optical Effect of Boundary Layers

The optical effect of a mass-transport boundary layer on light reflected from an underlying substrate is illustrated in Figure 5. Computationally, the continuously varying concentration in the (optically inhomogeneous) boundary layer can be represented by a series of (optically homogeneous) layers of uniform refractive index, with refraction and reflection of the light beam taking place at each interface between layers. Optical calculations have shown that for concentration gradients typically encountered in mass-transport boundary layers, reflection from within the boundary layer is negligible, and the principal effect is a change in the angle of incidence ϕ_{od} on the substrate. This effect depends on the refractive incides in the bulk fluid, n_{ob}, and at the interface, n_{oi}, and can be determined from the angle of incidence ϕ_o outside the boundary layer by use of Snell's law.

$$\sin \phi_{od} = \frac{n_{ob}}{n_{oi}} \sin \phi_o \quad . \tag{5}$$

The change in angle of incidence on the substrate, in turn, results in the measured changes in the ellipsometer parameters ψ and Δ. The independence of the boundary layer effect from the nature of the concentration profile or the thickness of the layer forms the basis of the present use of ellipsometry for the determination of interfacial concentrations.

Equipment

Measurements were made with a self-compensating automatic ellipsometer [5], Fig. 9. The light source was a 100-watt mercury short arc lamp. The 5461 Å line was selected by a narrow band interference filter. Glan-Thompson prisms in rotating mounts served as polarizer and analyzer. The two Faraday cells serve to electrically rotate the plane of polarization to reach compensation. The azimuths of rotation are the two measured parameters. A mica plate served as quarter wave compensator. Iris diaphrams have been used to define a light beam of 3 mm diameter which intersects the reflecting surface with an ellipse of approximately 3×6 mm. Cell windows were 6.3 mm thick quartz, and were oriented normal to the light beam and provided an angle of incidence of 75 deg. An RCA 931 A photomultiplier was used for light detection.

Mass-transport boundary layers were generated by the electrochemical deposition and dissolution of copper in aqueous $CuSO_4$ conditions under controlled transport conditions. A cross-section of the flow channel used for forced convection experiments is shown in Fig. 13. The trapezoidal cross-section had a hydraulic diameter of

1.21 cm. A 75 cm entrance length was used. Convection-free experiments were conducted with stagnant electrolyte in a similarly designed cell.

Experimental Procedures

Single crystal copper electrodes ((111),(100)) of 1×3 cm area were cast in epoxy holders and finished in a sequence of abrasive leveling, electropolishing, and mechanical polishing with 1 μm diamond paste. To avoid natural convection, the electrode surface under observation was oriented horizontally facing downward in the stagnant electrolyte. In the flow channel, the electrode was oriented vertically. To minimize surface oxidation, the 0.2 M $CuSO_4$ electrolyte was deoxygenated with a nitrogen stream saturated with water. This was particularly important for the case of forced convection, where diffusion of dissolved oxygen can result in significant rates of oxide formation. The electrolyte continuously contacted a copper surface in the electrolyte reservoir to minimize etching of the surface under observation caused by the $Cu - Cu^{++}$ disproportiation to Cu^{+}.

The optical effect of the mass-transport boundary layer was separated from that caused by changes in surface roughness by the use of current interruption techniques. In the flow cell, current pulses were applied to generate step changes in the interfacial concentration (Fig. D1). In the stagnant cell, the time-dependence of the interfacial concentration was followed by applying cathodic current densities of 5, 10, and 20 mA/cm^2 for varying time periods. At the end of each deposition period, a pump circulated the electrolyte in the cell to remove the diffusion layer. A refractometer[†] was used to determine the

[†]Bausch-Lomb Precision Refractometer, Catalogue Number 33-45-03.

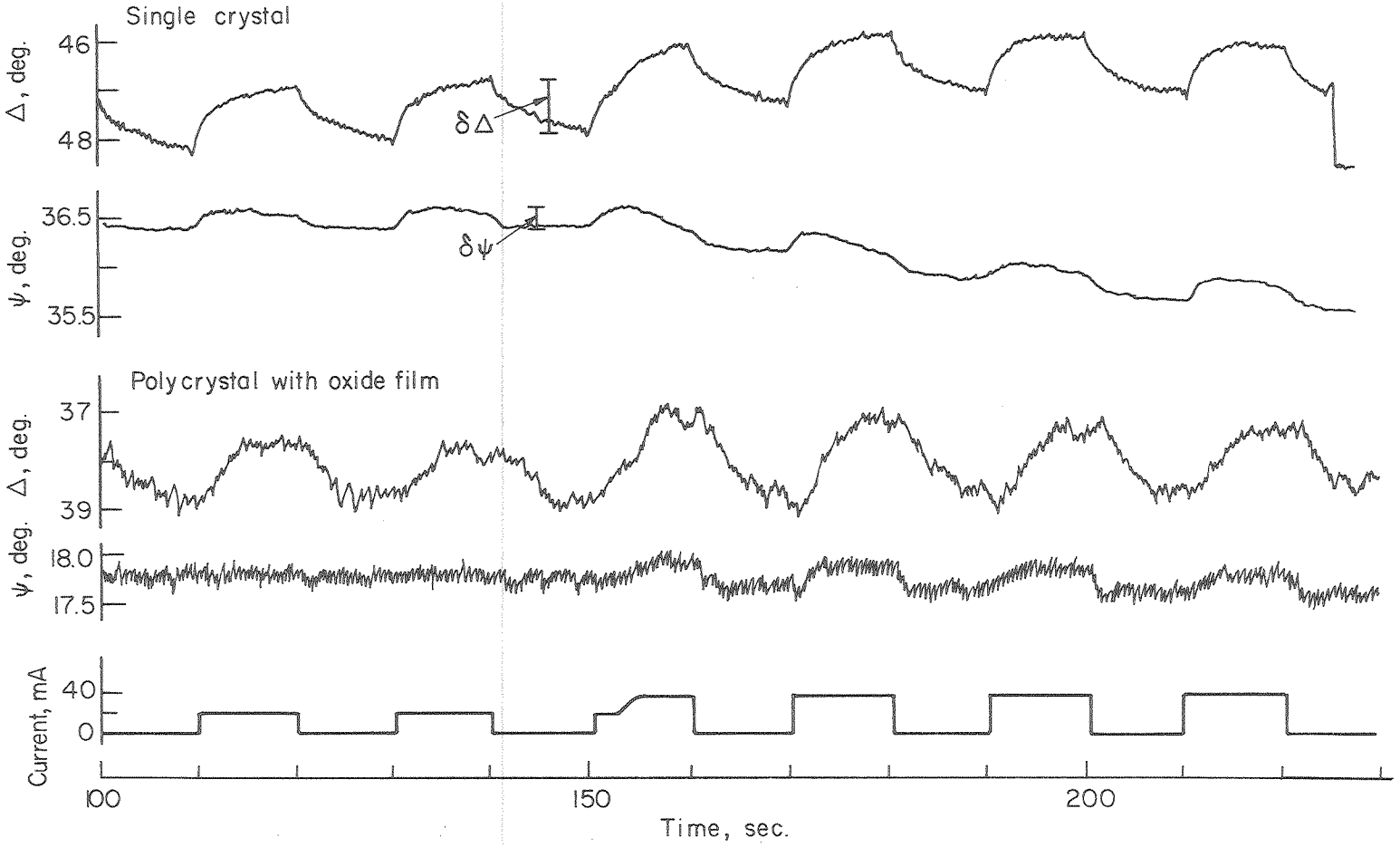

Figure D1. Experimental observation of cathodic convective diffusion boundary layer (Re > 500) by interruption technique. Cu deposition from 0.1 M $CuSO_4$. Single crystal $(III)_2$face. Polycrystalline Cu with oxide film. Electrode 3.3 cm^2.

XBL758-6998

dependence of refractive index on the $CuSO_4$ concentration. For $0 < C \leq 0.2$ M , (546.1 nm wavelength)

$$n_o = n_{H_2O} + 0.029\ C \qquad (6a)$$

The corresponding temperature dependence (for $20 \leq T \leq 30°C$) was found to be

$$n_o(T) = n_o(20°) - 0.00012\ (T - 20)\ . \qquad (6b)$$

Results

As indicated in Figure D1 the changes in Δ due to concentration changes, $\delta\Delta$, are much larger than the corresponding changes in ψ . The experimental data have been interpreted by substituting ϕ_{od} and n_{oi} from eqs. (5) and (6a) into eqs. (1) - (4) to reproduce the experimentally generated changes in Δ . The magnitude of $\delta\Delta$ depends on the optical constants of the reflecting surface [3]. Effective substrate optical constants were first determined from the values of Δ and ψ without the boundary layer, by the use of eqs. (1) - (3).

Figure D2 shows the changes in interfacial concentration as a function of $t^{1/2}$ for convection free copper deposition. The solid lines are given by the Sand equation [6] (constant transport properties) for a diffusion coefficient $D = 5\times10^{-6}\ cm^2/s$ and a transference number $t_+ = 0.385$. The deviation of the experimental data show a trend similar to interferometer results which could be interpreted by the use of concentration-dependent transport properties [7].

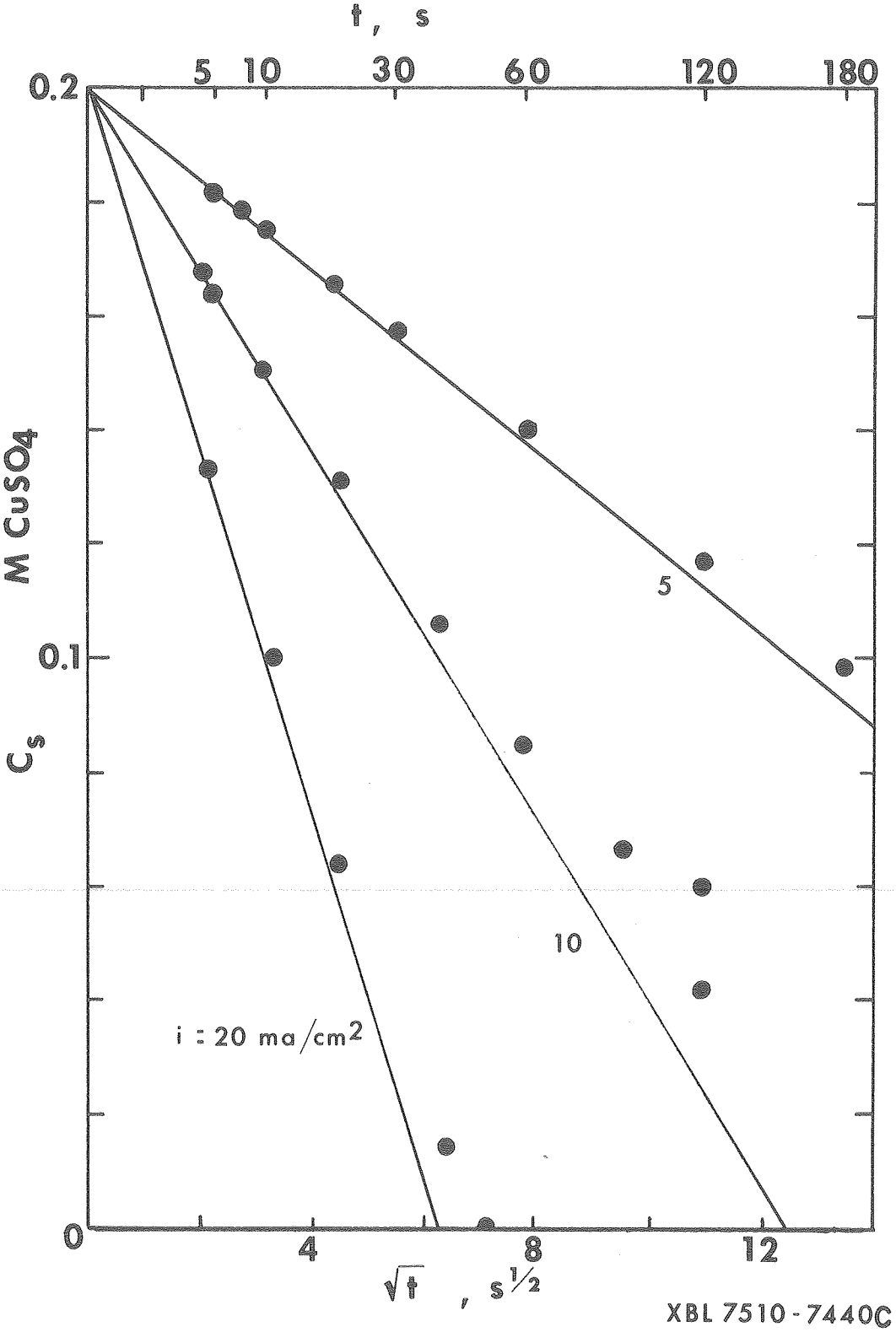

Figure D2. Experimental dependence of the interfacial $CuSO_4$ concentration C_s with $t^{1/2}$ (stagnant electrolyte). Electrode current density indicated next to solid curves given by Sand Eq. [12]. $D = 5 \times 10^{-6}$ cm^2/s, t+ = 0.385.

The forced-convection results are shown in Figure D3. Changes in concentration between the bulk fluid and interface are expressed as functions of the electrode current density i and Reynolds number, again for copper deposition. The solid lines represent the following Sherwood number correlations. In the laminar region, theory [8] gives

$$Sh = 1.23\ (ReSc\ d_n/x)^{1/3} \tag{7}$$

while in the turbulent region, the Chilton-Colburn analogy [9] and the integral method [10] with $v \propto y^{1/7}$ leads to

$$Sh = 0.0395\ Re^{3/4} \cdot Sc^{1/3} \ . \tag{8}$$

The Sherwood number has been expressed here as

$$Sh = \frac{i(1 - t_+)d_h}{zFD(C_b - C_i)} \ . \tag{9}$$

Bulk fluid properties $\rho = 1.027$ g/cc , $\nu = 0.0133$ cm^2/s , $D = 5.19\times10^{-6}$ cm^2/s , and $t_+ = 0.336$ have been used. The experimental results in the flow cell show a smaller concentration difference than predicted by the correlations. The increase in diffusion coefficient with decreasing concentration could account for this deviation.

To demonstrate the validity of the technique for interfacial concentrations greater than bulk concentrations, measurements were also conducted on the dissolution of copper. The results are presented below.

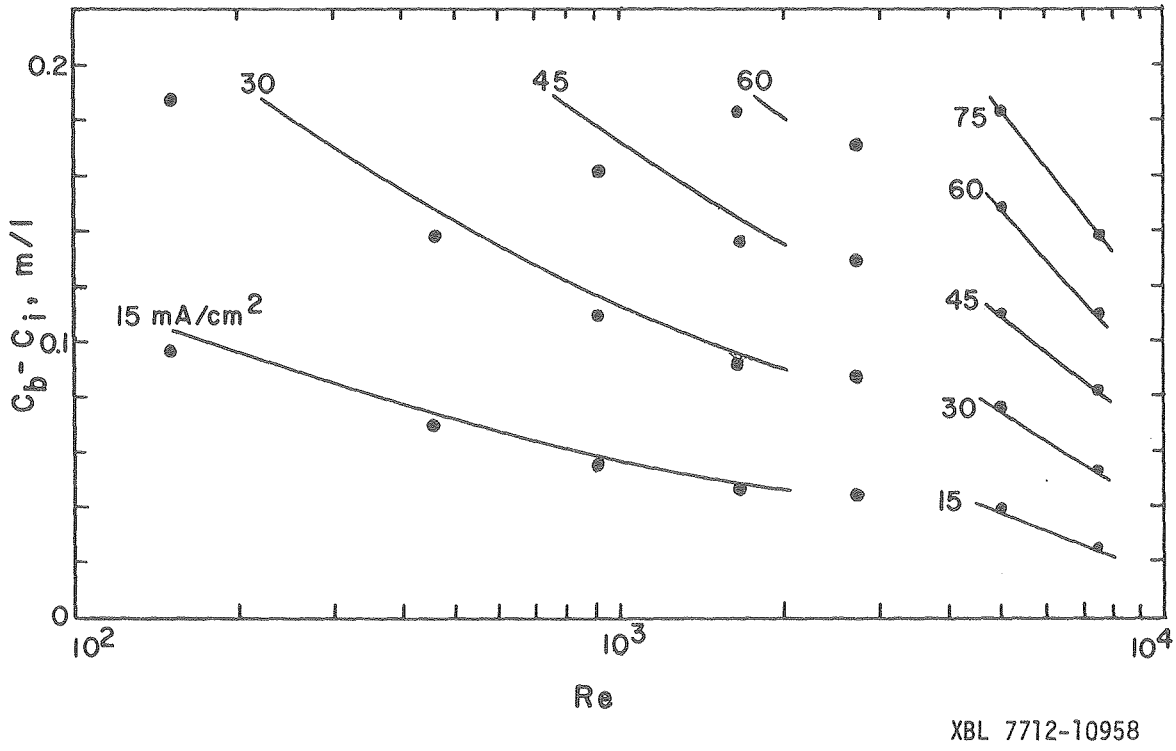

Figure D3. Experimental dependence of concentration difference on flow velocity for different current densities. Cathodic deposition from 0.2 M $CuSO_4$, channel flow.

Symmetry of Mass-Transport for Metal Deposition and Dissolution

(Re = 1600, 0.2 M bulk $CuSO_4$ concentration)

	Deposition		Dissolution	
i	$\delta\Delta$	$C_b - C_i$	$\delta\Delta$	$C_b - C_i$
15 mA/cm^2	-0.64 deg	0.045 moles/liter	0.59 deg	-0.045 moles/liter
30	-1.27	0.091	1.22	-0.094
45	-1.89	0.135	1.82	-0.145
60	-2.55	0.182	2.44	-0.188

Note that the ellipsometer parameter $\delta\Delta$ is not simply related to the concentration difference $C_b - C_i$ because of changes in the optical constants of the electrode surface.

Conclusions

Ellipsometry has been introduced as a new technique for the in situ measurement of local interfacial concentrations (or temperatures) under various transport conditions. The technique complements the observation of boundary layers by interferometry, where the interfacial refractive index may be difficult to derive precisely from the observations [11].

Model experiments conducted with the electrochemical deposition and dissolution of Cu have shown good agreement with predictions derived from established correlations. Minor disagreements can be attributed to the use of concentration-independent transport properties. For a practical resolution of an ellipsometer of 0.02 deg in the value

of Δ , 0.002 M changes in $CuSO_4$ concentration can be detected. For heat transfer in aqueous medium, the resolution is about 0.5 deg C.

The major difficulties associated with this technique are due to surface changes occurring during the generation of the mass-transport boundary layer. Equation (2) indicates the dependence of Δ and ψ on the reflecting surface refractive index n_s . Deposition and dissolution both change the surface topography, as do chemical reactions with dissolved materials such as oxygen.

The fast response of recently-developed automatic ellipsometers [3] is primarily responsible for the feasibility of mass transport studies, allowing the use of current-interruption techniques to separate out the effects of surface changes.

References

1. R. H. Muller, "Principles of Ellipsometry," in Advances in Electrochemistry and Electrochemical Engineering, Vol. 9, P. Delahay and C. W. Tobias, ed. (John Wiley & Sons, New York), pp. 167-226.

2. R. H. Muller and C. G. Smith, Surf. Sci. 56, 440 (1976).

3. R. H. Muller, Surf, Sci. 56, 19 (1976).

4. P. Drude, Ueber Oberflachenschickten, Ann. Der Physik und Chemis 36, 531-561, 865-897 (1889).

5. H. J. Mathieu, D. E. McClure, and R. H. Muller, Rev. Sci. Instrum. 45, 798 (1974).

6. H. J. S. Sand, Phil. Mag. 1 (6), 45 (1901).

7. F. R. McLarnon, R. H. Muller, and C. W. Tobias, Electrochim. Acta 21, 101 (1976).

8. J. Newman, Electrochemical Systems (Prentice-Hall, Inc., Englewood Cliffs, N.J., 1973), pp. 305-318.

9. C. H. Chilton and A. P. Colburn, Ind. Eng. Chem. 26, 1183 (1934).

10. R. E. Acosta, Ph.D. Thesis (U.C. Berkeley, 1974) LBL-2242.

11. F. R. McLarnon, R. H. Muller, and C. W. Tobias, J. Opt. Soc. Am. 65, 1011 (1976).

Appendix E. Concentration of Supporting Electrolyte at Electrode Surfaces

Introduction

The determination of the electrolyte composition at the cathode surface has immediate applications towards industrial electrorefining processes. In free convection, the rate of mass transfer is greatly influenced by the variation of the density of the electrolyte within the mass-transport boundary layer. Knowledge of the interfacial concentration of supporting electrolyte is necessary for the calculation of electrode current densities which are controlled by mass-transport.

Early measurements performed by pinhole sampling[1] and freezing the electrolyte[2] indicated that during copper deposition, the increase in H_2SO_4 concentration is 0.5 to 0.7 times the change in $CuSO_4$ concentration. Computations based on the technique of dimensional analysis[3] suggested a much lower value for the increase in acid concentration. Optical measurements by interferometry in a capillary cell[4] and during free convection[5] seem to confirm the larger changes in H_2SO_4 .

The degree of dissociation of the bisulfate ion greatly influences the suppression of Cu^{++} migration and the accumulation of H^+ at the electrode surface. Hseuh and Newman[4] obtained numerical solutions of the convective diffusion equation for boundary layer (rotating disc, forced convection) and penetration (stagnant diffusion) models for mass transport. Selman and Newman[6] similarly obtained solutions for free-convection boundary layers. The two cases of total and no dissociation of the bisulfate ion were treated. For complete dissociation, in the limit of well-supported electrolyte, the change in H_2SO_4 varied (for

the three boundary layer models) from 0.43 to 0.50 times the change in $CuSO_4$ concentration. For no dissociation, the proportionality constant varied from 0.16 to 0.27. The ionization constant for the bisulfate ion at infinite dilution, $K = 0.0103$, has been found by Raman spectroscopy[4] to increase by three orders of magnitude at 3 molar H_2SO_4 concentration. The larger experimental values cited[4,5] for the increase in H_2SO_4 should remain uncertain, as interferometry measurements in general include distortion by light deflection effects,[7] which complicate the derivation of interfacial concentrations.

The recent development of automatic ellipsometers with fast response times[8] has led towards a new technique for the determination of interfacial refractive indices. The $CuSO_4 - H_2SO_4$ system has been studied. The refractive index of the electrolyte within the boundary layer is generally a result of both the Cu^{++} and H^+ concentrations. To obtain unique interpretations of experimental data, measurements have been performed at limiting current, where the cuprous ion concentration (zero) is known.

Ellipsometry of Boundary Layers

Ellipsometry measures changes in the state of polarization of light reflecting from a surface. The experimentally determined parameters are the relative intensity parameter ψ and the relative phase Δ, which refer to different intensity changes and phase shifts for orthogonal components of the electric field vector.[9] An analysis of the optical effect of the mass-transport boundary layer has been presented earlier.[10] The basis for the numerical method used is illustrated in Figure 5.

The refractive index profile resulting from the concentration field may be viewed as an inhomogeneous film. This film may be approximated by a series of homogeneous films. Reflection and refraction occur at each interface. Computations indicate,[10] however, that for boundary layer thicknesses greater than about 10μm, reflection within the boundary layer becomes negligible. For this "thick-film" regime, which encompasses most transport conditions, the mass-transport boundary layer results in a modification of the interfacial angle of incidence. Changes in Δ and ψ may be characterized by using Snell's law to couple the interfacial refractive index with the appropriate bare substrate or film covered ellipsometer equations.[9] For boundary layer thicknesses greater than about 10μm, ellipsometry is sensitive to the interfacial refractive index but not to the refractive index profile or to the thickness of the boundary layer.

Changes in the optical properties of the substrate occur during the electrochemical generation of the diffusion layer. As ellipsometry is particularly sensitive to surface properties, care must be taken to separate the optical effect of the boundary layer from effects due to the changing substrate. The outlined experimental procedure sought to accomplish this separation. In addition, the magnitude of the changes in ψ and Δ due to changes in the interfacial refractive index depends on the substrate optical constant.[10]

Experimental Procedure

Mass-transport boundary layers were generated by galvanostatic copper deposition. Current interruption techniques were used to separate

surface changes from changes in the interfacial refractive index. Figure D1shows changes in Δ and ψ during deposition from a flowing electrolyte. The current was manually interrupted when the electrode potential began the sharp rise characteristic of secondary H_2 evolution, at which time the flowing electrolyte dissipated the diffusion layer. Measurements were made with an automatic self-compensating ellipsometer.[11]

Two transport conditions were investigated: diffusion through a stagnant, convection-free electrolyte (horizontal electrode facing down) and forced convection across a vertical electrode. Figure 13shows a view of the flow cell. Windows were oriented so that the light enters and leaves the cell at normal incidence and reflects from the surface at an angle of incidence of 75 degrees. The equivalent hydraulic diameter was 1.21 cm, and a 75 cm entrance length allowed development of the fluid velocity profile. The cell for stagnant electrolyte studies was similarly designed.

Single crystal copper electrodes ((100), (111)) of approximately 1 × 3 cm area were used. They were cut by electrochemical machining and cast in cylindrical epoxy mount. A combination of abrasives and anodic dissolution was used to polish the cathodes to a 1μm finish.

To minimize the surface chemical reaction, dissolved oxygen was removed from the electrolyte by stripping with water-saturated nitrogen. To reduce surface topography changes due to the $Cu - Cu^{++}$ disproportion to Cu^{+}, the electrolyte continuously contacted bulk copper. A refractometer[12] was used to correlate the concentrations of $CuSO_4$ and H_2SO_4 with the refractive index at 5461 Å wavelength.

Results

As indicated in Figure D1 the change $\delta\Delta$ due to the change in interfacial refractive index is larger than the corresponding value of $\delta\psi$,[10] and is therefore measured to greater accuracy by the 0.01 deg. resolution of the instrument. Effective substrate optical constants were first determined for the copper surface without the diffusion layer. The interfacial refractive index was determined from computations[10] by reproducing the value of $\delta\Delta$. Assuming the additivity of molar refractivities for $CuSO_4$ and H_2SO_4 , the concentration of H_2SO_4 was calculated from the refractive index at the surface.

Convectionless diffusion results are shown in Figure E1. Acid concentration (bulk values) was varied up to 6 molar. Solubility limits prevented larger acid concentrations for the 0.5M bulk copper sulfate curve. Electrode current densities of 30, 60, and 120 mA/cm^2 were used for the 0.1, 0.25 and 0.5 M $CuSO_4$ solutions to maintain deposition periods of about 5 sec. For comparison, the theoretical values of Hseuh and Newman[4] and Wilke et al.[3] are presented for 0.25 M bulk $CuSO_4$.

Convective diffusion results are presented below:

ACCUMULATION OF SULFURIC ACID

C_A^∞	Re	i	C_B^∞	$C_B^o - C_B^\infty$	$(C_B^o - C_B^\infty)/C_A^\infty$
0.176 M	750	30mA/cm^2	3.89 M	0.062±0.009	0.35±0.05
	6250	65		0.060	0.34
0.193	1080	40	1.02 M	0.067±0.007	0.35±0.04
	8600	80		0.071	0.37

ACKNOWLEDGEMENTS

This work was supported by the Division of Materials Sciences, Office of Basic Energy Sciences, U. S. Department of Energy.

I would like to thank Dr. Rolf Muller for his guidance and acknowledge his development of the automatic ellipsometer which was used in this dissertation. I would also like to thank Walter Giba and Lee Johnson for their assistance in numerous aspects of experimental work.

My thanks also go to Linda McGuire and Carol Payne for their help in typing this dissertation.

Results

As indicated in Figure D1 the change $\delta\Delta$ due to the change in interfacial refractive index is larger than the corresponding value of $\delta\psi$,[10] and is therefore measured to greater accuracy by the 0.01 deg. resolution of the instrument. Effective substrate optical constants were first determined for the copper surface without the diffusion layer. The interfacial refractive index was determined from computations[10] by reproducing the value of $\delta\Delta$. Assuming the additivity of molar refractivities for $CuSO_4$ and H_2SO_4 , the concentration of H_2SO_4 was calculated from the refractive index at the surface.

Convectionless diffusion results are shown in Figure E1. Acid concentration (bulk values) was varied up to 6 molar. Solubility limits prevented larger acid concentrations for the 0.5M bulk copper sulfate curve. Electrode current densities of 30, 60, and 120 mA/cm^2 were used for the 0.1, 0.25 and 0.5 M $CuSO_4$ solutions to maintain deposition periods of about 5 sec. For comparison, the theoretical values of Hseuh and Newman[4] and Wilke et al.[3] are presented for 0.25 M bulk $CuSO_4$.

Convective diffusion results are presented below:

ACCUMULATION OF SULFURIC ACID

C_A^∞	Re	i	C_B^∞	$C_B^o - C_B^\infty$	$(C_B^o - C_B^\infty)/C_A^\infty$
0.176 M	750	30mA/cm^2	3.89 M	0.062±0.009	0.35±0.05
	6250	65		0.060	0.34
0.193	1080	40	1.02 M	0.067±0.007	0.35±0.04
	8600	80		0.071	0.37

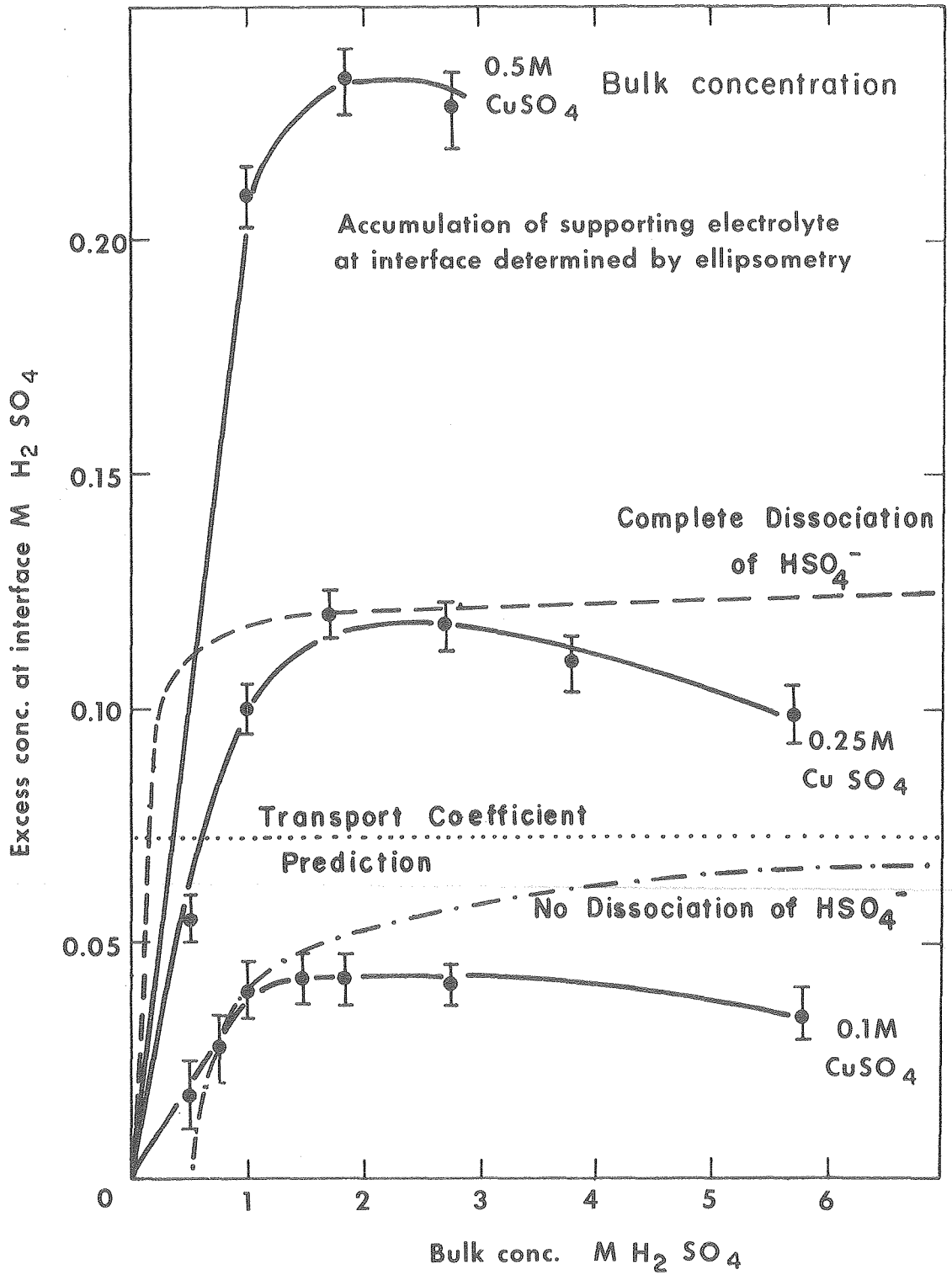

XBL 768-3276A

Figure 1. Accumulation of supporting electrolyte at the electrolyte-electrode interface. Cu deposition from $CuSO_4$ - H_2SO_4 mixtures, stagnant solution, limiting current. Broken curves, theoretical values based on complete or no dissociation of the bisulfite ion (Reference 4).

C_B^o and C_B^∞ refer to the interfacial and bulk fluid H_2SO_4 concentrations, while C_A^∞ is the bulk $CuSO_4$ concentration. Other flow velocities (characterized by the Reynolds number Re) were investigated, but the increase in H_2SO_4 concentration was constant for a given $CuSO_4$-H_2SO_4 solution. The large degree of uncertainty is primarily due to the roughening of the copper electrode during deposition.

Discussion

The results for both convectionless and convective diffusion indicate that the bisulfate ion is largely, but not completely dissociated. For forced convection, the value of 0.35 for $\left(C_B^o - C_B^\infty\right)/C_A^\infty$ lies between the values of 0.43 and 0.16 for complete and no dissociation.[4]

As previously mentioned, the large uncertainties in the measurements under forced convection are largely due to electrode surface changes. Roughening is greatly accentuated by the dissolved oxygen content of the electrolyte. The stripper used to remove oxygen was designed to treat the two liters of solution used in the stagnant cell system, and seemed inadequate for the 20 liter volume used for the flow cell.

Previous investigations[13] have indicated that the rate at which limiting current is reached effects the limiting current plateau. It is possible that the values presented here for the accumulation of acid have been influenced by the relatively fast approach to limiting current (5 sec).

While ellipsometry should be intrinsically more accurate than the methods previously cited,[1-5] unsteady state effects could alter the comparison of experimental results. Further studies should include the

rate and manner (potentiostatic vs galvanostatic) in which limiting current is reached. Because of changes in surface topography, towards which ellipsometry is particularly sensitive, rigorous deoxygenation of the electrolyte is necessary.

References

1. H. J. Reed, A. R. Graham, Trans. Electrochem. Soc. 80, 329 (1941).

2. A. Brenner, Tech. Proc. Amer. Electroptal. Soc. 95 (1940).

3. C. R. Wilke, M. Eisenberg, and C. W. Tobias, J. Electrochem. Soc. 106, 513 (1953).

4. L. Hseuh and J. Newman, Ind, Eng. Chem. Fundam. 10, 615 (1971).

5. Y. Awakura, M. Okoda, and Y. Kondo, J. Electrochem. Soc. 124, 1050 (1977).

6. J. Selman and J. Newman, J. Electrochem. Soc. 118, 1070 (1971).

7. F. R. McLarnon, R. H. Muller, and C. W. Tobias, Electrochim. Acta, 21, 101 (1976).

8. R. H. Muller, Surface Sci. 56, 19 (1976).

9. R. H. Muller, "Principles of Ellipsometry," in Advances in Electrochemistry and Electrochemical Engineering, Vol. 9, P. Delahay and C. W. Tobias, eds. (John Wiley & Sons, New York), pp. 167-226.

10. R. H. Muller and C. G. Smith, Surface Sci. 56, 440 (1976).

11. H. J. Mathieu, D. E. McClure, and R. H. Muller, Rev. Sci. Instrum. 45, 798 (1974).

12. Bausch-Lamb Precision Refractometer, Catalogue Number 33-45-03.

13. J. Selman, "Measurement and Interpretation of Limiting Currents," (Ph.D. Thesis, U.C. Berkeley, 1971) UCRL-20557.

Appendix F. Physical Properties of Anodic Film Materials

Optical Constants of Solid Film Materials (F1)

Compressed powders of known composition have been used to independently measure the optical constants of anodic film materials. A hydraulic press is used to compact materials in the form of powders in a cylindrical stainless steel die. The compacted material replicates the polished surfaces of the end plates. To avoid thermal decomposition of labile compounds, the pressing was done at room temperature. To facilitate removal from the die and subsequent handling of the fragile discs, the powders were pressed inside a brass ring placed on the lower end plate. The use of annealed rings has been found to minimize the relaxation of elastic deformation which causes strain-induced anisotropies in the samples. Other variables which affect the mechanical properties of the specimens were found to include pressure and the particle size and shape of the powder.

Optical constants determined by this method are shown in Table F1. Corrections for porosity effects have been based on the difference between the measured density of the compacted specimens and the theoretical density of the same material. Ellipsometer measurements were performed in air.

Molar Refractivity of Zincate

The concentration-refractive index relationship for zincate ($Zn(OH)_4^{=}$) was determined by measuring the refractive index of alkaline solutions containing known quantities of analytical grade ZnO powder. Measurements were performed using a refractometer (ref. G28) at

Table F1. Optical Constants of Solid Film Materials (546.1 nm)

Material	Densities		n - ik		
	specimen	theoretical	present	literature (real part)	ref.
Ag_2O	6.18 g/cm^2	7.14 g/cm^2	2.17-0.28i	2.10†	F2
CdO	5.37	8.15	2.50-0.01i	2.49	F3
ZnO	5.55	5.61	2.00-0.001i	2.01	F2
PbO_2	7.58	9.38	2.09-0.31i	2.23	F3
AgOH		5.7	1.87-0.0i††		
$Zn(OH)_2$		3.05	1.68-0.0i††		
$Cd(OH)_2$		4.79	2.13-0.0i††		
Ag		10.49	0.18-3.61i†††		
Zn		6.92	1.92-4.95i†††		
Cd		8.55	1.64-3.96i†††		

† Calculated from literature value for the molar refractivity, ref. F2.

†† Calculated using method given in ref. F2 (p. 10-258). AgOH was computed from Ag_2O refractive index, $Zn(OH)_2$ and $Cd(OH)_2$ from ZnO and CdO refractive indices.

††† Determined from ellipsometer measurements in air on polished metal surfaces.

wavelengths of 435.8, 546.1, and 539.2 nm, in 6 M and 8 M KOH solutions, and at 20° and 30°C. Zincate concentrations up to 0.6 M were measured; high concentrations could not be obtained by the dissolution of ZnO powder. The concentration-refractive index relationship was linear,

$$n = n_{ref} + 0.00575\ C_{Zn(OH)_4^{=}} .$$

The reference refractive index is the refractive index of the KOH solution at a given temperature and wavelength (F4).

Solubilities of the Solution-Phase Ag, Zn, and Cd Species

The solubilities used in computations (Table I, p. 83) were taken from the literature. The references for the solubilities are: silver - A23, A33; zinc - Z16; and cadmium - C1 to C4.

Transport Properties

The diffusion coefficients used in computations were those presented in Table I, p. 83. They agree reasonably well with literature values for the silver (A23), zinc (F5, F6), and cadmium species (C20). The viscosity and density of KOH solutions are given in ref. F7. For 6 M KOH, $\nu = .0145\ cm^2/s$ and $\rho = 1.238\ g/cm^3$ at 25°C.

References

F1. C. G. Smith and R. H. Muller, LBL-7355 (MMRD Annual Report, 1977) p. 248.

F2. J. A. Dean, Ed., Lange's Handbook of Chemistry (McGraw-Hill, New York, 1973), pp. 4-9 to 4-149, pp. 10-258 to 10-259.

F3. P. E. Liley, Y. S. Touloukian, and W. R. Gambell, Chemical Engineer's Handbook (McGraw-Hill, NY, 4th Ed., 1969) J. H. Perry, Ed., Sec. 3, p. 3-4.

F4. M. Sand, "Light Interference in Electrolyte Films on Metals," LBL-3589 (M.S. Thesis, U.C. Berkeley) 1975, p. 93.

F5. J. McBreen, Report N68-1517, Contract NAS 5-10231, Yardney Electric Corp., New York, June 1967.

F6. T. P. Dirkse, Technical Report AFAPL-TR-72-87, Contract No. S33615-70-C-1022, Project 3145, Calvin College, Grand Rapids, Mich., Dec. 1972.

F7. S. Falk and A. Salkind, Alkaline Storage Batteries (John Wiley & Sons, Inc., NY, 1969) p. 557.

Appendix G. Results and Interpretations of all Experiments

The following pages contain the interpretations of experimental observations on anodic film formation. A discussion of selected experiments has been presented in Sec. VI. The number of the experiment, e.g. Ag 80-1, has been used to determine the order in which the interpretations are listed. Stagnant cell experiments are indicated by the prefixes Ag 80, Cd 100, and Zn 70, and flow cell experiments are indicated by the prefixes Ag 300, Cd 400, and Zn 200. These interpretations were generated by the Fortran IV program RUFF.†

Coding has been used to choose among various alternatives in the representation of the electrode processes (Sec. IV). The key to the codes listed at the top of the output is given below.

Code 1

= 1., The experiment was conducted at constant current. The potential is read in for each experimental value of time, Δ and ψ.

= 2., The experiment was conducted at constant potential, and the electrode current density is read in.

Code 2

Describes the optical treatment of the secondary crystals. For the values given below, the positive value indicates that the Type I film has been treated as a homogeneous film, while the

†The program RUFF is listed in LBL-8083, in preparation.

negative value indicates that the Type I film has been treated as an inhomogeneous film with an assumed parabolic decrease with thickness of the film porosity.

= ±0., Small secondary crystals are treated using eqs. (50) and (51).

= ±1., Small secondary crystals are treated using eqs. (50) and (52).

= ±2., Coherent superposition of the reflection coefficients for the bare and covered portions of the surface (eq. (53)). The crystals are treated as homogeneous films, and the area fraction is given by eq. (52).

±2.5., Incoherent superposition (eq. (55)) of the reflectance ratios for the bare and covered portions of the surface. The crystals are treated as homogeneous films, and their surface coverage is given by eq. (52).

±3., The ray model (Appendix B) is used for the secondary crystals.

±4., The optical effect of the secondary crystals is neglected.

Code 3A

= 0., The porosity of the Type II film is constant with time.

= 4., The porosity decreases parabolically with time from 1 to the value POREI at time t_{NUC}.

Code 3

Describes the growth of the roughness layer.

= 1., The porosity of the layer is constant for the dissolution current i_d being larger than the film formation current i_f, and

the fraction of current FRUFF forming void volume results in an increase in the thickness of the layer. For $i_d < i_f$, the thickness is constant and the porosity increases.

= 2., For $i_d \geq i_f$ the description for the value 1 applies. For $i_d < i_f$, both the porosity and the thickness are constant.

= 3. to 6., The porosity of the layer is constant and the thickness increases, either indefinitely (= 3.), until TPACK (=4.), or until TDISS (=5.). For Code 3 = 6., the thickness increases from TNUC until TPACK.

= 7., The porosity increases from time $t = 0$ until TPACK with a constant thickness, then the thickness increases until TDISS with the porosity remaining constant.

Code 4

= 0., The Type II film has the refractive index TNPT (for silver and zinc, the hydroxides).

= 1., The Type II film has the refractive index TNF (for silver and zinc, the oxides).

Code 5

= 1., The hydration of the secondary crystals is a linear average of the refractive index of water and the non-porous material.

= 2., The Lorentz-Lorenz eqn. (eq. (60)) replaces the linear average in the description for the value 1.

Code 6

Directs the refractive indices used for the Type I film, the hydrate layer, and the secondary crystals. The Type I film is the oxide (TNF) for the values 1, 4, and 5, and is the hydroxide (TNF2) for the value 3. The hydrate layer is the hydroxide (TNF2) for all values except 4, when the layer is the oxide (TNF). The secondary crystals are the oxide for all values except 5, when the layer has the nonhydrated material refractive index TNPT.

Code 7

Directs the rate expressions for the formation of the secondary crystals and the optical effect of the hydrate layer.

= 0., The crystallization rate of the secondary crystals is proportional to their surface area (eq. (2a)).

= 1., The crystallization rate is constant (eq. (2b)).

= 2., At time TDIFF, the kinetics change from eq. (2a) to eq. (2b).

For the values 0-2, the hydrate layer was treated as a homogeneous film with its thickness given by eq. (30). For the following values in which the thickness TF2 has been set to -0.001, the hydrate layer determines the interfacial refractive index of the MTBL.

= 2.5, Same as 2, with the hydrate layer thickness TF2 = -0.001.

= 3.0, Same as Ø., with TF2 = -0.001.

= 3.5, Same as 1., with TF2 = -0.001.

Code 8

= 0., The optical effect of the hydrate layer begins at time t = TNUC.

= 3., The optical effect of the hydrate layer begins at TDIFF.

Code 9

= 0., The thickness of the Type I film is computed using an effective porosity which results from assuming a parabolic decrease in porosity with film thickness (eq. (27)).

= 1., The thickness is computed assuming a constant porosity.

Code 10

= 0., The optical averaging for statistical variations in the secondary crystal properties and for non-stoichiometry effects is on the coherent scale (eq. (53)).

= 1., The optical averaging is on the incoherent scale (eq. (55)).

Code 11

Directs the treatment of transient variations in the porosities of the Type I film and Hydrate layer, and the patchwise coverage of secondary crystals and/or non-stoichiometry.

The porosity of the hydrate layer decreases from 1 to POREF2 over the interval $0 < t < TDIFF$. After TDIFF, the hydrate layer is constant, or increases to 0.99 at TDISS for Code 11 = 2, 3, 6, 7, 12, 13, 16, or 17.

The porosity of the Type I film constant except for the values 1, 3, 5, 7. The porosity changes from POREFØ to FPACK linearly with time, from TNUC to TPACK for Code 11 = 1 or 3, and from TNUC to TDISS for Code 11 = 5 or 7.

For Code 11 = 5, 6, or 7, the fraction of the surface covered by secondary crystals increases parabolically with time from COVII at TNUC to 0.999 at TDISS. For Code 11 = 15, 16, or 17, the change is over the time interval TPACK to TDISS.

For Code 11 $\geq$ 10., a fraction of the electrode surface has the refractive index TNFA while the rest of the surface has the refractive index TNF. For TNUC < t < TPACK, the fraction is COVII. For TPACK < t < TDISS, the fraction increases parabolically with time from COVII to 0.99.

Code 12

= 0., The substrate refractive index is an effective value determined from the value of Δ and ψ at $t = 0$.

= 1., The substrate refractive index uses the values read from the input file.

Code 13

= 0., The formation of the Type I film from the hydrate layer has the constant rate RATF.

= 1., RATF = RATFO * COV(I,1), where COV(I,1) is the fraction of the surface covered by the Type I film (see Code 14).

Code 14

Directs the surface coverages of the Type II and Type I primary layers in relation to the fraction of the surface covered by secondary crystals (Code 11). For Code 11 $\geq$ 10., both primary layers cover the electrode surface. For Code 11 < 10., and Code 14.

= 0., The Type II film covers the surface, while the Type I film covers only the fraction of the surface covered by the secondary crystals (COV (I,1)).

= 1., Both Type II and Type I films have the surface coverage COV(I,1).

= 2., The Type I film covers the surface, while the Type I film has the coverage COV(I,1).

The columns at the bottom of the listings are the experimental values of time, current density, electrode potential, the relative phase Δ, and the relative amplitude parameter ψ, the theoretical (computed) values of Δ and ψ, the thicknesses in angstroms of the Type II, Type I, hydrate, and secondary crystal layers, and the coverage of the secondary crystals according to the projection along the surface normal.

#AG801# #2E-4 AMPS# #1MKOH,P2#

CODES, 1,2,3A,4,5,6,7,8 = 1.0, 2.0, 4.0, 1.0, 1.0, 1.0, 3.0, 0.0,
REYNOLDS NUMBER = 0.0
EFFECTIVE REFRACTIVE INDICES AND POROSITIES,
TYPE 2 FILM 2.170 -.2800 I .210
TYPE 1 FILM 2.170 -.2800 I .000
TYPE 1 HYDRATE 1.355 0.0000 I .980
SECONDARY CRYSTALS 1.878 -.1820 I .350
NUMBER OF SECONDARY SITES/SQCM .35E+09 LIMITING COVERAGE .527
CRYSTAL. RATE OF SEC. CRYSTALS (MA/SQCM), .07956
CRYSTAL. RATE OF TYPE2 FILM (MA/SQCM), .00619
SUPERSATURATION OF IONS, 9.860 ,TIME TO REACH(S) 3.47607
INITIAL DISSOLUTION CURRENT (MA/SQCM) .0129
TIMES, ONSET OF SEC. CRYSTALS(SEC) 42.28 PPT. CONSTANT (S) 15.50
DEHYDRATION RATE (MA/SQCM) .176
AVE. DISTANCE BETWEEN EXP. AND THEORY 6.325 (DEG)

		EXPERIMENT			THEORY		THICKNESSES(A)			
TIME(S)	I(MA/SQCM)	VOLTS	DEL	PSI	DEL	PSI	TYPE2	TYPE1(F)	TYPE1(H)	SECONDARY
0.00	.200	-.100	73.400	42.600	73.400	42.600	-1	0.0	-1	0.0
10.00	.200	.320	68.800	41.500	72.166	42.528	8.2	.0	.0	.0
20.00	.200	.320	67.000	40.700	70.050	42.411	22.9	.0	.0	.0
30.00	.200	.320	66.000	41.100	67.007	42.258	45.8	.0	.0	.0
40.00	.200	.320	65.200	42.800	62.760	42.091	82.2	.0	.0	.0
50.00	.200	.320	65.000	44.800	63.271	41.359	88.4	46.1	-.0	112.8
60.00	.200	.320	64.000	47.300	59.669	42.065	88.4	94.0	-.0	208.7
70.00	.200	.320	60.200	49.500	56.876	42.909	88.4	142.4	-.0	315.1
80.00	.200	.320	55.900	50.900	53.076	44.770	88.4	189.8	-.0	441.3
90.00	.200	.320	51.300	51.900	46.071	46.510	88.4	235.6	-.0	576.1
100.00	.200	.320	46.700	52.400	40.676	46.853	88.4	278.8	-.0	722.6
110.00	.200	.320	41.000	52.400	37.774	46.913	88.4	318.4	-.0	872.7
120.00	.200	.320	36.400	52.100	37.142	47.860	88.4	353.2	-.0	1027.3
130.00	.200	.320	33.200	51.600	36.282	50.044	88.4	382.1	-.0	1185.3
140.00	.200	.320	28.200	51.200	34.073	52.410	88.4	405.8	-.0	1345.0
150.00	.200	.320	25.200	50.800	31.593	54.316	88.4	417.3	-.0	1509.1
160.00	.200	.320	22.300	50.400	29.527	55.687	88.4	421.1	-.0	1675.9
170.00	.200	.320	19.700	49.500	26.368	56.685	88.4	421.1	-.0	1822.2
180.00	.200	.320	17.100	48.900	21.599	57.188	88.4	421.1	-.0	1949.9
190.00	.200	.320	15.700	48.500	16.001	56.935	88.4	421.1	-.0	2063.0
200.00	.200	.360	13.300	48.600	10.563	55.933	88.4	421.1	-.0	2165.1
210.00	.200	.360	11.600	48.200	6.965	54.934	88.4	421.1	-.0	2258.5
220.00	.200	.360	9.800	47.800	4.502	53.594	88.4	421.1	-.0	2344.9
230.00	.200	.360	8.600	47.300	3.111	52.117	88.4	421.1	-.0	2425.5
240.00	.200	.360	7.400	46.900	2.642	50.650	88.4	421.1	-.0	2501.2
250.00	.200	.360	5.400	46.200	2.918	49.293	88.4	421.1	-.0	2572.6
260.00	.200	.360	4.800	45.700	3.765	48.112	88.4	421.1	-.0	2640.4
270.00	.200	.360	3.600	45.000	5.019	47.143	88.4	421.1	-.0	2705.0
280.00	.200	.360	2.600	44.500						
290.00	.200	.360	1.000	43.600						
300.00	.200	.360	.600	42.600						
310.00	.200	.360	.200	41.600						
320.00	.200	.360	-.600	40.900						
330.00	.200	.360	-1.200	40.500						
340.00	.200	.360	-1.600	39.800						
350.00	.200	.360	-1.600	39.200						
360.00	.200	.360	-1.600	38.800						
370.00	.200	.360	-1.600	37.800						
380.00	.200	.360	-1.400	37.300						
390.00	.200	.360	-1.400	36.800						
400.00	.200	.360	-1.200	36.300						

AG 80-2,0.2MA,1MKOH,111

CODES, 1,2,3A,4,5,6,7,8 = 1.0, 2.0, 0.0, 1.0, 1.0, 1.0, 3.0, 0.0,
REYNOLDS NUMBER = 0.0
EFFECTIVE REFRACTIVE INDICES AND POROSITIES,
TYPE 2 FILM 2.170 -.2800 I .210
TYPE 1 FILM 2.170 -.2800 I .000
TYPE 1 HYDRATE 1.364 .0000 I .962
SECONDARY CRYSTALS 1.882 -.1836 I .344
NUMBER OF SECONDARY SITES/SQCM .39E+09 LIMITING COVERAGE .524
CRYSTAL. RATE OF SEC. CRYSTALS (MA/SQCM), .11000
CRYSTAL. RATE OF TYPE2 FILM (MA/SQCM), .00900
SUPERSATURATION OF IONS, 1.000 ,TIME TO REACH(S) .03577
INITIAL DISSOLUTION CURRENT (MA/SQCM) .0019
TIMES, ONSET OF SEC. CRYSTALS(SEC) 20.00 PPT. CONSTANT (S) 30.00
DEHYDRATION RATE (MA/SQCM) .173
AVE. DISTANCE BETWEEN EXP. AND THEORY 5.194 (DEG)

		EXPERIMENT			THEORY		THICKNESSES(A)			
TIME(S)	I(MA/SQCM)	VOLTS	DEL	PSI	DEL	PSI	TYPE2	TYPE1(F)	TYPE1(M)	SECONDARY
0.00	.200	0.000	74.000	42.100	74.000	42.100	-I	0.0	-I	0.0
10.00	.200	.330	69.400	41.400	68.816	41.875	35.8	.0	.0	.0
20.00	.200	.330	67.800	40.500	68.816	41.875	35.8	.0	.0	.0
30.00	.200	.330	66.800	41.300	68.236	41.383	35.8	95.7	-.0	.1
40.00	.200	.330	66.400	43.200	64.102	41.612	35.8	150.3	-.0	2.0
50.00	.200	.330	65.800	45.700	61.264	42.302	35.8	203.9	-.0	14.8
60.00	.200	.330	64.000	49.200	59.631	43.722	35.8	257.6	-.0	57.2
70.00	.200	.330	60.900	54.100	58.900	46.356	35.8	311.2	-.0	143.1
80.00	.200	.330	53.000	58.700	57.488	51.109	35.8	364.3	-.0	272.1
90.00	.200	.330	41.700	61.800	49.546	57.919	35.8	415.6	-.0	435.2
100.00	.200	.330	27.800	62.900	27.926	62.245	35.8	462.8	-.0	622.9
110.00	.200	.330	14.300	61.100	8.954	60.524	35.8	503.2	-.0	828.1
120.00	.200	.330	5.900	58.100	3.108	56.779	35.8	533.3	-.0	1046.0
130.00	.200	.330	.900	55.000	5.148	55.994	35.8	549.1	-.0	1273.3
140.00	.200	.330	-2.100	52.200						
160.00	.200	.330	-4.200	48.200						
180.00	.200	.330	-5.000	45.700						
220.00	.200	.330	-7.200	42.000						
260.00	.200	.330	-10.500	38.500						
300.00	.200	.330	-10.400	34.600						
360.00	.200	.330	-5.500	30.800						
420.00	.200	.330	.400	29.600						
540.00	.200	.330	7.400	29.500						
660.00	.200	.330	9.300	29.900						

AG 80-2,0.2MA,1MKJH,111

CODES, 1,2,3A,4,5,6,7,8 = 1.0, 2.0, 0.0, 1.0, 1.0, 1.0, 3.0, 0.0,
REYNOLDS NUMBER = 0.0
EFFECTIVE REFRACTIVE INDICES AND POROSITIES,
TYPE 2 FILM 2.170 -.2800 I .210
TYPE 1 FILM 2.170 -.2800 I .000
TYPE 1 HYDRATE 1.357 0.0000 I .975
SECONDARY CRYSTALS 1.925 -.1981 I .293
NUMBER OF SECONDARY SITES/SQCM .39E+09 LIMITING COVERAGE .659
CRYSTAL. RATE OF SEC. CRYSTALS (MA/SQCM), .10902
CRYSTAL. RATE OF TYPE2 FILM (MA/SQCM), .00659
SUPERSATURATION OF IONS, 1.782 ,TIME TO REACH(S) .11358
INITIAL DISSOLUTION CURRENT (MA/SQCM) .0015
TIMES, ONSET OF S.C. CRYSTALS(SEC) 20.00 ONSET OF PPT. (S) 27.37
DEHYDRATION RATE (MA/SQCM) .175
AVE. DISTANCE BETWEEN EXP. AND THEORY 8.277 (DEG)

			EXPERIMENT		THEORY		THICKNESSES(A)			
TIME(S)	I(MA/SQCM)	VOLTS	DEL	PSI	DEL	PSI	TYPE2	TYPE1(F)	TYPE1(H)	SECONDARY
0.00	.200	0.000	74.000	42.100	74.000	42.100	-I	0.0	-I	0.0
10.00	.200	.330	69.400	41.400	70.142	41.927	26.2	.0	.0	.0
20.00	.200	.330	67.800	40.500	70.126	41.927	26.2	.0	.0	.0
30.00	.200	.330	66.800	41.300	65.910	41.464	26.2	97.3	-.0	.1
40.00	.200	.330	66.400	43.200	61.603	41.645	26.2	151.1	-.0	1.9
50.00	.200	.330	65.800	45.700	58.594	42.245	26.2	205.1	-.0	13.9
60.00	.200	.330	64.000	49.200	56.803	43.513	26.2	259.3	-.0	53.4
70.00	.200	.330	60.900	54.100	55.954	45.904	26.2	313.4	-.0	133.1
80.00	.200	.330	53.000	58.700	54.607	50.280	26.2	367.2	-.0	252.2
90.00	.200	.330	41.700	61.800	47.502	56.671	26.2	419.4	-.0	402.4
100.00	.200	.330	27.800	62.900	27.812	61.176	26.2	468.2	-.0	575.1
110.00	.200	.330	14.900	61.100	8.582	60.265	26.2	511.1	-.0	763.9
120.00	.200	.330	5.900	58.100	.073	56.564	26.2	545.1	-.0	964.3
130.00	.200	.330	.900	55.000	-.307	55.050	26.2	567.0	-.0	1173.3
140.00	.200	.330	-2.100	52.200	1.402	56.035	26.2	573.3	-.0	1388.8
160.00	.200	.330	-4.200	48.200	-4.242	57.700	26.2	573.3	-.0	1719.2
180.00	.200	.330	-5.000	45.700	-14.064	55.060	26.2	573.3	-.0	1956.2
220.00	.200	.330	-7.200	42.000	-20.119	44.185	26.2	573.3	-.0	2308.4
260.00	.200	.330	-10.600	38.500	-12.030	35.957	26.2	573.3	-.0	2577.3
300.00	.200	.331	-10.400	34.600	-2.438	35.929	26.2	573.3	-.0	2799.7
360.00	.200	.330	-5.500	30.800	3.707	39.377	26.2	573.3	-.0	3078.9
420.00	.200	.330	.400	29.600	3.028	42.521	26.2	573.3	-.0	3315.1
540.00	.200	.330	7.400	29.500	18.872	37.956	26.2	573.3	-.0	3707.0
660.00	.200	.330	9.300	29.900	16.176	36.248	26.2	573.3	-.0	4030.3
-I	-I	-I	-I	-I						

AG 60-3.0,24A,1MKOP,100

CODES, 1,2,3A,4,5,6,7,8 = 1.0, 2.0, 3.0, 1.0, 1.0, 1.0, 3.0, 0.0,
KEY CELLS NUMBER = 0.0
EFFECTIVE REFRACTIVE INDICES AND POROSITIES,
TYPE 2 FILM 2.170 -.2800 I .210
TYPE 1 FILM 1.946 -.2042 I .271
TYPE 1 HYDRATE 1.366 .0000 I .960
SECONDARY CRYSTALS 1.456 -.1348 I .340
NUMBER OF SECONDARY SITES/SQCM .47E+09 LIMITING COVERAGE .790
CRYSTAL. RATE OF SEC. CRYSTALS (MA/SQCM). .06930
CRYSTAL. RATE OF TYPE2 FILM (MA/SQCM). .03450
SUPERSATURATION OF IONS. 2.310 ,TIME TO REACH(S) .19078
INITIAL DISSOLUTION CURRENT (MA/SQCM) .0035
TIMES, ONSET OF SEC. CRYSTALS(SEC) 50.00 PPT. CONSTANT (S) 60.00
DEHYDRATION RATE (MA/SQCM) .132
EFFECTIVE FILM CURRENT(MA/SQCM) .173
AVE. DISTANCE BETWEEN EXP. AND THEORY 7.445 (DEG)

			EXPERIMENT		THEORY		THICKNESSES(A)				
TIME(S)	I(MA/SQCM)	VOLTS	DEL	PSI	DEL	PSI	TYPE2	TYPE1(F)	TYPE1(H)	SECONDARY	COV
0.00	.200	0.300	70.800	42.300	70.800	42.330	-1	0.0	-1	0.0	0.000
10.00	.200	.320	68.800	42.000	67.829	42.153	21.6	.0	.0	.0	.000
20.00	.200	.320	66.200	41.500	65.114	42.036	43.1	.0	.0	.0	.000
30.00	.200	.320	63.200	41.600	62.617	41.951	64.7	.0	.0	.0	.000
40.00	.200	.350	60.900	41.300	60.379	41.899	86.3	.0	.0	.0	.000
50.00	.200	.350	62.100	41.300	60.379	41.899	86.3	.0	.0	.0	.000
60.00	.200	.350	64.000	42.300	64.203	41.775	86.3	103.4	-.0	.1	.000
70.00	.200	.350	67.000	45.000	62.089	42.209	86.3	158.3	-.0	1.7	.000
80.00	.200	.350	67.800	48.600	60.933	43.009	86.3	213.4	-.0	12.1	.000
90.00	.200	.350	65.400	55.000	60.725	44.346	86.3	268.5	-.0	45.6	.000
100.00	.200	.350	60.400	57.200	61.399	46.504	86.3	323.6	-.0	112.3	.001
110.00	.200	.350	61.600	61.300	62.451	50.069	86.3	378.5	-.0	211.1	.004
120.00	.200	.350	58.300	65.200	61.312	55.652	86.3	432.4	-.0	335.2	.010
130.00	.200	.350	42.500	67.400	52.455	62.363	86.3	484.0	-.0	477.6	.020
140.00	.200	.340	31.000	67.900	33.100	66.799	86.3	531.9	-.0	633.0	.035
150.00	.200	.350	19.900	67.700	12.409	66.538	86.3	574.1	-.0	797.8	.056
160.00	.200	.350	10.500	66.200	1.739	62.862	86.3	608.8	-.0	969.6	.082
170.00	.200	.340	3.000	63.900	1.041	60.271	86.3	633.0	-.0	1146.7	.115
180.00	.200	.340	-.400	62.000	3.929	60.025	86.3	645.0	-.0	1328.0	.155
190.00	.200	.330	-3.900	59.800	6.803	61.236	86.3	645.0	-.0	1504.8	.199
200.00	.200	.330	-5.900	57.900							
220.00	.200	.330	-8.800	54.200							
240.00	.200	.330	-10.600	51.700							
260.00	.200	.330	-11.800	49.200							
280.00	.200	.330	-12.700	47.200							
300.00	.200	.330	-13.700	45.300							
320.00	.200	.330	-13.400	40.100							
340.00	.200	.330	-11.700	35.200							
360.00	.200	.330	-8.700	32.400							
380.00	.200	.330	-7.100	31.300							
400.00	.200	.330	-7.700	31.300							
420.00	.200	.330	-6.900	31.700							

AG 30-5,.2MA,.MKOM,.CC

CODES, 1,2,3A,4,5,6,7,8 = 1.0, 2.0, 0.0, 1.0, 1.0, 1.0, 3.0, 0.0,
KEYNOLDS NUMBER = 0.0
EFFECTIVE REFRACTIVE INDICES AND POROSITIES,
TYPE 2 FILM 2.170 -.2800 I .210
TYPE 1 FILM 2.042 -.2364 I .256
TYPE 1 HYDRATE 1.360 0.0000 I .970
SECONDARY CRYSTALS 1.880 -.1848 I .340
NUMBER OF SECONDARY SITES/SQCM .47E+09 LIMITING COVERAGE .790
CRYSTAL. RATE OF SEC. CRYSTALS (MA/SQCM), .06514
CRYSTAL. RATE OF TYPE2 FILM (MA/SQCM), .00450
SUPERSATURATION OF IONS, 2.310 ,TIME TO REACH(S) .19078
INITIAL DISSOLUTION CURRENT (MA/SQCM) .002C
TIMES, ONSET OF SEC. CRYSTALS(SEC) 50.00 PPT. CONSTANT (S) 60.00
DEHYDRATION RATE (MA/SQCM) .032
EFFECTIVE FILM CURRENT(MA/SQCM) .190
AVE. DISTANCE BETWEEN EXP. AND THEORY 12.003 (DEG)

		EXPERIMENT			THEORY		THICKNESSES(A)				
TIME(S)	I(MA/SQCM)	VOLTS	DEL	PSI	DEL	PSI	TYPE2	TYPE1(F)	TYPE1(H)	SECONDARY	COV
0.00	.200	0.000	70.800	42.300	70.800	42.300	-1	0.0	-1	0.0	0.000
10.00	.200	.320	68.800	42.000	67.829	42.153	21.6	.0	.0	.0	.000
20.00	.200	.320	66.200	41.500	65.114	42.036	43.1	.0	.0	.0	.000
30.00	.200	.320	63.200	41.600	62.617	41.951	64.7	.0	.0	.0	.000
40.00	.200	.330	60.900	40.800	60.279	41.899	86.3	.0	.0	.0	.000
50.00	.200	.330	62.100	41.000	60.379	41.899	86.3	.0	.0	.0	.000
60.00	.200	.350	64.000	42.300	61.825	41.814	86.3	90.1	-.0	.1	.000
70.00	.200	.350	67.000	45.000	59.586	42.214	86.3	138.0	-.0	1.6	.000
80.00	.200	.350	67.800	48.600	58.183	42.958	86.3	186.0	-.0	11.6	.000
90.00	.200	.350	68.400	53.000	57.582	44.203	86.3	234.1	-.0	43.4	.000
100.00	.200	.350	66.400	57.200	57.672	46.238	86.3	282.2	-.0	106.4	.001
110.00	.200	.350	61.600	61.300	57.940	49.476	86.3	330.1	-.0	199.6	.003
120.00	.200	.380	53.300	65.200	58.037	54.557	86.3	377.3	-.0	316.6	.009
130.00	.200	.380	42.500	67.400	46.971	60.565	86.3	422.8	-.0	450.6	.018
140.00	.200	.380	31.000	67.900	28.643	64.281	86.3	465.6	-.0	596.8	.031
150.00	.200	.380	19.900	67.700	9.908	63.699	86.3	504.3	-.0	751.8	.050
160.00	.200	.380	10.500	66.200	-.612	59.926	86.3	537.4	-.0	913.3	.073
170.00	.200	.380	3.600	63.900	-2.297	56.927	86.3	563.2	-.0	1079.9	.102
180.00	.200	.380	-.400	62.000	-.760	56.207	86.3	580.0	-.0	1250.3	.137
190.00	.200	.380	-3.900	59.800	1.148	57.175	86.3	586.1	-.0	1423.9	.178
200.00	.200	.380	-5.900	57.900	.836	58.573	86.3	586.1	-.0	1581.1	.219
210.00	.200	.380	-8.800	54.200	-7.752	59.312	86.3	586.1	-.0	1825.8	.292
220.00	.200	.380	-10.600	51.700	-17.995	56.292	86.3	586.1	-.0	2018.3	.357
230.00	.200	.380	-11.800	49.200	-24.160	50.939	86.3	586.1	-.0	2179.8	.417
240.00	.200	.380	-12.700	47.200	-26.029	44.905	86.3	586.1	-.0	2320.9	.472
250.00	.200	.380	-13.700	45.300	-24.447	39.185	86.3	586.1	-.0	2445.9	.525
260.00	.200	.380	-13.400	40.100	-6.420	28.780	86.3	586.1	-.0	2761.3	.669
420.00	.200	.380	-11.700	35.200	6.506	31.167	86.3	586.1	-.0	3017.7	.799
430.00	.200	.380	-6.700	32.400	9.319	35.200	86.3	586.1	-.0	3236.9	.919
540.00	.200	.380	-1.200	31.300	29.575	35.109	86.3	586.1	-.0	3429.9	.790
630.00	.200	.380	3.700	31.300	26.271	35.957	86.3	586.1	-.0	3603.5	.790
650.00	.200	.380	5.600	31.700	23.013	36.004	86.3	586.1	-.0	3761.8	.790
-1	-1	-1	-1	-1							

```
 ##GA0-4#  #.#-  -.4P#  #14KOM,111#

COEFS, 1.2,3#,.#,#.#,7,8 =  1.0,  2.0,  -.0,  1.0,  1.0,  1.0,  3#.,  #.#,
SYMBOLIC NUMBER =      0.0
EFFECTIVE REFRACTIVE INDICES AND POROSITIES,
TYPE 2 FILM    2.17     -.23#  I              .21#
TYPE 1 FILM    2.170    -.2#0J I              .000
TYPE 1 HYDRATE    1.37#    0.0000 I              .94#
SECONDARY CRYSTALS    1.879    -.132# I              .34#
NUMBER OF SECONDARY SITES/SQCM      .6#.E+0#      LIMITING COVERAGE      .-63
CRYSTAL, RATE OF S.C. CRYSTALS (MA/SQCM),    -.81-1
CRYSTAL, RATE OF TYPE 2 FILM (MA/SQCM),    .02237
SUPERSATURATION OF IONS,  #.7## ,TIME TO REACH(S)    .69185
INITIAL DISSOLUTION CURRENT (MA/SQCM)      .0223
TIMES, CNST OF S.C. CRYSTALS(SLC) 19.-1 PPT. CONSTANT (S)  9.00
OXYDATION RATE (MA/SQCM)     .302
AVE. DISTANCE BETWEEN TYP. AND THEORY      3.692  (D&G)

                          EXPERIMENT                    THEORY              THICKNESSES(A)
TIME(S)   I(MA/SQCM)   VOLTS      DEL      PSI        DEL        PSI        TYPE2      TYPE1(F)   TYPE1(H)   SECONDARY     COV

   0.00       .400     -.1-0     7#.000    42.100    7#.000    42.100        -I         0.0          -I         0.0      0.000
  10.00       .400      .300     68.300    40.800    63.5#-    41.692      82.0         .0           .0          .0       .0#6
  20.00       .400      .300     67.200    41.-00    68.636    41.#30     14#.0        5J.9          -.0        59.0      .000
  30.00       .400      .300     65.000    49.500    64.833    43.206     1-#.0       13#.2          -.0       155.8      .003
  -0.00       .#0.      .3       62.2#-    73.-#-    62.228    48.-62     14#.0       221.6          -.0       306.2      .011
  50.00       .-00      .300     -7.100    60.600    -#.6#-    78.121     1-#.0       303.6          -.0       500.2      .030
  60.00       .#00      .300     16.100    60.#00    14.169    51.269     14#.0       37#.8          -.0       725.8      .063
  70.00       .400      .300     -3.200    -9.900    -2.422    53.220     14#.0       433.9          -.0       974.0      .113
  80.00       .-#0      .300     -6.-00    41.300
  90.00       .-#0      .3 -     -2.-.#    3#.1-
 100.00       .400      .300      3.#00    33.800
 110.00       .400      .300      9.000    33.200
 12#.#-       .4-#      .300     12.200    33.700
 130.#0       .-00      .300     13.3#0    3-.700
 140.00       .400      .300     14.300    33.600
 1#0.#.       .4-#      .300     13.300    3#.300
 160.00       .420      .300     12.600    35.900
 170.00       .430      .300     10.#00    37.300
 18#.-#       .4 0      .300      9.000    37.200
 190.00       .430      .300      7.#00    36.#00
 200.00       .400      .300      5.000    35.300
 21#.#-       .4 -      .300      4.#00    3#.400
 220.00       .430      .300      3.#00    34.#00
 230.00       .400      .300      3.203    34.000
 24#.#:       .4 -      .300      2.#00    33.000
 25#.00       .400      .300      2.#00    32.#00
 260.00       .400      .300      3.000    31.#00
 27#.#        .4-       .300      3.#00    31.-00
 280.00       .400      .300      5.000    31.200
 350.00       .400      .300      6.200    30.700
```

#AG30-4# #-3-# #MPS# #14KOM,111#

CODES, 1,2,3,4,5,6,7,8 = 1.0, 2.0, 4.0, 1.0, 1.0, 1.0, 3.0, 0.0,
REYNOLDS NUMBER = 0.0
EFFECTIVE REFRACTIVE INDICES AND POROSITIES,
TYPE 2 FILM 2.170 -.2500 I .210
TYPE 1 FILM 2.170 -.2500 I .000
TYPE 1 HYDRATE 1.33 .100 I .980
SECONDARY CRYSTALS 1.878 -.1323 I .349
NUMBER OF SECONDARY SITES/SQCM .64E+05 LIMITING COVERAGE .646
CRYSTAL, PART. OF SEC. CRYSTALS (MA/SQCM), .13.67
CRYSTAL, DIFF. OF TYPE 2 FILM (MA/SQCM), .00656
SUPERSATURATION OF IONS, .80 ,TIME TO REACH(S) .2063,
INITIAL DISSOLUTION CURRENT (MA/SQCM) .0099
TIME, CRIT OF SEC. CRYSTALS(SEC) 3.27 FPT, CONSTANT (S) 30.01
DEHYDRATION RATE (MA/SQCM) .316
AVE, DISTANCE BTWN EXP, AND THEORY 12.3 2 (DEG)

			EXPERIMENT		THEORY		THICKNESSES(A)				
TIME(S)	I(MA/SQCM)	VOLTS	DEL	PSI	DEL	PSI	TYPE2	TYPE1(F)	TYPE1(H)	SECONDARY	COV
0.00	.400	-.100	77.000	42.100	79.000	-2.100	-I	0.0	-I	0.0	0.000
10.00	.400	.300	58.900	40.800	70.278	-1.798	-.0	43.1	-.0	.1	.018
20.00	.400	.300	57.200	41.100	62.110	41.556	0.0	130.9	-.0	2.3	.000
30.00	.400	.300	55.500	49.400	57.801	42.222	0.0	231.8	-.0	20.6	.000
40.00	.400	.300	52.200	53.000	54.214	42.069	0.0	327.9	-.0	90.2	.001
50.00	.400	.300	47.100	60.600	52.357	53.263	0.0	423.7	-.0	244.3	.007
60.00	.400	.300	16.100	60.600	19.956	64.095	0.0	51.4	-.0	487.9	.028
70.00	.400	.300	-3.200	69.900	-13.066	5.384	0.0	586.4	-.0	884.7	.077
80.00	.400	.300	-6.600	61.300	-1.133	48.077	0.0	815.3	-.0	1175.2	.165
90.00	.400	.300	-2.400	56.100	4.961	51.361	0.0	615.3	-.0	1472.6	.259
100.00	.400	.300	3.600	53.800	1.193	53.078	0.0	615.3	-.0	1682.9	.338
110.00	.400	.300	9.000	53.200	-5.325	52.776	0.0	615.3	-.0	1810.9	.409
120.00	.400	.300	12.200	53.700							
130.00	.400	.300	13.300	54.700							
140.00	.400	.300	14.300	55.600							
150.00	.400	.300	13.900	56.300							
160.00	.400	.300	12.500	55.900							
170.00	.400	.300	10.900	57.300							
180.00	.400	.300	9.000	57.200							
190.00	.400	.300	7.000	55.900							
200.00	.400	.300	5.000	56.300							
210.00	.400	.300	4.200	55.700							
220.00	.400	.300	3.600	54.600							
230.00	.400	.300	3.200	54.000							
240.00	.400	.300	2.600	53.000							
250.00	.400	.300	2.300	52.200							
260.00	.400	.300	3.000	51.800							
270.00	.400	.300	3.800	51.200							
280.00	.400	.300	5.000	51.200							
290.00	.400	.300	6.200	50.700							

#AG80-12# #E=+.34V# #1MKOH,100#

CODES, 1,2,3A,4,5,6,7,8 = 2.0, 2.0, 0.0, 1.0, 1.0, 1.0, 3.0, 0.0,
REYNOLDS NUMBER = 0.0
EFFECTIVE REFRACTIVE INDICES AND POROSITIES,
TYPE 2 FILM 2.170 -.2800 I .210
TYPE 1 FILM 1.965 -.2103 I .249
TYPE 1 HYDRATE 1.385 0.0000 I .922
SECONDARY CRYSTALS 2.162 -.2772 I .010
NUMBER OF SECONDARY SITES/SQCM .59E+09 LIMITING COVERAGE .790
CRYSTAL. RATE OF SEC. CRYSTALS (MA/SQCM), .14592
CRYSTAL. RATE OF TYPE2 FILM (MA/SQCM), .00488
SUPERSATURATION OF IONS, 14.994 ,TIME TO REACH(S) -I
INITIAL DISSOLUTION CURRENT (MA/SQCM) -I
TIMES, ONSET OF SEC. CRYSTALS(SEC) 15.00 PPT. CONSTANT (S) 49.94
DEHYDRATION RATE (MA/SQCM) .286
EFFECTIVE FILM CURRENT(MA/SQCM) 2.378
AVE. DISTANCE BETWEEN EXP. AND THEORY 7.948 (DEG)

		EXPERIMENT			THEORY		THICKNESSES(A)				
TIME(S)	I(MA/SQCM)	VOLTS	DEL	PSI	DEL	PSI	TYPE2	TYPE1(F)	TYPE1(H)	SECONDARY	COV
0.00	4.000	.340	72.000	42.400	72.000	42.400	-I	0.0	-I	0.0	0.000
10.00	4.000	.340	66.600	41.700	67.892	42.191	29.3	.0	.0	.0	.000
20.00	4.000	.340	62.000	41.800	61.062	41.898	29.3	118.3	-.0	62.2	.000
30.00	4.000	.340	60.800	42.300	61.242	42.539	29.3	234.2	-.0	165.8	.003
40.00	3.000	.340	61.400	44.000	61.887	45.357	29.3	332.1	-.0	328.0	.012
50.00	3.000	.340	63.000	47.400	55.900	47.161	29.3	412.0	-.0	537.9	.032
60.00	3.000	.340	62.100	53.100	52.570	48.091	29.3	494.6	-.0	782.4	.067
70.00	2.000	.340	53.700	60.100	50.362	53.681	29.3	559.2	-.0	1051.7	.122
80.00	2.000	.340	31.600	64.400	39.510	59.985	29.3	603.7	-.0	1338.8	.197
90.00	2.000	.340	4.000	55.100	2.784	62.727	29.3	640.5	-.0	1639.0	.296
100.00	2.000	.340	-6.200	44.500	-21.922	44.113	29.3	667.3	-.0	1949.3	.418
110.00	2.000	.340	-5.400	35.300	-2.435	28.224	29.3	681.6	-.0	2267.2	.566
120.00	2.000	.340	1.400	30.800	14.597	30.084	29.3	681.6	-.0	2587.2	.737
130.00	2.000	.340	8.000	28.900	8.853	34.997	29.3	681.6	-.0	2843.3	.890
140.00	2.000	.340	13.400	28.800							
150.00	2.000	.340	17.100	29.000							
160.00	2.000	.340	19.200	29.800							
170.00	2.000	.340	20.200	30.600							
180.00	2.000	.340	19.200	31.800							
190.00	2.000	.340	17.200	32.600							
200.00	2.000	.340	13.900	33.000							
220.00	2.000	.340	10.200	33.600							
240.00	2.000	.340	9.800	32.200							
260.00	2.000	.340	8.000	31.200							
280.00	2.000	.340	6.400	31.000							
300.00	2.000	.340	5.400	30.200							
320.00	2.000	.340	5.200	29.900							

≠AG80-13≠ ≠E=+.3'V≠ ≠1MKOH,100≠

CODES, 1,2,3A,4,5,6,7,8 = 2.0, 2.0, 0.0, 1.0, 1.0, 1.0, 3.0, 0.0,
REYNOLDS NUMBER = 5.6
EFFECTIVE REFRACTIVE INDICES AND POROSITIES,
TYPE 2 FILM 2.170 -.2800 I .210
TYPE 1 FILM 2.017 -.2281 I .185
TYPE 1 HYDRATE 1.365 0.0000 I .960
SECONDARY CRYSTALS 1.878 -.1820 I .350
NUMBER OF SECONDARY SITES/SQCM .68E+09 LIMITING COVERAGE .790
CRYSTAL. RATE OF SEC. CRYSTALS (MA/SQCM), .00049
CRYSTAL. RATE OF TYPE2 FILM (MA/SQCM), .06000
SUPERSATURATION OF IONS, 1.67, ,TIME TO REACH(S) -I
INITIAL DISSOLUTION CURRENT (MA/SQCM) -I
TIMES, ONSET OF SEC. CRYSTALS(SEC) 3.50 PPT. CONSTANT (S) 15.00
DEHYDRATION RATE (MA/SQCM) 1.134
EFFECTIVE FILM CURRENT(MA/SQCM) 11.243
AVE. DISTANCE BETWEEN EXP. AND THEORY 2.070 (DEG)

		EXPERIMENT			THEORY		THICKNESSES(A)				
TIME(S)	I(MA/SQCM)	VOLTS	DEL	PSI	DEL	PSI	TYPE2	TYPE1(F)	TYPE1(H)	SECONDARY	COV
0.00	20.000	.550	73.000	41.800	73.000	41.800	-I	0.0	-I	0.0	0.000
2.00	20.000	.550	60.000	41.300	62.305	41.494	83.2	.0	.0	.0	.000
4.00	13.000	.550	56.300	41.400	57.237	41.596	83.2	72.3	-.0	13.4	.000
5.00	10.000	.550	54.100	41.600	56.352	41.818	83.2	123.1	-.0	10.9	.000
10.00	10.000	.550	54.300	42.900	57.030	42.911	83.2	210.2	-.0	11.7	.000
15.00	12.000	.550	58.700	48.200	60.879	47.415	83.2	327.9	-.0	12.7	.000
20.00	15.000	.550	59.500	66.200	59.374	63.601	83.2	475.2	-.0	13.7	.000
21.50	15.000	.550	50.200	70.500	49.704	72.185	83.2	524.3	-.0	14.0	.000
-I	-I	-I	-I	-I							

#AG80-15# #E=+.34# #1MKOH,P1#

CODES, 1,2,3A,4,5,6,7,8 = 2.0, 2.0, 0.0, 1.0, 1.0, 1.0, 3.0, 0.0,
REYNOLDS NUMBER = [illegible]
EFFECTIVE REFRACTIVE INDICES AND POROSITIES,
TYPE 2 FILM 2.170 -.2800 I .210
TYPE 1 FILM 1.964 -.2180 I .250
TYPE 1 HYDRATE 1.369 0.0000 I .953
SECONDARY CRYSTALS 1.880 -.1828 I .347
NUMBER OF SECONDARY SITES/SQCM .596+09 LIMITING COVERAGE .790
CRYSTAL, RATE OF SEC. CRYSTALS (MA/SQCM), .52887
CRYSTAL, RATE OF TYPE2 FILM (MA/SQCM), .00049
SUPERSATURATION OF IONS, 14.646 ,TIME TO REACH(S) -I
INITIAL DISSOLUTION CURRENT (MA/SQCM) -I
TIMES, ONSET OF SEC. CRYSTALS(SEC) 15.00 PPT. CONSTANT (S) 89.99
DEHYDRATION RATE (MA/SQCM) .419
EFFECTIVE FILM CURRENT(MA/SQCM) 11.307
AVE. DISTANCE BETWEEN EXP. AND THEORY 9.315 (DEG)

			EXPERIMENT		THEORY		THICKNESSES(A)				
TIME(S)	I(MA/SQCM)	VOLTS	DEL	PSI	DEL	PSI	TYPE2	TYPE1(F)	TYPE1(H)	SECONDARY	COV
0.00	10.000	.340	79.400	40.000	79.400	40.000	-I	0.0	-I	0.0	0.000
10.00	10.000	.340	61.000	40.000	78.686	39.997	2.9	.0	.0	.0	.000
20.00	10.000	.340	59.000	41.900	61.429	41.439	2.9	177.2	-.0	23.6	.278
30.00	10.000	.340	57.900	47.400	56.137	42.809	2.9	353.4	-.0	151.8	.803
40.00	12.000	.340	49.500	55.500	43.170	54.804	2.9	545.4	-.0	523.5	.838
45.00	12.000	.340	27.200	59.600	20.975	52.773	2.9	666.8	-.0	1048.8	.121
50.00	12.000	.340	5.400	57.200	14.168	55.578	2.9	739.3	-.0	1568.1	.271
60.00	16.000	.340	-12.100	36.200	-11.756	24.780	2.9	926.9	-.0	2666.7	.783
70.00	16.000	.340	5.900	27.300	13.636	24.409	2.9	1021.5	-.0	3971.7	.798
80.00	15.000	.340	24.000	28.000	24.168	24.476	2.9	1017.3	-.0	5068.1	.798
90.00	15.000	.340	30.800	31.800	19.641	23.967	2.9	1013.2	-.0	6804.2	.798
100.00	12.000	.340	30.400	35.000							
110.00	11.000	.340	28.000	37.200							
120.00	10.000	.340	24.000	38.600							
130.00	9.000	.340	20.600	38.300							
140.00	8.000	.340	17.700	38.100							
150.00	3.000	.340	16.300	38.000							
160.00	3.000	.340	15.700	37.500							
170.00	2.000	.340	15.500	37.000							

#AG80-15# #E=+.34# #1MKOH,P1#

CODES, 1,2,3A,4,5,6,7,8 = 2.0, 2.0, 0.0, 1.0, 1.0, 1.0, 3.0, 0.0,
REYNOLDS NUMBER = 0.0
EFFECTIVE REFRACTIVE INDICES AND POROSITIES,
TYPE 2 FILM 2.170 -.2800 I .210
TYPE 1 FILM 1.999 -.2219 I .208
TYPE 1 HYDRATE 1.366 0.0000 I .958
SECONDARY CRYSTALS 1.677 -.1150 I .589
NUMBER OF SECONDARY SITES/SQCM .47E+09 LIMITING COVERAGE .790
CRYSTAL. RATE OF SEC. CRYSTALS (MA/SQCM), .43719
CRYSTAL. RATE OF TYPE2 FILM (MA/SQCM), .00231
SUPERSATURATION OF ICNS, 3.408 ,TIME TO REACH(S) -I
INITIAL DISSOLUTION CURRENT (MA/SQCM) -I
TIMES, ONSET OF SEC. CRYSTALS(SEC) 15.00 PPT. CONSTANT (S) 84.16
DEHYDRATION RATE (MA/SQCM) .377
EFFECTIVE FILM CURRENT(MA/SQCM) 9.424
AVE. DISTANCE BETWEEN EXP. AND THEORY 12.467 (DEG)

			EXPERIMENT		THEORY		THICKNESSES(A)				
TIME(S)	I(MA/SQCM)	VOLTS	DEL	PSI	DEL	PSI	TYPE2	TYPE1(F)	TYPE1(H)	SECONDARY	COV
0.00	10.000	.340	79.400	40.000	79.400	40.000	-I	0.0	-I	0.0	0.000
10.00	10.000	.340	61.000	40.000	77.491	39.990	11.1	.0	.0	.0	.000
20.00	10.000	.340	59.000	41.900	61.937	40.352	11.1	152.2	-.0	58.2	.000
30.00	10.000	.340	57.900	47.400	56.010	42.257	11.1	303.3	-.0	280.2	.007
40.00	12.000	.340	49.500	55.500	38.741	50.725	11.1	467.6	-.0	807.8	.057
46.00	12.000	.340	27.200	59.600	33.194	45.047	11.1	570.9	-.0	1449.5	.184
50.00	12.000	.340	5.400	57.200	32.424	52.471	11.1	633.0	-.0	2037.0	.364
60.00	16.000	.340	-12.100	36.200	-23.201	31.727	11.1	794.8	-.0	3275.6	.941
70.00	16.000	.340	5.900	27.300	14.739	31.512	11.1	912.7	-.0	4705.2	.790
80.00	15.000	.340	24.000	28.000	23.813	26.529	11.1	909.3	-.0	6208.0	.790
90.00	15.000	.340	30.800	31.800	18.725	28.813	11.1	907.9	-.0	7178.9	.790
100.00	12.000	.340	30.400	35.000	17.161	27.000	11.1	907.9	-.0	7871.0	.790
110.00	11.000	.340	28.000	37.200	19.807	26.547	11.1	907.9	-.0	8376.9	.790
120.00	10.000	.340	24.000	38.600	21.237	27.092	11.1	907.9	-.0	8790.8	.790
130.00	9.000	.340	20.600	38.300	21.064	27.657	11.1	907.9	-.0	9134.3	.790
140.00	5.000	.340	17.700	38.100	20.424	27.894	11.1	907.9	-.0	9371.7	.790
150.00	3.000	.340	16.300	38.000	19.999	27.945	11.1	907.9	-.0	9502.0	.790
160.00	3.000	.340	15.700	37.500	19.690	27.946	11.1	907.9	-.0	9597.4	.790
170.00	2.000	.340	15.500	37.000	19.450	27.925	11.1	907.9	-.0	9675.5	.790
-I	-I	-I	-I	-I							

#A.8J-1.# #2E-4 AMPS# #.1MKOH,100#

CODES, 1,2,3#,4,5,6,7,8 = 1.0, 2.0, 0.0, 1.0, 1.0, 1.0, 3.0, 3.0,
REYNOLDS NUMBER = 0.0
EFFECTIVE REFRACTIVE INDICES AND POROSITIES,
TYPE 2 FILM 2.170 -.2300 I .210
TYPE 1 FILM 1.893 -.1887 I .326
TYPE 1 HYDRATE 1.341 0.0000 I .990
SECONDARY CRYSTALS 2.162 -.4772 I .010
NUMBER OF SECONDARY SITES/SQCM .63E+09 LIMITING COVERAGE .950
CRYSTAL. RATE OF SEC. CRYSTALS (MA/SQCM), .01900
CRYSTAL. RATE OF TYPE2 FILM (MA/SQCM), .0075
SUPERSATURATION OF IONS, 1.050 ,TIME TO REACH(S) .02961
INITIAL DISSOLUTION CURRENT (MA/SQCM) .0010
TIMES, ONSET OF SEC. CRYSTALS(SEC) 79.51 PPT. CONSTANT (S) 50.00
DEHYDRATION RATE (MA/SQCM) .105
EFFECTIVE FILM CURRENT(MA/SQCM) .177
ANG. DISTANCE BETWEEN EXP. AND THEORY 3.971 (DEG)

			EXPERIMENT		THEORY		THICKNESSES(A)				
TIME(S)	I(MA/SQCM)	VOLTS	DEL	PSI	DEL	PSI	TYPE2	TYPE1(F)	TYPE1(H)	SECONDARY	COV
0.00	.200	-.440	72.200	41.500	72.200	41.500	-1	0.0	-1	0.0	0.000
20.00	.200	.220	61.200	40.400	61.298	41.235	85.7	.0	.0	.0	.000
40.00	.200	.220	57.000	39.900	54.124	41.613	173.3	.0	.0	.0	.000
60.00	.200	.220	55.800	41.100	50.078	42.961	260.0	.0	.0	.0	.000
80.00	.200	.220	55.800	44.800	51.746	44.687	260.0	77.7	-.0	63.6	.003
100.00	.200	.280	57.300	50.800	51.710	48.993	260.0	176.3	-.0	114.8	.002
120.00	.200	.290	54.900	59.800	49.714	57.044	260.0	274.9	-.0	177.7	.004
140.00	.200	.290	24.400	72.700	33.115	68.429	260.0	372.9	-.0	249.0	.007
160.00	.200	.300	11.500	75.900	13.362	71.863	260.0	414.3	-.0	286.9	.010
180.00	.200	.310	-23.600	72.800	-21.052	70.707	260.0	469.9	-.0	337.2	.013
200.00	.200	.310	-48.300	59.100	-51.179	57.174	260.0	565.7	-.0	419.2	.021
220.00	.200	.340	-54.100	47.200	-58.120	43.928	260.0	659.8	-.0	504.4	.030
240.00	.200	.350	-55.100	37.200	-58.110	33.865	260.0	751.5	-.0	591.9	.041
260.00	.200	.350	-55.300	29.500	-55.343	26.605	260.0	840.8	-.0	681.4	.055
280.00	.200	.390	-52.200	22.700	-51.462	21.090	260.0	925.6	-.0	772.3	.070
300.00	.200	.390	-45.200	17.100	-45.409	16.700	260.0	1006.7	-.0	864.5	.088
320.00	.200	.460	-31.800	13.800	-36.195	13.197	260.0	1085.5	-.0	957.7	.108
340.00	.200	.480	-22.700	12.400	-21.822	10.629	260.0	1159.4	-.0	1051.8	.130
360.00	.200	.500	1.600	13.100							
380.00	.200	.500	12.800	14.400							
400.00	.200	.490	20.700	16.300							
420.00	.200	.490	25.100	18.100							
440.00	.200	.490	29.200	19.400							
460.00	.200	.490	30.100	20.400							

AG80-19,.6MA,1MKOH,111

CODES, 1,2,3A,4,5,6,7,8 = 1.0, 2.0, 0.0, 1.0, 1.0, 1.0, 4.0, 0.0,
REYNOLDS NUMBER = 0.0
EFFECTIVE REFRACTIVE INDICES AND POROSITIES,
TYPE 2 FILM 2.170 -.2800 I .210
TYPE 1 FILM 2.014 -.2271 I .189
TYPE 1 HYDRATE 1.410 0.0000 I .874
SECONDARY CRYSTALS 1.887 -.1853 I .338
NUMBER OF SECONDARY SITES/SQCM .70E+09 LIMITING COVERAGE .470
CRYSTAL. RATE OF SEC. CRYSTALS (MA/SQCM), .10142
CRYSTAL. RATE OF TYPE2 FILM (MA/SQCM), .00330
SUPERSATURATION OF IONS, 9.968 ,TIME TO REACH(S) .39469
INITIAL DISSOLUTION CURRENT (MA/SQCM) .0273
TIMES, ONSET OF SEC. CRYSTALS(SEC) 10.01 PPT. CONSTANT (S) 14.55
DEHYDRATION RATE (MA/SQCM) .589
AVE. DISTANCE BETWEEN EXP. AND THEORY 9.792 (DEG)

			EXPERIMENT		THEORY		THICKNESSES(A)			
TIME(S)	I(MA/SQCM)	VOLTS	DEL	PSI	DEL	PSI	TYPE2	TYPE1(F)	TYPE1(H)	SECONDARY
0.00	.600	.080	65.000	38.700	65.000	38.700	-1	0.0	-1	0.0
2.50	.600	.310	64.200	38.400	64.272	38.733	5.9	.0	.0	.0
10.00	.600	.350	62.000	40.300	62.174	38.836	23.6	.0	.0	.0
15.00	.600	.350	64.000	43.700	66.043	41.741	23.6	88.7	1208.3	57.6
20.00	.600	.350	67.900	50.600	67.374	45.229	23.6	183.3	1215.0	139.3
25.00	.600	.350	66.000	63.500	64.641	56.753	23.6	281.8	1204.7	247.1
30.00	.600	.350	29.900	73.900	22.851	67.222	23.6	378.6	1168.1	385.3
35.00	.600	.350	-16.900	64.000	-19.436	55.451	23.6	470.1	1103.2	542.4
40.00	.600	.350	-24.900	46.800	-18.395	39.916	23.6	552.2	1015.1	713.0
45.00	.600	.350	-21.400	35.300	-6.789	37.839	23.6	620.1	913.1	893.4
50.00	.600	.350	-12.900	29.200	-4.876	40.920	23.6	668.4	806.9	1081.1
55.00	.600	.350	-1.800	26.200	-7.323	44.857	23.6	691.5	704.0	1274.3
60.00	.600	.350	8.500	25.300						
70.00	.600	.350	22.200	26.500						
80.00	.600	.350	27.600	29.600						
100.00	.600	.350	25.600	34.400						
120.00	.600	.350	18.000	35.600						
140.00	.600	.350	13.300	33.700						
160.00	.600	.370	13.100	31.300						
180.00	.600	.390	15.100	29.600						
240.00	.600	.600	16.900	30.300						
300.00	.600	.600	19.900	31.200						
360.00	.600	.600	25.900	33.000						
420.00	.600	.560	29.800	31.400						

AG80-20 *6E-4 AMPS* *1MKOM,P2*

CODES, 1,2,3A,4,5,6,7,8 = 1.0, 2.0, 4.0, 1.0, 1.0, 1.0, 3.0, 3.0,
REYNOLDS NUMBER = 0.0
EFFECTIVE REFRACTIVE INDICES AND POROSITIES,
TYPE 2 FILM 2.170 -.2800 I .210
TYPE 1 FILM 2.169 -.2798 I .001
TYPE 1 HYDRATE 1.391 0.0000 I .910
SECONDARY CRYSTALS 2.169 -.2799 I .001
NUMBER OF SECONDARY SITES/SQCM .37E+09 LIMITING COVERAGE .952
CRYSTAL, RATE OF SEC. CRYSTALS (MA/SQCM), .39999
CRYSTAL, RATE OF TYPE2 FILM (MA/SQCM), .04994
SUPERSATURATION OF IONS, 9.034 ,TIME TO REACH(S) .32421
INITIAL DISSOLUTION CURRENT (MA/SQCM) .0141
TIME, ONSET OF SEC. CRYSTALS(SEC) 10.28 PPT. CONSTANT (S) 11.01
DEHYDRATION RATE (MA/SQCM) .588
AVE. DISTANCE BETWEEN EXP. AND THEORY 11.493 (DEG)

			EXPERIMENT		THEORY		THICKNESSES(A)				
TIME(S)	I(MA/SQCM)	VOLTS	DEL	PSI	DEL	PSI	TYPE2	TYPE1(F)	TYPE1(H)	SECONDARY	COV
0.00	.600	-.600	71.800	40.500	71.800	40.500	-1	0.0	-1	0.0	0.000
10.00	.600	.350	61.800	38.600	52.331	41.149	180.8	.0	.0	.0	.000
20.00	.600	.340	63.800	41.500	65.136	45.729	187.3	167.0	-.0	310.9	.207
25.50	.600	.340	66.400	48.600	58.371	51.843	187.3	225.4	-.0	507.4	.018
30.00	.600	.340	61.600	34.300	41.915	55.051	187.3	231.3	-.0	704.6	.034
36.00	.600	.340	29.700	63.700	25.912	57.922	187.3	341.2	-.0	970.2	.065
40.00	.600	.340	.100	59.900	20.584	59.315	187.3	350.9	-.0	1175.9	.095
50.00	.600	.380	-16.600	41.200	3.873	59.759	187.3	351.0	-.0	1618.8	.180
60.00	.600	.380	-4.400	33.400	-8.086	50.275	187.3	351.0	-.0	1901.1	.248
70.00	.600	.380	6.800	27.900	-4.915	41.357	187.3	351.0	-.0	2118.6	.308
80.00	.600	.380	15.300	29.200	3.362	36.831	187.3	351.0	-.0	2299.2	.363
90.00	.600	.380	18.700	31.400	10.070	35.710	187.3	351.0	-.0	2455.5	.414
100.00	.600	.380	18.900	33.200	13.323	35.857	187.3	351.0	-.0	2594.3	.462
110.00	.600	.380	17.100	34.600	12.734	35.197	187.3	351.0	-.0	2719.8	.508
120.00	.600	.380	14.300	35.600	12.271	35.138	187.3	351.0	-.0	2834.9	.552
130.00	.600	.380	10.900	35.700	9.755	35.571	187.3	351.0	-.0	2941.4	.594
140.00	.600	.380	8.000	35.200	6.864	34.423	187.3	351.0	-.0	3040.9	.635
150.00	.600	.380	5.800	34.100	4.141	32.756	187.3	351.0	-.0	3134.3	.674
160.00	.600	.380	5.000	33.300	1.985	30.744	187.3	351.0	-.0	3222.5	.713
170.00	.600	.380	5.000	31.900	.647	28.537	187.3	351.0	-.0	3306.2	.750
180.00	.600	.380	5.000	31.100	.251	26.314	187.3	351.0	-.0	3386.0	.787
190.00	.600	.380	6.600	27.700	.816	24.216	187.3	351.0	-.0	3462.1	.823
200.00	.600	.380	7.800	30.600	2.274	22.345	187.3	351.0	-.0	3535.2	.858
-1	-1	-1	-1	-1							

#AG80-30# #1E-3 AMPS# #6MKCM,1JO#

CODES, 1,2,3A,4,5,6,7,8 = 1.0, 2.0, 0.0, 1.0, 1.0, 1.0, 3.0, 0.0,
REYNOLDS NUMBER = 0.0
EFFECTIVE REFRACTIVE INDICES AND POROSITIES,
TYPE 2 FILM 2.170 -.2800 I .210
TYPE 1 FILM 1.974 -.2101 I .250
TYPE 1 HYDRATE 1.386 0.0000 I .999
SECONDARY CRYSTALS 1.878 -.1820 I .350
NUMBER OF SECONDARY SITES/SQCM .47E+09 LIMITING COVERAGE .300
CRYSTAL. RATE OF SEC. CRYSTALS (MA/SQCM), .15900
CRYSTAL. RATE OF TYPE2 FILM (MA/SQCM), .01274
SUPERSATURATION OF IONS, 2.310 ,TIME TO REACH(S) .09817
INITIAL DISSOLUTION CURRENT (MA/SQCM) .0252
TIMES, ONSET OF SEC. CRYSTALS(SEC) 6.16 PPT. CONSTANT (S) 13.05
DEHYDRATION RATE (MA/SQCM) 1.000
EFFECTIVE FILM CURRENT(MA/SQCM) .907
AVE. DISTANCE BETWEEN EXP. AND THEORY 4.898 (DEG)

		EXPERIMENT			THEORY		THICKNESSES(A)				
TIME(S)	I(MA/SQCM)	VOLTS	DEL	PSI	DEL	PSI	TYPE2	TYPE1(F)	TYPE1(H)	SECONDARY	COV
0.00	1.000	-.440	70.600	41.500	70.600	41.500	.0	.0	0.0	.0	0.000
5.00	1.000	.350	63.800	41.700	67.373	41.393	24.0	.0	.0	.0	.000
10.00	1.000	.380	55.100	42.000	55.855	41.540	24.0	154.8	-.0	50.4	.000
15.00	1.000	.370	53.300	42.300	52.625	42.402	24.0	250.4	-.0	100.4	.001
20.00	1.000	.370	60.000	50.200	53.003	51.648	24.0	474.8	-.0	209.6	.004
21.50	1.000	.330	60.500	55.500	51.935	56.529	24.0	522.8	-.0	256.4	.006
25.00	1.000	.350	34.300	68.900	26.445	70.843	24.0	634.5	-.0	351.8	.011
25.50	1.000	.330	21.400	70.800	19.293	72.194	24.0	650.2	-.0	370.2	.012
26.00	1.000	.340	7.000	70.000	8.565	72.907	24.0	666.0	-.0	388.6	.013
27.00	1.000	.350	-16.000	67.000	-13.682	72.054	24.0	697.3	-.0	424.0	.016
28.00	1.000	.360	-32.000	64.800	-30.750	68.590	24.0	728.5	-.0	459.6	.019
30.00	1.000	.380	-41.600	54.600	-47.507	59.439	24.0	790.5	-.0	526.7	.024
35.00	1.000	.380	-47.400	38.400	-55.253	39.240	24.0	943.4	-.0	674.7	.040
40.00	1.000	.410	-47.000	25.000	-50.749	26.711	24.0	1090.3	-.0	829.7	.060
45.00	1.000	.410	-40.400	15.700	-38.986	18.674	24.0	1229.3	-.0	990.1	.086
50.00	1.000	.420	-20.900	11.500	-20.075	13.785	24.0	1358.1	-.0	1154.7	.117
52.50	1.000	.420	-4.600	10.800	-7.585	12.442	24.0	1416.4	-.0	1244.3	.136
60.00	1.000	.460	26.600	15.100							
65.00	1.000	.500	29.500	20.000							
70.00	1.000	.520	28.500	21.400							
80.00	1.000	.570	23.500	24.200							
90.00	1.000	.570	21.700	24.900							
100.00	1.000	.570	22.700	26.100							
109.00	1.000	.570	24.000	27.600							

AG60-12 22-4 AMPS 6MKJH.100

CODES. 1.2.3A.4.5.6.7.8 = 1.0. -1.0. 0.0. 1.0. 1.0. 1.0. 1.0. 0.0.
CODES. 9.10.11.3.12.13.14 = 0.0. 0.0. 7.0. 3.0. 0.0. 0.0. 2.0.
REYNOLDS NUMBER = 3.0
EFFECTIVE REFRACTIVE INDICES AND POROSITIES.
TYPE 2 FILM 2.186 -.2000 I 0.000
TYPE 1 FILM 1.000 -.0147 I .297
TYPE 1 HYDRATE 1.334 -.0000 I .967
SECONDARY CRYSTALS 1.847 -.1656 I .394
ROUGHNESS .40 -1.5.7 I 0.000
NUMBER OF SECONDARY SITES/SQCM .746E+08 LIMITING COVERAGE .790
CRYSTAL. RATE OF SEC. CRYSTALS (MA/SQCM). .033
CRYSTAL. RATE OF TYPE. FILM (MA/SQCM). .005
SUPERSATURATION OF IONS. 2.31 .TIME TO PEACH(S) 2.45
INITIAL DISSOLUTION CURRENT (MA/SQCM) .2166
TIMES. LASET OF SEC. CRYSTALS(SEC) 3.5 RPT. CONSTANT (S) 2.0
TIME TO COMPLETE PATCH COVERAGE 291.6
TIME TO REACH COMPACT FILM I 677.6 S
TIME TO DISSIPATE HYDRATE LAYER 677.6 S
TPACK = 677.8 TDISS = 291.6
DEHYDRATION RATE (MA/SQCM) .016
EFFECTIVE FILM CURRENT(MA/SQCM) .023
WIDTH TO HEIGHT OF SEC. CRYSTALS. 1.000
INITIAL PATCH COVERAGE .299
FINAL POROSITY OF TYPE 1 FILM .000
MOLE FRACTION METAL IN PATCHES 0.000
PASSIVATION TIME 1000.00.
AVE. DISTANCE BETWEEN SAP. AND THEORY 1.135 (DEG)

		EXPERIMENT			THEORY		THICKNESSES(A)				
TIME(S)	I(MA/SQCM)	VOLTS	DEL	PSI	DEL	PSI	TYPE2	TYPE1(F)	TYPE1(H)	SECONDARY	COV
0.0	.200	-.340	69.000	41.700	69.000	41.700	0.0	0.0	0.0	0.0	0.000
20.0	.200	.250	67.800	40.800	67.67	4..9 5	0.0	4.0	3364.3	1236.4	.013
40.0	.200	.260	69.000	44.500	69.69	45.456	0.0	1.9	7193.5	1851.9	.030
60.0	.200	.270	66.100	49.000	66.924	49.009	0.0	20.2	7221.1	2189.8	.042
80.0	.200	.280	58.700	54.200	59.925	52.8 1	0.0	38.3	7249.	242..9	.051
100.0	.200	.290	46.900	56.600	46.538	5..939	0.0	3..4	7277.4	2590.3	.058
120.0	.200	.270	36.200	56.800							
140.0	.200	.280	27.700	56.200							
160.0	.200	.290	21.400	55.500							
180.0	.200	.270	16.200	54.800							
200.0	.200	.280	11.000	53.900							
220.0	.200	.270	6.500	53.000							
240.0	.200	.250	2.. 00	52.400							
260.0	.200	.250	-2.300	51.000							
280.0	.200	.250	-6.600	49.500							
300.0	.200	.260	-9.800	47.500							
320.0	.200	.260	-12.600	45.400							
340.0	.200	.260	-15.000	43.000							
360.0	.200	.260	-16.600	40.000							
380.0	.200	.260	-18.400	36.700							
400.0	.200	.260	-18.800	33.600							
420.0	.200	.260	-18.200	34.600							
440.0	.200	.260	-14.400	33.600							
460.0	.200	.260	-11.200	32.200							
480.0	.200	.260	-9.400	31.100							
520.0	.200	.260	-.400	29.100							
560.0	.200	.260	3.200	28.500							
600.0	.200	.260	7.000	27.800							
640.0	.200	.260	9.800	28.200							

```
 AC80-32   2F-4 A4PS   SMKC4,100

CODES, 1 2,3*,4,5,6,7,8 =  1.0,  -4.0,  0.0,  1.0,  1.0,  1.0,  3.0,  0.0,
CODES, 9 10,11,*,12,13,14 =  1.0,  0.0,  5.0,  3.0,  0.0,  0.0,  2.0,
REFLCTOS NUMBER =      3.0
EFFECTIV  REFRACTIVE INDICES AND POROSITIES,
TYPE 2 F LM   2.186   -1.0372 I              .120
TYPE 1 F LP   1.707   -.4145 I               .734
TYPE 1 M CRATE   1.420   0.6000 I                 .479
SECONDAR  CRYSTALS   1.845   -.6223 I                    .400
METCHNES      .460   -3.1517 I              0.000
NUMBER O  SECONDARY SITES/SQCM      .74E+08     LIMITING COVERAGE     .790
CRYSTAL. RATE OF SEC. CRYSTALS (MA/SQCM),      .048
CRYSTAL. RATE OF TYPE2 FILM (MA/SQCM),      .030
SUPERSAT RATION OF IONS,   2.00 ,TIME TO REACH(S)       7.36
INITIAL  ISSOLUTION CURRENT (MA/SQCM)      .0154
TIMES, O SET OF SEC. CRYSTALS(SEC)  105.0 PPT. CONSTANT (S)     2.0
TIME TO  COMPLETE PATCH COVERAGE     321.7
TIME TO  FACM COMPACT FILM I     300.0  S
TPACK =      300.0  TDISS =      321.7
DEPYDRAT ON RATE (MA/SQCM)     .085
EFFECTIV  FILM CURRENT(MA/SQCM)        .056
WIDTH TO  HEIGHT OF SEC. CRYSTALS,     1.000
INITIAL  ATCM COVERAGE      .3e4
FINAL PO OSITY OF TYPE I FILM     .600
PASSIVAT ON TIME      100.00
AVE. DIS ANCE BETWEEN EXP. AND THEORY      1.561  (DEG)
```

		EXPERIMENT			THEORY		THICKNESSES(A)				
TIME(S)	I(MA/SQCM)	VOLTS	DEL	PSI	DEL	PSI	TYPE2	TYPFL(F)	TYPEL(M)	SECONDARY	COV
120.0	.200	.270	36.200	56.800	35.850	54.472	0.0	71.3	-.0	1400.2	.027
140.0	.200	.290	27.700	56.200	28.542	55.618	0.0	155.2	-.0	1483.1	.030
160.0	.200	.290	21.400	55.500	21.564	55.697	0.0	232.8	-.0	1548.6	.033
180.0	.200	.270	16.200	54.800	15.536	55.031	0.0	305.6	-.0	1596.1	.035
200.0	.200	.270	11.000	53.900	10.517	53.993	0.0	373.7	-.0	1626.9	.037
220.0	.200	.270	6.500	53.000	6.192	52.847	0.0	437.4	-.0	1643.1	.037
240.0	.200	.250	2.100	52.400	2.159	51.749	0.0	496.9	-.0	1647.4	.037
260.0	.200	.250	-2.300	51.000	-1.925	50.802	0.0	552.5	-.0	1642.5	.037
280.0	.200	.250	-6.600	49.500	-6.298	50.128	0.0	604.4	-.0	1630.6	.037
300.0	.200	.260	-9.800	47.500	-11.007	49.913	0.0	653.1	-.0	1613.6	.036
320.0	.200	.260	-12.600	45.400	-11.066	44.876	0.0	698.8	-.0	1657.7	.038
340.0	.200	.260	-15.000	43.000	-17.447	44.383	0.0	765.0	-.0	1630.7	.037
360.0	.200	.260	-16.800	40.000	-14.734	39.008	0.0	830.6	-.0	1669.6	.038
380.0	.200	.260	-18.400	38.700							
400.0	.200	.260	-18.800	36.600							
420.0	.200	.260	-19.200	34.600							
440.0	.200	.260	-14.400	33.600							
460.0	.200	.260	-11.600	32.200							
480.0	.200	.260	-9.400	31.100							
520.0	.200	.260	-.400	29.100							
560.0	.200	.260	3.200	28.500							
600.0	.200	.260	7.000	27.800							
640.0	.200	.260	9.800	28.200							
680.0	.200	.260	11.400	28.300							

#=GPO-22= #2E-4 \#PS= #=4RC=.1DO=

CODES, 1=?,3A,4,5,6,7,8 = 1.0, 3.0, 4.0, 1.0, 1.0, 1.0, 5.0, 0.0,
KEYHOLES NUMBER = 0.0
EFFECTIVE REFRACTIVE INDICES AND PERESITIES,
TYPE 2 FILM 2.170 -.2300 I .210
TYPE 1 FILM 2.170 -.2300 I .000
TYPE 1 HYDRATE 1.409 0.0000 I .952
SECONDARY CRYSTALS 2.170 -.2300 I 0.000
NUMBER OF SECONDARY SITES/SQCM .74E+08 LIMITING COVERAGE .770
CRYSTAL, RATE OF SEC. CRYSTALS (MA/SQCM), .00003
CRYSTAL, RATE OF TYPE2 FILM (MA/SQCM), .05000
SUPERSATURATION OF IONS, 1.800 ,TIME TO REACH(S) .77733
EFFECTIVE DISSOLUTION CURRENT (MA/SQCM) .0053
TIMES, OFFSET OF SEC. CRYSTALS(SEC) 32.00 PPT. CONSTANT (S) 18.00
DEHYDRATION RATE (MA/SQCM) .111
EFFECTIVE FILM CURRENT(MA/SQCM) .072
AVE. DISTANCE BETWEEN EXP. AND THEORY 9.875 (DEG)

		EXPERIMENT			THEORY		THICKNESSES(A)				
TIME(S)	I(MA/SQCM)	VOLTS	DEL	PSI	DEL	PSI	TYPE2	TYPE1(F)	TYPE1(H)	SECONDARY	CCV
0.00	.200	-.340	69.000	41.700	69.000	41.700	-1	0.0	-1	0.0	0.000
20.00	.200	.250	67.800	40.400	65.310	41.565	29.0	.0	.0	.0	.000
40.00	.200	.260	66.000	44.500	72.844	40.980	45.3	55.4	2405.3	58.7	.327
60.00	.200	.270	68.100	49.000	76.912	38.177	45.3	120.2	3949.8	106.6	.885
80.00	.200	.280	54.700	54.200	52.717	39.855	45.3	185.7	5513.3	130.5	.790
100.00	.200	.290	46.900	56.600	47.256	45.317	45.3	251.8	6211.3	147.8	.790
120.00	.200	.270	36.200	56.800	43.676	47.840	45.3	318.2	6211.3	161.8	.790
140.00	.200	.290	27.700	56.200	38.563	51.120	45.3	384.8	6211.3	173.8	.790
160.00	.200	.290	21.400	55.500	33.147	54.360	45.3	451.6	6211.3	184.3	.790
180.00	.200	.270	16.200	54.800	18.768	56.304	45.3	518.6	6211.3	193.7	.790
200.00	.200	.270	11.000	53.900	7.921	55.530	45.3	585.7	6211.3	202.3	.790
220.00	.200	.270	6.600	53.000	.002	53.812	45.3	652.9	6211.3	210.2	.790
240.00	.200	.250	2.100	52.400	-5.201	51.884	45.3	720.2	6211.3	217.5	.790
260.00	.200	.250	-2.300	51.300	-9.527	50.086	45.3	787.6	6211.3	224.4	.790
280.00	.200	.250	-6.600	49.500	-10.501	48.502	45.3	855.0	6211.3	230.9	.790
300.00	.200	.260	-9.800	47.500	-11.348	47.166	45.3	922.5	6211.3	237.1	.790
320.00	.200	.260	-12.600	45.400	-11.185	46.157	45.3	990.1	6211.3	242.9	.790
340.00	.200	.260	-15.300	43.000	-10.194	45.591	45.3	1057.8	6211.3	248.5	.790
360.00	.200	.260	-16.800	40.000	-8.705	45.569	45.3	1125.5	6211.3	253.8	.790
380.00	.200	.260	-18.400	38.700							
400.00	.200	.260	-18.800	36.600							
420.00	.200	.260	-18.200	34.600							
440.00	.200	.260	-14.400	33.600							
460.00	.200	.260	-11.600	32.200							
480.00	.200	.260	-9.400	31.100							
500.00	.200	.260	-.400	29.100							
520.00	.200	.260	5.200	28.500							
540.00	.200	.260	7.000	27.900							
560.00	.200	.260	9.800	28.200							
580.00	.200	.260	11.400	28.300							

AG80-32 *2E-4 AMPS* *6MKOH,100*

CODES, 1,2,3A,4,5,6,7,8 = 1.0, 2.0, 4.0, 1.0, 1.0, 1.0, 5.0, 0.0,
REYNOLDS NUMBER = 0.0
EFFECTIVE REFRACTIVE INDICES AND POROSITIES,
TYPE 2 FILM 2.170 -.2800 I .210
TYPE 1 FILM 2.089 -.2509 I .104
TYPE 1 HYDRATE 1.405 0.0000 I .960
SECONDARY CRYSTALS 2.170 -.2800 I 0.000
NUMBER OF SECONDARY SITES/SQCM .74E+08 LIMITING COVERAGE .437
CRYSTAL. RATE OF SEC. CRYSTALS (MA/SQCM), .00014
CRYSTAL. RATE OF TYPE2 FILM (MA/SQCM), .02995
SUPERSATURATION OF ICNS, 3.135 ,TIME TO REACH(S) 4.52191
INITIAL DISSOLUTION CURRENT (MA/SQCM) .0127
TIMES, ONSET OF SEC. CRYSTALS(SEC) 32.00 PPT. CONSTANT (S) 18.00
DEHYDRATION RATE (MA/SQCM) .070
AVE. DISTANCE BETWEEN EXP. AND THEORY 11.173 (DEG)

			EXPERIMENT		THEORY		THICKNESSES(A)			
TIME(S)	I(MA/SQCM)	VOLTS	DEL	PSI	DEL	PSI	TYPE2	TYPE1(F)	TYPE1(H)	SECONDARY
0.00	.200	-.340	69.000	41.700	69.000	41.700	-1	0.0	-1	0.0
20.00	.200	.250	67.800	40.800	65.507	41.572	27.3	.0	.0	.0
40.00	.200	.260	69.000	44.500	71.035	41.468	45.2	29.7	2387.4	98.4
60.00	.200	.270	68.100	49.000	67.439	40.186	45.2	70.7	4759.2	178.7
80.00	.200	.280	58.700	54.200	53.845	42.861	45.2	113.1	6377.4	218.7
100.00	.200	.290	46.900	56.600	50.594	44.553	45.2	156.3	6377.4	247.8
120.00	.200	.270	36.200	56.800	45.665	46.243	45.2	200.1	6377.4	271.3
140.00	.200	.290	27.700	56.200	39.473	47.272	45.2	244.2	6377.4	291.4
160.00	.200	.290	21.400	55.500	33.234	47.505	45.2	288.7	6377.4	309.0
180.00	.200	.270	16.200	54.800	27.601	47.318	45.2	333.5	6377.4	324.8
200.00	.200	.270	11.000	53.900	22.283	47.070	45.2	378.5	6377.4	339.1
220.00	.200	.270	6.500	53.000	16.552	46.803	45.2	423.6	6377.4	352.4
240.00	.200	.250	2.100	52.400	9.830	46.190	45.2	469.0	6377.4	364.7
260.00	.200	.250	-2.300	51.000	2.281	44.676	45.2	514.5	6377.4	376.3
280.00	.200	.250	-6.600	49.500	-4.976	41.894	45.2	560.1	6377.4	387.2
300.00	.200	.260	-9.800	47.500	-10.561	38.040	45.2	605.8	6377.4	397.5
320.00	.200	.260	-12.600	45.400	-13.721	33.734	45.2	651.6	6377.4	407.3
340.00	.200	.260	-15.000	43.300	-14.408	29.575	45.2	697.5	6377.4	416.6
360.00	.200	.260	-16.800	40.000	-12.904	25.921	45.2	743.5	6377.4	425.6
380.00	.200	.260	-18.400	38.700						
400.00	.200	.260	-18.800	36.600						
420.00	.200	.260	-18.200	34.600						
440.00	.200	.260	-14.400	33.600						
460.00	.200	.260	-11.600	32.200						
480.00	.200	.260	-9.400	31.100						
520.00	.200	.260	-.400	29.100						
560.00	.200	.260	3.200	28.500						
600.00	.200	.260	7.000	27.800						
640.00	.200	.260	9.800	28.200						
680.00	.200	.260	11.400	28.300						

AG80-3E 6E-4 AMPS 6MKOH,111

CODES, 1,2,3A,4,5,6,7,8 = 1.0, 2.0, 0.0, 1.0, 1.0, 1.0, 3.0, 0.0,
REYNOLDS NUMBER = 0.0
EFFECTIVE REFRACTIVE INDICES AND POROSITIES,
TYPE 2 FILM 2.170 -.2800 I .210
TYPE 1 FILM 2.170 -.2800 I 0.000
TYPE 1 HYDRATE 1.410 0.0000 I .950
SECONDARY CRYSTALS 2.170 -.2800 I 0.000
NUMBER OF SECONDARY SITES/SQCM .39E+09 LIMITING COVERAGE .640
CRYSTAL. RATE OF SEC. CRYSTALS (MA/SQCM), .44000
CRYSTAL. RATE OF TYPE2 FILM (MA/SQCM), .00500
SUPERSATURATION OF IONS, 1.249 ,TIME TO REACH(S) .07978
INITIAL DISSOLUTION CURRENT (MA/SQCM) .0082
TIMES, ONSET OF SEC. CRYSTALS(SEC) 16.70 ONSET OF PPT. (S) 11.00
DEHYDRATION RATE (MA/SQCM) .390
AVE. DISTANCE BETWEEN EXP. AND THEORY 4.975 (DEG)

			EXPERIMENT		THEORY		THICKNESSES(A)			
TIME(S)	I(MA/SQCM)	VOLTS	DEL	PSI	DEL	PSI	TYPE2	TYPE1(F)	TYPE1(H)	SECONDARY
0.00	.600	-.500	67.800	41.400	67.800	41.400	-I	0.0	-I	0.0
10.00	.600	.250	66.000	41.400	65.319	41.326	19.9	.0	.0	.0
20.00	.600	.260	64.000	42.000	65.694	40.950	19.9	111.6	-.0	52.4
30.00	.600	.260	51.000	46.700	59.301	42.660	19.9	229.3	-.0	183.7
40.00	.600	.260	52.100	52.200	51.652	48.453	19.9	344.7	-.0	432.0
50.00	.600	.260	39.200	55.100	36.192	52.426	19.9	444.7	-.0	789.6
60.00	.600	.260	23.700	54.000	26.838	56.562	19.9	499.5	-.0	1231.5
70.00	.600	.260	13.400	50.600	13.116	57.135	19.9	499.5	-.0	1639.5
80.00	.600	.300	8.400	46.600	1.283	59.374	19.9	499.5	-.0	1908.4
90.00	.600	.300	7.000	43.400	1.226	42.952	19.9	499.5	-.0	2117.6
100.00	.600	.300	6.400	41.500	6.570	38.524	19.9	499.5	-.0	2292.2
110.00	.600	.300	6.500	39.700	11.921	36.847	19.9	499.5	-.0	2443.7
120.00	.600	.310	8.000	38.300	14.870	37.952	19.9	499.5	-.0	2578.6
130.00	.600	.330	9.400	37.600	15.614	39.637	19.9	499.5	-.0	2703.7
140.00	.600	.320	10.400	37.200						
150.00	.600	.310	10.000	37.700						
160.00	.600	.500	13.400	37.800						
170.00	.600	.490	16.500	35.900						
180.00	.600	.490	19.400	34.400						
190.00	.600	.500	21.100	33.200						
200.00	.600	.500	22.000	32.100						
210.00	.600	.500	22.400	31.200						
220.00	.600	.500	22.600	30.900						
230.00	.600	.500	23.000	30.800						
240.00	.600	.500	23.200	30.800						
250.00	.600	.500	23.600	30.900						
260.00	.600	.500	24.000	31.100						
270.00	.600	.500	24.200	31.200						
280.00	.600	.500	24.200	31.600						

AG80-35 6E-4 AMPS 6MKOH,111

CODES, 1,2,3A,4,5,6,7,8 = 1.0, 2.0, 0.0, 1.0, 1.0, 1.0, 3.0, 3.0,
KEYNOLDS NUMBER = 0.0
EFFECTIVE REFRACTIVE INDICES AND POROSITIES,
TYPE 2 FILM 2.170 -.2800 I .210
TYPE A FILM 2.139 -.2688 I .040
TYPE 1 HYDRATE 1.410 0.0000 I .950
SECONDARY CRYSTALS 2.170 -.2800 I .000
NUMBER OF SECONDARY SITES/SQCM .39E+09 LIMITING COVERAGE .843
CRYSTAL. RATE OF SEC. CRYSTALS (MA/SQCM), .36427
CRYSTAL. RATE OF TYPE2 FILM (MA/SQCM), .00959
SUPERSATURATION OF IONS, 2.270 ,TIME TO REACH(S) .26333
INITIAL DISSOLUTION CURRENT (MA/SQCM) .0148
TIMES, ONSET OF SEC. CRYSTALS(SEC) 16.70 ONSET OF PPT. (S) 17.60
DEHYDRATION RATE (MA/SQCM) .382
AVE. DISTANCE BETWEEN EXP. AND THEORY 5.186 (DEG)

		EXPERIMENT			THEORY		THICKNESSES(A)			
TIME(S)	I(MA/SQCM)	VOLTS	DEL	PSI	DEL	PSI	TYPE2	TYPE1(F)	TYPE1(H)	SECONDARY
0.00	.600	-.500	67.800	41.400	67.800	41.400	-1	0.0	-1	0.0
10.00	.600	.250	66.000	41.400	65.188	41.279	38.1	.0	.0	.0
20.00	.600	.260	64.000	42.000	65.145	41.033	38.1	104.7	-.0	76.0
30.00	.600	.260	61.400	46.700	59.451	42.865	38.1	220.9	-.0	222.2
40.00	.600	.260	52.100	52.200	51.242	48.098	38.1	335.1	-.0	465.9
50.00	.600	.260	39.200	55.100	38.232	52.157	38.1	435.5	-.0	792.4
60.00	.600	.260	23.700	54.000	26.629	57.165	38.1	500.2	-.0	1180.3
70.00	.600	.260	13.400	50.600	14.583	58.294	38.1	500.2	-.0	1606.2
80.00	.600	.300	8.400	46.600	1.204	51.930	38.1	500.2	-.0	1830.5
90.00	.600	.300	7.000	43.400	.100	44.237	38.1	500.2	-.0	2092.4
100.00	.600	.300	6.400	41.500	5.195	39.324	38.1	500.2	-.0	2268.6
110.00	.600	.300	6.600	39.700	10.804	37.317	38.1	500.2	-.0	2421.2
120.00	.600	.310	8.000	38.300	14.372	36.886	38.1	500.2	-.0	2530.6
130.00	.600	.330	9.400	37.600	15.711	36.982	38.1	500.2	-.0	2679.5
140.00	.600	.520	10.400	37.200						
150.00	.600	.510	10.000	37.700						
160.00	.600	.500	13.400	37.800						
170.00	.600	.490	16.600	35.900						
180.00	.600	.490	19.400	34.400						
190.00	.600	.500	21.100	33.200						
200.00	.600	.500	22.000	32.100						
210.00	.600	.500	22.400	31.200						
220.00	.600	.500	22.600	30.900						
230.00	.600	.500	23.000	30.800						
240.00	.600	.500	23.200	30.800						
250.00	.600	.500	23.600	30.900						
260.00	.600	.500	24.000	31.100						
270.00	.600	.500	24.200	31.200						
280.00	.600	.500	24.200	31.600						

AG300-02.14A/SQCM,2.35GPM,AG100-2

CODES. 1,2,3A,4,5,6,7,A = 1.0, 2.0, 4.0, 1.0, 1.0, 1.0, 3.0, 0.0,
REYNOLDS NUMBER = 10000.0
EFFECTIVE REFRACTIVE INDICES AND POROSITIES,
TYPE 2 FILM 2.170 -.2300 I .210
TYPE 1 FILM 2.145 -.2715 I .030
TYPE 1 HYDRATE 1.425 -.0000 I .917
SECONDARY CRYSTALS 1.878 -.1520 I .350
NUMBER OF SECONDARY SITES/SQCM .30E+09 LIMITING COVERAGE .729
CRYSTAL. RATE OF SEC. CRYSTALS (MA/SQCM) .26813
CRYSTAL. RATE OF TYPE 2 FILM (MA/SQCM). .07786
SUPERSATURATION OF IONS, 1.700 ,TIME TO REACH(S) .10975
INITIAL DISSOLUTION CURRENT (MA/SQCM) .2526
TIMES. ONSET OF SEC. CRYSTALS(SEC) 12.00 EPT. CONSTANT (S) 21.00
DEHYDRATION RATE (MA/SQCM) 1.000
EFFECTIVE FILM CURRENT(MA/SQCM) .533
AVE. DISTANCE BETWEEN EXP. AND THEORY 3.298 (DEG)

		EXPERIMENT			THEORY		THICKNESSES(A)				
TIME(S)	I(MA/SQCM)	VOLTS	DEL	PSI	DEL	PSI	TYPE2	TYPE1(F)	TYPE1(M)	SECONDARY	COV
0.00	1.000	.000	64.930	42.940	64.930	42.940	-1	0.0	-1	0.0	0.000
5.00	1.000	.340	58.760	41.980	59.124	42.574	94.0	.0	.0	.0	.000
10.00	1.000	.340	50.440	40.300	50.919	42.671	173.2	.0	.0	.0	.000
15.00	1.000	.340	53.380	41.290	54.236	41.217	212.0	82.0	-.0	104.9	.002
17.00	1.000	.340	56.030	43.570	57.660	47.267	212.0	118.9	-.0	251.7	.004
19.00	1.000	.340	58.350	44.850	59.159	48.646	212.0	137.6	-.0	291.8	.005
19.00	1.000	.340	58.760	47.670	60.428	50.253	212.0	154.8	-.0	332.8	.007
20.00	1.000	.340	62.960	50.240	61.409	52.077	212.0	172.3	-.0	374.1	.009
21.00	1.000	.340	64.293	54.111	62.091	54.098	212.0	189.5	-.0	416.0	.011
22.00	1.000	.340	64.360	58.050	60.435	56.404	212.0	207.4	-.0	458.4	.013
23.00	1.000	.340	59.320	62.450	58.038	58.878	212.0	225.1	-.0	501.2	.016
24.00	1.000	.340	49.980	62.250	54.580	61.461	212.0	242.5	-.0	544.2	.019
30.00	1.000	.220	10.740	61.440							

AG=CC-03,C.CMA/SGCM,2.2GPM,AGAGO-3

CCOES, 1,2,3A,4,5,6,7,8 = 1.C, 2.C, 4.C, 1.C, 1.O, 1.C, 3.O, O.O,
REYNOLDS NUMBER = 10500.0
EFFECTIVE REFRACTIVE INDICES AND POROSITIES,
TYPE 2 FILM 2.173 -.26CC I .21C
TYPE 1 FILM 2.154 -.2744 I .02C
TYPE A HYDRATE 1.414 0.CCCC I .980
SECONDARY CRYSTALS 1.852 -.1736 I .38C
NUMBER OF SECONDARY SITES/SGCM .62E+09 LIMITING COVERAGE .58C
STD. DEVIATION IN TNUC (COHERENT) 7.35 SEC
CRYSTAL. RATE OF SEC. CRYSTALS (MA/SGCM), .C7456
CRYSTAL. RATE OF TYPE2 FILM (MA/SGCM), .01938
SUPERSATURATION OF ICNS, 1.7CC ,TIME TO REACH(S) .455CC
INITIAL DISSOLUTION CURRENT (MA/SGCM) .2526
TIMES, ONSET OF SEC. CRYSTALS(SEC) 2C.C5 EFT. CONSTANT (S) 20.00
DEHYDRATION RATE (MA/SGCM) .6CC
EFFECTIVE FILM CURRENT(MA/SGCM) .33C
AVE. DISTANCE BETWEEN EXP. AND THEORY 2.888 (DEG)

			EXPERIMENT		THEORY		THICKNESSES(A)				
TIME(S)	I(MA/SGCM)	VOLTS	CEL	PSI	CEL	PSI	TYPE2	TYPE1(F)	TYPE1(H)	SECONDARY	COV
0.00	.600	-.340	67.550	42.750	67.550	42.750	-1	0.0	-1	0.0	0.000
5.00	.600	.280	64.510	43.220	64.176	43.441	19.6	.0	.0	.0	.000
10.00	.600	.280	60.990	41.570	61.188	43.054	53.4	.0	.0	.0	.000
20.00	.600	.300	61.160	42.080	59.744	42.822	141.9	.0	.0	.0	.000
30.00	.600	.300	61.420	46.880	58.101	44.463	192.5	87.6	-.0	236.8	.007
35.00	.600	.300	58.550	49.760	56.835	46.773	192.5	130.6	-.0	328.5	.012
40.00	.600	.300	54.120	53.010	53.462	50.109	192.5	172.5	-.0	423.7	.021
45.00	.600	.300	46.070	55.550	47.286	53.588	192.5	212.8	-.0	523.6	.032
50.00	.600	.300	37.080	57.110	39.503	56.374	192.5	251.0	-.0	627.2	.046
55.00	.600	.300	28.020	57.030	29.563	58.203	192.5	286.7	-.0	733.6	.062
60.00	.600	.300	20.470	56.190	18.851	58.267	192.5	319.1	-.0	842.2	.082
65.00	.600	.300	14.370	54.550	10.838	56.563	192.5	347.9	-.0	952.6	.105
70.00	.600	.300	10.470	53.160	7.335	54.499	192.5	372.2	-.0	1064.4	.131
75.00	.600	.300	7.770	51.700	6.928	53.290	192.5	391.7	-.0	1177.4	.160
80.00	.600	.300	5.460	50.460	7.826	53.117	192.5	405.6	-.0	1291.5	.193
85.00	.600	.300	5.460	50.460	9.161	53.699	192.5	413.3	-.0	1406.4	.229
90.00	.600	.300	5.540	49.240							
95.00	.600	.300	5.580	48.840							
100.00	.600	.300	5.750	48.640							
110.00	.600	.300	13.220	51.360							
115.00	.600	.300	23.170	52.660							
120.00	.600	.300	36.270	52.180							
125.00	.600	.300	46.770	49.100							
130.00	.600	.300	53.670	45.950							
135.00	.600	.300	56.550	42.390							
140.00	.600	.300	57.610	41.440							
150.00	.600	-.110	58.610	41.480							

AG300-03,0.6MA/SQCM,2.2GPM,AG100-3

CODES, 1,2,3A,4,5,6,7,8 = 1.0, 2.0, 4.0, 1.0, 1.0, 1.0, 3.0, 0.0,
REYNOLDS NUMBER = 1650C.0
EFFECTIVE REFRACTIVE INDICES AND POROSITIES,
TYPE 2 FILM 2.170 -.2800 I .210
TYPE 1 FILM 2.162 -.2772 I .010
TYPE 1 HYDRATE 1.397 0.0000 I .977
SECONDARY CRYSTALS 1.754 -.1407 I .498
NUMBER OF SECONDARY SITES/SQCM .36E+09 LIMITING COVERAGE .986
CRYSTAL. RATE OF SEC. CRYSTALS (MA/SQCM), .14456
CRYSTAL. RATE OF TYPE2 FILM (MA/SQCM), .05000
SUPERSATURATION OF IONS, 1.700 ,TIME TO REACH(S) .45500
INITIAL DISSOLUTION CURRENT (MA/SQCM) .2526
TIMES, ONSET OF SEC. CRYSTALS(SEC) 9.70 PPT. CONSTANT (S) 11.00
DEHYDRATION RATE (MA/SQCM) .599
EFFECTIVE FILM CURRENT(MA/SQCM) .337
AVE. DISTANCE BETWEEN EXP. AND THEORY 4.470 (DEG)

		EXPERIMENT			THEORY		THICKNESSES(A)				
TIME(S)	I(MA/SQCM)	VOLTS	DEL	PSI	DEL	PSI	TYPE2	TYPE1(F)	TYPE1(H)	SECONDARY	COV
0.00	.600	-.040	67.550	43.750	67.550	43.750	-1	0.0	-1	0.0	0.000
5.00	.600	.280	64.510	43.220	62.944	43.341	38.8	.0	.0	.0	.000
10.00	.600	.280	60.990	41.970	59.170	42.956	69.5	22.6	-.0	28.7	.000
20.00	.600	.300	61.180	42.080	57.471	42.867	69.5	109.8	-.0	96.0	.001
30.00	.600	.300	61.420	46.880	54.921	44.230	69.5	196.9	-.0	219.1	.003
35.00	.600	.300	58.590	49.760	54.439	46.105	69.5	239.9	-.0	329.0	.007
40.00	.600	.300	54.120	53.010	52.636	49.315	69.5	282.1	-.0	451.7	.014
45.00	.600	.300	46.070	55.550	46.898	53.253	69.5	322.9	-.0	583.7	.023
50.00	.600	.300	37.080	57.110	39.364	56.212	69.5	361.8	-.0	722.4	.035
55.00	.600	.300	28.030	57.080	30.081	58.082	69.5	398.1	-.0	866.2	.050
60.00	.600	.300	20.470	56.190	20.752	58.500	69.5	431.2	-.0	1013.9	.069
65.00	.600	.300	14.370	54.550	13.757	57.839	69.5	460.4	-.0	1164.6	.091
70.00	.600	.300	10.670	53.160	9.808	57.138	69.5	484.9	-.0	1317.9	.117
75.00	.600	.300	7.770	51.700	7.834	57.073	69.5	504.8	-.0	1473.1	.146
80.00	.600	.300	5.460	50.460	6.659	57.716	69.5	517.0	-.0	1630.1	.179
85.00	.600	.300	5.460	50.460	5.582	58.802	69.5	523.1	-.0	1788.5	.215
90.00	.600	.300	5.540	49.340							
95.00	.600	.300	5.580	48.840							
100.00	.600	.300	5.790	48.640							
110.00	.600	.300	13.220	51.360							
115.00	.600	.300	23.170	52.660							
120.00	.600	.300	36.270	52.180							
125.00	.600	.300	46.770	49.100							
130.00	.600	.300	53.670	45.550							
135.00	.600	.300	56.530	42.380							
140.00	.600	.300	57.610	41.440							
150.00	.600	-.110	58.610	41.480							

AG30C-5.0.6MA/SQCM,2.3GPM,AG111-3

CODES, 1,2,3A,4,5,6,7,8 = 1.0, 2.0, 4.0, 1.0, 1.0, 1.0, 3.0, 0.0,

REYNOLDS NUMBER = 10500.0

EFFECTIVE REFRACTIVE INDICES AND POROSITIES,

TYPE 2 FILM 2.170 -.2800 I .210

TYPE 1 FILM 2.154 -.2741 I . .021

TYPE 1 HYDRATE 1.410 0.0000 I .950

SECONDARY CRYSTALS 1.919 -.1960 I .300

NUMBER OF SECONDARY SITES/SQCM .47E+09 LIMITING COVERAGE .812

CRYSTAL. RATE OF SEC. CRYSTALS (MA/SQCM), .16894

CRYSTAL. RATE OF TYPE2 FILM (MA/SQCM), .00101

SUPERSATURATION OF ICNS, 1.000 ,TIME TO REACH(S) .10083

INITIAL DISSOLUTION CURRENT (MA/SQCM) .1486

TIMES, ONSET OF SEC. CRYSTALS(SEC) 1.00 PPT. CONSTANT (S) 24.95

DEHYDRATION RATE (MA/SQCM) .600

EFFECTIVE FILM CURRENT(MA/SQCM) .436

AVE. DISTANCE BETWEEN EXP. AND THEORY 8.586 (DEG)

		EXPERIMENT			THEORY		THICKNESSES(A)				
TIME(S)	I(MA/SQCM)	VOLTS	DEL	PSI	DEL	PSI	TYPE2	TYPE1(F)	TYPE1(H)	SECONDARY	COV
0.00	.600	-.060	66.920	43.560	66.920	43.560	-1	0.0	-1	0.0	0.000
5.00	.600	-.060	63.160	42.710	65.714	43.239	0.0	28.8	-.0	.1	.000
8.00	.600	-.060	60.390	42.070	63.660	42.940	0.0	63.4	-.0	1.1	.000
9.00	.600	.320	59.410	41.730	63.077	42.860	0.0	74.8	-.0	5.2	.000
10.00	.600	.320	58.820	41.600	62.542	42.791	0.0	86.3	-.0	14.8	.000
20.00	.600	.320	57.780	41.940	59.857	42.863	0.0	199.3	-.0	63.5	.000
30.00	.600	.320	58.360	47.750	59.997	45.733	0.0	311.3	-.0	169.9	.003
35.00	.600	.320	54.610	52.000	59.768	49.697	0.0	367.4	-.0	278.3	.007
40.00	.600	.320	43.990	56.430	55.727	55.975	0.0	421.8	-.0	404.6	.014
42.00	.600	.320	39.250	57.690	50.969	58.767	0.0	442.7	-.0	470.3	.020
44.00	.600	.320	33.950	58.440	43.654	61.198	0.0	462.8	-.0	537.3	.026
46.00	.600	.320	26.290	58.630	35.666	62.911	0.0	482.2	-.0	605.3	.032
48.00	.600	.320	19.480	58.370	27.279	63.897	0.0	500.7	-.0	674.1	.040
50.00	.600	.320	14.120	57.540	18.655	63.987	0.0	518.2	-.0	743.6	.049
52.00	.600	.320	9.970	56.740	10.988	63.205	0.0	534.5	-.0	813.8	.059
54.00	.600	.320	5.880	55.240	5.206	61.838	0.0	549.6	-.0	884.4	.069
56.00	.600	.320	1.990	53.760	1.515	60.307	0.0	563.4	-.0	955.5	.081
60.00	.600	.320	-1.990	50.660	-2.404	57.988	0.0	587.9	-.0	1089.6	.105
65.00	.600	.320	-5.100	46.930	-3.877	56.989	0.0	610.8	-.0	1255.9	.139
70.00	.600	.320	-5.440	43.440	-4.458	57.781	0.0	622.3	-.0	1424.2	.179
75.00	.600	.320	-4.480	41.260	-5.725	59.240	0.0	622.3	-.0	1591.9	.224
80.00	.600	.320	-2.920	39.200							
90.00	.600	.320	.640	37.160							
100.00	.600	.320	2.870	36.880							
110.00	.600	.320	-.480	36.090							
130.00	.600	.200	-2.190	35.140							
200.00	.600	.200	-.720	36.570							
240.00	.600	.200	-.510	41.540							
300.00	.600	.200	5.890	47.260							
315.00	.600	.200	21.520	50.570							
320.00	.600	.200	28.970	50.370							
325.00	.600	.200	36.870	49.720							
330.00	.600	.200	43.630	48.170							
340.00	.600	.200	53.410	43.810							
350.00	.600	-.110	57.240	41.120							

AG300-6,0.6MA/SQCM,1.0GPM,AG100-2

CODES, 1,2,3A,4,5,6,7,8 = 1.0, 2.0, 4.0, 1.0, 1.0, 1.0, 3.0, 0.0,
REYNOLDS NUMBER = 4600.0
EFFECTIVE REFRACTIVE INDICES AND POROSITIES,
TYPE 2 FILM 2.170 -.2800 I .210
TYPE 1 FILM 2.161 -.2769 I .011
TYPE 1 HYDRATE 1.391 0.0000 I .990
SECONDARY CRYSTALS 2.163 -.2777 I .008
NUMBER OF SECONDARY SITES/SQCM .36E+09 LIMITING COVERAGE .414
CRYSTAL. RATE OF SEC. CRYSTALS (MA/SQCM), .26052
CRYSTAL. RATE OF TYPE2 FILM (MA/SQCM), .10000
SUPERSATURATION OF IONS, 1.700 ,TIME TO REACH(S) .14770
INITIAL DISSOLUTION CURRENT (MA/SQCM) .1883
TIMES, ONSET OF SEC. CRYSTALS(SEC) 19.99 PPT. CONSTANT (S) 20.89
DEHYDRATION RATE (MA/SQCM) .286
EFFECTIVE FILM CURRENT(MA/SQCM) .390
AVE. DISTANCE BETWEEN EXP. AND THEORY 7.804 (DEG)

		EXPERIMENT			THEORY		THICKNESSES(A)				
TIME(S)	I(MA/SQCM)	VOLTS	DEL	PSI	DEL	PSI	TYPE2	TYPE1(F)	TYPE1(H)	SECONDARY	COV
0.00	.600	-.170	64.090	39.590	64.090	39.590	-I	0.0	-I	0.0	0.000
10.00	.600	.300	60.650	38.920	64.134	39.588	0.0	0.0	-.0	.0	.000
20.00	.600	.300	59.780	39.760	60.963	39.640	0.0	52.8	-.0	.4	.000
30.00	.600	.300	56.200	41.730	56.413	39.948	0.0	105.5	-.0	5.5	.000
40.00	.600	.300	51.480	42.860	52.947	40.475	0.0	158.3	-.0	30.7	.000
50.00	.600	.300	46.030	42.970	50.421	41.357	0.0	211.0	-.0	97.6	.001
60.00	.600	.300	41.780	43.260	48.336	42.959	0.0	263.5	-.0	215.6	.003
70.00	.600	.300	38.760	43.330	43.724	45.325	0.0	315.2	-.0	378.9	.010
80.00	.600	.300	35.750	43.200	35.515	45.920	0.0	364.4	-.0	576.3	.022
90.00	.600	.300	32.920	43.280	33.173	45.847	0.0	409.0	-.0	798.1	.043
100.00	.600	.300	29.870	43.760	31.891	48.004	0.0	446.1	-.0	1037.4	.072
110.00	.600	.300	27.230	44.070	27.283	50.744	0.0	472.5	-.0	1289.4	.112
120.00	.600	.300	24.580	44.480	19.029	52.251	0.0	484.5	-.0	1550.9	.162
130.00	.600	.300	22.750	44.730	11.033	50.735	0.0	484.5	-.0	1795.0	.216
140.00	.600	.300	20.510	45.160	8.936	48.324	0.0	484.5	-.0	1986.3	.265
150.00	.600	.300	18.290	45.310	10.281	46.508	0.0	484.5	-.0	2146.5	.310
160.00	.600	.300	15.660	45.550	12.734	45.703	0.0	484.5	-.0	2285.8	.351
170.00	.600	.300	12.650	45.490	15.003	45.662	0.0	484.5	-.0	2410.0	.390
180.00	.600	.300	10.050	45.340	16.636	46.040	0.0	484.5	-.0	2522.5	.427
190.00	.600	.300	7.050	45.100	17.610	46.588	0.0	484.5	-.0	2625.7	.463
200.00	.600	.300	4.060	44.770	18.040	47.163	0.0	484.5	-.0	2721.5	.498
210.00	.600	.300	1.300	44.150	18.059	47.691	0.0	484.5	-.0	2810.9	.531
220.00	.600	.300	-.830	43.150							
230.00	.600	.300	-2.910	41.580							
240.00	.600	.300	-5.100	41.590							

AG3CC/,0.6MA/SQCM,1.1GPM,111-2

CODES, 1,2,3A,4,5,6,7,8 = 1.0, 2.0, 0.0, 1.0, 1.0, 1.0, 3.0, 0.0,
REYNOLDS NUMBER = 4630.0
EFFECTIVE REFRACTIVE INDICES AND POROSITIES,
TYPE 2 FILM 2.170 -.2800 I .210
TYPE 1 FILM 2.154 -.2744 I .020
TYPE 1 MIXRATE 1.455 0.0000 I .950
SECONDARY CRYSTALS 2.005 -.2240 I .200
NUMBER OF SECONDARY SITES/SQCM .26E+05 LIMITING COVERAGE .640
STD. DEVIATION IN TAUC (COHERENT) 7.26 SEC
CRYSTAL. RATE OF SEC. CRYSTALS (MA/SQCM), .48342
CRYSTAL. RATE OF TYPE2 FILM (MA/SQCM), .10000
SUPERSATURATION OF ICAS, 1.700 ,TIME TO REACH(S) .14770
INITIAL DISSOLUTION CURRENT (MA/SQCM) .1883
TIMES, ONSET OF SEC. CRYSTALS(SEC) 19.96 PPT. CONSTANT (S) 20.00
DEHYDRATION RATE (MA/SQCM) .600
EFFECTIVE FILM CURRENT(MA/SQCM) .422
AVE. DISTANCE BETWEEN EXP. AND THEORY 7.528 (DEG)

			EXPERIMENT		THEORY		THICKNESSES(A)				
TIME(S)	I(MA/SQCM)	VOLTS	DEL	PSI	DEL	PSI	TYPE2	TYPE1(F)	TYPE1(M)	SECONDARY	COV
0.00	.600	-.150	48.310	39.560	48.310	39.560	-1	0.0	-1	0.0	0.000
5.00	.600	.300	45.680	39.720	43.207	40.356	87.2	.0	.0	.0	.000
10.00	.600	.300	43.600	40.500	43.034	42.058	190.0	.0	.0	.0	.000
15.00	.600	.300	46.020	43.190	45.791	44.925	292.8	.0	.0	.0	.000
20.00	.600	.300	48.020	48.790	51.911	47.625	292.8	22.7	-.0	64.2	.000
25.00	.600	.300	44.080	55.530	46.953	52.993	292.8	77.3	-.0	151.7	.001
30.00	.600	.300	29.160	60.360	36.752	60.047	292.8	131.5	-.0	278.1	.004
35.00	.600	.300	8.570	61.160	9.074	66.786	292.8	184.3	-.0	434.5	.009
40.00	.600	.300	-11.150	57.930	-16.908	58.733	292.8	234.4	-.0	612.6	.018
45.00	.600	.300	-18.120	53.150	-9.588	52.571	292.8	280.1	-.0	806.0	.031
50.00	.600	.300	-20.520	48.100	-7.845	53.587	292.8	319.3	-.0	1010.6	.049
60.00	.600	.300	-19.180	40.820	-19.689	50.965	292.8	379.7	-.0	1380.5	.091
65.00	.600	.300	-16.840	38.820	-24.065	47.093	292.8	388.7	-.0	1603.5	.123
70.00	.600	.300	-15.590	37.640	-24.854	43.147	292.8	388.7	-.0	1807.8	.157
75.00	.600	.300	-13.660	36.450	-22.795	39.835	292.8	388.7	-.0	1974.2	.187
100.00	.600	.300	-9.110	34.480	-4.846	34.543	292.8	388.7	-.0	2552.1	.312
130.00	.600	.300	-9.160	32.870	-.996	36.704	292.8	388.7	-.0	3012.4	.435
150.00	.600	.200	-9.860	31.850							
170.00	.600	.200	-10.360	32.890							
200.00	.600	.200	-7.540	34.750							
220.00	.600	.200	.320	36.040							
240.00	.600	.200	13.210	36.850							
270.00	.600	.200	26.290	37.950							
310.00	.600	.200	37.170	40.480							
350.00	.600	.200	46.970	41.260							
390.00	.600	-.100	50.620	40.960							

AG3CC7,0.6MA/SQCM,1.1GPM,111-2

CODES, 1,2,3A,4,5,6,7,8 = 1.0, 2.0, 0.0, 1.0, 1.0, 1.0, 3.0, 0.0,
REYNOLDS NUMBER = 4600.0
EFFECTIVE REFRACTIVE INDICES AND POROSITIES,
TYPE 2 FILM 2.170 -.2800 I .210
TYPE 1 FILM 2.154 -.2744 I .020
TYPE 1 HYDRATE 1.410 0.0000 I .950
SECONDARY CRYSTALS 1.996 -.2218 I .208
NUMBER OF SECONDARY SITES/SQCM .28E+09 LIMITING COVERAGE .614
CRYSTAL. RATE OF SEC. CRYSTALS (MA/SQCM), .45873
CRYSTAL. RATE OF TYPE2 FILM (MA/SQCM), .07421
SUPERSATURATION OF IONS, 1.682 ,TIME TO REACH(S) .14464
INITIAL DISSOLUTION CURRENT (MA/SQCM) .1863
TIMES, ONSET OF SEC. CRYSTALS(SEC) 17.25 PPT. CONSTANT (S) 19.41
DEHYDRATION RATE (MA/SQCM) .600
EFFECTIVE FILM CURRENT(MA/SQCM) .423
AVE. DISTANCE BETWEEN EXP. AND THEORY 8.175 (DEG)

			EXPERIMENT		THEORY		THICKNESSES(A)				
TIME(S)	I(MA/SQCM)	VOLTS	DEL	PSI	DEL	PSI	TYPE2	TYPE1(F)	TYPE1(H)	SECONDARY	COV
0.00	.600	-.150	48.310	39.560	48.310	39.560	-1	0.0	-1	0.0	0.000
5.00	.600	.300	45.680	39.720	43.401	40.302	83.1	.0	.0	.0	.000
10.00	.600	.300	43.600	40.500	40.309	41.879	166.1	.0	.0	.0	.000
15.00	.600	.300	46.020	43.190	37.980	45.131	249.2	.0	.0	.0	.000
20.00	.600	.300	48.020	48.790	44.578	48.199	249.2	42.7	-.0	240.6	.003
25.00	.600	.300	44.080	55.530	37.739	53.376	249.2	96.1	-.0	394.1	.008
30.00	.600	.300	29.160	60.360	22.738	57.260	249.2	146.8	-.0	573.0	.017
35.00	.600	.300	8.570	61.160	4.934	56.090	249.2	192.8	-.0	769.9	.031
40.00	.600	.300	-11.150	57.930	-4.342	53.914	249.2	231.7	-.0	979.7	.050
45.00	.600	.300	-18.120	53.150	-9.023	52.861	249.2	260.7	-.0	1199.2	.075
50.00	.600	.300	-20.520	48.100	-13.024	53.273	249.2	276.8	-.0	1425.9	.106
55.00	.600	.300	-19.180	40.820	-22.638	51.609	249.2	276.9	-.0	1839.2	.176
60.00	.600	.300	-16.840	38.820	-25.650	48.466	249.2	276.9	-.0	1990.3	.207
70.00	.600	.300	-15.550	37.640	-26.194	45.049	249.2	276.9	-.0	2121.3	.235
75.00	.600	.300	-13.660	36.450	-24.787	41.943	249.2	276.9	-.0	2237.9	.261
100.00	.600	.300	-9.110	34.480	-8.871	35.466	249.2	276.9	-.0	2692.5	.378
130.00	.600	.300	-9.160	32.870	-4.673	38.521	249.2	276.9	-.0	3089.6	.498
150.00	.600	.200	-9.860	31.850							
170.00	.600	.200	-10.360	32.890							
200.00	.600	.200	-7.540	34.750							
220.00	.600	.200	.330	36.040							
240.00	.600	.200	13.310	36.850							
270.00	.600	.200	26.290	37.950							
300.00	.600	.200	37.170	40.400							
330.00	.600	.200	46.970	41.260							
390.00	.600	-.100	50.620	40.960							

AG30013,1.0MA/SQCM,1.0GPM,100-2

CODES, 1,2,3A,4,5,6,7,8 = 1.0, 2.0, 4.0, 1.0, 1.0, 1.0, 3.0, 0.0,
REYNOLDS NUMBER = 1000.0
EFFECTIVE REFRACTIVE INDICES AND POROSITIES,
TYPE 2 FILM 2.170 -.2800 I .210
TYPE 1 FILM 2.013 -.2240 I .200
TYPE 1 HYDRATE 1.481 [illegible] I .930
SECONDARY CRYSTALS 1.878 -.1820 I .350
NUMBER OF SECONDARY SITES/SQCM .53E+09 LIMITING COVERAGE .810
STD. DEVIATION IN TNUC (COHERENT) 5.97 SEC
CRYSTAL. RATE OF SEC. CRYSTALS (MA/SQCM), .45000
CRYSTAL. RATE OF TYPE2 FILM (MA/SQCM), .06055
SUPERSATURATION OF IONS, 1.7[illegible] ,TIME TO REACH(S) .05317
INITIAL DISSOLUTION CURRENT (MA/SQCM) .0622
TIMES, ONSET OF SEC. CRYSTALS(SEC) 17.97 PPT. CONSTANT (S) 21.30
DEHYDRATION RATE (MA/SQCM) .990
EFFECTIVE FILM CURRENT(MA/SQCM) .798
AVE. DISTANCE BETWEEN EXP. AND THEORY 4.122 (DEG)

			EXPERIMENT		THEORY		THICKNESSES(A)				
TIME(S)	I(MA/SQCM)	VOLTS	DEL	PSI	DEL	PSI	TYPE2	TYPE1(F)	TYPE1(H)	SECONDARY	COV
0.00	1.000	-.050	64.090	41.900	64.090	41.900	-I	0.0	-I	0.0	0.000
1.00	1.000	.200	63.990	41.900	63.125	41.859	7.7	.0	.0	.0	.000
2.00	1.000	.290	62.390	41.740	61.829	41.811	17.3	.0	.0	.0	.000
3.00	1.000	.300	60.600	41.480	60.318	41.761	28.5	.0	.0	.0	.000
4.00	1.000	.300	58.210	41.210	58.603	41.720	41.3	.0	.0	.0	.000
5.00	1.000	.300	55.210	40.920	56.707	41.702	55.6	.0	.0	.0	.000
6.00	1.000	.300	53.220	40.660	54.681	41.753	71.5	.0	.0	.0	.000
7.00	1.000	.300	51.030	40.400	54.229	41.806	89.1	.0	.0	.0	.000
8.00	1.000	.300	50.440	40.280	53.807	41.959	108.6	.0	.0	.0	.000
9.00	1.000	.300	49.630	40.260	53.306	42.320	130.1	.0	.0	.0	.000
10.00	1.000	.300	49.430	40.260	52.435	42.985	153.9	.0	.0	.0	.000
11.00	1.000	.300	49.830	40.370	51.111	43.803	180.1	.0	.0	.0	.000
12.00	1.000	.300	50.790	40.890	50.172	44.220	209.0	.0	.0	.0	.000
13.00	1.000	.300	51.740	41.610	51.037	44.743	241.0	.0	.0	.0	.000
14.00	1.000	.300	53.260	42.750	52.913	45.210	276.5	.0	.0	.0	.000
15.00	1.000	.300	55.370	44.110	55.661	46.307	315.9	.0	.0	.0	.000
16.00	1.000	.300	57.470	45.670	58.743	48.368	359.7	.0	.0	.0	.000
17.00	1.000	.300	59.110	48.020	61.495	51.787	408.7	.0	.0	.0	.000
18.00	1.000	.300	62.840	51.850	63.206	56.432	436.9	17.9	-.0	96.1	.001
19.00	1.000	.300	64.280	54.000	66.311	60.314	436.9	44.7	-.0	162.7	.003
20.00	1.000	.300	66.270	59.000	68.834	64.640	436.9	70.5	-.0	241.7	.006
21.00	1.000	.300	66.850	63.260	70.297	69.216	436.9	94.9	-.0	329.4	.011
22.00	1.000	.300	64.360	69.390	64.800	74.491	436.9	118.6	-.0	423.5	.018
23.00	1.000	.300	48.440	75.030	44.640	79.782	436.9	141.0	-.0	522.1	.027
24.00	1.000	.300	-8.750	74.660	-2.051	79.912	436.9	161.3	-.0	624.3	.039
25.00	1.000	.300	-17.340	74.800	-19.578	72.008	436.9	179.2	-.0	729.2	.053
-I	-I	-I	-I	-I							

1 AG30013,1.0MA/SQCM,1.0GPM,100-2

CODES, 1,2,3A,4,5,6,7,8 = 1.0, 2.0, 4.0, 1.0, 1.0, 1.0, 3.0, 3.0,
REYNOLDS NUMBER = 1000.0
EFFECTIVE REFRACTIVE INDICES AND POROSITIES,
TYPE 2 FILM 2.170 -.2800 I .210
TYPE 1 FILM 2.146 -.2716 I .030
TYPE 1 HYDRATE 1.457 0.0000 I .854
SECONDARY CRYSTALS 1.878 -.1820 I .350
NUMBER OF SECONDARY SITES/SQCM .53E+09 LIMITING COVERAGE .437
CRYSTAL. RATE OF SEC. CRYSTALS (MA/SQCM), .38807
CRYSTAL. RATE OF TYPE2 FILM (MA/SQCM), .06210
SUPERSATURATION OF IONS, 1.700 ,TIME TO REACH(S) .05317
INITIAL DISSOLUTION CURRENT (MA/SQCM) .0622
TIMES, ONSET OF SEC. CRYSTALS(SEC) 12.00 PPT. CONSTANT (S) 21.19
DEHYDRATION RATE (MA/SQCM) 1.000
EFFECTIVE FILM CURRENT(MA/SQCM) .825
AVE. DISTANCE BETWEEN EXP. AND THEORY 5.859 (DEG)

		EXPERIMENT			THEORY		THICKNESSES(A)				
TIME(S)	I(MA/SQCM)	VOLTS	DEL	PSI	DEL	PSI	TYPE2	TYPE1(F)	TYPE1(H)	SECONDARY	COV
0.00	1.000	-.050	64.090	41.900	64.090	41.900	-I	0.0	-I	0.0	0.000
1.00	1.000	.200	63.990	41.900	63.125	41.859	8.4	.0	.0	.0	.000
2.00	1.000	.290	62.390	41.740	61.864	41.812	19.5	.0	.0	.0	.000
3.00	1.000	.300	60.600	41.480	60.436	41.765	32.9	.0	.0	.0	.000
4.00	1.000	.300	58.210	41.210	58.859	41.725	48.8	.0	.0	.0	.000
5.00	1.000	.300	55.210	40.920	57.164	41.701	67.3	.0	.0	.0	.000
6.00	1.000	.300	53.220	40.660	55.383	41.704	88.8	.0	.0	.0	.000
7.00	1.000	.300	51.030	40.400	53.564	41.756	113.8	.0	.0	.0	.000
8.00	1.000	.300	50.440	40.280	51.768	41.893	142.7	.0	.0	.0	.000
9.00	1.000	.300	49.630	40.260	50.088	42.130	176.3	.0	.0	.0	.000
10.00	1.000	.300	49.430	40.260	48.648	42.745	215.6	.0	.0	.0	.000
11.00	1.000	.300	49.830	40.370	47.600	43.854	261.7	.0	.0	.0	.000
12.00	1.000	.300	50.790	40.890	47.229	44.863	290.0	.0	.0	.0	.000
13.00	1.000	.300	51.740	41.610	50.469	46.632	290.0	37.2	-.0	.1	.000
14.00	1.000	.300	53.260	42.750	53.601	48.211	290.0	59.6	-.0	1.1	.000
15.00	1.000	.300	55.370	44.110	56.501	50.087	290.0	81.5	-.0	7.5	.000
16.00	1.000	.300	57.470	45.670	59.165	52.324	290.0	103.3	-.0	26.3	.000
17.00	1.000	.300	59.110	48.020	61.583	54.931	290.0	124.6	-.0	62.1	.000
18.00	1.000	.300	62.840	51.850	63.713	57.924	290.0	145.5	-.0	113.8	.001
19.00	1.000	.300	64.280	54.000	65.399	61.329	290.0	166.0	-.0	177.7	.003
20.00	1.000	.300	66.270	59.000	66.266	65.125	290.0	185.8	-.0	250.4	.006
21.00	1.000	.300	66.850	63.260	65.655	69.198	290.0	204.9	-.0	329.3	.011
22.00	1.000	.300	64.860	69.390	57.561	73.625	290.0	224.3	-.0	412.8	.017
23.00	1.000	.300	48.440	75.030	38.555	77.242	290.0	243.0	-.0	499.7	.025
24.00	1.000	.300	-8.750	74.660	7.502	77.744	290.0	260.5	-.0	589.2	.034
25.00	1.000	.300	-17.540	74.800	-17.855	73.427	290.0	275.4	-.0	680.7	.046
-I	-I	-I	-I	-I							

AG300-16, 1MA/SQCM, 6MKCH, AG110-2

CODES, 1,2,3A,4,5,6,7,8 = 1.0, 2.0, 4.0, 1.0, 1.0, 1.0, 3.0, 0.0,
REYNOLDS NUMBER = 1000.0

EFFECTIVE REFRACTIVE INDICES AND POROSITIES,

TYPE 2 FILM	2.170	-.2800 I	.210
TYPE 1 FILM	1.977	-.2109 I	.247
TYPE 1 HYDRATE	1.428	0.0000 I	.913
SECONDARY CRYSTALS	1.876	-.1820 I	.350

NUMBER OF SECONDARY SITES/SQCM .36E+09 LIMITING COVERAGE .670

CRYSTAL, RATE OF SEC. CRYSTALS (MA/SQCM), .32800
CRYSTAL, RATE OF TYPE2 FILM (MA/SQCM), .05551
SUPERSATURATION OF IONS, 2.310 ,TIME TO REACH(S) .09817
INITIAL DISSOLUTION CURRENT (MA/SQCM) .2558
TIMES, ONSET OF SEC. CRYSTALS(SEC) 5.63 PPT. CONSTANT (S) 18.53
DEHYDRATION RATE (MA/SQCM) .988
EFFECTIVE FILM CURRENT(MA/SQCM) .765
AVE. DISTANCE BETWEEN EXP. AND THEORY 1.251 (DEG)

			EXPERIMENT		THEORY		THICKNESSES(A)				
TIME(S)	I(MA/SQCM)	VOLTS	DEL	PSI	DEL	PSI	TYPE2	TYPE1(F)	TYPE1(H)	SECONDARY	COV
0.00	1.000	-.120	63.540	40.590	63.540	40.590	.0	.0	0.0	.0	0.000
5.00	1.000	.290	58.110	39.880	56.438	40.667	69.7	.0	.0	.0	.000
10.00	1.000	.290	56.280	40.130	55.822	41.392	80.0	133.1	-.0	124.8	.001
15.00	1.000	.290	60.030	43.620	60.093	44.477	80.0	263.9	-.0	253.1	.004
16.00	1.000	.290	60.960	44.740	60.991	45.699	80.0	289.0	-.0	303.6	.006
17.00	1.000	.290	61.620	46.960	61.650	47.155	80.0	313.7	-.0	355.4	.008
18.00	1.000	.290	61.670	48.660	61.966	48.810	80.0	337.9	-.0	408.2	.011
19.00	1.000	.290	60.970	52.550	61.293	50.693	80.0	362.2	-.0	462.0	.014
20.00	1.000	.290	59.240	54.110	59.363	52.795	80.0	387.0	-.0	516.4	.018
21.00	1.000	.290	56.010	56.740	56.639	54.988	80.0	411.3	-.0	571.5	.022
22.00	1.000	.290	53.230	58.590	52.897	57.193	80.0	435.2	-.0	627.0	.026
23.00	1.000	.290	47.640	60.280	47.848	59.279	80.0	458.5	-.0	683.0	.031
24.00	1.000	.290	41.980	62.600	42.118	61.133	80.0	481.2	-.0	739.4	.037
25.00	1.000	.290	37.260	63.430	36.446	62.837	80.0	503.3	-.0	796.0	.043
26.00	1.000	.290	31.100	64.560	29.731	64.191	80.0	524.7	-.0	853.0	.049
27.00	1.000	.290	22.030	64.740	22.232	65.021	80.0	545.4	-.0	910.2	.056
28.00	1.000	.290	15.430	64.460	14.563	65.234	80.0	565.2	-.0	967.6	.063
29.00	1.000	.290	7.090	63.660	7.466	64.880	80.0	584.2	-.0	1025.3	.071
30.00	1.000	.290	2.140	63.010	1.451	64.140	80.0	602.3	-.0	1083.1	.079
31.00	1.000	.290	-4.170	62.070	-3.361	63.236	80.0	619.4	-.0	1141.1	.087
32.00	1.000	.290	-7.480	61.360							

≠CO100-15≠ ≠4E-3 AMPS≠ ≠1MKOH≠

CODES, 1,2,3A,4,5,6,7,8 = 1.0, 2.0, 4.0, 1.0, 1.0, 1.0, 3.0, 0.0,
CODES, 9,10,11,3,12,13,14 = 0.0, 1.0, 7.0, 4.0, 1.0, 1.0, 1.0,
REYNOLDS NUMBER = 0.0
EFFECTIVE REFRACTIVE INDICES AND POROSITIES,
TYPE 2 FILM 2.130 0.0000 I .200
TYPE 1 FILM 2.121 0.0000 I 0.000
TYPE 1 HYDRATE 1.345 0.0000 I .932
SECONDARY CRYSTALS 2.130 0.0000 I 0.000
NUMBER OF SECONDARY SITES/SQCM .16E+09 LIMITING COVERAGE .790
CRYSTAL. RATE OF SEC. CRYSTALS (MA/SQCM), .18202
CRYSTAL. RATE OF TYPE2 FILM (MA/SQCM), .11578
SUPERSATURATION OF IONS, 2.300 ,TIME TO REACH(S) .00021
INITIAL DISSOLUTION CURRENT (MA/SQCM) .0004
TIMES, ONSET OF SEC. CRYSTALS(SEC) 10.0 PPT. CONSTANT (S) 2.0
TIME TO COMPLETE PATCH COVERAGE 90.8
TIME TO REACH COMPACT FILM I 71.2 S
TIME TO DISSIPATE HYDRATE LAYER 71.2 S
DEHYDRATION RATE (MA/SQCM) .3.4
EFFECTIVE FILM CURRENT(MA/SQCM) .268
CURRENT FRACTION FORMING ROUGHNESS .001
FINAL THICKNESS OF ROUGHNESS 4.2
WIDTH TO HEIGHT OF SEC. CRYSTALS, .536
INITIAL PATCH COVERAGE .380
FINAL POROSITY OF TYPE I FILM .011
AVE. DISTANCE BETWEEN EXP. AND THEORY 5.273 (DEG)

			EXPERIMENT		THEORY		THICKNESSES(A)				
TIME(S)	I(MA/SQCM)	VOLTS	DEL	PSI	DEL	PSI	TYPE2	TYPE1(F)	TYPE1(H)	SECONDARY	COV
10.0	.400	-.800	80.300	35.900	83.425	38.686	401.6	0.0	-.0	.0	.000
20.0	.400	-.800	78.000	37.400	91.056	36.137	401.6	50.5	-.0	2341.1	.025
30.0	.400	-.800	81.000	40.000	85.263	38.496	401.6	115.8	-.0	2560.2	.030
40.0	.400	-.800	85.600	43.700	80.903	41.734	401.6	168.4	-.0	2726.9	.034
50.0	.400	-.800	95.600	49.300	94.249	46.721	401.6	209.2	-.0	2841.2	.037
60.0	.400	-.800	110.400	56.500	110.118	53.325	401.6	240.6	-.0	2909.4	.039
70.0	.400	-.800	123.200	63.800	129.503	60.864	401.6	265.3	-.0	2941.0	.040
80.0	.400	-.800	155.200	69.600	154.892	65.858	401.6	284.8	-.0	2945.0	.040
90.0	.400	.870	163.500	69.400	173.313	69.609	401.6	301.8	-.0	2929.3	.040
93.00	.400	.980	170.500	69.400							

#CD10022# #1E-3 AMPS# #1MKOH#

CODES, 1,2,3A,4,5,6,7,8 = 1.0, 2.0, 4.0, 1.0, 1.0, 1.0, 3.0, 0.0,
CODES, 9,10,11,3,12,13,14 = 0.0, 1.0, 7.0, 4.0, 1.0, 1.0, 1.0,
REYNOLDS NUMBER = 0.0
EFFECTIVE REFRACTIVE INDICES AND POROSITIES,
TYPE 2 FILM 2.130 0.0000 I .200
TYPE 1 FILM 2.121 0.0000 I .015
TYPE 1 HYDRATE 1.441 0.0000 I .828
SECONDARY CRYSTALS 2.130 0.0000 I 0.000
NUMBER OF SECONDARY SITES/SQCM .30E+09 LIMITING COVERAGE .790
CRYSTAL. RATE OF SEC. CRYSTALS (MA/SQCM), .01425
CRYSTAL. RATE OF TYPE2 FILM (MA/SQCM), .02000
SUPERSATURATION OF IONS, 2.300 ,TIME TO REACH(S) .00003
INITIAL DISSOLUTION CURRENT (MA/SQCM) .0009
TIMES, ONSET OF SEC. CRYSTALS(SEC) 1.9 PPT. CONSTANT (S) 1.6
TIME TO COMPLETE PATCH COVERAGE 9.1
TIME TO REACH COMPACT FILM I 38.5 S
TIME TO DISSIPATE HYDRATE LAYER 38.5 S
DEHYDRATION RATE (MA/SQCM) .097
EFFECTIVE FILM CURRENT(MA/SQCM) .634
CURRENT FRACTION FORMING ROUGHNESS .000
FINAL THICKNESS OF ROUGHNESS 2.0
WIDTH TO HEIGHT OF SEC. CRYSTALS, 1.000
INITIAL PATCH COVERAGE .661
FINAL POROSITY OF TYPE I FILM .011
AVE. DISTANCE BETWEEN EXP. AND THEORY .574 (DEG)

		EXPERIMENT		THEORY		THICKNESSES(A)				
TIME(S)	I(MA/SQCM)	VOLTS	DEL	PSI	DEL	PSI	TYPE2	TYPE1(F)	TYPE1(H)	SECONDARY	COV
2.0	1.000	-.800	102.400	41.900	103.017	41.583	456.3	.0	-.0	119.4	.000
4.0	1.000	-.800	103.200	42.800	103.091	42.326	456.3	4.1	-.0	121.6	.000
6.0	1.000	-.800	104.800	43.100	104.069	43.666	456.3	7.5	-.0	120.8	.000
8.0	1.000	-.800	105.600	45.400	105.569	45.725	456.3	10.2	-.0	117.7	.000
10.0	1.000	-.500	106.000	47.100	105.985	47.281	456.3	13.2	-.0	116.8	.000
12.0	1.000	.500	104.800	48.200	105.058	47.703	456.3	17.7	-.0	119.4	.000
14.00	1.000	1.100	103.600	48.700							

#CC100-248# #6E-4 AMPS# #1MKOH#

CODES, 1,2,3A,4,5,6,7,8 = 1.0, 2.0, 4.0, 1.0, 1.0, 1.0, 3.0, 0.0,
CODES, 9,10,11,3,12,13,14 = 0.0, 1.0, 7.0, 4.0, 1.0, 1.0, 1.0,
REYNOLDS NUMBER = 0.0
EFFECTIVE REFRACTIVE INDICES AND POROSITIES,
TYPE 2 FILM 2.430 0.0000 I .200
TYPE 1 FILM 2.421 0.0000 I 0.000
TYPE 1 HYDRATE 1.366 0.0000 I .852
SECONDARY CRYSTALS 2.130 0.0000 I 0.000
NUMBER OF SECONDARY SITES/SQCM .10E+09 LIMITING COVERAGE .790
CRYSTAL. RATE OF SEC. CRYSTALS (MA/SQCM), .12129
CRYSTAL. RATE OF TYPE2 FILM (MA/SQCM), .33266
SUPERSATURATION OF IONS, 2.300 ,TIME TO REACH(S) .00009
INITIAL DISSOLUTION CURRENT (MA/SQCM) .0005
TIMES, ONSET OF SEC. CRYSTALS(SEC) 15.0 PPT. CONSTANT (S) 2.0
TIME TO COMPLETE PATCH COVERAGE 50.4
TIME TO REACH COMPACT FILM I 60.3 S
TIME TO DISSIPATE HYDRATE LAYER 60.3 S
DEHYDRATION RATE (MA/SQCM) .107
EFFECTIVE FILM CURRENT(MA/SQCM) .184
CURRENT FRACTION FORMING ROUGHNESS .001
FINAL THICKNESS OF ROUGHNESS 4.2
WIDTH TO HEIGHT OF SEC. CRYSTALS, 1.000
INITIAL PATCH COVERAGE .900
FINAL POROSITY OF TYPE I FILM .011
AVE. DISTANCE BETWEEN EXP. AND THEORY 1.369 (DEG)

		EXPERIMENT			THEORY		THICKNESSES(A)				
TIME(S)	I(MA/SQCM)	VOLTS	DEL	PSI	DEL	PSI	TYPE2	TYPE1(F)	TYPE1(H)	SECONDARY	COV
10.0	.600	-.820	107.000	45.000	105.966	45.388	463.8	0.0	-.0	.0	.000
20.0	.600	-.820	108.400	48.600	109.250	47.795	463.8	15.9	-.0	810.3	.007
30.0	.600	-.820	113.000	51.900	114.076	50.521	463.8	40.0	-.0	847.0	.007
40.0	.600	-.820	123.100	55.700	122.592	54.424	463.8	63.2	-.0	878.1	.008
50.0	.600	-.820	137.500	58.600	137.423	59.954	463.8	85.1	-.0	903.0	.008
60.00	.600	.800	144.700	59.100							

CD100-25 *2E-4 AMPS* *1MKOM*

CODES, 1,2,3A,4,5,6,7,8 = 1.0, 2.0, 4.0, 1.0, 1.0, 1.0, 3.0, 0.0,
CODES, 9,10,11,3,12,13,14 = 0.0, 1.0, 7.0, 4.0, 1.0, 1.0, 1.0,
REYNOLDS NUMBER = 0.0
EFFECTIVE REFRACTIVE INDICES AND POROSITIES,
TYPE 2 FILM 2.130 0.0000 I .200
TYPE 1 FILM 2.123 0.0000 I 0.000
TYPE 1 HYDRATE 1.377 0.0000 I .831
SECONDARY CRYSTALS 2.130 0.0000 I 0.000
NUMBER OF SECONDARY SITES/SQCM .21E+10 LIMITING COVERAGE .790
CRYSTAL, RATE OF SEC. CRYSTALS (MA/SQCM), .00415
CRYSTAL, RATE OF TYPE2 FILM (MA/SQCM), .J1000
SUPERSATURATION OF IONS, 2.300 ,TIME TO REACH(S) .00083
INITIAL DISSOLUTION CURRENT (MA/SQCM) .0004
TIMES, ONSET OF SEC. CRYSTALS(SEC) 2.0 PPT. CONSTANT (S) 1.4
TIME TO COMPLETE PATCH COVERAGE 91.6
TIME TO REACH COMPACT FILM I 99.5 S
TIME TO DISSIPATE HYDRATE LAYER 99.5 S
DEHYDRATION RATE (MA/SQCM) .010
EFFECTIVE FILM CURRENT(MA/SQCM) .179
CURRENT FRACTION FORMING ROUGHNESS .001
FINAL THICKNESS OF ROUGHNESS 5.1
WIDTH TO HEIGHT OF SEC. CRYSTALS, 1.000
INITIAL PATCH COVERAGE .616
FINAL POROSITY OF TYPE I FILM .011
AVE. DISTANCE BETWEEN EXP. AND THEORY .813 (DEG)

	EXPERIMENT				THEORY		THICKNESSES(A)				
TIME(S)	I(MA/SQCM)	VOLTS	DEL	PSI	DEL	PSI	TYPE2	TYPE1(F)	TYPE1(H)	SECONDARY	COV
10.0	.200	-.805	96.400	39.400	95.317	39.438	318.J	.0	-.0	348.6	.026
20.0	.200	-.805	95.200	40.200	94.896	40.029	318.J	2.1	-.0	386.9	.032
30.0	.200	-.805	96.600	41.200	95.235	40.696	318.J	4.1	-.0	422.8	.038
40.J	.200	-.805	97.600	42.400	96.718	42.106	318.J	6.0	-.0	455.6	.044
50.0	.200	-.805	98.800	44.100	98.926	43.625	318.J	7.7	-.0	484.9	.050
60.J	.200	-.700	99.200	45.200	99.926	45.226	318.J	9.3	-.0	510.4	.055
70.0	.200	-.300	100.600	46.800	100.678	47.183	318.J	10.7	-.0	532.1	.060
76.0	.200	-.100	101.000	47.800	100.902	48.356	318.J	11.5	-.0	543.7	.062
-I	-I	-I	-I	-I							

#CD100-26# #1E-4 AMPS# #1MKOH,#

CODES, 1,2,3A,4,5,6,7,8 = 1.0, 2.0, 4.0, 1.0, 1.0, 1.0, 3.0, 0.0,
CODES, 9,10,11,3,12,13,14 = 0.0, 1.0, 7.0, 4.0, 1.0, 1.0, 1.0,
REYNOLDS NUMBER = 0.0
EFFECTIVE REFRACTIVE INDICES AND POROSITIES,
TYPE 2 FILM 2.130 0.0000 I .200
TYPE 1 FILM 2.121 0.0000 I .020
TYPE 1 HYDRATE 1.345 0.0000 I .701
SECONDARY CRYSTALS 2.130 0.0000 I 0.000
NUMBER OF SECONDARY SITES/SQCM .10E+10 LIMITING COVERAGE .790
CRYSTAL. RATE OF SEC. CRYSTALS (MA/SQCM), .00273
CRYSTAL. RATE OF TYPE2 FILM (MA/SQCM), .10000
SUPERSATURATION OF IONS, 2.300 ,TIME TO REACH(S) .00332
INITIAL DISSOLUTION CURRENT (MA/SQCM) .0002
TIMES, ONSET OF SEC. CRYSTALS(SEC) 60.0 PPT. CONSTANT (S) 2.0
TIME TO REACH COMPACT FILM I 120.2 S
TIME TO DISSIPATE HYDRATE LAYER 191.1 S
DEHYDRATION RATE (MA/SQCM) .076
EFFECTIVE FILM CURRENT(MA/SQCM) .094
CURRENT FRACTION FORMING ROUGHNESS .200
FINAL THICKNESS OF ROUGHNESS 18.8
WIDTH TO HEIGHT OF SEC. CRYSTALS, .729
INITIAL PATCH COVERAGE .368
FINAL POROSITY OF TYPE I FILM .011
AVE. DISTANCE BETWEEN EXP. AND THEORY 10.490 (DEG)

		EXPERIMENT			THEORY		THICKNESSES(A)				
TIME(S)	I(MA/SQCM)	VOLTS	DEL	PSI	DEL	PSI	TYPE2	TYPE1(F)	TYPE1(H)	SECONDARY	COV
20.0	.100	-.830	100.200	40.200	101.172	38.476	219.3	0.0	-.0	.0	.000
40.0	.100	-.830	103.200	41.500	100.660	38.964	325.6	0.0	-.0	.0	.000
60.0	.100	-.830	106.800	43.500	102.097	39.136	409.3	0.0	-.0	.0	.000
80.0	.100	-.830	111.200	46.400	100.131	41.111	409.3	28.2	-.0	595.8	.019
100.0	.100	-.830	117.600	49.800	106.823	42.293	409.3	57.6	-.0	620.5	.020
120.0	.100	-.830	121.300	53.600	115.244	45.753	409.3	80.8	-.0	629.5	.021
140.0	.100	-.830	127.900	57.500	127.283	47.541	409.3	96.4	-.0	626.5	.021
160.0	.100	-.830	136.800	61.800	138.289	50.653	409.3	108.1	-.0	615.6	.020
180.0	.100	-.830	149.200	65.500	147.795	55.014	409.3	117.5	-.0	600.3	.019
200.0	.100	-.830	167.100	68.500	167.680	57.862	409.3	137.3	-.0	599.7	.019
220.0	.100	-.830	191.100	67.900	200.414	55.678	409.3	172.8	-.0	618.9	.020
240.0	.100	-.830	217.800	64.100	224.081	51.868	409.3	208.4	-.0	638.1	.022
260.0	.100	-.830	240.500	55.900	238.607	48.343	409.3	244.2	-.0	657.3	.023
280.0	.100	-.830	258.700	46.700	246.333	45.556	409.3	279.9	-.0	676.6	.024
300.0	.100	-.830	262.300	38.500	249.064	43.345	409.3	315.6	-.0	695.9	.026
320.0	.100	-.830	251.700	33.600	247.873	41.479	409.3	351.3	-.0	715.3	.027
340.0	.100	-.830	239.300	31.000	243.337	39.795	409.3	387.1	-.0	734.7	.029
360.0	.100	-.830	227.600	29.500	235.735	38.219	409.3	422.9	-.0	754.1	.030
380.0	.100	-.830	217.900	30.200	225.227	36.763	409.3	458.7	-.0	773.6	.032
400.0	.100	-.830	209.300	30.900	212.645	35.534	409.3	494.5	-.0	793.2	.033
420.0	.100	-.830	205.000	32.100	196.700	34.703	409.3	530.4	-.0	812.7	.035
440.00	.100	-.830	200.000	33.800							
480.00	.100	-.830	193.000	37.700							
520.00	.100	-.830	189.100	41.400							
560.00	.100	-.830	188.500	45.800							
600.00	.100	-.830	189.900	49.800							
640.00	.100	-.830	193.700	53.400							
680.00	.100	-.830	200.100	56.200							
720.00	.100	-.830	209.100	57.400							
760.00	.100	-.830	218.100	57.100							
800.00	.100	-.830	227.100	55.700							
840.00	.100	-.830	236.300	54.100							

#CD1CO-26# #1E-4 AMPS# #1MKOH,#

CODES, 1,2,3A,4,5,6,7,8 = 1.0, 2.0, 4.0, 1.0, 1.0, 1.0, 3.0, 0.0,
CODES, 9,10,11,3,12,13,14 = C.0, 1.0, 7.0, 4.0, 0.0, 1.0, 1.0,
REYNOLDS NUMBER = 0.0
EFFECTIVE REFRACTIVE INDICES AND POROSITIES,
TYPE 2 FILM 2.130 0.0000 I .200
TYPE 1 FILM 2.121 C.0000 I .020
TYPE 1 HYDRATE 1.345 0.0000 I .766
SECONDARY CRYSTALS 2.130 0.0000 I 0.000
NUMBER OF SECONDARY SITES/SQCM .10E+10 LIMITING COVERAGE .790
CRYSTAL. RATE OF SEC. CRYSTALS (MA/SQCM), .00242
CRYSTAL. RATE OF TYPE2 FILM (MA/SQCM), .10000
SUPERSATURATION OF IONS, 2.300 ,TIME TO REACH(S) .00332
INITIAL DISSOLUTION CURRENT (MA/SQCM) .0002
TIMES, ONSET OF SEC. CRYSTALS(SEC) 61.7 PPT. CONSTANT (S) 2.0
TIME TO REACH COMPACT FILM I 139.6 S
TIME TO DISSIPATE HYDRATE LAYER 186.4 S
DEHYDRATION RATE (MA/SQCM) .086
EFFECTIVE FILM CURRENT(MA/SQCM) .096
CURRENT FRACTION FORMING ROUGHNESS .200
FINAL THICKNESS OF ROUGHNESS 18.2
WIDTH TO HEIGHT OF SEC. CRYSTALS, .568
INITIAL PATCH COVERAGE .300
FINAL POROSITY OF TYPE I FILM .011
AVE. DISTANCE BETWEEN EXP. AND THEORY 11.957 (DEG)

		EXPERIMENT			THEORY		THICKNESSES(A)				
TIME(S)	I(MA/SQCM)	VOLTS	DEL	PSI	DEL	PSI	TYPE2	TYPE1(F)	TYPE1(H)	SECONDARY	COV
20.0	.100	-.830	100.200	40.200	108.634	39.584	95.2	0.0	-.0	.0	.000
40.0	.100	-.830	103.200	41.500	105.411	40.274	226.7	0.0	-.0	.0	.000
60.0	.100	-.830	106.800	43.500	104.407	40.618	330.4	0.0	-.0	.0	.000
80.0	.100	-.830	111.200	46.400	100.862	41.310	330.4	2.1	-.0	699.9	.016
100.0	.100	-.830	117.600	49.800	106.828	42.156	330.4	109.3	-.0	720.1	.017
120.0	.100	-.830	121.300	53.600	119.425	42.824	330.4	177.8	-.0	717.0	.017
140.0	.100	-.830	127.900	57.500	133.090	45.192	330.4	212.4	-.0	699.3	.016
160.0	.100	-.830	136.800	61.800	140.947	48.185	330.4	221.1	-.0	674.5	.015
180.0	.100	-.830	149.200	65.500	140.097	51.966	330.4	217.8	-.0	647.2	.014
200.0	.100	-.830	167.100	68.500	162.572	53.750	330.4	243.1	-.0	651.7	.014
220.0	.100	-.830	191.100	67.900	197.458	52.573	330.4	283.7	-.0	670.6	.015
240.0	.100	-.830	217.800	64.100	223.874	49.863	330.4	324.5	-.0	689.5	.015
260.0	.100	-.830	240.500	55.900	240.207	47.296	330.4	365.2	-.0	708.5	.016
280.0	.100	-.830	258.700	46.700	248.722	45.310	330.4	406.0	-.0	727.5	.017
300.0	.100	-.830	263.300	38.500	251.549	43.773	330.4	446.9	-.0	746.5	.018
320.0	.100	-.830	251.700	33.600	250.019	42.494	330.4	487.7	-.0	765.5	.019
340.0	.100	-.830	239.300	31.000	244.856	41.346	330.4	528.6	-.0	784.6	.020
360.0	.100	-.830	227.600	29.500	236.442	40.278	330.4	569.4	-.0	803.7	.021
380.0	.100	-.830	217.900	30.200	225.047	39.307	330.4	610.3	-.0	822.8	.022
400.0	.100	-.830	209.300	30.900	211.051	38.520	330.4	651.2	-.0	842.0	.023
420.0	.100	-.830	205.000	32.100	195.135	38.042	330.4	692.2	-.0	861.1	.024
440.00	.100	-.830	200.000	33.800							
480.00	.100	-.830	193.000	37.700							
520.00	.100	-.830	189.100	41.400							
560.00	.100	-.830	188.500	45.800							
600.00	.100	-.830	189.900	49.800							
640.00	.100	-.830	193.700	53.400							
680.00	.100	-.830	200.100	56.200							
720.00	.100	-.830	209.100	57.400							
760.00	.100	-.830	218.100	57.100							
800.00	.100	-.830	227.100	55.700							
840.00	.100	-.830	236.300	54.100							

CO 100-30 1E-3 AMPS 6MKOH

CODES, 1,2,3A,4,5,6,7,8 = 1.0, 0.0, 0.0, 1.0, 1.0, 1.0, 3.5, 0.0,
CODES, 9,10,11,3,12,13,14 = 0.0, 1.0, 7.0, 3.0, 1.0, 0.0, 1.0,
REYNOLDS NUMBER = 0.0
EFFECTIVE REFRACTIVE INDICES AND POROSITIES,
TYPE 2 FILM 2.130 0.0000 I .150
TYPE 1 FILM 2.007 0.0000 I 0.000
TYPE 1 HYDRATE 1.447 0.0000 I .874
SECONDARY CRYSTALS 1.892 0.0000 I .300
ROUGHNESS 1.640 -3.9570 I .001
NUMBER OF SECONDARY SITES/SQCM .19E+08 LIMITING COVERAGE .790
CRYSTAL. RATE OF SEC. CRYSTALS (MA/SQCM), .593
CRYSTAL. RATE OF TYPE2 FILM (MA/SQCM), .140
SUPERSATURATION OF IONS, 3.82 ,TIME TO REACH(S) .00
INITIAL DISSOLUTION CURRENT (MA/SQCM) .0016
TIMES, ONSET OF SEC. CRYSTALS(SEC) 1.5 PPT. CONSTANT (S) 2.0
TIME TO COMPLETE PATCH COVERAGE 138.0
TIME TO REACH COMPACT FILM I 66.3 S
TIME TO DISSIPATE HYDRATE LAYER 66.3 S
TPACK = 66.3 TDISS = 138.0
DEHYDRATION RATE (MA/SQCM) .297
EFFECTIVE FILM CURRENT(MA/SQCM) 1.531
CURRENT FRACTION FORMING ROUGHNESS .016
FINAL THICKNESS OF ROUGHNESS 26.8
WIDTH TO HEIGHT OF SEC. CRYSTALS, .400
INITIAL PATCH COVERAGE .904
FINAL POROSITY OF TYPE I FILM .467
MOLE FRACTION METAL IN PATCHES 0.000
PASSIVATION TIME 3000.00
AVE. DISTANCE BETWEEN EXP. AND THEORY 3.351 (DEG)

		EXPERIMENT			THEORY		THICKNESSES(A)				
TIME(S)	I(MA/SQCM)	VOLTS	DEL	PSI	DEL	PSI	TYPE2	TYPE1(F)	TYPE1(H)	SECONDARY	COV
10.0	1.000	-.920	91.600	38.800	92.832	43.427	415.2	.0	-.0	3401.4	.004
20.0	1.000	-.920	98.600	42.200	98.823	46.058	415.2	53.1	-.0	5088.4	.008
30.0	1.000	-.920	113.200	48.600	112.224	49.012	415.2	131.5	-.0	6069.6	.011
40.0	1.000	-.920	133.700	54.200	131.595	51.446	415.2	206.0	-.0	6801.3	.014
50.0	1.000	-.920	154.500	53.700	156.167	52.160	415.2	286.7	-.0	7395.5	.017
60.0	1.000	-.920	168.000	47.300							
70.0	1.000	-.920	174.400	37.200							
80.0	1.000	-.920	172.300	26.000							
90.0	1.000	-.920	149.100	17.600							
100.0	1.000	-.920	113.900	16.000							
110.0	1.000	-.920	90.800	20.200							
120.0	1.000	-.920	100.100	27.600							
130.0	1.000	-.920	107.100	34.000							
140.0	1.000	-.920	114.000	46.700							
150.0	1.000	-.920	123.000	48.200							
160.0	1.000	-.920	126.000	54.100							
170.0	1.000	-.920	138.400	60.600							
180.0	1.000	-.920	152.700	62.600							
190.0	1.000	-.920	171.500	61.700							
200.0	1.000	-.920	182.000	59.400							
210.0	1.000	-.920	185.500	57.200							
220.0	1.000	-.920	184.000	58.800							
230.0	1.000	.600	184.600	56.800							
240.0	1.000	.600	184.600	56.300							

CO 100-30 1E-3 AMPS 6MKOH

CODES. 1,2,3A,4,5,6,7,8 = 1. , 3. , . , 1. , 1. , 5. , 3.5, . ,
CODES. 9,10,11,12,A2,13,14 = 3. , 1.0, 1. , 3. , 1.0, 0.0, 1.0,
REYNOLDS NUMBER = 0.0
EFFECTIVE REFRACTIVE INDICES AND POROSITIES.
TYPE 2 FILM 3.173 -.3085 I .151
NON-STOICHIOMETRY N 3.173 -.396 I
TYPE 1 FILM 2.648 -.2615 I .293
TYPE 1 HYDRATE 1.535 0.0000 I .800
SECONDARY CRYSTALS 1.828 0. I .387
ROUGHNESS 1.481 -1.49 I .624
NUMBER OF SECONDARY SITES/SQCM .24E+06 LIMITING COVERAGE .790
CRYSTAL. RATE OF SEC. CRYSTALS (MA/SQCM). .423
CRYSTAL. RATE OF TYPE2 FILM (MA/SQCM). .145
SUPERSATURATION OF CNS. 3.82 ,TIME TO REACH(S) .0
INITIAL DISSOLUTION CURRENT (MA/SQCM) .1
TIMES. ONSET OF SEC. CRYSTALS(SEC) 1.5 PPT. CONSTANT (S) 2.0
TIME FOR INITIAL NON-STOICHIOMETRY 66.3
TIME TO COMPLETE PATCH COVERAGE 138.
TPACK = 66.3 TDISS = 138.0
DEHYDRATION RATE (MA/SQCM) .874
EFFECTIVE FILM CURRENT(MA/SQCM) 2.309
POROSITY OF ROUGH LAYER .624
CURREAT FRACTION FORMING ROUGHNESS .32
FINAL THICKNESS OF ROUGHNESS 764.9
WIDTH TO HEIGHT OF SEC. CRYSTALS. .422
INITIAL COVERAGE OF PATCHES .91
MOLE FRACTION METAL IN PATCHES .591
PASSIVATION TIME 3.
AVE. DISTANCE BETWEEN EXP. AND THEORY 6.511 (DEG)

		EXPERIMENT			THEORY		THICKNESSES(A)				
TIME(S)	I(MA/SQCM)	VOLTS	DEL	PSI	DEL	PSI	TYPE2	TYPE1(F)	TYPE1(H)	SECONDARY	COV
66.0	1.000	-.923	168.000	47.300	169.538	56.031	413.0	230.9	-.0	3928.7	.006
7 .	1.	-.92	174.4	37.2	176.367	37.556	413.	464.8	-.0	4949.9	.010
8..0	1.00	-.923	172.300	26.000	177.196	29.508	413.0	700.0	-.0	5666.3	.014
90.0	1.000	-.923	149.1	17.6	155. 53	19.487	413.	936.4	-.0	6236.5	.016
1 .	1.	-.92	113.9	16.	1 9.217	21.114	413.	1173.9	-.0	6718.1	.019
110.0	1.000	-.923	90.830	20.200	92.103	28.330	413.0	1412.6	-.0	7139.1	.021
120.0	1.	-.92	1 .1	27.6	98. 65	34.3 4	413.	1652.2	-.0	7515.5	.024
13 .	1.	-.92	1 7.1	34.	1 4.046	36.685	413.0	1892.7	-.0	7857.6	.026
140.0	1.000	-.920	114.000	46.700							
15 .	1.	-.92	123.	48.2							
16 .	1.	-.92	126.000	54.100							
170.0	1.000	-.920	138.400	60.600							
18 .	1.	-.92	152.7	62.6							
19 .	1.000	-.923	171.500	61.700							
200.0	1.000	-.920	182.000	59.400							
21 .	1.	-.92	185.5	57.2							
22..0	1.000	-.923	184.000	55.800							
230.0	1.000	.60	184.600	56.8							
24..0	1.	.6	184.6	56.3							

CD 100-32 2E-3 AMPS 6MKOH

CODES, 1,2,3A,4,5,6,7,8 = 1.0, 2.0, 0.0, 1.0, 1.0, 5.0, 3.5, 0.0,
CODES, 9,10,11,3,12,13,14 = 0.0, 1.0, 10.0, 3.0, 1.0, 0.0, 1.0,
REYNOLDS NUMBER = 0.0
EFFECTIVE REFRACTIVE INDICES AND POROSITIES,
TYPE 2 FILM 2.172 -.0102 I .150
NON-STOICHIOMETRY N 2.172 -.010 I
TYPE 1 FILM 1.805 -.0054 I .467
TYPE 1 HYDRATE 1.489 0.0000 I .861
SECONDARY CRYSTALS 2.130 0.0000 I 0.000
ROUGHNESS 1.456 -1.0897 I .725
NUMBER OF SECONDARY SITES/SQCM .24E+08 LIMITING COVERAGE .790
CRYSTAL. RATE OF SEC. CRYSTALS (MA/SQCM), .252
CRYSTAL. RATE OF TYPE2 FILM (MA/SQCM), .140
SUPERSATURATION OF IONS, 3.82 ,TIME TO REACH(S) .00
INITIAL DISSOLUTION CURRENT (MA/SQCM) .0014
TIMES, ONSET OF SEC. CRYSTALS(SEC) 1.5 PPT. CONSTANT (S) 2.0
TIME FOR INITIAL NON-STOICHIOMETRY 82.80
TIME TO COMPLETE PATCH COVERAGE 67.0
TPACK = 82.8 TDISS = 67.0
DEHYDRATION RATE (MA/SQCM) .600
EFFECTIVE FILM CURRENT(MA/SQCM) 2.391
POROSITY OF ROUGH LAYER .725
CURRENT FRACTION FORMING ROUGHNESS 1.000
FINAL THICKNESS OF ROUGHNESS 951.8
WIDTH TO HEIGHT OF SEC. CRYSTALS, .458
INITIAL COVERAGE OF PATCHES .05
MOLE FRACTION METAL IN PATCHES .050
PASSIVATION TIME 3000.00
AVE. DISTANCE BETWEEN EXP. AND THEORY 6.669 (DEG)

			EXPERIMENT		THEORY		THICKNESSES(A)				
TIME(S)	I(MA/SQCM)	VOLTS	DEL	PSI	DEL	PSI	TYPE2	TYPE1(F)	TYPE1(H)	SECONDARY	COV
5.0	.600	-.900	99.000	42.800	103.644	45.351	391.4	52.5	-.0	1492.9	.001
10.0	.600	-.900	117.400	48.600	120.535	49.220	391.4	156.1	-.0	2341.2	.003
15.0	.600	-.900	145.600	53.700	141.904	55.571	391.4	254.4	-.0	2816.4	.004
20.0	.600	-.900	177.400	50.000	179.019	57.071	391.4	370.9	-.0	3169.7	.005
25.0	.600	-.900	195.300	37.700	205.492	45.775	391.4	477.6	-.0	3458.1	.006
30.0	.600	-.900	200.800	25.200	206.351	31.094	391.4	584.5	-.0	3705.0	.007
35.0	.600	-.900	192.800	14.000	187.527	19.202	391.4	691.7	-.0	3922.8	.008
40.0	.600	-.900	153.300	8.400	148.470	13.705	391.4	799.1	-.0	4118.8	.009
45.0	.600	-.900	106.200	11.400	112.740	14.931	391.4	906.5	-.0	4297.7	.009
50.0	.600	-.900	91.800	16.600	96.354	18.005	391.4	1014.2	-.0	4462.8	.010
55.0	.600	-.900	95.300	21.600	92.033	20.768	391.4	1122.0	-.0	4616.6	.011
60.0	.600	-.900	98.300	25.600	94.887	22.936	391.4	1229.9	-.0	4760.7	.011
65.0	.600	-.800	105.000	27.600	102.256	24.238	391.4	1337.9	-.0	4896.6	.012
70.0	.600	-.620	105.400	30.400							

CO 100-36 6E-4 AMPS 6MKOH

CODES, 1,2,3A,4,5,6,7,8 = 1.0, 2.0, 0.0, 1.0, 1.0, 1.0, 3.5, 0.0,
CODES, 9,10,11,3,,12,13,14 = 0.0, 1.0, 7.0, 3.0, 1.0, 0.0, 1.0,
REYNOLDS NUMBER = 0.0
EFFECTIVE REFRACTIVE INDICES AND POROSITIES,
TYPE 2 FILM 2.130 0.0000 I .130
TYPE 1 FILM 2.054 0.0000 I .134
TYPE 1 HYDRATE 1.391 0.0000 I .929
SECONDARY CRYSTALS 1.852 0.0000 I .350
ROUGHNESS 1.635 -3.6822 I .020
NUMBER OF SECONDARY SITES/SQCM .22E+08 LIMITING COVERAGE .790
CRYSTAL. RATE OF SEC. CRYSTALS (MA/SQCM), .034
CRYSTAL. RATE OF TYPE2 FILM (MA/SQCM), .140
SUPERSATURATION OF IONS, 3.82 ,TIME TO REACH(S) .00
INITIAL DISSOLUTION CURRENT (MA/SQCM) .0016
TIMES, ONSET OF SEC. CRYSTALS(SEC) 1.5 PPT. CONSTANT (S) 2.0
TIME TO COMPLETE PATCH COVERAGE 54.1
TIME TO REACH COMPACT FILM I 53.4 S
TIME TO DISSIPATE HYDRATE LAYER 53.4 S
TPACK = 53.4 TDISS = 54.1
DEHYDRATION RATE (MA/SQCM) .262
EFFECTIVE FILM CURRENT(MA/SQCM) .805
POROSITY OF ROUGH LAYER .020
CURRENT FRACTION FORMING ROUGHNESS .001
FINAL THICKNESS OF ROUGHNESS .8
WIDTH TO HEIGHT OF SEC. CRYSTALS, .400
INITIAL PATCH COVERAGE .768
FINAL POROSITY OF TYPE I FILM .100
MOLE FRACTION METAL IN PATCHES 0.000
PASSIVATION TIME 3000.00
AVE. DISTANCE BETWEEN EXP. AND THEORY 2.102 (DEG)

		EXPERIMENT			THEORY		THICKNESSES(A)				
TIME(S)	I(MA/SQCM)	VOLTS	DEL	PSI	DEL	PSI	TYPE2	TYPE1(F)	TYPE1(H)	SECONDARY	COV
10.0	.600	-.930	87.700	41.800	86.721	44.715	459.6	.0	-.0	1419.6	.001
20.0	.600	-.930	99.800	46.700	99.279	47.968	459.6	66.0	-.0	2104.5	.002
30.0	.600	-.930	118.400	53.000	118.653	51.441	459.6	127.6	-.0	2472.4	.002
40.0	.600	-.930	144.000	56.400	144.316	54.023	459.6	183.7	-.0	2714.5	.003
50.0	.600	-.930	170.200	53.500	170.503	55.056	459.6	233.0	-.0	2880.1	.003
60.0	.600	-.930	185.600	45.000							
70.0	.600	-.930	193.700	35.200							
80.0	.600	-.930	195.700	26.400							
90.0	.600	-.930	192.300	19.500							
100.0	.600	-.930	178.300	15.100							
110.0	.600	-.930	149.000	12.600							
120.0	.600	-.930	115.900	14.400							
130.0	.600	-.930	99.000	18.500							
140.0	.600	-.930	91.900	23.100							
150.0	.600	-.930	93.300	28.200							
160.0	.600	-.930	97.700	32.500							
170.0	.600	-.930	100.100	37.700							
180.0	.600	-.930	105.600	42.600							
200.0	.600	-.930	118.600	53.100							
220.0	.600	-.930	136.800	60.600							
240.0	.600	-.930	161.600	61.000							
260.0	.600	-.930	179.600	5.300							
280.0	.600	-.930	187.500	9.100							
320.0	.600	-.930	193.600	.400							
360.0	.600	-.930	192.300	2.600							
400.0	.600	-.930	188.700	9.000							

CD 100-33 6E-4 AMPS 6MKOH

CODES, 1,2,3A,4,5,6,7,8 = 1.0, 2.0, 0.0, 1.0, 1.0, 1.0, 3.5, 0.0,
CODES, 9,10,11,3,12,13,14 = 0.0, 1.0, 10.0, 3.0, 1.0, 0.0, 1.0,
REYNOLDS NUMBER = C.0
EFFECTIVE REFRACTIVE INDICES AND POROSITIES,
TYPE 2 FILM 2.137 -.0016 I .150
NON-STOICHIOMETRY N 2.137 -.002 I
TYPE 1 FILM 1.848 -.0010 I .385
TYPE 1 HYDRATE 1.439 0.0000 I .929
SECONDARY CRYSTALS 1.856 -.0011 I .350
ROUGHNESS 1.476 -1.4057 I .645
NUMBER OF SECONDARY SITES/SQCM .68E+08 LIMITING COVERAGE .790
CRYSTAL. RATE OF SEC. CRYSTALS (MA/SQCM), .028
CRYSTAL. RATE OF TYPE2 FILM (MA/SQCM), .140
SUPERSATURATION OF IONS, 3.82 ,TIME TO REACH(S) .00
INITIAL DISSOLUTION CURRENT (MA/SQCM) .0011
TIMES, ONSET OF SEC. CRYSTALS(SEC) 1.5 PPT. CONSTANT (S) 2.0
TIME FOR INITIAL NON-STOICHICMETRY 82.8C
TIME TO COMPLETE PATCH COVERAGE 67.0
TPACK = 82.8 TDISS = 67.0
DEMYDRATION RATE (MA/SQCM) .386
EFFECTIVE FILM CURRENT(MA/SQCM) .422
POROSITY OF ROUGH LAYER .645
CURRENT FRACTION FORMING ROUGHNESS .334
FINAL THICKNESS OF ROUGHNESS 416.6
WIDTH TO HEIGHT OF SEC. CRYSTALS, .400
INITIAL COVERAGE OF PATCHES .C4
MOLE FRACTION METAL IN PATCHES .008
PASSIVATION TIME 3000.00
AVE. DISTANCE BETWEEN EXP. AND THEORY 5.736 (DEG)

		EXPERIMENT			THEORY		THICKNESSES(A)				
TIME(S)	I(MA/SQCM)	VOLTS	DEL	PSI	DEL	PSI	TYPE2	TYPE1(F)	TYPE1(H)	SECONDARY	COV
40.0	.600	-.930	144.000	56.400	139.818	39.675	441.4	135.9	-.0	1624.5	.003
50.0	.600	-.930	170.200	53.500	177.419	53.471	441.4	272.7	-.0	2046.7	.005
60.0	.600	-.930	185.600	48.000	187.062	45.696	441.4	409.0	-.0	2342.9	.006
70.0	.600	-.930	193.700	35.300	192.220	40.046	441.4	547.2	-.0	2578.7	.007
80.0	.600	-.930	195.700	26.400	195.536	34.207	441.4	685.0	-.0	2777.9	.008
90.0	.600	-.930	192.300	19.900	193.898	27.072	441.4	823.0	-.0	2951.9	.009
100.0	.600	-.930	178.300	15.100	180.474	19.429	441.4	961.3	-.0	3107.6	.010
110.0	.600	-.930	149.000	12.600	145.765	14.520	441.4	1099.8	-.0	3249.0	.011
120.0	.600	-.930	115.900	14.400							
130.0	.600	-.930	99.000	18.500							
140.0	.600	-.930	91.900	23.100							
150.0	.600	-.930	93.300	28.200							
160.0	.600	-.930	97.700	32.900							
170.0	.600	-.930	100.100	37.700							
180.0	.600	-.930	105.600	42.600							
200.0	.600	-.930	118.600	53.100							
220.0	.600	-.930	130.800	60.600							
240.0	.600	-.930	161.600	61.000							
260.0	.600	-.930	179.600	5.300							
280.0	.600	-.930	167.500	9.100							
320.0	.600	-.930	151.600	.400							
360.0	.600	-.930	192.300	2.600							
400.0	.600	-.930	188.700	9.600							
440.0	.600	-.930	182.600	5.500							
480.0	.600	-.930	174.200	5.800							
520.0	.600	-.700	171.600	25.400							

```
 CO=00-4.0.2MA/SQCM,2500 RE,0001

CODES, 1,2,3A,4,5,6,7,8 =  1.0,  0.0,  4.0,  1.0,  1.0,  1.0,  3.5,  0.0,
CODES, 9,10,11,12,13,14 =  0.0,  1.0,  7.0,  4.0,  1.0,  1.0,  1.0,
REYNOLDS NUMBER =  2500.0
EFFECTIVE REFRACTIVE INDICES AND POROSITIES,
TYPE 2 FILM   2.130   0.0000 I            .202
TYPE 1 FILM   2.122   0.0000 I            .012
TYPE 1 HYDRATE   1.387   0.0000 I            .916
SECONDARY CRYSTALS   1.552   0.0000 I            .250
NUMBER OF SECONDARY SITES/SQCM      .10E+09      LIMITING COVERAGE     .790
CRYSTAL. RATE OF SEC. CRYSTALS (MA/SQCM),    .15081
CRYSTAL. RATE OF TYPE2 FILM (MA/SQCM),    .18628
SUPERSATURATION OF IONS,  2.300 ,TIME TO REACH(S)     .00332
INITIAL DISSOLUTION CURRENT (MA/SQCM)      .0094
TIMES, ONSET OF SEC. CRYSTALS(SEC)    70.3 PPT. CONSTANT (S)     3.7
TIME TO COMPLETE PATCH COVERAGE     158.3
TIME TO REALM COMPACT FILM I     154.4  S
TIME TO DISSIPATE HYDRATE LAYER     154.4  S
DEHYDRATION RATE (MA/SQCM)     .200
EFFECTIVE FILM CURRENT(MA/SQCM)      .178
CURRENT FRACTION FORMING ROUGHNESS      .000
FINAL THICKNESS OF ROUGHNESS       5.0
WIDTH TO HEIGHT OF SEC. CRYSTALS,      .365
INITIAL PATCH COVERAGE      .735
FINAL POROSITY OF TYPE I FILM     .011
AVE. DISTANCE BETWEEN EXP. AND THEORY      4.545  (DEG)
```

		EXPERIMENT			THEORY		THICKNESSES(A)				
TIME(S)	I(MA/SQCM)	VOLTS	DEL	PSI	DEL	PSI	TYPE2	TYPE1(F)	TYPE1(H)	SECONDARY	COV
10.0	.200	-.870	82.920	35.900	84.302	38.063	215.5	0.0	-.0	.0	.000
20.0	.200	-.870	85.630	37.010	82.113	39.138	281.5	0.0	-.0	.0	.000
30.0	.200	-.870	84.260	37.830	81.863	40.142	333.6	0.0	-.0	.0	.000
40.0	.200	-.870	85.470	39.040	83.008	41.210	378.8	0.0	-.0	.0	.000
50.0	.200	-.870	86.460	40.570	85.467	42.402	419.7	0.0	-.0	.0	.000
60.0	.200	-.870	86.450	42.100	89.325	43.744	457.6	0.0	-.0	.0	.000
70.0	.200	-.870	90.120	43.790	94.777	45.223	493.3	0.0	-.0	.0	.000
80.0	.200	-.870	90.960	45.860	94.226	47.552	493.3	26.5	-.0	2622.4	.009
90.0	.200	-.870	92.800	48.010	94.519	47.682	493.3	36.1	-.0	3791.2	.019
100.0	.200	-.870	93.610	50.470	93.169	48.818	493.3	45.4	-.0	4467.8	.027
110.0	.200	-.870	94.410	52.940	92.641	50.116	493.3	54.2	-.0	4950.4	.033
120.0	.200	-.870	95.440	52.920	93.682	51.986	493.3	62.4	-.0	5316.9	.038
130.0	.200	-.870	93.920	58.680	95.233	54.116	493.3	69.9	-.0	5602.0	.042
140.0	.200	-.870	97.360	62.340	96.928	56.426	493.3	76.7	-.0	5825.1	.045
150.0	.200	-.870	97.430	66.030	98.219	58.820	493.3	82.8	-.0	5999.2	.048
160.0	.200	-.870	96.500	70.330	102.582	61.443	493.3	89.1	-.0	6156.1	.051
-1	-1	-1	-1	-1							

CU4005,0.4MA/SQCM,3000 RE,0001

CODES, 1,2,3A,4,5,6,7,8 = 1.0, 0.0, 4.0, 1.0, 1.0, 1.0, 3.5, 0.0,
CODES, 9,10,11,3,12,13,14 = 2.0, 1.0, 7.0, 4.0, 1.0, 1.0, 1.0,
REYNOLDS NUMBER = 3000.0
EFFECTIVE REFRACTIVE INDICES AND PERCENTITIES,
TYPE 2 FILM 2.150 0.0000 I .257
TYPE 1 FILM 2.150 0.0000 I 0.000
TYPE 1 HYDRATE 1.367 0.0000 I .935
SECONDARY CRYSTALS 2.123 0.0000 I .005
NUMBER OF SECONDARY SITES/SQCM .51E+05 LIMITING COVERAGE .790
CRYSTAL, RATE OF SEC, CRYSTALS (MA/SQCM), .01503
CRYSTAL, RATE OF TYPE2 FILM (MA/SQCM), .10644
SUPERSATURATION OF ICNS, 2.300 ,TIME TO REACH(S) 0.00000
INITIAL DISSOLUTION CURRENT (MA/SQCM) .0086
TIME, ONSET OF SEC, CRYSTALS(SEC) 20.3 PPT, CONSTANT (S) 2.0
TIME TO COMPLETE PATCH COVERAGE 98.2
TIME TO REACH COMPACT FILM I 169.8 S
TIME TO DISSIPATE HYDRATE LAYER 169.8 S
CEMYDRATION RATE (MA/SQCM) .196
EFFECTIVE FILM CURRENT(MA/SQCM) .349
CURRENT FRACTION FORMING ROUGHNESS .000
FINAL THICKNESS OF ROUGHNESS 5.0
RATIO TO HEIGHT OF SEC, CRYSTALS, .058
INITIAL PATCH COVERAGE .721
FINAL POROSITY OF TYPE I FILM 0.000
AVE, DISTANCE BETWEEN EXP, AND THEORY 3.131 (DEG)

			EXPERIMENT		THEORY		THICKNESSES(A)				
TIME(S)	I(MA/SQCM)	VOLTS	DEL	PSI	DEL	PSI	TYPE2	TYPE1(F)	TYPE1(H)	SECONDARY	COV
10.0	.400	-.870	75.130	35.070	79.039	38.225	244.3	0.0	-.0	.0	.000
20.0	.400	-.870	77.010	37.220	78.438	40.367	345.2	0.0	-.0	.0	.000
30.2	.400	-.870	80.440	39.610	78.210	41.367	345.2	37.3	-.0	719.1	.011
40.0	.400	-.870	84.480	41.930	82.883	43.186	345.2	72.3	-.0	1036.8	.024
50.0	.400	-.870	90.840	45.210	90.229	45.098	345.2	106.9	-.0	1218.4	.033
60.0	.400	-.870	99.820	44.930	100.219	47.218	345.2	139.3	-.0	1345.1	.040
70.0	.400	-.870	110.930	50.750	112.659	49.387	345.2	169.2	-.0	1438.7	.046
80.0	.400	-.870	125.210	53.850	126.532	51.480	345.2	196.3	-.0	1508.8	.050
90.0	.400	-.870	142.540	50.080	142.032	53.217	345.2	220.7	-.0	1561.1	.054
100.0	.400	-.870	161.600	56.610	158.314	55.086	345.2	245.9	-.0	1607.2	.057
110.0	.400	-.870	178.890	54.880	176.037	53.247	345.2	285.5	-.0	1675.8	.062
120.0	.400	-.870	191.410	51.410	193.686	50.112	345.2	322.1	-.0	1739.2	.067
130.0	.400	-.870	200.230	46.380	202.080	46.762	345.2	367.3	-.0	1796.3	.071
140.0	.400	-.870	204.110	40.180	206.497	43.765	345.2	408.9	-.0	1853.7	.076
150.0	.400	-.870	205.500	35.380	206.138	41.295	345.2	451.1	-.0	1900.0	.080
160.0	.400	-.870	204.960	30.310	202.803	39.337	345.2	493.7	-.0	1955.6	.084
170.0	.400	-.870	198.640	24.260	196.415	38.059	345.2	530.9	-.0	2002.8	.089
-1	-1	-1	-1	-1							

CO4066,1.0MA/SQCM,3000 RE,0001

CODES, 1,2,3,4,5,6,7,8 = 1.0, 2.0, 4.0, 1.0, 1.0, 1.0, 3.5, 0.0,
CODES, 9,10,11,12,13,14 = 0.0, 1.0, 7.5, 4.0, 1.0, 1.0, 1.0,
REYNOLDS NUMBER = 3000.0
EFFECTIVE REFRACTIVE INDICES AND POROSITIES,
TYPE 2 FILM 2.130 0.0000 I .610
TYPE 1 FILM 2.130 0.0000 I 0.000
TYPE 1 HYDRATE 1.387 0.0000 I .980
SECONDARY CRYSTALS 2.130 0.0000 I 0.000
NUMBER OF SECONDARY SITES/SQCM .70E+09 LIMITING COVERAGE .790
CRYSTAL. RATE OF SEC. CRYSTALS (MA/SQCM), .00499
CRYSTAL. RATE OF TYPE2 FILM (MA/SQCM), .00100
SUPERSATURATION OF IONS, 2.300 ,TIME TO REACH(S) 0.00000
INITIAL DISSOLUTION CURRENT (MA/SQCM) .0086
TIMES, ONSET OF SEC. CRYSTALS(SEC) 1.5 RFT. CONSTANT (S) 2.0
TIME TO COMPLETE PATCH COVERAGE 20.8
TIME TO REACH COMPACT FILM I 26.6 S
TIME TO DISSIPATE HYDRATE LAYER 26.6 S
DEHYDRATION RATE (MA/SQCM) .133
EFFECTIVE FILM CURRENT(MA/SQCM) .864
CURRENT FRACTION FORMING ROUGHNESS .000
FINAL THICKNESS OF ROUGHNESS 5.0
WIDTH TO HEIGHT OF SEC. CRYSTALS, .500
INITIAL PATCH COVERAGE .439
FINAL POROSITY OF TYPE I FILM 0.000
AVE. DISTANCE BETWEEN EXP. AND THEORY 4.565 (DEG)

			EXPERIMENT		THEORY		THICKNESSES(A)				
TIME(S)	I(MA/SQCM)	VOLTS	DEL	PSI	DEL	PSI	TYPE2	TYPE1(F)	TYPE1(H)	SECONDARY	COV
1.0	1.000	-.870	74.340	37.540	68.795	37.681	324.0	0.0	-.0	.0	.000
2.0	1.000	-.870	74.520	37.740	72.896	37.987	324.0	3.1	-.0	261.8	.001
3.0	1.000	-.870	74.720	37.840	73.312	38.324	324.0	6.0	-.0	446.6	.003
4.0	1.000	-.870	75.290	38.250	74.045	38.715	324.0	8.9	-.0	540.9	.005
5.0	1.000	-.870	75.460	38.650	75.024	39.156	324.0	11.7	-.0	607.3	.006
6.0	1.000	-.870	76.010	39.260	76.220	39.644	324.0	14.4	-.0	658.4	.008
7.0	1.000	-.870	76.340	40.170	77.606	40.174	324.0	16.9	-.0	699.0	.009
8.0	1.000	-.870	76.940	40.180	78.883	40.632	324.0	19.2	-.0	731.8	.009
9.0	1.000	-.870	77.300	40.760	79.880	41.051	324.0	21.4	-.0	758.5	.010
10.0	1.000	-.870	77.860	41.290	80.823	41.639	324.0	23.3	-.0	780.0	.011
15.0	1.000	-.870	81.380	45.250	83.997	44.368	324.0	29.0	-.0	836.3	.012
20.0	1.000	-.870	87.450	49.970	84.148	47.021	324.0	33.0	-.0	844.4	.012
25.0	1.000	-.880	93.190	55.760	92.528	49.687	324.0	46.9	-.0	902.2	.014
30.0	1.000	-.880	102.950	63.180	106.479	52.158	324.0	62.3	-.0	962.7	.016
35.0	1.000	-.890	118.630	58.790	123.481	53.836	324.0	77.8	-.0	1016.5	.018
40.0	1.000	-.850	142.470	61.040	141.615	54.309	324.0	93.3	-.0	1065.1	.020
45.0	1.000	-.850	165.310	59.640	159.440	53.882	324.0	108.9	-.0	1109.6	.022
50.0	1.000	-.850	177.810	55.940	174.418	52.151	324.0	124.5	-.0	1150.8	.023
55.0	1.000	-.800	186.650	50.730	185.628	49.791	324.0	140.2	-.0	1189.3	.025
60.0	1.000	-.850	188.930	43.140	193.675	47.220	324.0	155.9	-.0	1225.4	.026
65.0	1.000	.800	189.940	41.550	198.300	44.553	324.0	171.7	-.0	1259.5	.028
-1	-1	-1	-1	-1							

CO4000,1.0MA/SQCM,3000 RE,0001

COEFFS. 1,2,3,4,5,6,7,8 = 1.0, 3.0, 4.0, 1.0, 1.0, 1.0, 3.5, 3.0,
COEFFS. 9,10,11,12,13,14 = 3.0, 1.0, 7.0, 4.0, 1.0, 1.0, 1.0,
REYNOLDS NUMBER = 3000.0
EFFECTIVE REFRACTIVE INDICES AND POROSITIES.
TYPE 2 FILM 2.150 0.0000 I .010
TYPE 1 FILM 2.150 0.0000 I 0.000
TYPE 1 HYDRATE 1.390 0.0000 I .920
SECONDARY CRYSTALS 1.869 0.0000 I .920
NUMBER OF SECONDARY SITES/SQCM .652+09 LIMITING COVERAGE .790
CRYSTAL GROWTH RATE OF SEC. CRYSTALS (MA/SQCM). .03566
CRYSTAL RATE OF TYPE2 FILM (MA/SQCM). .00508
SUPERSATURATION OF ICE. 2.300 ,TIME TO REACH(S) 0.00000
INITIAL DISSOLUTION CURRENT (MA/SQCM) .0086
TIMES, UNDER LAY. SEC. CRYSTALS(SEC) 9.0 PPT. CONSTANT (S) 2.0
TIME TO COMPLETE PATCH COVERAGE 39.9
TIME TO REACH COMPACT FILM I 82.2 S
TIME TO DISSIPATE HYDRATE LAYER 82.2 S
DEHYDRATION RATE (MA/SQCM) 1.000
EFFECTIVE FILM CURRENT(MA/SQCM) .960
CURRENT FRACTION FORMING ROUGHNESS .000
FINAL THICKNESS OF ROUGHNESS 0.0
WIDTH TO HEIGHT OF SEC. CRYSTALS, .500
INITIAL PATCH COVERAGE .710
FINAL POROSITY OF TYPE I FILM 0.000
AVG. DISTANCE BETWEEN EXP. AND THEORY 7.561 (DEG)

		EXPERIMENT			THEORY		THICKNESSES(A)				
TIME(S)	I(MA/SQCM)	VOLTS	DEL	PSI	DEL	PSI	TYPE2	TYPE1(F)	TYPE1(H)	SECONDARY	COV
1.0	1.000	-.870	74.340	37.540	76.744	36.858	121.0	0.0	-.0	.0	.000
2.0	1.000	-.870	74.520	37.740	76.636	36.876	122.0	0.0	-.0	.0	.000
3.0	1.000	-.870	74.720	37.640	76.559	36.841	123.0	0.0	-.0	.0	.000
4.0	1.000	-.870	75.290	38.250	76.493	36.804	124.0	0.0	-.0	.0	.000
5.0	1.000	-.870	75.460	38.650	76.426	36.916	125.1	0.0	-.0	.0	.000
6.0	1.000	-.870	76.010	39.260	76.369	36.927	125.9	0.0	-.0	.0	.000
7.0	1.000	-.870	76.340	40.170	76.314	36.938	126.0	0.0	-.0	.0	.000
8.0	1.000	-.870	76.940	40.180	76.262	36.948	127.2	0.0	-.0	.0	.000
9.0	1.000	-.870	77.300	40.780	76.212	36.957	127.9	0.0	-.0	.0	.000
10.0	1.000	-.870	77.800	41.290	74.143	37.332	127.9	19.8	-.0	618.0	.008
15.0	1.000	-.870	81.380	45.250	72.770	38.980	127.9	100.9	-.0	1367.8	.039
20.0	1.000	-.870	87.450	49.970	77.694	40.819	127.9	182.8	-.0	1677.1	.058
25.0	1.000	-.860	93.180	55.760	83.400	43.105	127.9	259.4	-.0	1875.9	.073
30.0	1.000	-.860	102.950	53.180	103.916	45.032	127.9	326.2	-.0	2012.5	.084
35.0	1.000	-.850	118.000	56.790	122.690	48.046	127.9	389.4	-.0	2106.8	.092
40.0	1.000	-.850	142.470	61.060	142.177	50.355	127.9	446.7	-.0	2171.6	.098
45.0	1.000	-.850	165.610	59.640	166.344	48.337	127.9	536.7	-.0	2284.3	.108
50.0	1.000	-.850	177.810	55.940	179.369	45.593	127.9	635.4	-.0	2386.9	.118
55.0	1.000	-.800	186.650	50.730	185.203	43.621	127.9	736.1	-.0	2481.3	.128
60.0	1.000	-.850	188.630	43.140	189.906	42.381	127.9	836.8	-.0	2569.1	.137
65.0	1.000	.800	189.940	41.660	195.988	41.837	127.9	943.5	-.0	2651.2	.146
-1	-1	-1	-1	-1	-1						

```
 CD4009,4.0MA/SQCM,7000 RE,0001

CODES, 1,2,3A,4,5,6,7,8 =  1.0,  0.0,  4.0,  1.0,  1.0,  1.0,  3.5,  0.0,
CODES, 9,10,11,12,13,14 =  0.0,  1.0,  7.0,  4.0,  1.0,  1.0,  1.0,
REYNOLDS NUMBER =  3000.0
EFFECTIVE REFRACTIVE INDICES AND POROSITIES,
TYPE 2 FILM    2.150    0.0000 I            .010
TYPE 1 FILM    2.150    0.0000 I           0.000
TYPE 1 HYDRATE   1.392   0.0000 I             .990
SECONDARY CRYSTALS    2.150    0.0000 I            0.000
NUMBER OF SECONDARY SITES/SQCM      .27E+10      LIMITING COVERAGE     .790
CRYSTAL, RATE OF SEC. CRYSTALS (MA/SQCM),    .02481
CRYSTAL, RATE OF TYPE2 FILM (MA/SQCM),    .00100
SUPERSATURATION OF IONS,  2.300 ,TIME TO REACH(S)   0.00000
INITIAL DISSOLUTION CURRENT (MA/SQCM)      .0000
TIMES, ONSET OF SEC. CRYSTALS(SEC)    1.5  PPT. CONSTANT (S)    2.0
TIME TO COMPLETE PATCH COVERAGE       6.6
TIME TO REACH COMPACT FILM I      28.1  S
TIME TO DISSIPATE HYDRATE LAYER      28.1  S
DEHYDRATION RATE (MA/SQCM)    2.357
EFFECTIVE FILM CURRENT(MA/SQCM)     3.641
CURRENT FRACTION FORMING ROUGHNESS     .000
FINAL THICKNESS OF ROUGHNESS        5.0
WIDTH TO HEIGHT OF SEC. CRYSTALS,       .500
INITIAL PATCH COVERAGE      .759
FINAL POROSITY OF TYPE 1 FILM    0.000
AVE. DISTANCE BETWEEN EXP. AND THEORY       .526  (DEG)

                          EXPERIMENT                THEORY              THICKNESSES(A)
TIME(S)    I(MA/SQCM)    VOLTS     DEL      PSI      DEL      PSI      TYPE2     TYPE1(F)   TYPE1(H)   SECONDARY    COV

     1.0       4.000     -.930    70.380   37.990   69.960   37.173    122.3       0.0        -.0          .0       .000
     2.0       4.000     -.920    68.870   36.440   69.151   38.007    122.3      52.7        -.0       372.2       .010
     3.0       4.000     -.900    66.620   38.890   65.594   39.070    122.3      97.3        -.0       651.4       .027
     4.0       4.000     -.750    66.110   40.350   65.507   40.270    122.3     139.7        -.0       756.0       .039
     5.0       4.000     -.550    65.180   42.020   63.640   41.589    122.3     177.7        -.0       835.9       .048
     6.0       4.000     -.500    64.800   43.660   64.735   43.369    122.3     209.7        -.0       889.2       .054
     7.0       4.000      .860    70.370   43.150   70.400   45.390    122.3     245.3        -.0       937.8       .060
    -1         -1         -1       -1       -1
```

CD40010,1.0MA/SQCM,7000 RE,0001

CODES, 1,2,3A,4,5,6,7,8 = 1.0, 0.0, 4.0, 1.0, 1.0, 1.0, 3.5, 0.0,
CODES, 9,10,11,3,12,13,14 = 0.0, 1.0, 7.0, 4.0, 1.0, 1.0, 1.0,
REYNOLDS NUMBER = 7000.0
EFFECTIVE REFRACTIVE INDICES AND POROSITIES,
TYPE 2 FILM 2.130 0.0000 I .010
TYPE 1 FILM 2.130 0.0000 I 0.000
TYPE A HYDRATE 1.387 0.0000 I .981
SECONDARY CRYSTALS 2.130 0.0000 I 0.000
NUMBER OF SECONDARY SITES/SQCM .50E+09 LIMITING COVERAGE .790
CRYSTAL. RATE OF SEC. CRYSTALS (MA/SQCM), .00173
CRYSTAL. RATE OF TYPE2 FILM (MA/SQCM), .00100
SUPERSATURATION OF IONS, 2.300 ,TIME TO REACH(S) 0.00000
INITIAL DISSOLUTION CURRENT (MA/SQCM) .0097
TIMES, ONSET OF SEC. CRYSTALS(SEC) 1.5 PPT. CONSTANT (S) 2.0
TIME TO COMPLETE PATCH COVERAGE 40.0
TIME TO REACH COMPACT FILM I 6.7 S
TIME TO DISSIPATE HYDRATE LAYER 6.7 S
DEHYDRATION RATE (MA/SQCM) .178
EFFECTIVE FILM CURRENT(MA/SQCM) .762
CURRENT FRACTION FORMING ROUGHNESS .000
FINAL THICKNESS OF ROUGHNESS 5.0
WIDTH TO HEIGHT OF SEC. CRYSTALS, .500
INITIAL PATCH COVERAGE .457
FINAL POROSITY OF TYPE I FILM 0.000
AVE. DISTANCE BETWEEN EXP. AND THEORY 3.200 (DEG)

			EXPERIMENT		THEORY		THICKNESSES(A)				
TIME(S)	I(MA/SQCM)	VOLTS	DEL	PSI	DEL	PSI	TYPE2	TYPE1(F)	TYPE1(H)	SECONDARY	COV
0.0	1.000	-.860	76.010	39.310	75.902	41.852	479.2	.0	-.0	346.4	.001
10.0	1.000	-.860	76.840	41.620	76.445	43.226	479.2	19.8	-.0	534.9	.004
15.0	1.000	-.860	78.000	44.830	79.201	45.093	479.2	37.5	-.0	626.5	.005
20.0	1.000	-.860	80.340	48.470	82.489	47.405	479.2	52.5	-.0	680.6	.006
25.0	1.000	-.860	87.210	50.520	86.270	50.134	479.2	64.8	-.0	712.4	.006
30.0	1.000	1.330	93.730	58.690	90.465	53.245	479.2	74.8	-.0	729.7	.007
35.0	1.000	2.300	95.210	59.660	95.000	56.590	479.2	83.2	-.0	737.4	.007
40.0	1.000	2.520	95.960	60.340	99.869	60.267	479.2	90.4	-.0	738.8	.007
-1	-1	-1	-1	-1							

CURRENT=0.4MA/SQCM,T000 RE=.0001

CODES, A,B,C,D,E,F,G = 1.0, 0.0, 4.0, 1.0, 1.0, 1.0, 3.5, 0.0,
CODES, H,I,J,K,L,M,N = 3.0, 1.0, 7.0, 4.0, 1.0, 2.0, 1.0,
REYNOLDS NUMBER = 7000.0
EFFECTIVE REFRACTIVE INDICES AND POROSITIES,
TYPE 2 FILM 2.150 0.0000 I .010
TYPE 1 FILM 2.150 0.0000 I 0.000
TYPE 1 HYDRATE 1.367 0.0000 I .990
SECONDARY CRYSTALS 2.150 0.0000 I 0.000
NUMBER OF SECONDARY SITES/SQCM .31E+09 LIMITING COVERAGE .790
CRYSTAL, RATE OF SEC. CRYSTALS (MA/SQCM), .0010
CRYSTAL, RATE OF TYPE2 FILM (MA/SQCM), .0010
SUPERSATURATION OF ICES, 2.000 ,TIME TO REACH(S) 0.00000
INITIAL DISSOLUTION CURRENT (MA/SQCM) .0097
TIMES, ONSET OF SEC. CRYSTALS(SEC) 1.E5 PPT. CONSTANT (S) 2.0
TIME TO COMPLETE PATCH COVERAGE 66.0
TIME TO REACH COMPACT FILM 1 3.0 S
TIME TO DISSIPATE HYDRATE LAYER 3.0 S
CEMENTATION RATE (MA/SQCM) .307
EFFECTIVE FILM CURRENT(MA/SQCM) .280
CURRENT FRACTION FORMING ROUGHNESS .000
FINAL THICKNESS OF ROUGHNESS 5.0
WIDTH TO HEIGHT OF SEC. CRYSTALS, .500
INITIAL PATCH COVERAGE .260
FINAL POROSITY OF TYPE 1 FILM 0.000
AVE. DISTANCE BETWEEN EXP. AND THEORY 3.001 (DEG)

			EXPERIMENT		THEORY		THICKNESSES(A)				
TIME(S)	I(MA/SQCM)	VOLTS	DEL	PSI	DEL	PSI	TYPE2	TYPE1(F)	TYPE1(H)	SECONDARY	COV
1.0	.400	-.870	78.130	38.190	77.999	39.265	492.0	0.0	-.0	.0	.000
2.0	.400	-.870	77.520	38.270	79.604	39.358	492.0	2.0	-.0	181.1	.000
3.0	.400	-.870	77.910	38.370	78.497	39.417	492.0	4.0	-.0	309.6	.001
4.0	.400	-.870	78.110	38.370	78.651	39.302	492.0	6.0	-.0	376.3	.001
5.0	.400	-.870	78.330	38.460	78.816	39.394	492.0	8.0	-.0	424.8	.001
6.0	.400	-.870	78.290	38.560	78.982	39.393	492.0	9.9	-.0	463.7	.002
7.0	.400	-.870	78.290	38.680	79.149	39.300	492.0	11.9	-.0	496.5	.002
8.0	.400	-.870	78.280	38.780	79.317	39.914	492.0	13.8	-.0	524.8	.002
9.0	.400	-.870	78.470	38.880	79.487	40.035	492.0	15.6	-.0	549.8	.002
10.0	.400	-.870	78.600	38.990	79.658	40.163	492.0	17.5	-.0	572.0	.003
15.0	.400	-.870	79.800	39.810	80.506	40.902	492.0	25.7	-.0	655.0	.003
20.0	.400	-.870	80.710	41.130	81.377	41.618	492.0	32.7	-.0	707.1	.004
25.0	.400	-.870	82.220	42.370	82.267	42.909	492.0	38.4	-.0	739.6	.004
30.0	.400	-.870	83.100	44.090	83.179	44.174	492.0	43.1	-.0	758.5	.004
35.0	.400	-.870	84.350	46.120	84.121	45.512	492.0	46.9	-.0	768.0	.005
40.0	.400	-.870	85.000	48.250	85.107	47.220	492.0	50.1	-.0	771.0	.005
45.0	.400	-.870	87.050	50.290	86.154	48.994	492.0	52.9	-.0	769.5	.005
50.0	.400	-.870	88.270	52.710	87.281	50.922	492.0	55.3	-.0	765.0	.005
55.0	.400	-.870	89.240	55.280	88.506	52.995	492.0	57.4	-.0	758.5	.004
60.0	.400	-.870	90.490	58.330	89.841	55.194	492.0	59.4	-.0	750.8	.004
65.0	.400	-.870	92.300	61.380	91.298	57.502	492.0	62.3	-.0	742.2	.004
70.0	.400	-.870	94.330	64.700	92.858	59.927	492.0	71.1	-.0	756.0	.004
75.0	.400	-.870	97.610	68.320	101.371	60.035	492.0	84.2	-.0	774.1	.005
80.0	.400	-.870	103.080	72.530	107.954	62.032	492.0	91.3	-.0	791.3	.005
85.0	.400	-.870	110.670	76.350	115.562	64.050	492.0	101.4	-.0	807.8	.005
90.0	.400	-.870	123.610	79.770	124.350	65.974	492.0	111.5	-.0	823.6	.005
-1	-1	-1	-1		-1						

CU4001z,0.2MA/SqCM,7000 RE,3001

CODES, 1,2,3A,4,5,6,7,8 = 1.0, 0.0, 0.0, 1.0, 1.0, 1.0, 3.5, 0.0,
CODES, 9,10,11,3,A2,13,14 = 0.0, 1.0, 7.0, 4.0, 1.0, 1.0, 1.0,
REYNOLDS NUMBER = 7000.0
EFFECTIVE REFRACTIVE INDICES AND POROSITIES,
TYPE 2 FILM 2.130 0.0000 I .010
TYPE 1 FILM 2.130 0.0000 I .050
TYPE 1 HYDRATE 1.387 0.0000 I .910
SECONDARY CRYSTALS 2.130 0.0000 I 0.000
NUMBER OF SECONDARY SITES/SQCM .11E+09 LIMITING COVERAGE .790
CRYSTAL, RATE OF SEC. CRYSTALS (MA/SQCM), .00011
CRYSTAL, RATE OF TYPE2 FILM (MA/SQCM), .17311
SUPERSATURATION OF IONS, 2.300 ,TIME TO REACH(S) 0.00000
INITIAL DISSOLUTION CURRENT (MA/SQCM) .0097
TIMES, ONSET OF SEC. CRYSTALS(SEC) 32.3 PET. CONSTANT (S) 2.0
TIME TO COMPLETE PATCH COVERAGE 80.0
TIME TO REACH COMPACT FILM 1 259.6 S
TIME TO DISSIPATE HYDRATE LAYER 259.6 S
DEHYDRATION RATE (MA/SQCM) .010
EFFECTIVE FILM CURRENT(MA/SQCM) .042
CURRENT FRACTION FORMING ROUGHNESS .000
FINAL THICKNESS OF ROUGHNESS 5.0
WIDTH TO HEIGHT OF SEC. CRYSTALS, .500
INITIAL PATCH COVERAGE .013
FINAL POROSITY OF TYPE 1 FILM 0.000
AVE. DISTANCE BETWEEN EXP. AND THEORY 6.909 (DEG)

			EXPERIMENT		THEORY		THICKNESSES(A)				
TIME(S)	I(MA/SQCM)	VOLTS	DEL	PSI	DEL	PSI	TYPE2	TYPE1(F)	TYPE1(H)	SECONDARY	COV
10.0	.200	-.870	84.070	39.230	82.956	40.141	311.0	0.0	-.0	.0	.000
20.0	.200	-.870	83.390	40.210	83.289	40.396	348.+	0.0	-.0	.0	.000
30.0	.200	-.870	85.110	41.200	84.047	42.005	365.7	0.0	-.0	.0	.000
40.0	.200	-.870	82.850	41.990	82.054	42.195	385.7	1.7	-.0	147.0	.000
50.0	.200	-.870	82.400	42.680	81.400	42.964	385.7	3.9	-.0	223.7	.000
60.0	.200	-.870	82.100	43.170	80.873	42.374	385.7	5.0	-.0	264.3	.000
70.0	.200	-.870	81.920	43.560	79.836	43.424	385.7	7.3	-.0	291.2	.000
80.0	.200	-.870	81.470	44.350	79.117	43.532	385.7	9.2	-.0	317.5	.000
90.0	.200	-.870	82.020	44.930	78.081	44.213	385.7	11.0	-.0	332.0	.000
100.0	.200	-.870	81.020	44.930	77.239	44.330	385.7	13.3	-.0	351.4	.000
110.0	.200	-.870	80.720	46.320	76.482	44.449	385.7	15.2	-.0	366.8	.000
120.0	.200	-.870	80.280	46.810	75.634	44.571	385.7	17.7	-.0	384.8	.000
130.0	.200	-.870	79.240	47.380	74.819	44.594	385.7	20.0	-.0	399.5	.000
140.0	.200	-.870	78.380	48.050	73.951	44.618	385.7	22.2	-.0	413.2	.000
150.0	.200	-.870	77.740	48.530	73.083	44.944	385.7	24.3	-.0	426.1	.000
160.0	.200	-.870	76.530	49.300	72.184	45.072	385.7	26.7	-.0	438.2	.001
170.0	.200	-.870	75.050	49.690	71.256	45.202	385.7	29.0	-.0	449.7	.001
180.0	.200	-.870	73.610	50.020	70.318	45.333	385.7	31.3	-.0	460.6	.001
190.0	.200	-.870	71.580	50.370	69.346	45.465	385.7	33.6	-.0	471.1	.001
200.0	.200	-.870	69.520	50.610	68.347	45.598	385.7	35.9	-.0	481.1	.001
210.0	.200	-.870	67.530	50.760	67.317	45.732	385.7	38.2	-.0	490.7	.001
220.0	.200	-.870	64.590	50.580	66.255	45.867	385.7	40.5	-.0	499.9	.001
230.0	.200	-.870	61.630	50.400	65.157	46.003	385.7	42.8	-.0	508.6	.001
240.0	.200	-.870	57.920	50.220	64.020	46.139	385.7	45.2	-.0	517.4	.001
250.0	.200	-.870	52.430	49.300	62.840	46.274	385.7	47.5	-.0	525.7	.001
260.0	.200	-.870	47.160	49.070	61.659	46.408	385.7	49.9	-.0	533.8	.001
270.0	.200	-.870	43.010	47.920	61.919	46.547	385.7	52.4	-.0	541.6	.001
-1	-.	-1	-1	-1							

```
 CO 4CC15.C.2MA/SQCM.114C RE.UCC1

CCDES. 1.2.3A.4.5.6.7.8 =  1.0.  0.0.  0.C.  1.0.  1.0.  1.C.  3.5.  0.0.
CODES. 9.10.11.3.12.13.14 =  0.0.  1.0.  7.C.  4.0.  1.0.  0.0.  2.0.
REYNOLDS NUMBER =  1146.0
EFFECTIVE REFRACTIVE INDICES AND POROSITIES.
TYPE 2 FILM   2.13C   C.CCCC I            C.CCC
TYPE 1 FILM   1.748   0.COOC I             .793
TYPE 1 HYDRATE   1.389   0.COCO I             .990
SECONDARY CRYSTALS   2.13C   C.CCCC I              0.000
ROUGHNESS   1.705  -1.5855 I             .6CC
NUMBER OF SECONDARY SITES/SQCM      .12E+08      LIMITING COVERAGE     .790
CRYSTAL. RATE OF SEC. CRYSTALS (MA/SQCM).      .078
CRYSTAL. RATE OF TYPE2 FILM (MA/SQCM).      .002
SUPERSATURATION OF IONS.   3.E2 .TIME TO REACH(S)        .01
INITIAL DISSOLUTION CURRENT (MA/SQCM)      .C156
TIMES. ONSET OF SEC. CRYSTALS(SEC)     2.5 PPT. CONSTANT (S)     2.0
TIME TO COMPLETE PATCH COVERAGE      83.5
TIME TO REACH COMPACT FILM I      99.1  S
TIME TO DISSIPATE HYDRATE LAYER      94.1  S
TPACK =      99.1  TDISS =      83.5
DEHYDRATION RATE (MA/SQCM)     .012
EFFECTIVE FILM CURRENT(MA/SQCM)        .11C
POROSITY OF ROUGH LAYER     .60C
CURRENT FRACTION FORMING ROUGHNESS     .995
FINAL THICKNESS OF ROUGHNESS       433.3
WIDTH TO HEIGHT OF SEC. CRYSTALS.     1.0CC
INITIAL PATCH COVERAGE      .43C
FINAL POROSITY OF TYPE I FILM     .4CC
PORE FRACTION METAL IN PATCHES    0.000
PASSIVATION TIME     1CC0.00
AVE. DISTANCE BETWEEN EXP. AND THEORY       .156  (DEG)

                                EXPERIMENT                THEORY              THICKNESSES(A)
TIME(S)    I(MA/SQCM)    VOLTS      DEL      PSI        DEL      PSI       TYPE2    TYPE1(F)  TYPE1(M)  SECONDARY    COV

     10.0       .200      -.87C     57.22C    35.57C    57.231    35.709    179.6        .0        -.0     1022.8     .001
     20.0       .200      -.87C     57.6CC    25.87C    57.600    35.904    179.6        3.8       -.0     1551.7     .003
     30.0       .200      -.870     58.36C    36.38C    58.281    36.201    179.6        6.6       -.0     1811.4     .004
     40.0       .200      -.87C     59.14C    36.69C    59.150    36.616    179.6        9.1       -.0     1964.5     .005
     50.0       .200      -.870     59.9CC    37.20C    60.118    37.151    179.6       11.3       -.0     2054.1     .005
     60.0       .200      -.870     61.26C    37.71C    61.106    37.802    179.6       13.5       -.0     2102.3     .005
     70.0       .200      -.87C     62.21C    38.42C
     80.0       .200      -.870     63.38C    38.94C
     90.0       .200      -.870     64.32C    39.65C
    100.0       .200      -.870     66.07C    40.48C
    110.0       .200      -.870     67.40C    41.50C
    120.0       .200      -.87C     68.76C    42.02C
    130.0       .200      -.870     7C.C9C    42.04C
    140.0       .200      -.870     71.63C    43.96C
    150.0       .200      -.87C     72.96C    44.58C
    160.0       .200      -.870     75.30C    45.52C
    170.0       .200      -.870     77.41C    47.25C
    180.0       .200      -.870     79.72C    48.55C
    190.0       .200      -.870     81.22C    49.91C
    200.0       .200      -.870     84.71C    51.57C
    210.0       .200      -.870     87.78C    53.32C
    220.0       .200      -.870     9C.83C    55.07C
    230.0       .200      -.870     94.08C    56.71C
    240.0       .200      -.870     97.90C    58.64C
    250.0       .200      -.87C    1C2.2CC    6C.56C
    260.0       .200      -.870    107.3CC    62.28C
```

```
 CU 400,E-3,0.24M/SEC4,1140 RE,0001

CODES, A,B,3A,4,5,C,7,8 =  1.0,  3.0,  0.0,  1.0,  1.0,  3.0,  3.5,  0.0,
CODES, 9,10,11,12,13,14 =  3.0,  1.0,  7.0,  4.0,  1.0,  3.0,  2.0,
REYNOLDS NUMBER =  1140.0
EFFECTIVE REFRACTIVE INDICES AND POROSITIES,
TYPE 2 FILM    2.150   0.0000 I            0.000
TYPE 1 FILM    2.112   0.0000 I             .794
TYPE 1 HYDRATE   1.307   0.0000 I              .990
SECONDARY CRYSTALS    2.150   0.0000 I            0.000
ROUGHNESS    1.920  -1.5680 I             .599
NUMBER OF SECONDARY SITES/SEC4      .30E+08      LIMITING COVERAGE     .790
CRYSTAL RATE OF SEC. CRYSTALS (MA/SEC4),      .152
CRYSTAL RATE OF TYPE 2 FILM (MA/SEC4),      .002
SUPERSATURATION OF ION,    3.82 ,TIME TO REACH(S)        .01
INITIAL DISSOLUTION CURRENT (MA/SEC4)      .0156
TIMES, ONSET OF SEC. CRYSTALS(SEC)     2.5 PPT. CONSTANT (S)     2.0
TIME TO COMPLETE PATCH COVERAGE     107.1
TIME TO REACH COMPACT FILM I       7.2  S
TIME TO DISSIPATE HYDRATE LAYER       7.2  S
TPACK =       7.2  TDISS =      107.1
DEHYDRATION RATE (MA/SEC4)     .137
EFFECTIVE FILM CURRENT(MA/SEC4)         .251
POROSITY OF ROUGH LAYER     .599
CURRENT FRACTION FORMING ROUGHNESS     .533
FINAL THICKNESS OF ROUGHNESS       235.0
WIDTH TO HEIGHT OF SEC. CRYSTALS,     1.000
INITIAL PATCH COVERAGE      .575
FINAL POROSITY OF TYPE I FILM     .016
FCLE FRACTION METAL IN PATCHES   0.000
PASSIVATION TIME     1000.00
AVE. DISTANCE BETWEEN EXP. AND THEORY      1.279  (DEG)
```

		EXPERIMENT			THEORY		THICKNESSES(A)				
TIME(S)	I(MA/SEC4)	VOLTS	DEL	PSI	DEL	PSI	TYPE2	TYPE1(F)	TYPE1(H)	SECONDARY	COV
70.0	.200	-.870	62.210	38.460	62.515	38.060	179.0	.0	-.0	1472.4	.007
80.0	.200	-.870	63.380	38.940	63.174	38.764	179.0	22.6	-.0	1811.0	.010
90.0	.200	-.870	64.320	39.630	64.021	39.512	179.0	43.0	-.0	2020.9	.012
100.0	.200	-.870	66.070	40.480	64.697	40.346	179.0	61.5	-.0	2166.3	.014
110.0	.200	-.870	67.400	41.300	65.944	41.131	179.0	81.5	-.0	2290.4	.016
120.0	.200	-.870	68.760	42.020	67.061	41.802	179.0	105.8	-.0	2433.5	.018
130.0	.200	-.870	70.090	43.040	69.729	42.104	179.0	130.2	-.0	2562.2	.020
140.0	.200	-.870	71.630	43.960	72.115	42.646	179.0	154.7	-.0	2678.8	.022
150.0	.200	-.870	72.960	44.980	74.783	43.249	179.0	179.3	-.0	2786.1	.024
160.0	.200	-.870	75.300	45.920							
170.0	.200	-.870	77.410	47.250							
180.0	.200	-.870	79.720	48.390							
190.0	.200	-.870	81.220	49.910							
200.0	.200	-.870	84.710	51.270							
210.0	.200	-.870	87.780	53.220							
220.0	.200	-.870	90.830	55.070							
230.0	.200	-.870	94.080	56.710							
240.0	.200	-.870	97.900	58.640							
250.0	.200	-.870	102.300	60.760							
260.0	.200	-.870	107.300	62.260							
270.0	.200	-.870	113.260	64.070							
280.0	.200	-.870	122.580	66.090							
290.0	.200	-.870	131.420	68.220							
300.0	.200	-.870	141.510	69.950							
310.0	.200	-.870	149.830	71.220							
320.0	.200	-.870	158.770	72.300							

```
 CO 4CC15,0.2MA/SQCM,1140 RE,0001

CODES, 1.2,3A,4,5,6,7,8 =  1.  ,  .0,  6.0,  1.  ,  1.0,  1.  ,  3.5,  0.  ,
CODES, 9,10,11,3,12,13,14 =  0.0,  1.0, 10.0,  3.0,  1.0,  0.0,  1.0,
REYNOLDS NUMBER =  1140.0
EFFECTIVE REFRACTIVE INDICES AND POROSITIES,
TYPE 2 FILM   4.376  -2.0291 I          0.000
NON-STOICHIOMETRY N    4.376   -2.029 I
TYPE 1 FILM   4.376  -2.0291 I          0.000
TYPE 1 HYDRATE   1.393   0.0000 I           .990
SECONDARY CRYSTALS   4.376  -2.0291 I          0.000
ROUGHNESS   1.602  -3.3738 I           .148
NUMBER OF SECONDARY SITES/SQCM      .17E+09     LIMITING COVERAGE     .790
CRYSTAL. RATE OF SEC. CRYSTALS (MA/SQCM),      .172
CRYSTAL. RATE OF TYPE2 FILM (MA/SQCM),      .002
SUPERSATURATION OF IONS,   3.82 ,TIME TO REACH(S)        .01
INITIAL DISSOLUTION CURRENT (MA/SQCM)      .0156
TIMES, ONSET OF SEC. CRYSTALS(SEC)    2.5 PPT. CONSTANT (S)    2.0
TIME FOR INITIAL NON-STOICHIOMETRY      90.00
TIME TO COMPLETE PATCH COVERAGE    322.0
TPACK =     90.0  TDISS =     322.0
DEHYDRATION RATE (MA/SQCM)     .20
EFFECTIVE FILM CURRENT(MA/SQCM)        .42
POROSITY OF ROUGH LAYER     .148
CURRENT FRACTION FORMING ROUGHNESS     .002
FINAL THICKNESS OF ROUGHNESS      131.7
WIDTH TO HEIGHT OF SEC. CRYSTALS,      .280
INITIAL COVERAGE OF PATCHES       .12
MOLE FRACTION METAL IN PATCHES     .816
PASSIVATION TIME    3000.00
AVE. DISTANCE BETWEEN EXP. AND THEORY     2.588  (DEG)

                          EXPERIMENT                THEORY          THICKNESSES(A)
TIME(S)    I(MA/SQCM)   VOLTS     DEL      PSI       DEL       PSI       TYPE2     TYPE1(F)   TYPE1(H)   SECONDARY    COV

   170.0       .200     -.870    77.410   47.256    73.234    48.872    436.1      15.7        -.0      2435.9      .008
   180.0       .200     -.870    79.720   48.599    80.256    49.673    436.1      31.6        -.0      3069.0      .013
   190.0       .200     -.870    81.220   49.910    84.533    50.201    436.1      47.7        -.0      3513.2      .017
   200.0       .200     -.870    84.710   51.577    86.634    51.842    436.1      63.8        -.0      3866.8      .021
   210.0       .200     -.870    87.780   53.327    87.784    51.855    436.1      80.1        -.0      4165.3      .023
   220.0       .200     -.870    90.830   55.070    89.187    53.375    436.1      96.4        -.0      4426.3      .026
   230.0       .200     -.870    94.018   56.711    91.845    55.492    436.1     112.8        -.0      4659.7      .029
   240.0       .200     -.870    97.900   58.640    96.673    58.284    436.1     129.3        -.0      4871.8      .032
   250.0       .200     -.870   102.300   60.560   104.781    61.770    436.1     145.9        -.0      5066.9      .035
   260.0       .200     -.870   107.300   62.281
   270.0       .200     -.870   115.260   64.070
   280.0       .200     -.870   122.580   66.090
   290.0       .200     -.870   131.420   68.320
   300.0       .200     -.870   141.310   69.950
   310.0       .200     -.870   149.830   71.220
   320.0       .200     -.870   158.770   72.380
   330.0       .200     -.870   167.460   72.680
   340.0       .200     -.870   179.780   72.015
   350.0       .200     -.870   191.890   69.528
   360.0       .200     -.870   203.060   63.070
   370.0       .200     -.870   212.420   59.510
   380.0       .200     -.870   222.870   57.520
   390.0       .200     -.870   233.840   50.850
   400.0       .200     -.870   245.190   41.460
```

```
 CC4C.16,1.0)MA/SQCM,1140 RE,0001

CODES, 1,2,3A,4,5,6,7,8 =  1.0,  C.0,  0.0,  1.0,  1.0,  1.0,  3.5,  0.0,
CODES, 9,1?,11,3,12,13,14 =  1.0,  1.0,  7.0,  4.0,  1.0,  1.0,  2.0,
REYNOLDS NUMBER =  1140.0
EFFECTIVE REFRACTIVE INDICES AND PCROSITIES,
TYPE 2 FILM   2.13C   C.000  I                .000
TYPE 1 FILM   2.13C   C.0000 I                .000
TYPE 1 HYDRATE   1.404   0.000 I               .949
SECONDARY CRYSTALS   2.13  0.000 I             0.000
ROUGHNESS   1.919  -1.7026 I                .570
NUMBER OF SECONDARY SITES/SQCM      .11E+09     LIMITING COVERAGE     .79
CRYSTAL. RATE OF SEC. CRYSTALS (MA/SQCM),       .001
CRYSTAL. RATE OF TYPE2 FILM (MA/SQCM),      .002
SUPERSATURATION OF IONS,   3.82 ,TIME TO REACH(S)        .00
INITIAL DISSOLUTION CURRENT (MA/SQCM)      .0156
TIMES, ONSET OF SEC. CRYSTALS(SEC)     2.5 PPT. CONSTANT (S)     2.0
TIME TO COMPLETE PATCH COVERAGE      55.0
TIME TO REACH COMPACT FILM I      60.9  S
TIME TO DISSIPATE HYDRATE LAYER      60.9  S
TPACK =      63.9  TDISS =      55.0
DEHYDRATION RATE (MA/SQCM)     .348
EFFECTIVE FILM CURRENT(MA/SQCM)          .109
POROSITY OF ROUGH LAYER     .579
CURRENT FRACTION FORMING ROUGHNESS     .385
FINAL THICKNESS OF ROUGHNESS       224.6
WIDTH TO HEIGHT OF SEC. CRYSTALS,     1.000
INITIAL PATCH COVERAGE       .378
FINAL POROSITY OF TYPE I FILM     .000
POLE FRACTION METAL IN PATCHES    0.000
PASSIVATION TIME     1000.00
AVE. DISTANCE BETWEEN EXP. AND THEORY      .717  (DEG)
```

		EXPERIMENT			THEORY		THICKNESSES(A)				
TIME(S)	I(MA/SQCM)	VOLTS	DEL	PSI	DEL	PSI	TYPE2	TYPE1(F)	TYPE1(H)	SECONDARY	COV
5.0	1.000	-.870	69.170	36.430	69.460	37.232	387.0	.0	-.0	144.2	.000
10.0	1.000	-.87	69.330	37.030	69.424	37.687	387.	15.2	-.0	244.1	.001
15.0	1.000	-.870	70.030	38.230	69.623	38.349	387.0	30.9	-.0	291.4	.001
20.0	1.000	-.870	70.740	39.430	70.130	39.267	387.0	47.6	-.0	323.9	.001
25.0	1.000	-.87	71.22	41.03	71.091	40.578	387.	65.7	-.0	339.8	.001
30.0	1.000	-.870	72.080	42.930	72.774	42.177	387.0	85.7	-.0	351.7	.001
35.0	1.000	-.87	72.93	45.03							
40.0	1.000	-.87	73.12	47.92							
45.0	1.000	-.870	72.40	52.000							
50.0	1.000	-.87	72.84	58.680							
55.0	1.000	-.87	81.850	64.520							
60.0	1.000	-.870	98.730	65.380							

CD40016,1.0MA/SQCM,1140 RE,0001

CODES, 1,2,3A,4,5,6,7,8 = 1.0, 0.0, 0.0, 1.0, 1.0, 1.0, 3.5, 0.0,
CODES, 9,10,11,3,12,13,14 = 0.0, 1.0, 7.0, 4.0, 1.0, 0.0, 2.0,
REYNOLDS NUMBER = 1140.0
EFFECTIVE REFRACTIVE INDICES AND POROSITIES,
TYPE 2 FILM 2.130 0.0000 I 0.000
TYPE 1 FILM 2.130 0.0000 I .000
TYPE 1 HYDRATE 1.387 0.0000 I .893
SECONDARY CRYSTALS 2.130 0.0000 I 0.000
ROUGHNESS 1.932 -1.5998 I .596
NUMBER OF SECONDARY SITES/SQCM .11E+09 LIMITING COVERAGE .790
CRYSTAL, RATE OF SEC, CRYSTALS (MA/SQCM), .000
CRYSTAL, RATE OF TYPE2 FILM (MA/SQCM), .002
SUPERSATURATION OF ICNS, 3.82 ,TIME TO REACH(S) .00
INITIAL DISSOLUTION CURRENT (MA/SQCM) .0156
TIMES, ONSET OF SEC, CRYSTALS(SEC) 2.5 PPT, CONSTANT (S) 2.0
TIME TO COMPLETE PATCH COVERAGE 55.0
TIME TO REACH COMPACT FILM I 9.0 S
TIME TO DISSIPATE HYDRATE LAYER 9.0 S
TPACK = 9.0 TDISS = 55.0
DEHYDRATION RATE (MA/SQCM) .324
EFFECTIVE FILM CURRENT(MA/SQCM) .121
POROSITY OF ROUGH LAYER .596
CURRENT FRACTION FORMING ROUGHNESS 1.000
FINAL THICKNESS OF ROUGHNESS 307.1
WIDTH TO HEIGHT OF SEC, CRYSTALS, 1.000
INITIAL PATCH COVERAGE 1.000
FINAL POROSITY OF TYPE I FILM .000
MOLE FRACTION METAL IN PATCHES 0.000
PASSIVATION TIME 1000.00
AVE, DISTANCE BETWEEN EXP, AND THEORY 5.998 (DEG)

			EXPERIMENT		THEORY		THICKNESSES(A)				
TIME(S)	I(MA/SQCM)	VOLTS	DEL	PSI	DEL	PSI	TYPE2	TYPE1(F)	TYPE1(H)	SECONDARY	COV
35.0	1.000	-.870	72.930	45.030	72.038	43.991	387.0	.0	-.0	93.9	.000
40.0	1.000	-.870	73.120	47.920	71.800	45.643	387.0	37.4	-.0	118.3	.000
45.0	1.000	-.870	72.400	52.000	73.121	47.805	387.0	75.2	-.0	135.4	.000
50.0	1.000	-.870	72.840	58.680	76.593	50.804	387.0	113.3	-.0	149.0	.000
55.0	1.000	-.870	81.850	64.520	83.287	55.213	387.0	151.8	-.0	160.5	.000
60.0	1.000	-.870	98.730	65.360	100.944	60.992	387.0	189.8	-.0	170.6	.000
-I	-I	-I	-I	-I							

#ZN7C-10# #10MA.ES# #C.5M KCH#

CODES, 1.2.3A.4.5.6.7.8 = 1.0, 0.0, 0.0, 1.0, 1.0, 1.0, 3.5, 0.0,
CODES, 9.10.11.3.12.13.14 = 5.0, 0.0, 5.0, 7.0, 0.0, 0.0, 0.0,
REYNOLDS NUMBER = 0.0
EFFECTIVE REFRACTIVE INDICES AND POROSITIES,
TYPE 2 FILM 2.00 0.0000 I .000
TYPE 1 FILM 1.558 0.0000 I .143
TYPE 1 HYDRATE 1.364 0.0000 I .980
SECONDARY CRYSTALS 1.814 0.0000 I .279
ROUGHNESS 2.284 -3.6081 I .346
NUMBER OF SECONDARY SITES/SQCM .50E+07 LIMITING COVERAGE .790
CRYSTAL. RATE OF SEC. CRYSTALS (MA/SQCM), .04990
CRYSTAL. RATE OF TYPE2 FILM (MA/SQCM), .50000
SUPERSATURATION OF IONS, 2.300 ,TIME TO REACH(S) .25208
INITIAL DISSOLUTION CURRENT (MA/SQCM) .7074
TIMES, ONSET OF SEC. CRYSTALS(SEC) 1.0 PPT. CONSTANT (S) .9
TIME TO COMPLETE PATCH COVERAGE 25.8
TIME TO REACH COMPACT FILM I 3.0 S
TPACK = 3.0 TDISS = 25.8
DEHYDRATION RATE (MA/SQCM) 1.349
EFFECTIVE FILM CURRENT(MA/SQCM) *******
POROSITY OF ROUGH LAYER .518
CURRENT FRACTION FORMING ROUGHNESS .085
FINAL THICKNESS OF ROUGHNESS 103.4
WIDTH TO HEIGHT OF SEC. CRYSTALS, 1.000
INITIAL PATCH COVERAGE .200
FINAL POROSITY OF TYPE I FILM .010
POLE FRACTION METAL IN PATCHES 0.000
PASSIVATION TIME 1000.00
AVE. DISTANCE BETWEEN EXP. AND THEORY 2.859 (DEG)

			EXPERIMENT		THEORY		THICKNESSES(A)				
TIME(S)	I(MA/SQCM)	VOLTS	DEL	PSI	DEL	PSI	TYPE2	TYPE1(F)	TYPE1(H)	SECONDARY	COV
0.0	10.000	-.980	106.200	32.600	106.153	32.602	0.0	.0	0.0	.0	0.000
1.0	10.000	-1.050	103.000	31.900	102.129	32.937	0.0	21.6	-.0	.0	.000
2.0	10.000	-1.050	101.000	31.200	1.1.233	33.524	0.0	76.8	-.0	636.9	.000
3.0	10.000	-1.050	99.600	29.700	98.781	33.125	0.0	143.5	-.0	797.3	.000
4.0	10.000	-1.040	98.000	28.800	96.880	32.409	0.0	2[illegible]7.5	-.0	903.2	.000
5.0	10.000	-1.030	96.100	27.900	95.487	31.571	0.0	265.4	-.0	980.3	.000
6.0	10.000	-1.020	94.400	27.300	94.426	30.723	0.0	315.3	-.0	1038.0	.001
7.0	10.000	-1.000	92.900	26.800	93.483	29.917	0.0	356.5	-.0	1081.4	.001
8.0	10.000	-.990	90.900	26.500	92.455	29.170	0.0	389.2	-.0	1113.6	.001
9.0	10.000	-.950	89.100	26.200	91.162	28.492	0.0	413.8	-.0	1137.0	.001
10.0	10.000	-.970	86.700	25.900	89.459	27.897	0.0	431.2	-.0	1153.3	.001
11.0	10.000	-.920	84.300	25.900	87.241	27.424	0.0	442.3	-.0	1164.0	.001
12.0	10.000	-.890	82.300	25.900	84.472	27.143	0.0	448.6	-.0	1170.2	.001
13.0	10.000	-.880	80.300	26.100	81.236	27.146	0.0	450.6	-.0	1172.8	.001
14.0	10.000	-.850	78.600	26.600	77.777	27.525	0.0	449.1	-.0	1172.6	.001
15.0	10.000	-.660	77.000	26.900	74.481	28.328	0.0	445.[illegible]	-.0	1170.2	.001
15.5	10.000	.770	75.800	27.500	73.025	28.882	0.0	442.2	-.0	1168.4	.001
16.0	10.000	2.100	76.000	28.100							
16.5	10.000	3.100	74.600	28.700							
17.0	10.000	3.400	72.800	29.400							
18.0	10.000	3.400	72.200	30.100							
19.0	10.000	3.500	72.000	30.200							
20.0	10.000	3.600	71.800	30.400							
25.0	10.000	4.120	70.000	30.700							
30.0	10.000	4.770	68.200	30.800							
35.0	10.000	4.770	66.400	31.100							
40.0	10.000	5.020	64.700	31.300							

ZN7C-23 E=-1.0V 3.5% KOH

CODES, 1,2,3,4,5,6,7,8 = 2,1, 3,1, 1,0, 1,0, 1,0, 1,0, 0,0, 0,0,
CODES, 9,10,11,12,13,14 = 0,0, 0,0, 3,0, 4,0, 0,0, 0,0, 0,0,
REYNOLDS NUMBER = 3,
EFFECTIVE REFRACTIVE INDICES AND POROSITIES,
TYPE 2 FILM 2.88 -.0113 I .080
TYPE 1 FILM 2.72 -.111 I .010
TYPE 1 HYDRATE 1.377 0.0000 I .901
SECONDARY CRYSTALS 2.28 -.0104 I .080
NUMBER OF SECONDARY SITES/SQCM .5E+07 LIMITING COVERAGE .790
CRYSTAL, RATE OF SEC, CRYSTALS (MA/SQCM), 8.93091
CRYSTAL, RATE OF TYPE2 FILM (MA/SQCM), 4.14365
SUPERSATURATION OF IONS, 3.335 ,TIME TO REACH(S) .50000
INITIAL DISSOLUTION CURRENT (MA/SQCM) -1
TIMES, CHSEN OF SEC, CRYSTALS(SEC) 1.5 PPT, CONSTANT (S) 2.9
TIME TO REACH COMPACT FILM I 288.3 S
TIME TO DISSIPATE HYDRATE LAYER 288.3 S
TPACK = 288.3 TDISS = 1[illegible].0
DEHYDRATION RATE (MA/SQCM) 10.000
EFFECTIVE FILM CURRENT(MA/SQCM) -4.[illegible]
POROSITY OF ROUGH LAYER .390
CURRENT FRACTION FORMING ROUGHNESS .814
FINAL THICKNESS OF ROUGHNESS 186.1
WIDTH TO HEIGHT OF SEC, CRYSTALS, 1.000
FINAL POROSITY OF TYPE I FILM .182
MOLE FRACTION METAL IN PATCHES .080
PASSIVATION TIME 4.30
AVE, DISTANCE BETWEEN EXP, AND THEORY 1.038 (DEG)

		EXPERIMENT			THEORY		THICKNESSES(A)				
TIME(S)	I(MA/SQCM)	VOLTS	DEL	PSI	DEL	PSI	TYPE2	TYPE1(F)	TYPE1(H)	SECONDARY	COV
.1	10.000	-1.200	102.800	34.000	102.307	34.022	0.0	.0	0.0	.0	0.000
.5	10.000	-1.200	96.700	33.800	97.873	33.960	.8	0.0	85.5	.0	.000
1.0	9.000	-1.200	89.100	33.000	90.735	33.683	1.7	0.0	622.0	.0	.000
1.5	8.000	-1.200	86.000	32.900	87.288	33.401	2.5	0.0	1178.7	.0	.000
2.0	7.000	-1.200	91.200	33.200	90.111	33.740	2.5	22.5	1173.5	1218.1	.001
2.5	6.000	-1.200	92.800	33.400	92.716	33.969	2.5	42.6	1174.3	1221.7	.001
3.0	5.000	-1.200	94.000	33.600	94.615	34.104	2.5	58.0	1174.6	1225.3	.001
3.5	3.000	-1.200	94.300	33.900	92.878	34.124	2.5	67.1	1176.6	1229.0	.001
4.0	4.000	-1.200	92.600	34.200	92.577	34.126	2.5	67.2	1178.7	1229.0	.001
4.5	3.000	-1.200	91.000	34.400	91.695	33.902	2.5	67.2	1180.7	1229.0	.001
5.0	2.000	-1.200	91.200	34.400	91.633	33.888	2.5	67.2	1182.8	1229.0	.001
10.0	2.000	-1.200	91.200	34.500	91.167	33.823	2.5	67.5	1203.8	1229.0	.001
15.0	2.000	-1.200	91.200	34.500	90.765	33.777	2.5	67.7	1225.6	1229.0	.001
20.0	2.000	-1.2	91.2[illegible]	34.4[illegible]	9[illegible].394	33.747	2.5	68.[illegible]	1248.2	1229.0	.001
30.0	2.00	-1.200	91.100	34.400							
4[illegible].0	2.1[illegible]	-1.2[illegible]	91.0[illegible]	34.40[illegible]							
5[illegible].0	2.2	-1.20[illegible]	9[illegible].7[illegible]	34.400							
100.0	2.20	-1.200	88.000	34.400							
15[illegible].0	2.2[illegible]	-1.2[illegible]	84.[illegible]	33.8[illegible]							
200.0	2.20	-1.2[illegible]	80.600	32.700							
250.0	2.20	-1.200	78.30[illegible]	31.7							
3[illegible].0	2.2[illegible]	-1.2	76.[illegible]	3[illegible].7[illegible]							

ZN70-25 E=-1.0V 0.5M KOH

CODES, 1,2,3A,4,5,6,7,8 = 2.0, 0.0, 0.0, 1.0, 1.0, 1.0, 3.5, 0.0,
CODES, 9,10,11,3,12,13,14 = 0.0, 0.0, 10.0, 1.0, 0.0, 0.0, 0.0,
REYNOLDS NUMBER = 0.0
EFFECTIVE REFRACTIVE INDICES AND POROSITIES,
TYPE 2 FILM 2.268 -.0004 I .080
NON-STOICHIOMETRY N 2.268 -.030 I
TYPE 1 FILM 2.094 -.0003 I .187
TYPE 1 HYDRATE 1.395 0.0000 I .863
SECONDARY CRYSTALS 2.193 -.0003 I .080
NUMBER OF SECONDARY SITES/SQCM .50E+07 LIMITING COVERAGE .790
CRYSTAL. RATE OF SEC. CRYSTALS (MA/SQCM), .00100
CRYSTAL. RATE OF TYPE2 FILM (MA/SQCM), 4.10000
SUPERSATURATION OF IONS, 3.300 ,TIME TO REACH(S) .50000
INITIAL DISSOLUTION CURRENT (MA/SQCM) -I
TIMES, ONSET OF SEC. CRYSTALS(SEC) 1.5 PPT. CONSTANT (S) 2.9
TIME FOR INITIAL NON-STOICHIOMETRY 12.89
TIME TO COMPLETE PATCH COVERAGE 432.6
TPACK = 12.9 TDISS = 432.6
DEHYDRATION RATE (MA/SQCM) 10.000
EFFECTIVE FILM CURRENT(MA/SQCM) -.129
POROSITY OF ROUGH LAYER .490
CURRENT FRACTION FORMING ROUGHNESS .692
FINAL THICKNESS OF ROUGHNESS 403.4
WIDTH TO HEIGHT OF SEC. CRYSTALS, 1.000
INITIAL COVERAGE OF PATCHES .99
MOLE FRACTION METAL IN PATCHES .026
PASSIVATION TIME 1000.00
AVE. DISTANCE BETWEEN EXP. AND THEORY 1.754 (DEG)

	EXPERIMENT				THEORY		THICKNESSES(A)				
TIME(S)	I(MA/SQCM)	VOLTS	DEL	PSI	DEL	PSI	TYPE2	TYPE1(F)	TYPE1(H)	SECONDARY	COV
50.0	.220	-1.200	90.700	34.400	93.309	36.343	1.7	109.4	-.0	117.8	.000
100.0	.220	-1.200	88.000	34.400	86.763	35.051	1.7	109.4	-.0	117.8	.000
150.0	.220	-1.200	84.000	33.800	82.506	34.128	1.7	109.4	-.0	117.8	.000
200.0	.220	-1.200	80.600	32.700	79.777	33.271	1.7	109.4	-.0	117.8	.000
250.0	.220	-1.200	78.300	31.700	78.142	32.600	1.7	109.4	-.0	117.8	.000
300.0	.220	-1.200	76.000	30.700	77.295	31.849	1.7	109.4	-.0	117.8	.000
-I	-I	-I	-I	-I							

ZN70-25 ee=-1.2V* e0.5 M KCl*

CODES, 1,2,3a,4,5,c,7,8 = 2.0, 0.0, 4.0, 1.0, 1.0, 1.0, 3.5, 3.0,
CODEs 9,10,11,12,13,14 = 3.0, 0.0, 7.0, 4.0, 5.0, 1.1, 0.0,
REYNOLDS NUMBER = 0.0
EFFECTIVE REFRACTIVE INDICES AND POROSITIES,
TYPE 2 FILM 2.000 0.0000 I .090
TYPE 1 FILM 1.999 0.0000 I .010
TYPE 1 HYDRATE 1.376 0.0000 I .883
SECONDARY CRYSTALS 2.000 0.0000 I 0.000
NUMBER OF SECONDARY SITES/SQCM .50E+07 LIMITING COVERAGE .790
CRYSTAL. RATE OF SEC. CRYSTALS (MA/SQCM), .00012
CRYSTAL. RATE OF TYPE2 FILM (MA/SQCM), 1.22621
SUPERSATURATION OF IONS, 2.000 ,TIME TO REACH(S) .50000
INITIAL DISSOLUTION CURRENT (MA/SQCM) -1
TIMES, INSET OF SEC. CRYSTALS(SEC) 1.5 EXPT. CONSTANT (S) 1.0
TIME TO COMPLETE PATCH COVERAGE 74.9
TIME TO REACH COMPACT FILM I 203.4 S
TIME TO DISSIPATE HYDRATE LAYER 203.4 S
DEHYDRATION RATE (MA/SQCM) 1.190
EFFECTIVE FILM CURRENT(MA/SQCM) -18.931
POROSITY OF ROUGH LAYER .840
CURRENT FRACTION FORMING ROUGHNESS .597
FINAL THICKNESS OF ROUGHNESS 2724.3
WIDTH TO HEIGHT OF SEC. CRYSTALS, 1.000
INITIAL PATCH COVERAGE .522
FINAL POROSITY OF TYPE 1 FILM 0.000
PASSIVATION TIME 1000.00
AVE. DISTANCE BETWEEN EXP. AND THEORY 4.270 (DEG)

		EXPERIMENT			THEORY		THICKNESSES(A)				
TIME(S)	I(MA/SQCM)	VOLTS	DEL	PSI	DEL	PSI	TYPE2	TYPE1(H)	TYPE1(M)	SECONDARY	COV
1.0	0.000	-1.200	97.200	36.900	96.929	39.086	.0	.0	0.0	.0	0.000
2.0	0.000	-1.200	92.000	33.700	92.304	25.057	.0	5.5	-.0	35.2	.000
3.0	0.000	-1.200	89.000	34.500	89.411	27.710	.0	14.5	-.0	60.2	.000
4.0	0.000	-1.200	86.000	33.500	83.073	28.418	.0	24.9	-.0	73.3	.000
5.0	0.000	-1.200	84.100	32.900	81.738	29.102	.0	36.3	-.0	82.8	.000
6.0	0.000	-1.200	82.700	32.100	80.460	29.751	.0	47.0	-.0	90.5	.000
7.0	0.000	-1.200	81.000	31.600	79.278	30.351	.0	59.1	-.0	97.0	.000
8.0	0.000	-1.200	79.800	31.200	78.141	30.947	.0	70.5	-.0	102.8	.000
9.0	0.000	-1.200	78.300	30.900	77.054	31.477	.0	81.9	-.0	107.9	.000
10.0	0.000	-1.200	76.900	30.500	76.048	31.991	.0	93.1	-.0	112.5	.000
11.0	0.000	-1.200	75.700	30.200	75.120	32.459	.0	103.8	-.0	116.8	.000
12.0	0.000	-1.200	74.400	30.000	74.271	32.913	.0	114.2	-.0	120.7	.000
13.0	0.000	-1.200	73.600	30.000	74.229	32.174	.0	124.4	-.0	124.4	.000
14.0	0.000	-1.200	72.400	29.900	73.316	32.571	.0	134.4	-.0	127.8	.000
15.0	0.000	-1.200	71.400	29.900	72.624	32.948	.0	144.1	-.0	131.0	.000
16.0	0.000	-1.200	70.100	30.000	72.175	33.311	.0	153.7	-.0	134.0	.000
17.0	0.000	-1.200	69.100	30.000	71.960	33.655	.0	163.0	-.0	136.8	.000
18.0	0.000	-1.200	68.400	30.100	71.943	33.977	.0	171.9	-.0	139.5	.000
19.0	0.000	-1.200	67.700	30.200	72.030	34.279	.0	180.6	-.0	142.1	.000
20.0	0.000	-1.200	67.100	30.200	72.045	34.561	.0	189.1	-.0	144.5	.000
21.0	0.000	-1.200	66.700	31.400	66.977	35.368	.0	197.4	-.0	154.9	.000
30.0	0.000	-1.200	64.200	32.500	67.059	36.375	.0	250.2	-.0	163.1	.000
35.0	0.000	-1.200	63.000	33.300	67.331	37.291	.0	277.4	-.0	169.6	.000
40.0	0.000	-1.200	62.000	34.900	67.985	38.192	.0	295.7	-.0	174.8	.000
45.0	0.000	-1.200	61.400	35.900	68.881	39.040	.0	307.5	-.0	178.9	.000
50.0	0.000	-1.200	60.900	36.900	69.978	39.833	.0	314.3	-.0	182.0	.000
55.0	0.000	-1.200	71.500	37.200	70.964	40.133	.0	324.8	-.0	184.3	.000
60.0	0.000	-1.200	73.400	37.700	72.412	-1.030	.0	326.8	-.0	186.0	.000
65.0	0.000	-1.200	74.800	38.100	74.010	41.353	.0	325.6	-.0	187.2	.000

e2n70-25e e2E=-1.2e# e0.2 M KOH#

CUOF=e 1.2e3n+e3.e7e0 = 2.e0, 0.0, 4.e0, 1.C, 1.e0, 1.e0, 3.e3, 0.e0,
Cuoles, 3.1e3,1.e3,1.e4 = 0.e0, 0.e0, 7.C, 4.e0, 4.e0, 0.e0, 0.e0,
KEYCLES NUMBER = 0.e0
EFFECTIVE REFRACTIVE INDICES AND POROSITIES,
TYPE 2 FILM 2.0000 0.0000 I .C80
TYPE 1 FILM 1.6595 0.0000 I .C10
TYPE I HYDRATE 1.6335 0.0000 I .992
SECONDARY CRYSTALS 2.0000 0.0000 I C.CCC
NUMBER OF SECONDARY SITES/SQCM .e3E+08 LIMITING COVERAGE .790
CRYSTAL+ RATE OF SECO CRYSTALS (MA/SQCM), .32E74
CRYSTAL+ RATE OF TYPE2 FILM (MA/SQCM), 1.2C00C
SUPERSATURATION OF ILR+, 2.E3C +TIME TO REACH(S) .50000
INITIAL DISSOLUTION CURRENT (MA/SQCM) -1
TIME+ ONSET OF SECO CRYSTALS(SEC) 1.E PET. CONSTANT (S) 1.e0
TIME TO COMPLETE PATCH COVERAGE 71.e
TIME TO REACH COMPACT FILM T 235.7 S
TIME TO DISSIPATE HYDRATE LAYER 255.7 S
DEHYDRATION RATE (MA/SQCM) .971
EFFECTIVE FILM CURRENT(MA/SQCM) -.E47
POROSITY OF OUTER LAYER .E15
CURRENT FRACTAL FORMING ROUGHNESS .121
FINAL THICKNESS OF ROUGHNESS 525.2
RATIO TO HEIGHT OF SEC. CRYSTALS, 1.000
INITIAL PATCH COVERAGE .99J
FINAL POROSITY OF TYPE I FILM C.CCC
PASSIVATION TIME 1CC3.CW
AVG. DISTANCE BETWEEN EXP. AND THEORY 2.E2U (DEG)

TIME(S)	I(MA/SQCM)	VOLTS	EXPERIMENT SEL	EXPERIMENT PSI	THEORY SEL	THEORY PSI	THICKNESSES(A) TYPE2	TYPE1(F)	TYPE1(H)	SECONDARY	COV
72.e	1.e7CC	-1.e2CC	78.e3CC	29.e5CC	79.e7E	42.e39U	54.e+	495.e	-.e0	2613.e4	.e29
8C.e	1.e7JJ	-1.e2CC	6C.e03J	39.E0C	6J.e32E	42.e397	54.e+	257.9	-.e0	2671.e6	.e31
9C.e	1.e3CJ	-1.e2JC	8e.e1CJ	4C.e1CC	82.e247	43.e198	54.e+	280.9	-.e0	2780.9	.e33
1JC.e	1.e33C	-1.e2JJ	83.7CJ	4C.e3C3	84.e1e0	43.e46C	54.e+	303.6	-.e0	2882.2	.e36
11C.e	1.e33C	-1.e2JJ	85.9Ce	4C.e5CC	85.e99J	43.e62A	54.e+	326.9	-.e0	2976.8	.e38
12C.e	1.e2JJ	-1.e2CC	87.7JC	4C.e7CC	87.715	43.e644	54.e+	349.e	-.e0	3C65.8	.e4C
13C.e	1.e2JJ	-1.e2JC	89.eCJ	41.e1CC	89.e77	44.e372	54.e+	37C.9	-.e0	3149.9	.e42
14J.e	1.e2CC	-1.e2JJ	9C.e3JJ	41.e4CC	9C.e7c4	44.e352	54.e+	392.8	-.e0	3229.7	.e45
15J.e	1.e1JC	-1.e2JC	91.e6JJ	41.e5CC	92.e037	44.e4C4	54.e+	413.9	-.e0	3305.8	.e47
16C.e	1.e1JC	-1.e2JJ	92.e9JJ	42.eCCC	93.e288	44.e491	54.e+	435.9	-.e0	3378.5	.e49
17J.e	1.e0CJ	-1.e2CC	95.e9CJ	42.e2CC	94.e357	45.e195	54.e+	452.9	-.e0	3448.2	.e51
18J.e	1.e0JJ	-1.e2JC	97.e2CC	42.e4CC	95.e429	45.e316	54.e+	470.9	-.e0	3515.2	.e53
19C.e	1.e0CC	-1.e2CJ	98.e5JC	42.e6CC	96.e45C	45.e391	54.e+	489.e	-.e0	3579.8	.e55
2JC.e	1.e0CJ	-1.e2JC	98.e3CJ	43.e7CC	97.e622	46.e325	54.e+	507.7	-.e0	3642.1	.e57
21C.e	1.e0CJ	-1.e2JC	1CC.e3JJ	44.e3CC	99.e359	46.e825	54.e+	525.4	-.e0	3702.3	.e59
22C.e	1.e0JC	-1.e2JC	1C2.e5JC	44.e9CC	1C1.e788	47.e399	54.e+	545.e	-.e0	3760.7	.e61
23J.e	1.e0CJ	-1.e2JJ	1C4.e6JJ	45.e6CC	1C4.e65C	48.e353	54.e+	564.6	-.e0	3817.2	.e62
24C.e	1.e0JC	-1.e2JC	1C8.e4JJ	46.e9CC	1C9.e289	48.e3C1	54.e+	583.8	-.e0	3872.2	.e64
25C.e	1.e0JC	-1.e2JJ	111.e13J	46.e2CC	112.e965	49.e e54	54.e+	6C2.9	-.e0	3925.6	.e66
26C.e	1.e0JJ	-1.e2CC	119.1CJ	45.e6CC	118.e94C	3C.3e4	54.e+	622.1	-.e0	3977.7	.e68
27J.e	1.e0CJ	-1.e2JC	126.e0J	51.e3CC	126.e45J	51.e39C	54.e+	641.4	-.e0	4028.3	.e69
28J.e	1.e0CJ	-1.e2JC	133.e3CJ	52.7CC	135.e675	32.e3e4	54.e+	661.e	-.e0	4077.8	.e71
29C.e	1.e0JJ	-1.e2CC	147.eJJ	53.e6C	146.711	53.e59	54.e+	680.e	-.e0	4126.1	.e73
3JC.e	1.e0JJ	-1.e23C	1e3.2CC	54.eCCC	159.444	54.e3ee	54.e+	700.4	-.e0	4173.2	.e75
3C5.e	1.e0JJ	-1.e2CC	166.6CC	53.7CC	166.719	34.e212	54.e+	711.e	-.e0	4196.4	.e75
31C.e	1.e0JJ	-1.e2CJ	172.53J	53.2CC							
315.e	1.e0JJ	-1.e2JC	179.3JJ	51.9CC							
32J.e	1.e3CJ	-1.e2JC	185.1JC	5C.3JJ							
325.e	1.e3CC	-1.e2JJ	18e.93J	48.13J							

[illegible] 0.5 M KOH

```
CODES 1,2,3,4,5,6,7,8 =  2.0,  2.0,  4.0,  1.0,  1.0,  1.0,  3.5,  0.0,
CODES [illegible] =  0.0,  0.0,  7.0,  5.0,  1.0,  0.0,  0.0,
REYNOLDS NUMBER =      0.0
EFFECTIVE REFRACTIVE INDICES AND POROSITIES.
TYPE 2 FILM   1.0000   0.0000 I            .080
TYPE 1 FILM   1.999    0.0000 I            .010
TYPE  HYDRATE  [illegible].209   0.0000 I        .990
SECONDARY CRYSTALS   [illegible]   0.0000 I        .284
NUMBER OF SECONDARY SITES/SQCM     .982E07     LIMITING COVERAGE    .790
CRYSTAL. RATE OF SEC. CRYSTALS (MA/SQCM).   .08430
CRYSTAL. RATE OF TYPE2 FILM (MA/SQCM).  3.00000
SUPERSATURATION OF IONS.  2.300 ,TIME TO REACH(S)     .50000
INITIAL DISSOLUTION CURRENT (MA/SQCM)         -1
TIMES, ONSET OF SEC. CRYSTALS(SEC)     1.5 PPT. CONSTANT (S)    1.0
TIME TO COMPLETE PATCH COVERAGE     244.9
TIME TO REACH COMPACT FILM 1     195.9  S
TIME TO DISSIPATE HYDRATE LAYER     195.9  S
TPACK =      195.9  TDISS =      344.9
DEHYDRATION RATE (MA/SQCM)    2.047
EFFECTIVE FILM CURRENT(MA/SQCM)    -0.904
CURRENT FRACTION FORMING ROUGHNESS     .050
FINAL THICKNESS OF ROUGHNESS      1261.7
WIDTH TO HEIGHT OF SEC. CRYSTALS.     1.000
INITIAL PATCH COVERAGE     .284
FINAL POROSITY OF TYPE 1 FILM    0.000
PASSIVATION TIME      300.00
AVE. DISTANCE BETWEEN EXP. AND THEORY     4.364  (DEG)
```

			EXPERIMENT		THEORY		THICKNESSES(A)				
TIME(S)	I(MA/SQCM)	VOLTS	DEL	PSI	DEL	PSI	TYPE2	TYPE1(F)	TYPE1(H)	SECONDARY	COV
[illegible]	1.000	-1.200	166.030	55.700	171.564	51.012	225.2	689.7	-.0	3197.4	.010
[illegible]	1.000	-1.200	172.500	53.200	176.121	50.171	225.2	693.6	-.0	3187.7	.010
[illegible]	1.000	-1.200	179.300	51.900	180.570	49.159	225.2	697.7	-.0	3178.0	.010
[illegible]	1.000	-1.200	185.100	50.300	184.901	48.088	225.2	702.0	-.0	3168.3	.010
[illegible]	1.000	-1.200	189.900	48.100	189.105	46.970	225.2	706.3	-.0	3158.7	.010
[illegible]	1.000	-1.200	195.100	45.200	193.174	45.818	225.2	710.7	-.0	3149.0	.010
[illegible]	1.000	-1.200	199.000	42.300	197.105	44.642	225.2	715.1	-.0	3139.4	.010
[illegible]	1.000	-1.200	202.400	39.200	200.897	43.455	225.2	719.7	-.0	3129.8	.010
[illegible]	1.000	-1.200	204.800	37.100	204.420	42.234	225.2	725.6	-.0	3121.9	.030
[illegible]	1.100	-1.200	206.100	33.500	206.070	41.209	225.2	749.1	-.0	3137.0	.010
[illegible]	1.100	-1.200	206.000	30.500							
[illegible]	[illegible]	-1.200	205.400	27.200							
[illegible]	1.100	-1.200	203.100	24.500							
[illegible]	[illegible]	-1.200	201.100	21.500							
[illegible]	[illegible]	-1.200	197.000	19.000							
[illegible]	1.100	-1.200	172.300	17.200							
[illegible]	[illegible]	-1.200	57.300	15.600							
[illegible]	1.100	-1.200	140.700	13.300							
[illegible]	1.100	-1.200	124.400	[illegible]							
[illegible]	[illegible]	-1.200	109.600	17.000							
[illegible]	1.100	-1.200	96.000	19.000							
[illegible]	[illegible]	-1.200	[illegible]	21.000							
[illegible]	[illegible]	-1.200	[illegible]	[illegible]							
[illegible]	1.100	-1.200	[illegible]	25.600							
[illegible]	[illegible]	-1.200	[illegible]	26.000							
[illegible]	1.100	-1.200	75.000	26.000							
[illegible]	1.100	-1.200	[illegible]	27.400							
[illegible]	[illegible]	-1.200	[illegible]	28.000							
[illegible]	[illegible]	-1.200	[illegible]	28.100							

#ZN70-25# #E=-1.2V# #0.5 M KOH#

CODES, 1,2,3A,4,5,6,7,8 = 2.0, 2.0, 4.0, 1.0, 1.0, 1.0, 3.5, 0.0,
CODES, 9,10,11,3,12,13,14 = 0.0, 0.0, 10.0, 4.0, 1.0, 0.0, 0.0,
REYNOLDS NUMBER = 0.0
EFFECTIVE REFRACTIVE INDICES AND POROSITIES,
TYPE 2 FILM 2.098 -.0606 I .080
NON-STOICHIOMETRY N 2.098 -.061 I
TYPE 1 FILM 2.091 -.0600 I .010
TYPE 1 HYDRATE 1.343 0.0000 I .990
SECONDARY CRYSTALS 1.618 -.0225 I .629
NUMBER OF SECONDARY SITES/SQCM .56E+09 LIMITING COVERAGE .790
CRYSTAL. RATE OF SEC. CRYSTALS (MA/SQCM), .02510
CRYSTAL. RATE OF TYPE2 FILM (MA/SQCM), .03400
SUPERSATURATION OF ICNS, 2.300 ,TIME TO REACH(S) .50000
INITIAL DISSOLUTION CURRENT (MA/SQCM) -1
TIMES, ONSET OF SEC. CRYSTALS(SEC) 1.5 PPT. CONSTANT (S) 1.0
TIME FOR INITIAL NON-STOICHIOMETRY 497.98
TIME TO COMPLETE PATCH COVERAGE 500.0
TPACK = 498.0 TDISS = 500.0
DEHYDRATION RATE (MA/SQCM) 1.596
EFFECTIVE FILM CURRENT(MA/SQCM) .867
POROSITY OF ROUGH LAYER .057
CURRENT FRACTION FORMING ROUGHNESS .122
FINAL THICKNESS OF ROUGHNESS 336.7
WIDTH TO HEIGHT OF SEC. CRYSTALS, 1.000
INITIAL COVERAGE OF PATCHES .95
MOLE FRACTION METAL IN PATCHES .087
PASSIVATION TIME 3000.00
AVE. DISTANCE BETWEEN EXP. AND THEORY 5.874 (DEG)

		EXPERIMENT			THEORY		THICKNESSES(A)				
TIME(S)	I(MA/SQCM)	VOLTS	DEL	PSI	DEL	PSI	TYPE2	TYPE1(F)	TYPE1(H)	SECONDARY	COV
350.0	1.100	-1.200	206.200	33.300	217.709	26.695	131.3	1951.5	-.0	2606.6	.382
355.0	1.100	-1.200	206.600	30.500	214.047	24.474	131.3	1989.9	-.0	2619.0	.386
360.0	1.100	-1.200	205.400	27.200	208.991	22.286	131.3	2028.8	-.0	2631.3	.389
365.0	1.100	-1.200	203.300	24.500	202.300	20.184	131.3	2068.1	-.0	2643.5	.393
370.0	1.100	-1.200	202.100	21.500	193.683	18.261	131.3	2107.8	-.0	2655.6	.397
375.0	1.100	-1.200	191.300	19.000	182.898	16.649	131.3	2148.0	-.0	2667.5	.400
380.0	1.100	-1.200	173.300	17.200	169.964	15.515	131.3	2188.7	-.0	2679.4	.404
385.0	1.100	-1.200	157.300	15.600	155.467	15.013	131.3	2229.9	-.0	2691.1	.407
390.0	1.100	-1.200	140.700	15.300	140.600	15.222	131.3	2271.5	-.0	2702.8	.411
395.0	1.100	-1.200	124.400	16.600	126.663	16.087	131.3	2313.6	-.0	2714.4	.414
400.0	1.100	-1.200	109.600	17.000	114.453	17.456	131.3	2356.2	-.0	2725.8	.418
405.0	1.100	-1.200	96.800	19.000	104.136	19.144	131.3	2399.2	-.0	2737.2	.421
410.0	1.100	-1.200	92.200	21.000	95.514	20.991	131.3	2442.8	-.0	2748.4	.425
415.0	1.100	-1.200	88.100	22.000	88.287	22.881	131.3	2486.9	-.0	2759.6	.428
420.0	1.100	-1.200	84.000	25.800	82.179	24.733	131.3	2531.4	-.0	2770.7	.432
425.0	1.100	-1.200	79.600	26.000	76.970	26.501	131.3	2576.5	-.0	2781.7	.435
430.0	1.100	-1.200	75.000	26.800	72.499	28.158	131.3	2622.1	-.0	2792.6	.439
435.0	1.100	-1.200	71.000	27.400	68.651	29.695	131.3	2668.3	-.0	2803.4	.442
440.0	1.100	-1.200	65.600	28.000	65.343	31.111	131.3	2715.0	-.0	2814.2	.445
445.0	1.100	-1.200	59.700	28.100	62.521	32.414	131.3	2762.2	-.0	2824.8	.449
450.0	1.100	-1.200	54.600	27.900	60.146	33.617	131.3	2809.9	-.0	2835.4	.452
455.0	1.100	-1.200	48.900	27.500							
460.0	1.100	-1.200	41.100	26.700							
465.0	1.100	-1.200	33.100	26.100							
470.0	1.100	-1.200	26.500	24.600							
475.0	1.100	-1.200	17.600	22.800							
480.0	1.100	-1.200	6.800	20.000							
485.0	1.100	-1.200	-4.300	14.500							

```
  ZN7J-58   200MA   6M KCH

CODES, 1,2,3,4,5,6,7,8 =  1.0,  2.0,  4.0,  1.0,  1.0,  1.0,  3.5,  0.0,
CODES, 9,10,11,12,13,14 =  0.0,  0.0,  0.0,  4.0,  0.0,  0.0,  0.0,
KEYWORDS NUMBER =      0.0
EFFECTIVE REFRACTIVE INDICES AND POROSITIES,
TYPE 2 FILM   2.0000   0.0000 I            0.000
TYPE 1 FILM   1.0369   0.0000 I             .100
TYPE 1 HYDRATE      -I       -I I                .350
SECONDARY CRYSTALS   1.8820   0.0000 I                    .270
ROUGHNESS   2.0049  -1.8307 I                 .256
NUMBER OF SECONDARY SITES/SQCM      .40E+07     LIMITING COVERAGE     .790
CRYSTAL. RATE OF SEC. CRYSTALS (A/SQCM),  120.000
CRYSTAL. RATE OF TYPE2 FILM (MA/SQCM),  100.000
SUPERSATURATION OF IONS,   3.6) ,TIME TO REACH(S)      38.7,
INITIAL DISSOLUTION CURRENT (MA/SQCM)  ********
TIMES, ONSET OF SEC. CRYSTALS(SEC)    10.0 PPT. CONSTANT (S)   35.0
TPACK =      244.9   TDISS =       40.0
DEHYDRATION RATE (MA/SQCM)    4.000
EFFECTIVE FILM CURRENT(MA/SQCM)       0.000
POROSITY OF ROUGH LAYER     .250
CURRENT FRACTION FORMING ROUGHNESS     .110
FINAL THICKNESS OF ROUGHNESS      1435.7
WIDTH TO HEIGHT OF SEC. CRYSTALS,      .100
MOLE FRACTION METAL IN PATCHES    0.000
PASSIVATION TIME     2000.00
ADSORP. BY LANGMUIR, MAX. COVERAGE    .251
 BETA =      1.782  KCALS/MOLE
AVE. DISTANCE BETWEEN EXP. AND THEORY       .765  (DEG)

                                EXPERIMENT                THEORY          THICKNESSES(A)
TIME(S)    I(MA/SQCM)    VOLTS      DEL      PSI        DEL       PSI      TYPE2     TYPE1(F)   TYPE1(H)   SECONDARY    COV

     20.0     200.0000     -.0000    77.0700    24.0300    77.0770    24.0611     0.0          .0          0.0          .0    0.000
     40.0     200.0000     -.0000    82.1700    21.1000    82.0353    20.8357     0.0          .0          0.0          .0    0.000
     60.0     200.0000     -.0000    83.2500    21.0300    83.0306    20.8504     0.0          .0          0.0          .0    0.000
     80.0     200.0000     -.0000    82.8300    21.4000
    100.0     200.0000     -.0000    83.2400    21.3500
    120.0     200.0000     -.0000    83.0300    21.4000
    220.0     200.0000     -.0000    87.9900    23.9900
    240.0     200.0000     -.0000    82.5300    24.2000
    300.0     200.0000     -.0000    81.8700    23.2600
    320.0     200.0000     1.0000    74.9000    43.0700
```

[illegible]

[illegible] = 1.0, 1.0, 0.0, 1.0, 1.0, 1.0, 3.5, 0.C,
[illegible] = 0.0, 0.0, 0.0, 4.0, 0.0, 0.0, 0.0,
[illegible]
[illegible] REFRACTIVE INDICES AND POROSITIES,
[illegible] 0.000
[illegible] .200
[illegible] .200
[illegible] .600
[illegible] .074
[illegible] LIMITING COVERAGE .790
[illegible] 1.000
[illegible] 32.000
[illegible] TIME TO REACH(S) 20.34
[illegible] 745.4517
[illegible] 22.0 PPT. CONSTANT (S) 22.0
[illegible]
[illegible]
[illegible] 0.000
[illegible] .074
[illegible] .109
[illegible] 2550.4
[illegible] .170
[illegible] 0.000
[illegible] 1000.00
[illegible] .505
[illegible]
[illegible] 1.725 (DEG)

TIME	I(MA/SQCM)	VOLTS	EXPERIMENT DEL	EXPERIMENT PSI	THEORY DEL	THEORY PSI	THICKNESSES(A) TYPE2	TYPE1(F)	TYPE1(H)	SECONDARY	COV
[illegible]	[illegible]	[illegible]	76.700	24.000	76.250	24.740	0.0	.0	0.0	.0	0.000
[illegible]	[illegible]	[illegible]	82.100	21.100	81.215	20.322	0.0	.0	0.0	.0	0.000
[illegible]	[illegible]	[illegible]	90.500	21.000	88.653	20.418	0.0	.0	0.0	.0	0.000
[illegible]	[illegible]	[illegible]	92.300	21.400	91.631	20.556	0.0	.0	0.0	.0	0.000
[illegible]	[illegible]	[illegible]	93.200	21.500	94.457	20.552	0.0	.0	0.0	.0	0.000
[illegible]	[illegible]	[illegible]	96.500	21.900	99.308	20.698	0.0	.0	0.0	.0	0.000
[illegible]	[illegible]	[illegible]	97.900	23.900							
[illegible]	[illegible]	[illegible]	92.500	26.200							
[illegible]	[illegible]	[illegible]	[illegible]	35.200							
[illegible]	[illegible]	1.000	73.000	[illegible]							

ZR70-5% 200MA 6% KOH

COD-S, 1.0,2.0,3.0,4.0,5.0,6.0,7.0,8.0 = 1.0, 2.0, 0.0, 1.0, 1.0, 1.0, 0.5, 0.0,
CODES, 9.10,11.0,12.0,13.0,14.0 = 0.0, 0.0, 0.0, 0.0, 0.0, 0.0, 2.0,
REFLECTS NUMBER = 0.0
EFFECTIVE REFRACTIVE INDICES AND POROSITIES,
TYPE 2 FILM 2.000 0.0000 I 0.000
TYPE 1 FILM 1.930 0.0000 I .010
TYPE 1 HYDRATE 1.397 0.0000 I .825
SECONDARY CRYSTALS 1.594 0.0000 I .609
RODDIS 2.000 -1.7203 I .565
NUMBER OF SECONDARY SITES/SQCM .50E+06 LIMITING COVERAGE .790
CRYSTAL RATE OF SEC. CRYSTALS (MA/SQCM), 191.165
CRYSTAL RATE OF TYPE2 FILM (MA/SQCM), 191.000
SUPERSATURATION OF IONS, 1.82 ,TIME TO REACH(S) 8.45
INITIAL DISSOLUTION CURRENT (MA/SQCM) 50.3972
TIME CONST OF SEC. CRYSTALS(SEC) 0.3 PPT. CONSTANT (S) 29.0
TIME TO REACH COMPACT FILM I 35.7 S
TIME TO DISSIPATE HYDRATE LAYER 33.5 S
TPACK = 35.2 TDISS = 36.3
DEHYDRATION RATE (MA/SQCM) 1.0-4
EFFECTIVE FILM CURRENT(MA/SQCM) 84.772
POROSITY OF RODDIS LAYER .565
WIDTH OF HEIGHT OF SEC. CRYSTALS, .243
FINAL POROSITY OF TYPE 1 FILM .104
FLEE FRACTION, METAL IN PATCHES 0.300
PASSIVATION TIME 1000.00
AVE. DISTANCE BETWEEN EXP. AND THEORY 2.819 (DEC)

	EXPERIMENT			THEORY		THICKNESSES(A)				
TIME(S)	I(MA/SQCM)	VOLTS	DEL	PSI	DEL	PSI	TYPE2	TYPE1(F)	TYPE1(M)	SECONDARY	COV
25.0	200.000	-.000	92.500	28.200	92.444	30.690	0.0	104.3	-.0	31437.5	.322
50.0	200.000	-.500	90.500	55.200	80.024	33.333	0.0	92.6	-.0	39608.9	.511
75.0	200.000	1.000	73.000	43.200	73.234	43.403	0.0	75.4	-.0	45341.0	.670
-1	-1	-1	-1		-1						

```
 4A7(-6)   1.9MA,1.0(2   6M+.25MZAC

CODES, 1,2,3A,4,5,6,7,8 =  1.0,  2.0,  [illegible],  1.0,  1.0,  1.0,  3.5,  [illegible],
CODES, 9,1 ,11,3,12,13,14 =  [illegible],  [illegible],  [illegible],  4.0,  0.0,  0.0,  0.0,
REYNOLDS NUMBER =  [illegible]
EFFECTIVE REFRACTIVE INDICES AND POROSITIES,
TYPE 2 FILM   2.[illegible]  [illegible]  I  .300
TYPE 1 FILM   1.982   0.000) I  .030
TYPE 1 HYDRATE   -I   -I I  .35
SECONDARY CRYSTALS   1.82)   [illegible] I  .270
ROUGHNESS   2.284  -1.7563 I  .617
NUMBER OF SECONDARY SITES/SQCM  .4[illegible]7   LIMITING COVERAGE  .79
CRYSTAL, RATE OF SEC. CRYSTALS (MA/SQCM), 9[illegible]
CRYSTAL, RATE OF TYPE2 FILM (MA/SQCM), 27.7 [illegible]
SUPERSATURATION OF IONS,  2.7 ,TIME TO REACH(S)  27.9
INITIAL DISSOLUTION CURRENT (MA/SQCM)  431.2407
TIMES, ONSET OF SEC. CRYSTALS(SEC)  35.3 PPT. CONSTANT (S)  12[illegible]
TPACK =  273.5  TDISS =  29.
DEHYDRATION RATE (MA/SQCM)  1.000
EFFECTIVE FILM CURRENT(MA/SQCM)  [illegible]
POROSITY OF ROUGH LAYER  .617
CURRENT FRACTION FORMING ROUGHNESS  .144
FINAL THICKNESS OF ROUGHNESS  3452.[illegible]
WIDTH TO HEIGHT OF SEC. CRYSTALS,  .150
MOLE FRACTION METAL IN PATCHES  0.000
PASSIVATION TIME  1[illegible]
ADSORP. BY LANGMUIR, MAX. COVERAGE  .398
 BETA =  .627
AVE. DISTANCE BETWEEN EXP. AND THEORY  .619 (DEG)
```

			EXPERIMENT		THEORY		THICKNESSES(A)				
TIME(S)	I(MA/SQCM)	VOLTS	DEL	PSI	DEL	PSI	TYPE2	TYPE1(F)	TYPE1(H)	SECONDARY	COV
2.0	100.000	-1.20[illegible]	1 2.3[illegible]	26.5[illegible]	1 2.613	26.696	[illegible]	[illegible]	[illegible]	[illegible]	[illegible]
4.	1[illegible]	-1.20[illegible]	1 4.9[illegible]	22.8[illegible]	1 5.362	22.45[illegible]	.0	.0	0.0	.0	0.000
6.0	100.000	-1.200	111.7[illegible]	22.700	111.268	22.701	0.0	.0	0.0	.0	0.000
8.	1[illegible]	-1.20[illegible]	114.7[illegible]	23.4[illegible]	113.33[illegible]	23.131	[illegible]	[illegible]	[illegible]	[illegible]	[illegible]
1[illegible].0	1[illegible]	-1.2[illegible]	115.1[illegible]	23.700	1[illegible]4.872	23.306	0.0	.0	0.0	.0	0.000
20.0	100.000	-1.200	118.500	23.900	119.999	23.954	0.0	.0	[illegible]	[illegible]	[illegible]
3[illegible].0	[illegible]	-1.2[illegible]	119.1[illegible]	24.6[illegible]							
4[illegible].0	1[illegible]	-1.200	12[illegible].1[illegible]	25.[illegible]							
50.0	100.000	-1.200	124.000	26.300							
6[illegible].0	1[illegible]	-1.2[illegible]	125.[illegible]	26.1[illegible]							
70.0	100.000	-1.200	126.000	27.000							
80.0	100.000	-1.200	126.6[illegible]	28.[illegible]							
9[illegible].0	1[illegible]	-1.2[illegible]	127.[illegible]	27.7[illegible]							
100.0	100.000	-1.200	127.600	29.[illegible]00							
110.0	1[illegible]	-1.2[illegible]	128.4[illegible]	29.2[illegible]							
12[illegible].0	1[illegible]	-1.2[illegible]	129.[illegible]	29.7							
130.0	100.000	-1.200	129.600	30.300							
14[illegible].0	1[illegible]	-1.2[illegible]	127.[illegible]	31.1[illegible]							
15[illegible].0	1[illegible]	-1.2[illegible]	129.[illegible]00	32.2[illegible]							
160.0	100.000	-1.200	124.200	33.600							
17[illegible].0	1[illegible]	-1.2[illegible]	12[illegible].8[illegible]	38.							
18[illegible].0	100.000	-1.200	1[illegible].200	44.800							
183.0	100.000	-1.200	[illegible]5.700	53.460							

ZN7C-61 1.0M4A,1.0   6M+.25MZNC

CODES, 1,2,3A,4,5,6,7,8 = 1.[illegible], 1.0, 0.0, 1.0, 1.0, 1.0, 3.5, 0.0,
CODES, 9,10,11,3,12,13,14 = 0.0, 0.0, 3.0, 3.0, 0.0, 0.0, 0.0,
REYNOLDS NUMBER = [illegible]
EFFECTIVE REFRACTIVE INDICES AND POROSITIES,
TYPE 2 FILM 2.000 0.0000 I .080
TYPE 1 FILM 1.816 [illegible] I .179
TYPE 1 HYDRATE 1.434 0.000) I .852
SECONDARY CRYSTALS 1.933 [illegible] I .1[illegible]
ROUGHNESS 2.918 -2.235 I .6[illegible]7
NUMBER OF SECONDARY SITES/SQCM .4CE+07 LIMITING COVERAGE .790
CRYSTAL. RATE OF SEC. CRYSTALS (MA/SQCM), .[illegible]
CRYSTAL. RATE OF TYPE2 FILM (MA/SQCM), .[illegible]1025
SUPERSATURATION OF IONS, 2.07 ,TIME TO REACH(S) 27.90
INITIAL DISSOLUTION CURRENT (MA/SQCM) 27.7736
TIMES, ONSET OF SEC. CRYSTALS(SEC) 21.9 PPT. CONSTANT (S) 130.0
TIME TO REACH COMPACT FILM I 30.0 S
TIME TO DISSIPATE HYDRATE LAYER 3[illegible] S
TPACK = 30.0 TDISS = 79[illegible].7
DEHYDRATION RATE (MA/SQCM) .[illegible]59
EFFECTIVE FILM CURRENT(MA/SQCM) -12[illegible]6.893
POROSITY OF ROUGH LAYER .607
WIDTH TO HEIGHT OF SEC. CRYSTALS, 1.[illegible]
FINAL POROSITY OF TYPE I FILM .3[illegible]
PCLE FRACTION METAL IN PATCHES .080
PASSIVATION TIME 1[illegible].0
AVE. DISTANCE BETWEEN EXP. AND THEORY 1.034 (DEG)

		EXPERIMENT			THEORY		THICKNESSES(A)				
TIME(S)	I(MA/SQCM)	VOLTS	DEL	PSI	DEL	PSI	TYPE2	TYPE1(F)	TYPE1(H)	SECONDARY	COV
3[illegible].[illegible]	1[illegible].[illegible]	-1.2[illegible]	119.1[illegible]	24.6[illegible]	12[illegible].512	25.029	[illegible].	2.1	-.[illegible]	323.4	.6[illegible]
4[illegible].[illegible]	1[illegible].[illegible]	-1.2[illegible]	12[illegible].1[illegible]	25.[illegible]	122.465	25.606	0.0	6.7	-.0	489.6	.000
5[illegible].0	1[illegible].000	-1.200	124.000	26.000	123.728	26.157	0.0	11.7	-.0	585.7	.[illegible]00
6[illegible].[illegible]	1[illegible].[illegible]	-1.2[illegible]	125.[illegible]	26.1[illegible]	124.781	26.676	[illegible].	16.9	-.[illegible]	657.7	.0[illegible]
7[illegible].[illegible]	1[illegible].[illegible]	-1.2[illegible]	126.[illegible]	27.0[illegible]	125.678	27.165	0.0	22.4	-.0	716.6	.000
8[illegible].0	1[illegible].000	-1.200	126.600	28.000	126.456	27.624	0.0	28.[illegible]	-.[illegible]	767.2	.0[illegible]
9[illegible].[illegible]	1[illegible].[illegible]	-1.2[illegible]	127.[illegible]	27.7	127.143	28.[illegible]54	[illegible].	33.6	-.[illegible]	811.9	.0[illegible]
1[illegible].[illegible]	1[illegible].[illegible]	-1.200	127.6[illegible]	29.0[illegible]	127.759	28.458	0.[illegible]	39.4	-.0	852.1	.000
11[illegible].0	1[illegible].000	-1.200	128.400	29.2[illegible]	128.32[illegible]	28.837	[illegible].	45.1	-.[illegible]	888.8	.0[illegible]
12[illegible].[illegible]	1[illegible].[illegible]	-1.2[illegible]	129.[illegible]	29.7	128.638	29.195	[illegible].	5[illegible].9	-.0	922.8	.000
13[illegible].[illegible]	1[illegible].000	-1.200	129.6[illegible]	30.[illegible]0	129.321	29.521	0.0	56.6	-.0	954.4	.000
14[illegible].0	1[illegible].000	-1.2[illegible]	127.[illegible]	31.1[illegible]							
15[illegible].[illegible]	1[illegible].[illegible]	-1.2[illegible]	129.[illegible]	32.2[illegible]							
16[illegible].0	1[illegible].000	-1.2[illegible]	124.2[illegible]	33.60[illegible]							
17[illegible].[illegible]	1[illegible].[illegible]	-1.2	12[illegible].8	38.[illegible]							
18[illegible].[illegible]	1[illegible].[illegible]	-1.2	1[illegible]2.2	44.8							
18[illegible].[illegible]	1[illegible].000	-1.200	95.[illegible]00	53.400							

ANT-6? 1[illegible]MA,1[illegible] 6M*.254ZNO

CODES, 1,2,3A,4,5,6,7,8 = 1. , 2. , . , 1. , 1. , 1. , 3.5, . ,
CODES, 9,? ,11,3,12,13,14 = . , . , 3. , 3. , . , . , 2. ,
REYNOLDS NUMBER = [illegible]
EFFECTIVE REFRACTIVE INDICES AND POROSITIES,
TYPE 2 FILM 2.[illegible] [illegible] I .3[illegible]
TYPE 1 FILM 1.748 0.0000 I .015
TYPE 1 HYDRATE 1.388 [illegible] I .998
SECONDARY CRYSTALS 1.5[illegible] 0.[illegible] I .750
ROUGHNESS 2.825 -3.1535 I .6[illegible]7
NUMBER OF SECONDARY SITES/SQCM .4 E+ 7 LIMITING COVERAGE .79
CRYSTAL, RATE OF SEC. CRYSTALS (MA/SQCM), 93.29302
CRYSTAL, RATE OF TYPE2 FILM (MA/SQCM), 27.7[illegible]
SUPERSATURATION OF IONS, 2. 7 ,TIME TO REACH(S) 27.9
INITIAL DISSOLUTION CURRENT (MA/SQCM) 23.7971
TIMES, ONSET OF SEC. CRYSTALS(SEC) 21.5 PPT. CONSTANT (S) 57.4
TIME TO REACH COMPACT FILM I 25.9 S
TIME TO DISSIPATE HYDRATE LAYER 250.9 S
TPACK = 25 .5 TDISS = 184.9
DEHYDRATION RATE (MA/SQCM) .985
EFFECTIVE FILM CURRENT(MA/SQCM) -333.825
POROSITY OF ROUGH LAYER .6 7
WIDTH TO HEIGHT OF SEC. CRYSTALS, .129
FINAL POROSITY OF TYPE I FILM .59
MOLE FRACTION METAL IN PATCHES .[illegible]8
PASSIVATION TIME [illegible].30
AVE. DISTANCE BETWEEN EXP. AND THEORY 2.256 (DEG)

		EXPERIMENT			THEORY		THICKNESSES(A)				
TIME(S)	I(MA/SQCM)	VOLTS	DEL	PSI	DEL	PSI	TYPE2	TYPE1(F)	TYPE1(H)	SECONDARY	COV
15.[illegible]	[illegible]	-1.2[illegible]	129.[illegible]	32.20[illegible]	128.999	33.414	0.0	116.9	-.[illegible]	55277.8	.156
16[illegible].[illegible]	[illegible]	-1.2[illegible]	124.2[illegible]	33.6[illegible]	125.118	37.621	[illegible].[illegible]	289.7	-.[illegible]	69646.[illegible]	.248
17 .[illegible]	[illegible]	-1.2[illegible]	12[illegible].8[illegible]	38.0[illegible]	120.308	38.966	[illegible].[illegible]	510.5	-.[illegible]	79725.[illegible]	.323
18 .[illegible]	[illegible].[illegible]	-1.2[illegible]	102.2[illegible]	44.80[illegible]	102.233	43.961	0.0	794.9	-.[illegible]	87748.8	.394
183.	[illegible]	-1.2	95.7	53.4[illegible]							

```
 AR70-62   200KA,1000   6M*.25MZNO

CODES, 1,2,3,4,5,6,7,8 =  1.0,  2.0,  0.0,  1.0,  1.0,  1.0,  3.5,  0.0,
CODES, 9,10,11,12,13,14 =  0.0,  0.0,  0.0,  4.0,  0.0,  0.0,  0.0,
REYNOLDS NUMBER =      0.0
EFFECTIVE REFRACTIVE INDICES AND PERMITTIES,
TYPE 2 FILM    2.000    0.00000 I              .300
TYPE 1 FILM    2.000    0.00000 I              .190
TYPE 1 HYDRATE    1.307    0.0000 I              .350
SECONDARY CRYSTALS    1.000    0.0000 I              .270
ROUGHNESS    1.333   -1.0E-16 I              .696
NUMBER OF SECONDARY SITES/SEC-1      .403E+07      LIMITING COVERAGE     .790
CRYSTALS RATE OF SEC. CRYSTALS (MA/SEC-M), 90.000000
CRYSTALS RATE OF TYPE 2 FILM (MA/SEC-M), 27.77348
SUPERSATURATION OF ICNS,    4.03 ,TIME TO REACH(S)      38.49
INITIAL DISSOLUTION CURRENT (MA/SEC-M)  ********
TIMES, ONSET OF SEC. CRYSTALS(SEC)    39.5 PPT. CONSTANT (S)  120.0
TPACK =       2.0  TDISS =      290.0
OXYDATION RATE (MA/SEC-M)   38.027
EFFECTIVE FILM CURRENT(MA/SEC-M)       0.000
POROSITY OF ROUGH LAYER     .696
CURRENT FRACTION FORMING ROUGHNESS     .082
FINAL THICKNESS OF ROUGHNESS      373.6
WIDTH TO HEIGHT OF SEC. CRYSTALS,      .150
PORE FRACTION TOTAL AT PATCHES    0.000
PASSIVATION TIME      2000.00
AVERAGE BY LANGMUIR, MAX. COVERAGE    .838
 DELTA =      1.710  KCALS/MOLE
AVG. DISTANCE BETWEEN CAP. AND THEORY      1.273  (DEG)

                                EXPERIMENT                    THEORY              THICKNESSES(A)
TIME(S)     I(MA/SEC-M)    VOLTS      DEL      PSI        DEL        PSI       TYPE2     TYPE1(F)   TYPE1(H)   SECONDARY     COV

     2.0      200.000     -.930     90.500     29.300     88.334     28.456      0.0        .0         0.0         .0       0.000
     4.0      200.000     -.930     93.100     26.200     93.347     28.408      0.0        .0         0.0         .0       0.000
     6.0      200.000     -.930     93.100     26.200     96.495     28.419      0.0        .0         0.0         .0       0.000
     8.0      200.000     -.930     90.300     29.100     98.773     28.449      0.0        .0         0.0         .0       0.000
    10.0      200.000     -.910     99.100     27.900
    20.0      200.000     -.770    101.100     27.600
    30.0      200.000     -.720    104.500     27.700
    40.0      200.000     1.000    104.900     27.500
    50.0      200.000     -.180     99.900     27.100
    60.0      200.000     -.330     87.500     28.700
    70.0      200.000     -.830     73.300     35.500
    80.0      200.000     -.940     87.700     39.300
    90.0      200.000    -1.150     94.000     45.100
   100.0      200.000    -1.100     97.200     42.500
```

```
  ZNTO-e2   200MA,100C   SM=.25PZAC

CCOES, 1.e-3,e-3,e-2,7,5 =  1.0,  2.0,  4.0,  1.0,  1.0,  1.0,  5.5,  0.0,
CCOFS, 5.e-2,1.e-2,2.e-2,3,14 =  0.0,  0.0,  0.0,  4.0,  0.0,  0.0,  0.0,
KEYAGEUS NUMBER =      0.0
EFFECTIVE NONREACTIVE INDICES AND POROSITIES,
TYPE 2 FILM   2.000   0.0000 I            0.100
TYPE 1 FILM   2.000   0.0000 I            0.000
TYPE 1 INTERMEDIATE   1.445   0.0000 I            .822
SECONDARY CRYSTALS   1.020   0.0000 I            .270
ROUGHNESS   .e97e  -1.e-691 I            .e56
NUMBER OF SECONDARY SITES/SQCM      .40E+07      LIMITING COVERAGE     .790
CRYSTAL RATE OF SEC. CRYSTALS (MA/SQCM),  148.271
CRYSTAL RATE OF TYPE2 FILM (MA/SQCM),  166.709
SUPERSATURATION OF IONS,   2.69  TIME TO REACH(S)     13.70
INITIAL DISSOLUTION CURRENT (MA/SQCM)    82.5165
TIMES, ONSET OF SEC. CRYSTALS(SEC)     9.0 PPT. CONSTANT (S)    52.3
TPROM =      2.8  TOISS =      43.0
DEPOSITION RATE (MM/SEC.M)    2.e-6
EFFECTIVE FILM CURRENT(MA/SQCM)     114.950
POROSITY OF ROUGH LAYER     .695
CURRENT FRACTION PERFECT ROUGHNESS     .062
FINAL THICKNESS OF ROUGHNESS       377.4
WIDTH TO HEIGHT OF SEC. CRYSTALS,     .150
PORE FRACTION METAL IN PATCHES    0.000
PASSIVATION TIME      1000.00
RUSCKP. BY LANGMUIR, MAX. COVERAGE  0.000
 BETA =     1.e5e  KCALS/MOLE
AVG. DISTANCE BETWEEN EXP. AND THEORY       .766  (DEG)

                                EXPERIMENT                THEORY          THICKNESSES(A)
TIME(S)    I(MA/SQCM)   VOLTS      DEL      PSI        DEL       PSI       TYPE2     TYPE1(IP)  TYPE1(IM)  SECONDARY    COV

    10.0     200.000    -.910     99.100    27.900    99.097    27.916      0.0         .0         0.0         .0    0.000
    20.0     200.000    -.750    101.100    27.000   101.152    26.640      0.0       82.4         -.0    40804.3     .037
    30.0     200.000    -.720    101.600    27.700   100.399    27.569      0.0      206.2         -.0    81410.4     .059
    42.0     200.000     1.000    104.900    27.500
    54.0     200.000     -.130     99.900    27.100
    64.0     200.000     -.330     97.800    26.700
    80.0     200.000     -.360     98.300    25.500
    90.0     200.000     -.640     97.700    39.300
   100.0     200.000    -1.e50     94.800    43.100
   500.0     200.000    -1.e10     97.200    42.500
```

```
  ZN70-6SS   500MA,1010   6M*.25M2NO

CODES, 1,2,3A,4,5,6,7,8 =  1.0,  2.0,  4.0,  1.0,  1.0,  1.0,  3.5,  0.0,
CODES, 9,10,11,3,12,13,14 =  0.0,  0.0,  0.0,  4.0,  0.0,  0.0,  0.0,
REYNOLDS NUMBER =      0.0
EFFECTIVE REFRACTIVE INDICES AND POROSITIES,
TYPE 2 FILM    2.000    0.0000 I              0.000
TYPE 1 FILM    1.795    0.0000 I               .334
TYPE 1 HYDRATE    1.367    0.0000 I                .999
SECONDARY CRYSTALS    1.820    0.0000 I                    .270
ROUGHNESS    1.472    -.3668 I                 .339
NUMBER OF SECONDARY SITES/SQCM      .4028+07     LIMITING COVERAGE     .790
CRYSTAL, RATE OF SEC, CRYSTALS (MA/SQCM),  353.301
CRYSTAL, RATE OF TYPE2 FILM (MA/SQCM),  422.719
SUPERSATURATION OF ION,S,   2.03 ,TIME TO REACH(S)       1.09
INITIAL DISSOLUTION CURRENT (MA/SQCM)  225.9879
TIMES, OFSET OF SEC, CRYSTALS(SEC)    1.4 PPT, CONSTANT (S)   67.8
TMALK =      1.9  TDISS =      40.0
DEHYDRATION RATE (MA/SQCM)     .003
EFFECTIVE FILM CURRENT(MA/SQCM)      54.628
POROSITY OF ROUGH LAYER     .389
CURRENT FRACTION LEAKING ROUGHNESS     .001
FINAL THICKNESS OF ROUGHNESS        15.8
RATIO TO HEIGHT OF SEC, CRYSTALS,      .150
MOLE FRACTION METAL IN PATCHES   0.000
PASSIVATION TIME     1000.00
AVG,KMP, OF LANGMUIR, MAX, COVERAGE   0.000
 BETA =     0.000  KCALS/MOLE
AVG, DISTANCE BETWEEN PAP, AND THEORY     2.822  (DEG)

                                EXPERIMENT                    THEORY          THICKNESSES(A)
TIME(S)    I(MA/SQCM)    VOLTS     DEL      PSI        DEL        PSI      TYPE2     TYPE1(F)  TYPE1(M)  SECONDARY    COV

      .0      500.000    -.700     76.300     80.300     77.955     80.050      0.0        .0        0.0        .0     0.000
     1.00     500.000    -.690     79.500     27.100     78.041     29.886      0.0        .0        0.0        .0     0.000
     2.00     500.000     0.000     85.900     25.900     84.200     27.863      0.0        .0       -.0 17081.1     .007
     3.00     500.000    -.710     81.100     25.000
     4.00     500.000    -1.200     86.700     26.100
     5.00     500.000    -1.200     72.500     27.300
     6.00     500.000    -1.200     72.500     26.400
     7.00     500.000    -1.200     74.300     26.400
     8.00     500.000    -1.200     70.300     28.000
     9.00     500.000    -1.200     73.300     24.100
    10.00     500.000    -1.200     74.700     27.900
    11.00     500.000    -1.200     74.900     27.700
    20.00     500.000    -1.200     72.100     27.700
```

4M2C16.200MA/SQCM,3000 RE.1010 CRYSTAL

CODES, 1,2,3A,4,5,6,7,8 = 1.0, 0.0, 0.0, 1.0, 1.0, 1.0, 3.5, 0.0,
CODES, 9,10,11,3,12,13,14 = 0.0, 0.0, 0.0, 4.0, 0.0, 0.0, 0.0,
REYNOLDS NUMBER = 3000.0
EFFECTIVE REFRACTIVE INDICES AND POROSITIES,
TYPE 2 FILM 2.000 0.0000 I C.000
TYPE 1 FILM 2.000 0.0000 I C.000
TYPE 1 HYDRATE 1.340 0.0000 I .990
SECONDARY CRYSTALS 2.000 C.0000 I 0.000
ROUGHNESS 2.467 -2.3474 I .262
NUMBER OF SECUNDARY SITES/SQCM .10E+07 LIMITING COVERAGE .790
CRYSTAL, RATE OF SEC, CRYSTALS (MA/SQCM), .010
CRYSTAL, RATE OF TYPE2 FILM (MA/SQCM), .010
SUPERSATURATION OF IONS, 3.92 ,TIME TO REACH(S) 39.29
INITIAL DISSOLUTION CURRENT (MA/SQCM) ********
TIME, ONSET OF SEC, CRYSTALS(SEC) 27.0 PPT, CONSTANT (S) 2.0
TPACK = 2.2 TDISS = 12.0
DEHYDRATION RATE (MA/SQCM) 60.000
EFFECTIVE FILM CURRENT(MA/SQCM) 0.000
POROSITY OF ROUGH LAYER .262
CURRENT FRACTION FORMING ROUGHNESS .273
FINAL THICKNESS OF ROUGHNESS 821.0
WIDTH TO HEIGHT OF SEC, CRYSTALS, 1.000
MOLE FRACTION METAL IN PATCHES 0.000
PASSIVATION TIME 1000.00
ADSORP, BY LANGMUIR, MAX, COVERAGE .111
BETA = 2.715 KCALS/MOLE
AVE, DISTANCE BETWEEN EXP, AND THEORY 1.524 (DEG)

		EXPERIMENT			THEORY		THICKNESSES(A)				
TIME(S)	I(MA/SQCM)	VOLTS	DEL	PSI	DEL	PSI	TYPE2	TYPE1(F)	TYPE1(H)	SECONDARY	COV
2.0	200.000	-1.260	78.390	26.200	77.673	24.697	.0	0.0	0.0	.0	0.000
3.0	200.000	-1.260	81.040	24.630	80.080	24.579	.0	0.0	0.0	.0	0.000
4.0	200.000	-1.250	82.950	23.850	81.994	24.503	.0	0.0	0.0	.0	0.000
5.0	200.000	-1.240	84.580	23.670	83.600	24.452	.0	0.0	0.0	.0	0.000
10.0	200.000	-1.240	89.650	23.310	89.256	24.361	.0	0.0	0.0	.0	0.000
15.0	200.000	-1.220	92.420	23.510	93.002	24.376	.0	0.0	0.0	.0	0.000
20.0	200.000	-1.220	94.220	23.500	95.828	24.428	.0	0.0	0.0	.0	0.000
25.0	200.000	-1.220	96.000	23.580	98.099	24.495	.0	0.0	0.0	.0	0.000
30.0	200.000	-1.210	97.910	24.160							
35.0	200.000	-1.200	97.110	25.660							
40.0	200.000	-1.200	96.930	27.150							
45.0	200.000	-1.200	94.570	28.680							
50.0	200.000	-1.190	90.160	37.700							
55.0	200.000	-1.190	84.420	44.620							

ZN2+ 18.2[illegible] MA/SQCM,3.[illegible] RE,1.[illegible] CRYSTAL

CODES, 1,2,3A,4,5,6,7,8 = 1.[illegible], -2.[illegible], [illegible], 1.[illegible], 1.[illegible], 1.[illegible], 3.5, [illegible],
CODES, 9,10,11,3,12,13,14 = 0.0, 0.0, 7.0, 3.0, 1.0, 0.0, 2. ,
REYNOLDS NUMBER = 3[illegible]
EFFECTIVE REFRACTIVE INDICES AND POROSITIES,
TYPE 2 FILM 2.000 0.0000 I .[illegible]
TYPE 1 FILM 1.999 [illegible] I .[illegible]2
TYPE 1 HYDRATE 1.436 0.[illegible] I .45[illegible]
SECONDARY CRYSTALS 1.552 -.[illegible] I .673
ROUGHNESS 1.542 -2.5644 I .373
NUMBER OF SECONDARY SITES/SQCM .30E+07 LIMITING COVERAGE .796
CRYSTAL, RATE OF SEC. CRYSTALS (MA/SQCM), 84.1[illegible]
CRYSTAL, RATE OF TYPE2 FILM (MA/SQCM), .883
SUPERSATURATION OF IONS, .83 ,TIME TO REACH(S) 22.43
INITIAL DISSOLUTION CURRENT (MA/SQCM) 199.941
TIMES, ONSET OF SEC. CRYSTALS(SEC) 26.[illegible] PPT. CONSTANT (S) 2.0
TIME TO COMPLETE PATCH COVERAGE 74.3
TIME TO REACH COMPACT FILM I 25.[illegible] S
TIME TO DISSIPATE HYDRATE LAYER 25.0 S
TPACK = 25.[illegible] TDISS = 74.3
DEHYDRATION RATE (MA/SQCM) 122.186
EFFECTIVE FILM CURRENT(MA/SQCM) 3.952
POROSITY OF ROUGH LAYER .373
CURRENT FRACTION FORMING ROUGHNESS .40
FINAL THICKNESS OF ROUGHNESS 2641.6
WIDTH TO HEIGHT OF SEC. CRYSTALS, 1.0[illegible]
INITIAL PATCH COVERAGE .476
FINAL POROSITY OF TYPE I FILM .000
MOLE FRACTION METAL IN PATCHES .00[illegible]
PASSIVATION TIME 1000.00
AVE. DISTANCE BETWEEN EXP. AND THEORY 3.448 (DEG)

		EXPERIMENT			THEORY		THICKNESSES(A)				
TIME(S)	I(MA/SQCM)	VOLTS	DEL	PSI	DEL	PSI	TYPE2	TYPE1(F)	TYPE1(M)	SECONDARY	COV
31.0	200.000	-1.210	97.910	24.160	98.580	23.050	0.0	0.0	-.0	9310.2	.031
35.	20[illegible].[illegible]	-1.20[illegible]	97.11[illegible]	25.66	94.445	26.726	.	.	-.	9394.1	.031
45.[illegible]	2[illegible].[illegible]	-1.2[illegible]	94.572	28.680	94.833	33.430	.0	0.[illegible]	-.0	9348.2	.0331
50.0	200.000	-1.190	90.160	37.700	91.453	37.542	0.0	0.0	-.	9241.6	.03
55.[illegible]	20[illegible].[illegible]	-1.19[illegible]	84.42[illegible]	44.62	85.147	39.654	.	.	-.[illegible]	9 97.[illegible]	.[illegible]29
-I	-I	-I	-I	-I							

ZN20018,200MA/SQCM,3000 RE,1010 CRYSTAL

CODES, 1,2,3A,4,5,6,7,8 = 1.0, 2.0, 0.0, 1.0, 1.0, 1.0, 3.5, 0.0,
CODES, 9,10,11,3,12,13,14 = 0.0, 0.0, 7.0, 3.0, 1.0, 0.0, 2.0,
REYNOLDS NUMBER = 3000.0
EFFECTIVE REFRACTIVE INDICES AND POROSITIES,
TYPE 2 FILM 2.000 0.0000 I 0.000
TYPE 1 FILM 1.786 0.0000 I .399
TYPE 1 HYDRATE 1.448 0.0000 I .475
SECONDARY CRYSTALS 1.501 0.0000 I .750
ROUGHNESS 1.463 -2.5644 I .373
NUMBER OF SECONDARY SITES/SQCM .30E+07 LIMITING COVERAGE .790
CRYSTAL. RATE OF SEC. CRYSTALS (MA/SQCM), 16.778
CRYSTAL. RATE OF TYPE2 FILM (MA/SQCM), 8.269
SUPERSATURATION OF IONS, .21 ,TIME TO REACH(S) .23
INITIAL DISSOLUTION CURRENT (MA/SQCM) 50.5076
TIMES, ONSET OF SEC. CRYSTALS(SEC) 26.0 PPT. CONSTANT (S) 2.0
TIME TO COMPLETE PATCH COVERAGE 85.9
TIME TO REACH COMPACT FILM I 25.0 S
TIME TO DISSIPATE HYDRATE LAYER 25.0 S
TPACK = 25.0 TDISS = 85.9
DEHYDRATION RATE (MA/SQCM) 2.726
EFFECTIVE FILM CURRENT(MA/SQCM) 49.335
POROSITY OF ROUGH LAYER .373
CURRENT FRACTION FORMING ROUGHNESS .040
FINAL THICKNESS OF ROUGHNESS 3392.6
WIDTH TO HEIGHT OF SEC. CRYSTALS, 1.000
INITIAL PATCH COVERAGE .342
FINAL POROSITY OF TYPE I FILM .296
MOLE FRACTION METAL IN PATCHES 0.000
PASSIVATION TIME 1000.00
AVE. DISTANCE BETWEEN EXP. AND THEORY 4.800 (DEG)

		EXPERIMENT			THEORY		THICKNESSES(A)				
TIME(S)	I(MA/SQCM)	VOLTS	DEL	PSI	DEL	PSI	TYPE2	TYPE1(F)	TYPE1(H)	SECONDARY	COV
30.0	200.000	-1.210	97.910	24.160	97.521	22.587	0.0	.1	-.0	11018.9	.043
35.0	200.000	-1.200	97.110	25.660	98.909	33.697	0.0	52.7	-.0	16542.1	.096
45.0	200.000	-1.200	94.570	28.680	96.327	34.733	0.0	174.2	-.0	21262.5	.159
50.0	200.000	-1.190	90.160	37.700	88.680	38.159	0.0	261.7	-.0	22470.5	.178
55.0	200.000	-1.190	84.420	44.620	84.621	43.011	0.0	352.5	-.0	23246.6	.190
-I	-I	-I	-I	-I							

ZN20021,389MA/SQCM,9000 RE,POLY-2 CRYSTAL

CODES, 1,2,3A,4,5,6,7,8 = 1.0, 0.0, 0.0, 1.0, 1.0, 1.0, 3.5, 0.0,
CODES, 9,10,11,3,12,13,14 = 3.0, 0.0, 0.0, 4.0, 0.0, 0.0, 0.0,
REYNOLDS NUMBER = 900.0
EFFECTIVE REFRACTIVE INDICES AND POROSITIES,
TYPE 2 FILM 2.000 0.0000 I 0.000
TYPE 1 FILM 2.000 0.0000 I 0.000
TYPE 1-HYDRATE 1.390 0.0000 I .950
SECONDARY CRYSTALS 2.000 0.0000 I 0.000
ROUGHNESS 1.370 -1.7408 I .167
NUMBER OF SECONDARY SITES/SQCM .10E+07 LIMITING COVERAGE .790
CRYSTAL. RATE OF SEC. CRYSTALS (MA/SQCM), .010
CRYSTAL. RATE OF TYPE2 FILM (MA/SQCM), .010
SUPERSATURATION OF IONS, 3.16 ,TIME TO REACH(S) 6.35
INITIAL DISSOLUTION CURRENT (MA/SQCM) 822.9932
TIMES, ONSET OF SEC. CRYSTALS(SEC) 27.0 PPT. CONSTANT (S) 2.0
TPACK = 2.2 TDISS = 12.0
DEHYDRATION RATE (MA/SQCM) 120.000
EFFECTIVE FILM CURRENT(MA/SQCM) 0.000
POROSITY OF ROUGH LAYER .167
CURRENT FRACTION FORMING ROUGHNESS .034
FINAL THICKNESS OF ROUGHNESS 96.5
WIDTH TO HEIGHT OF SEC. CRYSTALS, 1.000
POLE FRACTION METAL IN PATCHES 0.000
PASSIVATION TIME 1000.00
ADSORP. BY LANGMUIR, MAX. COVERAGE .048
BETA = 3.251 KCALS/MOLE
AVE. DISTANCE BETWEEN EXP. AND THEORY .979 (DEG)

		EXPERIMENT			THEORY		THICKNESSES(A)				
TIME(S)	I(MA/SQCM)	VOLTS	DEL	PSI	DEL	PSI	TYPE2	TYPE1(F)	TYPE1(H)	SECONDARY	COV
0.0	400.000	-1.370	53.240	34.120	53.240	34.120	.0	0.0	0.0	.0	0.000
.3	400.000	-1.180	55.690	33.770	57.690	33.595	.0	0.0	0.0	.0	0.000
1.3	400.000	-1.120	58.970	33.310	59.595	33.331	.0	0.0	0.0	.0	0.000
2.3	400.000	-1.120	61.400	33.190	61.879	33.094	.0	0.0	0.0	.0	0.000
3.3	400.000	-1.110	63.210	33.310	63.595	32.929	.0	0.0	0.0	.0	0.000
4.3	400.000	-1.100	65.040	33.140	64.997	32.801	.0	0.0	0.0	.0	0.000
5.4	400.000	-1.090	67.270	33.100	66.307	32.688	.0	0.0	0.0	.0	0.000
6.3	400.000	-1.050	68.270	33.170	67.249	32.611	.0	0.0	0.0	.0	0.000
7.3	400.000	2.620	57.130	40.480							
8.3	400.000	2.810	40.100	52.510							
9.3	400.000	2.380	23.910	62.660							
10.3	400.000	2.330	8.780	63.170							
11.3	400.000	2.330	-6.470	63.300							
12.3	400.000	-.060	-12.860	63.470							
13.3	400.000	-.950	-11.880	63.570							
14.3	400.000	-1.370	43.260	64.670							
18.3	400.000	-1.370	55.440	38.990							
22.3	400.000	-1.370	55.520	38.020							

ZN2(021.4( )MA/SQCM,9.(RE,POLY-2 CRYSTAL

CODES, 1,2,3A,4,5,6,7,8 = 1.0, 2.0, 0.1, 1.0, 1.0, 1.0, 3.5, 0.1,
CODES, 9,10,11,3,12,13,14 = 0.0, 0.0, 7.0, 3.0, 1.0, 0.0, 2.0,
REYNOLDS NUMBER = 9...
EFFECTIVE REFRACTIVE INDICES AND POROSITIES,
TYPE 2 FILM 2.000 0.0000 I 0.000
TYPE 1 FILM 1.793 ...) I .358
TYPE 1 HYDRATE 1.458 0.0000 I .705
SECONDARY CRYSTALS 2.000 0.0 I .
ROUGHNESS 1.41 -2.9939 I .268
NUMBER OF SECONDARY SITES/SQCM .10E+08 LIMITING COVERAGE .790
CRYSTAL, RATE OF SEC, CRYSTALS (MA/SQCM), 152.535
CRYSTAL, RATE OF TYPE2 FILM (MA/SQCM), 20.000
SUPERSATURATION OF IONS, .68 ,TIME TO REACH(S) .29
INITIAL DISSOLUTION CURRENT (MA/SQCM) 65.2237
TIMES, ONSET OF SEC, CRYSTALS(SEC) 6.5 PPT, CONSTANT (S) 2.0
TIME TO COMPLETE PATCH COVERAGE 26.8
TIME TO REACH COMPACT FILM I 8.7 S
TIME TO DISSIPATE HYDRATE LAYER 8.7 S
TPACK = 8.7 TDISS = 26.8
DEHYDRATION RATE (MA/SQCM) 380.00
EFFECTIVE FILM CURRENT(MA/SQCM) 226.663
POROSITY OF ROUGH LAYER .268
CURRENT FRACTION FORMING ROUGHNESS .06
FINAL THICKNESS OF ROUGHNESS 1274.7
WIDTH TO HEIGHT OF SEC, CRYSTALS, 1.000
INITIAL PATCH COVERAGE .637
FINAL POROSITY OF TYPE I FILM .145
MOLE FRACTION METAL IN PATCHES 0.00
PASSIVATION TIME 1.0..
AVE, DISTANCE BETWEEN EXP, AND THEORY 2.14 (DEG)

		EXPERIMENT			THEORY		THICKNESSES(A)				
TIME(S)	I(MA/SQCM)	VOLTS	DEL	PSI	DEL	PSI	TYPE2	TYPE1(F)	TYPE1(H)	SECONDARY	COV
7.3	400.000	2.62	57.130	40.48	55.333	4..378	.	4.	-.	4158.4	. 2
8.3	4(..0	2.81	4..1..	52.51	41.916	51.254	.	2488.3	-.3	6306.2	.047
9.3	40..00.	2.380	23.91)	62.66.							
10.3	400.000	2.33	8.78.	63.17							
11.3	4 ..	2.33	-6.47	63.3							
12.3	400.00	-.061	-12.860	63.470							
13.3	4(...	-.95	-11.88.	63.57							
14.3	400.000	-1.370	43.260	64.67.							
18.3	400.000	-1.370	55.440	38.99							
22.3	4 ..	-1.37	55.52	38. 2							

ZN2[22.458MA/SQCM,.4560 RF.1000 CRYSTAL

CODES. 1.2.3A.4.5.6.7.8 = 1. . . . . 1. . 1. . 1. . 3.5. . .
CODES. 9.1 .11.3.12.13.14 = .0. 3.0. 0.. 4.. 0.0. 0.. 0..
KEYNOLDS NUMBER = 4560.0
EFFECTIVE REFRACTIVE INDICES AND POROSITIES.
TYPE 2 FILM 2.0[0.[[[I 0.0[.
TYPE 1 FILM 2.000 3.0000 I 0.000
TYPE 1 HYCRATE 1.39 . . I .99[
SECONDARY CRYSTALS 2.000 .0000[I 1.000
ROUGHNESS 2.398 -2.4197 I .181
NUMBER OF SECONDARY SITES/SQCM .1 E+ 7 LIMITING COVERAGE .79
CRYSTAL. RATE OF SEC. CRYSTALS (MA/SQCM), .[1
CRYSTAL. RATE OF TYPE2 FILM (MA/SQCM), .[1
SUPERSATURATION OF IONS, 3.45 ,TIME TO REACH(S) 5.81
INITIAL DISSOLUTION CURRENT (MA/SQCM) 901.1100
TIMES. ONSET OF SEC. CRYSTALS(SEC) 27.[PPT. CONSTANT (S) 2.
TPACK = 2.2 TDISS = 12.[
DEPYDRATION RATE (MA/SQCM) 137.400
EFFECTIVE FILM CURRENT(MA/SQCM) .[
POROSITY OF ROUGH LAYER .181
CURRENT FRACTION FORMING ROUGHNESS .300
FINAL THICKNESS OF ROUGHNESS 1317.4
WIDTH TO HEIGHT OF SEC. CRYSTALS, 1.00[
MOLE FRACTION METAL IN PATCHES 0.000
PASSIVATION TIME [.[.0.
ADSORP. BY LANGMUIR, MAX. COVERAGE .055
BETA = 3.114 KCALS/MOLE
AVE. DISTANCE BETWEEN EXP. AND THEORY 1.622 (DEG)

		EXPERIMENT			THEORY		THICKNESSES(A)				
TIME(S)	I(MA/SQCM)	VOLTS	DEL	PSI	DEL	PSI	TYPE2	TYPE1(F)	TYPE1(H)	SECONDARY	COV
.7	458.[[	-1.1[	73.75[	26.39	74.999	25.354	.	.	.	.	.
1.7	458.[[	-1.[8	82.63[	24.45	80.369	25.027	.	0.0	0.0	.[	0.000
2.7	458.000	-1.060	84.920	25.360	83.599	24.913	.0	0.0	0.0	.	.
3.7	458.[[[	-1.0[	84.62[	24.56	86.[63	24.857	.	.	.	.	.
4.[	458.[	-.96	85.850	24.37[	86.706	24.846	.0	0.[	0.0	.[	0.000
4.7	458.000	2.850	73.970	32.080							
5.7	458.[	2.76	55.45[	45.26							
6.7	458.00[	2.40[	37.730	58.450							
7.7	458.000	-.900	34.420	59.540							
8.7	458.[	-1.37	48.21[	55.82							
9.7	458.00[	-1.37[	54.990	46.09[							
10.7	458.000	-1.370	54.90[	41.9							
11.7	458.[	-1.37	54.[5	39.91							
12.7	458.000	-1.370	53.530	38.810							
13.7	458.[	-1.37[	53.28	39.4							
14.7	458.[	-1.37	53.38[	38.11							
22.7	458.000	-1.370	53.370	38.310							

ZN2C322,458MA/SQCM,4560 RE,1000 CRYSTAL

CODES, 1,2,3A,4,5,6,7,8 = 1.0, 2.0, 0.0, 1.0, 1.0, 1.0, 3.5, 0.0,
CODES, 9,10,11,3,12,13,14 = 0.0, 0.0, 7.0, 3.0, 1.0, 0.0, 2.0,
REYNOLDS NUMBER = 4560.0
EFFECTIVE REFRACTIVE INDICES AND POROSITIES,
TYPE 2 FILM 2.000 0.0000 I 0.000
TYPE 1 FILM 1.861 0.0000 I .240
TYPE 1 HYDRATE 1.463 0.0000 I .709
SECONDARY CRYSTALS 1.997 0.0000 I .005
ROUGHNESS 1.518 -2.3763 I .419
NUMBER OF SECONDARY SITES/SQCM .143+08 LIMITING COVERAGE .790
CRYSTAL, RATE OF SEC. CRYSTALS (MA/SQCM), 169.251
CRYSTAL, RATE OF TYPE2 FILM (MA/SQCM), 20.000
SUPERSATURATION OF IONS, .71 ,TIME TO REACH(S) .74
INITIAL DISSOLUTION CURRENT (MA/SQCM) 117.7222
TIMES, UNSLT OF SEC. CRYSTALS(SEC) 4.1 EFT. CONSTANT (S) 2.0
TIME TO COMPLETE PATCH COVERAGE 21.5
TIME TO REACH COMPACT FILM I 9.5 S
TIME TO DISSIPATE HYDRATE LAYER 9.5 S
TPACK = 9.5 TDISS = 21.5
DEHYDRATION RATE (MA/SQCM) 435.100
EFFECTIVE FILM CURRENT(MA/SQCM) 243.716
POROSITY OF ROUGH LAYER .419
CURRENT FRACTION FORMING ROUGHNESS .045
FINAL THICKNESS OF ROUGHNESS 972.2
WIDTH TO HEIGHT OF SEC. CRYSTALS, 1.000
INITIAL PATCH COVERAGE .655
FINAL POROSITY OF TYPE I FILM .100
MOLE FRACTION METAL IN PATCHES 0.000
PASSIVATION TIME 1000.00
AVE. DISTANCE BETWEEN EXP. AND THEORY 1.066 (DEG)

		EXPERIMENT			THEORY		THICKNESSES(A)				
TIME(S)	I(MA/SQCM)	VOLTS	DEL	PSI	DEL	PSI	TYPE2	TYPE1(P)	TYPE1(M)	SECONDARY	COV
4.7	458.000	2.650	73.970	32.080	73.541	30.790	0.0	2.3	-.0	3884.1	.025
5.7	458.000	2.760	52.450	45.290	55.656	45.196	0.0	2123.8	-.0	6324.4	.066
6.7	456.000	2.400	37.730	53.450							
7.7	453.000	-.900	34.420	59.540							
8.7	458.000	-1.370	48.210	53.820							
9.7	456.000	-1.370	54.990	46.090							
10.7	458.000	-1.370	54.900	41.900							
11.7	456.000	-1.370	54.050	39.610							
12.7	458.000	-1.370	53.530	38.810							
13.7	458.000	-1.370	53.230	39.400							
14.7	456.000	-1.370	53.360	38.110							
22.7	456.000	-1.370	53.370	38.110							

 &N200 I=.472MA/SQCM,ILOOO R=.1000

CODES= 1.2.3A.4.5.6.7.8 = 1.0, 0.0, 0.0, 1.0, 1.0, 1.0, 0.5, 0.0,
CODES= 9.10.11.12.13.14 = 0.0, 0.0, 0.0, 4.0, 0.0, 0.0, 0.0,
REYNOLDS NUMBER = 11000.0
EFFECTIVE REFRACTIVE INDICES AND POROSITIES,
TYPE 2 FILM 2.000 0.0000 I 0.000
TYPE 1 FILM 2.000 0.0000 I 0.000
TYPE 1 HYDRATE 1.356 0.0000 I .950
SECONDARY CRYSTALS 2.000 0.0000 I 0.000
ROUGHNESS 1.191 -1.6927 I 0.000
NUMBER OF SECONDARY SITES/SQCM .1D+07 LIMITING COVERAGE .790
CRYSTAL. RATE OF SEC. CRYSTALS (MA/SQCM), .010
CRYSTAL. RAT. OF TYPE2 FILM (MA/SQCM), .010
SUPERSATURATION OF IONS, 1.1) .TIME TO REACH(S) .36
INITIAL DISSOLUTION CURRENT (MA/SQCM) 287.2701
TIMES. ONSET OF SEC. CRYSTALS(SEC) 27.0 PPT. CONSTANT (S) 2.0
TPALK = 4.0 TDISS = 12.0
DEHYDRATION RATE (MA/SQCM) 141.600
EFFECTIVE FILM CURRENT(MA/SQCM) .009
WIDTH TO HEIGHT OF SEC. CRYSTALS, 1.000
POLE FRACTION METAL IN PATCHES 0.000
PASSIVATION TIME 1000.00
ADSORP. BY LANGMUIR, MAX. COVERAGE 0.000
 DETA = 5.000 KCALS/MOLE
AVE. DISTANCE BETWEEN EXP. AND THEORY .127 (DEG)

			EXPERIMENT		THEORY		THICKNESSES(A)				
TIME(S)	I(MA/SQCM)	VOLTS	DEL	PSI	DEL	PSI	TYPE2	TYPE1(F)	TYPE1(H)	SECONDARY	COV
0.0	472.000	-1.070	45.970	35.300	43.970	35.500	.0	0.0	0.0	.0	0.000
.1	472.000	-1.080	46.680	35.460	45.873	35.367	.0	0.0	0.0	.0	0.000
1.1	472.000	-1.060	49.750	35.010	49.743	34.962	.0	0.0	-.0	.0	.000
2.1	472.000	-1.060	49.950	35.030							
3.1	472.000	-1.060	49.940	35.120							
4.1	472.000	-1.060	49.940	35.120							
5.1	472.000	-1.060	49.940	35.120							
6.1	472.000	-1.060	49.940	35.120							
7.1	472.000	-1.060	49.710	35.490							
10.1	472.000	-1.060	48.480	35.700							
13.1	472.000	-1.060	47.200	36.350							
16.1	472.000	-1.060	45.030	38.210							
19.1	472.000	-1.060	42.150	41.400							
22.1	472.000	-1.060	40.470	44.540							
25.1	472.000	-1.060	39.840	47.910							
28.1	472.000	-1.060	38.140	51.690							
31.1	472.000	-1.060	18.860	56.740							
35.1	472.000	-1.060	11.710	67.580							

ZN2C.34,.472MA/SQCM,1[illegible] RE.[illegible]

CODES, 1,2,3A,4,5,6,7,8 = 1.0, -2.[illegible], [illegible], 1.0, 1.0, 1.0, 3.5, [illegible],
CODES, 9,1,.11,.2,12,13,14 = 3.0, 3.0, 5.0, 3.0, 1.0, 0.0, 2.0,
KEYNOLDS NUMBER = 11.00.2
EFFECTIVE REFRACTIVE INDICES AND POROSITIES,
TYPE 2 FILM 2.1[illegible] [illegible] I 3.[illegible]
TYPE 1 FILM 1.634 0.000) I .002
TYPE 1 HYDRATE 1.39[illegible] [illegible] I .99
SECONDARY CRYSTALS 1.881 0.3000 I .179
HOLGMESS 1.27) -4.090) I .[illegible]
NUMBER OF SECONDARY SITES/SQCM .55E+06 LIMITING COVERAGE .79
CRYSTAL, RATE OF SEC, CRYSTALS (MA/SQCM), 11.127
CRYSTAL, RATE OF TYPE2 FILM (MA/SQCM), 49.51.
SUPERSATURATION OF IONS, 1.22 ,TIME TO REACH(S) 5.44
INITIAL DISSOLUTION CURRENT (MA/SQCM) 469.0645
TIMES, ONSET OF SEC, CRYSTALS(SEC) 7.[illegible] PPT, CONSTANT (S) 2.[illegible]
TIME TO COMPLETE PATCH COVERAGE 12.4
TIME TO REACH COMPACT FILM I 25.2 S
TPACK = 25.2 TDISS = 12.4
DEHYDRATION RATE (MA/SQCM) 3.006
EFFECTIVE FILM CURRENT(MA/SQCM) 7.321
WIDTH TO HEIGHT OF SEC, CRYSTALS, 1.[illegible]
INITIAL PATCH COVERAGE .608
FINAL POROSITY OF TYPE I FILM .598
MOLE FRACTION METAL IN PATCHES .[illegible]
PASSIVATION TIME [illegible]
AVE, DISTANCE BETWEEN EXP, AND THEORY 2.512 (DEG)

			EXPERIMENT		THEORY		THICKNESSES(A)				
TIME(S)	I(MA/SQCM)	VOLTS	OEL	PSI	OEL	PSI	TYPE2	TYPE1(F)	TYPE1(H)	SECONDARY	COV
[illegible].1	472.[illegible]	-4.6.	48.68[illegible]	35.73[illegible]	49.[illegible]	37.866	[illegible].[illegible]	.[illegible]	-.[illegible]	3402.8	.001
13.1	472.[illegible]	-1.[illegible]6)	47.2[illegible]	36.350	48.975	38.953	[illegible].	1.2	-.[illegible]	3941.2	.[illegible]1
1[illegible].1	472.[illegible]	-1.6[illegible]	45.[illegible]	38.21[illegible]	43.778	39.824	.	2.7	-.[illegible]	4511.5	.0[illegible]1
19.1	472.[illegible]	-1.[illegible]0[illegible]	42.15[illegible]	41.40[illegible]							
22.1	472.[illegible][illegible]	-1.[illegible]6[illegible]	4[illegible].47[illegible]	44.94[illegible]							
25.1	472.[illegible]	-1.[illegible]6	39.84	47.51							
28.1	472.[illegible]7	-1.[illegible]6.	38.14[illegible]	51.89[illegible]							
31.1	472.[illegible][illegible]	-1.[illegible]6	13.66	66.74							
35.[illegible]	472.	-1.[illegible]6	[illegible].71	67.58							

```
 2N2:034,.72MA/SQCM,.1000 R=.1007

CODES, 1,2,3A,4,5,6,7,8 =  1. ,-2. ,  .1,  1.1,  1. ,  .1,  3.5,  3.0,
CODES, 9,10,11,12,13,14 =  0.0,  3.0,  5.0,  3.0,  1.0,  0.0,  3.0,
REYNOLDS NUMBER = 12  .0
EFFECTIVE REFRACTIVE INDICES AND POROSITIES,
TYPE 2 FILM   2.300   .0000 I            .0
TYPE 1 FILM   2.      .0000 I            .0
TYPE 1 HYDRATE   1.333   .0000 I          .990
SECONDARY CRYSTALS   1.521   .0000 I      .750
POLYMERSS   1.272  -.0090 I              .000
NUMBER OF SECONDARY SITES/SQCM     .2.6+ 8     LIMITING COVERAGE     .790
CRYSTAL, RATE OF SEC, CRYSTALS (MA/SQCM),     3.739
CRYSTAL, RATE OF TYPE2 FILM (MA/SQCM),     1.000
SUPERSATURATION OF ILNS,     .81  ,TIME TO REACH(S)       .95
INITIAL DISSOLUTION CURRENT (MA/SQCM)  3.7.9295
TIMES, ONSET OF SEC, CRYSTALS(SEC)   20.0 PPT, CONSTANT (S)     2.0
TIME TO COMPLETE PATCH COVERAGE      9  .
TIME TO REACH COMPACT FILM I      26.6  S
IPACK =      26.6  TDISS =      9  .0
DEHYDRATION RATE (MA/SQCM)  22.812
EFFECTIVE FILM CURRENT(MA/SQCM)       7.353
WIDTH TO HEIGHT OF SEC, CRYSTALS,      .1 1
INITIAL PATCH COVERAGE      .758
FINAL POROSITY OF TYPE I FILM     .  1
MOLE FRACTION METAL IN PATCHES    .  0
PASSIVATION TIME     2000.00
AVE, DISTANCE BETWEEN EXP, AND THEORY     3.119  (DEG)

                                EXPERIMENT                THEORY          THICKNESSES(A)
TIME(S)    I(MA/SQCM)   VOLTS      DEL      PSI        DEL        PSI      TYPE2      TYPE1(F)  TYPE1(H)  SECONDARY    COV

    22.1    472.  .    -1.  61     43.471     44.94      4  .333   46.574     .0         .4        -.0  11534.4    .009
    25.1    472.       -1.  .6     39.84      47.91      42.561     49.678     .0       268.2       -.0  18080.8    .023
    28.1    472.  .    -1.  .2     38.14      51.89      39.730     48.210     0.0      542.5       -.0  21731.5    .033
    32.1     472.      -1.  0      18.86      66.74
    35.1     472.  .   -1.  .      11.71      87.58
```

```
 AN2(39.50CMA/SQCM,91.0 RE,1.00

CODES, 1,2,3A,4,5,6,7,8 =  1.      .      .      1.      1.      1.      3.5,    .
CODES, 9,10,11,12,13,14 =  1.0,    1.,     2.,     4.,     5.0,    6.0,    7.,
REYNOLDS NUMBER =  9.33.)
EFFECTIVE REFRACTIVE INDICES AND POROSITIES,
TYPE 2 FILM    2.1.    1.3700 I              1.00
TYPE 1 FILM    2.      .    I                1.
TYPE 1 HYDRATE   1.69    .    I                .99
SECONDARY CRYSTALS   2.00    1.3900 I              1.00
ROUGHNESS   1.3+0    -.8992 I              .598
NUMBER OF SECONDARY SITES/SQCM      .3E+07     LIMITING COVERAGE     .79
CRYSTAL, RATE OF SEC, CRYSTALS (MA/SQCM),      .010
CRYSTAL, RATE OF TYPE2 FILM (MA/SQCM),      .1
SUPERSATURATION OF IONS,   3.9  ,TIME TO REACH(S)      6.2
INITIAL DISSOLUTION CURRENT (MA/SQCM)  ********
TIMES, ONSET OF SEC, CRYSTALS(SEC)    27.  PPT, CONSTANT (S)    2.
TPACK =      22.8  TDISS =      12.
DEPOSITION RATE (MA/SQCM) 15 .
EFFECTIVE FILM CURRENT(MA/SQCM)      .
POROSITY OF ROUGH LAYER     .598
CURRENT FRACTION FORMING ROUGHNESS     .  1
FINAL THICKNESS OF ROUGHNESS       45.2
WIDTH TO HEIGHT OF SEC, CRYSTALS,     1.
MOLE FRACTION METAL IN PATCHES     .
PASSIVATION TIME     1000.00
ADSORP, BY LANGMUIR, MAX, COVERAGE     .25
 BETA =      3.742  KCALS/MOLE
AVE, DISTANCE BETWEEN EXP, AND THEORY      1.054  (DEG)
```

			EXPERIMENT		THEORY		THICKNESSES(A)				
TIME(S)	I(MA/SQCM)	VOLTS	DEL	PSI	DEL	PSI	TYPE2	TYPE1(F)	TYPE1(M)	SECONDARY	COV
.0	5.0	-1.36	55.72	34.98	55.72	34.98	.0	0.0	0.0	.0	0.000
.3	500.00	-1.12	57.59	34.27	59.194	34.578	.0	0.0	0.0	.0	0.000
1.3	5 .0	-1. 8	62.92	33.3	61.566	34.22	.	0.0	0.0	.0	0.000
2.3	5 .0	-1.18	63.08	33.72	63.229	33.822	.0	0.0	0.0	.0	0.000
3.3	500.000	-1.18	63.66	33.92	63.639	33.544	.0	0.0	0.0	.0	0.000
7.3	5 .0	-1. 8	63.59	34.71							
9.3	500.00	-1.08	59.75	37.21							
11.3	500.00	-1. 8	58.24	41.							
13.3	5 .0	-1. 8	48.78	45.19							
14.3	500.00	-1.38	38.240	57.672							
15.3	5 .0	-1. 8	26.51	64.44							

```
  ZN 200 PM
CODES, 1,2,3,4,5,6,7,8 =  1.0,  2.0,  0.0,  1.0,  1.0,  1.0,  3.5,  0.0,
CODES, 9,10,11,3,12,13,14 =  3.0,  0.0,  7.0,  3.0,  1.0,  0.0,  2.0,
REYNOLDS NUMBER =  9000.0
EFFECTIVE REFRACTIVE INDICES AND POROSITIES,
TYPE 2 FILM    2.000    0.0000 I            0.000
TYPE 1 FILM    1.863    0.0000 I             .249
TYPE 1 HYDRATE    1.406    0.0000 I             .933
SECONDARY CRYSTALS    1.802    0.0000 I             .297
ROUGHNESS    1.577   -1.9744 I             .517
NUMBER OF SECONDARY SITES/SQCM      .223+08      LIMITING COVERAGE     .790
CRYSTAL, RATE OF SEC, CRYSTALS (MA/SQCM),  214.622
CRYSTAL, RATE OF TYPE2 FILM (MA/SQCM),   20.000
SUPERSATURATION OF IONS,    .81 ,TIME TO REACH(S)        .85
INITIAL DISSOLUTION CURRENT (MA/SQCM)  268.9456
TIMES, ONSET OF SEC, CRYSTALS(SEC)    5.5 PPT, CONSTANT (S)     2.0
TIME TO COMPLETE PATCH COVERAGE      43.6
TIME TO REACH COMPACT FILM I      14.7  S
TIME TO DISSIPATE HYDRATE LAYER      14.7  S
TPACK =      14.7  TDISS =      43.6
DEHYDRATION RATE (MA/SQCM) 475.000
EFFECTIVE FILM CURRENT(MA/SQCM)     239.988
POROSITY OF ROUGH LAYER     .517
CURRENT FRACTION FORMING ROUGHNESS     .064
FINAL THICKNESS OF ROUGHNESS     3447.9
WIDTH TO HEIGHT OF SEC, CRYSTALS,     1.000
INITIAL PATCH COVERAGE      .511
FINAL POROSITY OF TYPE I FILM     .066
MOLE FRACTION METAL IN PATCHES    0.000
PASSIVATION TIME     1000.00
AVE, DISTANCE BETWEEN EXP, AND THEORY      .253  (DEG)

                                  EXPERIMENT                THEORY          THICKNESSES(A)
TIME(S)    I(MA/SQCM)    VOLTS      DEL      PSI       DEL       PSI      TYPE2     TYPE1(F)  TYPE1(M)  SECONDARY    COV

     7.5    500.000    -1.080     63.593    34.710    63.614    34.917       0.0        5.7        -.0    7389.9     .139
     9.5    500.000    -1.080     59.750    37.210    59.912    37.057       0.0     2993.6        -.0   10888.5     .302
    11.5    500.000    -1.080     58.240    41.010    58.332    41.057       0.0     7267.5        -.0   12915.2     .425
    13.5    500.000    -1.080     46.780    46.190
    14.5    500.000    -1.080     38.240    57.670
    15.5    500.000    -1.080     28.510    64.440
```

4N2OC3*.5 JO4A/SQCM,9000 RL,1300

CODES, 1,2,3,4,5,6,7,8 = 1.0, 2.0, 0.0, 1.0, 1.0, 1.0, 3.5, 0.0,
CODES, 9,10,11,12,13,14 = 0.0, 0.0, 7.0, 3.0, 1.0, 0.0, 2.0,
PSYNOLOS NUMBER = 9000.0
EFFECTIVE REFRACTIVE INDICES AND POROSITIES,
TYPE 2 FILM 2.000 0.0000 I 0.000
TYPE 1 FILM 1.627 0.0000 I .150
TYPE 1 HYDRATE 1.394 0.0000 I .575
SECONDARY CRYSTALS 1.703 0.0000 I .438
ROUGHNESS 1.514 -2.2996 I .436
NUMBER OF SECONDARY SITES/SQCM .200+09 LIMITING COVERAGE .790
CRYSTAL, RATE OF SEC, CRYSTALS (MA/SQCM), 191.123
CRYSTAL, RATE OF TYPE2 FILM (MA/SQCM), 20.000
SUPERSATURATION OF IONS, .80 ,TIME TO REACH(S) .82
INITIAL DISSOLUTION CURRENT (MA/SQCM) 265.2765
TIMES, ONSET OF SEC, CRYSTALS(SEC) 5.5 RFT, CONSTANT (S) 2.0
TIME TO COMPLETE PATCH COVERAGE 31.2
TIME TO REACH COMPACT FILM I 10.0 S
TIME TO DISSIPATE HYDRATE LAYER 10.0 S
TPACK = 100.0 TDISS = 31.2
DEHYDRATION RATE (MA/SQCM) 475.000
EFFECTIVE FILM CURRENT(MA/SQCM) 76.955
POROSITY OF ROUGH LAYER .438
CURRENT FRACTION FORMING ROUGHNESS .032
FINAL THICKNESS OF ROUGHNESS 1984.8
WIDTH TO HEIGHT OF SEC, CRYSTALS, 1.006
INITIAL PATCH COVERAGE .111
FINAL POROSITY OF TYPE I FILM .496
PULE FRACTION METAL IN PATCHES 0.000
PASSIVATION TIME 1000.00
AVE, DISTANCE BETWEEN EXP, AND THEORY 2.393 (DEG)

			EXPERIMENT		THEORY		THICKNESSES(A)				
TIME(S)	I(MA/SQCM)	VOLTS	DEL	PSI	DEL	PSI	TYPE2	TYPE1(F)	TYPE1(H)	SECONDARY	COV
10.3	500.000	-1.080	48.780	49.190	49.347	49.300	0.0	5.5	-.0	13792.3	.452
14.3	500.000	-1.080	38.240	57.670	35.350	56.356	0.0	1012.5	-.0	15219.7	.550
15.3	500.000	-1.080	26.510	64.240	28.402	53.336	0.0	2645.6	-.0	16146.0	.619
-I	-I	-I	-I	-I							

TECHNICAL INFORMATION DEPARTMENT
LAWRENCE BERKELEY LABORATORY
UNIVERSITY OF CALIFORNIA
BERKELEY, CALIFORNIA 94720